THEORETICA CHIMICA ACTA

edenda curat

Hermann Hartmann

adiuvantibus
C. J. Ballhausen, København
R. D. Brown, Clayton
E. Heilbronner, Basel
J. Jortner, Tel-Aviv
J. A. A. Ketelaar, Amsterdam
M. Kotani, Tokyo
J. Koutecký, Praha
J. W. Linnett, Cambridge
E. E. Nikitin, Moskwa
R. G. Pearson, Evanston
B. Pullman, Paris
K. Ruedenberg, Ames
C. Sandorfy, Montreal
M. Simonetta, Milano
O. Sinanoğlu, New Haven

Vol. 25, 1972

Springer-Verlag · Berlin · Heidelberg · New York

The exclusive copyright for all languages and countries, including the right for photomechanical and any other reproductions, also in microform, is transferred to the publisher.

The use in this journal of registered or trade names, trademarks etc. without special acknowledgement does not imply that such names, as defined by the relevant protections laws, may be regarded as unprotected and thus free for general use.

Alle Rechte, einschließlich das der Übersetzung in fremde Sprachen und das der fotomechanischen Wiedergabe oder einer sonstigen Vervielfältigung, auch in Mikroform, vorbehalten. Jedoch wird gewerblichen Unternehmen für den innerbetrieblichen Gebrauch nach Maßgabe des zwischen dem Börsenverein des Deutschen Buchhandels e. V. und dem Bundesverband der Deutschen Industrie abgeschlossenen Rahmenabkommens die Anfertigung einer fotomechanischen Vervielfältigung gestattet. Wenn für diese Zeitschrift kein Pauschalabkommen mit dem Verlag vereinbart worden ist, ist eine Wertmarke im Betrage von DM 0,40 pro Seite zu verwenden. *Der Verlag läßt diese Beträge den Autorenverbänden zufließen.*

Die Wiedergabe von Gebrauchsnamen, Handelsnamen, Warenbezeichnungen usw. in dieser Zeitschrift berechtigt auch ohne besondere Kennzeichnung nicht zu der Annahme, daß solche Namen im Sinne der Warenzeichen- und Markenschutz-Gesetzgebung als frei betrachtet wären und daher von jedermann benutzt werden dürften.

Springer-Verlag Berlin Heidelberg New York
Printed in Germany by Brühlsche Universitätsdruckerei, Gießen
© by Springer-Verlag Berlin Heidelberg 1972

[illegible] /02
38963
[illegible] 24.4.[illegible] Hil

Index

Commentationes et Relationes

Alagona, G., Cimiraglia, R., Scrocco, E., Tomasi, J.: Theoretical Investigations on the Solvation Process. II. The Monohydrated Associates of Some Three-Membered Ring Molecules . . . 103
Anno, T.: On the Evaluation of the Energies of Hybridized Valence States . . . 248
Armstrong, D. R., Jamieson, J., Perkins, P. G.: The Electronic Structure of the Silyl Halides 396

Ballhausen, C. J., s. Güdel, H. U. . . . 331
Bender, C. F., s. McLaughlin, D. R., et al. . . . 352
Bertran, J.: Theoretical Study of the Photodimerization of Pyrimidine Bases . . . 372
Bessis, G., s. Tapia, O. . . . 130
Bingel, W. A.: Note on the Solution of Secular Problems with Two Non-Orthogonal Basis Functions . . . 196
Briggs, P. J., s. Melrose, M. P. . . . 181
Brown, R. D., Burden, F. R., Hart, B. T.: A Comparison of Lobe and Cartesian Gaussian Basis Sets for Molecular Calculations . . . 49
Burden, F. R., s. Brown, R. D., et al. . . . 49

Choplin, F., Kaufmann, G.: Etude LCAO MO CNDO 2 de la structure électronique de composés du titane . . . 54
Chu, S. Y.: SCF Calculations for H_2^+, Li_2^+ and LiH^+ with Atomic Basis Set Enlarged by Bond Function . . . 200
Cignitti, M., Paoloni, L.: The Electronic Structure of Groups of Isomeric Heteroaromatic Systems. IV. Structure and Spectra of Pyridones and Their N-Methyl Derivatives 277
Cimiraglia, R., s. Alagona, G., et al. . . . 103
Companion, A. L.: A Molecular Orbital Study of Bond Energies in Compounds of Sulfur and Fluorine . . . 268
Crasnier, F., s. Robinet, G., et al. . . . 259
Cremaschi, P., Gamba, A., Simonetta, M.: The Influence of Solvation on the Calculated Activation Energy for the Reaction $CH_3F + F^-$ . . . 237

Dacre, P. D., Elder, M.: Sulphur Dioxide. Notes on the Electronic Changes which Occur on Coordination . . . 254
Davis, R. E, Kim, K. S.: Fermi Resonance in the Carbonyl Band of Cyclopentanone . . . 89

Ecker, F., Hohlneicher, G.: Störungstheoretische Berechnung von Ionisierungsenergien und Elektronenaffinitäten mit Hilfe der Greenschen Zweipunktfunktion . . . 289
Elder, M., s. Dacre, P. D. . . . 254

Fraga, S., s. Lo, B. W. N. . . . 97, 391

Gamba, A., s. Cremaschi, P., et al. . . . 237
Gebelein, H., Jortner, J.: On the Relation between Non Adiabatic Unimolecular Reactions and Radiationless Processes . . . 143
Giessner-Prettre, C., Pullman, A.: Molecular Electrostatic Potentials: Comparison of *ab initio* and CNDO Results . . . 83
Goodisman, J.: Thomas-Fermi-Dirac Calculations for Molecules. II. One-Electron Energies for F_2 . . . 205
Gouterman, M., s. Schaffer, A. M. . . . 62
Güdel, H. U., Ballhausen, C. J.: Low Temperature Absorption Spectra of TcO_4^- and ReO_4^- in $KClO_4$ . . . 331

Hart, B. T., s. Brown, R. D., et al. . . . 49
Hinchliffe, A.: Further *ab initio* Calculations on the Allyl Radical . . . 138
Hohlneicher, G., s. Ecker, F. . . . 289
Hosoya, H.: Graphical Enumeration of the Coefficients of the Secular Polynomials of the Hückel Molecular Orbitals . . . 215
Hoyer, E., s. Reinhold, J. . . . 319
Hush, N. S., Williams, M. L.: Finite Electric Field Valence-Shell Calculations of Molecular Hyperpolarizabilities . . . 346

Jamieson, J., s. Armstrong, D. R., et al. 396
Jortner, J., s. Gebelein, H. 143
Jug, K., Lykos, P. G., McLean, A. D.: *Exponent Optimization for Π States of H_2* 10
— — — Optimal Double-Configuration Study of the Lowest Excited Π States of H_2. I. Potential Energy Curves and One-Electron Properties 17
— — — Optimal Double-Configuration Study of the Lowest Excited Π States of H_2. II. σ - π Separation 41
Kankare, J. J.: *Application of Coulson's Contour Integral Method to Linear Finite Polymers* 189
Kaufmann, G., s. Choplin, F. 54
Kim, K. S., s. Davis, R. E. 89
King, R. B.: Chemical Applications of Topology and Group Theory. VI. Polyhydral Water Networks in Clathrates and Semiclathrates 309
Kleiner, M.: A Note on the Relation between CI and Rayleigh-Schrödinger Perturbation Theory 121
Klopman, G., Polak, R.: *Semiempirical SCF Theory with "Scaled" Slater Orbitals. II. Molecular Calculations* 223
Kventsel, G. F., s. Ukrainsky, I. I. 360
Labarre, J.-F., s. Robinet, G., et al. 259
Ladd, M. F. C.: Charge Distributions in Polyatomic Ions 400
Leibovici, C., s. Robinet, G., et al. 259
Lo, B. W. N., Saxena, K. M. S., Fraga, S.: Complete Spin-Orbit Interaction in Many-Electron Atoms 97
— Fraga, S.: Nuclear Mass Effect in Many-Electron Atoms 391
Lykos, P. G., s. Jug, K., et al. 10, 17, 41
McLaughlin, D. R., Bender, C. F., Schaefer, H. F., III: *Geometry and Force Constant Determination from Correlated Wave Functions for Polyatomic Molecules: Ground States of H_2O and CH_2* 352
Mc Lean, A. D., s. Jug, K., et al. 10, 17, 41
Melrose, M. P., Briggs, P. J.: Integral Hellmann-Feynman Investigations of *trans* Bent Acetylene 181
Nelander, B.: A CNDO/2 Calculation on a Complex between Ethylene and Chlorine 382
Paoloni, L., s. Cignitti, M. 277
Perkins, P. G., s. Armstrong, D. R., et al. 396
Polak, R., s. Klopman, G. 223
Pullman, A., s. Giessner-Prettre, C. 83
Reinhold, J., Hoyer, E.: Angenäherte Berechnung der Dreizentren-Kernanziehungsintegrale in LCAO—MO-Verfahren für Koordinationsverbindungen 319
Reinsch, E.-A.: Das Kastenmodell als Grundlage für ein *ab initio*-Verfahren. III. Ergebnisse für das Wasserstoff- und Heliumatom 338
Robinet, G., Crasnier, F., Labarre, J.-F., Leibovici, C.: Analyse conformationnelle théorique de la diméthylsulfone, $(CH_3)_2SO_2$ 259
Saxena, K. M. S., s. Lo, B. W. N., et al. 97
Schaefer, H. F., s. McLaughlin, D. R., et al. 352
Schaffer, A. M., Gouterman, M.: Porphyrins XXV. Extended Hückel Calculations on Location and Spectral Effects of Free Base Protons 62
Scrocco, E., s. Alagona, G., et al. 103
Simonetta, M., s. Cremaschi, P., et al. 237
Tapia, O., Bessis, G.: Intermolecular Interactions-Dependence on Inter- and Intra-Molecular Distances. A Configuration Interaction Study of the $H_2 \cdots H_2$ System 130
Tomasi, J., s. Alagona, G., et al. 103
Ukrainsky, I. I., Kventsel, G. F.: Electronic Structure of Long Polyene Chains with an Impurity Atom 360
Walker, T. E. H.: On Open Shell Hartree-Fock Calculations 1
Williams, M. L., s. Hush, N. S. 346
Wirsam, B.: *Ab initio* Untersuchungen über Stabilität und Spektren des hypothetischen Moleküls Si_2H_2 169

Recensio

Fackler, J. P., Jr.: Symmetry in Coordination Chemistry. (Ref. H.-H. Schmidtke) 120

Theoret. chim. Acta (Berl.) 25, 1—9 (1972)
© by Springer-Verlag 1972

Commentationes

On Open Shell Hartree-Fock Calculations

T. E. H. WALKER*

Physical Chemistry Laboratory, South Parks Road, Oxford OX1 3QZ, England

Received July 20, 1971

The errors in open shell Hartree-Fock calculations are discussed. Various hamiltonians for single eigenvalue methods are considered, and it is shown that a better energy is obtained with those hamiltonians that correctly account for the open shell/closed shell interactions.

Die Fehler des Hartree-Fock-Verfahrens bei offenen Schalen werden diskutiert, indem verschiedene Hamilton-Operatoren für das Gesamtsystem betrachtet werden. Dabei zeigt sich, daß diejenigen Hamilton-Operatoren, die die Wechselwirkung zwischen offenen und abgeschlossenen Schalen am besten wiedergeben, auch die besten Energien liefern.

Discussion des erreurs dans les calculs Hartree-Fock à couche ouverte. On considère divers hamiltoniens pour les méthodes à valeur propre unique, et l'on montre qu'une meilleure énergie est obtenue avec les hamiltoniens qui rendent compte correctement de l'interaction couche ouverte-couche fermée.

1. Introduction

Although the Hartree-Fock equations for a closed shell atom or molecule may be solved fairly easily in principle, it is not so for open shell systems. This is due to the problem of the off-diagonal multipliers, which cannot be eliminated. Many authors have considered this [1, 2], and have developed methods which involve two coupled eigenvalue equations, one for the open and one for the closed shells. This approach has been successfully applied to many systems, but there are certain difficulties, namely lengthy computing time, and problems related to which sets of orbitals should be chosen for configuration interaction calculations.

An alternative method has been proposed by Roothaan [1], and also by Nesbet [3], which simplifies the Hartree-Fock equations to a single eigenvalue problem. This eliminates the off-diagonal multipliers, either by putting them equal to zero, or by incorporating them partially into the hamiltonian. These procedures are only strictly possible when the open shell orbitals are the only ones of their symmetry. Except for these particular cases, neglect of off-diagonal multipliers implies that the correct hamiltonian is not being used, and the energy obtained from the approximate Hartree-Fock equations is then corrected to allow for this [1].

A recent paper [4] has pointed out some consequences of this neglect of off-diagonal multipliers. The Fock matrix is no longer invariant to a unitary transformation of the orbitals, and one is not necessarily at liberty to choose the set of orbitals that diagonalises the matrix of lagrangian multipliers. This has resulted in calculations that give different total energies when different symmetry orbitals are used (even after correcting the energies as above), and discontinuous potential curves have been obtained when the symmetry changes with variation of normal coordinate [5]. Walker demonstrated [4] that the magnitude of the error depended on the number of closed shell orbitals with the same symmetry as the open shell, and on their type. Core closed shell orbitals gave rise to larger errors than valence orbitals, (in fact the error is roughly proportional to the orbital energy) and this was borne out by the results of some Hartree-Fock calculations.

---

* Present address: Department of Physics, University of Virginia, Charlottesville, Virginia, USA.

As has already been mentioned, single eigenvalue methods are much more convenient to use than those involving two eigenvalue equations, and it is of interest to investigate these errors in case they can be avoided in the future.

2. Theory

The total hamiltonian for an N-electron system is

$$\sum_{i=1}^{N} T_i + \sum_{i>j=1}^{N} v_{ij} \tag{2.1}$$

where T_i represents the terms due to kinetic energy and the attraction by the nucleus, and v_{ij} the interaction between electrons $(1/r_{ij})$. The Hartree-Fock method approximates this hamiltonian by replacing the two-body interaction v_{ij} by a single particle potential V, that is

$$H_0 = \sum_{i=1}^{n} (T_i + V_i) \tag{2.2}$$

with the eigenvalue equation $H_0\Phi_0 = E_0\Phi_0$, where Φ_0 is the determinant formed from the N lowest solutions of the eigenvalue equation

$$(T+V)\,\varphi_n = \varepsilon_n \varphi_n\,. \tag{2.3}$$

(Note that this equation is only obtained after choosing the set of orbitals that diagonalises the matrix corresponding to ε.) The Hartree-Fock potential is then defined by

$$\langle a|V|b\rangle = \sum_{n=1}^{N} \{\langle an|v|bn\rangle - \langle an|v|nb\rangle\} \tag{2.4}$$

with n denoting an occupied spinorbital.

Hence to first order the energy obtained from a Hartree-Fock calculation is

$$E_0 = \sum_{i=1}^{N} \varepsilon_i + \left\{\frac{1}{2}\sum_{i,j}^{N} [\langle ij|v|ij\rangle - \langle ij|v|ji\rangle] - \sum_{i=1}^{N} \langle i|V|i\rangle\right\} \tag{2.5}$$

$$= \sum_{i=1}^{N} \left[\langle n|T|n\rangle + \frac{1}{2}\langle n|V|n\rangle\right] = \frac{1}{2}\sum_{i=1}^{N} (\varepsilon_i^N + \varepsilon_i)\,. \tag{2.6}$$

This is not so for a single eigenvalue equation, because V' (we shall use primes systematically to refer to single eigenvalue calculations) is not defined as in (2.3). In this case, the bracketed part of (2.5) is not equal to $-\frac{1}{2}\sum_{i=1}^{N}\langle i|V|i\rangle$, but ncludes other terms. To determine these, we must consider the possible hamiltonians.

In the restricted Hartree-Fock method, orbitals with different spins, or those belonging to different degenerate components of the same representation – such as π^+, π^- in linear molecules – are constrained to have the same radial dependence. The hamiltonian is therefore the same for all electrons contained in he same space orbital. This is quite legitimate if there are only closed shells present, but not if there is one or more unpaired electron. Because exchange erms only arise between electrons of parallel spin, the hamiltonian for those electrons with the same spin as the unpaired electron should be different from hat for those with opposite spin.

The restricted Hartree-Fock potential, V', for a single eigenvalue calculation s defined so as to be the same for all electrons in spinorbitals of the same symmetry. If we consider a diatomic molecule with one unpaired σ electron in orbital x, possible hamiltonians are

$$\langle a_\sigma|V_1'|b_\sigma\rangle = \sum_{n=1}^{N-1}\{\langle an|v|bn\rangle - \langle an|v|nb\rangle\} + \langle ax|v|bx\rangle - \langle ax|v|xb\rangle\,, \tag{2.7a}$$

$$\langle a_\sigma|V_2'|b_\sigma\rangle = \sum_{n=1}^{N-1}\{\langle an|v|bn\rangle - \langle an|v|nb\rangle\} + \langle ax|v|bx\rangle - \frac{1}{2}\langle ax|v|xb\rangle \tag{2.7b}$$

and for both of these

$$\langle a_\pi|V'|b_\pi\rangle = \sum_{i=1}^{N}\{\langle an|v|bn\rangle - \langle an|v|nb\rangle\}\,. \tag{2.8}$$

The operators V_1', V_2' can also be written in the familiar J and K notation as

$$V_1' = \sum_{n=1}^{N-1}\left(J_n - \frac{1}{2}K_n\right) + J_x - K_x\,, \tag{2.9a}$$

$$V_2' = \sum_{n=1}^{N-1}\left(J_n - \frac{1}{2}K_n\right) + J_x - \frac{1}{2}K_x\,. \tag{2.9b}$$

The energy E' through first order from these hamiltonians is

$$E_1' = \frac{1}{2}\sum_{i=1}^{N}(\varepsilon_i^N + \varepsilon_i) + \frac{1}{2}\sum_{i=\sigma}\langle ix|v|xi\rangle\,, \tag{2.10a}$$

$$E_2' = \frac{1}{2}\sum_{i=1}^{N}(\varepsilon_i^N + \varepsilon_i) - \frac{1}{2}\langle xx|v|xx\rangle \tag{2.10b}$$

and it is immediately clear that the extra integrals needed in the energy expression involve the open shell electron, either with itself or with the closed shell electrons of the same symmetry.

These two different choices of hamiltonian introduce different errors into the energy. V_1' allows exactly for the interaction of the unpaired electron with itself, since $\langle ix|v|ix\rangle - \langle ix|v|xi\rangle = 0$ if $i = x$, but not for the interaction with closed shell electrons. The reverse is true for V_2', which accounts correctly for the closed shells but introduces a spurious contribution for the interaction of the open shell electron with itself. Although these errors are partially corrected by including the extra molecular integrals in the energy expression, there will still be residual terms corresponding to higher orders of perturbation theory.

Until recently it has always been assumed that these terms could be neglected. Kelly [6] included them in his many-body perturbation theory work on the oxygen atom, and showed that they were indeed small. However the large errors reported by Walker [4] and Dixon [5], when single eigenvalue methods were employed for polyatomic molecules, arise from second and higher orders, and this paper contains some further examples. Both the true Hartree-Fock hamiltonian, H, and the restricted hamiltonians, H', used in the single eigenvalue approximation are derived from one-body potentials. Thus if one was to write the Hartree-Fock wavefunction as a linear combination of determinants constructed from orbitals obtained from the restricted hamiltonian, only singly excited states contribute. We may then employ perturbation theory with the hamiltonian $H'' = V - V'$ to obtain the Hartree-Fock energy from the restricted wavefunctions.

Two kinds of restriction are involved in these calculations. The first, the requirement that the hamiltonian be the same for electrons with different spins, is common to both single and double eigenvalue methods. It corresponds to the neglect of spin polarisation. The second restriction is that the hamiltonian be the same for electrons in open and closed shells of the same symmetry. It is this second restriction that differentiates the single and double eigenvalue methods and introduces the molecular integrals into the energy expression.

3. Perturbation Calculations

The first order correction due to the perturbation $H'' = V - V'$ has already been discussed. An idea of its magnitude can be obtained from Table 1, where the results of some single eigenvalue calculations are given. The correction is much larger for the hamiltonian V_2', because the integrals $\langle xx|v|xx\rangle$ are larger than the exchange integrals $\langle ix|v|xi\rangle$ involved in the calculation for V_1'. The results for AlO, the only case in which both hamiltonians were used for a

Table 1. First order correction from $H'' = V - V'$ (a.u.)

Molecule	E_0'	E_1'	Total	Hamiltonian
BeH: $X^2\Sigma^+$ $1\sigma^2 2\sigma^2 3\sigma$	-15.1759042	0.0260388	-15.1498654	V_1'
CH$_3$: $^2A_1$ $1a_1^2 2a_1^2 3a_1 1b_1^2 1b_2^2$	-39.1525820	0.0760063	-39.0765757	V_1'
AlO: $X^2\Sigma^+$ $(1-6\sigma)^2 (1-2\pi)^4 7\sigma$	-316.8417385	0.0909992	-316.7507392	V_1'
AlO: $X^2\Sigma^+$	-316.6672300	-0.1694578	-316.8366878	V_2'

calculation on the same molecule, are particularly noticeable. Although the correction is much larger for V_2' than for V_1', the final energy is better, and we shall show that this is due to quicker convergence of the perturbation series. However the AlO results give quite a dramatic demonstration of the errors that can occur when single eigenvalue methods are used.

The second order contribution to the energy is

$$\varDelta E^2 = \sum_i \frac{\langle \Phi_0 | H'' | \Phi_i \rangle \langle \Phi_i | H'' | \Phi_0 \rangle}{E_0 - E_i} \tag{3.1}$$

where all singly excited states are to be included. If a non-restricted hamiltonian is employed these matrix elements are zero. Two different types of excitation can be distinguished, those in which the electron excited from an occupied spinorbital (q) to an unoccupied spinorbital (k) has spin parallel or antiparallel to the unpaired electron. These can be further subdivided into different symmetries of q. Table 2 gives the matrix elements $\langle \Phi_q^k | H'' | \Phi_0 \rangle$, where Φ_q^k represents the determinant formed by replacing an electron in q with one in k, and we have assumed one unpaired σ electron.

Table 3 shows the results for the second order energy for three molecules, whose wavefunctions were obtained with the hamiltonian V_1'. In the cases of BeH and AlO, only excitations to the first four unoccupied σ orbitals and first three π orbitals were considered, and these corrections would no doubt be increased if all single excitations were included. In CH_3, where only a minimum basis set was used, all excitations were included. To check the convergence, two further calculations were carried out. In BeH, the matrix of all excited states included in the second order calculation was diagonalised and the energy lowering found to be 0.003696 a.u., 97% of which was given by the second order term. In CH_3, the third order contribution was found to be +0.00014 compared to the second order −0.00659 a.u.

Table 2. Matrix elements of H''

Excitation	Spin	$V - V_1'$	$V - V_2'$
$q\sigma \to k\sigma$	α	0	$-\frac{1}{2}\langle qx \| v \| xk \rangle$
$q\sigma \to k\sigma$	β	$\langle qx \| v \| xk \rangle$	$+\frac{1}{2}\langle qx \| v \| xk \rangle$
$q\pi \to k\pi$	α	$-\frac{1}{2}\langle qx \| v \| xk \rangle$	$-\frac{1}{2}\langle qx \| v \| xk \rangle$
$q\pi \to k\pi$	β	$+\frac{1}{2}\langle qx \| v \| xk \rangle$	$+\frac{1}{2}\langle qx \| v \| xk \rangle$

Table 3. Second order correction from H'' (a.u.)

Molecule	$\varDelta E^2$	Hamiltonian
BeH	−0.0036	V_1'
CH_3	−0.0065	V_1'
AlO	−0.0058	V_1'
AlO	−0.0044	V_2'

There is also another means of checking the size of the total error introduced by using a single eigenvalue method. Cade and Huo [7] have reported calculations for BeH using the double eigenvalue method, and their energy was -15.15312 a.u. Our results with the same basis set was -15.14987 a.u., an error of 0.00325 a.u., which agrees well with the partial second order contribution of Table 3. (This error is not due to the different programmes, since a similar calculation on the $A^2\Pi$ state of BeH($|\sigma^2 2\sigma^2|\pi\rangle$ when the single eigenvalue hamiltonian is identical to that used in the eigenvalue method, gave results which agreed to five decimal places.) The difference, 0.00045 a.u. which remains, and which would be increased if all excited states were included, is due to the effect of using a restricted hamiltonian in the double eigenvalue method, that is of not including spin polarisation.

The error in the CH_3 single eigenvalue calculation was estimated in a previous paper [4] as 0.01 a.u. The fact that the second and third order contributions give slightly less than 70% of this is partially due to a minimum basis set being a bad approximation to the complete set of orbitals.

The calculations for AlO also allow a comparison of the two restricted hamiltonians. The difference between the two values of the total energy is 0.0859 a.u. (≈ 2.3 eV), which is large enough to be of importance when calculating excitation or ionization energies. The second order contributions only make up part of this difference, although they would be larger if all excitations were included. However it is possible to draw some general conclusions about the relative magnitudes of successive terms in the perturbation series.

If we write the energy denominator in Eq. (3.1) as $\Delta E(q,k,s)$ for the excitation of an electron in orbital q to orbital k with spin s (α or β), the second order energy becomes, using the matrix elements in Table 2.

$$\text{For } V_1' \quad \Delta E_1^2 = \sum_{q \neq x} \frac{|\langle qx|v|xk\rangle|^2}{\Delta E_1(q,k,\beta)}, \tag{3.2a}$$

$$\text{for } V_2' \quad \Delta E_2^2 = \frac{1}{4} \sum_{k \neq x} \frac{|\langle qx|v|xk\rangle|^2}{\Delta E_2(q,k,\alpha)} + \frac{1}{4} \sum_{q \neq x} \frac{|\langle qx|v|xk\rangle|^2}{\Delta E_2(q,x,\beta)} \tag{3.2b}$$

where we have assumed the unpaired electron has α spin. The summations over k include $k = x$ (with spin β) unless specifically excluded. To compare these two second order energies, some assumptions must be made about the relative magnitudes of the integrals and energy denominators in the two different calculations.

Since $\Delta E_2(q,k,\beta) = \Delta E_2(q,k,\alpha) + \langle qx|v|xq\rangle - \langle kx|v|xk\rangle$, the difference between the excitation energies will be small, and we can assume $\Delta E_2(q,k,\alpha) = \Delta E_2(q,k,\beta)$ in (3.2b). The expressions for ΔE^2 can then be written

$$\Delta E_1^2 = \sum_{k,q \neq x} \frac{|\langle qx|v|xk\rangle|^2}{\Delta E_1^2(q,k,\beta)} + \sum_{q \neq x} \frac{|\langle qx|v|xx\rangle|^2}{\Delta E_1^2(q,x,\beta)}, \tag{3.3a}$$

$$\begin{aligned} \Delta E_2^2 = {} & \frac{1}{2} \sum_{k,q \neq x} \frac{|\langle qx|v|xk\rangle|^2}{\Delta E_2^2(q,k,\beta)} + \frac{1}{4} \sum_{q \neq x} \frac{|\langle qx|v|xx\rangle|^2}{\Delta E_2^2(q,k,\beta)} \\ & + \frac{1}{4} \sum_{k \neq x} \frac{|\langle xx|v|xk\rangle|^2}{\Delta E_2(x,k,\alpha)}. \end{aligned} \tag{3.3b}$$

Table 4. Comparison of molecular integrals for different calculations on AlO (a.u.)

Integral $\langle qx\|v\|xk\rangle$		Calc. 1	Calc. 2
q	k		
6	8	−0.026809	−0.028206
5	8	−0.009270	−0.009658
4	8	−0.002473	−0.002066
3	8	−0.001855	−0.001784
2	8	0.001556	0.001458
1	8	−0.000157	−0.000161
6	7	0.011644	0.007808
5	7	−0.011294	−0.011482
4	7	−0.001809	−0.001421
3	7	−0.002088	−0.001690
2	7	0.001106	0.001145
1	7	0.000581	0.000471

Calc. 1 is with V_1', Calc. 2 with V_2'

Table 5. Comparison of energy denominators for different calculations on AlO (a.u.)

$\Delta E(q, k, \beta)$		Calc. 1	Calc. 2
q	k		
6	8	0.3704	0.3409
5	8	1.1006	1.0669
4	8	3.1471	3.1138
3	8	4.8411	4.8009
2	8	20.3853	20.3459
1	8	58.4207	58.4096
6	7	0.2274	0.1507
5	7	0.8899	0.8182
4	7	2.8484	2.7646
3	7	4.5401	4.3358
2	7	20.1146	19.9078
1	7	58.0943	57.8964

Calc. 1 is with V_1'; Calc. 2 with V_2'

Tables 4 and 5 give some representative values for the integrals and energy denominators for the two hamiltonians, and suggest that in most cases they are the same within about fifteen percent for both calculations. Hence we can deduce that $\Delta E_1^2 > \Delta E_2^2$ provided that

$$\frac{1}{2}\sum_{q,k\neq x}\frac{|\langle qx|v|xk\rangle|^2}{\Delta E_2(q,k,\beta)}+\frac{3}{4}\sum_{q\neq x}\frac{|\langle qx|v|xk\rangle|^2}{\Delta E_2(x,k,\beta)}>\frac{1}{4}\sum_{k\neq x}\frac{|\langle xx|v|xk\rangle|^2}{\Delta E_2(x,k,\alpha)}. \qquad (3.4)$$

One would expect this inequality to hold except for light atoms or molecules, when the summation over all q will contain very few terms. Table 6 shows the results for the two calculations on AlO in more detail. It confirms the arguments above, showing that $\Delta E_1^2 > \Delta E_2^2$, and that about half of ΔE_2^2 arises from the term

Table 6. Contributions to ΔE_1^2 and ΔE_2^2 for AlO (a.u.)

	ΔE_1^2	ΔE_2^2
Excitation $7\sigma \rightarrow k\sigma$	0	−0.002041
Total from other σ excitation	−0.005709	−0.002263
Total from π excitation	−0.000109	−0.000101
Grand total	−0.005818	−0.004405

$\frac{1}{4}\sum_{k\neq x}\frac{|\langle xx|v|xk\rangle|^2}{\Delta E(x,k,\alpha)}$. It is this term in light molecules that could invalidate the inequality (3.4). The assumptions about relative sizes of molecular integrals and energy denominators in the two calculations appear to be partially justified by the close agreement between the contributions from Π excitations.

However the difference between the limited second order contributions does not explain the discrepancy between the energies obtained for the two calculations, and higher order terms should be considered. While an actual calculation would be very tedious, there are two factors which suggest that $\sum_{n=3}^{\infty}\Delta E_1^n > \sum_{n=3}^{\infty}\Delta E_2^n$. Firstly, the matrix elements involved in the calculation of ΔE_2^n are a factor two smaller than the nonzero elements for ΔE_1^n. Secondly, although there are twice as many terms, because excitations of both spins contribute, they occur with opposite sign. There will therefore be some degree of cancellation in the higher orders of perturbation theory.

4. Conclusions

These results demonstrate the large errors that can occur when single eigenvalue methods are used, that is the hamiltonian is chosen to be the same for electrons in open and closed shells of the same symmetry. Moreover, these errors are the larger the more closed shells there are of the same symmetry as the open shell [4]. The same conclusions can be drawn from the behaviour of the Fock matrix under a unitary transformation of the orbitals, but the consideration of the second and higher order corrections may allow the errors to be minimised.

This work suggests that of the two hamiltonians considered here, V_2', which accounts correctly for the open shell/closed shell interactions, gives a better energy than V_1'. Although the two hamiltonians dealt with in this paper are the intuitively obvious ones, there are many others which could be used. It would be possible to employ as the Hartree-Fock potential V_3' defined by

$$\langle a_\sigma|V_3'|b_\sigma\rangle = \sum_{n=1}^{N-1}\{\langle an|v|bn\rangle - \langle an|v|nb\rangle\} + \langle ax|v|bx\rangle - \lambda\langle ax|v|xb\rangle$$

where λ is a variational parameter, chosen to minimise the total energy as given by $E_0' + E_1'$. Presumably this choice of λ would also minimise the magnitude of the second order correction to the energy.

The factors dealt with here are another aspect of the symmetry problems first raised by Löwdin [8]. He investigated the relationships between the symmetry orbitals used and the total energy for closed shell molecules, and showed that it was sometimes possible to obtain a lower energy by employing a lower symmetry. Cizek and Paldus [9, 10] and Hibbert and Coulson [11] have investigated the stability of the Hartree-Fock equations for both open and closed shell systems, and the former showed that for cyclic polyenes in the PPP approximation, the equations were always unstable to changes in symmetry. They were able to differentiate two types of instability for molecules with one unpaired electron, doublet and multiplet instability. The latter corresponds to spin polarisation and is always present, that is to say a lower energy will always be obtained if the restriction that electrons in the same orbitals have the same spatial dependence is lifted. Their doublet instability is formally related to the errors introduced by the single eigenvalue methods.

There is an interesting distinction between their work and this paper. They showed that the energy could be lowered by lowering the symmetry, but the reverse can be true for the errors discussed here. This follows because the open shell orbital may be the only one of its symmetry type in a high symmetry, but not in a lower one. For example, the ${}^2E'$ state in CH_3 has the configuration $(1a_1')^2\,(2a_1')^2\,(1e')^3\,(1a_2'')^2$, but in C_{2v} one component becomes ${}^2A_1$ with configuration $(1a_1)^2\,(2a_1)^2\,(1b_2)^2\,3a_1(1b_1)^2$. The off-diagonal multipliers connecting closed and open shells will be zero in D_{3h} but not in C_{2v}; thus in D_{3h} the single eigenvalue hamiltonian is exactly the same as the one in the double eigenvalue method.

In this paper we have only considered the energy, but other molecular properties may also be affected. Again singly excited states will contribute to the expectation value unless the correct Hartree-Fock hamiltonian is used. It is only likely that this will be important if the property is very dependent on the unpaired electron, or if contributions from spin polarisation are important.

Acknowledgements. The author would like to thank the Royal Commissioners for the Exhibition of 1851 and University College, Oxford for research fellowships.

References

1. Roothaan, C. J.: Rev. mod. Physics **32**, 179 (1960).
2. Hunt, W. J., Dunning, T. H., Goddard, W. A.: Chem. Physics Letters **4**, 231 (1969).
3. Nesbet, R. K.: Proc. Roy. Soc. (London) A **230**, 312, 322 (1955).
4. Walker, T. E. H.: Chem. Physics Letters **9**, 174 (1971).
5. Dixon, R. N.: Molecular Physics **20**, 113 (1971).
6. Kelly, H. P.: Physic. Rev. **144**, 39 (1966).
7. Cade, P. E., Huo, W. M.: J. chem. Physics **47**, 614 (1967).
8. Löwdin, P.-O.: Rev. mod. Physics **35**, 496 (1963).
9. Cizek, J., Paldus, J.: J. chem. Physics **47**, 3976 (1967).
10. Paldus, J., Cizek, J.: J. chem. Physics **52**, 2919 (1970).
11. Hibbert, A., Coulson, C. A.: J. Phys. B. **2**, 458 (1969).

T. E. H. Walker
Department of Physics
University of Virginia
McCormick Road
Charlottesville, Virginia 22901
USA

Theoret. chim. Acta (Berl.) 25, 10–16 (1972)
© by Springer-Verlag 1972

Exponent Optimization for Π States of H_2

KARL JUG*

Department of Chemistry, Illinois Institute of Technology, Chicago, Illinois 60616
and Department of Chemistry, Saint Louis University, Saint Louis, Missouri 63156

PETER G. LYKOS**

Department of Chemistry, Illinois Institute of Technology, Chicago, Illinois 60616

A. D. MCLEAN

IBM Research Laboratory, San Jose, California 95114

Received July 20, 1971

The total energy of the lowest ${}^1\Pi_u$, ${}^3\Pi_u$, ${}^1\Pi_g$, ${}^3\Pi_g$ states of H_2 was minimized in an extended Hartree-Fock procedure employing a double configuration wavefunction. The exponents of the basis functions 1s, 2s, $2p\sigma$, $2p\pi$, $3d\pi$ were optimized separately for all four states at various internuclear distances. The results show that the exponents are strongly state and distance dependent. They cannot be generally represented by atomic or equilibrium values. The details of the optimization process are presented.

Die Gesamtenergie der niedrigsten ${}^1\Pi_u$, ${}^3\Pi_u$, ${}^1\Pi_g$, ${}^3\Pi_g$ Zustände des H_2 wurde in einem erweiterten Hartree-Fock Verfahren mit einer Doppelkonfiguration minimisiert. Die Exponenten der Basisfunktionen 1s, 2s, $2p\sigma$, $2p\pi$, $3d\pi$ wurden unabhängig für alle vier Zustände bei verschiedenen Kernabständen optimisiert. Die Ergebnisse zeigen eine starke Zustands- und Abstandsabhängigkeit der Exponenten. Diese können nicht allgemein durch atomare oder Gleichgewichtswerte dargestellt werden. Die Einzelheiten des Optimisierungsverfahrens werden angegeben.

Minimisation de l'énergie totale des plus bas états ${}^1\Pi_u$, ${}^3\Pi_u$, ${}^1\Pi_g$, ${}^3\Pi_g$ de H_2 dans un procédé Hartree-Fock à deux configurations. Les exposants des fonctions de la base: 1s, 2s, $2p\sigma$, $2p\pi$, $3d\pi$ ont été optimisés séparément pour les quatre états pour différentes distances internucléaires. Les résultats montrent que les exposants dépendent fortement de l'état et de la distance. Ils ne peuvent pas être généralement représentés par des valeurs atomiques et des valeurs d'équilibre. Description des détails du processus d'optimisation.

1. Introduction

The purpose of the present series of papers was to study the consequences of exponent optimization in limited basis sets in the MO LCAO framework. We chose the lowest excited Π states of H_2 because this seemed to be the simplest case where such a comparative study would be interesting and feasible. In this paper we are concerned with the optimization process and the dependence of exponents on state and internuclear distance. Two subsequent papers give results for potential curves and one-electron properties [1] and $\sigma - \pi$ separation [2]. Our results suggest that in small basis sets exponent optimization of at least the dominant basis orbitals is necessary for each particular state and distance. Since we find the exponents strongly state and distance dependent, it seems to be impossible to represent them by atomic or single equilibrium values.

---

* On leave to: Institut für Theoretische Chemie, Universität Stuttgart.

** On leave to: Office of Computing Activities, National Science Foundation, Washington, D.C.

We used double-configuration wavefunctions of the type

$$\Psi = A\Phi_{\mathrm{HF}} + B\Phi_{\mathrm{HF'}}\,. \tag{1}$$

For the Π_u states $\Phi_{\mathrm{HF}} = (\sigma_g\pi_u)$, $\Phi_{\mathrm{HF'}} = (\sigma_u\pi_g)$ and for the Π_g states $\Phi_{\mathrm{HF}} = (\sigma_g\pi_g)$, $\Phi_{\mathrm{HF'}} = (\sigma_u\pi_u)$ were chosen. The terms in parentheses are the proper linear combinations of two determinants to define configurations of open-shell singlet and triplet states. The determinants are built up of MO's σ_g, σ_u, π_u, π_g. These MO's, below denoted by ψ, are given as linear combinations of atomic orbitals χ_μ with exponents ζ_μ

$$\psi_i = \sum_\mu C_{i\mu}\chi_\mu(\zeta_\mu)\,. \tag{2}$$

We used the following basis set of three σ AO's and two π AO's on each nucleus: $1s$, $2s$, $2p\sigma$, $2p\pi$, $3d\pi$. We then built up symmetry AO's where equivalent orbitals on each center were assigned the same exponents. The total energy of the double-configuration (1)

$$\begin{aligned} E_{\mathrm{ODC}} = {} & A^2\langle\Phi_{\mathrm{HF}}|H|\Phi_{\mathrm{HF}}\rangle + B^2\langle\Phi_{\mathrm{HF'}}|H|\Phi_{\mathrm{HF'}}\rangle \\ & + 2AB\langle\Phi_{\mathrm{HF}}|H|\Phi_{\mathrm{HF'}}\rangle \end{aligned} \tag{3}$$

was minimized with respect to coefficients C_μ and A and exponents ζ_μ in a multiconfiguration SCF procedure for various internuclear distances in the range of $R = 1.5$ to 10 Bohr. Details of the method can be found elsewhere [1, 3]. In this paper, we are primarily concerned with some qualitative and quantitative consequences of the exponent optimization problem.

2. Optimization Process

The optimization was performed in the following way. We started with the exponents of the subset $\{1s, 2s, 2p\sigma, 2p\pi, 3d\pi\}$ of the larger set $\{1s, 2s, 3s, 2p\sigma, 3d\sigma, 2p\pi, 3p\pi, 3d\pi, 4d\pi, 4f\pi\}$ of Zemke *et al.* [3] for $R = 2$ Bohr. First we optimized the exponent of the $1s$ AO by keeping the exponents of all the other orbitals fixed. By trial and error attempts, we searched for three exponent values for which the corresponding total energy contained a minimum. The optimal exponent was obtained by fitting a parabola through the three initial exponents. To make sure that the final exponent yields indeed a lower energy than any of the three initial values, the total energy was again calculated with all other exponents unchanged. Then, in sequence, the $2s$-, $2p\sigma$-, $2p\pi$- and $3d\pi$-exponents were optimized in the same way. No reoptimization of the exponents was attempted because of the expensive and time-consuming procedure. This means we relied on the assumption that each exponent optimization is independent of the others. This seems reasonable except perhaps for $1s$- and $2s$-orbitals. However, our goal was not high accuracy, rather it was to recognize the general problems of exponent optimization. In this spirit, most of the calculation was done in single precision except for a few cases where double-precision seemed to be necessary.

Table 1 contains the energy dependence and virial theorem of such an optimization for the $^1\Pi_u$ state at $R = 2$ Bohr. It is obvious that the $2p\pi$-orbital

Table 1. Exponent optimization for $^1\Pi_u$ state at 2 Bohr

$1s\sigma$	$2s\sigma$	$2p\sigma$	$2p\pi$	$3d\pi$	E_{ODC}	$\langle V\rangle/\langle T\rangle$
1.09	1.10	1.47	0.453	1.0	−0.713301	−2.0021
0.99					−0.712618	−1.9964
1.19					−0.713030	−1.9998
1.11	1.10				−0.713305	−2.0021
	1.20				−0.712039	−2.0049
	1.00				−0.713843	−2.0097
	0.90				−0.713640	−2.0257
	0.98	1.47			−0.713861	−2.0123
		1.37			−0.713549	−2.0151
		1.57			−0.714005	−2.0097
		1.67			−0.714008	−2.0073
		1.77			−0.713892	−2.0052
		1.63	0.453		−0.714022	−2.0083
			0.35		−0.709494	−2.0615
			0.6		−0.701948	−1.9048
			0.445	1.0	−0.714078	−2.0131
				1.1	−0.714131	−2.0128
				1.3	−0.714143	−2.0122
				1.45	−0.714101	−2.0118
			0.42	1.00	−0.713822	−2.0274
			0.442	1.23	−0.714152	−2.0142
1.09	1.10	1.47	0.453	1.0	−0.715675	Ref. [3]
	plus additional orbitals					
					−0.71859	experimental

plays the dominant role and changes in the $2p\pi$-orbital exponents cause significant changes in the total energy. Gradually less important are $1s$-, $2s$-, $2p\sigma$-orbital exponents, whereas the $3d\pi$-orbitals do not significantly influence the total energy upon exponent variation. From the virial theorem ratio $\langle V\rangle/\langle T\rangle$ in Table 1 we can also conclude that the location of the minimum of the potential curve is shifted to values $R > 2$ Bohr with increasing $\zeta_{2p\pi}$. This indicates a necessity for exponent optimization of the $2p\pi$-orbital exponent in the range of R values about the equilibrium distance.

We then proceeded to calculate points of the potential energy curves of all the four Π states at $R = 1.5, 1.8, 2.2, 3, 4, 5, 6, 7, 8, 10$ Bohr. With the above results of relative significance of the orbital exponents in mind, we optimized the $2p\pi$-exponents for all these distances, whereas the exponents of $1s$-, $2s$-, $2p\sigma$- and $3d\pi$-orbitals were optimized only at $R = 1.5, 3, 6, 10$ Bohr and interpolated for the other distances. We took the optimal set of one distance as the starting set for a neighbor distance. Some of the particular features of general interest are discussed.

The energy of the $^1\Pi_g$ state at 4 Bohr shows a rather flat minimum with respect to $2p\pi$-exponent variation. However, there is a significant dependence of $\langle V\rangle/\langle T\rangle$ on this exponent. Due to strong configuration interaction, the energy curve features a maximum in the range of internuclear distances $3.5 \leq R \leq 4.5$ Bohr. The location of this maximum depends significantly on exponent optimization. Similar conclusions hold for the $^3\Pi_g$ state. However, the $2p\pi$-exponents of $^1\Pi_g$

Table 2. Analysis of $^1\Pi_g$ and $^3\Pi_g$ state energies at 4 Bohr

	$^1\Pi_g$			$^3\Pi_g$		
	A	B	C	A	B	C
$\zeta_{2p\pi}$	0.444	0.455	0.236	0.444	0.300	0.254
E_{HF}	-0.56811	-0.56695	-0.60075	-0.58126	-0.60146	-0.60273
E_{CI}	-0.60514	-0.60480	-0.60348	-0.59976	-0.60561	-0.60499
E_{ODC}	-0.60586	-0.60619	-0.60364	-0.60132	-0.60636	-0.60554
$\langle V\rangle/\langle T\rangle$	-1.9277	-1.9263	-2.1856	-1.9131	-2.1167	-2.1686

A all exponents optimized for $^1\Pi_u$ state.
B $\zeta_{2p\pi}$ optimized for E_{ODC} for Π_g state.
C $\zeta_{2p\pi}$ optimized for E_{HF} for Π_g state.

and $^3\Pi_g$ at 4 Bohr differ from each other considerably and so does the location of the maxima. Since the location of the maxima seems to be of interest, we have also investigated the following point of view: Consider the energy of a single configuration Φ_{HF} as reference energy and optimize the $2p\pi$-exponent in order to obtain a minimum of the SCF energy of this configuration. With this exponent, proceed to the multi-configuration SCF procedure. The results for $^1\Pi_g$ and $^3\Pi_g$ states are in Table 2. It is clear from this table that the flat minimum of the E_{ODC} curve of $^1\Pi_g$ with respect to $\zeta_{2p\pi}$ does not imply a flat minimum of the E_{HF} curve. Quite the opposite is true, namely there is an important dependence of the latter energy on the choice of the $2p\pi$-exponent. For the $^1\Pi_g$ state this fact is more expressed since the optimal exponents $\zeta_{2p\pi}(\mathrm{ODC}) = 0.455$ for ODC optimization and $\zeta_{2p\pi}(\mathrm{HF}) = 0.236$ and for SCF optimization differ much more than for the $^3\Pi_g$ state. Comparing $\langle V\rangle/\langle T\rangle$ for E_{ODC} calculated with either ODC or SCF optimized $2p\pi$-exponents, we obtain a different internuclear distance R for the energy maximum in each case.

At 6 Bohr the Π_g states show another peculiarity. The $3d\pi$-orbital exponent was tentatively determined as 0.6 on the ODC level. We observed a distortion of the HF curve when this value was employed. The ODC energy curve was smooth. We checked this point and found that the distortion of the HF curve disappears for ζ values of about 0.65 to 0.7. This shows again that the SCF optimization follows a path different from ODC optimization.

For 10 Bohr a particular problem arises because of the asymptotic limits. All four Π states dissociate to hydrogen atom states ($1s$, $2p$) with $\zeta_{1s} = 1.00$ and $\zeta_{2p\pi} = 0.5$. The other orbitals are eliminated, *i.e.* their linear coefficients in the MO's decrease to zero. This requires a high degree of accuracy in the integrals if the optimal exponents of $2s$-, $2p\sigma$-, and $3d\pi$-orbitals are desired, since they contribute very little to the total energy. It is hard to predict to which limits these orbitals converge or even whether this is a meaningful question to ask.

3. Optimal Exponents

We have collected the results of our exponent optimization in Figs. 1–5. Here we have smoothed out the effect of interpolation for the exponents. The dashed part of Fig. 1 seems to be an artifact. The exponents should increase

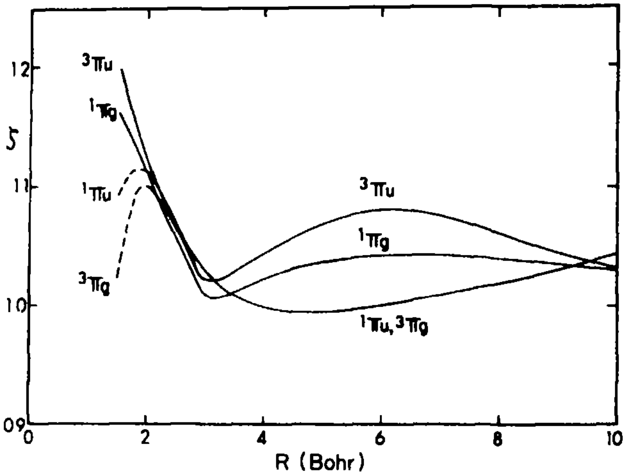

Fig. 1. Optimal 1s-orbital exponents ζ for Π states of H_2 in dependence of internuclear distance R

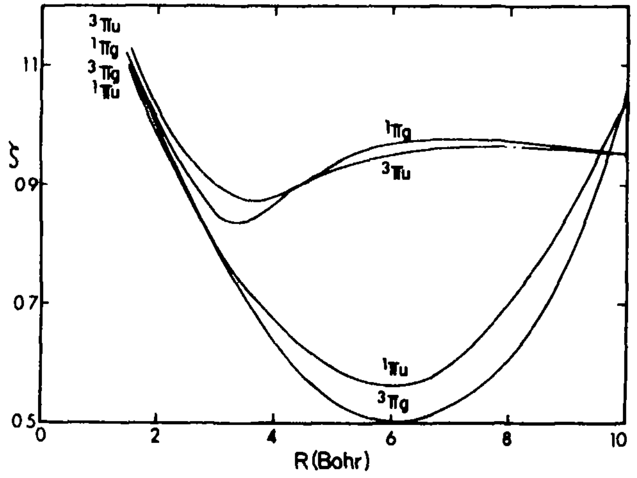

Fig. 2 Optimal 2s- orbital exponents ζ for Π states of H_2 in dependence of internuclear distance R

toward the united atom limit with decreasing internuclear distance. The curves for the $3d\pi$-orbitals are probably less accurate than for the orhers, because their energy contribution was very difficult to trace. The figures show clearly a high dependence of the optimal exponents on the internuclear distance. There is no way to make a good guess how they behave, except for the dominant orbitals at small and large *R*. There is a little *a priori* knowledge how significantly an orbital contributes to the total energy or another physical quantity at a particular distance. Some exponents would have to be optimized to four figures to guarantee six significant figures in the energy. There was no attempt made to achieve this goal, rather we were interested in the general features of nonlinear parameter optimization. There are indications that small sets of orbitals even

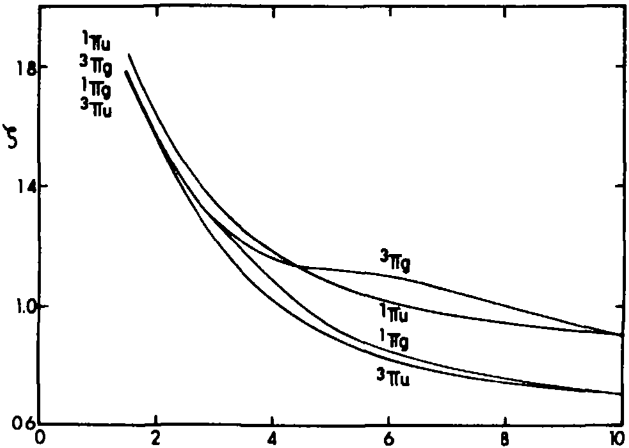

Fig. 3. Optimal $2p\sigma$-orbital exponents ζ for Π states of H_2 in dependence of internuclear distance R

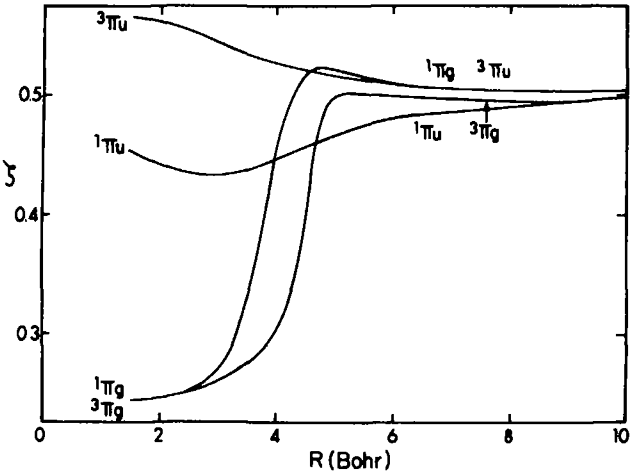

Fig. 4. Optimal $2p\pi$-orbital exponents ζ for Π states of H_2 in dependence of internuclear distance R

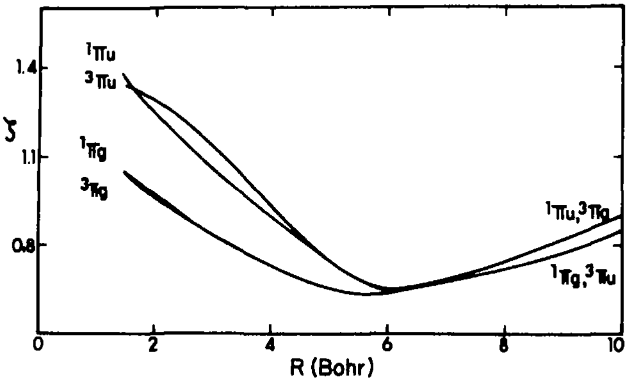

Fig. 5. Optimal $3d\pi$-orbital exponents ζ for Π states of H_2 in dependence of internuclear distance R

with optimized exponents are not necessarily superior to medium-sized sets with little optimization [3]. Perhaps the best compromise would be to optimize the exponents of a minimal basis set over the whole range of internuclear distances and then add a number of orbitals so that the larger set can take care of the features of potential curves by linear parameter optimization only.

Acknowledgements. This work was supported in part by a grant of the National Institutes of Health. The major portion of the computation was performed at the Common Research Computer Facility, Houston, and we thank its director Mr. G. Dolansky and his staff for their kind help and cooperation. We also thank Illinois Institute of Technology, Saint Louis University and IBM for computer time. The work would not have been completed without the help of Professor J. Hinze, Dr. A. C. Wahl, Dr. W. Zemke and Mrs. M. Owen who contributed with their advice and computation of sample cases. We thank Professor H. Silverstone for a discussion of the manuscript.

References

1. Jug, K., Lykos, P. G., McLean, A. D.: Optimal double-configuration study of the lowest excited Π states of H_2. I. Theoret. chim. Acta (Berl.) **25**, 17 (1972).
2. Optimal double-configuration study of the lowest excited Π states of H_2. II. Theoret. chim. Acta (Berl.) **25**, 41 (1972).
3. Zemke, W. T., Lykos, P. G., Wahl, A. C.: J. chem. Physics **51**, 5635 (1969).

Prof. K. Jug
Institut für Theoretische Chemie
Universität Stuttgart
D-7 Stuttgart 1
Relenbergstr. 32
Germany

heoret. chim. Acta (Berl.) 25, 17—40 (1972)
© by Springer-Verlag 1972

Optimal Double-Configuration Study of the Lowest Excited Π States of H_2

I. Potential Energy Curves and One-Electron Properties

KARL JUG*
Department of Chemistry, Illinois Institute of Technology, Chicago, Illinois 60616
and Department of Chemistry, Saint Louis University, Saint Louis, Missouri 63156

PETER G. LYKOS**
Department of Chemistry, Illinois Institute of Technology, Chicago, Illinois 60616

A. D. MCLEAN
IBM Research Laboratory, San Jose, California 95114

Received July 20, 1971

Various levels of approximation (Hartree-Fock, configuration interaction and double-configuration Hartree-Fock method) are compared for extensive and limited exponent optimization of the atomic orbitals of the wavefunctions. The potential energy curves for the lowest-lying $^1\Pi_u$, $^3\Pi_u$, $^1\Pi_g$, $^3\Pi_g$ states of the hydrogen molecule are presented. The shapes of the curves on the highest level of approximation, i.e. with the optimal double-configuration wavefunction, are basically in agreement with previous, more sophisticated and time-consuming work. The influence of the various approximations is also studied for several one-electron properties: charge distribution of the wavefunction along and perpendicular to the molecular axis, quadrupole moment and core attraction energy distribution. Differences arise to the work of Zemke *et al.* [1], who used a limited exponent optimization with a larger basis set, in the Π_g states where the π orbitals are very diffuse. The differences concern magnitude and location of minima and maxima of potential curves, as well as considerable changes in one-electron properties which depend strongly on the spatial distribution of the orbitals.

Verschiedene Approximationsstufen (Hartree-Fock, Konfigurationenwechselwirkung und Doppelkonfigurationen-Hartree-Fock-Methode) werden für ausgedehnte und begrenzte Exponentenoptimisierung von Atomorbitalen der Wellenfunktionen verglichen. Die Potentialkurven für die niedrigsten $^1\Pi_u$, $^3\Pi_u$, $^1\Pi_g$, $^3\Pi_g$ Zustände des Wasserstoffmoleküls werden angegeben. Die Form der Kurven im Rahmen der besten Näherung, d. h. mit Doppelkonfiguration, stimmen im wesentlichen mit früheren aufwendigeren Rechnungen überein. Der Einfluß der verschiedenen Approximationen wird auch an einigen Einelektroneneigenschaften studiert: Ladungsverteilung der Wellenfunktion längs und senkrecht zur Molekülachse, Quadrupolmoment und Verteilung der Rumpfenergie. Unterschiede erscheinen zur Arbeit von Zemke *et al.* [1], die einen größeren Basissatz mit begrenzter Optimisierung verwandten, bei den Π_g Zuständen, wo die π-Orbitale sehr diffus sind. Die Unterschiede betreffen roße und Lage der Minima und Maxima der Potentialkurven sowie beträchtliche Änderungen in lchen Einelektroneneigenschaften, die stark von der räumlichen Verteilung der Orbitale abhängen.

Comparaison de différents niveaux d'approximation (Hartree-Fock, interaction de configuration Hartree-Fock à deux configurations) pour des optimisations étendues et limitées des orbitales tomiques de base. Calcul des courbes d'énergie potentielle pour les plus bas états $^1\Pi_u$, $^3\Pi_u$, $^1\Pi_g$, $^3\Pi_g$ e la molécule d'hydrogène. Pour la fonction d'onde la plus raffinée: H.F. à deux configurations, la rme des courbes est en accord avec les résultats obtenus dans des travaux précédents plus complexes

---

* On leave to: Institut für Theoretische Chemie, Universität Stuttgart.

** On leave to: Office of Computing Activities, National Science Foundation, Washington, .C.

et plus coûteux. On étudie aussi l'influence des diverses approximations sur plusieurs propriétés monoélectroniques: distribution de charge le long de l'axe moléculaire et perpendiculairement à celui-ci, moment quadrupolaire et distribution de l'énergie d'attraction de coeur. On trouve des différences avec le travail de Zemke *et al.* (1), qui utilisent une plus grande base partiellement optimisée, pour les états Π_g où les orbitales π sont très diffuses. Les différences concernent la grandeur et la position des extrema des courbes de potentiel, ainsi que des variations importantes des propriétés monoélectroniques qui dépendent fortement de la distribution spatiale des orbitales.

1. Introduction

The purpose of this paper is to study various levels of approximation in the MO LCAO framework with the example of the lowest-lying $^1\Pi_u$, $^3\Pi_u$, $^1\Pi_g$, $^3\Pi_g$ states of the hydrogen molecule. Different types of wavefunctions were employed. The energies and expectation values of one-electron operators of a single-configuration type wavefunction Φ_{HF} are compared with those of a double-configuration wavefunction of CI type $\Psi_{\mathrm{CI}} = A_{\mathrm{CI}} \Phi_{\mathrm{HF}} + B_{\mathrm{CI}} \Phi_{\mathrm{HF'}}$ and of extended Hartree-Fock type $\Psi_{\mathrm{ODC}} = A_{\mathrm{ODC}} \Phi_{\mathrm{HF}} + B_{\mathrm{ODC}} \Phi_{\mathrm{HF'}}$. In the latter wavefunction the coefficients A and B are also subjected to a self-consistent iteration procedure. The configurations are built up of the proper linear combinations of determinants for each of the four Π states. Φ_{HF} and $\Phi_{\mathrm{HF'}}$ are chosen in such a way that they allow for proper dissociation of the molecular states in excited atomic states. The molecular orbitals used are the lowest σ_g, σ_u, π_u, π_g functions given as linear combinations of a small number of equivalent atomic orbitals on each center.

The present approach was used by Zemke *et al.* [1] to study primarily the $^1\Pi_u$ state, but also some of the characteristic features of the $^3\Pi_u$, $^1\Pi_g$ and $^3\Pi_g$ states. The present work is a generalization and complement of their study. Therefore we shall, in the next sections, be brief about the details of the method and emphasize only the differences arising in the present work. Most of the general features of the method are equal; the emphasis of the work of Zemke *et al.* [1] was on a limited exponent optimization of a medium-sized atomic basis set. Our objective was a full exponent optimization of a smaller basis set. Zemke *et al.* used the following atomic basis on each center $\{1s, 2s, 3s, 2p\sigma, 3d\sigma, 2p\pi, 3p\pi, 3d\pi, 4d\pi, 4f\pi\}$. They optimized the exponents for these 2×10 basis functions for the $^1\Pi_u$ state at $R = 2$ Bohr by minimizing the total energy of this state with a double-configuration function Ψ_{ODC} of extended Hartree-Fock type. They used these exponents for the study of all the other distances from $R = 1.5$ to 10 Bohr of the potential energy curve E_{ODC} of $^1\Pi_u$ and also the $^3\Pi_u$, $^1\Pi_g$ and $^3\Pi_g$ states. We employed a basis $\{1s, 2s, 2p\sigma, 2p\pi, 3d\pi\}$ on each nucleus. We optimized the exponents of the orbitals at a number of distances covering the potential curves from $R = 1.5$ to 10 Bohr. The optimization was performed separately for each of the four states. Details of the optimization can be found elsewhere [2]. For comparison, we have also calculated the properties of the $^3\Pi_u$, $^1\Pi_g$ and $^3\Pi_g$ states with the optimal exponents of the $^1\Pi_u$ states at the same distance.

We find the potential curves characterized properly in magnitude and location of minima and maxima for calculations based on optimized exponents. With comparative calculations with a single-state exponent set, here of the $^1\Pi_u$ state, for all four states we find larger inaccuracies in the magnitude than in the location of the minima. The location of the maxima with a small basis set is a difficult problem. One-electron properties are more uniform for all four states when calculated with a single-state exponent set instead of separate optimization. The $^1\Pi_u$ state exponent set leads to considerable inaccuracies for the Π_g states where diffuse π orbitals are involved. Details of Sections 3 and 4 lead us to the conclusion that exponent optimization of the dominant orbitals is necessary in small basis sets.

2. The Method

We use the Hamiltonian of the hydrogen molecule in the form consisting of kinetic energy T and nuclear attraction $-\frac{1}{r_a}-\frac{1}{r_b}$ of each electron, electronic repulsion $\frac{1}{r_{12}}$ and nuclear repulsion $\frac{1}{R}$

$$H = H_1 + H_2 + \frac{1}{r_{12}} + \frac{1}{R} \tag{2.1}$$

$$\text{with} \quad H_i = T_i - \frac{1}{r_{ai}} - \frac{1}{r_{bi}} \qquad i = 1, 2\,.$$

The approximate wavefunction is of double-configuration form

$$\Psi = A\Phi_1 + B\Phi_2 \tag{2.2}$$

where Φ_1 and Φ_2 are orthonormal. The total energy of the system is

$$E_{\text{total}} = \frac{1}{A^2+B^2}\{A^2 H_A + B^2 H_B + 2ABH_{AB}\} \tag{2.3}$$

$$\begin{aligned} \text{with} \quad H_A &= \langle\Phi_1|H|\Phi_1\rangle \\ H_B &= \langle\Phi_2|H|\Phi_2\rangle \\ H_{AB} &= \langle\Phi_1|H|\Phi_2\rangle\,. \end{aligned}$$

To obtain a minimal energy with respect to A and B, we have to solve

$$\begin{vmatrix} H_A - E & H_{AB} \\ H_{AB} & H_B - E \end{vmatrix} = 0\,. \tag{2.4}$$

We shall use a normalized wavefunction in the following.

Each configuration Φ_i consists of two determinants built up by a sigma MO σ_i and a pi MO π_i

$$^{1,3}\Phi_i = \tfrac{1}{2}\left\{\begin{vmatrix} \sigma_i(1) & \bar{\pi}_i(1) \\ \sigma_i(2) & \bar{\pi}_i(2) \end{vmatrix} \begin{matrix} - \\ + \end{matrix} \begin{vmatrix} \bar{\sigma}_i(1) & \pi_i(1) \\ \bar{\sigma}_i(2) & \pi_i(2) \end{vmatrix}\right\}. \tag{2.5}$$

The minus sign refers to the singlet, the plus sign to the triplet state and the bar to β spin. The MO set $\sigma_1, \sigma_2, \pi_1, \pi_2$ is assumed as orthonormal. With these wavefunctions, H_A, H_B and H_{AB} can be reduced to

$$\begin{aligned} H_A &= H_{\sigma_1} + H_{\pi_1} + J_{\sigma_1\pi_1} \pm K_{\sigma_1\pi_1} \\ H_B &= H_{\sigma_2} + H_{\pi_2} + J_{\sigma_2\pi_2} \pm K_{\sigma_2\pi_2} \\ H_{AB} &= J_{\sigma_1\sigma_2\pi_1\pi_2} \pm K_{\sigma_1\sigma_2\pi_1\pi_2} \,. \end{aligned} \tag{2.6}$$

For convenience, we have dropped the nuclear repulsion.

H_{σ_i} and H_{π_i} are the usual core integrals and J and K the Coulomb and exchange integrals

$$\begin{aligned} J_{\sigma_1\pi_1} &= (\sigma_1\sigma_1|\pi_1\pi_1)\,, \\ K_{\sigma_1\pi_1} &= (\sigma_1\pi_1|\pi_1\sigma_1)\,, \\ J_{\sigma_1\sigma_2\pi_1\pi_2} &= (\sigma_1\sigma_2|\pi_1\pi_2)\,, \\ K_{\sigma_1\sigma_2\pi_1\pi_2} &= (\sigma_1\pi_2|\pi_1\sigma_2)\,. \end{aligned}$$

If we subject the energy (2.3) to variation with respect to the MO's σ_i and π_i ($i = 1, 2$) preserving the orthonormality, we obtain the following set of equations

$$\begin{aligned} A^2(\mathbf{H}_1 + \mathbf{J}_{\pi_1} \pm \mathbf{K}_{\pi_1})\,\sigma_1(1) + AB(\mathbf{J}_{\pi_1\pi_2} \pm \mathbf{K}_{\pi_1\pi_2})\,\sigma_2(1) &= \lambda_{\sigma_1}\sigma_1(1) \\ B^2(\mathbf{H}_2 + \mathbf{J}_{\pi_2} \pm \mathbf{K}_{\pi_2})\,\sigma_2(1) + AB(\mathbf{J}_{\pi_2\pi_1} \pm \mathbf{K}_{\pi_2\pi_1})\,\sigma_1(1) &= \lambda_{\sigma_2}\sigma_2(1) \\ A^2(\mathbf{H}_1 + \mathbf{J}_{\sigma_1} \pm \mathbf{K}_{\sigma_1})\,\pi_1(2) + AB(\mathbf{J}_{\sigma_1\sigma_2} \pm \mathbf{K}_{\sigma_1\sigma_2})\,\pi_2(2) &= \lambda_{\pi_1}\pi_1(2) \\ B^2(\mathbf{H}_2 + \mathbf{J}_{\sigma_2} \pm \mathbf{K}_{\sigma_2})\,\pi_2(2) + AB(\mathbf{J}_{\sigma_2\sigma_1} \pm \mathbf{K}_{\sigma_2\sigma_1})\,\pi_1(2) &= \lambda_{\pi_2}\pi_2(2)\,. \end{aligned} \tag{2.7}$$

These are the extended Hartree-Fock equations in double-configuration form for this particular two-electron case [3]. The λ's are the Lagrange multipliers. The other multipliers vanish for symmetry reasons: As mentioned in the introduction, we used only one MO of each of the symmetry types σ_g, σ_u, π_u, π_g. The $\mathbf{J}$'s and $\mathbf{K}$'s are the usual Coulomb and exchange operators

$$\begin{aligned} \mathbf{J}_{\pi_1}\sigma_1(1) &= \left\langle \pi_1(2) \left| \frac{1}{r_{12}} \right| \pi_1(2) \right\rangle \sigma_1(1) \\ \mathbf{K}_{\pi_1}\sigma_1(1) &= \left\langle \pi_1(2) \left| \frac{1}{r_{12}} \right| \sigma_1(2) \right\rangle \pi_1(1) \\ \mathbf{J}_{\pi_1\pi_2}\sigma_2(1) &= \left\langle \pi_1(2) \left| \frac{1}{r_{12}} \right| \pi_2(2) \right\rangle \sigma_2(1) \\ \mathbf{K}_{\pi_1\pi_2}\sigma_2(1) &= \left\langle \pi_1(2) \left| \frac{1}{r_{12}} \right| \sigma_2(2) \right\rangle \pi_2(1) \qquad \text{etc.} \end{aligned}$$

After expansion of the MO's in atomic orbitals Eqs. (2.7) can be written in matrix form

$$\mathbf{F}_i\mathbf{C}_i = \mathbf{S}_i\mathbf{C}_i\lambda_i \qquad i = \sigma_1, \sigma_2, \pi_1, \pi_2 \tag{2.8}$$

where the double-configuration self-consistent field Hamiltonians are defined as

$$\begin{aligned} F_{\sigma_1} &= A^2(H_1 + Q_{\sigma_1}) + A\,B\,W_{\sigma_1} \\ F_{\sigma_2} &= B^2(H_2 + Q_{\sigma_2}) + A\,B\,W_{\sigma_2} \\ F_{\pi_1} &= A^2(H_1 + Q_{\pi_1}) + A\,B\,W_{\pi_1} \\ F_{\pi_2} &= B^2(H_2 + Q_{\pi_2}) + A\,B\,W_{\pi_2}. \end{aligned} \tag{2.9}$$

The repulsion energy matrix Q and coupling energy matrix W are obtained from contraction of supermatrix $\tilde{Q}$. For example

$$\begin{aligned} Q_{\sigma_1} &= D^{\dagger}_{\pi_1\pi_1}\tilde{Q}_{\pi_1\pi_1\sigma_1\sigma_1}, \\ W_{\sigma_1} &= (P_{\sigma_1\sigma_2}C_{\sigma_2})(S_{\sigma_1}C_{\sigma_1})^{\dagger} + (S_{\sigma_1}C_{\sigma_1})(P_{\sigma_1\sigma_2}C_{\sigma_2})^{\dagger} \\ \text{with}\quad P_{\sigma_1\sigma_2} &= D^{\dagger}_{\pi_1\pi_2}\tilde{Q}_{\pi_1\pi_2\sigma_1\sigma_2}, \\ D_{ij} &= C_iC_j^{\dagger} \qquad i,j = \sigma_1, \sigma_2, \pi_1, \pi_2, \\ \tilde{Q}_{ijkl} &= J_{ijkl} \pm K_{ijkl}. \end{aligned}$$

The J's and K's are the usual electronic repulsion integrals over atomic orbitals i, j, k, l. The formulas for the other cases are similar.

Solutions of the coupled Eqs. (2.8) yield the double-configuration self-consistent field MO's which allow us to calculate the energy and expection values of one-electron operators. The Hartree-Fock case is contained in the formalism with $A=0$ or $B=0$. In the following the energies H_A and H_B are denoted by E_{HF} and $E_{\mathrm{HF}'}$. The configuration interaction energy E_{CI} is then obtained by solving Eq. (2.4). The coupling energy H_{AB}, now denoted by E_{coupling}, has to be calculated separately. The final energy E_{ODC} referring to the MO's which are solutions of the coupled Eqs. (2.8) and (2.9) is obtained after self-consistent iteration of both linear AO coefficients C_i and configuration coefficient A. We employed an iteration procedure which alternately improves C_i and A in single steps.

In the following sections, we have chosen Φ_{HF} consisting of MO's σ_g and π_u for Π_u states and σ_g and π_g for Π_g states, whereas $\Phi_{\mathrm{HF}'}$ consists of σ_u and π_g for Π_u states and σ_u and π_u for Π_g states. The MO's are those belonging to lowest eigenvalue for each symmetry type of operator F of (2.9). The atomic basis set consists of symmetry adapted orbitals: three σ AO's $\{1s, 2s, 2p\sigma\}$ and two π AO's $\{2p\pi, 3d\pi\}$ on each center with equal exponents for equivalent orbitals.

3. Potential Energy Curves

The results of this paper are based on extensive exponent optimization of the symmetry adapted atomic basis set. The final exponents are collected in Table 1. The exponents of the $1s$, $2s$, $2p\sigma$ and $3d\pi$ orbitals were optimized at $R = 1.5, 2, 3$, 6 and 10 Bohr. For the other distances the exponents were interpolated linearly. The $2p\pi$-orbital exponents were optimized at all distances listed. All exponents

Table 1. Optimized exponents for three σ-orbital, two π-orbital basis sets of double configuration Π state wave functions of H_2

States ${}^1\Pi_u\,{}^3\Pi_u\,{}^1\Pi_g\,{}^3\Pi_g$

R	$1s\sigma$				$2s\sigma$				$2p\sigma$				$2p\pi$				$3d\pi$			
1.5	1.09	1.20	1.16	1.02	1.10	1.13	1.11	1.10	1.84	1.75	1.77	1.78	0.453	0.567	0.245	0.245	1.36	1.34	1.05	1.05
1.8	1.10	1.15	1.13	1.07	1.03	1.06	1.04	1.04	1.71	1.62	1.63	1.64	0.446	0.565	0.245	0.245	1.28	1.30	1.00	1.00
1.95	1.11	1.13	—	—	0.99	1.03	—	—	1.65	1.56	—	—	0.443	0.562	—	—	1.24	1.29	—	—
2.0	1.11	1.12	1.11	1.10	0.98	1.02	1.00	1.00	1.63	1.54	1.55	1.56	0.442	0.561	0.245	0.245	1.23	1.28	0.97	0.96
2.2	1.09	1.10	1.09	1.09	0.94	0.99	0.97	0.96	1.57	1.48	1.50	1.51	0.439	0.559	0.244	0.244	1.20	1.25	0.94	0.94
3.0	1.03	1.02	1.01	1.03	0.80	0.90	0.85	0.80	1.34	1.23	1.27	1.28	0.432	0.544	0.239	0.239	1.07	1.13	0.83	0.83
4.0	1.02	1.04	1.02	1.02	0.72	0.91	0.89	0.70	1.23	1.09	1.12	1.21	0.444	0.527	0.455	0.300	0.92	0.96	0.75	0.75
5.0	1.01	1.06	1.03	1.01	0.64	0.93	0.93	0.60	1.12	0.95	0.98	1.15	0.466	0.515	0.520	0.495	0.86	0.88	0.67	0.67
6.0	1.00	1.08	1.04	1.00	0.56	0.95	0.97	0.50	1.01	0.82	0.84	1.09	0.482	0.509	0.510	0.497	0.60	0.60	0.60	0.60
7.0	1.01	1.06	1.04	1.01	0.69	0.95	0.96	0.65	0.98	0.79	0.80	1.04	0.486	0.507	0.508	0.497	0.68	0.66	0.66	0.68
8.0	1.02	1.05	1.04	1.02	0.82	0.95	0.96	0.80	0.95	0.76	0.77	0.99	0.490	0.505	0.506	0.498	0.76	0.71	0.71	0.76
10.0	1.04	1.03	1.03	1.04	1.05	0.95	0.95	1.05	0.90	0.70	0.70	0.90	0.498	0.502	0.502	0.498	0.90	0.85	0.85	0.90

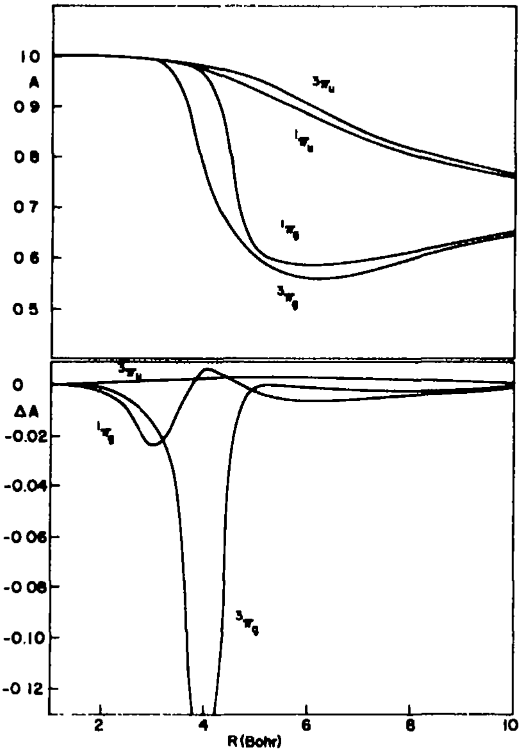

Fig. 1. ODC mixing coefficients A and differences ΔA between $^1\Pi_u$ based and optimal values

were determined by minimizing E_{ODC}, except $^1\Pi_g$ and $^3\Pi_g$ at $R=1.5$ to 3 Bohr. These exponents were optimized so to minimize E_{HF} rather than E_{ODC}. The reasons for doing so were purely economical. This part of the work involving integrals with such small exponents was finished only recently with a different program, whereas the other part was done two years ago. Our calculations indicate that we can safely assume that configuration interaction is so small for the range $R=1.5$ to 3 Bohr that not much improvement would result from optimizing E_{ODC}. In principle the values for the $2p\pi$-exponents would slightly increase.

Fig. 1 presents, on the ODC level, optimal coefficients A and differences $\Delta A = A' - A$ between mixing coefficients A' calculated with $^1\Pi_u$ exponents and optimal coefficients A. The results are also that the ODC approximation tries to mix the two configurations more than the CI approximation.

From the potential energy curves in the following tables this will become clearer. If Φ_{HF} is the dominant configuration, A is decreased when going from CI to ODC, otherwise it is increased. For the optimized exponents (Table 1) the configurations of the Π_g states are more strongly mixed than for the non-optimized exponents. The situation is reversed for the $^3\Pi_u$ state.

Tables 2–5 contain the self-consistent field energies E_{HF} and $E_{\text{HF'}}$ of the two configurations Φ_{HF} and $\Phi_{\text{HF'}}$, their configuration interaction energy E_{CI} and the optimum double-configuration energy E_{ODC} and the coupling energy E_{coupling}

Table 2. Potential energy curves and coupling energy for $^1\Pi_u$ state of H_2

R	E_{HF}	E_{HF}	E_{CI}	E_{ODC}	$E_{\mathrm{CI}}^{\mathrm{coupling}}$	$E_{\mathrm{ODC}}^{\mathrm{coupling}}$
1.5	0.69571	0.02498	−0.69612	−0.69700	−0.00082	−0.00260
1.8	−0.71136	−0.12102	−0.71198	−0.71301	−0.00125	−0.00330
1.95	−0.71249	−0.17596	−0.71326	−0.71433	−0.00155	−0.00369
2.0	−0.71223	−0.19217	−0.71307	−0.71415	−0.00167	−0.00383
2.2	0.70900	−0.24834	−0.71014	−0.71122	−0.00228	−0.00445
3.0	0.68040	−0.38819	−0.68378	−0.68447	−0.00668	−0.00809
4.0	0.64228	−0.46440	−0.65188	−0.65202	−0.01826	−0.01868
5.0	0.61376	0.49673	−0.63353	−0.63404	−0.03455	−0.03583
6.0	0.59494	−0.52087	−0.62097	−0.62701	−0.04133	−0.05193
7.0	0.58240	0.52254	−0.62109	−0.62475	−0.05557	−0.06220
8.0	0.57227	−0.52465	−0.62189	−0.62428	−0.06571	−0.07010
10.0	0.55476	0.52626	−0.62379	−0.62448	−0.08084	−0.08212

Table 3. Potential energy curves and coupling energies for $^3\Pi_u$ state of H_2

R	E_{HF}	E_{HF}	E_{CI}	E_{ODC}	$E_{\mathrm{CI}}^{\mathrm{coupling}}$	$E_{\mathrm{ODC}}^{\mathrm{coupling}}$
1.5	0.71334	0.03694	0.71383	−0.71426	−0.00098	−0.00185
1.8	−0.73012	0.09805	−0.73091	−0.73135	−0.00158	−0.00246
1.95	0.73169	−0.15015	0.73268	−0.73309	−0.00198	−0.00281
2.0	0.73156	−0.16590	−0.73263	0.73303	−0.00213	−0.00294
2.2	0.72869	0.22122	−0.73009	−0.73044	−0.00280	−0.00351
3.0	−0.70020	−0.37222	−0.70345	−0.70361	−0.00644	0.00680
4.0	−0.66119	−0.36585	−0.66829	−0.66847	−0.01371	−0.01421
5.0	−0.63179	−0.50908	0.64506	−0.64554	−0.02417	−0.02547
6.0	−0.61186	−0.53408	−0.63082	−0.63388	−0.03171	−0.03781
7.0	−0.59760	0.53971	−0.62643	−0.62886	−0.04327	−0.04825
8.0	0.58691	−0.54326	−0.62475	−0.62685	−0.05168	−0.05587
10.0	−0.57046	−0.54536	−0.62470	−0.62564	−0.06430	−0.06613

Table 4. Potential energy curves and coupling energies for $^1\Pi_g$ state of H_2

R	E_{HF}	E_{HF}	E_{CI}	E_{ODC}	$E_{\mathrm{CI}}^{\mathrm{coupling}}$	$E_{\mathrm{ODC}}^{\mathrm{coupling}}$
1.5	−0.63663	−0.05059	−0.63671	−0.63671	−0.00017	−0.00017
1.8	−0.65459	−0.18078	−0.65472	−0.65472	−0.00025	−0.00026
2.0	−0.65693	−0.25975	−0.65711	−0.65711	−0.00034	−0.00035
2.2	−0.65513	−0.31647	−0.65536	−0.65536	−0.00046	−0.00047
3.0	−0.63198	−0.46743	−0.63267	−0.63270	−0.00138	−0.00145
4.0	−0.56695	−0.55136	−0.60480	−0.60619	−0.04431	−0.04693
5.0	−0.54497	−0.56928	−0.61136	−0.61802	−0.05158	−0.06290
6.0	−0.54146	−0.57560	−0.61391	−0.62340	−0.05012	−0.06579
7.0	−0.53013	−0.57316	−0.61912	−0.62520	−0.06061	−0.07081
8.0	−0.52685	−0.56765	−0.62155	−0.62563	−0.06869	−0.07562
10.0	−0.52654	−0.55400	−0.62451	−0.62551	−0.08200	−0.08377

Table 5. Potential energy curves and coupling energies for ${}^3\Pi_g$ state of H_2

R	E_{HF}	$E_{HF'}$	E_{CI}	E_{ODC}	$E_{CI}^{coupling}$	$E_{ODC}^{coupling}$
1.5	−0.63693	−0.05220	−0.63698	−0.63703	−0.00010	−0.00019
1.8	−0.65497	−0.19146	−0.65505	−0.65511	−0.00015	−0.00028
2.0	−0.65739	−0.26142	−0.65750	−0.65757	−0.00020	−0.00036
2.2	−0.65569	−0.31790	−0.65583	−0.65592	−0.00028	−0.00046
3.0	−0.63303	−0.45860	−0.63346	−0.63366	−0.00085	−0.00127
4.0	−0.60143	−0.54674	−0.60558	−0.60634	−0.00775	−0.00931
5.0	−0.56160	−0.58410	−0.60960	−0.61253	−0.03331	−0.03903
6.0	−0.55573	−0.58957	−0.61560	−0.61962	−0.03629	−0.04386
7.0	−0.54934	−0.58753	−0.61942	−0.62247	−0.04384	−0.04975
8.0	−0.54745	−0.58224	−0.62140	−0.62362	−0.05120	−0.05553
100	−0.54629	−0.56944	−0.62366	−0.62444	−0.06375	−0.06528

for all four Π states with the optimal exponents for each state. With respect to the hierarchy of models HF, CI and ODC we observe that most of the correlation energy is in the step from HF to CI and little further energy decrease results from going from CI to ODC level. The difference between CI and ODC energies increases with increasing internuclear distance in the range $R = 1.5$ to 10 Bohr, reaching a maximum at $R = 6$ Bohr. From calculations not presented here, we can also learn that exponent optimization always improves E_{ODC} but the corresponding E_{HF} might be higher than the E_{HF} of a non-optimized exponent set. This is particularly true when configuration interaction becomes important. For ${}^3\Pi_u$ and ${}^3\Pi_g$ this is true for $R \geq 5$ Bohr, for ${}^1\Pi_g$ for $R \geq 4$ Bohr. The Hartree-Fock curves are in general far too high with the ODC optimized basis set and so there is little meaning in considering the difference between E_{ODC} and E_{HF} in our calculations as a good description of the correlation energy. With the (sometimes only little) improvement of E_{ODC} we sacrifice information about E_{HF}. With a larger basis set, even with limited exponent optimization, there seems to be more flexibility in linear combinations to represent *both* self-consistent field states HF and HF′ satisfactorily. This is particularly true for Π_g states, but also for the ${}^3\Pi_u$ state [4].

The complete set of potential curves for the four Π states is given in Figs. 2–5. The easiest way to describe them is to say that the E_{ODC} curves of ${}^1\Pi_u$ and ${}^3\Pi_u$ states calculated with the optimal exponents of Table 1, match almost exactly the results of Browne [5]. For the ${}^1\Pi_g$ states Browne [6] lists only values at 8 and 10 Bohr. Our values agree with those, too.

For ${}^1\Pi_u$ our results are inferior to those of Zemke *et al.* [1] for $R < 6$ Bohr. For larger distances our results are better because their fixed $2p\pi$ exponent could not converge to the proper limit. The difference between the two curves E_{ODC} and E''_{ODC} is, however, not considerable. Both curves show a minimum at about 1.95 Bohr quite in agreement with the extensive calculation by Kolos and Wolniewicz [7]. At larger distances both E_{ODC} and E''_{ODC} have a hump not visible in the figure. From the virial theorem ratio of potential and kinetic energy this maximum is located in our calculation at about 7.8 Bohr, whereas the more precise calculation by Kolos and Wolniewicz [7] locates it at 9 Bohr.

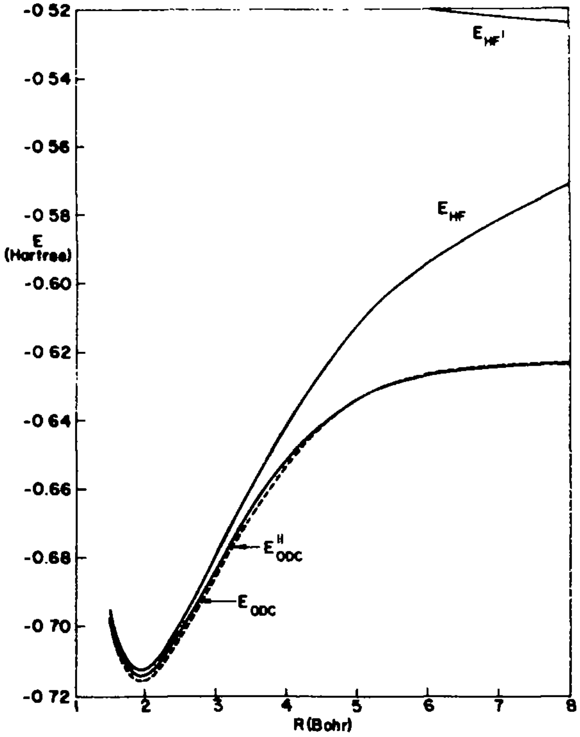

Fig. 2

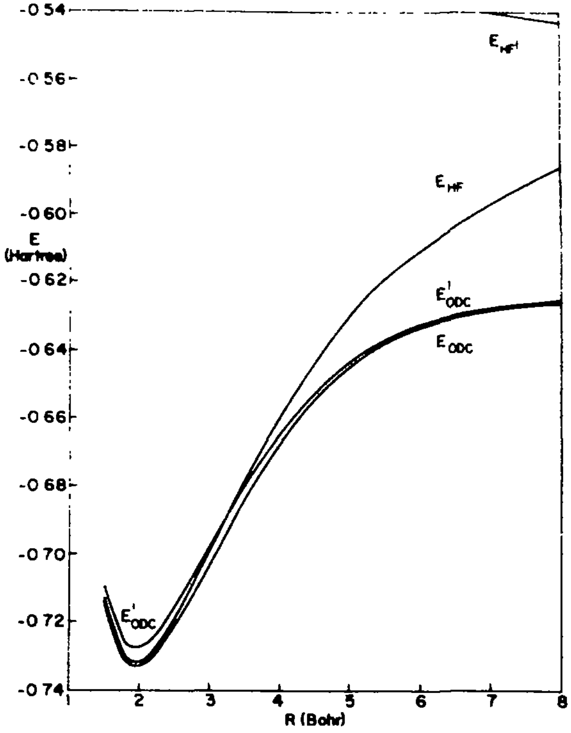

Fig. 3

Fig. 2. Potential energy curves of $^1\Pi_u$ state of H_2; E_{HF} and $E_{HF'}$ Hartree-Fock curves, E_{ODC} present optimal double-configuration curve, E''_{ODC} (dashed) curve of Ref. [1]

Fig. 3. Potential energy curves of $^3\Pi_u$ state of H_2; E_{HF} and $E_{HF'}$ Hartree-Fock curves, E_{ODC} present optimal double-configuration curve, E'_{ODC} curve with $^1\Pi_u$ exponents. E''_{ODC} (not shown because it almost coincides with E_{ODC}) curve of Ref. [1]

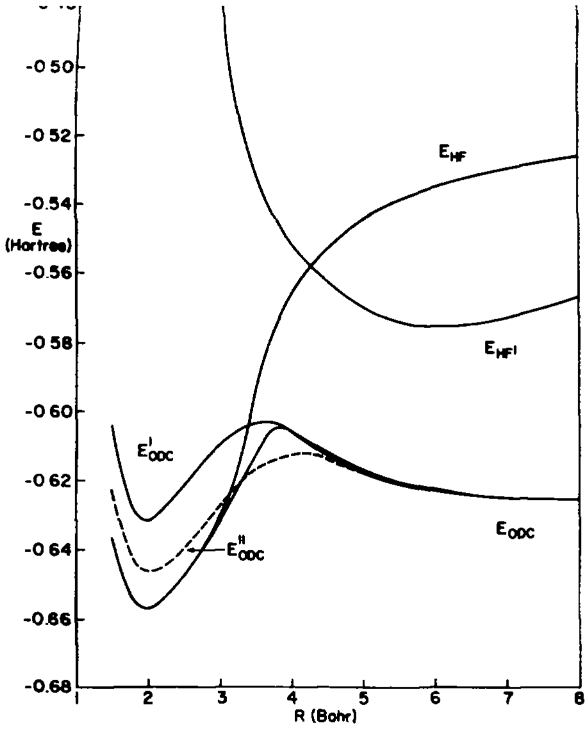

Fig. 4

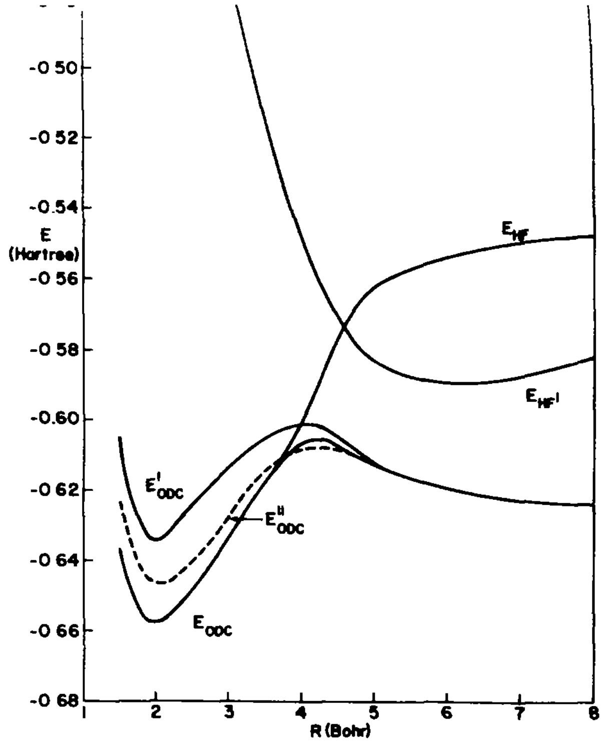

Fig. 5

Fig. 4. Potential energy curves of $^1\Pi_g$ state of H_2; E_{HF} and $E_{HF'}$ Hartree-Fock curves, E_{ODC} present optimal double-configuration curve of H_2, E'_{ODC} curve with $^1\Pi_u$ exponents, E''_{ODC} curve of Ref. [1]

Fig. 5. Potential energy curves of $^3\Pi_g$ state of H_2; E_{HF} and $E_{HF'}$ Hartree-Fock curves, E_{ODC} present optimal double-configuration curve of H_2, E'_{ODC} curve with $^1\Pi_u$ exponents, E''_{ODC} curve of Ref. [1]

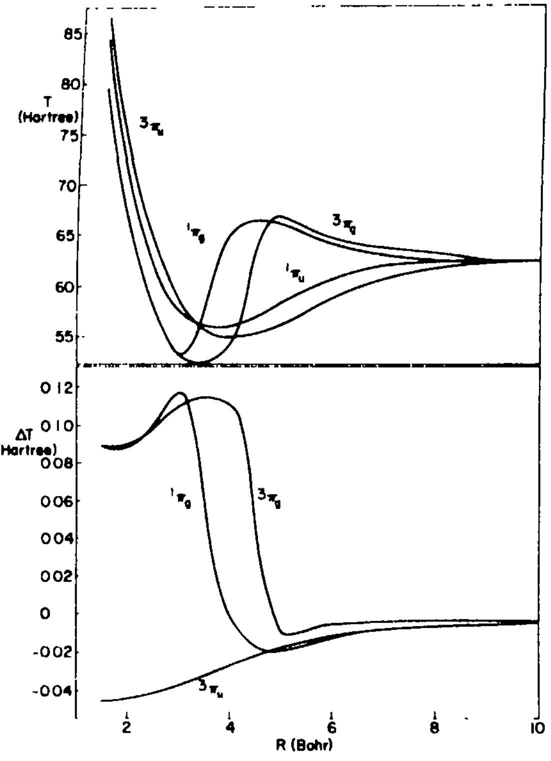

Fig. 6. ODC kinetic energies T and differences ΔT between $^1\Pi_u$ based and optimal values

The E_{ODC} potential curve for $^3\Pi_u$ is slightly lower than Zemke *et al.*'s denoted by E''_{ODC}. We prefered not to include it in the figure because it is almost indistinguishable from ours. Both curves have a minimum at $R = 1.95$ Bohr and no maximum. The potential curve E'_{ODC} for this state calculated with the exponents of $^1\Pi_u$ is quite inferior to both E_{ODC} and E''_{ODC} but locates the minimum correctly. However, here the virial theorem is not of much help since the internal distribution of kinetic and potential energy is way off the correct ratio for this case.

Most interesting are the Π_g states, where exponent optimization comes to full fruition at small internuclear distances. The fully optimized curve E_{ODC} is lower than Zemke's curve E''_{ODC}, which in turn is lower than the curve E'_{ODC}, based on the $^1\Pi_u$ optimization. All three curves show minima at about $R = 2.00$ Bohr which, for the $^3\Pi_g$ state, is in agreement with the more extensive calculation of Wright and Davidson [8]. For $^3\Pi_g$ there is a maximum between 4 and 5 Bohr which is correctly located on all three levels of approximation E_{ODC}, E'_{ODC} and E''_{ODC}. Quite interestingly, the larger basis set of Zemke *et al.* is more favorable than the present optimized set at some distances where strong configuration interaction occurs. We attribute this to the flexibility of linear optimization which can decrease the energy of *both* Hartree-Fock curves E_{HF} and $E_{HF'}$, whereas nonlinear parameter optimization seems to favor one curve at the costs of the other.

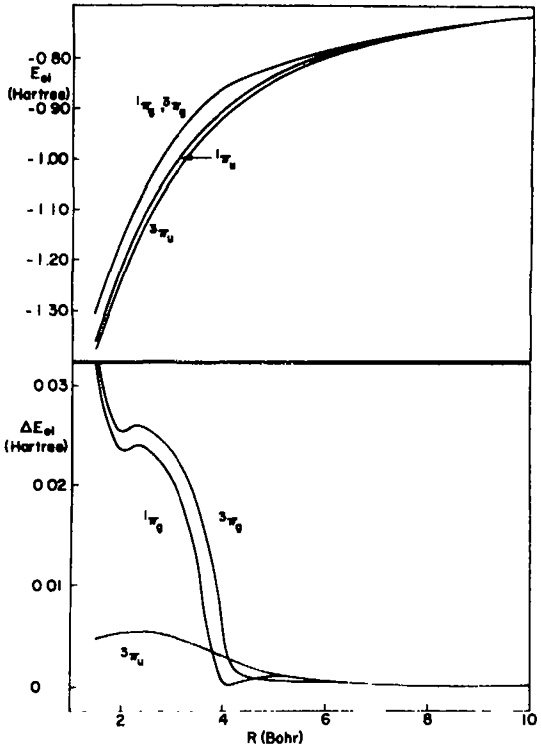

Fig. 7. ODC electronic energies E_{el} and differences ΔE_{el} between $^1\Pi_u$ based and optimal values

For larger distances $R \geqq 6$ Bohr our asymptotic set gains advantage over the unoptimized set by Zemke *et al.*

Similar consquences hold for the $^1\Pi_g$ state, where we locate the maximum at about 3.85 Bohr, whereas Zemke *et al.* located theirs tentatively at about 4.2 Bohr. Since they do not list values referring to the virial theorem, their choice is somewhat arbitrary. The precise location of the maximum has to await further investigation. The features of these curves are well-represented also in the less optimized E'_{ODC} curves although the location of the maxima undergoes a shift to smaller R values.

In the asymptotic limit of the ODC level all four states dissociate to the same atomic states. But $^1\Pi_u$ and $^3\Pi_g$ approach each other more closely and so do $^3\Pi_u$ and $^1\Pi_g$. This is expressed in the energies at 10 Bohr.

Figs. 6–8 contain the ODC energy breakdown and virial theorem for all four Π states with the optimal exponents and differences to $^1\Pi_u$ state based values of these quantities. Further calculations show an increase of kinetic energy when going from the HF level to the ODC levels for $^1\Pi_u$, $^3\Pi_u$ and $^3\Pi_g$ states. For $^1\Pi_g$ there is a surprising decrease of kinetic energy for $R \geqq 7$ Bohr. The increase of kinetic energies is certainly more than compensated by a decrease of potential energy. As far as a comparison of the two levels of exponent optimization is concerned, we can say that exponent optimization increases the kinetic

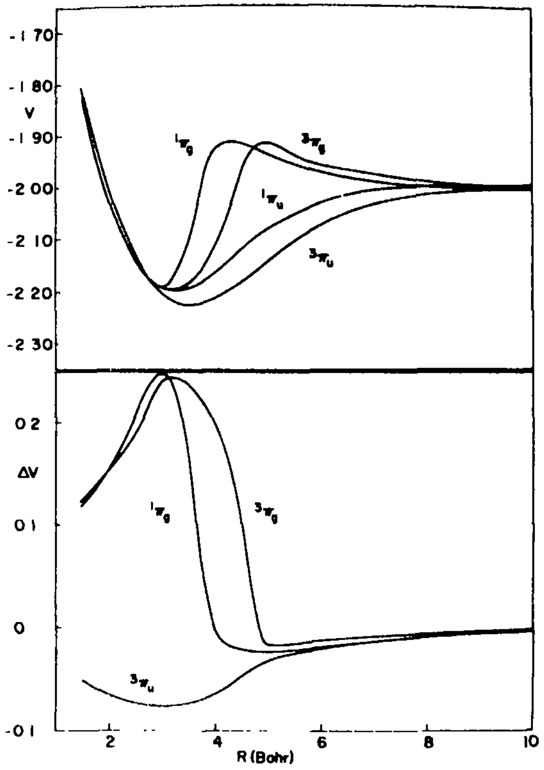

Fig. 8. ODC virial theorem ratios V and differences ΔV between $^1\Pi_u$ based and optimal values

energy of the $^3\Pi_u$ state, but decreases it for internuclear distances smaller than 4 Bohr, for the Π_g states. One might conclude that the wavefunction tries to contract upon exponent optimization for the $^3\Pi_u$ state and expand for the Π_g states. Details can be found in the next section.

4. Properties of One-Electron Operators

The density distribution perpendicular to the molecular axis can be analyzed by studying the expectation values of ϱ^2, the distribution along this axis by studying z_a^2.

Perpendicular to the molecular axis, measured by ϱ^2, there is a slight contraction in the Π_u states, whereas the Π_g states show a contraction for smaller distances and an expansion for larger distances when going from the HF level to the ODC level. Comparison of the four states shows again that $^3\Pi_u$ is more contracted than $^1\Pi_u$ whereas the Π_g are far more expanded (Fig. 9). The distributions of all four states come very close to each other when calculated with the exponents of $^1\Pi_u$.

Comparing the levels of approximation we find that when going from HF to ODC, $\langle z_a^2 \rangle$ increases for the Π_u states and decreases for the Π_g states. Simply speaking, the ODC functions on each atom for the Π_u states try to expand to

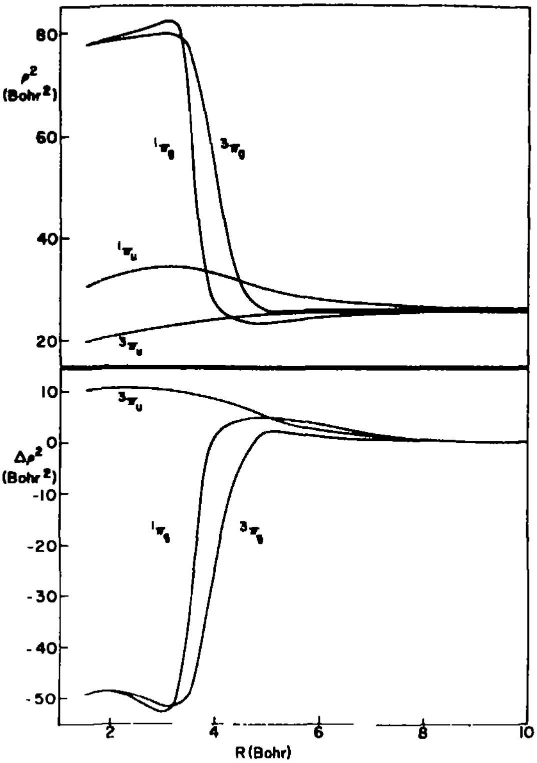

Fig. 9. ODC squares of wavefunction extensions ϱ^2 perpendicular to molecular axis and differences $\Delta\varrho^2$ between $^1\Pi_u$ based and optimal values

gain energy, whereas they try to contract for the Π_g states. This fact can be attributed to the different nodal character of the $\Phi_{HF'}$ admixture for Π_u and Π_g states. Comparing the extensions of Π_u states with Π_g states calculated with optimal exponents we can say that the Π_g states are more diffuse than the Π_u states and $^3\Pi_u$ is more contracted than the $^1\Pi_u$ state. It is no surprise to find that with the $^1\Pi_u$ optimized exponents the other three try to approach the extensions of $\langle z_a^2 \rangle$ of $^1\Pi_u$. For $^3\Pi_u \langle z_a^2 \rangle$ increases, whereas for the Π_g states it decreases (Fig. 10). Again we observe that the asymptotic limit shows at 10 Bohr where the ODC values of $\langle z_a^2 \rangle$ for $^1\Pi_u$ and $^3\Pi_g$ on one hand and $^3\Pi_u$ and $^1\Pi_g$ on the other hand are very close. This trend can be observed also for the other one-electron properties.

Quantities $\langle \varrho_a^2 \rangle$ and $\langle z_a^2 \rangle$ allow us to calculate the quadrupole moment $\langle 3z_a^2 - r_a^2 \rangle$ with respect to an atomic origin. The calculations show that the Π_u states are more expanded perpendicular to the direction of the molecular axis for small internuclear distances, and in the direction of the molecular axis for large internuclear distances. The Π_g states show a distribution which is always more expanded in the direction of the molecular axis than perpendicular to it.

The major portion of nuclear attraction energy $\left\langle \frac{1}{r_a} \right\rangle$ is due to attraction $\langle \sin^2\theta / r_a \rangle$ perpendicular to the molecular axis than to attraction along the

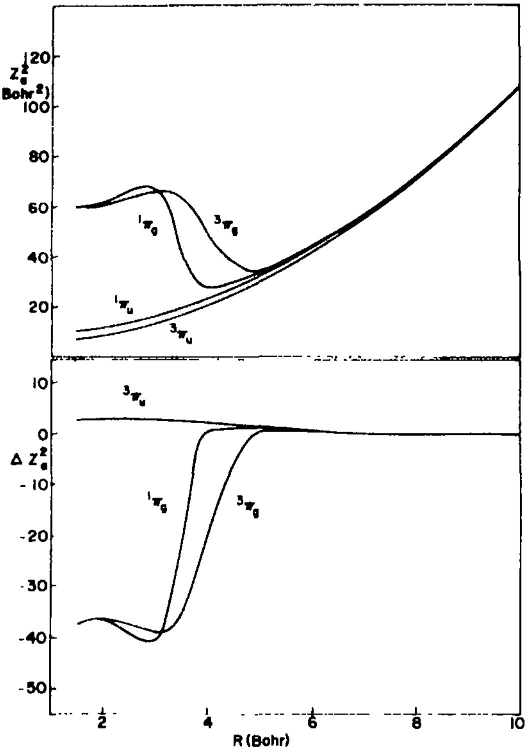

Fig. 10. ODC squares of wavefunction extensions z_a^2 parallel to molecular axis and differences Δz_a^2 between $^1\Pi_u$ based and optimal values

direction of the axis. The ratio $\langle \sin^2 \theta / r_a \rangle / \langle 1/r_a \rangle$ is very similar for all four states, being about 0.6. For comparison, in a spherical distribution this ratio would be 0.666. The expectation values for all four states are coming closer together if they are calculated with the $^1\Pi_u$ optimized exponents.

Tables 6 - 9 contain the eigenvalues of the double-configuration self-consistent field Hamiltonian F of (2.9). For the Hartree-Fock level, these are the orbital energies of the two MO's of Φ_{HF} and $\Phi_{HF'}$ calculated separately with $B = 0$ or $A = 0$. The ordering of the levels is $\lambda_{\sigma_g} < \lambda_{\sigma_u} < \lambda_{\pi_u} < \lambda_{\pi_g}$ except for the Π_g states at 10 Bohr where $\lambda_{\sigma_u} < \lambda_{\sigma_g}$. These levels should approach -0.38 for the σ MO's and -0.003 for the π MO's. There is no indication for these limits at 10 Bohr. The reason is that the electronic interaction is still very strong, i.e. in the order of 0.1 Hartrees; the kinetic energy has already approached the proper limits very closely. The only other remarkable feature is the positive orbital eigenvalue of the MO π_g of $^3\Pi_u$ at 2.2 Bohr with the optimal exponents, which disappears for a $^1\Pi_u$ exponent calculation. The ODC values are the Lagrange multipliers. For small distances, the two multipliers referring to orbitals of configuration Φ_{HF} are close to their corresponding SCF values, whereas the other two have no resemblance to the SCF values. The more mixing occurs between the two configurations Φ_{HF} and $\Phi_{HF'}$ the more the Lagrange multipliers decrease for the

Table 6. Eigenvalues of ${}^1\Pi_u$ state of H_2

R	σ_g	σ_u	π_u	π_g	
1.5	−1.02222	−0.43665	−0.11454	−0.01860	HF
	−1.02359	−0.00290	−0.11699	−0.00227	ODC
1.8	−0.93406	−0.47430	−0.11230	−0.02505	
	−0.93560	−0.00392	−0.11537	−0.00292	
1.95	−0.89591	−0.48713	−0.11120	−0.02600	
	−0.89750	−0.00455	−0.11461	−0.00330	
2.0	−0.88398	−0.49048	−0.11083	−0.02600	
	−0.88558	−0.00478	−0.11436	−0.00343	
2.2	−0.83939	−0.49993	−0.10942	−0.02490	
	−0.84099	−0.00585	−0.11346	−0.00404	
3.0	−0.70392	−0.50736	−0.10410	−0.02209	
	−0.70391	−0.01381	−0.11093	−0.00793	
4.0	−0.59252	−0.48930	−0.09766	−0.01920	
	−0.58291	−0.04279	−0.11158	−0.01958	
5.0	−0.52220	−0.47062	−0.09069	−0.01959	
	−0.49221	−0.09654	−0.11480	−0.03824	
6.0	−0.47983	−0.47708	−0.08403	−0.03033	
	−0.43009	−0.14979	−0.11701	−0.05573	
7.0	−0.45774	−0.44925	−0.07762	−0.02637	
	−0.38778	−0.19182	−0.11590	−0.06898	
8.0	−0.44396	−0.43427	−0.07024	−0.02614	
	−0.36112	−0.22038	−0.11478	−0.07891	
10.0	−0.42671	−0.41799	−0.05438	−0.02641	
	−0.33111	−0.25657	−0.11336	−0.09315	

Table 7. Eigenvalues of ${}^3\Pi_u$ state of H_2

R	σ_g	σ_u	π_u	π_g	
1.5	−0.98849	−0.42247	−0.13276	−0.00680	HF
	−0.98948	−0.00210	−0.13449	−0.00170	ODC
1.8	−0.90092	−0.44642	−0.13177	−0.00230	
	−0.90208	−0.00300	−0.13403	−0.00229	
1.95	−0.86394	−0.45370	−0.13113	−0.00035	
	−0.86515	−0.00355	−0.13369	−0.00263	
2.0	−0.85239	−0.45592	−0.13089	−0.00009	
	−0.85362	−0.00376	−0.13355	−0.00275	
2.2	−0.80907	−0.46241	−0.12989	0.00182	
	−0.81031	−0.00474	−0.13301	−0.00333	
3.0	−0.68155	−0.48000	−0.12467	−0.00593	
	−0.68196	−0.01147	−0.13020	−0.00677	
4.0	−0.58474	−0.48564	−0.11716	−0.02151	
	−0.57947	−0.03099	−0.12717	−0.01487	
5.0	−0.52749	−0.48025	−0.10891	−0.03264	
	−0.50568	−0.06952	−0.12462	−0.02828	
6.0	−0.49220	−0.48287	−0.10094	−0.04386	
	−0.44518	−0.12015	−0.12010	−0.04424	
7.0	−0.47047	−0.46333	−0.09272	−0.04393	
	−0.39668	−0.16891	−0.11532	−0.05915	
8.0	−0.45706	−0.45163	−0.08488	−0.04516	
	−0.36362	−0.20418	−0.11144	−0.07035	
10.0	−0.44199	−0.43719	−0.07034	−0.04631	
	−0.32668	−0.24583	−0.10678	−0.08487	

Table 8. Eigenvalues of $^1\Pi_g$ state of H_2

R	σ_g	σ_u	π_u	π_g	
1.5	−1.13635	−0.49951	−0.09414	−0.05539	HF
	−1.13629	−0.00025	−0.00018	−0.05555	ODC
1.8	1.04359	−0.52773	−0.09376	−0.05544	
	−1.04344	−0.00041	−0.00028	−0.05569	
2.0	0.99060	−0.54276	−0.09332	−0.05542	
	−0.99034	−0.00059	−0.00039	−0.05575	
2.2	−0.94358	−0.55509	−0.09270	−0.05541	
	−0.94315	−0.00086	−0.00053	−0.05584	
3.0	−0.79876	−0.58012	−0.08994	−0.05541	
	−0.79615	−0.00384	−0.00181	−0.05663	
4.0	−0.59110	−0.49236	−0.10624	−0.02197	
	−0.38974	0.25473	−0.09090	−0.05927	
5.0	−0.52912	0.46234	−0.09248	−0.02147	
	0.25565	−0.35225	−0.11903	−0.06763	
6.0	0.49956	0.45476	−0.08538	−0.03004	
	−0.22853	0.36530	−0.11989	−0.07187	
7.0	−0.45856	−0.44506	−0.07729	−0.02483	
	−0.22768	−0.36112	−0.11911	−0.07776	
8.0	−0.43739	−0.43710	−0.06940	−0.02441	
	−0.23749	−0.35042	−0.11738	−0.08408	
10.0	−0.41827	−0.42537	−0.05428	−0.02605	
	−0.26029	−0.32995	−0.11452	−0.09476	

Table 9. Eigenvalues of $^3\Pi_g$ state of H_2

R	σ_g	σ_u	π_u	π_g	
1.5	−1.13606	−0.50099	−0.09579	−0.05567	HF
	−1.13601	−0.00025	−0.00018	−0.05585	ODC
1.8	−1.04301	−0.52924	−0.09534	−0.05581	
	−1.04289	−0.00040	−0.00027	−0.05608	
2.0	−0.98993	−0.54397	−0.09495	−0.05586	
	−0.98972	−0.00055	−0.00036	−0.05621	
2.2	−0.94258	−0.55624	−0.09425	−0.05596	
	−0.94225	−0.00077	−0.00047	−0.05640	
3.0	−0.79718	−0.58079	−0.09138	−0.05651	
	0.79535	−0.00299	−0.00142	−0.05761	
4.0	−0.65900	−0.55180	−0.10159	−0.05649	
	−0.62118	−0.04814	−0.01577	−0.06183	
5.0	−0.53888	−0.48251	−0.10747	−0.03852	
	−0.23116	−0.35058	−0.10614	−0.05219	
6.0	−0.50540	−0.47139	−0.09947	−0.04469	
	−0.20069	−0.36807	−0.11008	−0.05680	
7.0	−0.47303	−0.46149	−0.09184	−0.04463	
	−0.20288	−0.36241	−0.10997	−0.06357	
8.0	−0.45573	−0.45341	−0.08415	−0.04558	
	−0.21739	−0.34857	−0.10832	−0.07125	
10.0	−0.43786	−0.44148	−0.06981	−0.04606	
	−0.24691	−0.32383	−0.10555	−0.08417	

configuration Φ_{HF} and increase for the configuration $\Phi_{HF'}$ in absolute value, so that σ_g approaches σ_u and π_u approaches π_g. The asymptotic limits should be -0.25 for σ and -0.06125 for π. Again we observe that the eigenvalues for all four states are close together when all are calculated with ${}^1\Pi_u$ exponents.

Tables 10–13 contain the eigenvectors. For all four states we observe little change in the coefficients of configuration Φ_{HF} when going from the HF level to the ODC level. The changes increase with increasing configuration interaction. They are relatively larger for the less important AO's $2s$, $2p\sigma$ and $3d\pi$ than for the dominant $1s$ and $2p\pi$. The HF' MO's show decreasing change for the $1s$ and $2p$ with increasing interaction, i.e. they are more stabilized by configuration interaction. There is, at all distances an important change in the coefficients of $2s$, $2p\sigma$ and $3d\pi$ AO's of this configuration $\Phi_{HF'}$. For large distances the coefficients of $1s$ and $2p\pi$ should approach $1/\sqrt{2}$, whereas the other coefficients should vanish. At 10 Bohr this trend becomes apparent. At small distances the most remarkable fact is the great difference in the coefficients of the σ MO's for ${}^1\Pi_g$ and ${}^3\Pi_g$ states which has no counterpart in the energy. It could very well be that the way in which the $1s$, $2s$, $2p\sigma$ exponents for 1.5 Bohr were obtained had an influence on the coefficients. One might conclude that the dependence of the linear coefficients on the exponents is expressed in such a way that the coefficients can take care of a redistribution of the charge so that there is almost no energy change when going from ${}^1\Pi_g$ to ${}^3\Pi_g$. We also emphasize that we did not reoptimize after obtaining the first optimized set of exponents. The discrepancy between ${}^1\Pi_g$ and ${}^3\Pi_g$ coefficients at 1.5 Bohr disappears when results of the Π_g states are based on the ${}^1\Pi_u$ state exponents.

5. Conclusion

The purpose of the present paper was a characterization of the features of the four lowest-lying Π states of the hydrogen molecule. We employed a double-configuration wavefunction and three levels of approximation, namely HF, CI and ODC for energies and one-electron properties. We compared these properties for two sets of exponents: one set based on optimization of the ${}^1\Pi_u$ state and taken also for all the other states and the other set based on optimization of all four states separately.

We found that the potential curves E_{CI} and E_{ODC} are characterized properly with maxima and minima on the CI and ODC level, and also the HF level is represented properly by the E_{HF} and $E_{HF'}$ curves. The emphasis on the accuracy of the HF level is decreased when the accuracy of the ODC level is increased. This can be seen from a comparison of the results for the ${}^3\Pi_u$ and Π_g states with ${}^1\Pi_u$ exponents and optimal exponents. The location of the maxima and minima of the potential curves is also dependent on the exponents. We find minima for Π_u and Π_g states properly at $R=1.95$ and $R=2.00$ with the optimal exponents. The maxima for ${}^1\Pi_u$ at $R=7.8$ Bohr, for ${}^1\Pi_g$ at $R=3.8$ Bohr and ${}^3\Pi_g$ at $R=4.2$ Bohr are less secured. They probably depend on the choice of the basis set.

An analysis of the one-electron properties shows uniformity for the four states when calculated with the same set of exponents, whereas significant differ-

Table 10. Eigenvectors of $^1\Pi_u$ state of H_2

R	σ_g			σ_u			π_u		π_g		
	1s	2s	2p	1s	2s	2p	2p	3d	2p	3d	
1.5	0.73563	−0.23537	0.05673	0.92149	0.59895	−0.02590	0.50601	−0.00416	4.0973	0.22399	HF
	0.73514	−0.23455	0.05622	1.02400	0.38657	−0.03350	0.50606	−0.00479	1.0399	−0.46189	ODC
1.8	0.68366	−0.16236	0.06141	0.87386	0.42024	−0.02861	0.50839	−0.00548	3.5594	0.24313	
	0.68318	−0.16144	0.06066	0.92885	0.32705	−0.02231	0.50848	−0.00643	1.0119	−0.45349	
1.95	0.65929	−0.12716	0.06348	0.85195	0.36426	−0.02809	0.50970	−0.00610	3.3437	0.24838	
	0.65885	−0.12620	0.06259	0.88722	0.31000	−0.02002	0.50982	−0.00725	1.0217	−0.44254	
2.0	0.65509	−0.11981	0.06417	0.84817	0.34366	−0.02736	0.51014	−0.00622	3.2710	0.24767	
	0.65466	−0.11883	0.06322	0.87781	0.30114	−0.01886	0.51028	−0.00745	1.0367	−0.43656	
2.2	0.65464	−0.11017	0.06568	0.85530	0.24702	−0.02263	0.51198	−0.00645	2.9821	0.23613	
	0.65424	−0.10912	0.06453	0.86601	0.24078	−0.01459	0.51216	−0.00799	1.1263	−0.40243	
3.0	0.65932	−0.08053	0.06787	0.85276	0.02661	−0.00209	0.52064	−0.00651	2.1238	0.15040	
	0.65925	−0.07928	0.06548	0.83378	0.07490	−0.00150	0.52112	−0.00976	1.4008	−0.20675	
4.0	0.66542	−0.03639	0.05887	0.79156	−0.01557	0.01366	0.53558	−0.00275	1.4514	0.03129	
	0.66595	−0.03513	0.05408	0.77140	0.03097	0.00903	0.53717	−0.01042	1.3765	−0.01945	
5.0	0.68208	−0.01890	0.04377	0.75604	−0.02427	0.02077	0.55352	0.00986	1.1015	−0.03959	
	0.68323	−0.01811	0.03652	0.74199	0.00755	0.01103	0.55802	−0.00840	1.1600	0.01645	
6.0	0.69772	−0.01521	0.02741	0.73590	−0.02280	0.02884	0.55666	0.05821	0.64387	−0.31344	
	0.69829	−0.01451	0.02115	0.72751	−0.00500	0.00993	0.58067	−0.00446	1.0343	0.04262	
7.0	0.70031	−0.00253	0.01532	0.71999	−0.00656	0.02451	0.57755	0.06606	0.81020	−0.13201	
	0.70029	−0.00193	0.01105	0.71153	0.00670	0.00855	0.60140	−0.00437	0.90921	−0.00779	
8.0	0.69414	0.01168	0.00817	0.70410	0.00957	0.01982	−0.60340	0.06386	0.82119	−0.05513	
	0.69326	0.01299	0.00515	0.69660	0.01935	0.00675	0.62102	−0.00316	0.84504	0.00085	
10.0	0.67057	0.04084	0.00379	0.67325	0.03937	0.01074	0.65043	0.03767	0.77303	−0.00905	
	0.66733	0.04452	0.00123	0.66735	0.04607	0.00306	0.65495	−0.00093	0.77417	−0.00052	

Table 11. Eigenvectors of $^3\Pi_u$ state of H_2

R	σ_g			σ_u			π_u		π_g		
	1s	2s	2p	1s	2s	2p	2p	3d	2p	3d	
1.5	0.61854	−0.09745	0.05942	0.77707	0.77644	−0.01791	0.50696	0.01313	3.8216	0.32743	HF
	0.61880	−0.09755	0.05902	0.95421	0.05215	−0.13646	0.50705	0.01246	1.2314	−0.35500	ODC
1.8	0.61709	−0.08332	0.06355	0.78749	0.54458	−0.02079	0.51034	0.01282	3.1278	0.29443	
	0.61756	−0.08358	0.06298	0.95866	0.00034	−0.09517	0.51050	0.01187	1.2578	−0.31273	
1.95	0.61616	−0.07591	0.06523	0.79271	0.45930	−0.01854	0.51214	0.01287	2.8073	0.25658	
	0.61675	−0.07626	0.06456	0.95187	−0.01520	−0.07946	0.51233	0.01176	1.3154	−0.27793	
2.0	0.61855	−0.07675	0.06570	0.79825	0.42932	−0.01751	0.51274	0.01296	2.7215	0.24657	
	0.61920	−0.07714	0.06500	0.95343	−0.02545	−0.07483	0.51294	0.01179	1.3227	−0.26808	
2.2	0.61673	−0.06545	0.06690	0.79929	0.34646	−0.01219	0.51536	0.01327	2.3903	0.20006	
	0.61760	−0.06601	0.06603	0.93716	−0.03130	−0.05710	0.51563	0.01182	1.3688	−0.21945	
3.0	0.63283	−0.05053	0.06901	0.81305	0.12094	0.00899	0.52648	0.01620	1.6077	0.06023	
	0.63531	−0.05236	0.06718	0.89885	−0.08820	−0.01812	0.52717	0.01316	1.3992	−0.06221	
4.0	0.60335	0.03054	0.06129	0.72416	0.10188	0.02196	0.54088	0.02396	1.2066	−0.01808	
	0.60938	0.02572	0.05785	0.77828	−0.00138	0.00261	0.54307	0.01607	1.2402	0.00832	
5.0	0.59207	0.07947	0.04926	0.66740	0.11100	0.02680	0.55679	0.03214	1.0305	−0.03851	
	0.60279	0.07024	0.04386	0.70647	0.04820	0.01020	0.56184	0.01508	1.0797	0.01353	
6.0	0.58870	0.10854	0.03605	0.63576	0.11904	0.03091	0.55849	0.06801	0.72052	−0.23142	
	0.60288	0.09524	0.02985	0.66120	0.08082	0.01221	0.57972	0.01649	0.98468	0.02627	
7.0	0.61436	0.09431	0.02460	0.63626	0.10066	0.02390	0.58057	0.07043	0.81495	−0.10066	
	0.63144	0.07662	0.01873	0.66445	0.06323	0.00946	0.60321	0.00891	0.88864	0.00580	
8.0	0.62963	0.08454	0.01676	0.63767	0.09037	0.01877	0.60388	0.06986	0.81296	−0.04601	
	0.64833	0.06404	0.01163	0.66624	0.05460	0.00724	0.62357	0.00481	0.83460	0.00169	
10.0	0.65261	0.06340	0.00556	0.65151	0.06708	0.00893	0.65018	0.04238	0.77180	−0.00436	
	0.67367	0.03891	0.00279	0.67916	0.03434	0.00275	0.65580	0.00142	0.77251	0.00043	

Table 12 Eigenvectors of $^1\Pi_g$ state of H_2

R	σ_g			σ_u			π_u		π_g		
	1s	2s	2p	1s	2s	2p	2p	3d	2p	3d	
1.5	0.66531	−0.15486	0.06159	0.82924	0.70297	−0.02592	0.49892	0.05946	6.3776	0.05858	HF
	0.66525	−0.15477	0.06155	0.85861	0.61339	−0.03792	0.50244	−0.02819	6.3757	0.05812	ODC
1.8	0.65120	−0.12628	0.06742	0.82913	0.46927	−0.03082	0.49908	0.05796	5.3501	0.06252	
	0.65113	−0.12616	0.06735	0.83467	0.46351	−0.02888	0.50300	−0.01570	5.3472	0.06169	
2.0	0.64675	−0.11271	0.07054	0.83589	0.35148	−0.02828	0.49926	0.05723	4.8409	0.06332	
	0.64666	−0.11256	0.07044	0.82666	0.38282	−0.02266	0.50338	−0.00941	4.8367	0.06210	
2.2	0.64702	−0.10355	0.07225	0.84259	0.25803	−0.02236	0.49945	0.05710	4.4299	0.06245	
	0.64692	−0.10336	0.07211	0.82121	0.31361	−0.01626	0.50387	−0.00625	4.4242	0.06068	
3.0	0.66438	−0.09136	0.07670	0.86430	0.01740	0.00010	0.50011	0.06106	3.3092	0.04350	
	0.66424	−0.09097	0.07623	0.83364	0.08310	−0.00037	0.50675	−0.00660	3.2916	0.03716	
4.0	0.64645	−0.02363	0.07924	0.77532	0.01353	0.00617	0.52309	0.04589	1.1294	−0.13740	
	0.64451	−0.01287	0.05793	0.75966	0.04255	0.00954	0.53823	−0.00623	1.2532	−0.06940	
5.0	0.63436	0.02443	0.07404	0.71980	0.03074	0.00603	0.54194	0.06582	0.61233	−0.34944	
	0.63740	0.03418	0.03583	0.70817	0.04859	0.00895	0.57065	−0.01077	0.95518	−0.08590	
6.0	0.64040	0.04169	0.06213	0.69356	0.03761	0.00537	0.54678	0.09398	0.56872	−0.36491	
	0.64320	0.04941	0.02490	0.68432	0.05032	0.00857	0.58765	−0.00432	0.92424	−0.03486	
7.0	0.65295	0.04494	0.04794	0.68354	0.03815	0.00298	0.57140	0.09232	0.75157	−0.18362	
	0.65284	0.05160	0.01705	0.67572	0.04850	0.00667	0.60608	0.00072	0.88035	−0.00544	
8.0	0.66225	0.04410	0.03468	0.67830	0.03892	0.00131	0.59735	0.08831	0.78991	−0.09137	
	0.65906	0.05106	0.01197	0.67141	0.04764	0.00481	0.62463	0.00172	0.83326	0.00017	
10.0	0.68054	0.03066	0.01194	0.68414	0.02837	0.00183	0.64910	0.04860	0.77038	−0.01339	
	0.67436	0.03809	0.00401	0.67813	0.03557	0.00156	0.65586	0.00090	0.77258	0.00087	

Table 13. Eigenvectors of $^3\Pi_g$ state of H_2

R	σ_g			σ_u			π_u		π_g		
	1*s*	2*s*	2*p*	1*s*	2*s*	2*p*	2*p*	3*d*	2*p*	3*d*	
1.5	0.80812	−0.31896	0.06115	1.00623	0.51229	−0.02620	0.49881	0.06128	6.3608	0.05447	HF
	0.80807	−0.31888	0.06111	1.01924	0.45513	−0.03787	0.44334	−0.57120	6.3582	0.05385	ODC
1.8	0.70128	−0.38548	0.06645	0.89683	0.39252	−0.02825	0.49891	0.06022	5.3257	0.05580	
	0.70123	−0.38530	0.06639	0.89000	0.37822	−0.03892	0.45640	−0.47702	5.3219	0.05478	
2.0	0.65394	−0.12108	0.06979	0.84492	0.34526	−0.02647	0.49881	0.06229	4.8163	0.05515	
	0.65390	−0.12098	0.06970	0.83146	0.34469	−0.03824	0.46401	−0.43406	4.8113	0.05373	
2.2	0.64531	−0.10165	0.07143	0.84216	0.26532	−0.02172	0.49914	0.06040	4.3933	0.05116	
	0.64527	−0.10154	0.07130	0.82602	0.26846	−0.03602	0.47170	−0.38570	4.3870	0.04925	
3.0	0.64371	−0.06725	0.07556	0.84450	0.04902	−0.00101	0.49947	0.06598	3.2500	0.02248	
	0.64383	−0.06716	0.07513	0.83702	0.03444	−0.02111	0.49675	−0.25595	3.2329	0.01654	
4.0	0.64516	−0.01723	0.06798	0.77962	0.01331	0.01101	0.50433	0.06726	2.0455	0.03568	
	0.64795	−0.01920	0.06488	0.79085	−0.02411	0.00325	0.52560	−0.07599	1.9902	0.01037	
5.0	0.65284	0.01430	0.05501	0.73598	0.02457	0.00887	0.54273	0.05295	0.82358	−0.20835	
	0.68676	−0.02040	0.02758	0.74570	−0.00526	0.00668	0.56910	−0.02256	0.95564	−0.10903	
6.0	0.67357	0.01597	0.04333	0.72069	0.01692	0.00842	0.55417	0.07170	0.72799	−0.23195	
	0.70202	−0.01943	0.01496	0.72741	−0.00844	0.00640	0.58714	−0.01225	0.91067	−0.06155	
7.0	0.66767	0.03829	0.03009	0.69902	0.03079	0.00775	0.57968	0.06793	0.83342	−0.08851	
	0.70622	−0.00959	0.00845	0.71197	0.00589	0.00548	0.60449	−0.00427	0.88244	−0.01716	
8.0	0.65784	0.05538	0.02159	0.67924	0.04394	0.00641	0.60670	0.06066	0.82483	−0.03412	
	0.69807	0.00718	0.00483	0.69663	0.01958	0.00425	0.62310	−0.00179	0.83637	−0.00626	
10.0	0.63909	0.07587	0.01128	0.64750	0.06848	0.00440	0.65088	0.03450	0.77380	−0.00334	
	0.66855	0.04314	0.00229	0.66686	0.04661	0.00161	0.65491	−0.00046	0.77405	−0.00141	

ences between the states begin to show when their properties are calculated for each with its own optimal exponents.

There are problems with exponent optimization which are difficult to resolve, in particular, the dependence of the exponents on each other and the dependence of the linear coefficients on the exponents. We find exponent optimization necessary when the MO's are much more diffuse or contracted than either limit for large or small internuclear distances so that a prediction for intermediate distances is not possible. This happens to be the case for the Π_g states at the energy minimum. From our results we conclude that it would be best to optimize the exponents of the dominant orbitals, here $1s$ and $2p\pi$, and add a larger number of further functions which are not optimized but which allow us by linear coefficient optimization to describe the features of potential curves properly.

Acknowledgement. This work was supported in part by a grant of the National Institutes of Health. The major portion of the work was performed at the Common Research Computer Facility, Houston and we thank its director Mr. G. Dolansky and his staff for their kind help and cooperation. We also thank Illinois Institute of Technology, Saint Louis University and IBM for computer time. The work would not have been completed without the help of Professor J. Hinze, Dr. A. C. Wahl, Dr. W. Zemke and Mrs. M. Owen. We thank Professor H. Silverstone for a discussion of the manuscript.

References

1. Zemke, W. T., Lykos, P. G., Wahl, A. C.: J. chem. Physics **51**, 5635 (1969).
2. Jug, K., Lykos, P. G., McLean, A. D.: Exponent optimization for Π states of H_2. Theoret. chim. Acta (Berl.) **25**, 10 (1972).
3. Veillard, A., Clementi, E.: Theoret. chim. Acta (Berl.) 7, 133 (1967).
4. Zemke, W. T.: Ph. D. Thesis, Illinois Institute of Technology, Chicago (1969).
5. Browne, J. C.: J. chem. Physics **40**, 43 (1964).
6. J. chem. Physics **41**, 1583 (1964).
7. Kolos, W., Wolniewicz, L.: J. chem. Physics **43**, 2429 (1965).
8. Wright, W. M., Davidson, E. R.: J. chem. Physics **43**, 840 (1965).

Prof. K. Jug
Institut für Theoretische Chemie
Universität Stuttgart
D-7 Stuttgart 1
Relenbergstr. 32
Germany

Theoret. chim. Acta (Berl.) 25, 41—48 (1972)
© by Springer-Verlag 1972

Optimal Double-Configuration Study of the Lowest Excited Π States of H_2

II. $\sigma - \pi$ Separation

Karl Jug*
Department of Chemistry, Saint Louis University, Saint Louis, Missouri 63156

Peter G. Lykos**
Department of Chemistry, Illinois Institute of Technology, Chicago, Illinois 60616

A. D. McLean
IBM Research Laboratory, San Jose, California 95114

Received July 20, 1971

The $\sigma - \pi$ separation of energies and one-electron properties of the four lowestlying Π states of the hydrogen molecule considered in the preceding paper [1] is presented. The calculations are based on separate exponent optimization for all four states. The values of the σ electron properties of the four states are much closer than those of the π electrons. The degree of uniformity of the π electron property values increases when a lesser level of approximation based on a single-state (${}^1\Pi_u$) exponent set is used. The assumption of equal parameter values for different states in semiempirical π electron methods is valid only on this level. Conclusions based on this assumption cannot lead us to a representative description of the antibonding character of molecular states.

Die $\sigma - \pi$-Separierung von Energien und Einelektroneneigenschaften der vier niedrigsten Π Zustände des Wasserstoffmoleküls, die in der vorhergehenden Arbeit [1] betrachtet worden sind, wird angegeben. Die Rechnungen basieren auf getrennter Exponentenoptimisierung für alle vier Zustände. Die σ-Elektroneneigenschaften der vier Zustände sind untereinander ähnlicher als die der π-Elektronen. Auch diese werden sich ähnlicher auf einer niedrigeren Approximationsstufe, die auf einem einzigen (${}^1\Pi_u$) Exponentensatz basiert. Nur auf dieser Stufe kann die Annahme gleicher Parameterwerte für verschiedene Zustände in semiempirischen π-Methoden gerechtfertigt werden. Folgerungen aus dieser Annahme können uns nicht zu einer repräsentativen Beschreibung des antibindenden Charakters von Molekülzuständen führen.

Séparation $\sigma - \pi$ des énergies et des propriétés monoélectroniques pour les quatre plus bas états Π de la molécule d'hydrogène envisagés dans l'article précédent. Les calculs sont fondés sur une optimisation séparée des exposants pour les quatre états. Les valeurs des propriétés des électrons σ des quatre états sont plus voisines que celles des électrons π. Le degré d'uniformité des propriétés des électrons π augmente lorsque l'on emploie un degré d'approximation inférieur fondé sur un ensemble d'exposants d'un seul état (${}^1\Pi_u$). L'hypothèse d'une identité des valeurs des paramètres pour les différents états dans les méthodes à électrons π semi-empiriques n'est validée qu'à ce niveau. Les conclusions fondées sur cette hypothèse ne peuvent nous conduire à une description représentative du caractère antiliant des états moléculaires.

---

[*] On leave to: Institut für Theoretische Chemie, Universität Stuttgart.

[**] On leave to: Office of Computing Activities, National Science Foundation, Washington, D.C.

Accession number
38963

1. Introduction

The purpose of this paper is to investigate the basis of approximate molecular orbital theories where groups of electrons are separated from other groups. The most popular separation is the one of σ and π electrons, particularly in hydrocarbons. The conditions for a $\sigma-\pi$ separation were formulated by Lykos and Parr [2]. The Π states of H_2 are the simplest case where such a separation can be studied. In the following two sections we shall discuss the $\sigma-\pi$ separation of energies and one-electron properties and the consequences for approximate molecular orbital theories. In essence, we cannot support the assumption of equal parameter values for different states in semiempirical MO methods as valid in molecules.

2. $\sigma-\pi$ Separation

Figs. 1 2 contain kinetic (T_σ, T_π) and total electronic (E_σ, E_π) energy of the σ electron and the π electron and their interaction ($E_{\sigma\pi}$) for the four Π states with the optimal exponents listed in Table 1 of the preceding paper [1] on the ODC level.

Comparing the σ and π energies of the four Π states with each other, yields the following important result. The σ part E_σ of the total electronic energy shows almost no fluctuation over the whole range of internuclear distances. This is true

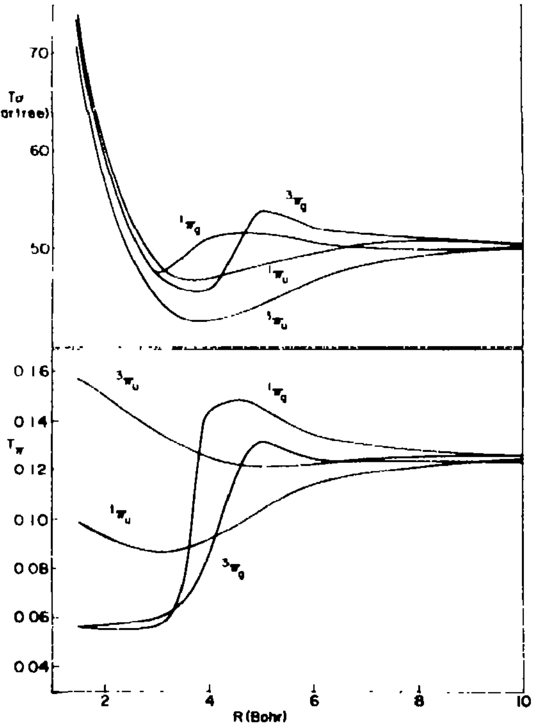

Fig. 1. σ and π part of kinetic energy

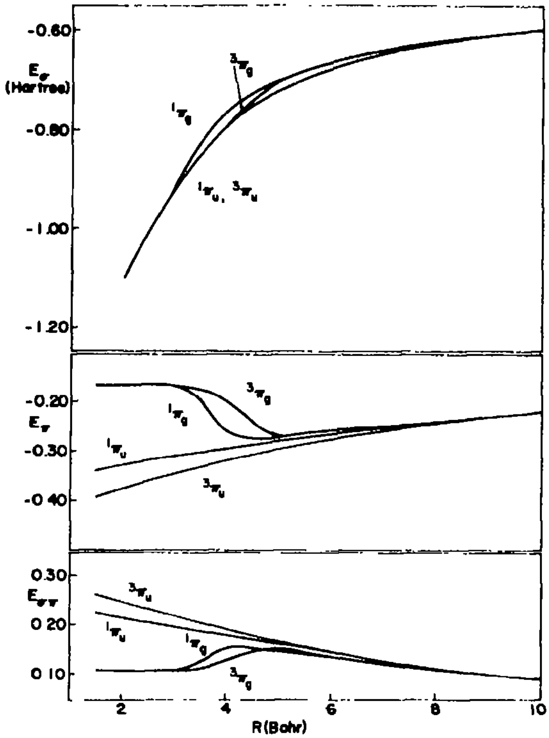

Fig. 2. σ and π part of electronic energy and $\sigma-\pi$ interaction energy

to lesser degree for T_σ. The energy differences between the four states arise from E_π and $E_{\sigma\pi}$. E_π is increasing in the order $^3\Pi_u$, $^1\Pi_u$, $^3\Pi_g$ or $^1\Pi_g$ for all distances on the HF level and for distances smaller than 8 Bohr on the ODC level where the asymtotic limits have not been reached closely. $E_{\sigma\pi}$ shows the opposite trend. With the optimal exponents for each state the differences between the Π_u and Π_g states are rather large, whereas the values of the $^3\Pi_u$ and Π_g states are fairly close to the $^1\Pi_u$ values if the energies for all four states are calculated with the $^1\Pi_u$ exponents. In particular, the Π_g states gain total energy decrease upon exponent optimization by a decrease in electronic interaction $E_{\sigma\pi}$ which is somewhat reduced by the increase in core energy E_π. For HF and CI levels, we obtain similar results except for $E_{\sigma\pi}$. The electronic interaction is decreasing from HF to CI and finally ODC. The effect increases with internuclear distance. The proper dissociation of the states is based on a decrease in electronic interaction.

We present in Table 1 a subdivision of $E_{\sigma\pi}$ in intraconfigurational and interconfigurational parts. It is interesting to note that the intraconfigurational part shows almost no difference for all three levels, HF, CI and ODC. The interconfigurational part is always negative and tends to reduce the total electronic interaction. Again we find a tendency to uniformity if these energies are calculated for all four states with the $^1\Pi_u$ exponents.

To complete the picture of $\sigma-\pi$ separation, we also mention the results for one-electron properties. The density distribution of the σ electron perpendicular

Table 1. Subdivision of $E_{e\pi}$

	${}^1\Pi_u$		${}^3\Pi_u$		${}^1\Pi_g$		${}^3\Pi_g$		
R	E_{intra}	E_{inter}	E_{intra}	E_{inter}	E_{intra}	E_{inter}	E_{intra}	E_{inter}	
2.0	0.21740	0.0	0.24872	0.0	0.11091	0.0	0.11159	0.0	HF
	0.21734	−0.00167	0.24819	−0.00213	0.11093	−0.00034	0.11160	−0.00020	CI
	0.21749	−0.00383	0.24816	−0.00294	0.11109	−0.00035	0.11181	−0.00036	ODC
4.0	0.20208	0.0	0.20929	0.0	0.20397	0.0	0.13597	0.0	
	0.20227	−0.01826	0.20927	−0.01371	0.20346	−0.04431	0.13642	−0.00775	
	0.20118	−0.01868	0.20861	−0.01421	0.20234	−0.04693	0.13734	−0.00931	
6.0	0.19773	0.0	0.18304	0.0	0.17851	0.0	0.17229	0.0	
	0.19409	−0.04133	0.18351	−0.03171	0.19395	−0.05012	0.18140	−0.03629	
	0.19686	−0.05193	0.18430	−0.03781	0.20186	−0.06579	0.18223	−0.04386	
8.0	0.18305	0.0	0.16996	0.0	0.19004	0.0	0.17113	0.0	
	0.18514	−0.06571	0.17043	−0.05168	0.18755	−0.06869	0.17017	−0.05120	
	0.18437	−0.07010	0.16988	−0.05587	0.18812	−0.07562	0.16966	−0.05553	
10.0	0.17365	0.0	0.15813	0.0	0.18221	0.0	0.16236	0.0	
	0.17705	−0.08084	0.15979	−0.06430	0.17764	−0.08200	0.15988	−0.06375	
	0.17666	−0.08212	0.15986	−0.06613	0.17731	−0.08377	0.15981	−0.06528	

Table 2. Density distribution ϱ^2 (Bohr^2) of σ and π electrons perpendicular to molecular axis

	${}^1\Pi_u$		${}^3\Pi_u$		${}^1\Pi_g$		${}^3\Pi_g$	
R	$(\varrho^2)_\sigma$	$(\varrho^2)_\pi$	$(\varrho^2)_\sigma$	$(\varrho^2)_\pi$	$(\varrho^2)_\sigma$	$(\varrho^2)_\pi$	$(\varrho^2)_\sigma$	$(\varrho^2)_\pi$
2.0	1.291	31.169	1.415	19.240	1.321	77.554	1.322	76.934
	1.292	31.166	1.416	19.238	1.321	77.563	1.322	76.940
	1.295	31.121	1.414	19.229	1.322	77.463	1.322	76.817
4.0	1.886	31.574	2.192	22.269	2.013	21.098	1.996	51.564
	1.874	31.204	2.181	22.084	1.894	24.567	1.978	52.491
	1.885	31.245	2.146	22.163	1.944	25.232	1.959	51.435
6.0	1.995	27.168	2.308	24.488	2.177	22.445	2.237	22.076
	1.960	26.396	2.257	23.983	1.985	23.687	2.045	24.528
	1.972	25.995	2.172	23.590	1.998	22.779	1.908	24.165
8.0	2.003	26.352	2.190	24.877	2.735	20.777	2.248	21.229
	1.979	24.823	2.162	23.580	2.001	23.269	2.140	24.052
	1.997	25.007	2.057	23.638	2.020	23.355	1.979	24.183
10.0	1.979	25.536	2.133	25.111	2.005	21.836	2.092	22.158
	1.972	24.134	2.130	23.779	1.991	23.726	2.068	24.152
	1.987	24.185	2.022	23.823	2.018	23.787	1.985	24.193

to the molecular axis $\langle\varrho^2\rangle_\sigma$ and along the molecular axis $\langle z_a^2\rangle_\sigma$ is fairly equal for all four states. Great differences arise for the distribution of the π electron. The wavefunction is more contracted for ${}^3\Pi_u$ than ${}^1\Pi_u$, whereas for the Π_g states the functions are much more expanded than for ${}^1\Pi_u$. This is valid for both $\langle\varrho^2\rangle_\pi$ and $\langle z_a^2\rangle_\pi$. Table 2 shows the representative results for ϱ^2. The differences between the four states are greatly reduced when the ${}^1\Pi_u$ state exponents are used for all four states. Similar results are obtained for z_a^2.

Qualitatively the same conclusions hold for the quantities $\left\langle \frac{1}{r_a} \right\rangle$ and $\left\langle \frac{\sin^2\theta}{r_a} \right\rangle$. The σ parts are equal and the differences in the π part between Π_g and Π_u states arise from expansion of the π orbital in the Π_g states accompanied by a decrease in the above expectation values.

3. Consequences for Approximate Molecular Orbital Methods

Approximate molecular orbital methods are dealing with groups of electrons, which have certain features in common and can be treated separately from the others. π-electrons, σ-electrons, lone pairs, non-bonding $1s$-electrons are such groups. Conditions for a separation of π-electrons from σ-electrons were formulated by Lykos and Parr [2]. They include (A) the wavefunction Φ is an antisymmetrized product of σ part Φ_σ and π part Φ_π, (B) all three functions Φ, Φ_σ, Φ_π are normalized, (C) Φ_σ and Φ_π can be represented by linear combinations of configurations which are built up by sets of mutually exclusive subsets of orbitals for σ and π electrons. The total energy can be separated in σ part, π part and $\sigma-\pi$ interaction

$$E_{\text{total}} = E_\sigma + E_\pi + E_{\sigma\pi}\,. \tag{3.1}$$

The latter part can be considered as the π electron energy $E'_\pi = E_\pi + E_{\sigma\pi}$. In cases where the σ function Φ_σ does not change under π-electron excitation for all Π-states under consideration, energy differences can conveniently be written as

$$\Delta E = E'_{\pi_1} - E'_{\pi_2} \tag{3.2}$$

n the ODC level, condition (A) does not hold, however, (3.2) may still be valid. This is used as a justification of semiempirical methods in which experimental nsition energies between Π-states have been used to determine the parameters the method [3]. Let us briefly outline the implications for H_2. Fig. 2 shows that , is constant for all four states and we can consider the σ part as frozen. The nplest type of approximation, the Hückel method, uses orbital energies as presentative for ground and excited Π-states. In particular, in diatomic molecules e orbital energies ε are representing two states in the following way

$$\varepsilon_\pm = \alpha \pm \beta \tag{3.3}$$

d the state energy difference ΔE is

$$\Delta E = \varepsilon_- - \varepsilon_+ = -2\beta\,. \tag{3.4}$$

we consider the effective underlying Hamiltonian as the SCF operator and the O's as symmetrically orthogonalized [4], the π part of H_2 can indeed be written as

$$\begin{aligned} \varepsilon_{\pi_g} &= \alpha_{\pi_g} - \beta_{\pi_g} \\ \varepsilon_{\pi_u} &= \alpha_{\pi_u} + \beta_{\pi_u} \end{aligned} \tag{3.5}$$

where α and β have the usual meaning and ε is the SCF orbital energy. If we identify $\varepsilon_- = \varepsilon_{\pi_g}, \varepsilon_+ = \varepsilon_{\pi_u}$ and assume $\alpha_{\pi_g} = \alpha_{\pi_u} = \alpha$ and $\beta_{\pi_g} = \beta_{\pi_u} = \beta$ we obtain Eqs. (3.3) with the consequence that

$$\begin{aligned} \beta &= \tfrac{1}{2}(\varepsilon_{\pi_u} - \varepsilon_{\pi_g}) \\ \alpha &= \tfrac{1}{2}(\varepsilon_{\pi_u} + \varepsilon_{\pi_g}), \end{aligned} \tag{3.6}$$

We have now to ask the question whether these α's and β's have any resemblance to the theoretically calculated $\alpha_{\pi_g}, \alpha_{\pi_u}, \beta_{\pi_g}, \beta_{\pi_u}$ values based on the atomic basis sets $\{2p, 3d\}$ and $\{1s, 2s, 2p\}$ and the coefficients and exponents given in the preceding paper [1]. In Hückel methods, β adjustment is done at the equilibrium positions of the molecule. Let us take for convenience $R = 2$ Bohr as such a distance. With the optimal $2p\pi$-exponents for the four states $\zeta_{{}^1\Pi_u} = 0.442, \zeta_{{}^3\Pi_u} = 0.561, \zeta_{{}^1\Pi_g} = 0.245, \zeta_{{}^3\Pi_g} = 0.245$ we would not expect resemblance of α_{π_g} and α_{π_u} or β_{π_g} and β_{π_u}. Table 3 shows α and β parameter values for ${}^1\Pi_u$ and ${}^1\Pi_g$ states calculated with optimal exponents for each state. We find ${}^1\Pi_g$ much less antibonding than ${}^1\Pi_u$ bonding contrary to the usual Hückel type assumptions. The orbital energy ε for the π_g orbital equals the $3d$ energy of the hydrogen atom, although it is mainly composed of highly expanded $2p\pi$ orbitals.

Table 3. α and β parameter values (Hartree) at $R = 2$ Bohr

	${}^1\Pi_u$	${}^1\Pi_g$	Empirical from (3.6)
α	0.0696	- 0.0728	- 0.0831
β	0.0413	0.0174	0.0277
$\bar{\alpha}$	0.108	0.090	
$\bar{\beta}$	−0.106	−0.088	-

Non-orthogonal parameters with bar.

If we take the ${}^1\Pi_u$ state exponents as a basis for our calculation, the various α and β parameters will be more uniform. Most semiempirical methods take for granted that the atomic orbitals used for the ground state can be used with the same exponents for excited states also. The choice of the same parameters for ground and excited states is then a simple consequence. Yet, from our present study we expect that also in hydrocarbons the assumption of equal exponents for all possible Π states is unrealistic and might be completely misleading. Huzinaga [5] showed that different exponents should be used for bonding and antibonding orbitals in ethylene.

Let us also show the implications for the Pariser-Parr method [6] where β is calculated by the state energy difference.

$$\Delta E = E^{\text{total}}_{\Pi_g} - E^{\text{total}}_{\Pi_u} = -2\beta .$$

We would have to take the difference between the ODC level energies with the optimal exponents for Π_u and Π_g states as the empirical energy difference. Fig. 3

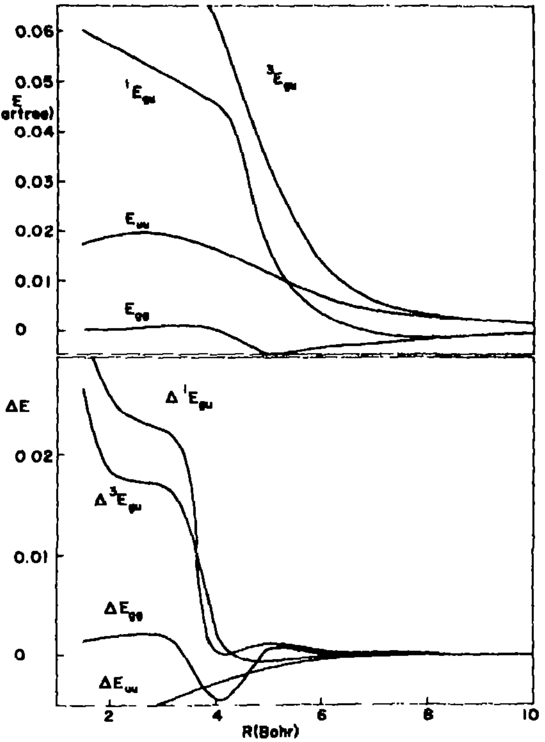

Fig. 3. ODC singlet-singlet $^1E_{gu}$, triplet-triplet $^3E_{gu}$ and singlet-triplet E_{uu}, E_{ug} transition energies and differences ΔE between $^1\Pi_u$ based and optimal values

shows these differences for all possible combinations. The β calculated in such a way is at best an average of the β's for Π_g and Π_u states. It cannot be interpreted as representative for either Π_u or Π_g. On the other hand, if we calculate all quantities with the same exponent set, the energy difference between two states is completely misrepresented. So the β's based on equal exponents for all states do not yield good excitation energies. The differences between optimal and $^1\Pi_u$ based excitation energies are also in Fig. 3.

We do not try to find further similarities with hydrocarbons, because H_2 is not a representative system. Further studies including 2s-, $2p\sigma$- and $2p\pi$-interactions, might be done along the same lines for ethylene.

We feel that exponent optimization in a minimal basis set is necessary, because it is difficult to predict whether the atomic orbitals in a molecule are more contracted, as in $^3\Pi_u$ state, or more expanded, as in the $^1\Pi_u$ and Π_g states, than in the free atom. Large basis sets do not require such a careful exponent optimization. However, they involve a large number of parameters. We do not expect that parametrization schemes can be simplified to such a degree as Hückel or Pariser-Parr methods suggest.

Acknowledgement. This work was supported in part by a grant of the National Institutes of Health. We thank Professor H. Silverstone for a discussion of the manuscript.

References

1. Jug, K., Lykos, P. G., McLean, A. D.: Theoret. chim. Acta (Berl.) **25**, 17 (1972).
2. Lykos, P. G., Parr, R. G.: J. chem. Physics **24**, 1166; **25**, 1301 (1956).
3. For a review see e.g. Jug, K.: Theoret. chim. Acta (Berl.) **14**, 91 (1969).
4. Löwdin, P. O.: J. chem. Physics **18**, 365 (1950).
5. Huzinaga, S.: J. chem. Physics **36**, 453 (1962).
6. Pariser, R., Parr, R. G.: J. chem. Physics **21**, 466, 767 (1953).

Prof. K. Jug
Institut für Theoretische Chemie
Universität Stuttgart
D-7 Stuttgart 1
Relenbergstr. 32
Germany

Theoret. chim. Acta (Berl.) 25, 49—53 (1972)
© by Springer-Verlag 1972

A Comparison of Lobe and Cartesian Gaussian Basis Sets for Molecular Calculations

R. D. Brown, F. R. Burden, and B. T. Hart
Department of Chemistry, Monash University, Clayton, Victoria, Australia, 3168

Received August 3, 1971

Lobe gaussian and cartesian gaussian basis sets, of approximately minimal basis Slater accuracy, have been compared for molecular calculations. The basis sets were constructed so that they only differed in the representation of the angular dependence of the p function.

Calculation of total energy and several one-electron properties for a series of nine molecules shows that, for molecular calculations, the lobe and cartesian gaussian representations are equivalent.

Lobe- und cartesische Gauß-Basissätze mit näherungsweise der gleichen Genauigkeit wie minimale Slater-Basissätze wurden für den Fall von Rechnungen an Molekülen verglichen.

Die Basissätze wurden so konstruiert, daß sie nur in der Darstellung der Winkelabhängigkeit der p-Funktion voneinander abwichen.

Berechnungen der Gesamtenergie und verschiedener Einelektron-Eigenschaften einer Serie von neuen Molekülen zeigen, daß "Lobe"- und cartesische Gaußrepräsentationen für Rechnungen an Molekülen äquivalent sind.

Introduction

Since Boys [1] first pointed out the computational advantages in using gaussian functions for *ab initio* molecular orbital calculations, there has been a steady increase in the use of these functions so that currently most *ab initio* calculations on large molecules have employed gaussian basis sets in preference to Slater type orbitals (e.g. [2]). However during this time of renewed interest in gaussian functions, many different gaussian basis sets have appeared in the literature with little attempt to compare their accuracy in molecular calculations [3].

In the course of an investigation on the use of small gaussian basis sets that will give the same accuracy as a minimal basis set of Slater type orbitals (STO's) with substantial gains in computation time [4], we have found it necessary to compare the use of gaussian lobe functions and cartesian gaussian functions (spherical gaussians) for molecular calculations.

During the preparation of the results to be reported here, a report by Shih *etal.* [5] appeared in which the accuracy of lobe and cartesian gaussian bases for atomic calculations was investigated. Our work is an extension of the comparison of lobe and cartesian gaussians to molecular calculations where we seek to judge the ability of these two *atomic* basis sets to describe the molecular environment.

In keeping with the trend of using calculated one-electron properties as a more sensitive indication of the accuracy of a wavefunction [6], we have calculated the total energy and relevant one electron properties for several polyatomic molecules. The implications of these results will be discussed.

Basis Sets

The lobe (LG) and cartesian gaussian (CG) functions both employ the same radial function $\exp(-\alpha r^2)$ but have different angular functions. The CG may be directly compared with Slater type atomic orbitals in that the atomic function is obtained by combining the radial part with the appropriate spherical harmonic $Y_{lm}(\theta, \varphi)$

$$\varphi_{lm}^{CG} = N_l r^l \exp(-\alpha r^2)\, Y_{lm}(\Theta, \varphi) \qquad (1)$$

where

$$N_l = 2^{n+1} [(2n-1)!!]^{-\frac{1}{2}} \quad (2\pi)^{-\frac{1}{4}} \alpha^{\frac{2n+1}{4}}$$

$$(2n-1)!! = 1.3. \ldots (2n-1).$$

The LG s-type function is of the same form as the s-type CG. The LG p-type function is obtained by placing pairs of s-type functions equidistant above and below the orbital centre [7]

$$\varphi_p^{LG} = N \{\exp[-\alpha(r-R^0)^2] - \exp[-\alpha(r+R^0)^2]\} \qquad (2)$$

where

R^0 = distance of the lobe from the orbital origin.

$$N = \left(\frac{2\alpha}{\pi}\right)^{\frac{3}{4}} \left|2 - 2\exp\left(\frac{-\alpha R^2}{2}\right)\right|^{\frac{1}{2}}.$$

R = distance between the two lobes.

It has been shown [5, 8] that on substituting $R^0 = \gamma\alpha^{-\frac{1}{2}}$, where γ is an arbitrary constant, into Eq. (2) and expanding the function in a Taylor series one obtains in the limit, as γ approaches zero, the same expression as the corresponding CG. Shih *et al.* have pointed out that one needs to balance the value of γ so that it is small enough to allow only the first term of the Taylor series to be important but large enough to allow the molecular integrals to be calculated accurately. We have used the value of $\gamma = 0.03$ suggested by Whitten [8] and also used by Shih *et al.* [5], to obtain the lobe positions for the p type LG functions.

In keeping with our desire to produce small gaussian sets of minimal basis Slater accuracy we have used basis sets consisting of a 1s function, a 2s function and three 2p functions for each first row atom. We have used the contracted sets produced by Stewart [9] and have employed the usual scaling technique [3 b] with exponents taken from Clementi and Raimondi [10]. As will be shown in a subsequent paper [4] we have found a five component 1s function, a three component 2s function, three component 2p functions for the heavy atoms, and a three component function for hydrogen, yield results which are very comparable with minimal basis Slater calculations [4, 11]. We will designate the heavy atom LG basis sets by [5, 3, 3] LG and the CG sets by [5, 3, 3] CG.

As the LG and CG basis sets chosen, only differ in their representation of the p-type function, one would expect molecular calculations involving these sets to highlight any deficiencies in the lobe representation.

Computer programs written by us were used for the LG and CG integral, SCF and one-electron property calculations. All programs have been thoroughly tested for speed and accuracy against other similar programs.

Results and Discussion

In an attempt to investigate the correspondence of the LG and CG basis sets in *all* regions of space, we have used the calculated wavefunctions to obtain one-electron properties that are sensitive to the region close to the nucleus (e.g. $\langle r^{-1}\rangle$, $\langle r^{-3}\rangle$), together with those that are more sensitive probes of the wavefunction away from the nucleus (e.g. $\langle r^2\rangle$). The total energy is also reported although this is known to be a rather insensitive criterion of the wavefunction accuracy.

Calculations have been performed on the following series of nine common closed shell small molecules:

$$H_2O,\ NH_3,\ HF,\ HCN,\ H_2CO,\ CO,\ NOF,\ OF_2,\ O_3.$$

The latter four nonhydrogen containing molecules have been included in an attempt to ascertain whether the hydrogen representation has any unusual effect on the performance of the basis sets under discussion.

We have calculated $\langle r\rangle$, $\langle r^2\rangle$, $\langle r^{-1}\rangle$, $\langle r^{-3}\rangle$, and the associated one-electron properties for each molecule using both basis sets and as the results show similar trends we felt it better to quote comparisons rather than actual values for each operator. We have therefore recorded in Table 1 maximum percentage difference and maximum absolute difference in each of the one electron properties, as calculated using the LG and CG basis sets, over the range of the nine molecules tested. The actual values of the one-electron properties calculated may be obtained from the authors. It should be noted that the values tabulated are the maximum differences found and in general the differences between the two basis sets were somewhat less than these tabulated values.

The total energies were found to differ in the 6th or 7th significant digit representing a maximum energy difference of 1 × 10^{-4}% which is quite insignificant

Table 1. Summary of the differences between LG basis and CG basis calculations

Property[b]	Maximum percentage difference	Maximum absolute difference
E total	0.001	0.0003 a.u.
ε_i	0.1	0.0003 a.u.
$\langle r\rangle$[a]	0.1	0.001 a.u.
μ		0.003 D.
$\langle r^{-1}\rangle$[a]	0.003	0.001 a.u.
σ^d av [c]		0.02 p.p.m.
$\langle r^{-3}\rangle$[a]	0.3	0.003 a.u.
eqQ[c]		0.005 M.Hz.
$\langle r^2\rangle$[a]	0.2	0.007 a.u.
χ^d_{av}[d]		0.006[e]

[a] Electronic contribution only.

[b] Origins: H_2O, NH_3, HF heavy atom;
NOF, OF_2, O_3 – central atom.

[c] Property calculated at N or O.

[d] Property calculated at the centre of mass.

[e] Units of 10^{-6} emu.mol^{-1}.

when one realizes that the basis sets employed here produce total energies which are some 0.5–0.6% from the Hartree-Fock limit. In looking at the actual integrals, it is found that generally the maximum difference in the one- and two-electron integrals is in the 4th or 5th significant digit with the LG values smaller. Hence it would seem that the self consistency procedure for obtaining the one electron orbital energies and total energy allows the differences in basic integral values to be partially averaged out.

For all molecules the individual orbital energies were found to differ by less than 0.1%.

Calculated values for $\langle z\rangle^e$ and dipole moment for each molecule also indicated that the difference between basis sets is small; the maximum relative difference in $\langle z\rangle$ being around 0.1% which corresponds to a maximum absolute difference of 0.003 *D* in the dipole moment. This small difference between basis sets is again quite insignificant when one notes the difficulty in calculating precise dipole moments even with large gaussian and STO basis sets.

We have also noted that these calculations mirror minimal basis Slater (MBS) calculations on dipole moment even to the poor dipole moment (c.f. experiment) for FNO and CO. This correspondence with MBS calculations will be reported in a future publication.

Because of the close similarity in total energy calculated with the basis sets, one would expect the electronic contributions to the potential at each atom to also be in close agreement. We found the difference in $\langle r^{-1}\rangle$ values occurred in the 5th or 6th significant figure with the LG values always the smaller.

Since the basis sets only differ in the representation of a *p* function, it would seem that near the nucleus, the LG *p* function is slightly inferior to the CG *p* function.

It was also noticeable that the absolute difference in the $\langle r^{-1}\rangle$ values at the heavy nuclei were greater than at hydrogen due presumably to the higher nuclear charge on the heavy atom accentuating any slight changes in the representation of the electron distribution.

The computed values of the electric field gradient tensor q (which is directly proportional to $\langle r^{-3}\rangle$) again show the difference between the basis sets is in the 4th or 5th significant figure. This corresponds to a maximum absolute difference of 0.003 a.u. in the field gradient and a maximum difference of 0.005 MHz in the calculated heavy atom nuclear quadrupole coupling constants.

As the field gradient has shown to be a sensitive probe of the electron density in the vicinity of the nucleus, the above small differences between the two basis sets would allow one to conclude that the representation around the nucleus is essentially the same with either type of *p* function.

Neumann and Moskowitz [6] have suggested, on the basis of accurate calculations on H_2O, H_2CO and CO, that the operator r^2 is a rather insensitive test of the accuracy of the wavefunction. However it does give a means of comparing the wavefunctions, from the two basis sets, in the region away from the nucleus.

Our results for $\langle r^2\rangle$ once again show the small difference in the two basis sets with the LG basis producing wavefunctions which are slightly more diffuse than those given by the CG basis. The relative differences in $\langle r^2\rangle$ values are less than

0.10% which is quite small in view of the fluctuations in calculated $\langle r^2 \rangle$ even with large basis sets [6]. This differences in $\langle r^2 \rangle$ would mean a difference of 0.006[1] in the average diamagnetic susceptibility χ^d_{av}.

Conclusion

We have shown that the differences in calculated molecular properties using (i) cartesian gaussians and (ii) gaussian lobe functions scaled to the cartesian gaussians (using the formula $R^0 = 0.03\,\alpha^{-\frac{1}{2}}$ where R^0 is the distance of the lobe from the nuclear centre and α is the gaussian exponent) as basis sets, are quite small. The basis sets used were of approximately minimal Slater accuracy and only differed in the representation of the p-type function. By surveying the regions close to the nucleus (with $\langle r^{-1} \rangle$ and $\langle r^{-3} \rangle$) and those further out (with $\langle r^2 \rangle$) we have shown that the two basis sets are essentially the same for molecular calculations.

It is our conclusion that the representation of a p orbital with a gaussian lobe function obtained using the above formula is, for molecular calculations, the same as that with the corresponding cartesian gaussian. We find, with our computer programs, calculations emplyoing LG basis sets are very slightly faster than those with CG basis sets.

References

1. Boys, S. F.: Proc. Roy. Soc. (London) A **200**, 542 (1950).
2. a) Buenker, R. J., Whitten, J. L., Petke, J. D.: J. chem. Physics **49**, 2261 (1968).
   b) Peyerimhoff, S. D., Buenker, R. J.: Theoret. chim. Acta (Berl.) **19**, 1 (1970).
   c) Demuynch, J., Veillard, A.: Chem. Physics Letters **6**, 204 (1970).
   d) Robin, M. B., Basch, H., Knebler, N. A., Wiberg, K. B., Ellison, G. B.: J. chem. Physics **51**, 45 (1969).
3. a) Dunning, T. H.: J. chem. Physics **53**, 2823 (1970).
   b) O-ohata, K., Taketa, H., Huzinaga, S.: J. physic. Soc. Japan **21**, 2306 (1966).
   c) Stewart, R. F.: J. chem. Physics **50**, 2485 (1969).
   d) Ditchfield, W., Hehre, W. J., Pople, J. A.: J. chem. Physics **52**, 5001 (1970).
4. Brown, R. D., Burden, F. R., Hart, B. T.: To be published.
5. Shih, S., Buenker, R. J., Peyerimhoff, S. D., Wirsam, B.: Theoret. chim. Acta (Berl.) **18**, 277 (1970).
6. a) Neumann, D. B., Moskowitz, J. W.: J. chem. Physics **49**, 2056 (1968).
   b) — — J. chem. Physics **50**, 2216 (1969).
   c) Aung, S., Pitzer, R. M., Chan, S. J.: J. chem. Physics **49**, 2071 (1968).
7. Whitten, J. L.: J. chem. Physics **44**, 359 (1966).
8. Petke, J. D., Whitten, J. L., Douglas, A. W.: J. chem. Physics **51**, 256 (1969).
9. Stewart, R. F.: J. chem. Physics **52**, 431 (1970).
10. Clementi, E., Raimondi, D. L.: J. chem. Physics **38**, 2686 (1963).
11. Klessinger, M.: Theoret. chim. Acta (Berl.) **15**, 353 (1969).

Prof. Dr. R. D. Brown
Department of Chemistry
Monash University
Clayton, Victoria, Australia 3168

---

[1] In units of 10^{-6} emu. mol^{-1}.

Theoret. chim. Acta (Berl.) 25, 54 --61 (1972)
© by Springer-Verlag 1972

Etude LCAO MO CNDO 2 de la structure électronique de composés du titane

F. Choplin et G. Kaufmann
Laboratoire de Chimie Minérale et Structurale - Groupe de Spectrochimie Moléculaire
2. rue Blaise Pascal, 67 Strasbourg, France

Reçu le 26 octobre 1971

A LCAO MO CNDO 2 Study of Titanium Complexes

The authors have studied the compounds $TiCl_4$ and $TiCl_4$, 2 HCN, using a modified GTO–CNDO 2 technique suitable for application to transition elements. The results concerning the bond length Ti–Cl and the order of molecular levels in $TiCl_4$ are in agreement with experimental values. A. Mulliken population analysis on $TiCl_4$, 2 HCN indicates that the Ti–N bond has practically pure σ character.

Les auteurs ont étudié les molécules $TiCl_4$ et $TiCl_4$, 2 HCN au moyen de la méthode GTO–CNDO 2 modifiée en vue de son application aux éléments de transition. Les résultats concernant la distance TiCl et l'ordre des niveaux moléculaires dans $TiCl_4$ sont en accord satisfaisant avec l'expérience. L'analyse de population sur le complexe $TiCl_4$, 2 HCN décrit la liaison TiN comme une liaison faible à caractère presque uniquement σ.

Die Moleküle $TiCl_4$ und $TiCl_4$, 2 HCN wurden mit Hilfe einer verbesserten "GTO–CNDO 2" Methode im Rahmen einer Anwendung auf die Übergangselemente untersucht. Die Ergebnisse in bezug auf den Ti–Cl-Bindungsabstand und das Orbitalschema in $TiCl_4$ sind in guter Übereinstimmung mit den experimentellen Werten. Die Mullikensche Populationsanalyse für $TiCl_4$, 2 HCN deutet auf eine relativ schwache Ti–N Bindung mit fast reinem σ-Charakter hin.

1. Introduction

La structure électronique des complexes d'éléments de transition est un domaine très étudié de la chimie de coordination. Actuellement, de nombreux calculs ont été déjà effectués, faisant appel soit à la théorie du champ des ligands, [1], soit à la théorie des orbitales moléculaires. A cause de la complexité et de la durée des calculs mis en oeuvre, celleci est le plus souvent appliquée sous forme approchée ou semi empirique, comme c'est le cas pour la méthode de Ballhausen et Gray [2], ou la méthode CNDO [6]. Un certain nombre d'études non empiriques ont été entreprises, sur des composés comme $CuCl_4^{2-}$ [3], MnO_4^- [4], $Ni(CN)_4^{2-}$ [5], mais elles sont encore limitées par des considérations pratiques. La methode CNDO 2, très utilisée pour les molécules faisant intervenir des éléments de la première et de la deuxième ligne [6], avait, jusqu'à présent, fourni des résultats peu encourageants pour des complexes de métaux de transition tels que $TiCl_4$ et VCl_4 [7, 8]. Sa modification récente par Allen et coll. [9], et son application à des complexes octaédriques du type XF_6^{4-} et X^{2+}, 6 H_2O [10, 11], a permis d'obtenir des résultats corrects concernant la géométrie, l'ordre des niveaux moléculaires et la définition de la covalence de ces molécules.

Le but de notre travail est de reprendre les approximations introduites par ces auteurs, et de les appliquer à l'étude de la structure électronique du tétrachlorure de titane et de son complexe avec l'acide cyanhydrique: $TiCl_4$, $2HCN$. La méthode est testée par rapport à $TiCl_4$, principalement en ce qui concerne la géométrie et l'ordre des orbitales moléculaires. Nous pouvons ainsi comparer les composés avant et après coordination, et proposer une interprétation qualitative de la nature des liaisons dans le complexe d'addition.

2. Partie théorique

Les équations classiques de la méthode CNDO2 [6] sont modifiées de façon à tenir compte de l'intervention, sur le métal de transition, de deux couches de valence ($3d$, et $4s-4p$) [9]. Dans notre travail, une modification supplémentaire intervient au niveau du choix des orbitales atomiques, et nous utilisons pour les décrire des combinaisons linéaires de fonctions gaussiennes. Celles correspondant au titane ($4s$, $3d$) sont tirées des travaux de Veillard et coll. [12], et les fonctions $4p$ (Ti) sont calculées à partir d'un critère de recouvrement maximum. Pour les autres atomes C, H, N, Cl, nous utilisons les bases données par Roos et coll. [13].

Par rapport aux travaux précédents [9–11], l'utilisation de fonctions gaussiennes permet de calculer explicitement les intégrales coulombiennes du type $\gamma 3d 3d$ (monocentriques) et $\gamma' 3d_A S_B$ (bicentrique) alors que dans les travaux précités ces quantités sont calculées à partir de la fonction $3s$ du métal central. Si cette dernière approximation est valable pour des métaux de transition riches en électrons d, il nous est apparu qu'elle ne pouvait convenir dans le cas du titane. Dans ce cas, en effet, le calcul SCF sur $TiCl_4$ diverge.

Les paramètres β_0 retenus pour le titane ont été optimisés de façon à obtenir une valeur de la distance TiCl la plus proche de la valeur expérimentale

$$\beta_0(3d) = 0.5374 \text{ u.a.} \qquad \beta_0(4s, 4p) = 0.318 \text{ u.a.}$$

Les paramètres β_0 pour les autres atomes sont tirés des travaux de Pople [6], de même que les potentiels d'ionisation I_μ et affinités électroniques A_μ. Pour le titane, ces quantités ont été calculées à partir des données spectroscopiques.

La convergence correcte des vecteurs propres étant difficile à obtenir, nous avons utilisé un procédé décrit par Chesnut et coll. [14]. Pour chaque cycle du processus SCF, on emploie une matrice densité $P^{(n)}$ définie par:

$$P^{(n)} = P^{(n-1)} + \delta(P^{(n')} - P^{(n-1)})$$

$P^{(n-1)}$ matrice densité entrant au $n^{\text{ième}}$ cycle,
$P^{(n')}$ matrice densité sortant du $n^{\text{ième}}$ cycle,
$P^{(n)}$ matrice densité entrant au $(n+1)^{\text{ième}}$ cycle,
δ facteur constant pris égal à 0.7.

Afin d'étudier les liaisons dans le complexe, nous avons procédé à une analyse de population selon Mulliken [15] sur les vecteurs propres C', obtenus par déorthogonalisation de la base [16]

$$C' = S^{-1/2} C .$$

C représente les vecteurs propres issus du calcul CNDO.

Tous les calculs ont été effectués sur le programme FORTRAN V SESOS 5 écrit par les auteurs pour ordinateurs IBM 360 et UNIVAC 1108 (Centre de Calcul de l'Institut de Mathématiques, et Centre de Recherches Nucléaires, Strasbourg).

3. Résultats et discussion

a) *Tétrachlorure de titane*

L'étude du tétrachlorure de titane a porté sur deux points: distance de liaison TiCl et ordre des niveaux moléculaires. La valeur expérimentale de cette distance est de 2.17 Å, et la valeur calculée est de 2.40 Å. La différence relative de 10% apparait acceptable, compte tenu des résultats précédemment obtenus par cette méthode pour des complexes octaédriques de métaux de transition [11].

Etant donné que la valeur de la distance TiCl dans le complexe $TiCl_4$, 2 HCN est de 2.22 Å, nous avons retenu la structure électronique obtenue pour $TiCl_4$ avec dTiCl = 2.17 Å, afin de permettre la comparaison entre les composés avant et après coordination. En effet, le nombre de paramètres intervenant dans une optimisation de géométrie du complexe est trop important pour permettre un calcul complet, et il serait alors aberrant de comparer les valeurs 2.22 et 2.40.

L'ordre des niveaux moléculaires ne varie pas lorsque la distance TiCl est comprise entre 2.0 et 2.30 Å (Fig. 1). Au dela de cette valeur, le dernier niveau occupé n'est plus un niveau t_1 mais un niveau t_2. Pour la distance obtenue à l'énergie minimale, l'ordre des niveaux occupés est:

$$a_1 < t_2 \ll a_1 < e < t_2 < t_1 < t_2 .$$

Pour la valeur dTiCl expérimentale (2.17 Å), l'ordre des niveaux avec leurs énergies (en u.a.) est le suivant:

$$1a_1 < 1t_2 \ll 2a_1\ (0.618) < 1e\ (-0.608) < 2t_2\ (-0.583) < 3t_2\ (-0.563) < 1t_1\ (-0.529) .$$

Cet ordre est à rapprocher de celui obtenu par étude du spectre photoélectronique de $TiCl_4$ [17]

$$e < a_1 < t_2 < t_2 < t_1 .$$

Les énergies correspondantes sont de −0.433 u.a. (t_1), −0.470 u.a., −0.486 u.a., −0.513 u.a. (a_1). On observe, comme il est courant dans le cadre des calculs CNDO [6, 18], une valeur absolue des énergies théoriques plus importante que celle des énergies expérimentales correspondantes. Cependant le rangement des niveaux est respecté, sauf en ce qui concerne une inversion e/a_1, mais avec une faible différence d'énergie entre ces deux niveaux (0.01 u.a.).

Si l'on compare ces résultats à ceux de Becker et coll. [7], on observe dans leur calcul une répartition de ces cinq niveaux entre −0.55 et −0.88 u.a., avec une énergie extrêmement basse pour l'orbitale $2t_2$, qui se retrouve très en dessous du niveau $2a_1$.

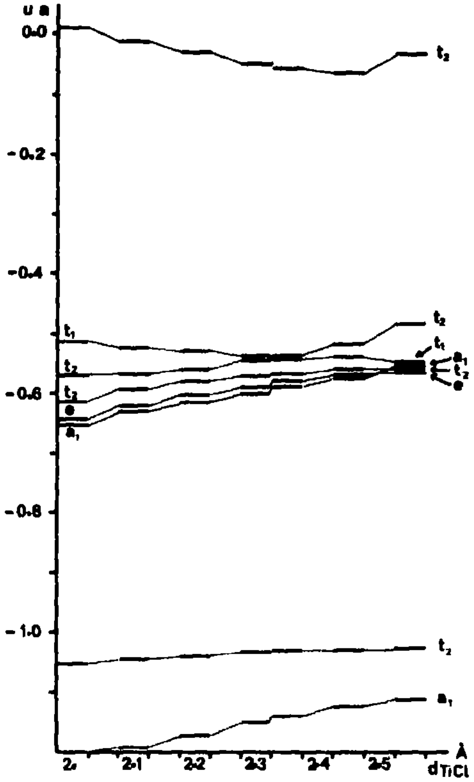

Fig. 1. Ordre des niveaux moléculaires dans $TiCl_4$

Pour la valeur 2.17 Å de la distance TiCl, l'ordre est:

$$1t_2 < 1a_1 < 2t_2 < 2a_1 < 1e < 3t_2 < t_1 .$$

Dans notre cas, nous obtenons une répartition des cinq orbitales étudiées dans un domaine d'énergies relativement restreint (−0.615 à −0.529), ce qui correspond bien au domaine expérimental (−0.513 à −0.433), compte tenu de l'abaissement des valeurs énergétiques, défaut intrinsèque de la méthode CNDO.

D'autre part, aucun des travaux précités ne fournit de valeur optimale pour la distance TiCl.

En ce qui concerne la structure électronique du tétrachlorure de titane, on observe une charge assez importante de 1.56 sur le titane, correspondant à un métal à un degré d'oxydation 4. En l'absence de déorthogonalisation, cette charge est de 1.27. Ce résultat est à rapprocher de celui obtenu par Clack et coll. [10] pour le complexe Ti^{III} 6 H_2O où la charge sur le titane est de 0.96. La population électronique 4*p* paraît cependant un peu forte, si on la compare à celle obtenue pour de nombreux complexes de métaux de transition. Il est possible que le critère de recouvrement maximum soit insuffisant pour déterminer la fonction 4*p*, ce qui peut entrainer des erreurs lors de la déorthogonalisation, puisque celle ci fait intervenir directement la matrice des intégrales de recouvrement.

b) *Complexe* $TiCl_4$, 2 HCN

Le complexe formé peut avoir deux structures: une forme *cis* (Fig. 2A) et une forme *trans* (Fig. 2B). Nous avons essayé de déterminer la structure la plus stable au moyen du calcul. Si on reporte sur le composé trans les longueurs de liaison données pour la forme *cis* [19], on obtient une différence d'énergie de 0.004 u.a. en faveur de la forme *cis* (110.614 contre 110.610 u.a.). Cette différence est insuffisante et peut être facilement inversée si l'on fait varier les paramètres géométriques du composé *trans*. Dans le cas du composé *cis*, nous avons envisagé une variation de l'angle θ (voir Fig. 2A), et l'énergie minimale est obtenue pour $\theta \simeq 40^\circ$ ($E = -110.640$ u.a.), mais là encore la différence $Ecis - Etrans$ est trop minime pour nous permettre de conclure. La valeur de l'angle θ diffère notablement de la valeur expérimentale (θ exp. $\simeq 13^\circ$) et correspond à une déformation assez faible du tétraèdre $TiCl_4$ lors de la coordination avec les molécules d'acide cyanhydrique. Cependant, le calcul que nous avons effectué ne tient pas compte des interactions intermoléculaires existant dans le cristal, et la valeur expérimentale ne peut pas servir exactement de référence.

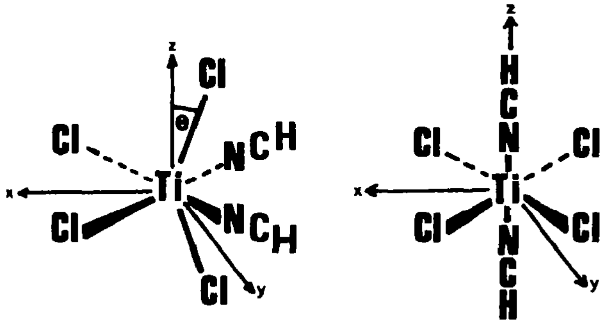

2A forme cis 2B forme trans

Fig. 2A et B. Structure du complexe $TiCl_4$, 2 HCN

L'analyse de population effectuée après déorthogonalisation montre les effets suivants (cf. Tableau 1): un transfert global de 0.10 *e* s'effectue du groupement HCN vers le titane. Ce transfert provient de tous les atomes puisque la charge positive sur le carbone augmente de 0.10 *e* et celle sur l'hydrogène de 0.04 *e*. On note une augmentation de la charge négative sur l'azote de 0.04 *e*. Au niveau de la liaison CN, la population électronique passe de 1.46 *e* (HCN libre) à 1.56 *e*, et ceci est à rapprocher de l'augmentation de la fréquence νCN dans le complexe [21], qui passe de 2097 cm^{-1} à 2134 cm^{-1}. Cette augmentation correspond à un transfert électronique $\sigma + \pi$ du carbone vers l'azote, avec prédominance de la population σ (le rapport σ/π (CN) passe de 0.63 dans HCN libre à 0.71 dans le complexe) [22, 23].

L'ensemble des électrons apportés par les deux molécules d'acide cyanhydrique se répartit uniformément sur le groupement $TiCl_4$. La charge négative augmente sur les atomes de chlore, et la population de la liaison TiCl diminue lorsqu'on

Tableau 1. Populations électroniques

		$TiCl_4$	HCN	$TiCl_4$ 2 HCN
Ti	*s*	0,31	—	0,21
	px	0,15	—	0,16
	py	0,15	—	0,14
	pz	0,15	—	0,26
	dx^2-y^2	0,17	—	0,12
	dxy	0,44	—	0,53
	dz^2	0,17	—	0,69
	dyz	0,44	—	0,14
	dxz	0,44	—	0,19
	q	1,56	—	1,56
Cl_1	*s*	1,97	—	1,99
	p	5,42	—	5,44
	q	−0,39	—	−0,43
Cl_2	*s*	1,97	—	1,99
	p	5,42	—	5,46
	q	−0,39	—	−0,45
N	*s*	—	1,80	1,75
	px	—	1,16	1,20
	py	—	1,16	1,19
	pz	—	1,06	1,08
	q	—	−0,18	−0,22
C	*s*	—	1,19	1,16
	px	—	0,87	0,85
	py	—	0,88	0,85
	pz	—	0,95	0,93
	q	—	0,11	0,21
H	*s*	—	0,93	0,89
	q	—	0,07	0,11

passe de $TiCl_4$ au complexe. Ce fait correspond à l'abaissement de la fréquence de vibration νTiCl, qui passe de 498 cm^{-1} (dans $TiCl_4$) à 330, 380 cm^{-1} (dans le complexe) [21].

La liaison TiN possède une population électronique faible de 0.112 *e*, contenant un pourcentage σ de 0.85, le reste étant constitué par un recouvrement $p_\pi p_\pi$. Ce schéma donne donc une liaison σ à peu près pure entre l'azote et le titane, liaison constituée par un transfert des électrons $2s$(N) et $2p\sigma$(N) vers le titane. Les faibles transferts électroniques mis en jeu indiquent une liaison faible, ne contenant pas de participation $d_\pi(\mathrm{Ti}) \rightarrow p_\pi(\mathrm{N})$, qui constitue un facteur de stabilisation dans de nombreux complexes d'éléments de transition. Ces conclusions rejoignent celles des études expérimentales effectuées sur le complexe qui décrivent ce dernier comme peu stable, partiellement décomposé en ses constituants à température ordinaire, et totalement dès 80° C [20].

Le modèle développé ici ne tenant pas compte des interactions dans le cristal, il ne peut mettre en évidence la liaison hydrogène entre H et un atome de chlore d'une molécule voisine. Cette interaction conduit à une diminution de la force

Tableau 2. *Populations de liaison et fréquences de vibration*

	HCN	$TiCl_4$ [21]	$TiCl_4$, 2 HCN [21]
νCN cm^{-1}	2097	—	2134
pop CN	1,466	—	1,562
νTiCl cm^{-1}		498,5	330, 380
pop TiCl	---	0,441	0,393/0,357
νTiN cm^{-1}	--	--	281
pop TiN	—	–	0,112
νCH cm^{-1}	3311	--	3173
pop CH	0,811	--	0,818

de liaison CH dans le complexe, alors que notre calcul montre un renforcement de celle-ci, par suite d'un transfert électronique des électrons de l'hydrogène vers le carbone.

4. Conclusion

A partir des approximations récentes introduites dans la méthode CNDO [9], en vue de son extension aux éléments de transition, nous avons étudié la molécule de tétrachlorure de titane et de son complexe avec l'acide cyanhydrique. Les résultats concernant $TiCl_4$ sont en accord satisfaisant avec l'expérience, compte tenu des erreurs que l'on peut attendre d'une telle méthode: en particulier, la distance de liaison TiCl est à 10% de la valeur expérimentale, mais l'ordre des niveaux moléculaires correspond à celui obtenu par étude du spectre photoélectronique de cette molécule. Le nombre de renseignements expérimentaux sur le complexe $TiCl_4$, 2 HCN est insuffisant pour permettre une vérification complète des fonctions d'onde obtenues pour ce composé. Cependant, l'étude des populations électroniques permet de confirmer un certain nombre de propriétés mises en évidence de manière qualitative. Comme dans le cas des complexes octaédriques, une étude extensive sur les complexes tétraédriques devrait permettre de confirmer les approximations introduites dans la méthode CNDO2 appliquée à de telles molécules.

Remerciements. Nous remercions Monsieur le Professeur Jeannin et Monsieur Constant de l'Université de Toulouse, pour avoir mis à notre disposition, avant publication, leurs résultats sur la structure cristalline du complexe $TiCl_4$, 2 HCN, et pour les discussions fructueuses à ce sujet.

Bibliographie

1. Davies, D. R., Webb, G. A.: Coord. chem. Rev. **6**, 95 (1971).
2. Ballhausen, C. J., Gray, H. B.: Molecular orbital theory. New York, Amsterdam: W. A. Benjamin 1965.
3. Demuynck, J., Veillard, A.: Chem. Physics Letters **6**, 204 (1970).
4. Hillier, I. H., Saunders, V. R.: Chem. Physics Letters **9**, 219 (1971).
5. Demuynck, J., Veillard, A., Vinot, G.: Chem. Physics Letters **10**, 522 (1971).
6. Pople, J. A., Segal, G. A.: J. chem. Physics **43**, 5136 (1965).
7. Becker, C. A. L., Ballhausen, C. J., Trajberg, I.: Theoret. chim. Acta (Berl.) **13**, 355 (1969).
   — Dahl, J. P.: Theoret. chim. Acta (Berl.) **14**, 26 (1969).

8. Dahl, J. P., Johansen, H.: Theoret. chim. Acta (Berl.) **11**, 26 (1968).
9. Allen, G. C., Clack, D. W.: J. chem. Soc. (London) (A) **1970**, 2668.
10. Clack, D. W., Farrimond, M. S.: J. chem. Soc. (London) (A) **1971**, 299.
11. Allen, G. C., Clack, D. W., Farrimond, M. S.: J. chem. Soc. (London) (A) **1971**, 2728.
12. Roos, B., Veillard, A., Vinot, G.: Theoret. chim. Acta (Berl.) **20**, 1 (1971).
13. — Siegbahn, P.: Theoret. chim. Acta (Berl.) **17**, 209 (1970).
14. Chesnut, D. B., Wormer, P. E. S.: Theoret. chim. Acta (Berl.) **20**, 250 (1971).
15. Mulliken, R. S.: J. chem. Physics **23**, 1833 (1955).
16. Löwdin, P. O.: J. chem. Physics **18**, 365 (1950).
17. Cox, P. A., Evans, S., Hamnett, A., Orchard, A. F.: Chem. Physics Letters **7**, 414 (1970).
18. Absar, I., van Wazer, J. R.: J. physic. Chem. **75**, 1360 (1971).
19. Constant, G. C., Jeannin, Y.: Acta crystallogr. (à paraître).
20. — — Communication privée.
21. Kawai, K., Kanesaka, I.: Spectrochim. Acta **25** A, 1265 (1969).
22. Reedijk, J., Zuur, A. P., Groeneveld, W. L.: Rec. Trav. Chim. Pays Bas **86**, 1127 (1967).
23. Purcell, K. F.: J. Amer. chem. Soc. **89**, 247 (1967).

Dr. F. Choplin
Laboratoire de Chimie Minérale et Structurale
Groupe de Spectrochimie Moléculaire
2, rue Blaise Pascal
F-67 Strasbourg, France

Theoret. chim. Acta (Berl.) 25, 62–82 (1972)
© by Springer-Verlag 1972

Porphyrins XXV. Extended Hückel Calculations on Location and Spectral Effects of Free Base Protons*

A. M. SCHAFFER** and M. GOUTERMAN

Department of Chemistry, University of Washington, Seattle, Washington 98105

Received June 14, 1971

Extended Hückel calculations for the free bases of porphin, phthalocyanine, tetrabenzporphin, and tetrazaporphin show: (i) A marked effect of carbon-nitrogen skeletal distortions is expected on the Q_x–Q_y (i.e. visible) band splitting that may account for observed environment effects; (ii) bridged structures will show very little splitting without either incipient bond formation between central hydrogen and bridge nitrogen or considerable skeletal distortion; (iii) while solution phthalocyanine may be bridged, the vapor is not; (iv) $n-\pi^*$ transitions introduced by the bridge aza nitrogens may be the cause of Soret band broadening of phthalocyanine and tetrazaporphin. Band polarizations with respect to the skeleton are discussed.

Rechnungen mit der erweiterten Hückeltheorie für die freien Basen von Porphin, Phthalocyanin, Tetrabenzporphin und Tetrazaporphin zeigen, 1. daß eine Verzerrung des C–N-Gerüstes einen deutlichen Effekt auf die Aufspaltung des Q_x–Q_y-Bandes zeitigen sollte, 2. daß verbrückte Strukturen kaum eine Aufspaltung hervorbringen sollten wenn nicht beginnende Bindungsbildung zwischen den zentralen Wasserstoff- und den Brücken-Stickstoffatomen oder beträchtliche Verzerrungen des Gerüstes vorliegen, 3. daß Phthalocyanin vielleicht in flüssigem Zustand verbrückt ist, dagegen im gasförmigen nicht und 4. daß $n\pi^*$-Übergänge, die von den Brücken-Azastickstoffatomen induziert werden, die Ursache der Soret-Bandenverbreiterung von Phthalocyanin und Tetrazaporphin sein können. Schließlich werden Bandpolarisierungen bezüglich des C–N-Gerüstes diskutiert.

Des calculs de Hückel Etendu pour les bases libres de la porphine, de la phtalocyanine, de la tétrabenzoporphine et de la tétraazaporphine montrent que:

1) un effet marqué des distorsions du squelette carbone-azote est à attendre sur la séparation de la bande $Q_x - Q_y$ (c'est-à-dire visible), ce qui peut rendre compte des effets d'environnement observés.

2) les structures pontées présenteront peu de séparation s'il n'y a pas soit formation d'un début de liaison entre l'hydrogène central et l'azote du pont soit une distorsion considérable du squelette.

3) alors que la phtalocyanine en solution peut être pontée, elle ne l'est pas en phase vapeur.

4) les transitions $\pi \rightarrow \pi^*$ introduites par les azotes aza du pont peuvent être la cause de l'élargissement de la bande de Soret de la phtalocyanine et de la tétraazaporphine.

On discute les polarisations des bandes par rapport au squelette.

Background

Square planar porphyrins and related square planar compounds such as phthalocyanine (Pc), tetrabenzporphin (TBP), and tetrazaporphin (TAP) show an electronic absorption in the visible (Q band) and another in the near uv (B or Soret band). It has long been known that replacement of the metal by two hydrogens, which reduces the symmetry from D_{4h} to D_{2h}, splits these bands into four components Q_x, Q_y, B_x, B_y [1]. The splitting is quite different for the Q and B regions; it varies very greatly among the four skeletons listed; and for the Q band of H_2Pc (free base phthalocyanine), it differs considerably between solution and vapor phase [1, 2].

---

* Submitted by A.M.S. in partial fulfillment of the requirement for the Ph. D. degree granted by the Department of Chemistry, University of Washington.

** Present address: see end of paper.

The location of the free base protons has been the subject of long debate. Proposed structures are: (i) two pyrrole and two aza groups, which we shall refer to as *bonded*; (ii) shared protons, which we shall refer to a *bridged*; (iii) hydrogen bonded models somewhere between. Finally we note that x-ray work has shown that there can be substantial D_{2h} skeletal distortion in the free base. The purpose of this paper is to use the extended Hückel (EH) model to explore the effect of proton location and skeletal distortion on the free base spectrum.

Various theoretical studies of the free base problem have been undertaken using the self-consistent molecular orbital Pariser-Parr-Pople (SCMO–PPP) method [3, 4]. The more recent studies [3b, 4] correctly predict the magnitude of the Q_x, Q_y splitting in free base porphin (H_2P) and indicate a wider B_x, B_y splitting than was believed earlier [1]. Simple Hückel calculations have been made on phthalocyanine [5], and using this model Chen [6] explicitly considered the effect of bonded and bridged protons on the phthalocyanine spectrum. He concluded that the protons were bridged. However, we believe that Chen chose somewhat arbitrarily the α and β values for the bridged case. This paper draws its inspiration from Chen's work. But here we use the extended Hückel model to study the problem. Moreover, as we shall see, we find that small D_{2h} skeletal distortions can have effects on $Q_x - Q_y$ splitting comparable to the bridged hydrogens.

Finally we note that there is considerable experimental interest in the H_2Pc crystal primarily because of its photoconductivity both in the ir and visible regions [7, 8]. Consequently, attempts have been made to calculate the band structure of this crystal [9, 10] in order to test the theories of production of charge carriers and their mode of transport. However, a knowledge of the molecular wavefunction is required to calculate the band structure of the excess electrons and holes. Sukigara and Nelson [9] used a PPP wavefunction of bonded H_2Pc while Chen [10] has used his Hückel wavefunction for the bridged model of H_2Pc. As we shall show, our extended Hückel calculations provide some important cautions for crystal calculations.

Although Hückel and extended Hückel models have been used to calculate spectra [6, 11], there is an intrinsic difficulty with a one electron model. It is long known [1] that the Q and B states of porphyrins are not single electron transitions but are based on the transitions $a_{2u}(\pi) \rightarrow e_g(\pi^*)$ and $a_{1u}(\pi) \rightarrow e_g(\pi^*)$ heavily mixed together by two electron terms. This mixing decreases in the order $H_2P > H_2TAP \sim H_2TBP > H_2Pc$, where the Q bands are reasonably closer to purer one electron transitions. Yet we shall ignore two electron terms and interpret the $Q_x - Q_y$ splitting simply in terms of the energy gap between $b_{2g}(\pi^*)$ and $b_{3g}(\pi^*)$ [the labels for the two $e_g(\pi^*)$ orbitals in D_{2h} symmetry]. Now we might note that the EH model does not always predict the energy gap between the top filled orbitals $b_{1u}(\pi)$ and $a_u(\pi)$ [D_{2h} labels] in accord with more exact SCMO–PPP calculations or with deduction from experiment. However, we believe that calculations of the splitting of $e_g(\pi^*)$ by D_{2h} distortion will be more successful since symmetry forces the $e_g(\pi^*)$ orbitals to be degenerate in the metal case; thus, all we ask from the EH model is to correctly predict the effect of the D_{2h} perturbation.

While the EH model may be expected to be qualitatively correct, detailed quantitative agreement is not to be expected. However, our aim here is to throw some new light on the extensive spectral and crystallographic studies that have been done on free base systems. Moreover we are encouraged by the fact that EH calculations used judiciously have in the past made fairly accurate predictions about molecular geometry of porphyrin systems [12].

The EH program used for most of these calculations has been previously described [11].

Free Base Porphin

The crystal structures of free base porphyrins have been extensively studied. We did calculations based on three sets of x-ray coordinates: Coordinates I are D_{4h}, based on tetragonal H_2TPP (free base tetraphenyl porphin) determined by Hamor, Hamor, and Hoard [13]; coordinates II are D_{4h}, based on H_2P (free base porphin) of Webb and Fleischer [14]; coordinates V are D_{2h} based on triclinic H_2TPP studied by Silvers and Tulinsky [15]. (The D_{2h} and D_{4h} labels refer to the carbon-nitrogen skeleton.) The crystal symmetry of these molecules requires tetragonal H_2TPP to have four equivalent pyrrole rings, triclinic H_2TPP to have a center of inversion, while H_2P has no required molecular symmetry. Recent work by Chen and Tulinsky [16] indicates that H_2P may be closer to the D_{2h} structure of triclinic H_2TPP than to the D_{4h} structure earlier reported [14]. As a result we have calculated two structures closely related to II: coordinates III were obtained from II by moving the pyrrole nitrogens farther from the center and the aza nitrogens closer; coordinates IV were obtained with the reverse distortion. Case III corresponds to the type of distortion found for H_2TPP [15] and indicated for H_2P [16].

It is clear from the evidence in all studies that the central H atoms are localized on a diagonally opposed pair of N atoms with a bond distance in the range 0.90 to 0.95 Å. Fig. 1 gives a generalized atom numbering scheme for D_{4h} skeletons and skeletons with D_{2h} distortions which have planes of symmetry passing through the central nitrogens. The numbers 1 and 8 can be either H or C atoms depending on the molecule. Likewise atom number 5 can be either C or N, while atom 4 does not occur in the aza molecules. The planar porphin coordinates found for the three different crystal structures are presented in Table 1. Since the N-H bond distance is the least accurately determined, a range of values to reasonable changes of the N-H distance. For a given set of coordinates, changing the N_9–H_{20} bond distance by 0.05 Å does not reverse the order of the top filled and lowest empty MO's and does not change the energy of any MO by more than 0.015 eV.

An MO energy level diagram for free base porphin with coordinates I, II, and V is given in Fig. 2. To illustrate the effect of the central hydrogens, the energy level pattern of Zn porphin [11] is also included. Comparison with ZnP shows that the four orbitals responsible for the visible and near uv absorption intensity

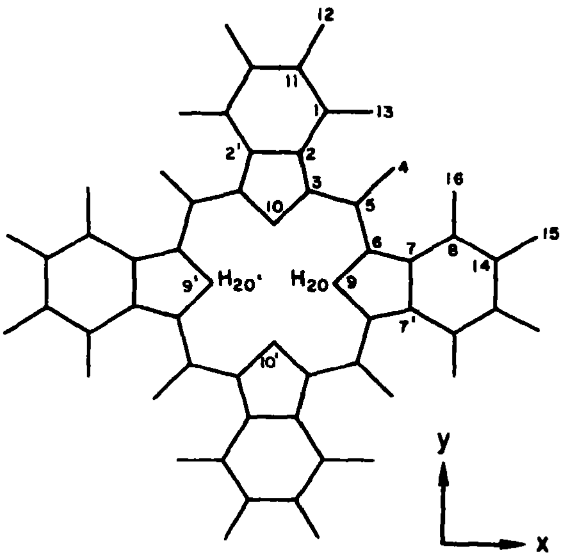

Fig. 1. Skeletal numbering for D_{4h} calculations and D_{2h} distortions preserving x, y symmetry axes

Table 1. Coordinates (x, y) for various Fig. 1 skeletons in Å

Atom	$\mathrm{I}(D_{4h})$[a]		$\mathrm{II}(D_{4h})$[b]		$\mathrm{V}(D_{2h})$[c]		$\mathrm{VI}(D_{4h})$[d]		$\mathrm{XIII}(D_{4h})$[e]		$\mathrm{XVIII}(D_{4h})$[f]	
	x	y	x	y	x	y	x	y	x	y	x	y
1 (H, C)	1.325	5.084	1.309	5.104	1.317	5.111	1.390	5.335	1.394	5.429	1.445	4.888
2 (C)	0.681	4.217	0.671	4.233	0.674	4.244	0.695	4.131	0.695	4.219	0.681	4.120
3 (C)	1.098	2.839	1.104	2.858	1.092	2.849	1.098	2.692	1.098	2.839	1.085	2.692
4 (H_5)	3.208	3.208	3.184	3.184	3.176	3.218			3.208	3.208		
5 (C, N)	2.444	2.444	2.420	2.420	2.430	2.440	2.387	2.387	2.444	2.444	2.387	2.387
6 (C)	2.839	1.098	2.858	1.104	2.897	1.121	2.692	1.085	2.839	1.098	2.692	1.085
7 (C)	4.217	0.681	4.233	0.671	4.254	0.678	4.131	0.695	4.219	0.695	4.120	0.681
8 (H, C)	5.084	1.325	5.104	1.309	5.180	1.233	5.334	1.390	5.429	1.394	4.888	1.445
9 (N)	2.054	0.000	2.053	0.000	2.100	0.000	1.910	0.000	2.054	0.000	1.910	0.000
10 (N)	0.000	2.054	0.000	2.053	0.000	2.030	0.000	1.910	0.000	2.051	0.000	1.910
11 (C)							0.695	6.539	0.695	6.639		
12 (H)							1.235	7.474	1.237	7.578		
13 (H)							2.470	5.335	2.478	5.429		
14 (C)							6.539	0.695	6.639	0.695		
15 (H)							7.474	1.235	7.578	1.237		
16 (H)							5.335	2.470	5.429	2.478		
20 (H)	1.104	0.000	1.103	0.000	1.150	0.000	0.960	0.000	1.104	0.000	0.910	0.000

[a] Tetragonal H_2TPP [13]. The D_{4h} label refers to symmetry of carbon-nitrogen skeleton.
[b] H_2P [14].
[c] Triclinic H_2TPP [15].
[d] H_2Pc, average of Robertson's D_{2h} coordinates [21].
[e] H_2TBP, derived from coordinates I.
[f] H_2TAP, derived from coordinates VI.

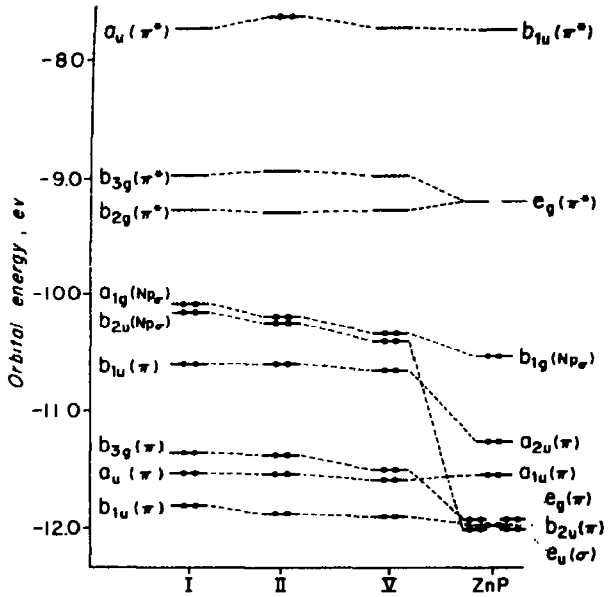

Fig. 2. Top filled and lowest empty MO's of H_2P and ZnP. For full geometry see Table 1

changes as follows: One $e_g(\pi^*)$ of ZnP rises in energy while the energy of the other goes down a bit; $a_{2u}(\pi)$ rises in energy while the energy of $a_{1u}(\pi)$ stays fixed. The energy splitting of the orbitals $b_{2g}(\pi^*)$ and $b_{3g}(\pi^*)$ is that expected by perturbation theory: $b_{2g}(\pi^*)$, which has non-zero coefficients on the pyrrole nitrogens, is at lower energy than is $b_{3g}(\pi^*)$, which has non-zero coefficients on the aza nitrogens. That $a_{1u}(\pi)$ is unaffected is also expected, since it has zero coefficient on all central nitrogens. However the shift of $a_{2u}(\pi)$ to higher energy is not necessarily expected. It also occurs in SCMO–PPP calculations, when free base is compared to metalloporphin [3].

The energy level diagram also indicates the presence of two low lying $n \rightarrow \pi^*$ transitions, including the symmetry allowed $b_{3u}(\sigma) \rightarrow b_{2g}(\pi^*)$. Although these are predicted to be in the near ir, our EH calculations generally underestimate the energy of charge transfer transitions [17]. Consequently, the allowed $n \rightarrow \pi^*$ transition may appear in the Soret region and be obscured by stronger $\pi \rightarrow \pi^*$ bands, a possibility suggested by Sundbom [4] on the basis of theoretical work and by Antenson [18] who, on the basis of the sharpness of Q_x at low temperature, concluded that Q_x is the lowest singlet state.

Although it is reasonably clear that the H atoms in free base porphyrins are bonded, EH calculations on the bridged model are useful for comparison purposes. The N–H bond distance was varied from 1.45 to 1.53 Å. In this configuration there are four equivalent N atoms and the D_{2h} perturbation due to H atoms is much less severe. The π electron system is essentially D_{4h}; therefore, it is not surprising that the splitting of the lowest empty $e_g(\pi^*)$ orbitals is only about 16 cm^{-1}.

Table 2. Calculated and experimental values of Q_x, Q_y and Δ for free base porphins

Coordinates[a]	Q_x (cm^{-1})	Q_y (cm^{-1})	Δ[b] (cm^{-1})
I (D_{4h}, H_2TPP)	11190	13580	2390
II (D_{4h}, H_2P)	10520	13190	2660
III (D_{2h}, H_2P)[c]	10400	12790	2390
IV (D_{2h}, H_2P)[d]	10630	13560	2930
V (D_{2h}, H_2TPP)	11110	12790	1680
H_2P (vapor, 393° C)	15930[e]	19550	3610
H_2P (benzene, 25° C)	16200	19200	3000
H_2TPP (vapor, 448° C)	15060	18310	3250
H_2TPP (oil, 304° C)	15200	18100	2900
H_2TPP (oil, 30° C)	15400	18320	2830
H_2TPP (benzene, 25° C)	15380	18250	2860

[a] See Table 1 for full geometry.

[b] The calculated value is the $b_{3g}(\pi^*) - b_{2g}(\pi^*)$ energy gap while the experimental value is the $Q_x - Q_y$ splitting.

[c] Identical to II except with N(9): $x = 2.083$, $y = 0$ and N(10): $x = 0$, $y = 2.023$.

[d] Identical to II except with N(9): $x = 2.023$, $y = 0$ and N(10): $x = 0$, $y = 2.083$.

[e] All experimental values from Ref. [19].

Because of the contribution of two electron terms, it is naive to interpret the experimental splitting of the Q_x and Q_y bands in terms of the energy difference Δ between the empty orbitals $b_{2g}(\pi^*)$ and $b_{3g}(\pi^*)$. Nonetheless since the observed splitting and calculated Δ both arise from the lifting of the D_{4h} degeneracy, we believe they should be qualitatively correlated. Thus when the bridged model gives $\Delta = 16$ cm^{-1}, as just mentioned, we believe that a splitting of this order of magnitude would be expected for a real molecule with this structure.

Table 2 gives calculated transition energies $b_{1u}(\pi) \rightarrow b_{2g}(\pi^*)$, $b_{3g}(\pi^*)$ for several skeletal geometries, the splitting values Δ, and the experimental values [19]. The calculated Δ values are comparable to experimental. There are marked changes of calculated Δ with changes in the carbon-nitrogen skeleton. Experimentally Δ changes with substituents, with temperature, and in going from solution to vapor. We believe that some of the effect of substituent and all of the effect of temperature and phase change should be attributed to changes in the carbon-nitrogen skeleton.

Although we are confident that observed changes in $Q_x - Q_y$ splitting can be related to changes in the carbon-nitrogen skeleton, because of the crudity of the model, the relation of particular geometries to particular experimental conditions is on less firm ground. We note that calculated values of Δ are higher using H_2P rather than H_2TPP geometry, consistent with experiment. Chen and Tulinsky's [16] recent work on H_2P indicates that the pyrrole nitrogens are separated by a greater distance than the aza nitrogens. This result plus chemical intuition suggests that the change in $Q_x - Q_y$ splitting that occurs in going from solution to vapor is due to a change such as from coordinates III to coordinates II. That is, in solution the carbon-nitrogen skeleton is D_{2h} with pyrrole nitrogens moved farther from the center and aza nitrogens moved closer. However in vapor, we propose that thermal motion causes the free base porphyrin to take on a more geometrically symmetrical configuration.

Other spectral correlations might be mentioned. The low energy transition $b_{1u}(\pi) \rightarrow b_{2g}(\pi^*)$ is predicted to be polarized along the x axis; consequently, the Q_x band should be polarized along the proton axis. This agrees with the results from the polarization reflection studies of Anex and Umans [20]. It is also interesting to note that the EH model correctly predicts the Q_y band to be more intense than the Q_x band. This result is a consequence of the fact that both $b_{1u}(\pi)$ and $b_{3g}(\pi^*)$ are strongly localized on N_{10}.

Free Base Phthalocyanine

In a classical two-dimensional analysis Robertson [21] determined the x-ray structure of free base phthalocyanine. Although the experimental uncertainty of ± 0.03 Å is large by today's standards, the carbon-nitrogen skeleton is most likely D_{2h}. Robertson, however, did not directly observe the inner protons. There are two possible bonding schemes for these H atoms. They can be bonded directly to two of the four nitrogen atoms, or each hydrogen can be shared by two neighboring nitrogens.

The position of the central hydrogens is still a matter of some controversy. Both proponents of the bridged and bonded model have used experimental evidence to buttress their conclusions. Fleischer [22] has performed a refinement on Robertson's original data and has concluded that the hydrogens are in a bridged position. This view is supported by Berezin [23] who proposed a model in which the internally dissociated protons are shared by six nitrogen atoms. Sharp and Landon [24] also used the bridged H model to characterize the spectroscopic properties of a new polymorph of H_2Pc. From a neutron diffraction study of H_2Pc, however, Hoskins, Mason, and White [25] have found evidence of four half-hydrogens which lie very nearly on a line which join centrosymmetrically related pyrrole nitrogen atoms. Gurinovich [26], studying the N H stretching frequency in a variety of porphyrin type compounds, found that as the molecule becomes more complicated the value of ν(N–H) decreases. This suggested to him that the shift of ν(N–H) of H_2Pc relative to H_2P is not due to intramolecular H bonding. Although Hoskins *et al.* make a compelling argument for the bonded model in H_2Pc crystals, there is no reason to believe that the H atom position is the same in solution, vapor, and crystal. Thus, calculations were performed for both bonded and bridged models.

a) Bonded Model

The coordinates for the bonded model are given in Table 1 using the numbering of Fig. 1: coordinates VI are a D_{4h} average of the D_{2h} values obtained by Robertson. Coordinates VII and VIII were obtained from VI by moving the pyrrole nitrogen atoms farther apart by 0.02 Å (VII) and 0.05 Å (VIII). The aza nitrogens were moved closer together by the same amount for each case. The NH bond distance was set at 0.95 Å, and variation of this value over ± 0.05 Å had little effect on the result.

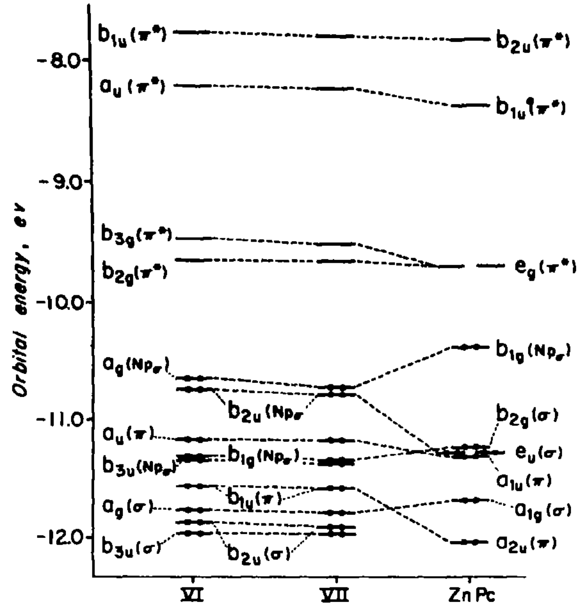

Fig. 3. Top filled and lowest empty MO's of bonded H_2Pc and ZnPc. For full geometry see Table 1

An MO energy level diagram for H_2Pc with coordinates VI and VII is given in Fig. 3 along with ZnPc [17b]. Comparison with ZnPc shows that free base formation affects the four orbitals responsible for the visible and near uv absorption intensity in a very similar manner as in porphin, Fig. 2: The orbital $b_{3g}(\pi^*)$, with non-zero coefficients on the aza nitrogens, is at higher energy than $b_{2g}(\pi^*)$ with non-zero coefficients on the pyrrole nitrogens. Also the orbital $a_{2u}(\pi)$ in ZnPc rises strongly in energy while $a_{1u}(\pi)$ only rises slightly. The latter, as in porphin, has nodes at the central nitrogen atoms.

One important difference between ZnP and ZnPc, as shown by SCMO-PPP calculations, is that in ZnP the top filled orbitals $a_{1u}(\pi)$ are very close in energy while in ZnPc $a_{2u}(\pi)$ is far lower in energy than $a_{1u}(\pi)$. In ZnPc the Q bands are basically one electron transitions $a_{1u}(\pi) \to e_g(\pi^*)$. Although free base formation causes $a_{2u}(\pi)$ to rise in energy relative to ZnPc, we believe that in H_2Pc the Q bands will still be due to transitions $a_u(\pi) \to b_{2g}(\pi^*)$, $b_{3g}(\pi^*)$. In this case the lower energy Q_x band will be polarized perpendicular to the H–H axis while in H_2P it is polarized parallel to the H- H axis[1,2].

Table 3 gives the calculated values of Q_x and Δ for coordinates VI, VII, and VIII plus the corresponding experimental results [2]. The transition energies of

---

[1] In this paper we follow the general convention that refers to the lower energy Q band as Q_x and upper one Q_y, without implying an absolute orientation. The reader should note in each case the polarization predicted. (We note that in chlorophyll the reduced ring is conventionally placed on the x axis forcing the protons on the y axis and making the lower energy band y polarized. For this reason it is generally called Q_y.)

[2] *Note Added in Proof:* Recent PPP calculations by M. Sundborn (Ph. D. Thesis) predict the lower energy Q_x band is polarized parallel the H–H axis, contrary to what the extended Hückel calculations suggest.

Table 3. Calculated and experimental values of Q_x, Δ, and the polarization for various geometries of free base phthalocyanine

Geometry[a]	Coordinates H_{20} (x, y)	Q_x (cm^{-1})	Δ (cm^{-1})	Polarization[b]
VI	0.960, 0.000	12310	1440	y
VII[c]	0.970, 0.000	12430	1270	y
VIII[d]	0.985, 0.000	12560	1120	y
IX	1.081, 0.000	13090	−17	x(L)
IX	1.910, 0.000	13460	88	y(M)
IX	2.110, 0.000	13280	374	y(M)
IX	2.426, 0.000	13090	761	y(M)
X	1.380, 0.000	13100	72	M
X	2.030, 0.000	13300	335	M
X	2.210, 0.000	13160	612	M
X	0.000, 1.325	12990	242	M
XI	1.830, 0.000	13340	480	M
XI	1.977, 0.000	13150	632	M
XII	1.030, 0.000	12690	577	M
XII	1.830, 0.000	13090	582	M
XII	2.030, 0.000	13020	819	M
XII	2.21, 0.000	12880	1120	M
XII	0.000, 1.775	13260	617	M
XII	0.000, 2.110	13370	197	M
H_2Pc in CLNP Ref. [43]		14330	730	
H_2Pc vapor Ref. [2a]		14580	1490	

[a] Full geometry given in Tables 1 and 4.

[b] Polarization of lowest energy Q band given with respect to axes, Figs. 1 and 4; x(L) refers to bridged structure with D_{4h} carbon-nitrogen skeleton.

[c] Identical to VI (bonded H_2Pc) except N_9: $x = 1.92$, $y = 0$; N_{10}: $x = 0$, $y = 1.90$.

[d] Identical to VI except N_9: $x = 1.935$, $y = 0$; N_{10}: $x = 0$, $y = 1.885$.

the EH model should more properly be compared to the average of the excited singlet and triplet energies than to the excited singlets alone. Although phosphorescence of H_2Pc has not been observed, results for metal phthalocyanines [27] indicate that the triplet should be in the region 9000 to 10000 cm^{-1}. When this is averaged in with the observed singlet, the result agrees reasonably well with the EH transition energy. The difference in energy Δ between $b_{2g}(\pi^*)$ and $b_{3g}(\pi^*)$ corresponds quite well to the energy gap between Q_x and Q_y observed in vapor but tends to be larger than the gap observed in solution, as shown in Table 3.

b) Bridged Model

The coordinates of the bridged model are given in Table 4 using the numbering of Fig. 4. The following coordinates were used: Coordinates IX form the same D_{4h} carbon-nitrogen skeleton as VI; coordinates X are the D_{2h} carbon-nitrogen coordinates reported by Robertson [21]; coordinates XI and XII are slight variants of X with bond lengths and angles within Robertson's experimental error. Unlike the bonded model, the proper distance of the central hydrogens from the nitrogens is not apparent. Moreover in the D_{2h} model the distance

Table 4. Coordinates (L, M) for various Fig. 4 skeletons in Å

Atom	IX (D_{4h})[a]		X (D_{2h})[b]		XI (D_{2h})[c]		XII (D_{2h})[c]		XX (D_{2h})[d]	
	L	M	L	M	L	M	L	M	L	M
1 (H, C)	2.789	4.755	2.75	4.77	2.726	4.772	2.726	4.772	2.595	4.496
2 (C)	2.429	3.412	2.41	3.42	2.404	3.422	2.390	3.422	2.415	3.419
3 (C)	1.136	2.671	1.145	2.64	1.141	2.642	1.136	2.642	1.145	2.640
5 (C, N)	0.000	3.376	0.000	3.32	0.000	3.32	0.000	3.316	0.000	3.320
6 (C)	2.671	1.136	2.71	1.13	2.704	1.139	2.704	1.139	2.710	1.130
7 (C)	3.412	2.429	3.405	2.45	3.405	2.458	3.390	2.458	3.386	2.458
8 (H, C)	4.755	2.789	4.73	2.84	4.745	2.840	4.745	2.840	4.448	2.671
9 (N)	1.351	1.351	1.38	1.325	1.380	1.325	1.380	1.325	1.380	1.325
10 (C, N)	3.376	0.000	3.43	0.000	3.430	0.000	3.430	0.000	3.430	0.000
12 (H)	2.026	5.519	1.974	5.52	1.950	5.520	1.950	5.520		
13 (C)	4.132	5.115	4.08	5.17	4.081	5.154	4.081	5.154		
14 (H)	4.412	6.158	4.341	6.217	4.342	6.201	4.342	6.201		
15 (C)	5.115	4.132	5.07	4.20	5.081	4.190	5.081	4.190		
16 (H)	6.158	4.412	6.117	4.498	6.128	4.488	6.128	4.488		
17 (H)	5.519	2.026	5.506	2.09	5.521	2.090	5.521	2.090		
20 (H)	0.68–2.426	0.000	0.68–2.21	0.000	1.03–1.975	0.000	0.53–2.21	0.000	1.830	0.000

[a] H_2Pc, D_{4h} average of [21], a rotation of coordinates VI.

[b] H_2Pc, Ref. [21].

[c] H_2Pc, slight distortion of coordinates X.

[d] H_2TAP, derived from coordinates X.

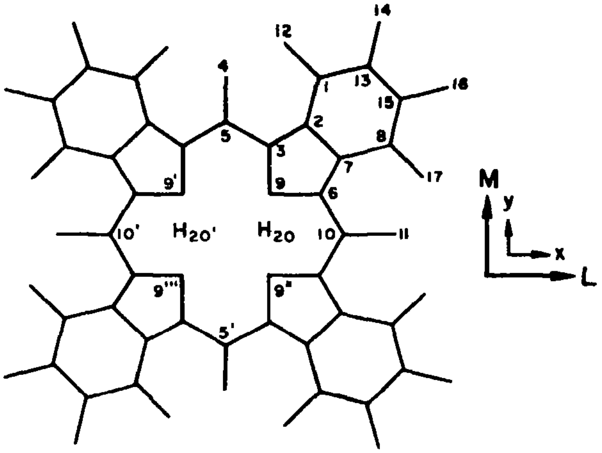

Fig. 4 Skeletal numbering for bridged models and D_{2h} distortions preserving L, M symmetry axes. For D_{2h} distortion, Robertson [21] found the N_9 $N_{9'}$ distance to be 2.76 Å and the N_9 $N_{9''}$ distance to be 2.65 Å

between N_9 and $N_{9'}$ is 2.76 Å while the N_9 $N_{9''}$ distance is 2.65 Å. It is not clear whether the H atoms belong on the M axis between N_9–$N_{9'}$ or on the L axis between N_9–$N_{9''}$. Accordingly we varied the distance of the hydrogens from the center, and in the D_{2h} geometry the axis upon which they were placed.

Table 3 gives the energy gap $b_{3g}(\pi^*) - b_{2g}(\pi^*) \equiv \Delta$ for different carbon-nitrogen skeletons and various distances of the protons from the center. More values are given in Ref. [17b]. For a D_{4h} carbon-nitrogen skeleton (IX), $|\Delta|$ is under 100 cm^{-1} until the distance between central hydrogen and bridged nitrogen is under ~ 1.3 Å. As the distance between the central hydrogens and bridge nitrogens decreases, the energy of $b_{3g}(\pi^*)$ rises above $b_{2g}(\pi^*)$ exactly as in bonded H_2Pc. To reach $\Delta \sim 730$ cm^{-1}, corresponding to the observed solution $Q_x - Q_y$ splitting, this distance has to be reduced to 0.95 Å.

For the D_{2h} model, Δ depends on the specific carbon-nitrogen geometry, the position of the central hydrogens, and the axis upon which these hydrogens are placed. For the carbon-nitrogen skeletons studied and for the hydrogen distance from the center varying from 0.68 Å to 2.43 Å we have obtained Δ values between -270 cm^{-1} and $+1120$ cm^{-1}. We have done calculations on NiPc using D_{2h} coordinates XII and obtained a splitting of 400 cm^{-1} [28]. It would seem, then, that if the distance of the hydrogen atoms from the bridged nitrogens is larger than ~ 1.3 Å, the primary cause for any significant Δ value is the D_{2h} distortion of the carbon-nitrogen skeleton. *Therefore to obtain the experimental Δ value of 730 cm^{-1} from a bridged model, either there is an incipient* NH *bond with the bridge nitrogens or there is substantial D_{2h} distortion of the carbon-nitrogen skeleton.*

The energy level pattern for different geometries of the bridged model are given in Fig. 5. As in the bonded model (*vide ante*) we interpret the two Q bands as $a_u(\pi) \to b_{2g}(\pi^*)$, $b_{3g}(\pi^*)$. If the splitting of $b_{2g}(\pi^*)$, $b_{3g}(\pi^*)$ is due to incipient bond formation between the central hydrogens and bridge nitrogens, then as in the

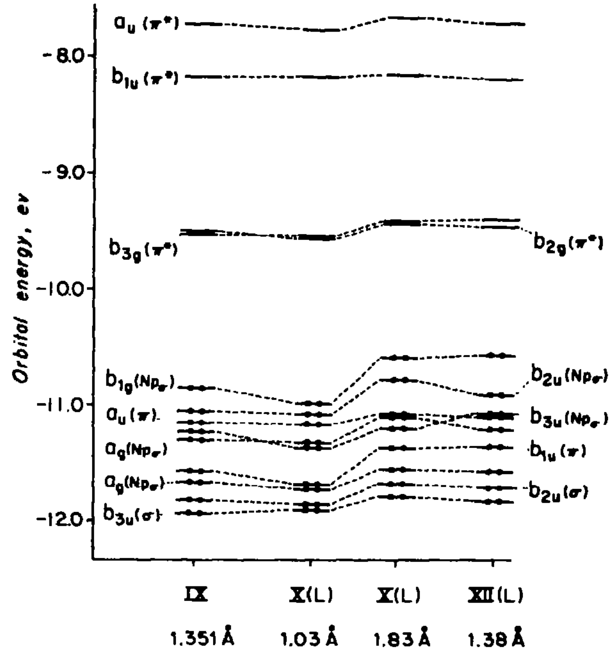

Fig. 5. Top filled and lowest empty MO's for bridged H_2Pc. The coordinates and distance of the hydrogens from the center are given. Full geometry may be found in Table 4

bonded model, the orbital $b_{2g}(\pi^*)$ with non-zero coefficients on the bonded nitrogens will be at lower energy and the lower energy transition will be polarized perpendicular to the H–H axis. In Fig. 4, if the splitting is due to incipient NH bond formation, placing the hydrogens on the *L* axis makes the lower energy transition polarized parallel to *M*. The Robertson distortion shown in Fig. 4 also tends to put $b_{2g}(\pi^*)$ at lower energy than $b_{3g}(\pi^*)$, so that if the protons are placed on the *L* axis of the D_{2h} model the two effects cooperate to enhance splitting. Our calculations suggest that the experimental splitting of $730\,\mathrm{cm}^{-1}$ can be obtained from the Robertson distortion alone, from incipient NH bond formation alone, or from both effects acting cooperatively. For the effects to act cooperatively, the hydrogen atoms must be on the *L* axis of the Robertson carbon-nitrogen skeleton in Fig. 4.

There are three geometric parameters which significantly influence the calculated results in bridged H_2Pc with D_{2h} skeletal symmetry. From the results of free base tetrazaporphin calculations (*vide infra*), it will be seen that the most important of these is the coordinates of the atoms in the inner ring: C_3, N_5, C_6, N_9, and N_{10}. Another factor, although less important, is the inclination of the benzene rings toward the *M* molecular axis. When calculations were done for a constant set of inner ring coordinates, Δ increases as the benzene rings were foreshortened in the *M* direction. The final parameter, which has already been discussed in detail, is the position of the central hydrogen atoms.

c) Postion of $n-\pi^*$ Transitions

In normal phthalocyanine solution spectra, the half-widths of the Q and B bands are approximately 400 and 5000 cm^{-1} respectively. Hochstrasser and Marzzacco [29] have proposed that the presence of $n\rightarrow\pi^*$ transitions, even though forbidden, under allowed $\pi\rightarrow\pi^*$ transitions broadens the latter. Although the MO diagrams for both bonded (Fig. 3) and bridged (Fig. 5) indicate the possibility of $n\rightarrow\pi^*$ transitions under both the Q and B bands, only the B shows temperature independent broadening. However, Fielding and MacKay [30, 31], in a study of the single crystal absorption of H_2Pc, observed weak transitions not split by the crystalline field in the 4000 to 10000 cm^{-1} region. Since the extinction coefficients of these bands are larger than those usually associated with singlet-triplet transitions, Fielding and MacKay assigned them to symmetry forbidden transitions which should be allowed to some extent in a single crystal. Although we do predict $n\rightarrow\pi^*$ transitions in this region, the strong fluorescence of H_2Pc suggests that no other singlets lie under the first $\pi\rightarrow\pi^*$ transition. In addition, our EH method generally underestimates the energy of $n-\pi^*$ transitions [17].

d) Relation to Experimental Spectra

Before attempting to summarize our conclusions, let us list some of the pertinent spectral behavior of H_2Pc [2]. (1) There is a strong variation in the Q_x-Q_y splitting which is more environment than temperature dependent. For example, in silicone oil over the temperature range 297° K to 577° K the splitting varies only from 730 to 770 cm^{-1}. (2) In going from solution to vapor Q_y is blue shifted about 1000 cm^{-1} while Q_x is blue shifted normally (about 250 cm^{-1}). (3) The Q_y band shows anomalous broadening with temperature although the relative Q_x, Q_y intensities are preserved. This latter effect has tentatively been attributed to vibronic coupling between the Q_x, Q_y states [2a].

From the results of our calculations we can suggest three structural changes to account for the striking increase in Q_x-Q_y splitting on going from vapor to solution:

(1) Both structures are bonded. In vapor the carbon-nitrogen skeleton is D_{4h} and in solution D_{2h}, with the pyrrole nitrogens more separated than the aza nitrogens.

(2) Both structures are bridged. In the vapor the total splitting results from cooperation between a D_{2h} Robertson type distortion and incipient bond formation between central hydrogen and bridged nitrogen.

(3) In solution H_2Pc is bridged, most likely with a Robertson D_{2h} distortion with protons on the L axis, while in the vapor H_2Pc is bonded, most likely with D_{4h} carbon-nitrogen skeleton.

Which of these three explanations is most likely? Our bridged calculations of Δ include a range that readily encompasses the observed solution Q_x-Q_y splitting of ~700 cm^{-1}. They are never as large as the ~1500 cm^{-1} vapor splitting, and they only approach this value with central hydrogens essentially bound to the bridged nitrogens. Since such a bond seems chemically unreasonable, *we rule out a bridged structure for the vapor* and reject explanation (2). However our bonded calculation of Δ give values as low as 1100 cm^{-1}, and conceivably 700 cm^{-1} could be achieved. Thus though our calculations indicate explanation (3), the inaccuracy of our method prevents us from ruling out explanation (1).

A great amount of work has been done on crystal and film H_2Pc. Our calculations on the bridged model show that values of Δ comparable to experiment lead to a lower energy band polarized parallel to M axis. Lyons, Walsh, and White [32] obtained better agreement between the experimental polarized spectra of single crystal of β–H_2Pc and spectra calculated using a point dipole approximation if they assumed the lower energy transition is polarized along the L axis. Their conclusion, however, is not completely unambiguous, for there is great difficulty in even correctly assigning the transitions in crystal spectra. Lucia and Verderame [33] observed that the Δ of thin films of β–H_2Pc is approximately the same as the vapor, and they have suggested that the Q_x and Q_y states are each red-shifted by about 600 cm^{-1} in the crystal site then split by about 200 to 500 cm^{-1} under the factor group (Davydov splittings). This explanation seems to imply that the structure of the free base in the vapor closely resembles that in the crystal, and it is the solution results that are anomalous. Sharp and Landon [24] have stated that the spectra of thin films of α–H_2Pc should be most closely related to solution spectra since the α-form is a metastable and less ordered polymorph than the usually studied β H_2Pc. However, the Δ of α–H_2Pc is almost 2000 cm^{-1} which is closer to the vapor rather than the solution results.

Recent X-ray work on metal phthalocyanines [34, 35] indicates that the phthalocyanine skeleton is fairly flexible. Consequently, the phthalocyanine ring geometry may be very sensitive to changes in the molecular environment. The strong dependence of the $Q_x - Q_y$ splitting upon solvent may be a reflection of such geometry changes. Edwards [2] found that Δ is much more environment than temperature dependent. For example, Δ is 699, 767, 870, 909, and 1487 cm^{-1} in HMPA (300° K), 1–CLNP (300° K), Kr (20° K), Ar (20° K), and vapor respectively. These experimental results plus the calculations reported here make clear that "isolated molecule" energies suitable for crystal calculations may be dependent on crystal packing, which can affect the carbon-nitrogen skeletal geometry and in turn the proton positions. It may be that neither the vapor nor the solution $Q_x - Q_y$ split correspond to the "isolated molecule" suitable for a zeroth order wavefunction for a particular solid phase. Since the Davydov splitting for a crystal phase will be comparable to the $Q_x - Q_y$ splitting, which is not clearly known, understanding the crystal spectra of H_2Pc will be difficult. Metallophthalocyanines pose a much simpler problem.

e) Relation to Theory of Chen and Berezin

Using the simple Hückel model, Chen [6] successfully reproduced the observed absorption spectra of H_2Pc with a bridged hydrogen model by slightly raising the Coulomb integral α value of the adjacent bridge nitrogens. Our EH calculations show that the protons *lower* the α value of the adjacent bridge nitrogens. Moreover they show that unless the hydrogen-bridge nitrogen distance becomes comparable to normal bond lenghts, a carbon-nitrogen skeleton distortion is also necessary if the observed 730 cm^{-1} splitting is to be achieved. We also note that Chen placed the bridged hydrogens on the M axis of the D_{2h} skeleton (Fig. 4), while our calculations show the L axis to be more likely.

Berezin [23] proposed that the internally dissociated H atoms are stabilized in the presence of the negative electrostatic field produced by its two dissociated electrons. Maximum stabilization would therefore probably occur when the proton was situated equidistant from the three N atoms (N_9, $N_{9''}$, and N_{10}). Our calculations show that such geometry gives too small a splitting for a D_{4h} carbon-nitrogen skeleton.

Free Base Tetrabenzporphins

Although work on the X-ray structure of tetrabenzporphin was begun by Robertson [36], no detailed analysis of a TBP has been published. It was therefore necessary to make some assumptions about the structure of H_2TBP on the basis of what is known about other free bases. Coordinates XIII (Table 1) are derived from the H_2TPP D_{4h} coordinate of Hamor, Hamor, and Hoard [13] with C_2–C'_2 and C_7–C'_7 increased to 1.39 Å so that the outer benzo rings can achieve the normal hexagonal benzene geometry. Coordinates XIV and XV were obtained from XIII by moving the pyrrole nitrogens farther apart by 0.06 Å (XIV) and 0.10 Å (XV) and the aza nitrogens closer together by the same amounts respectively. Coordinates XVI are derived from the D_{4h} geometry of H_2Pc, coordinates VI. All these cases are bonded with an NH distance of 1 Å. Coordinates XVII were derived from the bridged D_{2h} coordinates of H_2Pc, XII.

Fig. 6 gives the energy level scheme for ZnTBP [17b] and several geometries of H_2TBP. Unlike ZnP but like ZnPc, the top filled MO is $a_{1u}(\pi)$ a result found by SCMO–PPP calculations [3]. Just as for H_2P and H_2Pc, the effect of free base formation is to raise the lower energy $a_{2u}(\pi)$ of the ZnTBP. We see in Fig. 6 that the order of $a_u(\pi)$, $b_{1u}(\pi)$ (the top filled orbitals of H_2TBP) is dependent on geometry. As shown in Table 5, the splitting of $b_{2g}(\pi^*)$ and $b_{3g}(\pi^*)$ is slightly larger for bonded H_2TBP than for either bonded H_2P or H_2Pc. In bridged H_2TBP the splitting is smaller than in bridged H_2Pc. The larger splitting for bonded H_2TBP is due to greater localization of the $e_g(\pi^*)$ orbitals onto the central nitrogen atoms. For all geometries in Table 5, the splitting Δ is rather larger than the 1395 cm^{-1} $Q_x - Q_y$ splitting given by Solov'ev *et al.* [37]. In addition to this, they observe the B band clearly split into two components, whose separation is 1000 cm^{-1}. This is the only one of the four free bases studied herein that shows clear B band splitting.

The polarization of the transitions relative to the H–H axis is determined by which orbital $b_{1u}(\pi)$ or $a_u(\pi)$ is higher in energy. Because the energies are so close, the neglected two electron terms will be important, and we cannot answer this question within the present model.

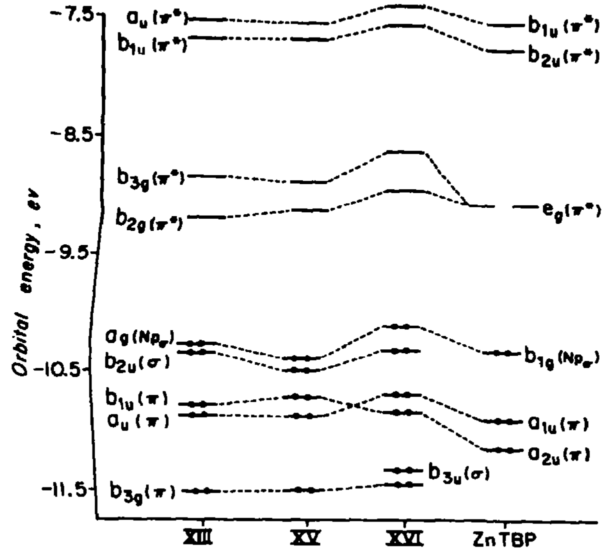

Fig. 6. Top filled and lowest empty MO's of H_2TBP and ZnTBP. Geometry of XIII given in Table 1 while XV and XVI are described in text

Table 5. Calculated and experimental values of Q_x, Δ, and the polarization for various geometries of free base tetrabenzporphin

Geometry	Q_x (cm^{-1})	Δ (cm^{-1})	Polarization
XIII[a]	13020	2663	x
XV[b]	12850	2279	x
XV[c]	12930	1914	x
XVI[d]	14150	2759	y
XVII[e]	14660	99	M
H_2TBP in pyridine Ref. [37]	15020	1395	
H_2TBP in CLNP Ref. [41]	14970	1363	

[a] Bonded H_2TBP, full geometry given in Table 1.
[b] Identical to XIII except N_9: $x = 2.08$, $y = 0$; N_{10}: $x = 0$, $y = 2.02$; H_{20}: $x = 1.08$, $y = 0$.
[c] Identical to XIII except N_9: $x = 2.10$, $y = 0$; N_{10}: $x = 0$, $y = 2.00$; H_{20}: $x = 1.10$, $y = 0$.
[d] Bonded H_2TBP, derived from coordinates VI (Table 1).
[e] Bridged H_2TBP, derived from coordinates XII (Table 4) with H_{20}: $x = 1.83$, $y = 0$.

Free Base Tetrazaporphins

No complete structural analysis of a tetrazaporphin has been published although preliminary investigations have been made on the X-ray structure of various aza substituted porphyrins [36, 38]. There is thus a fairly large uncertainty in the geometry of this molecule; e.g., the central protons in H_2TAP may be either bonded or bridged, while the skeletal geometry may be similar to H_2P, as was assumed in earlier calculations [3a], or it may be more closely related to H_2Pc. Consequently, a fairly wide range of atomic coordinates derived

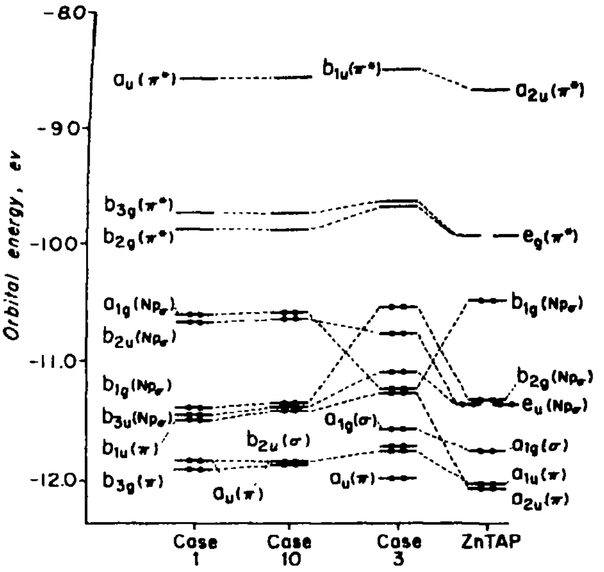

Fig. 7. Top filled and lowest empty orbitals of ZnTAP and H_2TAP. Description of geometry given in Tables 1, 4, and 6

from bonded H_2P, bonded H_2Pc, and bridged H_2Pc were used. Coordinates XVIII (Table 1) were derived from D_{4h} coordinates VI of H_2Pc. Coordinates XIX were derived from D_{4h} coordinates I of H_2TPP. Coordinates XX, XXI, XXII were bridged structures obtained from D_{2h} coordinates X, XI, XII of H_2Pc. Coordinates XXIII have the D_{2h} distortion of the carbon-nitrogen skeleton as in XX, but the central hydrogen atoms are bonded. In all cases the C_2-C'_2 and C_7-C'_7 bond (C_2-C_7 in bridged model) have the porphin bond distance of 1.362 Å.

Fig. 7 compares the calculated MO's for bonded and bridged H_2TAP with ZnTAP. As in previous cases the $a_{2u}(\pi)$ orbital of ZnTAP rises in energy in the free base. The splitting of the empty orbitals $b_{2g}(\pi^*)$ and $b_{3g}(\pi^*)$ is the same as in the comparable H_2Pc skeletons. In the bonded cases, therefore, the lowest energy Q transition is polarized parallel to the proton axis. In the bridged cases with the H-H axis parallel to L, the same is true. With the D_{2h} carbon-nitrogen skeleton XX and the H-H axis parallel to M, a negligible splitting occurs. The polarization predicted for the bonded cases agrees with that predicted by SCMO-PPP calculations [3] and is like H_2P. As in H_2Pc, there is a fairly large number of $n \rightarrow \pi^*$ transitions predicted to be in the region of the Q and B bands. If we again assume that we have underestimated the energy of these transitions, the diffuseness of the B and N bands in H_2TAP [39, 40] may be caused by these underlying $n \rightarrow \pi^*$ transitions.

Table 6 compares the calculated values of Q_x and for various geometries of H_2TAP with experimental results. Comparing these values with those in Table 3, one finds that the calculated splitting for bonded H_2TAP is less than that for bonded H_2Pc with a similar geometry, but the reverse is true for bridged H_2Pc

Table 6. Calculated and experimental value of Q_x and Δ for various geometries of free base tetrazaporphins

Case	Geometry	Coordinates H_{20} (x, y)	Q_x (cm^{-1})	Δ (cm^{-1})	Polarization
1	XVIII[a]	0.91, 0.000	12740	1110	x
2	XIX[b]	1.054, 0.000	9530	1085	x
3	XX[c]	1 83, 0.000	13030	295	L
4	XX	0.000, 1.83	13020	10	L
5	XXI[d]	1.03, 0.000	14830	553	L
6	XXI	1.83, 0.000	12840	653	L
7	XXII[e]	1.83, 0.000	12840	819	L
8	XXII	2.03, 0.000	12130	1144	L
9	XXII	2.21, 0.000	11510	1522	L
10	XXIII[f]	0.695, 0.667	12480	1193	[g]
11	XXIII	0.900, 0.505	12640	1121	[g]
H_2TAP in pyridine Ref. [39]			16030	1960	
H_2TAP in chlorobenzene Ref. [40]			16210	2140	

[a] Bonded H_2TAP, derived from geometry VI. Full coordinates given in Table 1.

[b] Bonded H_2TAP, derived from geometry I.

[c] Bridged H_2TAP, derived from geometry X. Full coordinates given in Table 4.

[d] Bridged H_2TAP, derived from geometry XI.

[e] Bridged H_2TAP, derived from geometry XII.

[f] Geometry of carbon-nitrogen skeleton same as XX, but central hydrogen atoms are bonded.

[g] Polarization parallel to axis connecting pyrrole nitrogens.

and H_2TAP. This result is a natural consequence of the percent composition of the lowest empty $e_g(\pi^*)$ orbitals in ZnTAP and ZnPc which have a 21.8% N_9, 31.3% N_5 and 24% N_9, 24.7% N_5 composition, respectively. The best agreement with the experimental values is obtained either from the bonded model or from the bridged model XXII with a relatively short H_{20}–N_4 distance. Although these EH calculations are not able to unambiguously assign the best configuration, it must be remembered that Weiss *et al.* [3a] obtained a calculated Δ of 1870 cm^{-1} by assuming a bonded geometry. Our results indicate that small changes in ring geometry will lead to measurable changes in Δ. The 181 cm^{-1} increase in the $Q_x - Q_y$ splitting upon changing the solvent from pyridine to chlorobenzene [39, 40] can be interpreted on this basis.

Computer time for these EH calculations is normally reduced by assuming that the molecule of interest has two planes of symmetry. In all previously discussed calculations, this requirement has been met. If we consider a bonded configuration of H_2TAP or H_2Pc with the D_{2h} skeletal symmetry of Robertson [21], the resulting structure does not have two planes of symmetry. This structure is important, however, in order to test our previous assumption that in the bonded model the perturbation due to the central H atoms is much greater than that due to the distortion of the skeleton. Since calculations on such a structure of H_2Pc would be too costly, we considered the case of H_2TAP with C_{2h} molecular symmetry.

As can be seen from the results of such a calculation (Table 6 and Fig. 7), the properties of this configuration should be very similar to those of bonded H_2TAP with D_{4h} skeletal symmetry. This result confirms that indeed the main perturbation on the molecule is the bonding protons. From a study of the intrinsic polarization of the fluorescence of H_2TAP [41], it was concluded that the symmetry of the molecule was D_{2h}. Although the molecular symmetry of the configuration under consideration is formally C_{2h}, the symmetry of the π electron orbitals is essentially still D_{2h}. Consequently, the selection rules for such a configuration should be effectively equivalent to one that is formally D_{2h}.

The neutron diffraction study on H_2Pc indicates that the protons are not exactly on the line connecting the two nitrogen atoms, N_9–$N_{9'''}$ of Fig. 4. Physically, this corresponds to an increase in the amount of H-bonding with the bridged nitrogen atoms. Although the effect of placing H_{20} and $H_{20'}$ closer to N_{10} and $N_{10'}$ respectively (case 11) is slight, it does result in a smaller calculated value of Δ. The MO diagram for bonded H_2TAP with D_{2h} skeletal symmetry (case 10) closely resembles that of bonded H_2TAP with D_{4h} skeletal symmetry (case 1), even with respect to the $N_{p\sigma}$ orbitals. Although the above discussion is specifically about H_2TAP, similar results are expected for C_{2h} H_2Pc.

Other Work

A Mulliken population analysis [42] for various geometries of H_2P, H_2Pc, H_2TBP, and H_2TAP are reported elsewhere [17b]. The charge density of all atoms except the central hydrogens and the pyrrole nitrogens are fairly insensitive to changes in geometry. Generally, we find that the net charge of the pi electron SCMO PPP calculations for H_2P [3] and H_2Pc [9] correlates with the net charge for all valence electrons in the EH model. Ref. [17b] also includes the following: additional calculations on various geometries of H_2Pc; a population analysis for the top filled and lowest empty orbitals of H_2P and H_2Pc; and a more complete discussion of some of our results.

Conclusions

We have discussed the splitting of the two Q bands in the free bases of four porphyrin related skeletons in terms of the energy gap between the vacant orbitals $b_{2g}(\pi^*)$, $b_{3g}(\pi^*)$ that are the degenerate $e_g(\pi^*)$ of the metal. We have been led to the following conclusions:

(1) The splitting is determined not only by the central H atoms but by distortions of the carbon-nitrogen skeleton. Changes in these distortions can account for the dependence of the $Q_x - Q_y$ split on environment.

(2) To obtain splittings of $700\,\mathrm{cm}^{-1}$ or more by a bridged structure, either there is incipient NH bond formation between central hydrogen atoms and bridge nitrogens or there is substantial D_{2h} distortion. Both effects may work cooperatively, but even so they cannot explain the large $Q_x - Q_y$ splitting observed in vapor of H_2Pc.

(3) Because of the sensitivity of $Q_x - Q_y$ splitting to environment in H_2Pc, the "isolated molecule" splitting suitable for the crystal may not correspond to either vapor or solution observations.

(4) $n-\pi^*$ transitions occur at lower energies in H_2TAP and H_2Pc than in H_2P or H_2TBP and may account for the great broadening of the Soret region of the former two compared to the latter.

(5) The only case where a bridged structure is likely is solution H_2Pc. Even here the calculations do not altogether rule out a bonded structure.

Acknowledgments. The research was supported in part by Public Health Services Research Grant GM-14292 from the Institute of General Medical Sciences. Professor E. R. Davidson let us use a new symmetrized extended Hückel program that he prepared for our C_{2h} calculation.

References

1. Paper I: Gouterman, M.: J. molecular Spectroscopy **6**, 138 (1961).
2a. Paper XV: Edwards, L., Gouterman, M.: J. molecular Spectroscopy **33**, 292 (1970).
b. Edwards, L.: Ph. D. Thesis, Committee on Chem. Phys., Harvard University, 1969.
3a. Paper III: Weiss, C., Kobayashi, H., Gouterman, M.: J. molecular Spectroscopy **16**, 415 (1965).
b. Paper XXIV: McHugh, A. J., Gouterman, M., Weiss, C.: Theoret. chim. Acta (Berl.) **24**, 346—370 (1972).
4. Sundbom, M.: Acta chem. Scand. **22**, 1317 (1968).
5a. Mathur, S. C.: J. chem. Physics **45**, 3470 (1966).
b. — McKannon, E. C.: Int. J. Quant. Chem. Symp. (No. 1), 247 (1967).
c. Klasino, L., Nowakowski, J.: J. chem. Physics **49**, 3326 (1968).
6. Chen, I.: J. molecular Spectroscopy **23**, 131 (1967).
7. Day, P., Williams, R. J. P.: J. chem. Physics **37**, 567 (1962).
8. Harrison, S. E.: J. chem. Physics **50**, 4739 (1969).
9. Sukigara, M., Nelson, R. C.: Molecular Physics **17**, 387 (1969).
10. Chen, I.: J. chem. Physics **51**, 3241 (1969).
11. Paper IV: Zerner, M., Gouterman, M.: Theoret. chim. Acta (Berl.) **4**, 44 (1966).
12. Paper V: — — Inorg. Chem. **5**, 1699 (1966).
13. Hamor, M. J., Hamor, T. A., Hoard, J. L.: J. Amer. chem. Soc. **86**, 1938 (1964).
14. Webb, L. E., Fleisher, E. B.: J. Amer. chem. Soc. **87**, 667 (1965).
15. Silvers, S., Tulinsky, A.: J. Amer. chem. Soc. **86**, 927 (1964).
16a. Chen, B.: Ph. D. Thesis, Department of Chemistry, Michigan State University, 1971.
b. — Tulinsky, A.: To be published.
17a. Schaffer, A. M., Gouterman, M.: Theoret. chim. Acta (Berl.) **18**, 1 (1970).
b. — Ph. D. Thesis, Department of Chemistry, University of Washington, 1972.
18. Antenson, J. E.: Ph. D. Thesis, Department of Chemistry, University of Pennsylvania, 1969.
19a. Paper XVI: Edwards, L., Gouterman, M., Dolphin, D. H.: J. molecular Spectroscopy **35**, 90 (1970).
b. Paper XVII: — Dolphin, D. H., Gouterman, M., Adler, A. D.: J. molecular Spectroscopy **38**, 16 (1971).
20. Anex, B. G., Umans, R. S.: J. Amer. chem. Soc. **86**, 5026 (1964).
21. Robertson, J. M.: J. chem. Soc. **1936**, 1195.
22. Fleischer, E. B.: Chem. Comm. **1970**, 105.
23. Berezin, B. D.: Russ. J. physic. Chem. **39**, 165 (1965).
24. Sharp, J. H., Landon, M.: J. physic. Chem. **72**, 3230 (1968).
25. Hoskins, B. F., Mason, S. A., White, J. C. B.: Chem. Comm. **1969**, 554.
26. Gurinovich, I. F.: Zh. Prikl. Spektrosk. **6**, 657 (1967).
27. Vincett, P. S., Voigt, E. M., Rieckoff, K. E.: J. chem. Physics **55**, 4131 (1971).
28. Schaffer, A. M.: Unpublished calculation.
29. Hochstrasser, R. M., Marzzacco, C.: J. chem. Physics **49**, 971 (1968).
30. Fielding, P. E., MacKay, A. G.: J. chem. Physics **38**, 2777 (1963).
31. — — Aust. J. Chem. **17**, 750 (1964).
32. Lyons, L. E., Walsh, J. R., White, J. W.: J. chem. Soc. **1960**, 167.

33. Lucia, E. A., Verderame, F. D.: J. chem. Physics **48**, 2674 (1968).
34. Vogt, L. H., Jr., Zalkin, A., Templeton, D. H.: Inorg. Chem. **6**, 1725 (1967).
35. Brown, C. J.: J. chem. Soc. (A), **1968**, 2488, 2494.
36. Robertson, J. M.: J. chem. Soc. **1939**, 1809.
37. Solov'ev, K. N., Shkirman, S. F., Kachura, T. F.: Bull. Acad. Sci. USSR, Phys. Ser. **27**, 763 (1963).
38. Woodward, I.: J. chem. Soc. **1940**, 601.
39. Stern, A., Pruckner, F.: Z. physik. Chem. (Leipzig) **178** A, 420 (1937).
40. Linstead, R. P., Whalley, M.: J. chem. Soc. **1952**, 4839.
41. Gurinovitch, G. P., Sevchenko, A. N., Solov'ev, K. N.: Optics and Spectroscopy **10**, 396 (1961).
42. Mulliken, R. S.: J. chem. Physics **23**, 1833, 1841 (1955).
43. Lucia, E. A., Marino, C. P., Verderame, F. D.: J. molecular Spectroscopy **26**, 133 (1968).
44. Barrett, P. A., Linstead, R. P., Rundall, F. G., Tuey, G. A. P.: J. chem. Soc. **1940**, 1079.

Dr. Arnold M. Schaffer
Department of Chemistry
University of Houston
Houston, Texas 77004, USA

Prof. Dr. Martin Gouterman
Department of Chemistry
University of Washington
Seattle, Washington 98105, USA

Theoret. chim. Acta (Berl.) 25, 83 –88 (1972)
© by Springer-Verlag 1972

Molecular Electrostatic Potentials: Comparison of *ab initio* and CNDO Results

C. GIESSNER-PRETTRE and A. PULLMAN
Institut de Biologie Physico-Chimique, Laboratoire de Biochimie Théorique associé au C.N.R.S.
13, rue P. et M. Curie, Paris 5è, France

Received November 15, 1971

The possibilities of utilization of CNDO wave functions for computing molecular electrostatic potentials are studied by comparison with *ab initio* results for H_2O and H_2CO.

Les possibilités d'utilisation de fonctions d'onde CNDO pour le calcul des potentiels électrostatiques moléculaires sont étudiées par comparaison avec des résultats *ab initio* pour H_2O et H_2CO.

Die Möglichkeiten der Verwendung von CNDO-Wellenfunktionen zur Berechnung molekularer elektrostatischer Potentiale werden durch Vergleich mit *ab initio* Rechnungen für H_2O und H_2CO untersucht.

Several nonempirical studies using wavefunctions from either STO minimal basis sets [1–3] or GTO basis sets [4, 5] have shown that the value of the electrostatic potential created by the electronic distribution and the nuclear charges of a molecule in the different regions of the space surrounding it gives valuable informations about the sites involved in protonation or in reactions with electrophilic agents. Large-scale non-empirical computations of this sort being unfortunately precluded, we have set out to investigate the possibilities of the CNDO-method in this field: in a preliminary study [6] we have determined within the CNDO/2 semi-empirical framework the isopotential curves for adenine and guanine and have observed that they allow a very neat distinction between the two molecules as to the most probable regions for electrophilic attack, in remarkable conformity with the known experimental facts. On the other hand, the CNDO maps for adenine agree qualitatively with the corresponding *ab initio* maps available [4]. However, some differences appear upon detailed comparison, particularly as concerns the depth of the potential wells and the location of the bottom of these wells.

These differences led us to search for their origin and to try to find an approximation for the calculation of the electrostatic potential from CNDO/2 wave functions which would be in closer agreement with non empirical results. For performing this test we chose water and formaldehyde. For water, non-empirical isopotential maps from a wave function expressed in a minimal STO basis are available for comparison [7]. The choice of formaldehyde was made, aside from the small size of the molecule and the existence in the literature of several *ab initio* minimal STO wave functions which could be used to calculate the non empirical isopotential maps [8, 9], because the structure of protonated formaldehyde is experimentally known [10].

Computational Details

The interaction energy between a molecular distribution and an external unitary positive charge placed at point P is given by [2]:

$$V_P = \sum_A \frac{Z_A}{R_{PA}} - \sum_{\mu\nu} P_{\mu\nu} \int \frac{\chi_\mu \chi_\nu}{r_P} \mathrm{d}\tau ,$$

where the first summation runs over the nuclei of the molecule and the second is carried over all the electrons of the molecule. The integrals appearing in the second summation are the nuclear attraction integrals of a hydrogen nucleus on the distribution $\chi_\mu \chi_\nu$. If the wave functions utilized to calculate the $P_{\mu\nu}$ elements of the density matrix are obtained from CNDO/2, Z_A has to be taken equal to the number of valence electrons.

Approximation I. If one chooses to stay exactly within the CNDO/2 approximations, only the diagonal elements of the density matrix are retained and the nuclear attraction integrals are approximated by minus the repulsion integrals between s orbitals. This was the approximation we used previously [6], in which:

$$V_P = \sum_A \left(\frac{Z_A}{R_{PA}} - P_{AA} \gamma_{AH} \right).$$

This approximation corresponds to Fig. 1.

Approximation II. Another possibility is to keep the same elements of the density matrix, but to abandon the γ-approximation and to use instead the corresponding correct nuclear attraction integrals V_{AH} over s atomic orbitals (so as to retain the spherical symmetry of the interaction). The corresponding maps are those of Fig. 2.

Approximation III. Instead of averaging the nuclear attraction integrals on each atom A, all the nuclear attraction integrals are computed exactly and introduced in the summation with the corresponding $P_{\mu\nu}$ element, provided that χ_μ

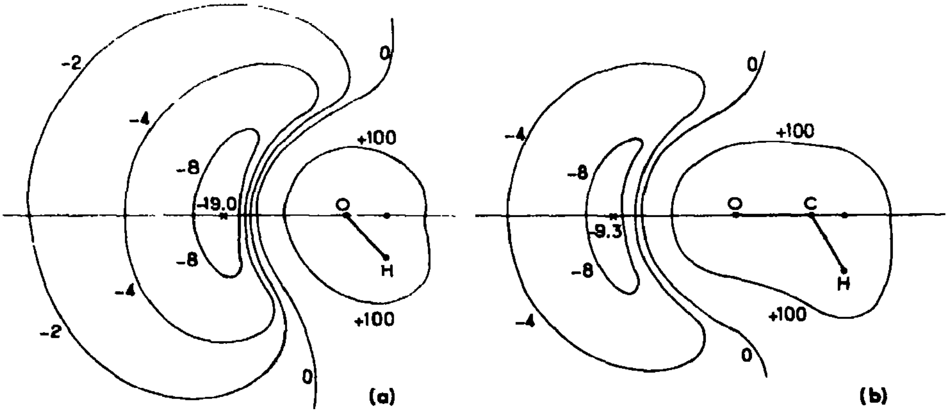

Fig. 1a and b. Electrostatic molecular potential energy maps for a) water molecule, b) formaldehyde, using Approx. I. Energies are in kcal/mole. The upper part of the figure corresponds to the y or z plane, the lower part to the molecular plane

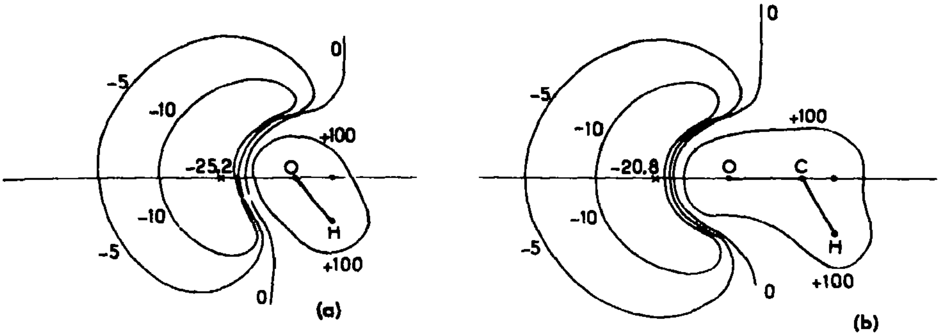

Fig. 2. Same as Fig. 1. Approx. II

and χ_ν are located on the same atom. The only nuclear attraction terms left out are the three-center terms. This approximation corresponds to the maps of Fig. 3.

Approximation IV. The first three approximations utilize the usual CNDO/2 density matrix made with the coefficients admittedly considered as coefficients over Slater orbitals in spite of the ZDO approximation. Now, the CNDO eigenvectors may be conceived instead [11] as expressed in terms of orthogonalized orbitals λ derived from Slater orbitals χ by the Löwdin's transformation [12]. Thus, one may retransform the CNDO coefficients into coefficients over Slater orbitals by the matrix product:

$$C^\chi = S^{-1/2} C^\lambda ,$$

where S is the overlap matrix over the Slater orbitals, and use these "deorthogonalized" coefficients for calculating a new density matrix. This approach was utilized for studying charges and dipole moments [13, 14], and very recently, density distributions [20].

If one uses this deorthogonalized density matrix for the computation of the potentials, all the nuclear attraction integrals must be retained since the two-center distributions $\chi_\mu \chi_\nu$ are no longer zero. This approximation of the potential V_P differs from an exact computation only by the freezing of the 1*s* electrons into the nuclei and by the fact that the density matrix is obtained through a CNDO deorthogonalization process instead of a complete *ab initio* SCF procedure. This approximation corresponds to Fig. 4.

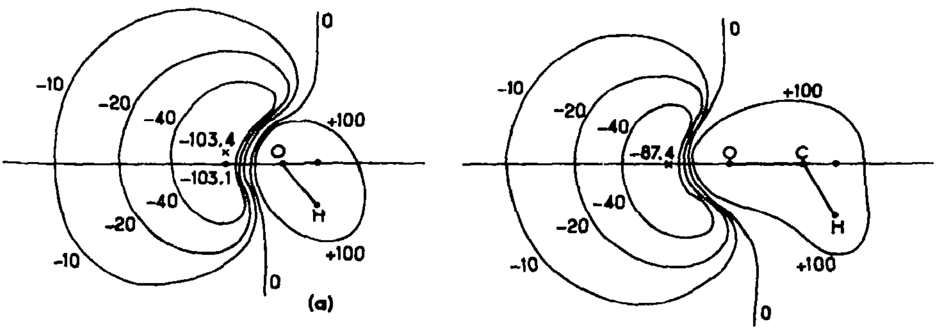

Fig. 3. Same as Fig. 1. Approx. III (b)

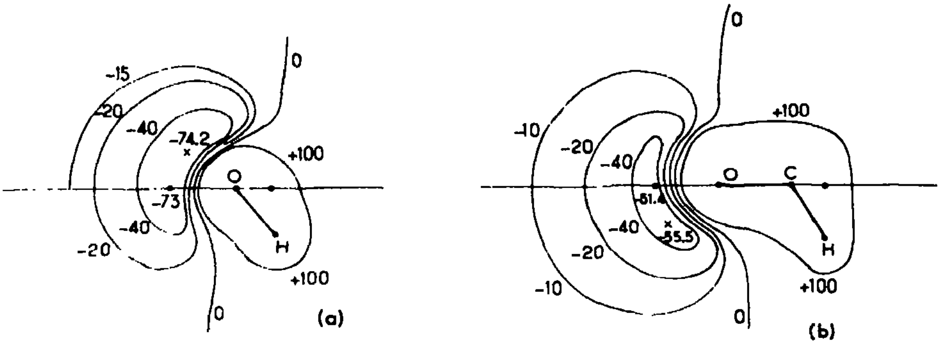

Fig. 4. Same as Fig. 1. Approx. IV

Reference ab initio Computations. The reference curves for H_2O (Fig. 5a) are those of Bonaccorsi *et al.* [7], corresponding to the molecule-optimized Slater basis set of Aung, Pitzer and Chan [15].

For H_2CO we have computed the isoenergy values using two different wave functions: one in a Slater minimal basis set (best atom ζ's with $\zeta_H = 1.2$) [8], the other in a molecule-optimized Slater basis (isotropic) [9]. The corresponding maps are those of Figs. 5b1, and 5b2 respectively.

For these potential computations (and those of Approx. IV), we have used an adaptation of a part of an integral program written by Stevens [16].

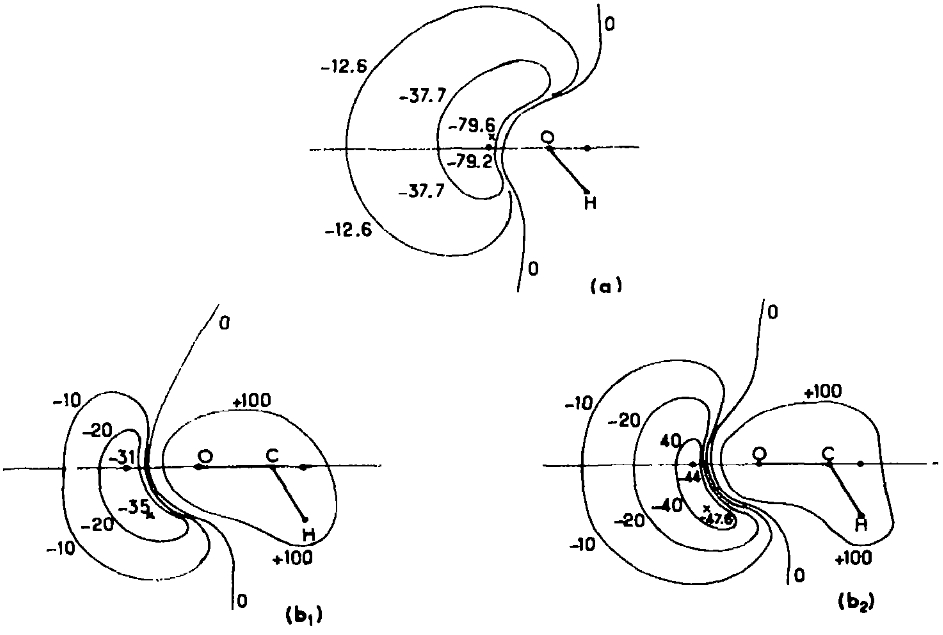

Fig. 5a and b. Non-empirical electrostatic potential energy maps for: a H_2O of Ref. [7], b1 H_2CO (Slater exponents, $\zeta_H = 1.2$), b2 H_2CO (optimized isotropic basis)

Results and Discussion

The maps of Approx. I (full CNDO) show a similar behaviour for the two molecules: the potential wells are rather shallow and located on the molecular axis. These results when compared to the non-empirical ones of Bonaccorsi *et al.* for water and ours for formaldehyde show that the computed values are too small (in absolute value) and that the bottoms of the wells are located too far from the oxygen atoms when approximating the nuclear integrals by the γ-values. This appears as a general deficiency of Approx. I, which has partly been discussed before [6]. As expected, replacing the γ's by the average V_{AH}-values (Approx. II) increases the numerical potential values and brings the minima closer to the molecule (Fig. 2). But in the two approximations, the minima are located on the molecular symmetry axis for both molecules whereas the *ab initio* calculations find the bottoms of the potential wells away from the molecular axis, somewhat above (and below) the molecular plane in the case of water, and in the molecular plane but clearly away from the C=O axis in the case of formaldehyde (Fig. 5). For this molecule the non-empirical isopotential maps are in agreement with experimental findings on the structure of protonated formaldehyde: high resolution proton magnetic resonance indicates unambiguously [10] an unsymmetrical structure for the protonated species[1].

As concerns the non-empirical curves it is interesting to note that the location of the potential well is very similar whatever basis set is utilized. From a qualitative point of view the two sets of curves are very similar, but they differ in the extension of the attractive zone and in the numerical value of the minima. The greater extension occurs for the optimized basis and is probably related to the fact that the optimized exponents for the oxygen atom are smaller than the corresponding Slater exponents.

Approx. III leads to numerical values of the potentials which are much larger than in the preceeding computations, and even larger than the *ab initio* values. For water the largest potential is now slightly off the molecular plane. But for formaldehyde the molecular axis is still found to be the most attractive region for a positve charge.

If we turn now to Approx. IV, we observe a better quantitative agreement with non-empirical calculations. The numerical agreement between the two types of calculations shows that the accuracy of the representation of the core electrons (the 1*s* electrons from oxygen and carbon atoms in the present cases) plays a negligible role on the value of the electrostatic potential at the distances considered. On the other hand, the introduction of the two-center distributions seems required for obtaining the directionality of the attraction energy when the bottoms of the potential wells are very small depressions in a rather deep arc-shaped valley, as it is the case in the neighbourhood of oxygen atoms.

As far as the depth of potential wells is concerned, Approx. IV appears in better agreement with the values obtained from the wave function using an optimized basis set than those from a wave function using regular Slater exponents.

---

[1] The experimental evidence on the geometry of H_3O^+ is less clearcut: crystal data indicate pyramidal structures but the free ion is claimed to be planar [17–19] with very easy distortion.

Conclusion

These calculations show that one way to obtain *quantitatively* good isopotential maps from a CNDO/2 wavefunction is to transform the eigenvectors from the orthogonal basis set into a regular Slater basis and to introduce all the integrals. Although the calculation of nuclear integrals is very rapid for one point of space, the large number of points required for a map renders the computer time necessary for such calculations rapidly prohibitive when the size of the molecule increases. However, for large molecules this approximation might be useful for the exploration of a relatively small region of space where a preliminary study has shown that the potential well has the largest probability to be found. Such an exploratory study may be performed very rapidly using Approx. II. (The use of Approx. I, which is less good, and slower, may be preferred only when consistency with other CNDO results is desired).

Acknowledgements. We gratefully acknowledge the help of Dr. J. Beaudet in the program introducing all the nuclear integrals. We thank also Professor Stevens for communicating us the formaldehyde eigenvectors used for the maps of Fig. 5b2.

References

1 Bonaccorsi, R., Petrongolo, E., Scrocco, E., Tomasi, J.: Quantum aspects of heterocyclic compounds in chemistry and biochemistry, Jerusalem Symposia, Vol. II, 181 (1970).
2. Scrocco, E., Tomasi, J.: J. chem. Physics **52**, 5270 (1970).
3. -- Theoret. chim. Acta (Berl.) **20**, 331 (1971).
4. Pullman, A., Scrocco, E., Tomasi, J.: Theoret. chim. Acta (Berl.), in press.
5. - -- Chem. Physics Letters **12**, 622 (1972).
6. Giessner-Prettre, C., Pullman, A.: C. R. Acad. Sci. **272**c, 750 (1971).
7. Bonaccorsi, R., et al.: Private communication and Ref. [3].
8. Aung, S., Pitzer, R. M., Chan, S. I.: J. chem. Physics **45**, 3457 (1966).
9. Switkes, E., Stevens, R. M., Lipscomb, W. N.: J. chem. Physics **51**, 5229 (1969).
10. Olah, G. A., O'Brien, D. H., Calin, M.: J. Amer. chem. Soc. **89**, 3582 (1967).
11. Pople, J. A., Segal, G. A.: J. chem. Physics **43**, S 136 (1965).
12. Löwdin, P. O.: J. chem. Physics **18**, 365 (1950).
13. Giessner-Prettre, C., Pullman, A.: Theoret. chim. Acta (Berl.) **11**, 159 (1968).
14. Shillady, D. D., Billingsley, F. P., Bloor, J. E.: Theoret. chim. Acta (Berl.) **21**, 1 (1961).
15. Aung, S., Pitzer, R. M., Chan, S. I.: J. chem. Physics **49**, 2071 (1961).
16. Stevens, R. M.: J. chem. Physics **52**, 1397 (1970).
17. Grahn, R.: Arkiv fysik **19**, 147 (1961).
18. de Paz, M., Ehrenson, S., Friedman, L.: **52**, 3362 (1970).
19. Moskowitz, J. M., Harrison, M. C.: J. chem. Physics **43**, 3550 (1965).
20. MacIver, J. W., Jr., Coppens, P., Novak, D.: Chem. Physics Letters **11**, 82 (1971).

Prof. Dr. A. Pullman
Institut de Biologie Physico-Chimique
13, rue Pierre et Marie Curie
Paris 5è, France

Theoret. chim. Acta (Berl.) 25, 89—96 (1972)
© by Springer-Verlag 1972

Fermi Resonance in the Carbonyl Band of Cyclopentanone

R. E. Davis and Kwang Sup Kim*

Department of Chemistry, Purdue University, West Lafayette, Indiana 47907

Received November 16, 1971

The relative carbonyl stretching frequency shifts in the infrared spectra of cyclopentanone (CP) and O^{18}-CP have been measured in various solvents. The plot of these shifts versus those of acetophenone shows that the doublet in the carbonyl stretching region of CP is caused by Fermi resonance and the splitting does not take place in O^{18}-CP. In the vapor phase no doublet was observed in CP or O^{18}-CP.

Using these results, the vibrational energy diagrams of CP and O^{18}-CP are proposed and the energy difference between the unperturbed resonating levels (δ^0) and interaction terms (H_{ij}) were obtained. These values agree well with those obtained from the intensity data.

Die relativen Frequenzverschiebungen der Carbonylstreckschwingung im Infrarotspektrum des Cyclopentanons (CP) und O^{18}-CP werden in verschiedenen Lösungsmitteln gemessen. Beim Auftragen dieser Werte gegen die des Acetophenons zeigt sich, daß das Dublett im Bereich der Carbonylstreckschwingung des CP durch Fermiresonanz hervorgerufen wird und bei O^{18}-CP keine Aufspaltung stattfindet. In der Dampfphase wurde weder bei CP noch bei O^{18}-CP ein Dublett beobachtet.

Aufgrund dieser Ergebnisse wird ein Schwingungsenergiediagramm von CP und O^{18}-CP vorgeschlagen und die Energiedifferenz zwischen den ungestörten Resonanzzuständen (δ^0) und den Wechselwirkungstermen (H_{ij}) erhalten. Diese Werte stimmen mit den aus Intensitätsmessungen erhaltenen gut überein.

The carbonyl stretching region of the infrared and Raman spectra of cyclopentanone (CP) contains a doublet band. This splitting has been investigated [1, 2] extensively by examining the effects of solvent, concentration, and temperature on the doublet and by comparing the infrared and Raman spectra of CP and $CP-\alpha:\alpha:\alpha':\alpha'-d_4$. It was concluded that the doublet is caused by Fermi resonance and does not involve conformational isomerism, dimolecular association through hydrogen bonding, dipole-dipole interaction or enolization of the ketone. According to a microwave study, CP has one major conformational structure of C_2 symmetry in the ground state [3]. Although the dimeric association by a dipole-dipole interaction in CCl_4 was reported recently [4], its contribution to the doublet is not significant as confirmed in previous works [1, 2].

In the course of a study of the infrared carbonyl bands of various ketones, we have had occasion to synthesize and study the infrared absorptions of O^{18}-CP in comparison with those of O^{16}-CP. With these spectral data in the carbonyl stretching region, the Fermi interaction of CP and O^{18}-CP has been studied using its solvent perturbation.

Several O^{18}-labelled ketones such as benzoyl chloride [5, 6], *p*-benzoquinone [7] and tetramethylcyclobutane-1,3-dione [8] have been used for study of the

---

* Taken in part from the Ph. D. Thesis of K. S. Kim, Jan. 1971. Paper X. Vibrational Effects in Carbonium Ion Reactions. Paper IX. Davis, R. E., Pfaffenberger, C. R. C.: Theoret. chim. Acta (Berl.) 20, 364 (1971).

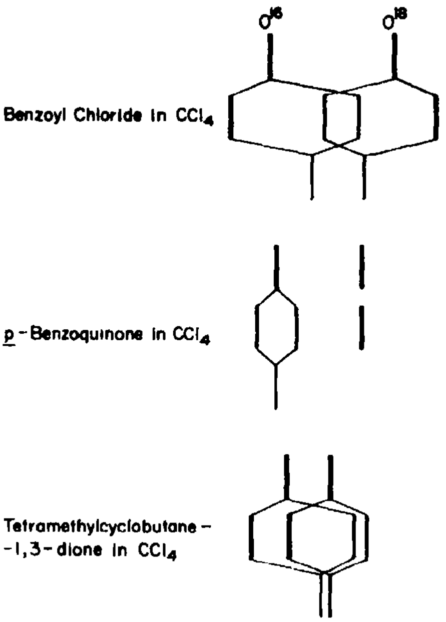

Fig. 1. Schematic interacting energy levels in the carbonyl stretching region of benzoyl chloride, *p*-benzoquinone and tetramethylcyclobutane-1,3-dione

doublet splittings of their normal ketones in the carbonyl stretching region. The interacting energy levels can be represented by the schematic diagram (Fig. 1). The energy levels and the intensities of O^{18}-ketones depend on the degree of the relative shifts of the resonating carbonyl and overtone or combination levels caused by O^{18}-substitution. The overtone or combination bands of benzoyl chloride are effected very much by O^{18}-substitution while those of *p*-benzoquinone and tetramethylcyclobutanedione (TMDO) remain at the almost same locations. This information is useful for the vibrational assignment with group-theoretical considerations and selection rules for TMDO [8]. However, this kind of consideration is not successful for CP because of many numerically possible combinations and its low molecular symmetry.

CP in solvents is similar to *p*-benzoquinone due to the large separation of the resonating levels by O^{18}-substitution (see Fig. 2). In the vapor phase the carbonyl band is shifted to a higher level; the interaction in O^{16}-CP is weakened significantly and it may be negligible (Fig. 3). The same behavior is observed in O^{18}-CP. The half-band width and the relative locations of three sub-bands are almost equal to those of O^{16}-CP (Fig. 3 and Table 1). If there is interaction in the vapor phase, the band would be complex and broad due to the contribution from rotational states. These behaviors are shown schematically in Fig. 4.

With different solvents, the carbonyl band can be shifted. In Fig. 5, the relative frequency shifts ($\Delta\nu/\nu$) calculated on the basis of the vapor state frequency are plotted against those of acetophenone [9]. In the case of O^{16}-CP in which the

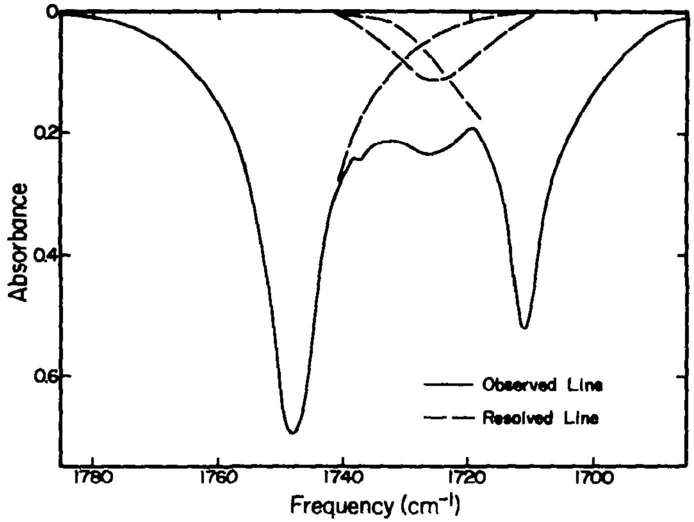

Fig. 2. Infrared spectrum of partially O^{18}-substituted cyclopentanone in the carbonyl stretching region, 0.04 cc/cc CS_2, 0.05 mm thick matched KBr cell

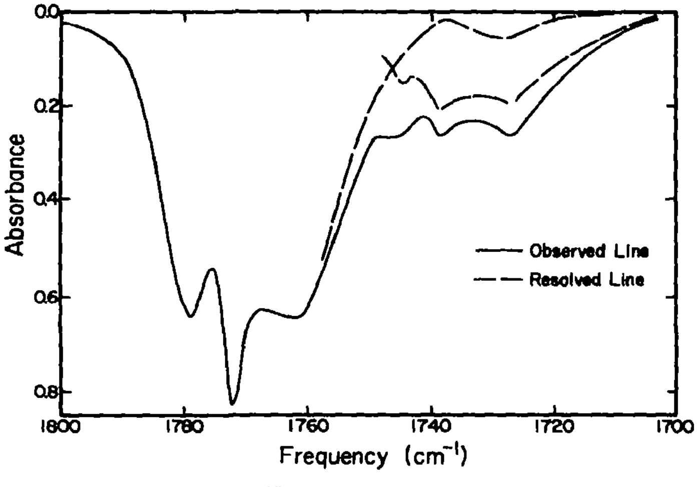

Fig. 3. Infrared spectrum of partially O^{18}-substituted cyclopentanone in vapor phase in the carbonyl stretching region, 15 mm Hg, 10 cm cell with CsBr windows

resonating levels are very close, the carbonyl level can be lower and higher than the other level interacting with it. The latter level depends only weakly upon the nature of solvent. Therefore, the stronger band has been assigned as the carbonyl absorption O^{18}-CP gives a good straight line as ketones do whose carbonyl band does not involve Fermi resonance [9]. O^{16}-CP shows the same tendency as O^{18}-CP in the low and high relative shifts ($\Delta\nu/\nu$). However, the line is not connected in the middle region (the broken line of Fig. 5). This effect takes place in solvents

Table 1. Infrared data in the carbonyl stretching region of O^{16}- and O^{18}-cyclopentanones and the calculated parameters

Point No.	Solvent	ν_{16}	ν_c	ν_{18}	ϱ	δ	δ^0	H_{ij}	a
	Vapor	1776 1771[a] 1759		1743 1738[a] 1725					
1	Cyclohexane	1753	1724	1714	13.78	29	17	11.7	0.89
2	Carbon disulfide	1747	1725	1709	5.77	22	12	9.2	0.88
3	Nitromethane	1733	1747	1706	1.49	14	2	6.9	0.76
4	Chloroform	1729	1745	1703	1.30	16	2	7.9	0.75
5	Bromoform	1726	1743	1703[b] 1699	1.49	17	1	8.5	0.73
6	Benzene	1747	1728	1710	4.73	19	11	7.7	0.89
7	Carbon tetrachloride	1749	1726	1711	5.2	23	13	8.9	0.89
8	Acetonitrile	1746	1733	1707	1.06	13	1	6.5	0.73

[a] Used as standard.

[b] Doublet of equal intensities. Average value was used.

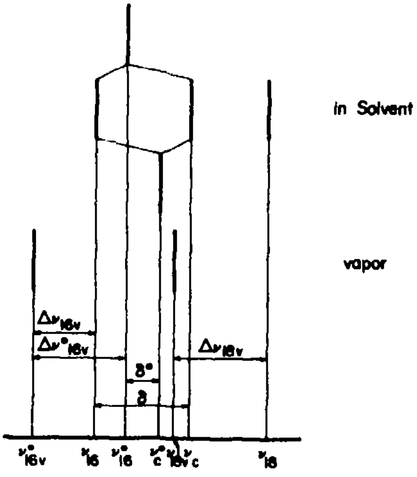

Fig. 4. Schematic interacting energy levels of O^{16}- and O^{18}-cyclopentanones in solvent and vapor phase in the carbonyl stretching region

which would be expected to lower the resonating carbonyl level to the overtone or combination level. The shift ($\Delta\nu^0_{16v}$) of O^{16}-CP can be assumed to be equal to $\Delta\nu_{18v}$, and the frequencies of the resonating levels (ν^0_{16} and ν^0_c) can be determined (Table 1). The extrapolation to $\delta^0 = 0$ in a plot of ϱ against δ^0 gives $\varrho = 1$ (Fig. 6(a)) (ϱ = the intensity of strong band/that of weak band). These two behaviors are those which can be expected from the Fermi resonance scheme which is shown in Fig. 4.

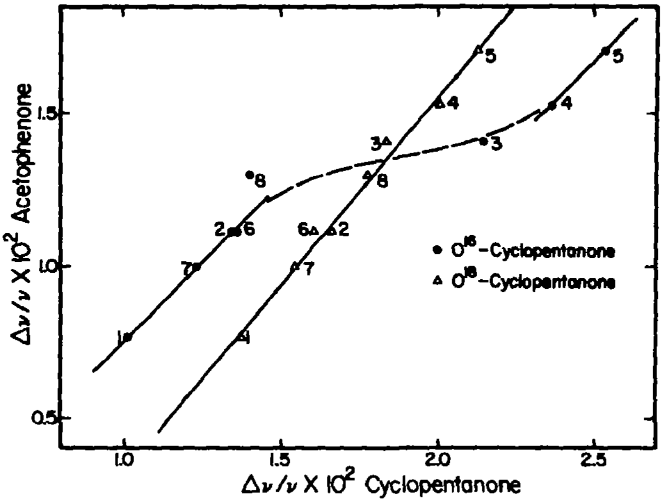

Fig. 5. Plot of the relative frequency shift of O^{16}- and O^{18}-cyclopentanones versus that of acetophenone

If the resonating levels (ψ_i^0 and ψ_j^0) have very nearly the same energy, the effect can be calculated from the first-order perturbation theory. The solution may be written as [10, 11]

$$E_{i,j}=\tfrac{1}{2}(E_i^0+E_j^0)+\tfrac{1}{2}\sqrt{(E_i^0-E_j^0)+4|H_{ij}|^2}\,, \tag{1}$$

where

$$E_i^0=\langle\psi_i^0|\hat{H}|\psi_i^0\rangle$$

$$E_j^0=\langle\psi_j^0|\hat{H}|\psi_j^0\rangle$$

and

$$H_{ij}=\langle\psi_i^0|\hat{H}|\psi_j^0\rangle$$

$\hat{H}$ includes the perturbation operator.

The eigenfunctions after interaction are

$$\psi_i=a\psi_i^0-b\psi_j^0$$

$$\psi_j=b\psi_i^0+a\psi_j^0\,, \tag{2}$$

where

$$a=[\delta+\delta^0/2\delta]^{1/2}$$

and

$$b=[\delta-\delta^0/2\delta]^{1/2}\,.$$

Subscripts i and j indicate the carbonyl and overtone or combination band respectively. If the resonating overtone or combination level (ψ_j^0) is assumed to have negligible intrinsic intensity [12],

$$\varrho=I_i/I_j=a^2/b^2 \tag{3}$$

and combining Eqs. (2) and (3),

$$\delta^0=\delta(\varrho-1)/(\varrho+1)\,. \tag{4}$$

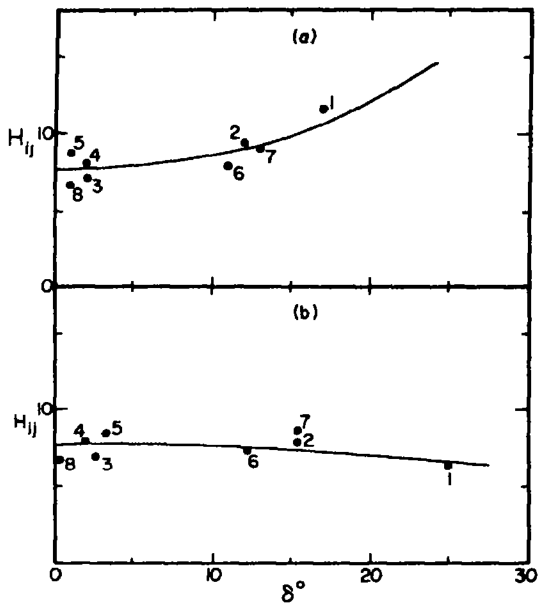

Fig. 6. Plot of H_{ij} versus δ^0. a was obtained from the scheme in Fig. 4 and b from the intensity data

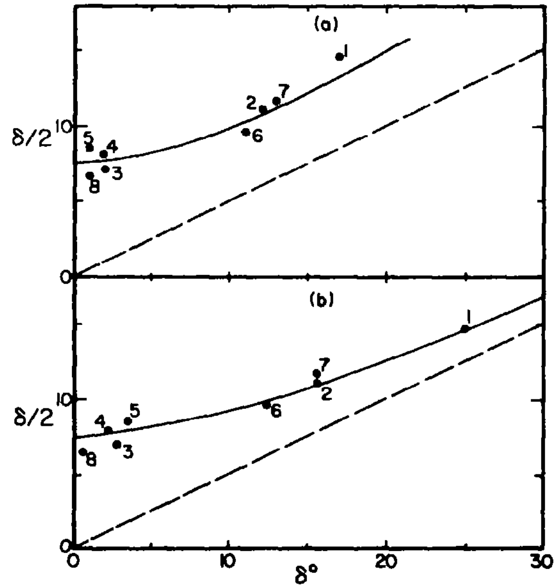

Fig. 7. Plot of $\delta/2$ versus δ^0. a was obtained from the scheme in Fig. 4 and b from the intensity data

Using these equations, δ^0, H_{ij} and a can be calculated (Table 2). These values are plotted in (b) of Figs. 6 and 7, in comparison with those (a) obtained from the scheme in Fig. 4. They agree well, but discrepancies are found when δ^0 is large, e.g. in nonpolar solvents. According to Fermi resonance theory, H_{ij} will decrease

Table 2. Calculated parameters from intensity data

Point No.	Solvent	δ^0	H_{ij}	a
1	Cyclohexane	25.1	6.2	0.97
2	Carbon disulfide	15.5	7.8	0.92
3	Nitromethane	2.8	6.9	0.77
4	Chloroform	2.1	7.9	0.75
5	Bromoform	3.4	8.3	0.77
6	Benzene	12.4	7.2	0.91
7	Carbon tetrachloride	15.6	8.5	0.92
8	Acetonitrile	0.4	6.5	0.72

(Fig. b) and $\delta/2$ will approach to the broken line (Fig. 7) as δ^0 increases. Therefore the values from ϱ data give a better agreement when δ^0 is large. That is, the postulated energy scheme (Fig. 4) may not be completely valid in the nonpolar solvent because ν_{18} get close to ν_c^0 and the interaction may take place between them.

Experimental

Preparation of O^{18}-CP: O^{16}-CP was sealed in a glass tube with dry tetrahydrofuran, "normalized" (low deuterium content) H_2O^{18} and perchloric acid as catalyst. This mixture was heated for 10 h on a steam bath. CP was isolated in purity of 99.5% or better by gas chromatography (6 ft. column of 20% diisodecylphthalate on 60–80 Chromosorb P). The exchange reaction were carried out by D. Samuel of the Weizmann Institute of Science, Rehovoth, Israel. This product was found to contain 38.2% O^{18}-CP by mass spectrometric analysis.

Spectrography: Spectra were measured on a Perkin-Elmer Model 421 spectrophotometer with a dual grating interchange. Solvent absorptions were removed by using matched KBr cells, 0.05 mm thick. The calibration was performed by using water vapor. Overlapped bands were resolved by a graphical method on an assumption of their symmetric shapes to determine the location and the relative absorbance of each band. For ϱ, the maximum relative absorbance of each band was used.

Acknowledgement. The author wishes to express his thanks to his major professor, R. E. Davis, for guidance throughout the course of this work. He also wishes to express his thanks to Prof. Walter F. Edgell for valuable discussions and the use of his infrared spectrophotometer.

Dr. David Samuel provided the O^{18} water and Mrs. I. Wassermann performed the exchange reaction.

References

1. Angell, C. L., Krueger, P. J., Lauzon, R., Leitch, L. C., Noack, K., Smith, R. J. D., Jones, R. N.: Spectrochim. Acta **15**, 926 (1959).
2. Allen, G., Ellington, P. S., Meakins, G. D.: J. chem. Soc. (London) **1960**, 1909.
3. Kim, H., Gwinn, W. D.: J. chem. Physics **51**, 1815 (1969).
4. Lynch, R. L., Christian, S. D., Affsprung, H. E.: J. physic. Chem. **73**, 3263 (1969).
5. Pinchas, S., Samuel, D., Weiss-Broday, M.: J. chem. Soc. (London) **1961**, 2382.
6. Rao, C. N. R., Venkataraghavan, R.: Spectrochim. Acta **18**, 273 (1962).

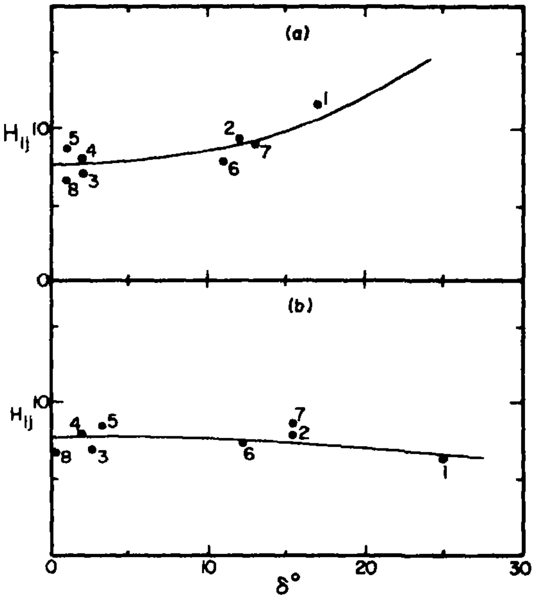

Fig. 6. Plot of H_{ij} versus δ^0. *a* was obtained from the scheme in Fig. 4 and *b* from the intensity data

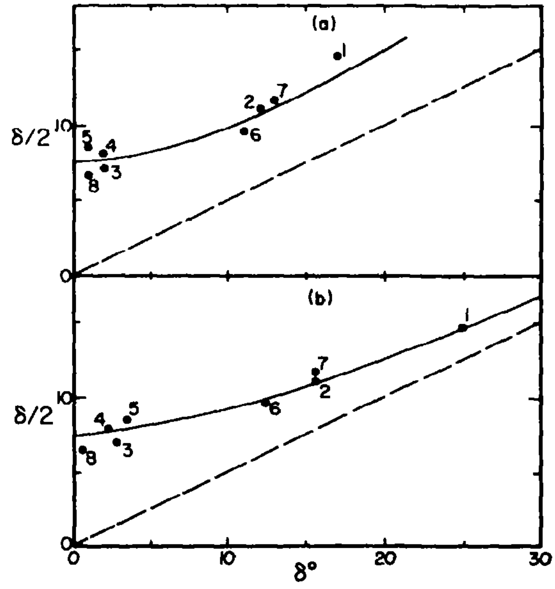

Fig. 7. Plot of $\delta/2$ versus δ^0. *a* was obtained from the scheme in Fig. 4 and *b* from the intensity data

Using these equations, δ^0, H_{ij} and a can be calculated (Table 2). These values are plotted in (b) of Figs. 6 and 7, in comparison with those (a) obtained from the scheme in Fig. 4. They agree well, but discrepancies are found when δ^0 is large, e.g. in nonpolar solvents. According to Fermi resonance theory, H_{ij} will decrease

Table 2. Calculated parameters from intensity data

Point No.	Solvent	δ^0	H_{ij}	a
1	Cyclohexane	25.1	6.2	0.97
2	Carbon disulfide	15.5	7.8	0.92
3	Nitromethane	2.8	6.9	0.77
4	Chloroform	2.1	7.9	0.75
5	Bromoform	3.4	8.3	0.77
6	Benzene	12.4	7.2	0.91
7	Carbon tetrachloride	15.6	8.5	0.92
8	Acetonitrile	0.4	6.5	0.72

(Fig. b) and $\delta/2$ will approach to the broken line (Fig. 7) as δ^0 increases. Therefore the values from ϱ data give a better agreement when δ^0 is large. That is, the postulated energy scheme (Fig. 4) may not be completely valid in the nonpolar solvent because ν_{18} get close to ν_c^0 and the interaction may take place between them.

Experimental

Preparation of O^{18}-CP: O^{16}-CP was sealed in a glass tube with dry tetrahydrofuran, "normalized" (low deuterium content) H_2O^{18} and perchloric acid as catalyst. This mixture was heated for 10 h on a steam bath. CP was isolated in purity of 99.5% or better by gas chromatography (6 ft. column of 20% di-isodecylphthalate on 60-80 Chromosorb P). The exchange reaction were carried out by D. Samuel of the Weizmann Institute of Science, Rehovoth, Israel. This product was found to contain 38.2% O^{18}-CP by mass spectrometric analysis.

Spectrography: Spectra were measured on a Perkin-Elmer Model 421 spectrophotometer with a dual grating interchange. Solvent absorptions were removed by using matched KBr cells, 0.05 mm thick. The calibration was performed by using water vapor. Overlapped bands were resolved by a graphical method on an assumption of their symmetric shapes to determine the location and the relative absorbance of each band. For ϱ, the maximum relative absorbance of each band was used.

Acknowledgement. The author wishes to express his thanks to his major professor, R. E. Davis, for guidance throughout the course of this work. He also wishes to express his thanks to Prof. Walter F. Edgell for valuable discussions and the use of his infrared spectrophotometer.

Dr. David Samuel provided the O^{18} water and Mrs. I. Wassermann performed the exchange reaction.

References

1. Angell, C. L., Krueger, P. J., Lauzon, R., Leitch, L. C., Noack, K., Smith, R. J. D., Jones, R. N.: Spectrochim. Acta **15**, 926 (1959).
2. Allen, G., Ellington, P. S., Meakins, G. D.: J. chem. Soc. (London) **1960**, 1909.
3. Kim, H., Gwinn, W. D.: J. chem. Physics **51**, 1815 (1969).
4. Lynch, R. L., Christian, S. D., Affsprung, H. E.: J. physic. Chem. **73**, 3263 (1969).
5. Pinchas, S., Samuel, D., Weiss-Broday, M.: J. chem. Soc. (London) **1961**, 2382.
6. Rao, C. N. R., Venkataraghavan, R.: Spectrochim. Acta **18**, 273 (1962).

7. Becker, E. D., Ziffer, H., Charney, E.: Spectrochim. Acta **19**, 1871 (1963).
8. Kim, K. S.: Ph. D. Thesis, Purdue University, 1971.
9. Bellamy, L. J., Williams, R. L.: Trans. Faraday Soc. **55**, 16 (1959).
10. Davydov, A. S.: Quantum mechanics transl. by I. V. Schensted, Chpt. 8. Ann Arbor, Michigan: Neo Press 1966.
11. Herzberg, G.: Infrared and Raman spectra, p. 215. New York: D. Van Nostrand 1945.
12. Overend, J.: Infrared spectroscopy and molecular structure, ed. by M. Davis. Chpt. X. New York: Elsevier 1963.

Prof. Dr. R. E. Davis
Department of Chemistry
Purdue University
West Lafayette, Indiana 47907, USA

Theoret. chim. Acta (Berl.) 25, 97—102 (1972)
© by Springer-Verlag 1972

Complete Spin-Orbit Interaction in Many-Electron Atoms*

B. W. N. Lo, K. M. S. Saxena, and S. Fraga
Division of Theoretical Chemistry, Department of Chemistry, University of Alberta, Edmonton 7, Alberta, Canada

Received July 6, 1971

The complete spin-orbit coupling constants have been evaluated, including both the spin-own orbit and the spin-other orbit terms, for all the positive ions, neutral systems, and negative ions from He to Kr, as well as for various isoelectronic series.

Für alle positiven und negativen Ionen und für die neutralen Atome von He bis Kr sowie für verschiedene isoelektronische Serien werden die kompletten Spin-Bahn-Kopplungskonstanten einschließlich der Spin-Bahn-Wechselwirkung verschiedener Elektronen berechnet.

Introduction

Because of its importance, as the main contributor to the splitting of the terms of a multiplet, the spin-orbit interaction in many-electron atoms has received great attention.

The *complete* spin-orbit interaction consists of one-body spin-orbit couplings and two-body, mutual spin-orbit interactions, the latter including both direct and exchange terms. Horie [8] developed the formulation for the two-body, mutual spin-orbit interactions between the open-shell electrons; in the literature this contribution is known under the designation of *spin-other-orbit* interaction. Blume and Watson [2], on the other hand, treated the one-body couplings and the remaining two-body, mutual interactions, which behave (including both the direct and exchange terms) as an effective one-body spin-orbit coupling; in the literature this contribution is known under the designation of *spin-own-orbit* interaction. The most extensive calculations have been carried out by Fraga and co-workers [6, 11, 14], but unfortunately only the spin-own-orbit interaction (without the exchange terms) was considered in that work. On the other hand, Blume and Watson [3], Froese-Fischer [7], and Malli [10] have evaluated the complete spin-orbit interaction for a limited number of systems, using Hartree-Fock functions.

The purpose of the present work is to report now the values of the complete spin-orbit interaction for all the positive ions, neutral atoms, and negative ions from He to Kr, as well as for a number of isoelectronic series.

---

* This work has been supported in part by the National Research Council of Canada.

Theoretical Considerations

The spin-orbit hamiltonian for a many-electron atom is

$$\mathscr{H}_{so} = \tfrac{1}{2}\alpha^2 \sum_i \left\{ Z r_i^{-3} (\boldsymbol{l}_i \cdot \boldsymbol{s}_i) - \sum_{j \neq i} r_{ij}^{-3} (\boldsymbol{r}_{ij} \times \boldsymbol{p}_i) \cdot (\boldsymbol{s}_i + 2\boldsymbol{s}_j) \right\},$$

where the summations extend to all the electrons in the system, characterized by the momentum ($\boldsymbol{p}$), angular momentum ($\boldsymbol{l}$), and spin angular momentum ($\boldsymbol{s}$) vector operators; r_i defines the position of electron i with respect to the nucleus (with charge Z) and r_{ij} is the interelectronic distance between electrons i and j. The fine structure constant is represented by α.

The spin-orbit interaction for a given state may be expressed,

$$(vSLJ|\mathscr{H}_{so}|vSLJ) = (-1)^{S+L+J} \begin{Bmatrix} S & S & 1 \\ L & L & J \end{Bmatrix} (vSL\|\mathscr{H}_{so}\|vSL),$$

in terms of 6-j symbols and double-barred matrix elements. The state under consideration is labelled by the total quantum numbers S, L, J, and the seniority number, v.

The spin-orbit coupling constant, λ, is defined by the relation

$$(vSLJ|\mathscr{H}_{so}|vSLJ) = \lambda\Gamma,$$

with

$$\Gamma = \tfrac{1}{2}[J(J+1) - L(L+1) - S(S+1)],$$

so that

$$\lambda = [S(S+1)(2S+1)L(L+1)(2L+1)]^{-\frac{1}{2}} (vSL\|\mathscr{H}_{so}\|vSL),$$

which can be transformed into

$$\lambda = \eta_1 \zeta_c + \eta_2 M^{(0)} + \eta_3 M^{(2)}$$

(for configurations involving up to d electrons). The spin-own-orbit parameter, ζ_c, defined by Blume and Watson [2], includes the spin-orbit coupling of the electrons in the nuclear coulombic field and the direct and exchange terms of the effective one-body couplings arising from the two-body interactions not included in the spin-other-orbit contribution of Horie [8]; the latter is given by the last two terms in the above expression. The radial integrals, $M^{(k)}$, have been defined by Marvin [12].

The values of the coefficients $\eta(vSL)$ can be determined from the formulas obtained by Horie [8] for the double-barred matrix elements. The corresponding values for up to half-filled shells are presented in Table 1. The values for the conjugated configurations can be obtained by the relations.

$$\eta_1(l^m) = -\eta_1(l^n),$$

$$\eta_2(l^m) = \eta_2(l^n) + [2(m+n) - 6]\,\eta_1(l^n),$$

$$\eta_3(d^m) = \eta_3(d^n) - \tfrac{12}{7}\,\eta_1(d^n),$$

with $m + n = 2(2l+1)$, where l is the orbital angular momentum quantum number of the shell under consideration. These expressions are valid only for p^n and d^n configurations. (The values in Table 1 might also be obtained from the coefficients given by Barnes *et al.* [1].)

Table 1. Values of the parameters $\eta(l^n vSL)$ for some important configurations[a]

Configuration	State[b]	η_1	η_2	η_3
p^1	${}^2_1P$	1		
p^2	${}^3_2P$	$\frac{1}{2}$	-6	
p^3	${}^2_3D$	0	$-\frac{37}{5}$	
	${}^2_1P$	0	-5	
d^1	${}^2_1D$	1		
d^2	${}^3_2F$	$\frac{1}{2}$	$-\frac{27}{7}$	$\frac{51}{49}$
d^3	${}^4_3F$	$\frac{1}{3}$	$-\frac{38}{7}$	$-\frac{6}{49}$
d^4	${}^5_4D$	$\frac{1}{4}$	-6	$\frac{3}{7}$

[a] *These parameters vanish for the states* ${}^1D(p^2)$, ${}^1S(p^2)$, ${}^4S(p^3)$, and ${}^6S(d^5)$.

[b] The seniority number, v, is given as a left subscript.

Results and Discussion

Tables 2–5 collect all the values of λ for the systems under consideration, with comparison to the experimental values obtained from the data of Moore [13], as given by Fraga and co-workers [5, 14]; the latter are given in brackets. The values[1] of ζ_c and $M^{(k)}$ have been obtained from the analytical Hartree-Fock functions of Clementi [4] and Malli [9].

Calculations have also been carried out for the first positive ion of the configurations $K(2)\,L(8)\,3s^2\,3p^6\,3d^n\,4s^2$. The corresponding absolute values are: Ti, $3d^1$ ${}^2D$, 147 (93); V, $3d^2$ ${}^3F$, 101; Cr, $3d^3$ ${}^4F$, 88 (84); Mn, $3d^4$ ${}^5D$, 85 (87); Co, $3d^6$ ${}^5D$, 158 (144); and Ni, $3d^7$ ${}^4F$, 256. (The experimental values are given in parentheses.)

The agreement with the experimental values, excellent for the light elements, deteriorates as one progresses along the periodic system, reflecting the fact that the LS coupling is not appropriate for the heavy elements.

For simplicity, no comparison is made here with the results of Blume and Watson [3], but it must be mentioned that the agreement is excellent, better for the light elements than for the heavy atoms: the largest difference is 4 cm^{-1} for Cl, Ga, and Se. The exception, however, is Br, where the present value is 2211 cm^{-1} while Blume and Watson [3] predict a value of 2194 cm^{-1}; it is evident that the difference (17 cm^{-1}) between both theoretical results is negligible relative to the difference (well over 200 cm^{-1}) with the experimental result of 2454 cm^{-1}.

In addition, it should be pointed out that the relative weights of the direct and exchange terms within the spin-own-orbit contribution are similar to those observed by Blume and Watson [3]; for that reason the discussion is not repeated here. It should be sufficient to mention that a simple comparison (for systems with the open shell occupied by only one electron, where the spin-other-orbit interaction vanishes) with the values of Malli and Fraga [11], that included only the direct terms, reveals that the exchange contribution may be as high as 30% (relative to the uncorrected value) for B, decreasing to about 3% for heavier atoms.

---

[1] The values of all the radial integrals needed have been collected in the Technical Report TC-7105, Department of Chemistry, University of Alberta. This Technical Report has been placed at the Depository of Unpublished Data, National Science Library, National Research Council, Ottawa 7, Canada K1A OR6. A limited number of copies is available upon request.

Table 2. Absolute values[a] (in cm^{-1}) of the spin-orbit coupling constant, λ, for positive ions, neutral atoms, and negative ions

Configuration[b]	State	Positive ions		Neutral atoms		Negative ions	
		System	λ	System	λ	System	λ
$2p^1$	^2P	C	43	B	10		
			[43]		[11]		
$2p^2$	^3P	N	42	C	14	B	2
			[45]		[15]		
$2p^3$	^2D	O	11	N	5	C	2
	^2P		7		3		1
$2p^4$	^3P	F	171	O	81	N	31
			[160]		[74]		
$2p^5$	^2P	Ne	517	F	268	O	120
			[521]		[269]		
$3p^1$	^2P	Si	169	Al	62		
			[191]		[75]		
$3p^2$	^3P	P	140	Si	65	Al	19
			[159]		[75]		
$3p^3$	^2D	S	2	P	1	Si	0.4
	^2P		1		0.7		0.3
$3p^4$	^3P	Cl	319	S	183	P	90
			[324]		[188]		
$3p^5$	^2P	A	896	Cl	549	S	302
			[955]		[587]		
$3d^1$	^2D			Sc	77		
					[67]		
$3d^2$	^3F	Sc	31	Ti	59	Sc	27
			[27]		[54]		
$3d^3$	^4F	Ti	32	V	55	Ti	30
			[30]		[51]		
$3d^4$	^5D	V	35	Cr	56	V	33
			[36]		[53]		
$3d^6$	^5D	Mn	77	Fe	112	Mn	75
			[62]		[104]		
$3d^7$	^4F	Fe	131	Co	186	Fe	129
			[117]		[181]		
$3d^8$	^3F	Co	244	Ni	338	Co	242
			[227]		[333]		
$3d^9$	^2D	Ni	608	Cu	821		
			[603]				
$4p^1$	^2P	Ge	1018	Ga	464		
			[1178]		[551]		
$4p^2$	^3P	As	725	Ge	399	Ga	139
			[740]		[426]		
$4p^3$	^2D	Se	1	As	0.7	Ge	0.3
	^2P		0.8		0.5		0.2
$4p^4$	^3P	Br	1269	Se	829	As	472
			[1570]		[995]		
$4p^5$	^2P	Kr	3226	Br	2211	Se	1381
			[3581]		[2457]		

[a] The values for p^n, with $n > 3$, and d^n, with $n > 5$, are negative.

[b] The positive ions of the transition elements (from Sc through Ni) have configurations $4s^0\,3d^n$.

Table 3. Absolute values[a] (in cm^{-1}) of the spin-orbit coupling constant, λ, for the isoelectronic series[b] $2p^n$

System	$2p^1$, ^2P	$2p^2$, ^3P	$2p^4$, ^3P	$2p^5$, ^2P
B	10			
	[11]			
C	43	14		
	[43]	[15]		
N	118	42		
	[116]	[45]		
O	263	100	81	
	[258]	[105]	[74]	
F	507	202	171	268
	[497]	[210]	[160]	[269]
Ne		365	318	517
		[382]	[301]	[521]
Na			543	906
			[512]	[909]
Mg			869	1477
			[185]	[1484]
Al				2281
				[2293]

[a] The values are negative for $n > 3$.
[b] With configurations $K(2)\,2s^2\,2p^n$.

Table 4. Absolute values[a] (in cm^{-1}) of the spin-orbit coupling constant, λ, for the isoelectronic series[b] $3p^n$

System	$3p^1$, ^2P	$3p^2$, ^3P	$3p^4$, ^3P	$3p^5$, ^2P
Al	62			
	[75]			
Si	169	65		
	[191]	[75]		
P	338	140		
	[373]	[159]		
S	586	252	183	
	[633]	[284]	[188]	
Cl	930	411	319	549
	[995]	[458]	[324]	[587]
A		625	506	896
		[699]	[507]	[955]
K			756	1362
			[744]	[1441]
Ca			1079	1969
			[1037]	[2077]
Sc				2741
				[2885]

[a] The values are negative for $n > 3$.
[b] With configurations $K(2)\,L(8)\,3s^2\,3p^n$.

Table 5. Absolute values[a] (in cm^{-1}) of the spin-orbit coupling constant, λ, for the isoelectronic series[b] $3d^n$

System	$3d^1$, ^2D	$3d^2$, ^3F	$3d^3$, ^4F	$3d^4$, ^5D	$3d^6$, ^5D	$3d^7$, ^4F	$3d^8$, ^3F	$3d^9$, ^2D
Sc	86	31						
	[79]	[27]						
Ti	158	63	32					
	[154]	[60]	[30]					
V	253	106	57	35				
	[248]	[105]	[56]	[36]				
Cr	377	163	91	57				
	[383]	[165]	[92]	[58]				
Mn	535	236	135	87	76			
	[542]	[240]	[135]	[90]	[62]			
Fe			189	125	115	131		
			[192]	[133]	[100]	[117]		
Co				172	162	189	244	
				[186]		[176]	[227]	
Ni					221	262	344	608
							[322]	[603]
Cu					292	349	465	833
								[829]
Zn						455	612	1107

[a] The values are negative for $n > 5$.

[b] With configurations $K(2)\ L(8)\ 3s^2\ 3p^6\ 3d^n$.

References

1. Barnes, J. A., Carroll, B. L., Flores, L. M., Hedges, R. M.: Atomic Data **2**, 1 (1970).
2. Blume, M., Watson, R. E.: Proc. Roy. Soc. (London) A **270**, 127 (1962).
3. Proc. Roy. Soc. (London) A **271**, 565 (1962).
4. Clementi, E.: Tables of atomic functions. San Jose: IBM 1965.
5. Fraga, S., Malli, G.: Many-electron systems: Properties and interactions. Philadelphia: W. B. Saunders Co. 1968.
6. , Thorhallsson, J., Fisk, C.: Canad. J. Physics **47**, 1415 (1969).
7. Froese-Fischer, C.: Canad. J. Physics **45**, 1501 (1967).
8. Horie, H.: Progr. theoret. Physics (Kyoto) **10**, 296 (1953).
9. Malli, G.: Canad. J. Physics **44**, 3121 (1966).
10. J. chem. Physics **48**, 1088 (1968).
11. – , Fraga, S.: Theoret. chim. Acta (Berl.) **7**, 80 (1967).
12. Marvin, H. H.: Physic Rev. **71**, 102 (1947).
13. Moore, C. E.: Natl. Bur. Standards (U.S.), Circ. No. 467 (1949).
14. Thorhallsson, J., Fisk, C., Fraga, S.: J. chem. Physics **48**, 2925 (1968).

Prof. Dr. S. Fraga
Division of Theoretical Chemistry
University of Alberta
Edmonton 7, Alberta, Canada

Theoret. chim. Acta (Berl.) 25, 103—119 (1972)
© by Springer-Verlag 1972

Theoretical Investigations on the Solvation Process

II. The Monohydrated Associates of Some Three-Membered Ring Molecules

GIULIANO ALAGONA, RENZO CIMIRAGLIA, EOLO SCROCCO, and JACOPO TOMASI
Laboratorio di Chimica Quantistica ed Energetica Molecolare del C.N.R.,
Via Risorgimento 35, I-51100 Pisa, Italy

Received December 23, 1971

The conformation energies for monohydrated associates $M \cdot H_2O$, where M stands for oxirane, aziridine, oxaziridine and cyclopropene, have been obtained by using an electrostatic method, tested in a preceding paper, which relies on SCF molecular potentials calculated exactly. Stable associates have been found in the heterogroup region as well as near the bent bonds (single or double).

A discussion is made on the errors in calculating thermodynamic properties for such associates in gas phase by using *a priori* calculations. As a numerical example the free energy change in the association process is compared for two monohydrated associates of aziridine.

Die Konformationsenergien für Anlagerungsverbindung $M \cdot H_2O$, wobei M für Oxiran, Aziridin, Oxaziridin und Cyclopropen steht, werden mit einer elektrostatischen Methode berechnet. Dieses Verfahren wurde in einer vorhergehenden Veröffentlichung getestet und beruht auf exakt berechneten SCF-Molekülpotentialen. Stabile Anlagerungsverbindungen wurden für Konformationen gefunden, bei denen das Wassermolekül in der Nähe der Heterogruppe oder der gezogenen Einfach- oder Doppelbindung liegt. Die Fehler bei der Berechnung thermodynamischer Eigenschaften für derartige Anlagerungsverbindungen in der Gasphase werden abgeschätzt. Als ein numerisches Beispiel wird die Differenz der freien Energie bei der Anlagerung für zwei Anlagerungsverbindungen von Aziridin und Molekül Wasser verglichen.

1. Introduction

In a preceding paper [1] (hereafter called I) we proposed and tested a simple procedure useful to obtain a qualitative prediction of the most stable conformations of molecular hydration associates. Such a procedure must be considered only as a guide to reducing the number of geometries to be examined with correct quantum-mechanical methods.

The simple case of a monohydration associate AB where A stands for water and B is a molecule having at least a polar (hydrophilic) group is studied here using the electrostatic approach of paper I. Once the distance between the water molecule and the group chosen for solvation is determined, it is assumed that the changes of the interaction energy with orientation are solely controlled by the shape of the electrostatic fields generated by the two molecules. According to this assumption (the "electrostatic assumption"), the interaction energy can be written as:

$$\Delta E = \int d\tau_1 \left[\varrho_A(x_1) - \sum_\alpha Z_\alpha \delta(x_1 - x_\alpha)\right] \cdot \int d\tau_2 \left[\varrho_B(x_2) - \sum_\beta Z_\beta \delta(x_2 - x_\beta)\right] \cdot \frac{1}{|x_1 - x_2|} \tag{1}$$

$\varrho_A(x_1)$ and $\varrho_B(x_2)$ are the electronic density functions of the two single molecules, $\sum_{\alpha}^{\text{nucl}} Z_\alpha \delta(x_1 - x_\alpha)$ is the nuclear charge density distribution of A, etc. The second integral of the right-hand side of Eq. (1) represents the electrostatic potential produced by molecule B. One can therefore write:

$$\Delta E = \int d\tau_1 \left[\varrho_A(x_1) - \sum_\alpha Z_\alpha \delta(x_1 - x_\alpha) \right] V_B(x_1). \tag{2}$$

A partial justification of this assumption may be drawn, *a posteriori*, by examining the partition of the hydrogen-bond energy of associates thus far performed on *ab initio* calculations. From such analysis on H_2O dimer [2], formamide dimer [3], and H_2CO-H_2O associate [4], it was actually found that the coulombic portion of the interaction energy (i.e. the electrostatic energy) is nearly equal to the SCF interaction energy for large separations, beginning from distances a little greater than the equilibrium one. This trend is due to a cancellation, in this distance range, of the exchange, polarization and charge transfer portion of the energy[1]. At the equilibrium distance the coulombic portion becomes greater than the SCF interaction energy: for the three associates here considered the differences are, respectively: 1.4 kcal/mole (22%), 1.2 kcal/mole (16%) and 1.2 kcal/mole (34%).

As regards the variation of the interaction energy with respect to the reciprocal orientation of the two partners, the available data on the three systems considered, show that the SCF interaction energy and its coulombic portion run in a noticeably parallel fashion [1 4]. A unique exception concerns a set of conformations of the H_2CO-H_2O associate (model B of Ref. [4]), where however the O···H···O distance undergoes remarkable changes during the rotation involved.

As a practical method to calculate the electrostatic interaction energy, in I it was proposed to use an approximation of Eq. (2), where the molecular potential $V_B(x_1)$ is rigorously obtained *via* SCF MOLCAO calculations and the water molecule charge distribution (molecule A in Eq. (2)) is replaced by a suitable point-charge set which has the same dipole and quadrupole moments as those of a SCF wavefunction. This point-charge distribution also adequately reproduces in the neighbouring regions the same electrostatic potential as is calculated from a SCF wavefunction of H_2O. The interaction energy is then reduced to the simple sum:

$$\Delta E = \sum_k q_k(k)\, V_B(k), \tag{3}$$

where q_k are the values of the point charges, which are placed at the points k.

In paper I this procedure was checked, with fairly encouraging results, on the water dimer. In the present paper we will use Eq. (3) firstly to search for the most stable conformations of monohydration associates for some three-membered ring molecules, secondly to obtain a first guess about the most important contributions to the thermodynamic properties of such associates. The electrostatic potentials

---

[1] We have adopted here the terminology of Ref. [4] to which reference is made for detailed definitions. We note here that the electrostatic energy as defined by Kollman and Allen [5] in their analysis of H_2O and HF dimers is somewhat different.

V_B of the cyclic molecules here considered are taken from previous SCF MOLCAO calculations [6, 7]; the point charge model for H_2O is the same as in paper I.

The electrostatic method does not allow one to find the equilibrium distances between the two associated molecules. Reasonable distances, selected with reference to the experimental one of other hydrogen-bond associates, were employed throughout our calculations, but, as a result of several checks with other distances, we can state that the main conclusions of the conformational analysis do not depend considerably on the value employed.

2. Choice of a Reference System for the Geometry of the Associates

The associates between three membered ring molecules and water, both species being considered as rigid bodies, possess six internal degrees of freedom, three for determining the position of a point in the H_2O molecule -- which we always chose as the oxygen nucleus – and three for describing the orientation of water with respect to the organic molecule.

For the first three degrees of freedom we chose polar systems differing according to the hydration zone we are interested in. All polar systems employed have the polar axis lying on the ring plane, perpendicular to a bond and passing through the opposite nucleus (an arrow in the figures indicates the positive direction). When hydration of a heterogroup is considered, the origin of the reference system will be in the heteroatom nucleus whereas, when the hydration of a ring bond is considered, it will be in this very bond. In all cases the azimuthal ϕ angles will be measured from the ring plane. Typical examples are shown in Figs. 1 and 11.

As regards the second three degrees of freedom, we shall describe them by three rotation angles about three orthogonal axes ξ, η and ζ defined as follows: the η axis connects the O nucleus of water to the polar system center, the ζ axis is parallel to the ring plane and the ξ axis is determined by the left-handedness of the system.

Associates having the same values of the polar coordinates will be referred to as *conformations* belonging to the same *configuration*. Given a configuration, a starting conformation must be defined; this will be done in the text according to the particular cross-section of the energy hypersurface we are interested in. In such a way it is possible to define each set of conformations considered in this paper in terms of rotations around an axis alone. For the reader's convenience we have reported for each cross section (Figs. 1–12) a sketch of the starting conformation together with an indication of the direction of axes and of the rotation involved. Such a sketch will be also useful for a complete definition of the azimuthal ϕ angles, allowance being made that we assume as origin the molecular half-plane on the left of the figure.

3. Monohydrates of Oxirane: $(CH_2)_2O \cdot H_2O$

Chemical intuition suggests that association of oxirane with a water molecule will occur through a hydrogen-bond where the H_2O molecule acts as a proton donor and the oxygen atom of oxirane as acceptor group. We actually find the

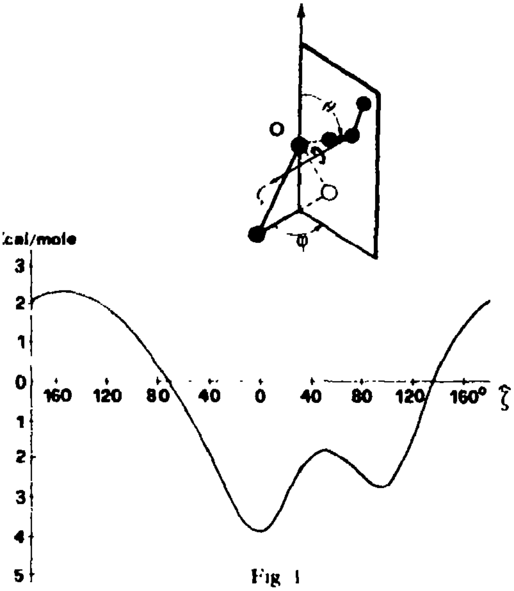

Fig. 1

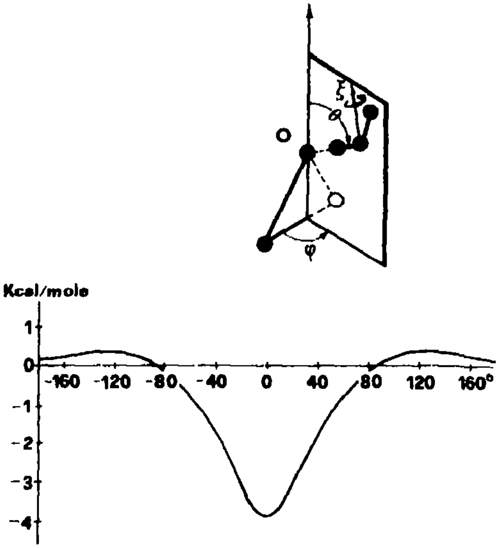

Fig. 2

Fig. 1. Interaction energy between oxirane and water in the associate $(CH_2)_2O \cdot H_2O$. Rotation of the H_2O molecule around its ζ axis. For the position of H_2O see the text

Fig. 2. Interaction energy in the associate $(CH_2)_2O \cdot H_2O$. Rotation of the H_2O molecule around its ξ axis

most stable associate ($\Delta E = -3.8$ kcal/mole) at $\phi = 90°$ and $\theta = 63°$ (or in the equivalent position at $\phi = 270°$, $\theta = 63°$), i.e. with a direction of the O—O axis almost corresponding to that of an oxirane O lone pair[2]. Moreover, in the most stable conformation the O—H bond directly involved in the association is exactly collinear with the O—O axis. This can be verified by the aid of Figs. 1, 2, 3 where some cross-sections of the energy hypersurface, related to conformations pertaining to the most stable configuration, are reported.

Fig. 1 refers to conformations differing among them by a rotation about the ζ axis. The starting conformation (sketched in the figure) is the most stable: the H_2O molecule lies in the plane perpendicular to the ring with a O—H bond pointing directly towards the heteroatom. The second minimum, relating to a rotation of $\zeta = 96°$, again corresponds to an almost linear hydrogen bond. The non equivalence of the two minima and the slight deviation from linearity of the second stable conformation ($\hat{\zeta} = 96°$ instead of 104°) are presumably due to destabilizing electrostatic effects of the CH_2—CH_2 group.

A rotation around ξ axis is decidedly hindered (see Fig. 2), the starting conformation being at the bottom of a fairly deep hole. On the contrary the rotation around η axis (Fig. 3) is almost free: the barrier height is 1.4 kcal/mole.

The picture of the association of water to the ring oxygen obtained with the present method corresponds to a classical linear hydrogen bond. It may be of

---

[2] The localization of the molecular orbitals of oxirane, performed in Ref. [6], leads to a couple of oxygen lone pair orbitals having its charge centers at $\theta = 68°$ ($\phi = 90°$ and 270°).

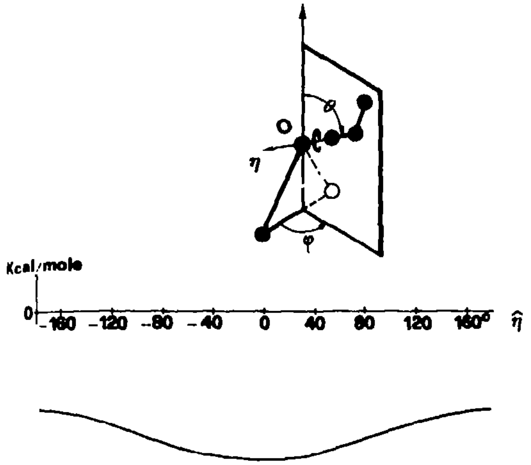

Fig. 3

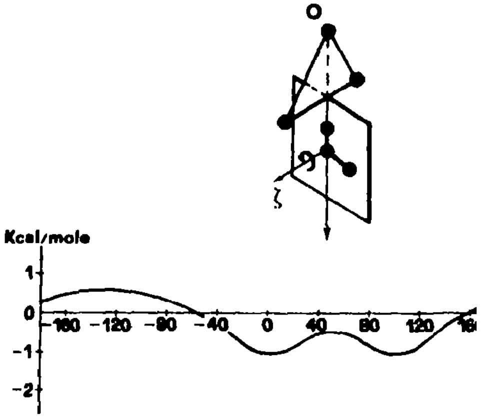

Fig. 4

Fig. 3. Interaction energy in the associate $(CH_2)_2O \cdot H_2O$. Rotation of the H_2O molecule around its η axis

Fig. 4. Interaction energy between $(CH_2)_2O$ and H_2O. Hydrocarbon zone: rotation around ζ axis

some interest to point out that the "bifurcated" associate, with the H_2O molecule perpendicular to the ring plane and with the two O–H bonds symmetrically pointing towards the two lone pairs, is not favoured.

For all the configurations thus far considered the r value was kept constant at $r = 2.76$ Å; this value, as above said, was selected according to experimental values of other hydrogen bonds, but as a check we have repeated the calculations using larger and smaller values ($\Delta r = \pm 0.2$ Å) and found that the position of the minima and the shape of energy hypersurface did not change significantly.

The electrostatic potential maps of oxirane (Figs. 10 and 11 of Ref. [6]) show that the direction of the hydrogen bonds does not correspond exactly either to the direction of the minima of $V(x)$ ($\theta \simeq 54°$) or to the directions of larger potential gradient. It is convenient to point out here that we shall not search close relations between potential gradient and geometry of associates because it would correspond to reducing the H_2O charge distribution to a single point dipole. It is a well known fact that such an approximation is largely unsatisfactory for several reasons, the first being that it is not able to reproduce the directional properties of the hydrogen bond.

Keeping in mind such cautionary remarks, one can however use the shape and the sign of the electrostatic potential to obtain a first indication of the regions of the outer molecular space where association is more probable. For example, from Figs. 10 and 11 of Ref. [6] a second minimum of $V(x)$ for oxirane in the region near the bent C–C bond is evident. The hydration of the C–C bond is indeed possible according to our model. The most stable configuration corresponds to $\theta = 0°$ in its polar system. The stabilization energy is decidedly lower than in the preceding case (-1.1 kcal/mole against -3.8 kcal/mole). As an example the rotation around ζ axis is shown in Fig. 4. The two minima correspond to two symmetrical conformations, both having an O – H bond along the C_2 symmetry axis of oxirane, while the H_2O molecule lies in the plane perpendicular to the ring. This is the best configuration we have found in this region. The electrostatic model does not evidence noticeable barriers for rotations around η axis; a single minimum appears for rotations around ζ axis (corresponding to the best conformation of Fig. 4). In this case, again, the shape of the conformation curves are not heavily dependent on the r value; the curve reported in Fig. 4 refers to an r value such as to allow a penetration of the van der Waals spheres of about 10%.

In this molecule each CH_2 group is surrounded by a region of positive $V(\mathbf{x})$ values (see again Fig. 10 in Ref. [6]) which could in principle lead to associates where the H_2O molecule acts as proton acceptor. In this zone we find so small a stabilization energy (~0.2 kcal/mole) as not to deserve here a more detailed analysis.

4. Monohydrates of Aziridine: $(CH_2)_2NH \cdot H_2O$

When compared with oxirane, the situation for aziridine monohydrates is more complex. In the heterogroup region it will now be possible to have hydrogen bonds with the H_2O molecule acting both as proton acceptor (N – H bond region) and as donor (N lone pair region).

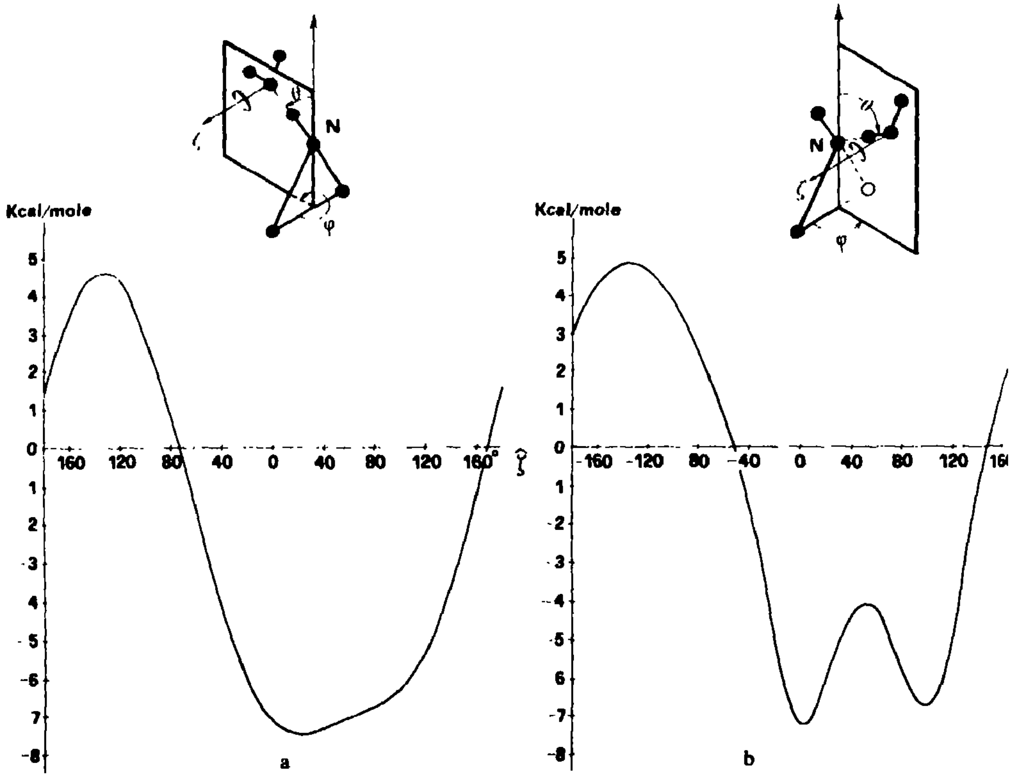

Fig. 5a and b. Interaction energy in the associate $(CH_2)_2NH \cdot H_2O$. Rotation of the H_2O molecule around its ζ axis. a Association to the NH bond, b association to the N lone pair

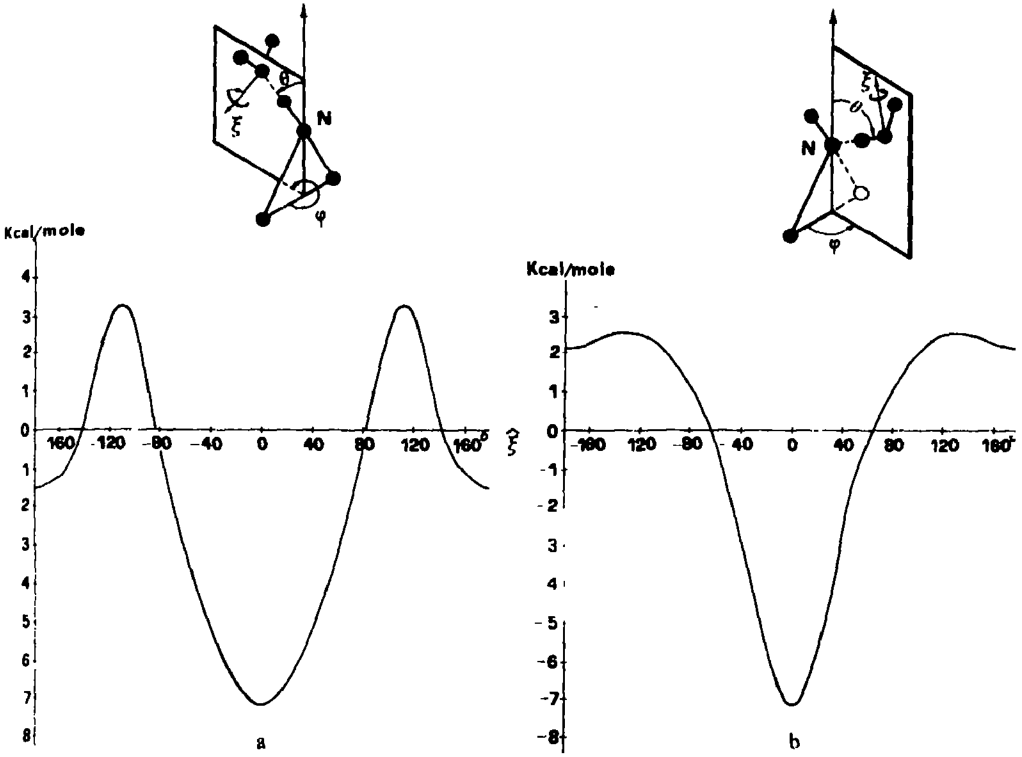

Fig. 6a and b. As Fig. 5, rotations around ξ axes

We actually find in the N–H region a minimum of -7.3 kcal/mole at $\phi = 270°$ and $\theta = 68°$ (the H_2O oxygen nucleus exactly lies in the line of the N–H bond), the most stable conformation having an oxygen lone pair almost collinear with the N–H bond. In the N lone pair region the minimum is found at $\phi = 90°$ and $\theta = 62°$ [3]; its value is nearly the same as in the preceding case (-7.1 kcal/mole) but, as it will be shown immediately, the shape of the energy hypersurface is decidedly different.

In order to facilitate comparisons between the two associates, the conformation energy graphs are reported two by two in Figs. 5a, b; 6a, b; 7a, b. Figs. 5 refer to rotations around ζ axis. Fig. 5a shows a trend of the stabilization energy very close to that found in the corresponding rotation of dimeric water (paper I, Fig. 6) [4]; we note that in the present case the starting conformation has the O lone pair center exactly collinear with the N–H bond. Fig. 5b is similar to the corresponding one of oxirane (Fig. 1 of this paper), although differences in depth and curvature are evident.

---

[3] The charge center of the N lone pair localized orbital lies at $\theta = 56°$, while the minimum of $V(x)$ is at $\theta = 55°$ (see Ref. [6]).

[4] The electrostatic model there employed was tailored on minimal basis set SCF wavefunctions: it is gratifying to observe that the far more accurate calculations of Hankins, Moskowitz and Stillinger on the H_2O dimer [8] confirm the shape of the curve in question.

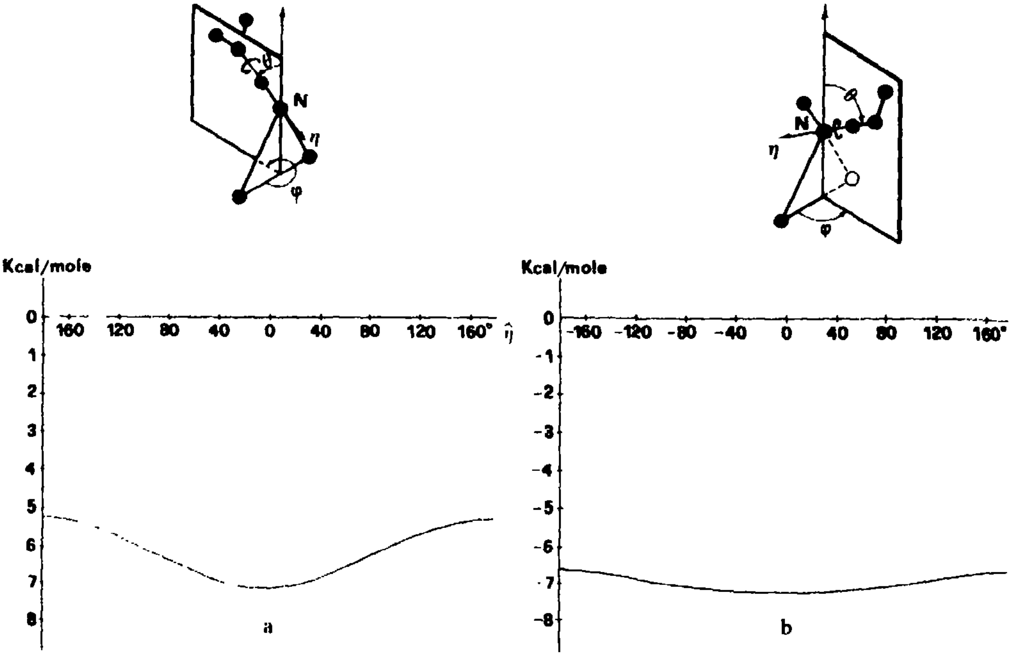

Fig. 7a and b. As Fig. 5, rotations around η axes

Rotations about ξ and η axes are reported in Figs. 6 and 7; in both cases the difference between the two associates are evident and will not be further discussed here. It is clear that such differences in the shape of the energy hypersurface between the two associates, if confirmed by more accurate calculations, could produce sensible differences in their thermodynamic stabilities. This topic will be considered later.

Solvation of the CH_2–CH_2 group leads in aziridine to results very similar to those found in oxirane (Fig. 4). The minimum is slightly lower than in oxirane ($\Delta E \simeq -1.8$ kcal/mole) and corresponds to the same configuration. Oxirane had two equivalent conformations while in aziridine the most stable one has the H_2O molecule lying in the half plane which also contains the N lone pair.

5. Monohydrates of Oxaziridine: $CH_2ONH \cdot H_2O$

The main interest in studying the hypothetical water associates of CH_2ONH lies in the fact that oxaziridine contains at the same time in its ring the two heterogroups (O and NH) already seen separately.

The most stable configuration in the oxygen zone is found at $\phi = 90°$, $\theta = 63°$ ($\Delta E = -3.7$ kcal/mole). A second minimum is found at $\phi = 270°$, $\theta = 57°$ ($\Delta E = -3.5$ kcal/mole); this little difference in the minima is presumably due to the different electrostatic interaction with the NH bond and the N lone pair orbital. In this case, again, a correspondence between the most stable configuration and

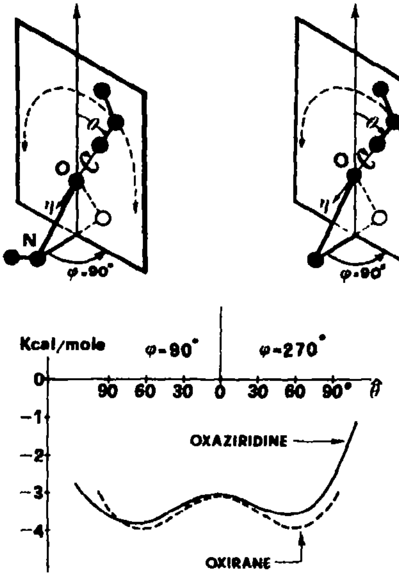

Fig. 8. Comparison of the stabilization energies in $(CH_2)_2O$ and CH_2ONH monohydrates with association in the O ring region

the direction of lone pairs can be found: the localized lone pair orbitals of Ref. [7] have charge centers at $\phi \simeq 90^\circ$, $\theta \simeq 67^\circ$ and $\phi \simeq 270^\circ$, $\theta \simeq 67^\circ$ respectively.

Configuration curves are similar in oxirane and oxaziridine. In the first case the barrier heigth between the two equivalent configurations is about 0.9 kcal/mole while for oxaziridine associates we found that the higher of the two different barriers is about 0.7 kcal/mole. Fig. 8 reports for both molecules the stabilization energies for the best conformation of each configuration considered. In all cases the $\hat{\xi}$ and $\hat{\zeta}$ optimum angles are equal to zero, while the orientation of H_2O around the hydrogen bond changes with θ angle and at the minimum corresponds to $\hat{\eta} = 240^\circ$ for oxaziridine and to $\hat{\eta} = 0^\circ$ for oxirane. The curves here reported refer to the best configurations we have found; however an analysis of the stabilization energy for configurations having the H_2O oxygen nucleus in planes different from that shown in Fig. 8 showed a relatively high freedom in the motion relating to the ϕ coordinate.

Conformation curves for the oxaziridine associate in this oxygen zone are not reported; they are very similar to the corresponding one of oxirane (see Figs. 1–3).

The most stable configuration for the associate in the N–H region corresponds to $\phi = 270^\circ$, $\theta = 68^\circ$ (i.e. the same values as in the aziridine monohydrate), with a stabilization energy of -7.6 kcal/mole. Fig. 9 shows the rotations around ζ axis, starting from the conformation having the water O lone pair charge center on the N–H···O axis; the resemblance with Fig. 5a is very close. Also in this case the best conformation has not the lone pair charge center exactly collinear with the hydrogen bond axis: the angle between the N–H straigth line and the oxygen lone pair center direction, which was about 20° in the aziridine case is now 30°.

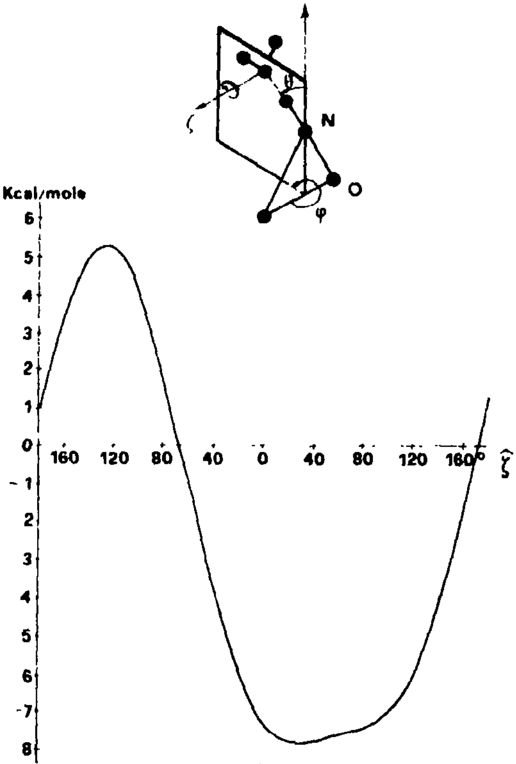

Fig 9

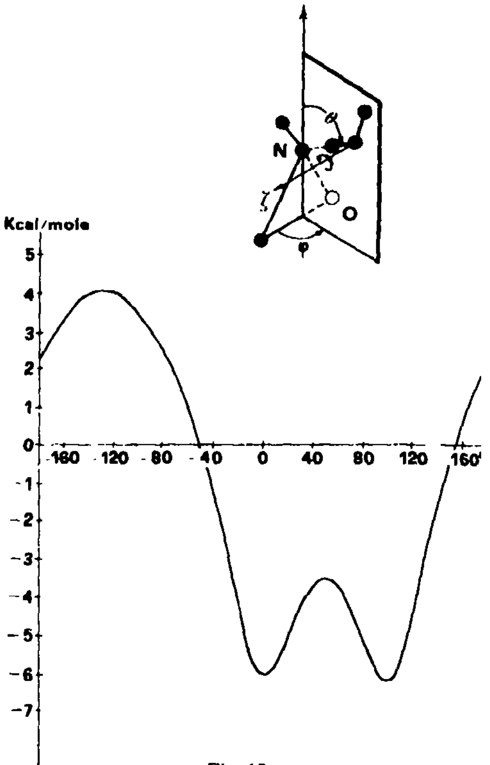

Fig. 10

Fig. 9. Interaction energy between CH_2NHO and H_2O. Association in the NH region

Fig. 10. Interaction energy between CH_2NHO and H_2O. Association in the N lone pair region

Rotations around η axis (almost free) and around ζ axis (a deep hole) are very similar to the corresponding ones of the aziridine monohydrate and are not reported here.

The association in the N lone pair region leads to a minimum at $\phi = 90°$, $\theta = 63°$ ($\Delta E = -6.1$ kcal/mole). Such configuration is at the bottom of a relatively deep hole with respect to the ϕ coordinate. Also in this case two conformations, nearly equivalent and both corresponding to linear $O-H \cdots N$ bonds, are possible. Such conformations are evident in Fig. 10; a comparison with Fig. 5b shows that interactions with the oxygen atom of the ring lead to a small stabilization of the conformer having the second H atom pointing downwards. Other sections of the interaction energy hypersurface (rotations about η and ζ axes) are again very similar to the corresponding one of aziridine and are not reported here.

From the comparison between oxaziridine and the two molecules of oxirane and aziridine, we could state, as a sort of conclusion, that both the geometry of most stable associate and the interaction energy do not change drastically when substitutions are made in a molecule. The changes we found can be explained in terms of electrostatic effects of the substituent groups.

6. Monohydrates of Cyclopropene: $(CH)_2CH_2 \cdot H_2O$

For a study about the hydration of hydrocarbon groups we chose cyclopropene instead of the saturated analogue cyclopropane because the association near the C–C single bond has been already seen in oxirane and aziridine while the C=C double bond presents obvious interesting features[5].

The electrostatic potential $V(x)$ for cyclopropene has four nearly equivalent minima. The first two are in the region of the double bond and are symmetrically placed on either side of the ring plane (see Fig. 17 of Ref. [6]); the presence of such minima may be related to a description of a strained double bond system in terms of two banana bonds. The other two minima are near each C–C single bond, and are placed in the ring plane (see Fig. 18 of Ref. [6]).

We found four configurations of water monoassociate having practically the same energy. The first couple corresponds to the two double bond potential minima. In a polar reference frame centered on the midpoint of the C=C bond and with polar axis pointing outwards (see also Fig. 11) the best configurations are at $\theta = 50°$ (the minima of $V(x)$ are at $\theta = 58°$ and the banana bond charge centers at $\theta = 71°$) and $\phi = 90°$ and 270°. The energy changes for variations of θ are very small and the barrier heigth at $\theta = 0°$ is of the order of 0.5 kcal/mole. The best conformation ($\Delta E = -2.9$ kcal/mole) has the H_2O molecule in the plane perpendicular to the ring, with a O–H bond pointing approximately towards the C=C midpoint while the other H nucleus is at a θ angle greater than the O nucleus. A secondary minimum corresponds to a hydrogen bond made with the other O–H bond: see Fig. 11 where the starting conformation has the H$\hat{O}$H angle bisector pointing towards the polar axes center.

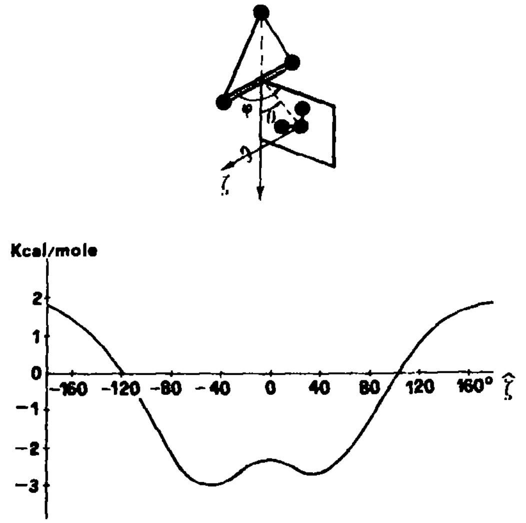

Fig. 11. Interaction energy between $(CH)_2CH_2$ and H_2O. Association in the C–C double bond region

---

[5] It is perhaps superfluous to remark that the trend of association of water to C–C and C=C bonds will surely change in going to unstrained molecules.

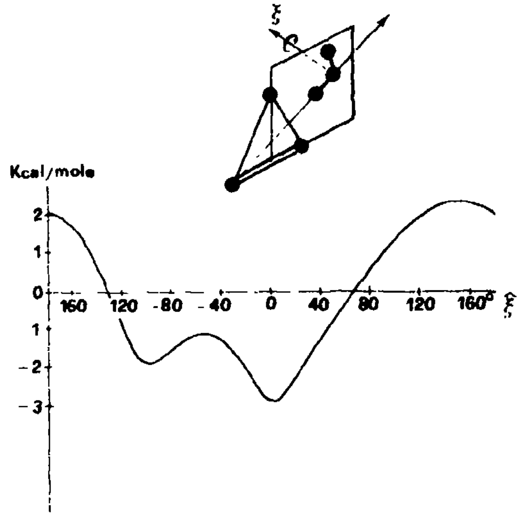

Fig. 12 As Fig. 11, association in the C–C single bond region

The second couple of symmetrical configurational minima is related to water association near the two C–C single bonds. One of such two configurations is depicted in Fig. 12 ($\theta = 0°$). In the best conformation ($\Delta E = -2.9$ kcal/mole) the H_2O molecule lies in the cyclopropene ring plane with an OH bond perpendicular to the C–C bond. The second OH bond, is directed as shown in the sketch of Fig. 12. Rotations around ξ axis show a second conformational minimum having the other OH almost perpendicular to the C–C bond.

Hydration of the CH_2 group leads to stabilization energies always less than 1 kcal/mole and no minima have been found; in this region the energy hypersurface presents a saddle point.

All results for cyclopropene have been checked by changing the distance of the water molecule from the relevant functional group (C=C and C–C) in the range 2.5 3.4 Å. Changes in the shape of the conformation (and configuration) curves are not observed, while, as expected, the absolute values of ΔE show an r dependence analogous to that found in paper I for water dimer.

7. Thermodynamic Stability of the Associates

a) Error Analysis with Use of SCF *Energies*

Thermodynamic information about the associates could be obtained through statistical methods once the potential energy hypersurface is known. In order to estimate the reliability of results, an analysis of the errors arising from the approximate knowledge of the energy hypersurface is demanded.

As an example, we will consider the problem of the thermodynamic stability of an associate, AB, in comparison either with the single species A and B, or with other associates.

The stability of the associate is directly related to the Gibbs free energy change in the association reaction

$$\mathrm{A} + \mathrm{B} \rightarrow \mathrm{AB}\,. \tag{4}$$

Assuming ideal gas behaviour and the molecules in their standard states, one gets:

$$\Delta F^{\circ} = F^{\circ}_{\mathrm{AB}} - (F^{\circ}_{\mathrm{A}} + F^{\circ}_{\mathrm{B}}) = -D - RT \ln \frac{f^{\mathrm{AB}} N}{f^{\mathrm{A}} f^{\mathrm{B}}}\,, \tag{5}$$

where N is Avogadro's number, D the dissociation energy of AB and the f's are the molecular partition functions, *measured from the bottom* of the energy hypersurface.

The formation of the associate leads to six intermolecular vibration modes which have no counterparts in the separated molecules. These intermolecular degrees of freedom originate in 3 rotational and 3 translational modes of the individual molecules which disappear when association takes place and can be interpreted, in a first approximation, as a stretching mode (ν_{σ}), four bending (ν_{δ} and ν_{γ}) and one torsional (ν_{τ}) mode. The other vibrational modes of the associate have analogs in motions already present in A or B. As a first approximation, one may assume the corresponding contribution to the partition function unchanged in going from separated molecules to the associate[6].

Eq. (5) may be therefore simplified:

$$\Delta F^{\circ} = -D - RT \ln \left[N \cdot \prod_{\alpha}^{3} \frac{f^{\mathrm{AB}}_{\mathrm{tr}_{\alpha}} f^{\mathrm{AB}}_{\mathrm{rot}_{\alpha}}}{f^{\mathrm{A}}_{\mathrm{tr}_{\alpha}} f^{\mathrm{A}}_{\mathrm{rot}_{\alpha}} f^{\mathrm{B}}_{\mathrm{tr}_{\alpha}} f^{\mathrm{B}}_{\mathrm{rot}_{\alpha}}} \cdot \prod_{\beta}^{6} f^{\mathrm{AB}}_{\mathrm{vib}_{\beta}} \right]. \tag{6}$$

Where the three values of α label the three inertia axes and the index β the six intermolecular vibration modes.

If calculated with *a priori* methods, practically all the terms of Eq. (6) are subject to errors:

a) Uncertainties in the geometry of the chemical species involved in reaction (4) are reflected in f_{rot} terms, through the corresponding inertia moments. If one assumes that the geometries of both A and B are known and that the association does not alter them appreciably, errors are essentially due to the uncertainty in the equilibrium distance between A and B. Assuming a comparatively large uncertainty range ($\Delta r = \pm 0.2$ Å), for monohydration associates like those here considered the overall error in the rotational term $\Delta RT \ln f^{\mathrm{AB}}_{\mathrm{rot}}$ amount to about 0.01 kcal/mole. Uncertainties in the reciprocal equilibrium orientation of A and B give rise to somewhat smaller errors.

---

[6] It is well know that the formation of a hydrogen bond considerably changes some vibration frequencies. In particular the stretching of the X–H bond may change of some hundreds of wave numbers. The contribution which such frequency shift gives to ΔF^0 can be evaluated as

$$\Delta[RT \ln f_{v}] = -\tfrac{1}{2} Nhc \cdot \Delta n - \Delta[RT \ln(1 - e^{-x})] \simeq -\tfrac{1}{2} Nhc \cdot \Delta n$$

(N being Avogadro's number, $x = hcn/kT$ and Δn the shift in question measured in cm^{-1}). The contribution is practically proportional to Δn because the frequency of the N–H stretching vibration is of the order of 3000 cm^{-1} and therefore the exponential term is completely negligible. Assuming for our weak hydrogen bonds a shift of 50–250 cm^{-1} one gets a contribution of ~0.07–0.36 kcal/mole for ΔF^0. This will be taken into account later.

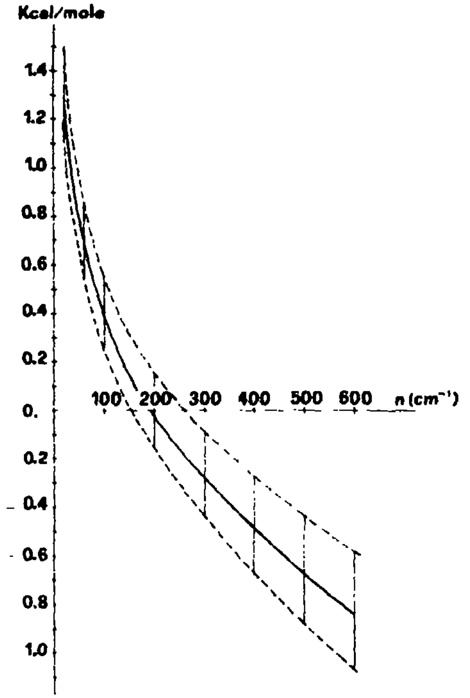

Fig. 13. Free energy contribution for a single harmonic vibration mode and its error bounds, assuming the error in the force constant to be 50%

b) More complicated is the analysis of the errors involved in the vibrational terms. Errors are due to uncertainties in quite a large portion of the potential energy hypersurface, which are propagated in a different manner according to the scheme adopted to evaluate frequencies (see, for example, Ref. [9]). Assuming here the harmonic approximation and a complete separation of the motions, the error may be reduced to be dependent, for each vibrational degree of freedom, on a single parameter, say the force constant k or the corresponding frequency ν. It is easy to show that the error in the free energy change, due to a single vibrational mode, when energies are measured from the potential hypersurface minimum, is:

$$\Delta(RT\ln f_{\mathrm{vib}_B}) \simeq -\tfrac{1}{2}Nhc\,\frac{1+e^{-x_B}}{1-e^{-x_B}}\,\Delta n\,. \tag{7}$$

With such error limits we find the situation depicted in Fig. 13: the free energy contribution due to a harmonic oscillator (full line) at a given calculated frequency n actually lies between the two dashed curves. For each vibrational degree the average error amounts to about ± 0.2 kcal/mole. If one assumes the error to be the same also for roto-vibrational modes the errors of all the intermolecular degrees of freedom and of the additional intramolecular X—H frequency changes produce an uncertainty conspicuous if compared with the expected ΔF° values (about ± 1 kcal/mole).

c) The last, but not least, source of error originates in the dissociation energy (D) of the associate. Such a value may be expected to be sufficiently accurate only when using very good SCF calculations.

As an overall impression, approximate thermodynamic previsions on the stability of associates seem to be a very delicate problem. However when one is concerned in the *relative* stability of different associates, a rather large compensation among errors may be expected and therefore the hope of getting reliable results is not quite unrealistic.

b) Error Analysis with Use of the Electrostatic Approximation

If we now pass on to analyze the electrostatic picture, it is evident that the method employed in this paper is too crude to give directly a prevision of sufficient precision for the free energy of formation. It may be however regarded as a guide to more rigorous calculations and may give a first guess to the *relative* stability of different associates.

From paper I the electrostatic method turns out to be able to give a description of the geometry of the associate sufficient for the rotational contribution, if the distances for hydrogen bonds are fixed according to experimental data. For the vibrational terms the error bounds assumed in the preceding section seem to be sufficient to include also the additional errors arising from the electrostatic approximation. As an example, in Table 1, a comparison is made among quadratic force constants for H_2O dimer as calculated with the electrostatic method and with two different MOLCAO SCF minimal basis set wavefunctions. As a further check we may quote a comparison with the accurate wavefunctions of Hankins, Moskowitz and Stillinger [8]. For the two sets of conformations reported in this paper (curve A and B, the reader is referred to the quoted paper for the identification of the curves) we have calculated the free energy contribution (by means of a numerical integration in the WKB approximation) and found: $RT \ln f = 0.09$ kcal/mole for curve A and 0.32 kcal/mole for curve B. The same sections of the energy hypersurface, as calculated with the electrostatic model give, in the order, 0.04 and 0.26 kcal/mole[7].

Table 1. Comparison of quadratic force constants for intermolecular vibrations in $(H_2O)_2$[a]

Force constant	Ref. [5] SCF	Ref. [1] SCF	Ref. [1] Electrostatic
$\partial^2 \varepsilon/\partial \theta_1^2$	0.040986	0.0344	0.0274
$\partial^2 \varepsilon/\partial \chi_1^2$	0.029775	0.0345	0.0344
$\partial^2 \varepsilon/\partial \theta_2^2$	0.011711	0.0066	0.0050
$\partial^2 \varepsilon/\partial \chi_2^2$	0.016972	–	0.0164
$\partial^2 \varepsilon/\partial \phi^2$	0.001444	–	0.0006
$\partial^2 \varepsilon/\partial R^2$	0.022877	0.0269	–

[a] The notation is the same as in Ref. [5]. All values in a.u.

---

[7] Both our electrostatic curve and curve B of Ref. [8] have quite a similar shape and the small differences between the partition functions are mainly due to our extrapolation of the higher portions of curve B of Ref. [8].

Table 2. Contributions to ΔF^0 for two different associates of aziridine[a]

Type of motion	Associate I	Associate II
	$-RT\ln f$	
$\gamma(\xi)$	-0.0002	$+0.1073$
$\gamma(\eta)$	$+0.2221$	$+0.7979$
$\tau(\zeta)$	-0.5339	-0.5234
$\delta(\xi)$	-1.5256	-1.3016
$\delta(\eta)$	-1.5515	-1.1758
$\sigma(\zeta)$	$+0.0755$	$+0.0755$
$\sum_{p}^{6} RT\ln f^{AB}_{vib_p}$	-3.31	-2.02
$\sum_{x}^{3} RT\ln \frac{f^{AB}_{rot_x}}{f^{A}_{rot_x} f^{B}_{rot_x}}$	1.55	1.53
$\sum_{x}^{3} RT\ln \frac{f^{AB}_{tr_x}}{f^{A}_{tr_x} f^{B}_{tr_x}}$	41.65	41.65
$RT\ln N$	32.64	32.64
$-D$	-7.3	-7.1
ΔF^0	-0.05	1.42

[a] Expressed in kcal/mole.

In order to give a rough idea of the thermodynamic stability of the monohydrates considered in this paper, we have selected the two most stable associates of aziridine, the first (associate I) having the H_2O molecule attached to the N–H bond and the second (associate II) bound through the N lone pair. Assuming that in both cases during the association process the two molecules approach each other along the N–H–O axis direction (i.e. along the electrostatically most favoured channel) with the H_2O molecule disposed according to the most stable conformation, it is easy to visualize how six external modes of the separated molecules transform into six intermolecular vibrations.

The potential curves for associate I corresponding to $\gamma(\xi)$, $\gamma(\eta)$ and $\tau(\zeta)$ motions have been already reported (Figs. 4a, 5a and 6a); curves for $\delta(\xi)$ and $\delta(\eta)$ are not reported for brevity; the curve corresponding to the stretching vibration $[\sigma(\zeta)]$ is not obtainable from the electrostatic model and the corresponding contribution to ΔF was evaluated from a Morse function obtained from the stretching SCF curve of $(H_2O)_2$ with the D parameter taken from the present calculations. The corresponding contributions to ΔF^0 are reported in Table 2: they are calculated, according to the case, either in the harmonic approximation, or as rotators (restricted or free) or numerically in the WKB approximation.

The same procedure was utilized for associate II and the results are again reported in Table 2. At the bottom of this Table one can find also the other terms necessary to calculate ΔF^0 according to Eq. (6), the rotational contribution for the associates being related to the most stables geometries for I and II found in Sect. 4, and the dissociation energies being the corresponding stabilization energies reported in the same section.

According to the electrostatic model the most stable associate has the H_2O molecule bound through the N–H bond (associate I). The equilibrium constants for the two associates are $K_I = 1.093$ and $K_{II} = 0.092$. Such values do not seem completely outside any chemical plausibility, but it is necessary to repeat here that we have been mainly concerned in their relative – rather than absolute – values.

References

1. Bonaccorsi, R., Petrongolo, C., Scrocco, E., Tomasi, J.: Theoret. chim. Acta (Berl.) **20**, 331 (1971).
2. Petrongolo, C., Scrocco, E., Tomasi, J.: Unpublished results.
3. Dreyfus, M., Pullman, A.: Theoret. chim. Acta (Berl.) **19**, 20 (1970).
4. Morokuma, K.: J. chem. Physics **55**, 1236 (1971).
5. Kollman, P. A., Allen, L. C.: Theoret. chim. Acta (Berl.) **18**, 399 (1970).
6. Bonaccorsi, R., Scrocco, E., Tomasi, J.: J. chem. Physics **52**, 5270 (1970).
7. — — — Theoret. chim. Acta (Berl.) **21**, 17 (1971).
8. Hankins, D., Moskowitz, J. W., Stillinger, F. H.: J. chem. Physics **53**, 4544 (1970).
9. Gerrat, J., Mills, I. M.: J. chem. Physics **49**, 1719 (1968).
10. Del Bene, J., Pople, J. A.: J. chem. Physics **52**, 4858 (1970).

Prof. Dr. J. Tomasi
Laboratorio di Chimica
Quantistica ed Energetica
Moleculare del C.N.R.
Via Risorgimento 35
I-56100 Pisa, Italy

Theoret. chim. Acta (Berl.) 25, 120 (1972)
© by Springer-Verlag 1972

Recensio

John P. Fackler, Jr.: Symmetry in Coordination Chemistry. New York and London: Academic Press 1971. 139 Seiten, Preis $4.95.

Symmetriebetrachtungen sind ein nützliches und weit verbreitetes Mittel zur Bestimmung der Struktur- und Bindungseigenschaften von Molekülen. Koordinationsverbindungen eignen sich wegen der meist hohen Symmetrie- und Orbitalentartungen hierfür besonders gut. Das vorliegende Büchlein ist ein einführender Text in die Theorie der Symmetrie, die an Hand einfacher Beispiele demonstriert wird. Die Theorie ist also nicht axiomatisch aufgebaut, sondern wird aus den experimentellen Befunden deduziert, wobei soweit als möglich von mathematischen Formulierungen Abstand genommen wird. Ein solches Vorgehen mag bei den einführenden Kapiteln, in denen die Molekülsymmetrie, die Symmetrieoperationen, die Klassifizierung der Symmetrie, die Symmetriegruppen und die Elektronentheorie der Atome und Ionen besprochen werden, für den lernenden Chemiker didaktisch von Vorteil sein, jedoch läßt sich in den folgenden Kapiteln Darstellungstheorie, Schwingungsstruktur und Bindungseigenschaften (Ligandenfeld- und MO-Theorie) ein unformalistischer, episch beschreibender Textaufbau weniger rechtfertigen. Nach Meinung des Rezensenten hätte eine weitgehendere Konzession an die Mathematik, die dem Autor vielleicht nur schwer abzuringen wäre, dem Verständnis dieser Themen eher genutzt als geschadet.

Für ein einführendes Studium der Symmetrieeigenschaften und ihrer Anwendungsmöglichkeiten auf Koordinationsverbindungen der Übergangselemente eignet sich das Buch jedoch in hervorragender Weise. Es kann zu diesem Zweck und auch wegen des mäßigen Anschaffungspreises empfohlen werden. Wer aufgrund dieses Vorstudiums ein Interesse an dem Stoff findet und tiefer in das Verständnis der Dinge eindringen will, muß auf umfassendere Lehrbücher zurückgreifen, von denen es eine ganze Reihe auf dem Büchermarkt gibt.

H.-H. Schmidtke

Eingegangen am 14 Januar 1972

Theoret. chim. Acta (Berl.) 25, 121 –129 (1972)
© by Springer-Verlag 1972

Commentationes

A Note on the Relation between CI and Rayleigh-Schrödinger Perturbation Theory

M. Kleiner

Department of Chemistry, The University, Sheffield S3 7HF, England

Received July 6, 1971

Energy expressions to the 4th order of accuracy are derived from a partitioned CI matrix; these expressions are identical in each order, to the corresponding formulas derived in the frame of Rayleigh-Schrödinger perturbation theory.

Von einer aufgespaltenen CI-Matrix werden Energieausdrücke bis zur 4. Ordnung entwickelt. Diese Ausdrücke sind für jede Ordnung identisch mit den im Rahmen der Rayleigh-Schrödingerschen Störungstheorie entwickelten Formeln.

1. Introduction

One of the main deficiencies in the Hartree-Fock method is that a single determinant represents a wave function, which in principle must be approximated by an infinitely long expansion. To correct this inadequacy more terms are needed, which are conventionally introduced by means of admitting configuration interaction (CI). Numerous studies have confirmed the favourable effect that either full or judicious inclusion of CI has on the wave function and on the expectation values derived from it. Recent detailed studies have been made on Benzene [1] and on CO [2]. Although CI admission is in principle a straightforward process, in practice the labour involved may quickly become prohibitively expensive. Suppose $2N$ electrons and K atomic orbitals are involved ($K \geqq N$), then for full CI (limiting ourselves to singlet states only) in a basis that extends over all possible eigenfunctions of the S^2 operator, one has to build and diagonalize a matrix of size

$$M = \sum_{L=0}^{t} \binom{K-2L}{N-L} \binom{K}{2L} \frac{(2L)!}{L!\,(L+1)!} \qquad \begin{array}{ll} t = K-N, & K < 2N \\ t = N, & K \geqq 2N \end{array} \tag{1}$$

corresponding to all possible $0, 1, 2, 3, \ldots, 2N$ excitations[1]. Even for a relatively small system comprized of 4 electrons and 6 orbitals (say, LiH in a double zeta basis), Eq. (1) yields $M = 105$, which is already quite large. It is concluded that except for very small systems, the effort needed to overcome the CI size barrier may outweigh that invested in computing the basic molecular integrals. Clearly a simplifying procedure is needed; in looking for a device to reduce the CI scheme to manageable dimensions one may resort to Perturbation Theory [3–6]. According to standard Rayleigh-Schrödinger perturbation theory (henceforth RS) and with the familiar notation ($\boldsymbol{H} = \boldsymbol{H}^0 + \varepsilon \boldsymbol{H}'$; $\varepsilon \to 1$), one has for the correct energy of a perturbed level $\boldsymbol{n}$:

---

[1] General expressions for M, the dimension of a CI problem over a basis of S^2 operator eigenfunctions, as a function of K, N and S ($2S+1$ being the state multiplicity) have been previously given by Mulder [17], and by other authors listed in his paper. The derivation of Eq. (1) in the present communication is similar in approach to that given by [17], but differs from it in some details. It is therefore documented in the Appendix.

$$E_n = E_n^0 + \varepsilon E_n' + \varepsilon^2 E_n'' + \cdots = E_n^0 + \langle \psi_n^0 | \boldsymbol{H}' | \psi_n^0 \rangle + \sum_{m \neq n} \frac{\langle \psi_n^0 | \boldsymbol{H}' | \psi_m^0 \rangle^2}{E_n^0 - E_m^0} + \cdots \tag{2}$$

where the power of ε determines the order of the perturbation. To make the connection with CI one formally equates integrals of type H'_{nm} in (2) with the nm'th CI matrix element; thus the molecular Hamiltonian implicitly assumes the role of a perturbation between the energy levels. Recently this procedure was examined in detail [7–11]. The numerical results obtained by these authors suggest that in many cases it would be feasible to apply second (or higher) order perturbation theory to proceed beyond the SCF limit. In view of these encouraging results, it would be useful to elaborate on the formal relation between the CI and RS methods, in the particular context of MO calculations. While the relation is well understood from the RS tail, it is not as clear when one assumes no knowledge of RS. Our starting point therefore will be the CI *matrix*; it will be stepwise and approximately diagonalized. At each stage the expressions for the resulting eigenvalues will be examined and the various matrix elements involved assigned numerical values in a manner that will indicate the relation to RS, subject to the particular partitioning described next.

2. Approximate Diagonalization

The CI matrix is constructed according to Slater's rules [12]. Zero's are put either for matrix elements of two states differing in more than two orbitals, or according to Brillouin's theorem, for $\left\langle \mathrm{G.S.} | H | E \overset{n}{\underset{m}{\uparrow}} \right\rangle$; the symbol $E \overset{n}{\underset{m}{\uparrow}}$ stands for: E = state; m = orbital excited from; n = orbital excited to; $\uparrow$ = excitation. Virtual orbitals are used for building the various excited states [13]. For the diagonal elements, closed expressions for states of type $E \overset{c}{\underset{a}{\uparrow}} \overset{d}{\underset{b}{\uparrow}}$ $a \neq b$, $c \neq d$ or lesser complexity have been given [14]. $\boldsymbol{B}$ is now the CI matrix (Fig. 1).

We have now a Hermitian matrix with the property: diagonal elements $\gg$ off-diagonal elements. The matrix $\boldsymbol{B}$ is in the mathematical sense "perturbed" [15] and we may assume that it can be expanded in a converging matrix series; ε is a small parameter which labels "order",

$$\boldsymbol{B} = \boldsymbol{B}^0 + \varepsilon \boldsymbol{B}^{\mathrm{I}} + \varepsilon^2 \boldsymbol{B}^{\mathrm{II}} + \cdots \tag{3}$$

where the $\boldsymbol{B}$'s do not depend on ε. Let $\boldsymbol{S}$ be an as yet undetermined unitary matrix of the form

$$\boldsymbol{S} = \boldsymbol{S}^0 + \varepsilon \boldsymbol{S}^{\mathrm{I}} + \varepsilon^2 \boldsymbol{S}^{\mathrm{II}} + \cdots . \tag{4}$$

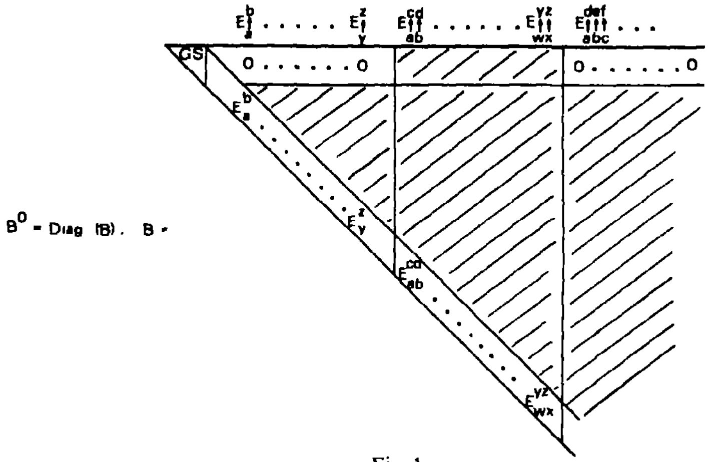

Fig. 1

We adjust S in such a way that

$$A = SBS^{-1} \qquad A = \text{Diag}(\lambda_1 \ldots \lambda_m). \tag{5}$$

S can always be chosen[2] to yield $A_{nn} = \lambda_n$, i.e. the eigenvalues of A and B are identical in magnitude and order along the diagonal. It is suggested from (3), (4) and (5) that A can also be expanded in terms of a converging matrix series

$$A = A^0 + \varepsilon A^{\text{I}} + \varepsilon^2 A^{\text{II}} + \cdots \tag{6}$$

all the A's being diagonal. Our aim now is to compute A. Substitution into a rearranged (5) the series on the right of (3), (4) and (6) yields

$$(A^0 + \varepsilon A^{\text{I}} + \varepsilon^2 A^{\text{II}} + \cdots)(S^0 + \varepsilon S^{\text{I}} + \varepsilon^2 S^{\text{II}} + \cdots) = (S^0 + \varepsilon S^{\text{I}} + \varepsilon^2 S^{\text{II}} + \cdots)(B^0 + \varepsilon B^{\text{I}} + \cdots) \tag{7}$$

if (7) is to hold identically in the successive powers of ε, the following sequence of matrix equations must hold

$$A^0 S^0 = S^0 B^0 \tag{8}$$

$$A^0 S^{\text{I}} + A^{\text{I}} S^0 = S^0 B^{\text{I}} + S^{\text{I}} B^0 \tag{9}$$

$$A^0 S^{\text{II}} + A^{\text{I}} S^{\text{I}} + A^{\text{II}} S^0 = S^0 B^{\text{II}} + S^{\text{I}} B^{\text{I}} + S^{\text{II}} B^0 . \tag{10}$$

$$. \; . \; . \; . \; . \; . \; . \; . = . \; . \; . \; . \; . \; . \; . \; . \tag{11}$$

The only quantities in these equations which are known from the outset are the elements of B, i.e. the elements of the CI matrix. It is possible, however, with the help of Eqs. (8–11) to set up one after the other the A's and the S's to determine A to any degree of accuracy. Now, as we cannot separate the different orders of the B's, we are left with some freedom to assign their values, subject to (3) as constraint. This can be done in a manner that suits the context of a particular problem. To obtain full agreement with expressions derived from RS [9] one must choose for the $\boldsymbol{B}$'s

---

[2] By elementary row and column operations.

$$B^0_{ij} = \begin{cases} \neq 0, & i=j \quad \text{(and not degenerate)} \\ =0, & i \neq j \end{cases}$$
$$B^{\mathrm{I}}_{ij} = \begin{cases} =0, & i=j \\ \neq 0, & i \neq j \end{cases} \tag{12}$$
$$\boldsymbol{B}^{\mathrm{II}} = \boldsymbol{B}^{\mathrm{III}} = \cdots = 0 \,.$$

This choice can of course be made independently of the RS method. Previously the flexibility in partitioning the Hamiltonian in the context of CI was noted by [7].

3. Diagonalization to First Order

Let $\varepsilon \to 0$ so that $\boldsymbol{B} \to \boldsymbol{B}^0$ and $\boldsymbol{S} \to \boldsymbol{S}^0$. Then since the eigenvalues of $\boldsymbol{A}$ are the same as those of $\boldsymbol{B}$ (identity also in order along the diagonal, as is in (5) above) $\boldsymbol{A}^0 = \boldsymbol{B}^0$ and (8) becomes

$$\boldsymbol{B}^0 \boldsymbol{S}^0 = \boldsymbol{S}^0 \boldsymbol{B}^0 \,. \tag{13}$$

As $\boldsymbol{S}$ must be unitary for any ε it follows that when $\varepsilon \to 0$, $\boldsymbol{S}^0$ is unitary. It can be verified (see Appendix) that a unitary matrix ($\boldsymbol{S}^0$) which commutes with a non-degenerate diagonal matrix ($\boldsymbol{B}^0$ in (13)) must be diagonal itself and each of its diagonal elements be of modulus unity. We choose

$$\boldsymbol{S}^0 = \mathbf{1} \,. \tag{14}$$

Now it follows from (13) and (14) that (9) takes the form

$$\boldsymbol{B}^0 \boldsymbol{S}^{\mathrm{I}} - \boldsymbol{S}^{\mathrm{I}} \boldsymbol{B}^0 = \boldsymbol{B}^{\mathrm{I}} - \boldsymbol{A}^{\mathrm{I}} \,. \tag{15}$$

The nn'th element on both sides of (15) can be written

$$\sum_i B^0_{ni} S^{\mathrm{I}}_{in} - \sum_i S^{\mathrm{I}}_{ni} B^0_{in} = B^{\mathrm{I}}_{nn} - A^{\mathrm{I}}_{nn} = 0 \tag{16}$$

since $\boldsymbol{B}^0$ is diagonal. Hence

$$A^{\mathrm{I}}_{nn} = B^{\mathrm{I}}_{nn} \,. \tag{17}$$

If powers of ε higher than the first are neglected, (6) reduces to $\boldsymbol{A} = \boldsymbol{A}^0 + \varepsilon \boldsymbol{A}^{\mathrm{I}}$, or, in view of Eqs. (2) and (17)

$$\lambda_n = B^0_{nn} + \varepsilon B^{\mathrm{I}}_{nn} \,. \tag{18}$$

Eq. (18) is identical to the expression corrected to first order in the RS method. According to the convention adopted for the $\boldsymbol{B}$'s in Eqs. (12), $B^{\mathrm{I}}_{nn} = 0$ and (18) reduces to

$$\lambda_n = B^0_{nn} \tag{19}$$

– a similar expression was derived on different grounds in [3]. It should be noted that here, $B^{\mathrm{I}}_{nn}=0$ was adopted as a basic assumption due to our particular partitioning of the CI matrix and does not follow from the quality of the zero order wave function.

4. Diagonalization to Second Order

It can be verified from (9), (13) and (16) (see Appendix) that[3]

$$S^{\mathrm{I}}_{ij}=\begin{cases}0, & i=j\\ \dfrac{B^{\mathrm{I}}_{ij}}{B^{0}_{ii}-B^{0}_{jj}}, & i\neq j.\end{cases} \tag{20}$$

From a rearranged (10) and taking advantage of (14) one finds

$$\mathbf{A}^{\mathrm{II}}=\mathbf{B}^{\mathrm{II}}+\mathbf{S}^{\mathrm{I}}\mathbf{B}^{\mathrm{I}}-\mathbf{A}^{\mathrm{I}}\mathbf{S}^{\mathrm{I}}+\mathbf{S}^{\mathrm{II}}\mathbf{B}^{0}-\mathbf{B}^{0}\mathbf{S}^{\mathrm{II}} \tag{21}$$

for the diagonal elements of $\mathbf{A}^{\mathrm{II}}$ one need consider only (22) (as $\mathbf{A}^{\mathrm{I}}\mathbf{S}^{\mathrm{I}}$ vanishes along the diagonal and $\mathbf{B}^{0}$ is diagonal)

$$(\mathbf{A}^{\mathrm{II}})_{nn}=B^{\mathrm{II}}_{nn}+(\mathbf{S}^{\mathrm{I}}\mathbf{B}^{\mathrm{I}})_{nn}=B^{\mathrm{II}}_{nn}+\sum_{i\neq n}\frac{B^{\mathrm{I}}_{ni}B^{\mathrm{I}}_{in}}{B^{0}_{nn}-B^{0}_{ii}} \tag{22}$$

thus, to the second power of ε the diagonal elements of $\mathbf{A}$ take now the full form

$$\lambda_n=B^{0}_{nn}+\varepsilon B^{\mathrm{I}}_{nn}+\varepsilon^2\left|B^{\mathrm{II}}_{nn}+\sum_{i\neq n}\frac{B^{\mathrm{I}}_{ni}B^{\mathrm{I}}_{in}}{B^{0}_{nn}-B^{0}_{ii}}\right| \tag{23}$$

when the convention in (12) is introduced (23) is reduced to (24) – an expression derived from RS by Moller-Plesset [3], and used by Nesbet [4] for the approximate diagonalization of large matrices.

$$\lambda_n=B^{0}_{nn}+\sum_{i\neq n}\frac{B^{\mathrm{I}}_{ni}B^{\mathrm{I}}_{in}}{B^{0}_{nn}-B^{0}_{ii}}\,. \tag{24}$$

5. Diagonalization to Third and Fourth Order

From (10), (13) and (14) one obtains

$$\mathbf{A}^{0}\mathbf{S}^{\mathrm{II}}-\mathbf{S}^{\mathrm{II}}\mathbf{B}^{0}=\mathbf{B}^{\mathrm{II}}-\mathbf{A}^{\mathrm{II}}+\mathbf{S}^{\mathrm{I}}\mathbf{B}^{\mathrm{I}}-\mathbf{A}^{\mathrm{I}}\mathbf{S}^{\mathrm{I}} \tag{25}$$

which leads, noting that the $\mathbf{A}$'s are diagonal, to

$$S^{\mathrm{II}}_{ij}=\begin{cases}0, & i=j\\ \dfrac{B^{\mathrm{II}}_{ij}}{B^{0}_{ii}-B^{0}_{jj}}+\dfrac{1}{B^{0}_{ii}-B^{0}_{jj}}\left(\displaystyle\sum_{l\neq i}\frac{B^{\mathrm{I}}_{il}B^{\mathrm{I}}_{lj}}{B^{0}_{ii}-B^{0}_{ll}}-\frac{B^{\mathrm{I}}_{ii}B^{\mathrm{I}}_{ij}}{B^{0}_{ii}-B^{0}_{jj}}\right), & i\neq j\end{cases} \tag{26}$$

substituting to (10) and, as only diagonal elements of $\mathbf{A}^{\mathrm{III}}$ are needed (this eliminates terms originating from $\mathbf{A}^{\mathrm{I}}\mathbf{S}^{\mathrm{II}}$, $\mathbf{A}^{\mathrm{II}}\mathbf{S}^{\mathrm{I}}$ and causes disappearance of $\mathbf{S}^{\mathrm{II}}\mathbf{B}^{0}-\mathbf{B}^{0}\mathbf{S}^{\mathrm{II}}$) we have

---

[3] As we are not interested in "Expectation Values" here, the columns of $\mathbf{S}$ matrices will not be renormalized at successive intermediate steps.

$$\begin{aligned} A_{nn}^{\mathrm{III}} = B_{nn}^{\mathrm{III}} + \sum_j S_{nj}^{\mathrm{I}} B_{jn}^{\mathrm{II}} + \sum_j S_{nj}^{\mathrm{II}} B_{jn}^{\mathrm{I}} &= B_{nn}^{\mathrm{III}} + 2 \sum_{j \neq n} \frac{B_{nj}^{\mathrm{I}} B_{jn}^{\mathrm{II}}}{B_{nn}^0 - B_{jj}^0} \\ &+ \sum_{j \neq n} \sum_{l \neq n} \frac{B_{nl}^{\mathrm{I}} B_{lj}^{\mathrm{I}} B_{jn}^{\mathrm{I}}}{(B_{nn}^0 - B_{ll}^0)(B_{nn}^0 - B_{jj}^0)} - \sum_{j \neq n} \frac{B_{nn}^{\mathrm{I}} B_{nj}^{\mathrm{I}} B_{jn}^{\mathrm{I}}}{(B_{nn}^0 - B_{jj}^0)^2} \end{aligned} \tag{27}$$

on introduction of the conditions specified in (12) the first two terms on the right hand of (27) disappear, and one remains with the third order expression in the RS theory. However, because of B_{nn}^{I}, the last term also disappears and only one term is left. Thus we have the third order correction for λ_n

$$A_{nn}^{\mathrm{III}} = \sum_{j \neq n} \sum_{l \neq n} \frac{B_{nl}^{\mathrm{I}} B_{lj}^{\mathrm{I}} B_{jn}^{\mathrm{I}}}{(B_{nn}^0 - B_{ll}^0)(B_{nn}^0 - B_{jj}^0)} \tag{28}$$

a simplification that viewed from RS [3, 7, 8] results from the particular nature of the variationally obtained SCF energy. A similar treatment yields for S_{ij}^{III} and for A_{nn}^{IV}, the correction to 4th order

$$S_{ij}^{\mathrm{III}} = \begin{cases} 0, & i = j \\ \dfrac{1}{B_{ii}^0 - B_{jj}^0} \left(\displaystyle\sum_{k \neq i} \sum_{l \neq i} \frac{B_{il}^{\mathrm{I}} B_{lk}^{\mathrm{I}} B_{kj}^{\mathrm{I}}}{(B_{ii}^0 - B_{ll}^0)(B_{ii}^0 - B_{kk}^0)} - \sum_{l \neq i} \frac{B_{il}^{\mathrm{I}} B_{li}^{\mathrm{I}} B_{ij}^{\mathrm{I}}}{(B_{ii}^0 - B_{ll}^0)(B_{ii}^0 - B_{jj}^0)} \right), & i \neq j \end{cases} \tag{29}$$

$$\begin{aligned} A_{nn}^{\mathrm{IV}} = &\sum_{i \neq n} \sum_{j \neq n} \sum_{l \neq n} \frac{B_{nl}^{\mathrm{I}} B_{ij}^{\mathrm{I}} B_{jl}^{\mathrm{I}} B_{in}^{\mathrm{I}}}{(B_{nn}^0 - B_{ii}^0)(B_{nn}^0 - B_{jj}^0)(B_{nn}^0 - B_{ll}^0)} \\ &- \sum_{i \neq n} \sum_{j \neq n} \frac{B_{ni}^{\mathrm{I}} B_{in}^{\mathrm{I}} B_{nj}^{\mathrm{I}} B_{jn}^{\mathrm{I}}}{(B_{nn}^0 - B_{ii}^0)(B_{nn}^0 - B_{jj}^0)^2} . \end{aligned} \tag{30}$$

6. Discussion

A scheme was described in which the CI matrix served as a starting point for the derivation of energy expressions identical to those obtained in the RS frame. A particular partitioning of the CI matrix allowed for the simplifications similar to those due to Moller-Plesset [3].

It must be emphasized, following [16], that this identity is formal, as it depends on the partitioning of the CI matrix. It appears that the CI method is related to the "Variation Perturbation" method [16], which encompasses RS as a special case. We now consider briefly the reasoning which leads to the partitioning adopted in (12). For concreteness the expression in (27) is examined. It was initially derived for a Hamiltonian of the general form $\boldsymbol{B} = \boldsymbol{B}^0 + \varepsilon \boldsymbol{B}' + \varepsilon^2 \boldsymbol{B}'' + \cdots$. To make the CI method compatible with ordinary RS, where only 1st order perturbation is usually admitted, we must put $\boldsymbol{B}^{\mathrm{II}} = \boldsymbol{B}^{\mathrm{III}} = \cdots = 0$ and retain only $\boldsymbol{B} = \boldsymbol{B}^0 + \varepsilon \boldsymbol{B}'$. The role of the perturbing matrix $\boldsymbol{B}'$, is to help us assess the effect of extending the basis by adding configurations. At this stage only the last two terms on the left of (27) remain, forming the usual 3rd order correction in RS. A further simplification is obtained from (18). Although (18) in itself is a simple result in RS, it has important implications in the CI context, as it assures that the eigenvalues of $\boldsymbol{B}$ corrected to first order are "diagonal". It follows that provided $\boldsymbol{B}^0$ is taken to be the diagonal part of the original CI matrix, one may put $B^{\mathrm{I}}_{nn} = 0$. This choice allows us to simulate the Moller-Plesset [3] results, and to drop the 4th term in (27) leading to the single term expression in (28).

The arguments given above formally justify regarding a CI study for some state n equivalent to an ordinary RS treatment with the following characteristics: $H = H^0 + \varepsilon H'$; $\langle \psi_n^0 | H' | \psi_n^0 \rangle = 0$. Eqs. (28) and (30) must therefore be derivable by any of the methods available for construction of correction expressions in RS. One may choose to operate within the scheme of rules formulated by Huby[4] [18]. To apply his "derivation by inspection" method, and using his notation, we define a projection operator

$$Q_0 = \sum_{i \neq n} |\psi_i^0\rangle\langle\psi_i^0|, \qquad (Q_0^2 = Q_0) \tag{31}$$

(i.e. Q_0 is the projector onto the space orthogonal to the state n which is presently under investigation) and an inverse operator $\boldsymbol{a}$

$$\boldsymbol{a} = (E_n^0 - H^0)^{-1}, \quad \left((E_n^0 - H^0)^{-1}\psi_i^0 = \frac{1}{E_n^0 - E_i^0}\,\psi_i^0\right) \tag{32}$$

now it is well known [19] that if

$$E_n' = E_n'' = \cdots = E_n^{(N-1)'} = 0 \tag{33}$$

then the N'th order correction is given by

$$E_n^{N'} = \left\langle \psi_n^0 \middle| H' \left(\frac{Q_0}{\boldsymbol{a}} H'\right)^{N-1} \middle| \psi_n^0 \right\rangle \tag{34}$$

where (33) reads

$$\langle \psi_n^0 | H' | \psi_n^0 \rangle = \left\langle \psi_n^0 \middle| H' \frac{Q_0}{\boldsymbol{a}} H' \middle| \psi_n^0 \right\rangle = \cdots = \left\langle \psi_n^0 \middle| H' \left(\frac{Q_0}{\boldsymbol{a}} H'\right)^{N-2} \middle| \psi_n^0 \right\rangle = 0 .$$

If however only corrections up to the k'th order vanish, $K < N - 1$, then additional terms (with the correct sign) must be added to expression (34), which arise from all possible "Bra-ket"-ing internal H' factors in (34), according to the prescription in [18]. For E_n''' we thus have

$$E_n''' = \left\langle \psi_n^0 \middle| H' \frac{Q_0}{\boldsymbol{a}} H' \frac{Q_0}{\boldsymbol{a}} H' \middle| \psi_n^0 \right\rangle + (-1) \left\langle \psi_n^0 \middle| H' \frac{Q_0}{\boldsymbol{a}} \langle H' \rangle \frac{Q_0}{\boldsymbol{a}} H' \middle| \psi_n^0 \right\rangle \tag{35}$$

however

$$\left\langle \psi_n^0 \middle| H' \frac{Q_0}{\boldsymbol{a}} \langle H' \rangle \frac{Q_0}{\boldsymbol{a}} H' \middle| \psi_n^0 \right\rangle = \left\langle \psi_n^0 \middle| H' \frac{Q_0}{\boldsymbol{a}^2} H' \middle| \psi_n^0 \right\rangle \langle \psi_n^0 | H' | \psi_n^0 \rangle = 0$$

$$(H'_{nn} = 0 \text{ by assumption})$$

and only the first term in (35) survives, which is identical to (28). This identity is easily seen after substituting for Q_0 and $\boldsymbol{a}$ their values defined in (31) and (32).

---

[4] The author is indebted to a referee for bringing to his attention the papers by Mulder [17] and Huby [18].

Similarly for $E_n^{4'}$ one obtains

$$\begin{aligned}
E_n^{4'} = & \left\langle \psi_n^0 \middle| H' \frac{Q_0}{a} H' \frac{Q_0}{a} H' \frac{Q_0}{a} H' \middle| \psi_n^0 \right\rangle \\
& - \left\langle \psi_n^0 \middle| H' \frac{Q_0}{a} \langle H' \rangle \frac{Q_0}{a} H' \frac{Q_0}{a} H' \middle| \psi_n^0 \right\rangle \\
& - \left\langle \psi_n^0 \middle| H' \frac{Q_0}{a} H' \frac{Q_0}{a} \langle H' \rangle \frac{Q_0}{a} H' \middle| \psi_n^0 \right\rangle \\
& - \left\langle \psi_n^0 \middle| H' \frac{Q_0}{a} \left\langle H' \frac{Q_0}{a} H' \right\rangle \frac{Q_0}{a} H' \middle| \psi_n^0 \right\rangle \\
= & \left\langle \psi_n^0 \middle| H' \frac{Q_0}{a} H' \frac{Q_0}{a} H' \frac{Q_0}{a} H' \middle| \psi_n^0 \right\rangle \\
& - \left\langle \psi_n^0 \middle| H' \frac{Q_0}{a^2} H' \middle| \psi_n^0 \right\rangle \left\langle \psi_n^0 \middle| H' \frac{Q_0}{a} H' \middle| \psi_n^0 \right\rangle .
\end{aligned} \tag{36}$$

Expression (36) is identical to (30) obtained for the fourth order correction by the approximate diagonalization method. The assertion that perturbation corrections may be derived from a CI matrix independently of the RS method is therefore shown to be correct.

Appendix

1. To derive the expression on the right side of (1). Consider $2N$ electrons and K atomic orbitals, and look at a case where L pairs out of the N available are distributed in $2L$ orbitals, each orbital is occupied by a single electron. This can be effected in $\binom{K}{2L}$ ways. Meanwhile the rest of the $N-L$ pairs can be distributed in $\binom{K-2L}{N-L}$ ways between the vacant orbitals. The total number of ways to achieve a situation of $(N-L)$ orbitals doubly occupied and $2L$ orbitals singly occupied is $\binom{K-2L}{N-L}\binom{K}{2L}$. To each of these situations correspond several linearly independent S^2 eigenfunctions, whose total number has been given by [20]. For $2L$ electrons outside a closed shell and a singlet state this number is $\binom{2L}{L} - \binom{2L}{L-1} = \frac{(2L)!}{L!(L+1)!}$. Multiplying this number by the number of realized situation and summing over all L yields

$$M = \sum_{L=0}^{t} \binom{K-2L}{N-L}\binom{K}{2L} \frac{(2L)!}{L!(L+1)!} \qquad \begin{array}{ll} t = K-N, & K < 2N, \\ t = N, & K \geqq 2N . \end{array}$$

Judging by several numerical checks this expression is identical to that given by Mulder's [17] closed formula,

$$M = \frac{K+1}{(N+1)(K-N+1)} \binom{K}{N}^2 .$$

2. To show that $\boldsymbol{S}^0$ is diagonal and each S^0_{ii} is of modulus unity. Starting with $\boldsymbol{S}^0\boldsymbol{B}^0 = \boldsymbol{B}^0\boldsymbol{S}^0$, one obtains on performing multiplication: $S^0_{ij}(B^0_{ii} - B^0_{jj}) = 0$. As $\boldsymbol{B}^0$ is not degenerate, $S^0_{ij} = 0$. Also $\boldsymbol{S}^0$ being unitary leads to $S^{0*}_{ii} \cdot S^0_{ii} = 1$, hence $S^0_{ii} = 1 \cdot \exp(\pm i\theta)$; choose $\theta = 0$.

3. To find S^{I}_{ij}. Since B^0 is diagonal it follows from (16) that S^{I}_{ij} satisfies

$$B^0_{ii}S^{\mathrm{I}}_{ij} - S^{\mathrm{I}}_{ij}B^0_{jj} = B^{\mathrm{I}}_{ij}; \qquad S^{\mathrm{I}}_{ij} = \frac{B^{\mathrm{I}}_{ij}}{B^0_{ii} - B^0_{jj}}.$$

Similarly, for S^{I}_{ii}: $B^0_{ii}S^{\mathrm{I}}_{ii} - S^{\mathrm{I}}_{ii}B^0_{ii} = 0$ and S^{I}_{ii} is arbitrary. Choose $S^{\mathrm{I}}_{ii} = 0$ to satisfy orthogonality constraints: $\langle S^0_i | S^{\mathrm{I}}_i \rangle = 0$. This choice will persist for $S^{\mathrm{II}}_{ii}, S^{\mathrm{III}}_{ii}, \ldots$.

Acknowledgements. The author wishes to thank Dr. D. B. Cook for critically reading the manuscript, Dr. C. D. H. Chisholm for useful discussion, and the Science Research Council for their support.

References

1. Buenker, R. J., Whitten, J. L., Petke, J. D.: J. chem. Physics **49**, 2261 (1968).
2. Grimaldi, F., Lecourt, A., Moser, C.: Int. J. quant. Chemistry **1** *S*, 153 (1967).
3. Moller, C., Plesset, M. S.: Physic. Rev. **46**, 618 (1934).
4. Nesbet, R. K.: Proc. Roy. Soc. (Lond.) *A* **230**, 312 (1955).
5. Anno, T., Sadd, A.: J. chem. Physics **29**, 1170 (1958).
6. Grimaldi, F.: J. chem. Physics **43** *S*, 59 (1965).
7. Claverie, P., Diner, S., Malrieu, J. P.: Int. J. quant. Chemistry **1**, 751 (1967).
8. Gershgorn, Z., Shavitt, I.: Int. J. quant. Chemistry **2**, 751 (1968).
9. Diner, S., Malrieu, J. P., Claverie, P.: Theoret. chim. Acta (Berl.) **13**, 1 (1969).
10. Masson, A., Levy, B., Malrieu, J. P.: Theoret. chim. Acta (Berl.) **18**, 193 (1970).
11. Giessner-Prettre, C., Pullman, A.: Theoret. chim. Acta (Berl.) **20**, 378 (1971).
12. Slater, J. C.: Quantum theory of molecules and solids, Vol. 1, pp. 285-290, New York: McGraw-Hill 1963.
13. Roothaan, C. C. J.: Rev. mod. Physics **23**, 69 (1951).
14. Murrell, J. N., Lenore-McEwen, K.: J. chem. Physics **25**, 1143 (1956).
15. Wilkinson, J. H.: The algebraic eigenvalue problem, p. 66, Oxford: Clarendon Press 1965.
16. McWeeny, R., Sutcliffe, B. T.: Methods of molecular quantum mechanics, pp. 36-39, London and New York: Academic Press 1969.
17. Mulder, J. J. C.: Molecular Physics **10**, 479 (1966).
18. Huby, R.: Proc. physic. Soc. (London) **78**, 529 (1961).
19. Messiah, A.: Quantum mechanics, Vol. 2, p. 686, Amsterdam: North-Holland Publishing Co. 1965.
20. Eckart, C.: Rev. mod. Physics **2**, 305 (1930).

Dr. M. Kleiner
Department of Chemistry
The University
Sheffield S3 7HF, England

Theoret chim. Acta (Berl.) 25, 130–137 (1972)
© by Springer-Verlag 1972

Intermolecular Interactions-Dependence on Inter- and Intra-Molecular Distances. A Configuration Interaction Study of the $H_2 \cdots H_2$ System

O. Tapia* and G. Bessis**
Centre de Mécanique Ondulatoire Appliquée, 23, rue du Maroc, Paris 19e, France

Received September 9, 1971

The potential energy curves for two H_2 molecules are calculated by a SCF-MO-LCGO-CI procedure. The orientational and internal geometry dependence of the interaction energy is studied. Numerical results show: a) that repulsive interaction energy increases with increased intramolecular dimensions and b) that it has a rough additivity dependence with the number of stretched partners. The attractive interaction energies display a behavior similar to the repulsive one. A simple qualitative explanation for this fact is advanced.

Die Potentialkurven für zwei H_2-Moleküle werden mit Hilfe eines SCF-MO-LCGO-CI-Verfahrens berechnet. Die Abhängigkeit der Wechselwirkungsenergie von der Orientierung sowie der inneren Geometrie der beiden Moleküle wird untersucht. Die numersichen Ergebnisse zeigen: a) die abstoßende Wechselwirkungsenergie steigt mit wachsenden intramolekularen Dimensionen, und b) dieser Energieanteil zeigt ungefähr Additivität entsprechend der Zahl der gestreckten Wechselwirkungspartner. Die anziehenden Anteile der Wechselwirkung zeigen ähnliches Verhalten wie die abstoßenden. Eine einfache qualitative Erklärung für dieses Verhalten wird vorgeschlagen.

Les courbes d'énergie potentielle du système formé de deux molécules H_2 sont déterminées par la méthode SCF-MO-LCGO-CI et la dépendance de l'énergie d'interaction en fonction de l'orientation et de la géométrie est explicitée. Les résultats montrent que: a) la partie répulsive de l'énergie d'interaction croît avec les dimensions intramoléculaires du système, b) la dépendance est, grosso modo, additive en fonction du nombre de partenaires «étirés». La partie attractive de l'énergie d'interaction présente le même comportement que dans le cas répulsif. Une tentative d'explication qualitative simplifiée de ces résultats est présentée.

1. Introduction

An increased interest in the knowledge of the internal geometry dependence of intermolecular forces has been raised, principally due to work of Bratos *et al.* [1], on vapor-solution infrared (IR) frequency shifts and band shape. They have shown that these shifts depend on the difference between the mean energies of the solute-solvent interaction in the two vibrational states implied in the IR transition. Speaking pictorially these shifts depend on the variation of the intermolecular forces with the effective size of the interacting molecules. Also, in connection with chemical reaction mechanism, a vibrational excitation mechanism has been suggested for the exchange reaction $H_2 + D_2$ in presence of argon atoms [2, 3]. These developments showed the interest to undertake a study of intermolecular forces and their dependence on the distance, orientation and internal geometry from a theoretical point of view. In previous papers [4, 5], Pauli repulsive interaction between two H_2 molecules in their electronic ground state has been investigated using a SCF-MO-LCGO procedure. For this type of system, repulsive forces predominate at short range distances, and the SCF-MO method is the adequate theoretical tool for the calculation of the intermolecular potential energy. At intermediate distances, however, Van der Waals forces become important. It has been shown by London [6] that these forces come out from dynamic electronic correlations. The SCF-MO scheme does not take into account this kind of correlation and a configuration interaction (CI) is needed to introduce it. The $H_2 \ldots H_2$ system is considered here as a model because it has the main features of four centers molecular interactions and nevertheless one is still able to make rather exact calculations. This system has been often considered and parallel calculations have been carried out by Magnasco *et al.* [12, 13] using a restricted basis of Slater orbitals for a different set of distances and geometries. Reference to their work and conclusions has been reported in our preceeding paper [5].

---

* Permanent address: Carrera de Quimica, Facultad de Quimica Farmacia, Universidad de Chile, Casilla 233, Santiago, Chile.

** Permanent address: Laboratoire de Spectroscopie et de Luminescence, Université Claude Bernard, Lyon I, Villeurbanne, France.

In Section 2, we present the method, models and details of the calculations. Section 3 contains the results and discussion of the dependence of the potential energy on intermolecular distance and orientation. The intramolecular distance dependence of the interaction energy is discussed in Section 4, and for reasons further discussed only the linear geometrical configuration is studied.

2. Method, Models and Calculations

a) Wave Function

The wave function of the composite system is taken as a linear combination of a zero$^{\text{th}}$ order, singly and doubly excited electronic configurations state functions

$$\psi = C_0\psi_0 + \sum_S C_S\psi_S + \sum_D C_D\psi_D \,. \tag{1}$$

The coefficients C_0, C_S, C_D are determined variationally. ψ_0 stands for the SCF closed shell electronic wave function of the ground state represented by a single Slater determinant. ψ_S and ψ_D stand for singly and doubly excited state functions. The virtual SCF-MO's have been used to build up the ψ_S and ψ_D functions. The total Hamiltonian, H, once diagonalized in this basis, the lowest energy eigenvalue represents the ground electronic energy, $E_{\text{SCF-CI}}$. In the CI calculation, we consider only up to diexcited electronic configurations. The reason follows from a second order perturbation analysis of $E_{\text{SCF-CI}}$ in terms of essentially localized MO's at long range distances. One can show that the total energy can be written approximately

$$E_{\text{SCF-CI}} \approx E_{\text{SCF}} - \sum_D \frac{|\langle\psi_0|H|\psi_D\rangle|^2}{E_D^0 - E_0^0}\,, \tag{2}$$

where $E_{\text{SCF}} = \langle\psi_0|H|\psi_0\rangle$ and E_D^0 and E_0^0 are the expectation values of the hamiltonian taken over a non interacting unperturbed system. The second term of Eq. (2), $E^{(2)}$, is an approximation to the dynamic electronic correlation energy.

If the limit of our approximate basis seems to be severe, however a study of this expression, using essentially localized MO's, shows that the Van der Waals interaction energy, which behaves asymptotically like $-1/R^6$, is accounted for. Owing to the fact that the dielectronic integrals involved are exactly calculated, mainly all second order dispersion effects are implicitly contained in within the limits of our approximate basis. Of course to take a full account of the Van der Waals interaction term, a more extended basis would be required.

b) Models

The dependence of potential energy on orientational and intermolecular distance has been considered by analysing four geometrical configurations, a) rectangular configuration (D_{2h}), b) perpendicular configuration (C_{2v}), c) linear configuration ($D_{\infty h}$) and d) *T*-configuration (C_{2v}). The standard symbols are used to indicate the corresponding symmetry point group, Fig. 1. The internal geometry dependence is studied by considering one or both partner molecules at an intramolecular distance, r, greater than the equilibrium distance, $r_0 = 1.4166$ a.u. This model is a consequence of the assumption that a vibrationally excited state has a vibration amplitude greater then the fundamental one. The value $r = 1.6$ a.u. for the stretched molecule (*s*) is considered.

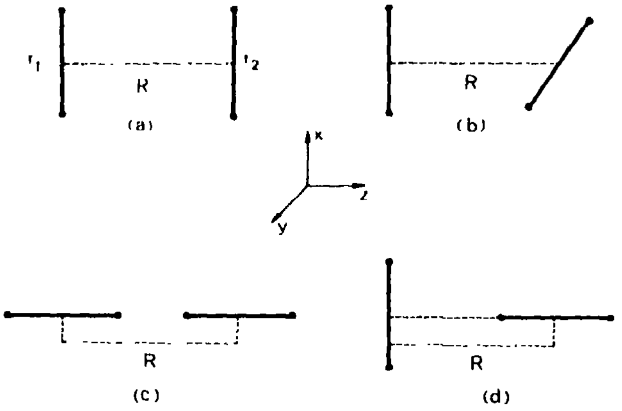

Fig. 1. Geometrical conformation, frame of reference, parameters: R intermolecular distance, r_1 and r_2 intramolecular distances

c) Calculations

A Gaussian orbital basis set has been used to expand the MO's. In this basis all the electronic many centers integrals could be calculated exactly, so that one of the most serious drawback of intermolecular calculations is taken away. We have considered twenty four Gaussian functions. Six centered on each hydrogen atom; (three of *s*-type and three of *p*-type: p_x, p_y, p_z). The rather great number of points of the energy curve to be calculated prevents any attempt to optimize the Gaussian exponents. More details concerning this basis could be found elsewhere [5]. For all geometric configurations, the same CI basis set built up from the first six supermolecule SCF-MO's is used. This number of MO's allows us to build all singly and doubly excited configurations which can be accomodated in the computer core storage; this amounts to 117 Slater determinants arranged in 45 S^2-operator eigenfunctions with $S = 0$. A CI Fortran program for CDC 3600 computer has been written [7]. It needs as input, the "Basint" tape of Gaussian integrals and the SCF-MO coefficients. These inputs are directly obtained from IBMOL program [8].

3. Distance and Orientation Dependence of the Potential Energy. Results and Discussion

For all geometrical configurations the SCF energy, E_{SCF}, and the configuration interaction energy, E_{SCF-CI}, are collected in Table 1 as a function of intermolecular distance, R. This distance is expressed in units of the H_2 equilibrium distance as $L = R/r_0$. The point $L = 20.0$ is calculated in order to check the behavior of the composite system at very long range distance. We remark that E_{SCF} at this distance corresponds to almost two non interacting H_2 molecules. E_{SCF} for the two isolated H_2 molecules is 2.2510089 a.u. which compares fairly well with E_{SCF} $(L = 20)$ from Table 1, and it is quite independent of the different orientations. For the geometries considered: rectangular and linear, the CI calculation leads to nearly the same value of E_{SCF-CI} $(L = 20)$. The imposition to MO's of a lower overall symmetry seems to play an important role in the calculation of the total energy: $2\,E_{SCF-CI}(H_2) = 2.2703348$ a.u. Nevertheless the orientational independent value of E_{SCF-CI} $(L = 20)$ suggests that one still have a meaningful shape for the intermolecular potential. In this calculation, this later value is taken as the energy of two almost independent molecules.

A glance at the columns of E_{SCF-CI} (Table 1) shows a very different behavior of the potential energy for the molecules orientations considered. The rectangular and perpendicular configurations do not display a characteristic minimum in the experimental Van der Waals region [9]. Our results, for the linear configuration, compare fairly well with experimental ones [9]. For the same case, Wilson *et al.* [10] do not succeded to get any minimum. The potential energy curve has a minimum located at about 3.45 Å. Gordon *et al.*, quote an experimental determined value of 3.34 Å. The dissociation energy in our scheme is equal to $E_{min} = 50.5 \times 10^{-23}\,J$, matching rather well the experimental value of $51.5 \times 10^{-23}\,J$ [9]. The T-configuration energy curve shows a lesser depth at a larger distance $R = 3.75$ Å.

These very different results, when orientation is varied, could be understood if one consider the MO's involved in the calculations. In Fig. 2, we present a MO diagram of these orbitals which shows schematically the nodal planes. For sake of simplicity two geometries are discussed: the linear and the rectangular one. In spite of the total σ-character of all MO's involved in calculations, to each one a different local symmetry can be assigned. This is indicated in the Fig. 2 using a reference frame as defined on Fig. 1. Incidentally one can see that at very

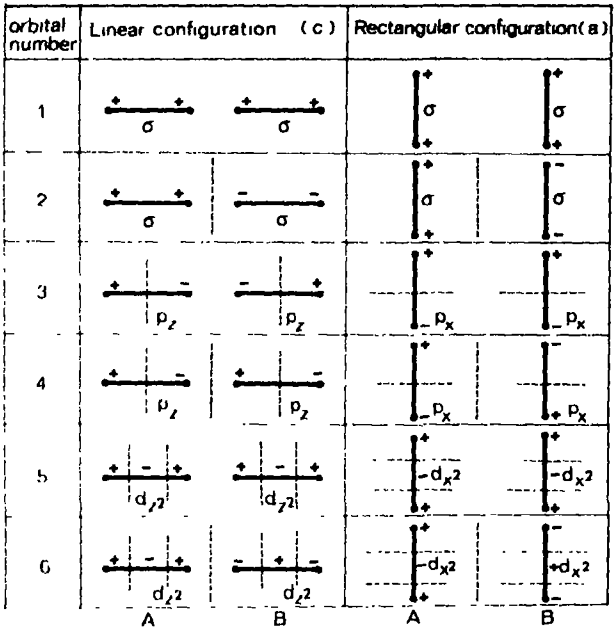

Fig. 2. Molecular orbitals diagram. For each molecular orbital local symmetry is indicated, and the nodal plane is represented by broken lines. Sign variations are indicated

long distances, where intermolecular overlaps are negligible, the linear combination of molecular orbitals taken by pairs, $(1 \pm 2), (3 \pm 4), (5 \pm 6)$ would give the localized MO's with local symmetry indicated on Fig. 2. Now, if we consider in $E^{(2)}$ the terms corresponding to the Van der Waals attraction between molecules, it contains, associated with the appropriate denominators, for the linear configuration, two electrons integrals of the type

$$\left\langle \sigma_A(1)\, p_{Z_A}(1) \left| \frac{1}{r_{12}} \right| \sigma_B(2)\, p_{Z_B}(2) \right\rangle$$

and

$$\left\langle \sigma_A(1)\, d_{Z_A^2}(1) \left| \frac{1}{r_{12}} \right| \sigma_B(2)\, d_{Z_B^2}(2) \right\rangle,$$

and for the rectangular configuration

$$\left\langle \sigma_A(1)\, p_{X_A}(1) \left| \frac{1}{r_{12}} \right| \sigma_B(2)\, p_{X_B}(2) \right\rangle$$

and

$$\left\langle \sigma_A(1)\, d_{X_A^2}(1) \left| \frac{1}{r_{12}} \right| \sigma_B(2)\, d_{X_B^2}(2) \right\rangle.$$

In the region where the multipolar expansion of $1/r_{12}$ is valid, we can retain the leading dipole-dipole interaction operator $V_{dd} = \frac{1}{R^3}(X_1 X_2 + Y_1 Y_2 - 2Z_1 Z_2)$. It follows, for the second order interaction energy, that $E^{(2)}_{\text{linear}} \approx 4E^{(2)}_{\text{rectangular}}$ when we use our MO's basis set. The contributions coming from MO's, whose local symmetry allows the interaction along the direction of the intermolecular axis, and which have a higher energy than that used by us, are fundamental in order to get a Van der Waals minimum. Work is in progress to test numerically this contention.

The main point is that this kind of "frozen CI basis", which does not take into account the change of symmetry, cannot reproduce the orientational dependence of attractive intermolecular forces.

4. Internal Geometry Dependence of Intermolecular Interactions

a) Numerical Results

The success in getting a significant contribution to the interaction correlation energy for the linear configuration, allows us to undertake the study of internal geometry dependence of attractive and Pauli repulsion interaction energy. In Table 2, the values of E_{SCF} and $E_{\text{SCF-CI}}$ are given for different intermolecular distances R and the following cases: a) both molecules at equilibrium distance $r_1 = r_2 = r_0$, b) one stretched molecule $r_1 = 1.6$ a.u., for the other $r_2 = r_0$ and c) both molecules stretched $r_1 = r_2 = 1.6$ a.u. Also E_{SCF} for two isolated H_2 molecules in the three cases is indicated. The E_{SCF} for the stretched systems (b) and (c) at the distance $L = 20$ represents rather well two non interacting molecules. The three total energy curves present a minimum nearly at the same intermolecular distance. The depth of the potential is independent of the variation of the internal parameters. The SCF potential energy curve corresponds to a repulsive state between the two H_2 molecules.

The variation of interaction energy with respect to case (a) is presented in Table 3. The total interaction energy, $U_{\text{SCF-CI}}(L, r_1, r_2)$, is defined as:

$$U_{\text{SCF-CI}}(L, r_1, r_2) = E_{\text{SCF-CI}}(L, r_1, r_2) - E_{\text{SCF-CI}}(20.0, r_1, r_2). \tag{3}$$

The correlation interaction energy, $U_{\text{corr}}(L, r_1, r_2)$ is defined to be:

$$U_{\text{corr}}(L, r_1, r_2) = U_{\text{SCF-CI}}(L, r_1, r_2) - U_{\text{SCF}}(L, r_1, r_2),$$

where U_{SCF} comes from formula (3) with SCF instead of SCF-CI energies. Finally, the variation of the interaction energy $\Delta U(L, r_1, r_2)$ is defined by the formula:

$$\Delta U(L, r_1, r_2) = U(L, r_1, r_2) - U(L, r_0, r_0). \tag{4}$$

The comparison of ΔU_{SCF}, at a given distance L, for the cases (b) and (c) shows us that this quantity is rather additive with the number of stretched molecules. This same result was found for the rectangular and perpendicular configurations [5]. The repulsive energy increases with increased internal dimension in accordance with our previous results [5]. It is worth to note that, the additivity of repulsive energy with the number of stretched molecules is more accurately reproduced for the rectangular and perpendicular configuration than it is for the linear one. This result seems not surprising because one could expect a great electronic cloud deformation in the linear case, this obviously could shade any kind of additivity.

The new results concern the correlation interaction energy: the attractive $U_{corr}(L, r_1, r_2)$ increases with increasing values of r_1 and or r_2. A glance at Table 3 shows us that ΔU_{corr}, at a given distance, is also a roughly additive function over all the ranges studied. It seems that molecules retain a certain identity inside the composite system.

Table 1. E_{SCF} and $E_{SCF\,CI}$ values for the geometrical configurations: a) rectangular, b) perpendicular, c) linear, d) T, as a function of intermolecular distance L in R/r_0 units

L	a		b		c		d	
	E_{SCF}	$E_{SCF\,CI}$	E_{SCF}	$-E_{SCF\,CI}$	$-E_{SCF}$	$-E_{SCF\,CI}$	$-E_{SCF}$	$-E_{SCF\,CI}$
1.5	2.0784015	2.1007100	2.0892859	2.1059093	1.7473396	1.7869960	2.0652882	2.0837133
2.0	2.1910301	2.2114234	2.1934048	2.2121826	2.1440852	2.1732333	2.1862722	2.204925
3.0	2.2449125	2.2644072	2.2451236	2.2639088	2.2413293	2.2620255	2.2442769	2.2636663
4.0	2.2504927	2.2698157	2.2505365	2.2696830	2.2501745	2.2713600	2.2505509	2.2699905
5.0	2.2509628	2.2701892	2.2509771	2.2701715	2.2509032	2.2708407	2.2510103	2.2703179
6.0	2.2510009	2.2702014	2.2510066	2.2701994	2.2509880	2.2703126	2.2510263	2.2702342
20.0	2.2510088	2.2702012	2.2510080		2.2510086	2.2702011	2.2510085	·

Table 2. SCF and SCF CI energies in a.u. Variation with both, intermolecular L and intramolecular distances r_1, r_2. For comparison, E_{SCF} for two isolated H_2 molecules is indicated in the last row

L	Normal molecules $r_1 = r_2 = r_0$		One stretched molecule $r_1 = 1.6$ a.u., $r_2 = r_0$		Two stretched molecules $r_1 = r_2 = 1.6$ a.u.	
	$-E_{SCF}$	$-E_{SCF\,CI}$	$-E_{SCF}$	$-E_{SCF\,CI}$	$-E_{SCF}$	$-E_{SCF\,CI}$
3.5	2.2481432	2.2695262	2.2414195	2.2649886	2.2346822	2.2604253
4.0	2.2501745	2.2713600	2.2437478	2.2670295	2.2373082	2.2626580
4.5			2.2444251	2.2669503	2.2381021	2.2625769
5.0	2.2509032	2.2708907	2.2446272	2.2664151	2.2383473	2.2619743
6.0	2.2509880	2.2703126	2.2447315	2.2657678	2.2384739	2.2612156
20.0	2.2510086	2.2702011	2.2447569	2.2656275	2.2385041	2.2610468
$2H_2$	2.2510089		2.2447561		2.2385043	-

Table 3. ΔU_{SCF} and correlation interaction energy ΔU_{corr}. Variation of interaction energy, with respect to the intermolecular distance L and the intramolecular distances r_1, r_2 in a.u.

L	One stretched molecule $r_1 = 1.6$ a.u., $r_2 = r_0$		Two stretched molecules $r_1 = r_2 = 1.6$ a.u.	
	ΔU_{SCF}	$-\Delta U_{corr}$	ΔU_{SCF}	$-\Delta U_{corr}$
3.5	0.01283	0.01379	0.02603	0.02746
4.0	0.00475	0.01136	0.00985	0.02215
5.0	0.00069	0.00467	0.00140	0.00923
6.0	0.00012	0.00089	0.00026	0.00181

b) Discussion

The increase of attractive intermolecular energy with the internal dimensions can be understood in terms of molecular properties of the partners, particularly their dipolar polarizabilities. Since our numerical results on the variation of attractive interaction energy with the number of stretched molecules seems to support the idea of a certain independence of the partners, and with the hypothesis that, roughly, the main contribution to the correlation interaction energy is of a second order dispersion type, U_{corr} can be represented by the London term $U_{\text{corr}} \approx -C^{(6)}_{H_2-H_2}/R^6$. The $C^{(6)}$ coefficient being intimately connected with dipolar-polarizabilities. Proceeding with the Slater-Kirkwood formula, one gets the expression

$$-U_{\text{corr}}R^6 \approx \tfrac{3}{4}\bar{E}\alpha_{H_2} \cdot \alpha_{H_2}\,, \tag{5}$$

where $\bar{E}$ is an average excitation energy and α the polarizability of isolated molecules. Ishiguro *et al.*, studied the variation of polarizabilities with interatomic distance for the H_2 molecule [11]. They found that α_{H_2} is an increasing function of interatomic distance. Formula (5) shows that, at a given distance, U_{corr} must increase with internal dimensions. This behavior prompts a qualitative picture. When bonds are formed, electrons flow to the interatomic region and become tightly bound, exactly the opposite is going on when atoms are stretched from their equilibrium positions. The molecule become larger and more easily polarizable. But if this is so, in a given point of space, between the interacting molecules, the electron density increases when one (or both) molecule (*s*) is stretched, then, the Pauli repulsion energy increases. This picture seems to be in agreement with the numerical results obtained on calculations of this type of forces [4, 5].

Acknowledgements. The authors would like to thank Professor S. Bratos for several suggestions and helpful discussions. The computer time for this work was supported by the C.M.O.A. of Paris, and Professor R. Daudel, Director of this Laboratory, is much acknowledged.

References

1. Bratos, S., Rios, J., Guissani, I.: J. chem. Physics **52**, 439 (1970).
2. Bauer, S. A., Ossa, E.: J. chem. Physics **45**, 434 (1966).
3. Burcat, A., Lifshitz, A.: J. chem. Physics **47**, 3079 (1967).
4. Tapia, O., Bessis, G., Bratos, S.: Compt. Rend. Ac. Sc. (Paris) B **268**, 813 (1969).
5. — — — Int. J. quant. Chemistry S4, 289 (1971).
6. London, F.: Trans. Faraday Soc. **38**, 8 (1937).
7. Bessis, G.: Unpublished work.
8. Clementi, E., Veillard, A.: Rep. I.B.M. Research Laboratory, San José (USA).
9. Gordon, R. G., Cashion, J.: J. chem. Physics **44**, 1190 (1966).
10. Woodrow Wilson, C., Jr., Goddard III, W. A.: J. chem. Physics **51**, 716 (1968).
11. Ishiguro, E., Arai, T., Mizushima, M., Kotani, M.: Proc. physic. Soc. (London) **ALXV**, 178 (1952).
12. Magnasco, V., Musso, G. F.: J. chem. Physics **46**, 4015; **47**, 1723; **47**, 4629 (1967).
13. — — McWeeny, R.: J. chem. Physics **47**, 4617 (1967).

Prof. Dr. G. Bessis
Laboratoire de Spectroscopie et luminescence
Faculté des Sciences de Lyon
Université Claude Bernard
F-69 Villeurbanne, France

Theoret chim. Acta (Berl.) 25, 138–142 (1972)
© by Springer-Verlag 1972

Further *ab initio* Calculations on the Allyl Radical

A. Hinchliffe

Chemistry Department, U.M.I.S.T., Manchester M60 1QD, England

Received October 21, 1971

Further *ab initio* calculations of proton coupling constants using the LCGO technique are presented for the allyl radical, showing varying degrees of success.

Es werden weitere *ab initio* Rechnungen für die Proton-Kopplungskonstante angegeben wobei die LCGO-Methode auf das Allylradikal mit unterschiedlichem Erfolg angewandt wird.

Introduction

In a previous publication [1] the results of preliminary *ab initio* calculations of ESR hyperfine coupling constants in the allyl radical were presented. Each Slater type orbital (STO) was represented by a linear combination of two Gaussian orbitals (GTOs), and two different linear combinations (contractions) were reported. Considering the relative lack of sophistication of the wavefunctions employed, the results were found to be in fair agreement with experiment, and compared well with the results obtained from semi empirical calculations.

In this publication we present the results of similar calculations employing more accurate wavefunctions. The reason for extending the calculations by using a larger number of GTOs in the contraction is that, whereas small contractions are clearly very poor for energy calculations, this gives little guide as to their usefulness for the calculation of molecular properties; thus hopefully it should be possible to use very simple wavefunctions for the *ab initio* calculation of certain molecular properties, although the converse may be true.

Method

A number of differet contractions were tried in order to assess the sensitivity of the proton ESR coupling constants. The STO hydrogen exponent was assumed to be 1.2 throughout, instead of the free atom value 1.0; A number of contractions exist in the literature for free atoms, the ones used in the present work being given in Table 1 [2, 3]. Thus each STO was approximated by GTO where $n = 2, 3, 4, 5, 6$ (referred to as A, B, C, D, E) and a further calculation was performed (F) to check that the proton coupling constant calculation is insensitive to the precise form of the carbon 1*s* orbital. For this calculation, the carbon 1*s* orbitals were approximated as 6 GTO whilst the valence orbitals were approximated by 3 GTO.

All integrals were calculated using a version of IBMOL 4 [4] specially rewritten for the University of Manchester ICL 1906 Å computer, running under the GEORGE III operating system [1]. It is unfortunately impossible to report the exact mill times taken for integral calculation, as this figure cannot be obtained

Table 1. Contractions used

H		K_c		S_c		X_c		
d	α	d	α	d	α	d	α	
0.4301	1.2266	0.4301	27.6756	0.7471	0.3412	0.4523	1.1418	A
0.6789	0.2183	0.6789	4.9262	0.2856	0.1296	0.6713	0.2824	
0.1543	3.2078	0.1677	69.6723	-0.2888	8.3652	0.2332	2.3235	B
0.5353	0.5843	0.5434	12.4425	0.7008	0.3794	0.5743	0.5014	
0.4446	0.1581	0.4320	3.2222	0.3734	0.1223	0.4132	0.1318	
0.0568	7.5123	0.0649	158.7920	-0.0874	32.1659	0.0997	4.6202	C
0.2601	1.3747	0.2815	28.8682	-0.2444	5.5509	0.3560	1.0573	
0.5328	0.3819	0.5339	7.8246	0.6465	0.4253	0.5289	0.3113	
0.2916	0.1267	0.2707	2.4906	0.4479	0.1346	0.2545	0.0988	
0.0221	16.2804	0.0267	331.7210	-0.0221	109.0350	0.0437	8.4706	D
0.1354	2.9833	0.1322	60.6526	-0.0994	19.4645	0.1906	1.9972	
0.3318	0.8333	0.3580	16.7641	-0.2188	4.9297	0.4054	0.6365	
0.4826	0.2845	0.4736	5.5702	0.6386	0.4343	0.4439	0.2220	
0.1936	0.1072	0.1632	2.0004	0.4602	0.1366	0.1576	0.0791	
0.0092	33.2684	0.0092	750.6175	-0.0042	73.1160	0.0079	15.4981	E
0.0494	6.0997	0.0494	137.6249	-0.0207	13.4087	0.0514	4.0416	
0.1685	1.7065	0.1685	38.5025	-0.0515	3.7681	0.1898	1.4461	
0.3705	0.5862	0.3705	13.2266	0.3346	0.5389	0.4050	0.6045	
0.4165	0.2276	0.4165	5.1363	0.5621	0.2446	0.4013	0.2764	
0.1303	0.0938	0.1303	2.1154	0.1713	0.1166	0.1052	0.1307	

from the computer to any degree of accuracy. As a rough approximation however, for $n = 2$ the two electron integrals took 180 seconds whilst for $n = 4$ the mill time was approximately 2000 seconds.

The self consistent field method used to calculate the wavefunctions was the Unrestricted Hartree Fock (UHF) method [5] which averaged 200 sec to obtain accuracy in the density matrices to 5 decimals, depending on the goodness of the initial guesses for the density matrices. As before, the allyl radical was assumed to be planar with regular geometry, all CC bond lengths 1.4 Å, all CH bond lengths 1.08 Å. No attempt was made to find the lowest energy conformation, although it was not expected that any change in geometry would affect the results significantly.

Results and Discussion

The nuclear repulsion energy was 64.83595 a.u., whilst the electronic energies are given in Table 2. The best energy was given by the $n = 5$ set, this contraction corresponding to the best $n = 5$ contraction for the carbon atom in its ^3p state [3]. The $n = 6$ set was slightly inferior, due to the different method of finding the contraction [2]. For large systems however, the small improvements in energy and wavefunction that result from using $n > 4$ seem hardly justifiable in the face of the increased cost of the calculation (proportional to n^4 approximately).

Table 2

Basis	$\langle S^2\rangle_{ba}$	$\langle S^2\rangle_{aa}$	Energy	Density at nucleus
A	1.0252	0.7632	−176.5639	0.262
B	0.9657	0.7548	−179.6109	0.362
C	0.9902	0.7580	−180.6720	0.429
D	0.9954	0.7587	−180.9997	0.495
E	1.0597	0.7679	−180.9893	0.486
F	0.9645	0.7548	−180.7283	0.368

Energies and density at nucleus in atomic units.

Table 3

Basis	1	2	3
A	−26.79	−26.89	+19.06
	−8.78	−8.81	+6.49
B	−28.35	−28.61	+20.14
	−9.32	−9.41	+6.86
C	−36.76	−37.14	+26.21
	−12.06	−12.18	+8.88
D	−42.45	−42.96	+29.99
	−13.91	−14.08	+10.18
E	−53.95	−54.30	+39.94
	−17.64	−17.76	+13.67
F	−28.33	−28.59	+20.10
	−9.32	−9.40	+6.78
Experiment	−13.93	−14.83	+4.06

Proton coupling constants (gauss).

UHF calculations, as is well known [5] are not accurate descriptions of spectroscopic states, since they are not spin eigenfunctions. Such wavefunctions can be improved by the spin annihilation technique of Amos and Snyder [5]. Values of $\langle S^2\rangle_{ba}$ and $\langle S^2\rangle_{aa}$ in the notation of [5] are given in Table 2: spin annihilation generally makes a large improvement in the value of $\langle S^2\rangle$.

The results for Basis A ($n = 2$) were reported previously [1], but unfortunately there was an error in the coupling constants reported in [1], for that particular basis set. We report here the corrected values in Table 3, together with the results for the other basis sets.

In general, the coupling constants calculated *before* spin annihilation are too large, whilst the ones calculated after spin annihilation are in much better agreement with experiment. The results for the central proton become less good as n increases, and a general unwelcome trend is obvious from the table, that the coupling constants increase in modulus as n increases. This is because the one and two electron integrals for all except the carbon 1*s* orbitals change little as n increases, so consequently the molecular orbital coefficients change little as n increases. However, the density of the hydrogen $1s$ orbital at the nucleus changes by 100%, as can be seen from Table 2. For comparison, the exact value for a Slater hydrogen $1s$ orbital $\sqrt{\zeta^3/\pi}\, e^{-r}$ is $\zeta^3/\pi = 0.55$ for $\zeta = 1.2$. The density at the nucleus is seriously in error, even for the most accurate contraction taken ($n = 5$). Further, the shapes of GTOs and STOs around the nucleus is quite different.

Treating the density at the nucleus as a variable parameter still gives the same overall pattern of coupling constants, and does not correctly reproduce their experimental ratio.

As before [1] we may compare our results with the results of a semi empirical calculation using the Pariser-Parr integrals [6]. The Pariser-Parr model may be regarded as using an *orthogonalised* basis of π type atomic orbitals $(\bar{\varphi}_1 \dots \bar{\varphi}_m)$ for the construction of π molecular orbitals. These are related to the non-orthogonal $2p_z$ orbitals $(\varphi_1 \dots \varphi_m)$ by the transformation

$$(\bar{\varphi}_1 \dots \bar{\varphi}_m) = (\varphi_1 \dots \varphi_m) S^{-\frac{1}{2}}$$

where $S_{ij} = \langle \varphi_i | \varphi_j \rangle$ is the matrix of overlap integrals. *Ab initio* calculations are generally performed using a non orthogonal basis, for ease of computation, and if $P_1(r)$, $Q_1(r)$ are the one electron charge and spin density functions respectively [7], where

$$\begin{aligned} P_1(r) &= \Sigma\, \varphi_i^*(r)\,(P_1)_{ij}\,\varphi_j(r) \\ Q_1(r) &= \Sigma\, \varphi_i^*(r)\,(Q_1)_{ij}\,\varphi_j(r) \end{aligned} \qquad (1)$$

and P_1, Q_1 are their matrix representations, and also

$$\begin{aligned} P_1(r) &= \Sigma\, \bar{\varphi}_i^*(r)\,(P_1)_{ij}\,\bar{\varphi}_j(r) \\ Q_1(r) &= \Sigma\, \bar{\varphi}_i^*(r)\,(Q_1)_{ij}\,\bar{\varphi}_j(r) \end{aligned} \qquad (2)$$

then

$$\begin{aligned} \bar{P}_1 &= S^{\frac{1}{2}} P_1 S^{\frac{1}{2}} \\ \bar{Q}_1 &= S^{\frac{1}{2}} Q_1 S^{\frac{1}{2}} \end{aligned} \qquad (3)$$

so the elements of $\bar{P}_1$, $\bar{Q}_1$ obtainable from our *ab initio* calculation by (3) should be directly comparable to the semi empirical results.

For the semi empirical calculation we find

$$\bar{P}_1 = \begin{pmatrix} 1.000 & 0.693 & 0.000 \\ & 1.000 & 0.693 \\ & & 1.000 \end{pmatrix} \quad \bar{Q}_1 = \begin{pmatrix} 0.551 & 0.000 & -0.425 \\ & -0.102 & 0.000 \\ & & 0.551 \end{pmatrix}$$

whilst for the $n = 5$ *ab initio* calculations we obtain

$$\bar{P}_1 = \begin{pmatrix} 1.000 & 0.671 & 0.000 \\ & 1.000 & 0.671 \\ & & 1.000 \end{pmatrix} \quad \bar{Q}_1 = \begin{pmatrix} 0.570 & 0.000 & -0.370 \\ & -0.140 & 0.000 \\ & & 0.570 \end{pmatrix}$$

which compare reasonable well. It is interesting to note that, assuming the proton coupling constants can be calculated using McConnell's relation [8] with a proportionality constant -22.5 gauss, the "experimental" diagonal elements of $\bar{Q}_1$ are 0.58, −0.16 and 0.58, which compare alomost exactly with our calculation. It is also interesting to note that the diagonal elements of $\bar{P}_1$ are 1.000. The discrepancy in the *ab initio* calculation of coupling constants arises because of the relatively inaccurate representation of the σ system.

References

1 Hinchliffe, A. Chem. Physics Letters (in press).
2 Stewart, R. F. J. chem. Physics **52**, 431 (1970).
3 J. chem. Physics **50**, 2485 (1969).
4 QCPE program No 92, Indiana University, U.S.A.
5 Amos, A. T., Snyder, L. C.: J. chem. Physics **46**, 3144 (1967).
6 Pariser, R., Parr, R. G.: J. chem. Physics **21**, 466 (1953).
7 McWeeny, R., Sutcliffe, B. T.: Methods of molecular quantum mechanics, p. 87. Academic Press 1970
8 McConnell, H. M. J. chem. Physics **28**, 1188 (1958).

Dr. A. Hinchliffe
Chemistry Department U.M.I.S.T.
Manchester, M60 1QD, England

Theoret. chim. Acta (Berl.) 25, 143--168 (1972)
© by Springer-Verlag 1972

On the Relation between Non Adiabatic Unimolecular Reactions and Radiationless Processes

HELMUT GEBELEIN* and JOSHUA JORTNER

Department of Chemistry, Tel-Aviv University, Tel-Aviv, Israel

Received September 30, 1971

In this paper we present the results of a theoretical study of non adiabatic unimolecular dissociation processes with applications to the decomposition of $N_2O(^1\Sigma)$ to yield $N_2(^1\Sigma_g)$ and $O(^3P)$. Such unimolecular reactions which involve a change in the electronic state can be handled by the theory of thermally excited intramolecular radiationless decay processes in analogy to molecular predissociation and electronic relaxation in the statistical limit. General criteria were advanced for describing the decay probability of a single vibronic level in terms of Fermi's golden rule and for specifying the (high pressure) unimolecular rate constant in terms of a thermally averaged transition probability. The quantum mechanical rate constant for the non adiabatic reaction is characterized by a preexponential factor determined by the interstate coupling matrix element and by a temperature dependent activation energy. At low temperatures the activation energy is equal to the continuum onset, and the reaction involves a tunnelling process. In the high temperature limit a general demonstration of the Franck Condon principle for thermal reactions was provided, whereupon the non radiative transition occurs at the intersection of the potential surfaces. Numerical calculations for a one dimensional model system for the thermal decomposition of N_2O were performed utilizing the semiclassical approximation and confirm our general conclusions. A two dimensional linear model has been developed representing the rate constant in terms of a convolution of two generalized line shape functions, which enabled us to study the distribution of vibrational energy among the diatomic N_2 molecules resulting from the thermal decomposition of N_2O. Some predictions concerning the determination of single level decay probabilities and vibrational distribution of the molecular products are presented.

In dieser Arbeit werden die Ergebnisse einer theoretischen Untersuchung nicht adiabatischer unimolekularer Zerfallsreaktionen mitgeteilt und auf den Zerfall von $N_2O(^1\Sigma)$ zu $N_2(^1\Sigma_g)$ und $O(^3P)$ angewandt. Solche unimolekularen Reaktionen, bei denen sich der Elektronenzustand ändert, können mit der Theorie thermisch angeregter intramolekularer strahlungsloser Zerfallsprozesse in Analogie zu molekularer Prädissoziation und elektronischer Relaxation im statistischen Limit behandelt werden. Kriterien zur Beschreibung der Zerfallswahrscheinlichkeiten eines einzelnen Vibrationszustands unter Berücksichtigung von Fermis Golden Rule werden entwickelt sowie die unimolekulare Geschwindigkeitskonstante (im Hochdruckbereich), wobei thermisch gemittelte Übergangswahrscheinlichkeiten berücksichtigt werden, mitgeteilt. Die quantenmechanische Geschwindigkeitskonstante für die nicht adiabatische Reaktion wird durch einen präexponentialen Faktor, der durch die Matrixelemente der Kopplung beider Zustände bestimmt ist und durch eine temperaturabhängige Aktivierungsenergie charakterisiert. Bei tiefer Temperatur stimmt die Aktivierungsenergie mit der Energie der Kontinuumsgrenze überein, die Reaktion verläuft über einen Tunneleffekt. Für hohe Temperaturen wurde ein allgemeiner Beweis des Franck-Condon-Prinzips für thermische Reaktionen gegeben, wonach der strahlungslose Übergang beim Schnittpunkt der Potentialflächen auftritt. Rechnungen für ein eindimensionales Modell des N_2O Zerfalls wurden in der semiklassischen Näherung durchgeführt und bestätigen unsere Folgerungen. Ein zweidimensionales Modell wurde entwickelt, das die Geschwindigkeitskonstante als Faltungsintegral zweier verallgemeinerter Linienformintegrale wiedergibt. Dadurch wurde es ermöglicht, die Verteilung der Vibrationsenergie auf die zweiatomigen N_2 Moleküle, die bei dem thermischen Zerfall von N_2O enstehen, zu studieren. Einige Voraussagen über die Bestimmung der Zerfallswahrscheinlichkeiten eines Vibrationszustandes und die Vibrationsverteilung der molekularen Produkte werden mitgeteilt.

---

* Present address: Institut für physikalische Chemie, Frankfurt, Robert-Mayer-Straße 11, Germany.

1. Introduction

The key physical idea underlying recent theoretical studies [1] of intramolecular radiationless transitions in large molecules is that electronically excited zero order molecular states are non stationary (or metastable) being degenerate with and irreversibly coupled to a quasi-continuum of zero order levels corresponding to lower electronic configurations. This work has established the formal analogy between electronic relaxation processes (i.e. internal conversion and intersystem crossing) and radiationless molecular decomposition processes (i.e. predissociation and autoionization). Forty years ago, Rosen [2], Langer [3] and Rice [4] proposed that thermal unimolecular decomposition reactions can be considered as an Auger process, in complete analogy to predissociation and autoionization. This approach has been revived lately in the work of Mies and Kraus [5-7] who stress the point that the "activated state" in chemical kinetics is equivalent to the concept of a resonance state in scattering theory, and is thus amenable to theoretical treatment by the Fano configuration scheme. Mies and Kraus [5-7] consider the activated molecule in unimolecular decomposition in terms of a vibrationally excited zero order molecular state located above the threshold dissociation energy. A different class of unimolecular decomposition process involve a change in the electronic state. The best documented reactions of this type [8-12] (see Table 1) pertain to the thermal decomposition of some linear triatomics to yield an oxygen atom and a closed shell diatomic molecule.

$$XYO(^1\Sigma) \rightarrow XY(^1\Sigma) + O\,.$$

The dissociation energy, D of the ground state molecule $XYO(^1\Sigma)$ yielding $XY(^1\Sigma)$ and an excited $O(^1D)$ oxygen atom, usually exceeds the experimental Arrhenius [13] activation energy, E_A. There exists, however, a non bonding triplet state [8-12] dissociating into $XY(^1\Sigma)+O(^3P)$ yielding a ground state oxygen atom. The repulsive potential surface intersects the bound ground state potential curves at energies well below the dissociation limit, providing a proper rationalization for the low activation energy. The intramolecular interstate coupling is envisaged to be induced by weak spin-orbit interaction [8-12], so that following the usual conventional nomenclature adopted in chemical kinetics [11] (which semantically is not quite appropriate) one refers to such a process as a non adiabatic reaction. In this context the Landau-Zener [14, 15] formalism for non adiabatic processes (such as predissociation) was applied by Stearn and Eyring [8] for the thermal decomposition of N_2O. The predissociation probability calculated by the Landau-Zener formula was identified with the transmission coefficient κ in the absolute reaction theory, so that the high pressure rate constant, k, is given by [8] $k=(\kappa k_B T/h)(Z^*/Z)\exp(-E_A/k_B T)$. The ratio Z^*/Z of the partition functions for the activated complex and for the bound molecule is close to unity. An application of the unimolecular reaction rates theories of Hinshelwood, Kassel, Rice and Ramsperger [16-18] to the thermal decomposition of N_2O was given by Gill and Laidler [9]. A useful review of these theories is presented by Troe and Wagner [12]. In an interesting recent work, Gilbert and Ross [19] have proposed that the formalism of intramolecular radiationless processes can be applied for the study of non adiabatic unimolecular decomposition processes,

Table 1. Experimental data for nonadiabatic unimolecular rate constants of some triatomic molecules (Ref. [12])

ΔH_0[kcal/mole]	D(XY–O) or D(XY–S) [kcal/mole]	T[°K]	$k_\infty \left[\frac{1}{\text{sec}}\right]$ expt	$k \left[\frac{1}{\text{sec}}\right]$ theory[a]
Reaction: $N_2O(^1\Sigma^+) \rightarrow N_2(^1\Sigma^+) + O(^3P)$				
38.6 ± 0.1	$N_2(^1\Sigma^+) \rightarrow$ $N_2(^1\Sigma^+) + O(^1D)$	888	$7.47 \ 10^{-4}$	2.8×10^{-3}
	83.5 ± 0.1	1400–2000	$1.6 \times 10^{11} \exp\left(-\frac{60}{RT}\right)$	$4.1 \times 10^{11} \exp\left(-\frac{59}{RT}\right)$
Reaction: $CO_2(^1\Sigma^+) \rightarrow CO(^1\Sigma^+) + O(^3P)$				
125.8 ± 0.6	$CO_2(^1\Sigma^+) \rightarrow$ $CO(^1\Sigma^+) + O(^1D)$ 171.1 ± 0.6	2800–3700	$2.10^{11} \exp\left(-\frac{110}{RT}\right)$	
Reaction: $CS_2(^1\Sigma^+) \rightarrow CS(^1\Sigma^+) + S(^3P)$				
91.5 ± 5	$CS_2(^1\Sigma^+) \rightarrow$ $CS(^1\Sigma^+) + S(^1D)$ 118 ± 5	1950–2800	$8.10^{12} \exp\left(-\frac{89}{RT}\right)$	
Reaction: $COS(^1\Sigma^+) \rightarrow CO(^1\Sigma^+) + S(^3P)$				
	$COS(^1\Sigma^+) \rightarrow$ $CO(^1\Sigma^+) + S(^1D)$ 97.6 ± 1	1550–2700	$3.7 \times 10^{11} \exp\left(-\frac{68.3}{RT}\right)$	

[a] Theoretical value for a one dimensional system characterized by a Morse type N_2–O potential for the initial state and the crossing of the band and repulsive potentials occurring at $E_0 = 21023$ cm^{-1}.

performing some approximate numerical calculations for the thermal decomposition of N_2O. In the present paper, we shall pursue further the formal analogy between non adiabatic high pressure unimolecular decomposition reactions and molecular radiationless processes. The main goals and accomplishments of the present work are:

a) The theory of predissociation [20–24] will be applied for the study of non adiabatic unimolecular processes. The only difference between the two types of processes involves the excitation mode of the decaying states, which is optical in the case of predissociation and thermal for unimolecular decomposition.

b) Microscopic rate constant for the decay of individual zero order vibronic levels cannot be handled by the Landau-Zener formula [14, 15] which provides an averaged level, neglecting the oscillatory nature of these transition probabilities [19]. The *WKB* semi-classical approximation which was successfully applied by Child [23] for predissociation will be adopted by us to derive analytic expression for the microscopic rate constant for simple model systems.

c) Quantum mechanical rate expression will be derived for the decay in a two electronic level system without invoking the concept of an activated complex.

d) The general features of the rate expression for non adiabatic unimolecular decomposition will be elucidated. In the low temperature limit the process corresponds to tunnelling between two zero order states, being completely analogous to the common situation encountered for electronic relaxation in large aromatic molecules. In the high temperature limit, a semi-classical approximation for nuclear motion can be adopted and the major contribution to the rate constant originates from the vicinity of the crossing of the potential surface.

e) The nature of the activation energy and its temperature dependence will be established.

f) From the practical point of view numerical calculations will be performed for a model system pertaining to the unimolecular decomposition of N_2O.

g) From the point of view of general methodology, we shall establish the conditions for the application of the Fermi golden rule to the study of unimolecular decomposition processes.

2. A Physical Model for Non Adiabatic Unimolecular Decay

To describe a unimolecular decomposition process, which involves a change in the electronic state of a triatomic molecule, we shall proceed in a manner completely analogous to the treatment of electronic relaxation [1] and decomposition processes [20–24]. We shall specify an appropriate zero order basis set to describe the approximate vibronic levels of the physical system. The choice of this basis set is in principle arbitrary, being just a matter of convenience. The total Hamiltonian $\boldsymbol{H}$ can be dissected in the form

$$\boldsymbol{H} = \boldsymbol{H}_0 + \boldsymbol{V} \tag{2.1}$$

where the zero order basis set of $\boldsymbol{H}_0$ corresponds to pure spin states (of different spin configurations) in the Born-Oppenheimer approximation (see Fig. 1). The eigenfunctions of $\boldsymbol{H}_0$ can be represented as a product of electronic wave functions, φ, and vibrational wave functions, χ,

$$\begin{aligned} |i\alpha\rangle &= \varphi_i(\boldsymbol{r}, \boldsymbol{R})\, \chi_{i\alpha}(\boldsymbol{R}) \\ |f\beta\rangle &= \varphi_f(\boldsymbol{r}, \boldsymbol{R})\, \chi_{f\beta}(\boldsymbol{R}) \end{aligned} \tag{2.2}$$

where the indices i and f represent the initial and the final electronic states, respectively. The vibrational wavefunctions $\chi_{i\alpha}(\boldsymbol{R})$ and $\chi_{f\beta}(\boldsymbol{R})$ in the initial and final electronic states correspond (approximately) to the eigenvalues of the adiabatic potentials $V_i(\boldsymbol{R}) = \langle\varphi_i|\boldsymbol{H}_0|\varphi_i\rangle$ and $V_f(\boldsymbol{R}) = \langle\varphi_f|\boldsymbol{H}_0|\varphi_f\rangle$. Finally $\boldsymbol{r}$ and $\boldsymbol{R}$ represent the electronic and the nuclear coordinates respectively. The potential $V_i(\boldsymbol{R})$ is bound and the eigenstates $|i\alpha\rangle$ are discrete. The final state potential $V_f(\boldsymbol{R})$ is repulsive at least for one degree of freedom, so that the eigenstates $|f\beta\rangle$ are continuous. The corresponding energies of the zero order states will be denoted by $E_{i\alpha}$ and by $E_{f\beta}$.

The intramolecular coupling term consists of two parts

$$\boldsymbol{V} = \boldsymbol{T}_R + \boldsymbol{H}_{so} \tag{2.3}$$

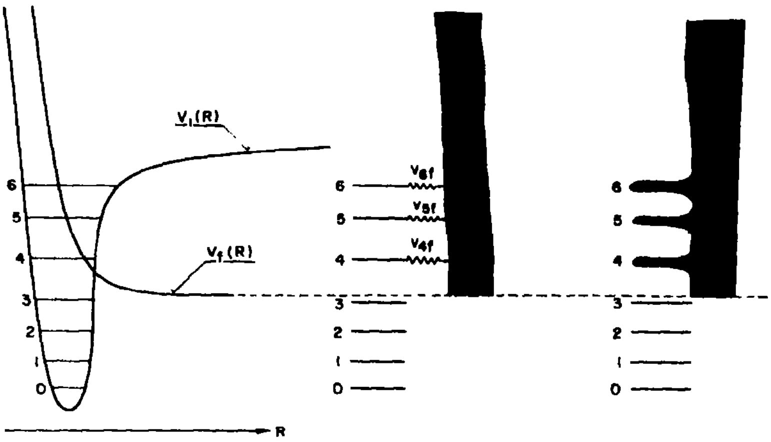

(a) Potential surfaces (b) Zero order energy levels (c) Resonances

Fig. 1. A schematic description of the resonance states involved in unimolecular decomposition. a One dimensional potential surfaces. b Zero order energy levels corresponding to the two electronic states. Near resonance coupling between discrete and continuum zero order levels is designated by arrows. c Non overlapping resonances appear above the continuum threshold. These states diagonalize the total molecular Hamiltonian

where T_R is the nuclear kinetic energy operator and H_{so} is the spin orbit coupling operator. Now we assert that:

(A) Relaxation within a two electronic level system can be considered, whereupon off resonance second order coupling of $|i\alpha\rangle$ and $|f\beta\rangle$ with higher electronic states can be disregarded [25].

As the non adiabatic coupling term T_R conserves spin states, the relevant coupling term between near resonance states $|i\alpha\rangle$ and $|f\beta\rangle$ involves just the spin orbit coupling and second order mixed type terms involving coupling via T_R and H_{so} with higher electronic states are neglected. Thus the relevant interstate coupling terms are

$$\begin{aligned} V_{i\alpha,f\beta} &= \langle i\alpha| T_R + H_{so} |f\beta\rangle \\ &= \int dR\, \chi_{i\alpha}(R) \left[\int dr\, \varphi_i(r,R)\, H_{so}\, \varphi_f(r,R)\right] \chi_{f\beta}(R)\,. \end{aligned} \tag{2.4}$$

To simplify this result we assume that

(B) The electronic matrix element of the spin orbit coupling operator

$$\langle H_{so}(R)\rangle = \int dr\, \varphi_i(r,R)\, H_{so}\, \varphi_f(r,R) \tag{2.5}$$

is assumed to be a slowly varying function of the nuclear coordinates R and will be taken as a constant $\langle H_{so}(R)\rangle \equiv \langle H_{so}\rangle$ in the double integral (2.4).

This assumption is equivalent to the Condon approximation in the calculation of molecular optical transition moments. Recent studies [25] have indicated that for the case of non adiabatic coupling between two electronic states of the same spin via T_R the application of the Condon approximation is not justified. However, for the case of coupling via H_{so} between two different spin states this approximation seems to be reasonable. Thus Eq. (2.4) is recast in the form

$$V_{i\alpha,f\beta}=\langle H_{so}\rangle \int dR\,\chi_{i\alpha}(R)\chi_{f\beta}(R) \tag{2.4a}$$

which takes the simple form of an electronic matrix element multiplied by a vibrational overlap Franck Condon factor [26].

The zero order states $|i\alpha\rangle$ which are quasidegenerate with the continuum states $|f\beta\rangle$, are metastable. Thus we encounter the extreme case of the statistical limit [1] where the density of states in the dissipative channel $|f\beta\rangle$ is a continuous function of the energy, and the physical situation is completely analogous to that of predissociation [21, 22]. Invoking assumption (A) the width $\Gamma_{i\alpha}$ of a zero order state $|i\alpha\rangle$ is given in terms of time dependent perturbation theory by the Fermi golden rule

$$\Gamma_{i\alpha}=2\pi\sum_{\beta}|V_{i\alpha,f\beta}|^2\,\delta(E_{i\alpha}-E_{f\beta}) \tag{2.6}$$

and making use of assumption (B) (Eq. 2.4a) we get

$$\Gamma_{i\alpha}=2\pi|\langle H_{so}\rangle|^2\sum_{\beta}|\int dR\,\chi_{i\alpha}(R)\chi_{f\beta}(R)\delta(E_{i\alpha}-E_{f\beta}). \tag{2.6a}$$

It is important to note at this point that the decay probability of an "initially prepared" zero order state $|i\alpha\rangle$ can be expressed in terms of the width (2.6) by $\Gamma_{i\alpha}/\hbar$, only provided that it is justified to consider the decay of a single resonance. We thus invoke the basic assumption.

(C) The spacing between the resonances considerably exceeds their widths. Denoting by $E_{i\alpha}-E_{i(\alpha+1)}$ the energy spacing between the adjacent order states $|i\alpha\rangle$ and $|i(\alpha+1)\rangle$ we imply that

$$\Gamma_{i\alpha}\ll|E_{i\alpha}-E_{i(\alpha+1)}| \tag{2.7}$$

for all α. Condition (2.7) provides us with the basic relation necessary for describing the decay process in terms of the perturbation theoretical results (2.6), so that the decay probability $W_{i\alpha}$ of the zero order state $|i\alpha\rangle$ is then given by

$$W_{i\alpha}=\Gamma_{i\alpha}/\hbar=2\pi/\hbar|\langle H_{so}\rangle|^2\sum_{\beta}\int dR\,\chi_{i\alpha}(R)\chi_{f\beta}(R)\delta(E_{i\alpha}-E_{f\beta}). \tag{2.8}$$

Thus, when interference effects between resonances can be disregarded, each zero order state can be described as an independently decaying resonance, its decay pattern being exponential and being characterized by the reciprocal decay time (2.8). The applicability of restriction (2.7) will imply that the thermally averaged rate constant will invoke a preexponential factor which involves the interstate coupling matrix element. This physical situation is often referred to in chemical kinetics as a non adiabatic transition [11]. The usual semiclassical description of a non adiabatic transition is provided [11] by implying that the splitting of the zero order potential surfaces at the intersection point is "small". Levich and Dogonadze [27] in their beautiful theoretical study of electron transfer processes in solution have provided a complete semiclassical criterion for the applicability of the non adiabatic kinetic scheme in terms of the Landau Zener theory, and similar conditions were also provided by Nikitin [28]. Considering unimolecularily decaying states as resonances, Eq. (2.7) provides a necessary and sufficient quantum mechanical condition for the applicability of the non adiabatic limit. To the best of our knowledge a complete quantum mechanical formulation of the adiabatic case was not yet provided. In this context, Mies and Kraus [5] have provided a simpliefied model (equal resonance spacings and widths) which exhibits the transition from the adiabatic to the non adiabatic case. For the physical case under consideration, which involves a spin forbidden transition between two different electronic states of a triatomic molecule the resonance widths are $\Gamma_{i\alpha} \sim 1$–$10\,\mathrm{cm}^{-1}$ (see Sect. 4), while the spacing between adjacent resonances corresponds to the vibrational frequency $\sim 1000\,\mathrm{cm}^{-1}$, thus the non adiabacity condition (2.7) is fulfilled.

Up to this point we have been concerned with the decay of an initially prepared isolated resonance, without referring to the "preparation" of the decaying states. We now focus attention on thermal excitation by collisions with inert molecules (which do not modify the zero order molecular levels or the intramolecular spin orbit coupling). Two further assumptions are introduced at this point:

(D) Thermal vibrational excitation (and relaxation) rates considerably exceed the non radiative decay probabilities, whereupon

$$\Gamma_{i\alpha}/\hbar \ll \frac{1}{\tau_v} \tag{2.9}$$

where τ_v is the vibrational relaxation time.

(E) The width of each resonance is considerably lower than the thermal energy $k_B T$, in the temperature range of interest [5–7]:

$$\Gamma_{i\alpha} \ll k_B T. \tag{2.10}$$

Condition (2.9) provides us with the conventional basic assumption for the applicability of unimolecular rate theory in the high pressure limit. Eq. (2.10) implies that the thermal population of all molecular eigenstates (of H) which correspond to the same resonance is equal.

The high pressure thermally averaged rate constant, k, is now given in the form

$$k = \sum_{\alpha} \exp(-E_{i\alpha}/k_B T)\, W_{i\alpha} / \sum_{\alpha} \exp(-E_{i\alpha}/k_B T) \tag{2.11}$$

where the microscopic rate constants $W_{i\alpha}$ (Eq. (2.8)) represent the predissociation probability for the zero order $|i\alpha\rangle$ state.

3. A One Dimensional Model

To pursue the formal analogy between decomposition of a thermally activated zero order vibrational level of a triatomic linear molecule XYO($^1\Sigma$) and predissociation we shall first limit ourselves to a one dimensional model, considering only the displacement R along the Y–O linear coordinate. We thus assume that only this single R coordinate is reactive while all the other modes remain unchanged. This "diatomic molecule model" for the decomposition of a triatomic

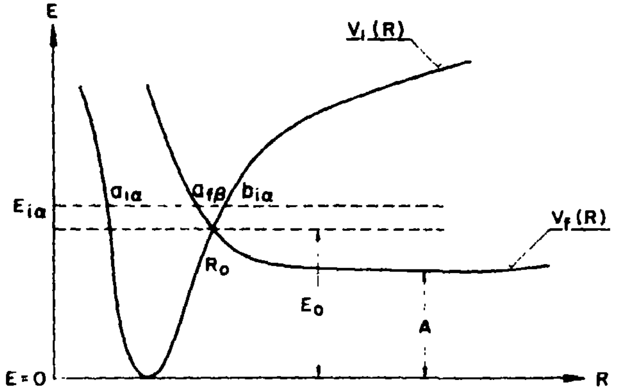

Fig. 2. Relevant parameters for the semiclassical calculation of vibrational overlap integrals between two one dimensional potential surfaces

linear molecule implies that: a) the X Y separation is the same in the triatomic molecule XYO($^1\Sigma$) and in the resulting dissociation product XY($^1\Sigma$). This approximation can be relaxed as demonstrated in Sec. 4. b) The linear predissociation process along the XYO axis of the linear molecule is considered. This assumption neglects the role of the bending modes of the XYO molecules which can lead to predissociation off the linear axes.

Considering the one dimensional model the microscopic rate constant (or transition probability) (2.8) takes the simple form

$$W_{i\alpha} = 2\pi/\hbar \, |\langle H_{so}\rangle|^2 \, |\langle \chi_{i\alpha}(R) | \chi_{f\beta}(R)\rangle|^2 \tag{3.1}$$

where $\chi_{i\alpha}(R)$ (characterized by the energy $E_{i\alpha}$) and $\chi_{f\beta}(R)$ (characterized by the energy $E_{f\beta}$) are now the eigenfunctions belonging to the one dimensional (bound) potential $V_i(R)$ and to the (repulsive) potential $V_f(R)$, respectively. We are essentially left with the calculation of the square of the Franck Condon vibrational overlap integral between the bound vibrational state $\chi_{i\alpha}(R)$ and the continuum states $\chi_{f\beta}(R)$ which are quasidegenerate with it [20, 23]. It will be convenient for the sake of bookkeeping to set $\chi_{i\alpha}(R)$ to be normalized to unity and to choose $\chi_{f\beta}(R)$ as a continuum state of $V_f(R)$ which is normalized by the delta function of energy. Thus Eq. (3.1) then takes the form

$$W_{i\alpha} = 2\pi/\hbar \, |\langle H_{so}\rangle|^2 \, |\int \chi_{i\alpha}(R)\chi_{f\beta}(R) dR|^2 \, . \tag{3.1a}$$

We will evaluate Eq. (3.1a) with the help of the *WKB* method recently utilized by Child [33] for the case of predissociation of O_2. In the semiclassical approximation the wave functions are (see Fig. 2):

$$\chi_{i\alpha}(R) = \left(\frac{2\mu\omega}{\pi P_{i\alpha}(R)}\right)^{1/2} \sin\left(\frac{1}{\hbar}\int\limits_{R}^{a_{i\alpha}} P_{i\alpha}(r) dr + \frac{\pi}{4}\right) \tag{3.2a}$$

$$\chi_{f\beta}(R) = \left(\frac{2\mu}{\pi\hbar P_{f\beta}(R)}\right)^{1/2} \sin\left(\frac{1}{\hbar}\int\limits_{a_{f\beta}}^{R} P_{f\beta}(r) dr + \frac{\pi}{4}\right). \tag{3.2b}$$

Here $P_\gamma(R) = [2\mu(E_\gamma - V_\gamma(R))]^{1/2}$; $\gamma = i\alpha, f\beta$ are the momenta associated with the two states. ω is the classical oscillation frequency

$$\frac{2\pi}{\omega} = 2\hbar\left(\frac{\partial\beta}{\partial E}\right) = 2\mu \int_{a_{i\alpha}}^{b_{i\alpha}} \frac{dr}{P_{i\alpha}(r)} = (2\mu)^{1/2} \int_{a_{i\alpha}}^{b_{i\alpha}} \frac{dr}{[E_{i\alpha} - V_i(r)]^{1/2}} \tag{3.3}$$

taken at the energy $E = E_{i\alpha}$. β assumes the values $(v + 1/2)\pi$ for the bound states by the Bohr quantization condition. In the region of the intersection point $R = R_0$ (characterized by the energy E_0) of the potential curves $V_i(R)$ and $V_f(R)$, the wavefunctions (3.2) are replaced by the corresponding Airy functions

$$Ai(\xi) = \frac{1}{\pi} \int_0^\infty \cos\left(\frac{u^3}{3} + u\xi\right) du \tag{3.4}$$

where the parameter ξ is defined by

$$\xi = \left(R + \frac{E}{F}\right)(2\mu F/\hbar^2)^{1/2} \tag{3.5}$$

while the force is

$$F = -\left(\frac{\partial V}{\partial R}\right)_{R = R_0} \tag{3.6}$$

and V can take either the value of $V_i(R)$ (and then we shall take (3.6) as F_i and (3.5) as $\xi_{i\alpha}$) or the value of V_f (whereupon we shall denote (3.6) by F_f and (3.5) by $\xi_{f\beta}$). In the vicinity of the crossing point R_0 we have

$$\chi_{i\alpha}(R) = (\pi\hbar\omega)^{1/2} (2\mu/\sqrt{F_i}\,\hbar^2)^{1/2}\, Ai(-\xi_{i\alpha})\,, \tag{3.7a}$$

$$\chi_{f\beta}(R) = (2\mu/\sqrt{F_f}\,\hbar^2)^{1/2}\, Ai(-\xi_{f\beta})\,. \tag{3.7b}$$

The major contribution to the integral (3.1) originates from the region $R = R_0$ around the energy of the crossing point $E \simeq E_0$. Utilizing (3.4) the predissociation decay probability can then be recast in the form

$$W_{i\alpha} = \frac{\pi K}{\sqrt{E^*\,(\partial\beta/\partial E)}} |Ai(t)|^2 \tag{3.8}$$

where

$$K = \frac{2\pi^2 (2\mu)^{1/2} |\langle H_{so}\rangle|^2}{\hbar^2(F_i - F_f)} \tag{3.9}$$

and

$$E^* = |\hbar F_i F_f/(2\mu)^{1/2}(F_i - F_f)|^{2/3} \tag{3.10}$$

while the linear parameter

$$t = -(E_{i\alpha} - E_0)/E^* \tag{3.11}$$

represents the deviation of the energy of the zero order level $|i\alpha\rangle$ from the intersection point. Eqs. (3.8)–(3.11) are based on the linear extrapolation $V_j(R) = E_0 - F_j(R)$ $(j = i, f)$, thus well above the crossing point we have to apply

Eq. (3.2) and the transition probability takes the form

$$W_{i\alpha} = \frac{K}{(E_{i\alpha} - E_0)^{1/2} (\partial \beta / \partial E)} \sin^2 \left[\Phi(E_{i\alpha}) + \frac{\pi}{4} \right] \tag{3.12}$$

$\Phi(E)$ is the phase integral

$$\Phi(E_{i\alpha}) = \frac{1}{\hbar} \int_{a_{f\beta}}^{b_{i\alpha}} [2\mu(E_{i\alpha} - V_+(R))]^{1/2} dR \tag{3.13}$$

and $V_+(R) = V_f(R)$ for $R < R_0$ and $V_+(R) = V_i(R)$ for $R > R_0$. In the region of the crossing point $\Phi = 2/3|t|^{3/2}$ and Eq. (3.12) reduces to (3.8). Thus Eq. (3.8) was used for the calculation of the predissociation probability of zero order states characterized by energy $E_{i\alpha} \leq E_0$ while Eq. (3.12) was utilized in the energy region $E_{i\alpha} > E_0$.

4. Numerical Calculations for N_2O

To provide a numerical estimate of the reaction rate $N_2O(^1\Sigma) \rightarrow N_2(^1\Sigma_g) + O(^3P)$ we have chosen one dimensional surfaces similar to those given by Stearn and Eyring [8] and by Gilbert and Ross [19]. We took only a single coordinate corresponding to the N_2 O mode to be reactive, and described the bound state by a Morse potential and alternatively by a harmonic potential. The parameters for these potentials are given in Fig. 3. The repulsive state was specified in terms

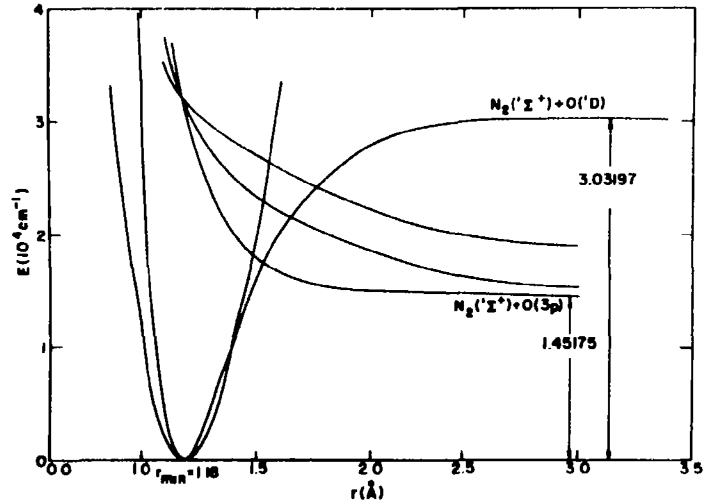

Fig. 3 Morse and harmonic potentials for $N_2O(^1\Sigma)$ and repulsive potentials for $N_2(^1\Sigma^+) + O(^3P)$. The formulas are (see text) $V_i(R) = 30319.7\,(1 - e^{-4\cdot(1.18)})^2$ for the Morse potential and $V_i(R) = \frac{1}{2}210425\,(r - 1.18)^2$ for the ground state Harmonic potential. The three repulsive potentials have the form $V_f(R) = A + \frac{B}{r^n}$ with $A = 14517.5$ [cm^{-1}], $B_1 = 54000$, $B_2 = 29700$, $B_3 = 22600$, $n_1 = 6.72$, $n_2 = 3.12$, $n_3 = 1.45$. The crossing points for the Morse potential are $E_0^{(1)} = 17523$ cm^{-1}, $E_0^{(2)} = 21023$ cm^{-1}, $E_0^{(3)} = 24524$ cm^{-1} while for the harmonic potential we took $E_0^{(1)} = 16995$ cm^{-1}, $E_0^{(2)} = 21022$ cm^{-1}, $E_0^{(3)} = 25262$ cm^{-1}

of a R^{-n} potential

$$V_f(R) = A + \frac{B}{R^n}. \tag{4.1}$$

The value of $A = 14517\,\text{cm}^{-1}$ was taken from the known thermochemical data (Table 1). The value of B and n (Fig. 3) were determined by: a) Taking the crossing point E_0 of the two potential curve to be located at 50, 60 or 70 kcal/mole. b) Using the observed onset for the optical dissociation continuum for the transition $N_2O(^1\Sigma) \rightarrow N_2(^1\Sigma) + O(^3P)$, located by Sponer and Bonner [29] at 4.0 eV, to correspond to the repulsive potential at the equilibrium distance of the N–O bond of $N_2O(^1\Sigma)$. Finally, the spin orbit coupling term was taken to be $|H_{so}| \simeq 100\,\text{cm}^{-1}$.

In Fig. 4 we present the microscopic rate constants Eq. (3.1) for different $|i\alpha\rangle$ levels calculated by the semiclassical approximation. It is apparent that this is not a smooth function of the energy, but rather a strongly oscillation function, as expected for the case of predissociation [23, 24]. The detailed features of the relative and absolute widths of different vibronic levels depend on the nature of the potential surfaces. The most important qualitative conclusion originating from these results is that it is not justified to use the Landau Zener formalism for the calculation of the thermally averaged rate constant, which is based on a "coarse graining" procedure assuming that $W_{i\alpha}$ is a smoothly varying function of the energy $E_{i\gamma}$. In Table 2, we display our numerically calculated thermally

Table 2. Calculated rate constants for the unimolecular decomposition of N_2O at different temperatures. [Units of k are sec^{-1}].

T[°K]	k_1	k_2	k_3	k_4	k_5	k_6
100	9.33(−84)	7.74(−102)	1.98(−131)	6.77(−86)	7.73(−101)	3.72(−132)
200	2.69(−39)	1.52(−50)	2.42(−62)	1.69(−39)	3.05(−51)	1.41(−65)
300	2.32(−23)	1.09(−30)	4.11(−38)	1.85(−38)	1.13(−31)	7.60(−41)
400	4.74(−15)	1.75(−20)	6.66(−26)	3.33(−15)	1.87(−21)	3.09(−28)
500	5.40(−10)	2.62(−14)	1.43(−18)	3.38(−10)	3.07(−15)	1.24(−20)
600	1.33(−6)	3.50(−10)	1.09(−13)	7.59(−7)	4.49(−11)	1.47(−15)
700	3.60(−4)	3.14(−7)	3.31(−10)	1.92(−4)	4.32(−8)	6.20(−12)
800	2.46(−2)	5.20(−5)	1.36(−7)	1.24(−2)	7.61(−6)	3.25(−9)
900	6.69(−1)	2.81(−3)	1.48(−5)	3.23(−1)	4.30(−4)	4.27(−7)
1000	9.53(0)	6.93(−2)	6.35(−4)	4.43(0)	1.10(−2)	2.14(−5)
1500	9.53(0)	6.93(−2)	6.35(−4)	4.43(0)	1.10(−2)	2.14(−5)
1500	2.85(+4)	1.11(+3)	5.51(+1)	1.13(+4)	1.90(+2)	2.85(0)
2000	1.81(+6)	1.58(+5)	1.78(+4)	6.70(+5)	2.87(+4)	1.16(+3)
2500	1.35(+7)	2.05(+6)	3.98(+5)	4.66(+6)	3.76(+5)	2.97(+4)
3000	7.41(+7)	1.57(+7)	4.22(+6)	2.46(+7)	2.93(+6)	3.45(+5)
4000	6.87(+8)	2.16(+8)	8.48(+7)	2.20(+8)	4.15(+7)	7.89(+6)
5000	2.68(+9)	1.06(+9)	5.22(+8)	8.52(+8)	2.11(+8)	5.37(+7)
6000	5.41(+9)	2.49(+9)	1.41(+9)	1.71(+9)	5.07(+8)	1.56(+8)
8000	1.61(+10)	9.07(+9)	6.21(+9)	5.15(+9)	1.96(+9)	7.82(+8)
10000	3.21(+10)	2.04(+10)	1.55(+10)	1.06(+10)	4.69(+9)	2.18(+9)

k_1 = Morse potential $E_0 = 17523\,\text{cm}^{-1}$, k_2 = Morse potential $E_0 = 21022\,\text{cm}^{-1}$, k_3 = Morse potential $E_0 = 24524\,\text{cm}^{-1}$, k_4 = Harmonic potential $E_0 = 16995\,\text{cm}^{-1}$, k_5 = Harmonic potential $E_0 = 21022\,\text{cm}^{-1}$, k_6 = Harmonic potential $E_0 = 25262\,\text{cm}^{-1}$.

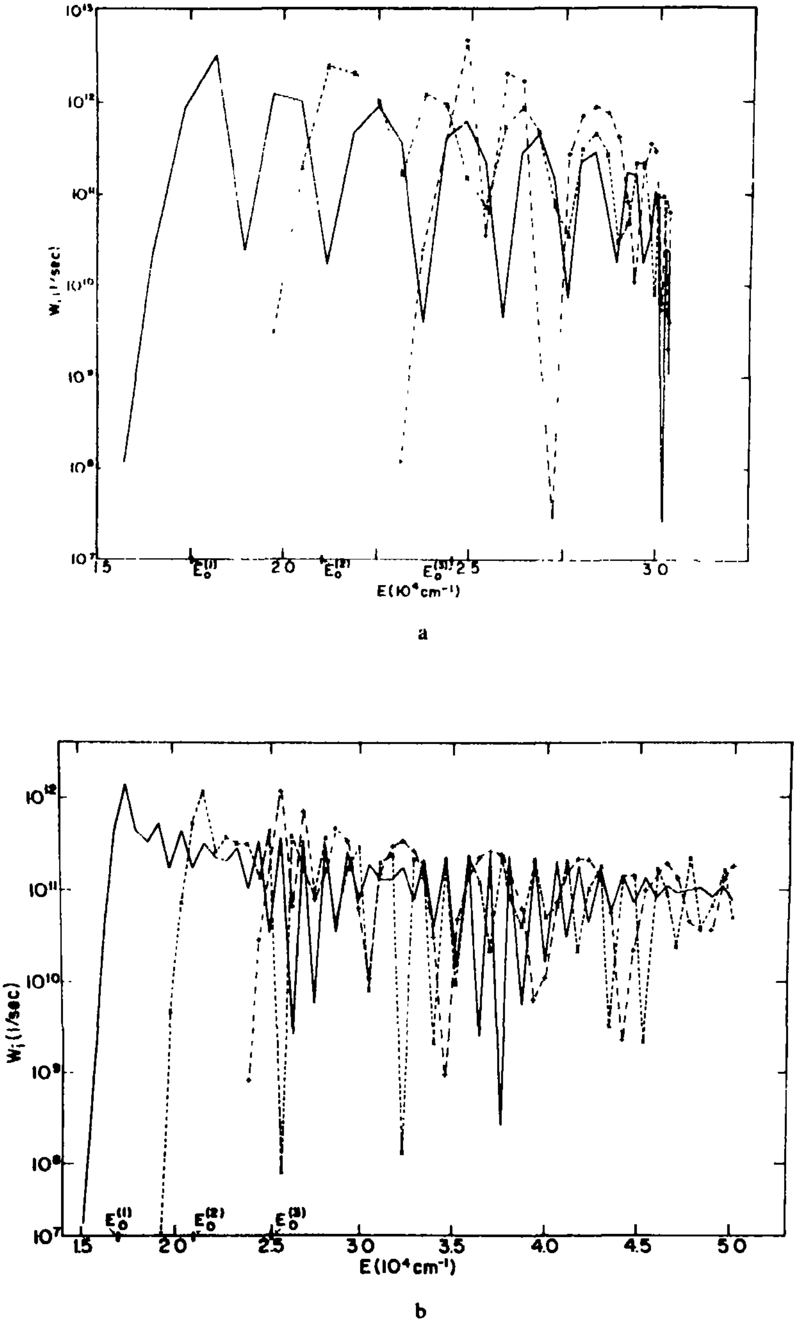

Fig. 4. a Microscopic rate constants for Morse potentials. —— $E_0 = 17523$ cm^{-1}; – – – $E_0 = 21023$ cm^{-1}; –· · $E_0 = 24524$ cm^{-1}. b Microscopic rate constants for the harmonic potential. —— $E_0 = 16995$ cm^{-1}; – – $E_0 = 21022$ cm^{-1}; · · · $E_0 = 25262$ cm^{-1}

averaged unimolecular rate constants (Eq. (2.11)) for N_2O. The following points are pertinent:

a) The energy at the crossing point E_0 determines the high temperature activation energy (see Fig. 5 and subsequent discussion), thus at a constant temperature the rate constant (for a given $V_f(R)$ potential) increases with decreasing the crossing point energy E_0.

b) Anharmonicity effects tend to increase the rate constant. For a given value of E_0 and constant temperature the rate constant calculated for a Morse potential exceeds the value calculated for the harmonic potential by a numerical factor 3–10. the deviation increases with increasing E_0. These anharmonicity effects on the vibrational overlap Franck-Condon integrals are well documented in the theory of electronic relaxation processes [30].

c) In the temperature region 1400°–2000° K the experimental [31] high pressure rate constant for the decomposition of N_2O is

$$k_\infty(\text{expt}) = 1.6\times 10^{11}\exp\left(-\frac{(60/\text{kcal})}{k_BT}\right).$$

The theoretical value for the Morse potential and $E_0 = 60$ kcal/mole is

$$k(\text{calc}) = 4.1\times 10^{11}\exp\left(-\frac{59/\text{kcal}}{k_BT}\right)$$

in the same temperature region. This almost perfect agreement between theory and experiment should not be taken too seriously in view of the approximation involved in the oversimplified one dimensional theoretical model.

The activation energy, defined in the conventional manner, turns out from our theoretical calculations to be temperature dependent. The apparent activation energy $\tilde{E}_A$, was defined in the conventional manner

$$\tilde{E}_A = -\partial \ln k/\partial(1/k_BT) \qquad (4.2)$$

where k is the theoretical rate constant. Utilizing Eq. (2.11) one easily obtains the formula previously given by Gilbert and Ross [19]

$$\tilde{E}_A = \frac{\sum\limits_\alpha W_{i\alpha}E_{i\alpha}\exp(-E_{i\alpha}/k_BT)}{\sum\limits_\alpha W_{i\alpha}\exp(-E_{i\alpha}/k_BT)} - \frac{\sum\limits_\alpha E_{i\alpha}\exp(-E_{i\alpha}/k_BT)}{\sum\limits_\alpha \exp(-E_{i\alpha}/k_BT)} = \frac{\langle WE\rangle}{k} - \langle E\rangle \qquad (4.3)$$

where the square brackets represent averaged mean values.

In Fig. 5 we present the temperature dependence of the activation energy. The following points should be noted:

a) At low temperature where $k_BT \ll \hbar\omega$ (ω representing the vibrational frequency, as discussed in Section 5) the activation energy takes the value

$$\tilde{E}_A = A; \qquad k_BT \ll \hbar\omega \qquad (4.4a)$$

corresponding to the onset of the dissipative continuum (see Eq. (4.1)).

b) At higher temperatures the activation energy increases monotonously until it flattens up at high temperatures.

c) The constant value of the activation energy reached at high temperatures, i.e. when $k_BT \gg \hbar\omega$ (see Section 5) is very close to the energy E_0 of the crossing

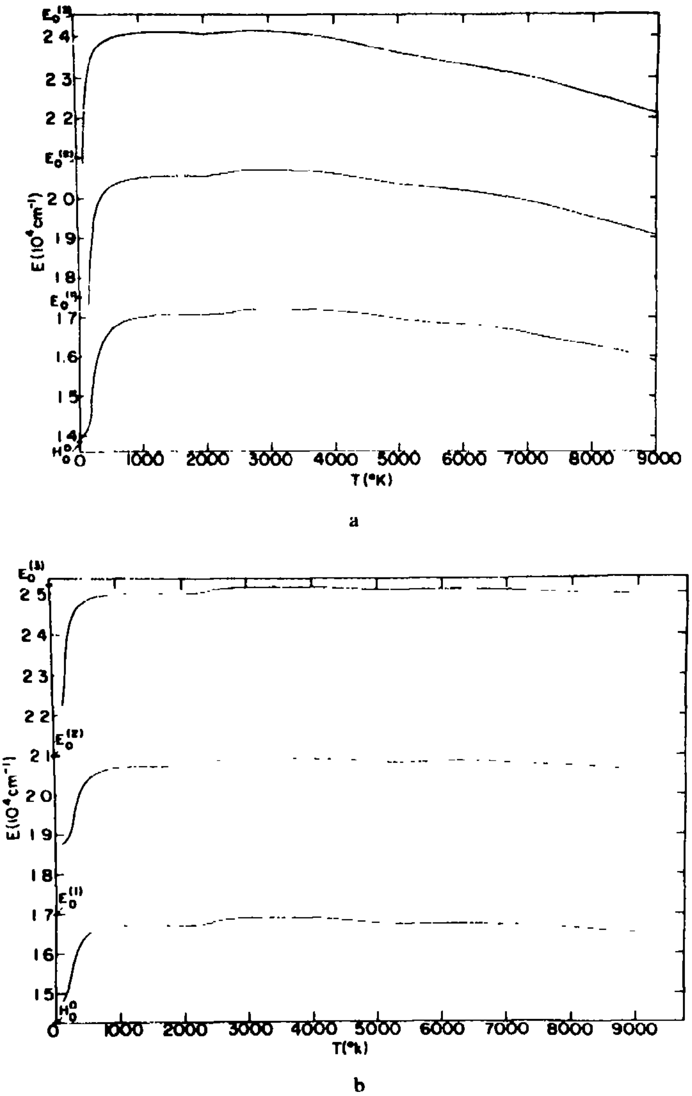

Fig. 5. a Activation energy derived for the Morse potential defined in Fig. 4a. b Activation energy derived for the harmonic potential defined in Fig. 4b

point of the potential surfaces, so that

$$\tilde{E}_A \approx E_0 ; \qquad k_B T \gg \hbar\omega . \tag{4.4b}$$

To be more precise, we may utilize the general formula for the high temperature rate constant (see Section 5) which reads

$$k = k_0 T^{-\gamma} \exp(-E_0/k_B T) \tag{4.5}$$

where k_0 is a numerical constant and γ is a half integer determined by the number, n, of the vibrational degrees of freedom in the initial states, $\gamma = n/2$. Thus, the high temperature activation energy obtained from (4.5) is

$$\tilde{E}_A = E_0 - \gamma k_B T. \tag{4.6}$$

Thus the apparent high temperature activation energy is expected to be somewhat lower than the crossing point energy E_0 in accordance with the behavior exhibited in Fig. 5.

d) The decrease of the apparent activation energy at very high temperature (see Fig. 5) has no physical significance and is attributed to arise from the truncation of the basis set of the initial vibrational levels including a finite number of vibrational levels in the present calculations. Indeed, there is a pronounced effect of the number of vibrational states taken into account. In the case of a Morse potential, the number (~ 50) of the vibrational levels is not very high, the decrease of the activation energy with temperature at very high temperatures is faster than in the case of a harmonic potential, where we have included 200 levels in our calculations. These mathematical artifacts can be improved but not completely removed by extending the size of the zero order basis set corresponding to the initial vibronic levels. It should, however, be pointed out that for a real life situation at extremely high temperature when $k_B T$ is of the order of the $^1\Sigma$ ground state dissociation energy, D, direct thermally induced dissociation $N_2O \rightarrow N_2(^1\Sigma) + O(^1D)$ will become the dominant decompositions mechanism.

The most important conclusions arising from the present discussion of the activation energy involve the distinction between the low temperature case $\hbar\omega \gg k_B T$ and the high temperature case $\hbar\omega < k_B T \ll D$. In the low temperature limit the unimolecular decomposition of the triatomic N_2O molecule occurs by quantum mechanical decay of very few bound zero order states which are located just above the continuum threshold, A, into the continuum. On the other hand, in the high temperature limit, the major contribution to the decay rate originates from the contribution of the intersection point of the two zero order potential surfaces. These conclusions are identical with the theory of radiationless processes in solid state [32] and molecular physics [33].

5. Comments on the High Temperature Activation Energy

The general expression for the non radiative thermally averaged decay probability, which under the conditions specified in Section 2 is equal to the unimolecular rate constant, can be displayed in the general form

$$k = \frac{2\pi}{\hbar Z} |\langle H_{so} \rangle|^2 \sum_\alpha \sum_\beta \exp(-E_{i\alpha}/k_B T) |S_{i\alpha,f\beta}|^2 \delta(E_{i\alpha} - E_{f\beta}) \tag{5.1}$$

where $S_{i\alpha,f\beta}$ is the (multidimensional) vibrational overlap integral with the continuum wavefunction being volume normalized), while $Z = \sum_\alpha \exp(E_{i\alpha}/k_B T)$ being the partitition function. Eq. (5.1) can in general be handled by recasting the thermally averaged transition probability in terms of a Fourier transform of a generating function [32–34]. Following the general methods developed by

Kubo and Toyozawa [32] and by Lax [34] one can represent (5.1) in the form

$$k = \frac{|\langle H_{so}\rangle|^2}{h^2} \sum_{\alpha} \frac{\exp(-E_{i\alpha}/k_B T)}{Z} \int_{-\infty}^{\infty} dt \left\langle \chi_{i\alpha} \middle| \exp\left(\frac{i}{\hbar} H_f t\right) \exp\left(-\frac{i}{\hbar} H_i t\right) \middle| \chi_{i\alpha} \right\rangle \tag{5.2}$$

where H_i and H_f represent the molecular nuclear Hamiltonians $H_j = T_R + V_j(R)$ $(j = i, f)$ in the initial and in the final states. This expression can be written in a closed analytical form only for the case of two harmonic potentials, which is not very useful for the problem at hand. However, it was previously demonstrated that in the high temperature limit a closed expression of (5.2) can be derived for a general form of the nuclear potentials [32, 34]. The high temperature limit is realized [32, 34] when the variation of the potential energy in the initial state within the averaged De Broglie wavelength $\hbar/(\mu k_B T)^{1/2}$ is negligible relative to the thermal energy $k_B T$, so that [32]

$$\left(\hbar/(\mu k_B T)^{1/2} \frac{\partial}{\partial R}\right)^n V_i(R) \ll k_B T \,. \tag{5.3}$$

For all integer values of n note that for $n = 2$ Eq. (5.3) yields the well known condition

$$\hbar\omega \ll k_B T \tag{5.4}$$

for the validity of the high temperature limit, which was utilized in the qualitative discussion in Section 4. When condition (5.3) is satisfied, one can neglect the commutator $[T_R, V_i(R)]$ in the exponent of the matrix element of (5.2), whereupon

$$\begin{aligned} &\frac{1}{\hbar} \int_{-\infty}^{\infty} \left\langle \chi_{i\alpha} \middle| \exp\left(\frac{i}{\hbar} H_f t\right) \exp\left(-\frac{i}{\hbar} H_i t\right) \middle| \chi_{i\alpha} \right\rangle dt \\ &= \frac{1}{\hbar} \int_{-\infty}^{\infty} \left\langle \chi_{i\alpha} \middle| \exp\left[\frac{i}{\hbar} (V_f - V_i) t\right] \middle| \chi_{i\alpha} \right\rangle dt = \int dR |\chi_{i\alpha}|^2 \, \delta(V_f(R) - V_i(R)) \,. \end{aligned} \tag{5.5}$$

Furthermore, we can replace the summation over α states by the classical expression

$$\begin{aligned} \frac{1}{Z} \sum_{\alpha} |\chi_{i\alpha}|^2 \exp(-E_{i\alpha}/k_B T) &= \exp(-V_i(R)/k_B T)/Z \\ &= \exp(-V_i(R)/k_B T) / \int dR \exp(-V_i(R)/k_B T) \,. \end{aligned} \tag{5.6}$$

Eq. (5.2) with the aid of Eqs. (5.5) and (5.6) takes the following limiting form at high temperatures

$$k = \frac{|\langle H_{so}\rangle|^2}{\hbar} \frac{\int dR \exp(-V_i(R)/k_B T)\, \delta(V_f(R) - V_i(R))}{\int dR \exp(-V_i(R)/k_B T)} \,. \tag{5.7}$$

The following comments should be made at this point:

a) The high temperature rate constant is valid for any form (and dimension) of the potential surfaces for the initial and final states.

b) This rate constant was derived for the case of interstate coupling which is independent of the nuclear coordinates. When the zero order states are coupled by the nuclear kinetic energy operator, $\langle \boldsymbol{H}_{so} \rangle$ in (5.7) is replaced by the matrix elements of the nuclear momentum and by a temperature dependent factor.

c) Eq. (5.7) provides the most general proof that in the high temperature limit the non radiative transition takes place in the configuration where the two potential surfaces intersect, i.e. along the hypersurface where

$$V_i(\boldsymbol{R}) = V_f(\boldsymbol{R}). \tag{5.7}$$

d) Condition (5.7) is usually referred to as the Franck-Condon principle for thermal reaction which involve a change in the electronic states. This principle played a crucial role in the understanding of electron transfer processes in solution [36, 37, 27]. However, from the present discussion it is obvious that this argument is much more general.

For the sake of comparison with the results of the numerical calculations of Section 4, let us specialize to the one dimensional case setting $\boldsymbol{R} = R$. Recasting the high temperature partition function in the approximate form corresponding to a harmonic potential characterized by a force constant κ,

$$\int dR \exp(-V_i(R)/k_B T) \approx (\pi k_B T/\kappa)^{1/2}$$

and utilizing the well known properties of the delta function, Eq. (5.7) is reduced to the simple form

$$\begin{aligned} k &= \frac{|\langle \boldsymbol{H}_{so} \rangle|^2}{\hbar} \left(\frac{\kappa}{4\pi k_B T} \right)^{1/2} \frac{\exp(-V_i(R_0)/k_B T)}{\left| \frac{\partial}{\partial R} (V_f(R) - V_i(R)) \right|_{R=R_0}} \\ &= \frac{|\langle \boldsymbol{H}_{so} \rangle|^2}{\hbar} \left(\frac{\pi \mu \omega^2}{k_B T} \right)^{1/2} \frac{\exp(-E_0/k_B T)}{\left| \frac{\partial}{\partial R} (V_f(R) - V_i(R)) \right|_{R=R_0}} \end{aligned} \tag{5.8}$$

where E_0 and R_0 correspond again to the distance and energy of the crossing point of the one dimensional potential surfaces. Thus in this high temperature limit the activation energy in the one dimensional model is just E_0 while the apparent activation energy being $E_0 - k_B T/2$. Finally, it is worthwhile to notice that the high temperature unimolecular rate constant is determined by $|(F_f - F_i)|^{-1}$ in a manner analogous to the result of the semiclassical approximation (Eq. (3.12)), and also to the Landau Zener formula.

6. A Two Dimensional Linear Model for the Unimolecular Decomposition of N_2O

The one dimensional model for the unimolecular decomposition of N_2O can be extended to include the role of the N-N vibration, still maintaining that the dissociation in the final state occurs along the N-N-O ($^1\Sigma$) axes. Gilbert and Ross [19] have performed approximate numerical calculations for a two dimensional model. In what follows we shall present some general results for such a model, which may be of interest for the understanding of the nature of the distribution vibrational energy among the N_2 molecules resulting from the thermal decomposition of N_2O. This problem, which cannot be handled by the simple one dimensional model, is of considerable theoretical and experimental interest.

Denoting by R the N–O and by X the N–N distance, the two dimensional potentials representing the initial and the final states are

$$V_i(R, X) = f_1(R) + f_2(X) \tag{6.1}$$

$$V_f(R, X) = A + \frac{B}{R^n} + \tilde{f}_2(X) \tag{6.2}$$

where $f_1(R), f_2(X)$ and $\tilde{f}_2(X)$ can be chosen to be either Morse or harmonic potentials. The ground state potential (6.1) is similar to that previously used for some triatomic molecules. $f_1(R)$ corresponds to the bound N–O potential in the ground state. It should be noted that the bound N–N potentials $f_2(X)$ and $\tilde{f}_2(X)$ in the initial and final states may differ both in their equilibrium distance, in the vibrational frequency (for a harmonic potential) or in the characteristic reciprocal length and the effective dissociation energy (for a Morse Potential). In this approximate representation the X and R modes are independent and the vibrational wave functions are

$$\chi_{i\alpha\alpha'}(R, X) = \chi_{i\alpha}(R)\,\chi_{i\alpha'}(X), \tag{6.3a}$$

$$\chi_{f\beta\beta'}(R, X) = \chi_{f\beta}(R)\,\chi_{f\beta'}(X), \tag{6.3b}$$

while the corresponding energies are given by

$$E_{i\alpha\alpha'} = E_{i\alpha} + E_{i\alpha'}, \tag{6.4}$$

$$E_{f\beta\beta'} = E_{f\beta} + E_{f\beta'}, \tag{6.5}$$

We now require two indices to specify each vibrational state. Note that as before $\chi_{f\beta}(R)$ represents an unbound state.

The unimolecular rate constant is now given by

$$k = \frac{2\pi}{h} |\langle H_{so}\rangle|^2 \tag{6.6}$$

$$\cdot \frac{\sum\limits_{\alpha}\sum\limits_{\alpha'}\sum\limits_{\beta}\sum\limits_{\beta'} \exp\left(-\frac{E_{i\alpha}+E_{i\alpha'}}{k_B T}\right) |\langle\chi_{i\alpha}|\chi_{f\beta}\rangle|^2 |\langle\chi_{i\alpha'}|\chi_{f\beta'}\rangle|^2 \,\delta(A + E_{f\beta} + E_{f\beta'} - E_{i\alpha} - E_{i\alpha'})}{\sum\limits_{\alpha}\sum\limits_{\alpha'} \exp\left(-\frac{E_{i\alpha}+E_{i\alpha'}}{k_B T}\right)}$$

Rewriting the delta function in (6.6) in terms of a convolution integral involving two delta functions we have

$$k = \frac{2\pi}{h Z_\alpha Z_{\alpha'}} |\langle H_{so}\rangle|^2 \int d\varepsilon \sum_{\alpha}\sum_{\beta} \exp\left(-\frac{E_{i\alpha}}{k_B T}\right) \tag{6.7}$$

$$\cdot |\langle\chi_{i\alpha}|\chi_{f\beta}\rangle|^2 \,\delta(A + E_{f\beta} - E_{i\alpha} + \varepsilon) \sum_{\alpha'}\sum_{\beta'} \exp\left(-\frac{E_{i\alpha'}}{k_B T}\right) |\langle\chi_{i\alpha'}|\chi_{f\beta'}\rangle|^2 \,\delta(E_{f\beta'} - E_{i\alpha'} - \varepsilon)$$

where $Z_\alpha Z_{\alpha'}$ is the product of the two partition functions in the denominator of (6.6).

It will be convenient at this stage to define two auxiliary functions.

$$F(\varepsilon)=\frac{1}{Z_\alpha}\sum_\alpha \exp\left(-\frac{E_{i\alpha}}{k_BT}\right)|\langle\chi_{i\alpha}|\chi_{f\beta}\rangle|^2\,\delta(A+E_{f\beta}-E_{i\alpha}+\varepsilon)\,, \tag{6.8}$$

$$G(\varepsilon)=\frac{1}{Z_{\alpha'}}\sum_{\alpha'} \exp\left(-\frac{E_{i\alpha'}}{k_BT}\right)|\langle\chi_{i\alpha'}|\chi_{f\beta'}\rangle|^2\,\delta(E_{f\beta'}-E_{i\alpha'}-\varepsilon) \tag{6.9}$$

and to rewrite (6.7) in the concise form

$$k=\frac{2\pi}{\hbar}|\langle H_{so}\rangle|^2\int d\varepsilon F(\varepsilon)\,G(\varepsilon)\,. \tag{6.10}$$

Thus the quantum mechanical rate constant for the present model can be expressed in terms of a convolution integral involving two generalized line shape functions. The line shape functions $F(\varepsilon)$ (Eq. (6.8)) can be evaluated by the numerical methods described in Sections 3 and 4 which are based on the semiclassical approximation. Obviously $F(\varepsilon)$ involves the decay of the N–O zero order vibronic into the continuum, however, now the N–N modes come in and the onset energy A for tunnelling can be reached by different combinations of N–O and N–N modes. Thus the metastable decaying states correspond to a combination of both N–O and N–N vibrationally excited states. The role of the N–N modes is incorporated in terms of the generalized line shape function $G(\varepsilon)$ (Eq. (6.9)). An explicit expression for $G(\varepsilon)$ can be provided assuming that the N–N vibrations in the initial and final states are harmonic both being characterized by a reduced mass μ_2 and the same frequency ω_2, while the origins of the N–N potentials are displaced by (ΔX) in these two electronic states. In this simple case one gets the Fourier integral [32–36]

$$G(\varepsilon)=\int dt\exp(-i\varepsilon t/\hbar)\exp\left\{-\frac{\Delta^2}{2}\Big|\coth\left(\frac{\hbar\omega_2}{2k_BT}\right)(1-\cos\omega_2 t)-i\sin\omega_2 t\right\} \tag{6.11}$$

where the reduced displacement is defined by

$$\Delta=\left(\frac{\mu_2\omega_2}{\hbar}\right)^{1/2}\Delta X\,. \tag{6.11a}$$

In the simple case when $\Delta=0$, thus the two N–N potentials are not displaced between the two electronic states $G(\varepsilon)=\delta(\varepsilon)$ and Eq. (6.10) is reduced to

$$k=\frac{2\pi}{\hbar}|\langle H_{so}\rangle|^2 F(0) \tag{6.12}$$

which is just the result of the one dimensional model discussed in Section 3. It is also interesting to note that in a manner completely analogous to the theoretical study of optical selection in electronic relaxation [39], the present formalism can be extended to provide the vibrational population of the N_2 molecules resulting from the unimolecular decomposition. We can define the rate $k_{\beta'}$ for the production of the N_2 in the β' vibrational state, so that

$$k_{\beta'} = \frac{2\pi}{\hbar} |\langle H_{so}\rangle|^2 \int d\varepsilon F(\varepsilon)\, G_{\beta'}(\varepsilon) \tag{6.13}$$

where

$$G_{\beta'}(\varepsilon) = \frac{1}{Z_{\alpha'}} \sum_{\alpha'} \exp\left(-\frac{E_{i\alpha'}}{k_B T}\right) |\langle \chi_{i\alpha'} | \chi_{f\beta'}\rangle|^2\, \delta(E_{f\beta'} - E_{i\alpha'} + \varepsilon)\,. \tag{6.14}$$

From the formal point of view the decomposition processes resulting in different vibrational levels of the N_2 product correspond to different decay channels and $k = \sum_{\beta'} k_{\beta'}$. Now in the simple case $\Delta = 0$ we have $G_{\beta'}(\varepsilon) = (\exp(-E_{i\alpha'}/k_B T))\,\delta(\varepsilon)/Z_{\alpha'}$ whereupon Eq. (6.13) takes the simple form

$$k_{\beta'=\alpha'} = k\, \frac{\exp(-E_{i\alpha'}/k_B T)}{Z_{\alpha'}} \tag{6.15}$$

so that the vibrational states of the N_2 product assume a Boltzmann distribution characteristic of the ground state. In real life the situation when $\Delta \neq 0$ a more complex distribution (6.13) is obtained.

7. Discussion

In this paper we consider a general theoretical scheme for the nonadiabatic unimolecular decomposition of some triatomic molecules, which involve a change in the electronic state, and is thus amenable to study in terms of a thermally induced intramolecular radiationless decomposition, in complete analogy to molecular predissociation (classified by Herzberg [38] as case I c) and to electronic relaxation in the statistical limit. We have advanced some simple general criteria (Eq. (2.7)) for describing the decay process in terms of Fermi's golden rule, and were able to present general expressions for the decay probability of a single vibronic level (Eq. (2.8)) and for the thermally averaged unimolecular rate constant (Eq. (2.11)). The general quantum mechanical rate expression (2.11) for the non adiabatic reaction (subjected to restriction (2.7)) is characterized by a pre-exponential factor which is determined by the square of the interstate coupling matrix elements, in a manner analogous to electronic relaxation process [1], and as was previously asserted on the basis of transition state theory for this class of reactions [11]. The general behavior of the rate constant at low and high temperatures is of considerable interest. At low temperatures the rate constant is determined by tunnelling from the small number of zero order vibrational levels $\{i\tilde{\alpha}\}$ just above the continuum threshold A, so that $E_{i\tilde{\alpha}} \gtrsim A$ whereupon

$$k \approx \frac{2\pi}{\hbar} |\langle H_{so}\rangle|^2 \sum_{\{\tilde{\alpha}\}} \frac{|\langle \chi_{i\tilde{\alpha}} | \chi_{f\beta}\rangle|^2}{Z_\alpha} \exp(-A/k_B T) \tag{7.1}$$

while at high temperatures the general rate constant (5.7) represents non radiative transition occurring at the intersection of the two potential surfaces. Note that the notion of an activated complex does not enter into these considerations and this concept can be defined only in the high temperature limit as corresponding to the configuration satisfying Eq. (5.7).

We have then proceeded to present the results of model calculations for the unimolecular decomposition of N_2O adopting one or two dimensional linear models. Applying the semiclassical approximation the microsopic rate constant calculated for the one dimensional model result in an oscillatory function of the energy and cannot be handled within the framework of the Landau-Zener [14, 15] approximate scheme. This conclusion concurs with the results of the original work of Gilbert and Ross [19], however, we believe that some of our arguments (Section 2 and 6), the physical models and the computational method employed by us are somewhat more general. The numerical results obtained herein for the one dimensional model confirm our general considerations. Similar results for thermally induced predissociation of a diatomic molecule (see appendix) also provide support to our general conclusions. In particular, it is important to notice that the calculated apparent activation energy varies from the value of A corresponding to the continuum onset at low temperatures to a value close to E_0, which represents the intersection point of the two one dimensional surfaces, at high temperatures.

An important conclusion originating at this point is that unimolecular reaction rates which correspond to processes involving a change in the electronic states, cannot be described over a broad temperature region in terms of the Arrhenius equation, and experimental activation energies can be compared to the theoretical data only over a narrow temperature range.

The one dimensional and the two dimensional linear models employed herein are admittedly crude, but they are very helpful in the elucidation of the gross features of the physical problem at hand. In particular, it is important to notice that in describing the potential surfaces for the initial and the final states we have completely discarded the conventional notion of normal modes [8]. As the decaying resonance states involve an admixture of highly excited vibrational ground state levels and continuum states, the use of normal modes (which is only valid for a small number of low lying bond vibrational levels) is quite useless in this context. The use of vibrational modes corresponding to different bonds was utilized in the semiquantitative description of molecular ground state potential surfaces [8, 38]. It was felt for some time that the highly excited vibronic levels of a lower electronic configuration which act as a dissipative channel in intramolecular electronic relaxation processes in large molecules are inadequately described in terms of normal modes, however, the problem of an alternative description of nuclear motion in a large molecule was not yet resolved.

We were able to provide a theoretical scheme for the linear dissociation process, the inclusion of the N–N vibrational mode being of considerable interest in relation to the vibrational states of the N_2 molecules which result from the unimolecular dissociation of N_2O. In the case when the N–N coordinate remains unchanged between the initial and the final states the partition of the N_2 vibrational states in the final product will be the same as in the initial ground state molecule.

The most serious sin of omission involved in the present treatment is the complete disregard of the doubly degenerate ground state bending vibration which will result in non linear dissociation (i.e. to an $O(^3P)$ atom flying apart at an angle

$\Theta < \pi$ relative to the $N_2(^1\Sigma)$ molecular axes). This problem can be handled (at least within the framework of the harmonic approximation) by assigning additional out of plane imaginary frequencies for the N–O motion. This interesting problem deserves a further study.

Any theoretical study should be tested in terms of the correlations it provides for the available experimental data and, most important, in terms of the suggestions for new experiments. The following comments are now in order:

a) The activation energy for the nonadiabatic unimolecular dissociation of N_2O, CO_2, CS_2 and COS should vary in the range $\Delta H_0^0 \leqq A \leqq E_A \leqq E_0 \leqq D$ (see Table 1). The only exception of this general conclusion (i.e. $E_A < D$) involves the high pressure dissociation of the CO_2 molecule [40] where $E_A = 110$ kcal/mole while $\Delta H_0^0 = 126$ kcal/mole. As the experimental data were obtained from shock wave experiments autocatalytic effects cannot be excluded. A further experimental study of k, for this reaction will be desirable.

b) The thermally averaged rate constant is rather uniformative and it will be very interesting to obtain direct experimental information concerning the energy dependence of the microscopic rate constants $W_{i\alpha}$ for the decay of a single vibronic zero order ground state level. In view of anharmonicity effects these highly excited vibrational levels located above the continuum onset A may be accessible to optical excitation by either one photon absorption or, alternatively, by multiphoton absorption utilizing intense high power laser light sources. Such experiments of laser induced unimolecular decay of a single vibronic level will be of considerable value. Such optical selection experiments seem to be feasible by combining modern laser techniques with sensitive mass spectrometric detection methods.

c) The distribution of vibrational energy among the diatomic molecules resulting from conventional thermal dissociation or by optical selection of a single level (above A) is of considerable interest for the test of the general theory outlined in Section 6. To monitor the vibrationally excited states of homonuclear N_2 resulting from N_2O dissociation one can utilize antistokes Raman scattering from a laser. In the cases of nonadiabatic unimolecular decomposition of CO_2, CS_2 or COS one can monitor directly the infrared emission from the resulting heteronuclear molecule. In the suggested thermal experiments vibrational relaxation of the products by the buffer gas has to be taken into account.

In conclusion, we would like to state that the formalism developed for nonradiative processes can be successfully applied to nonadiabatic unimolecular reactions. The present treatment is by no means limited to triatomic molecules. In the case of large molecular systems, it might be sometimes feasible to consider a "submolecule" within a large molecule (leaving out all the vibrational modes which are unchanged between the two electronic states) and to treat unimolecular thermally induced nonadiabatic decomposition or optically excited predissociation in large molecules by the adaptation of theoretical scheme employed in the present work.

Acknowledgments. One of us (H. Gebelein) is grateful for a grant from Deutsche Forschungsgemeinschaft. We are greatly indebted to Professor I. G. Ross and to Dr. R. G. Gilbert for stimulating discussions and for prepublication information. We wish to thank Professor J. W. Moskowitch, Mr. A. Nitzan, Mr. A. Moalein and Mr. S. Muchamel for very helpful discussions.

Appendix

Some Calculations on the Collision Induced Predissociation of $O_2(^3\Sigma_u^-)$

In the Schumann-Runge band of O_2 a line broadening due to predissociation can be experimentally observed. Murrell and Taylor [24] calculated this line broadening by numerical evaluation of the Franck-Condon factors and investigated the influence of the form of the repulsive potential while Child [23] has applied the *WKB* method for this system. We repeated this calculation with the method outlined for a *RKR* potential [41, 23] a Morse-potential and a harmonic potential. From the results for the line broadening in Fig. 6, it can be seen that the pattern of the line broadening is quite sensitive to the different bound state potentials as well as to the absolute value of the crossing point. The absolute values for the line broadening were calculated with a spinorbit interaction value of 70 cm^{-1} as for this value the absolute line broadening is in best agreement with the experimental results. The line broadening $\Delta\nu$ is given by the formula

$$\Delta\nu_i = \hbar W_i \tag{A.1}$$

We next turn our attention to the problem of collision induced predissociation [42] of $O_2(^3\Sigma_u^-)$ electronically excited states initially excited optically in the pres-

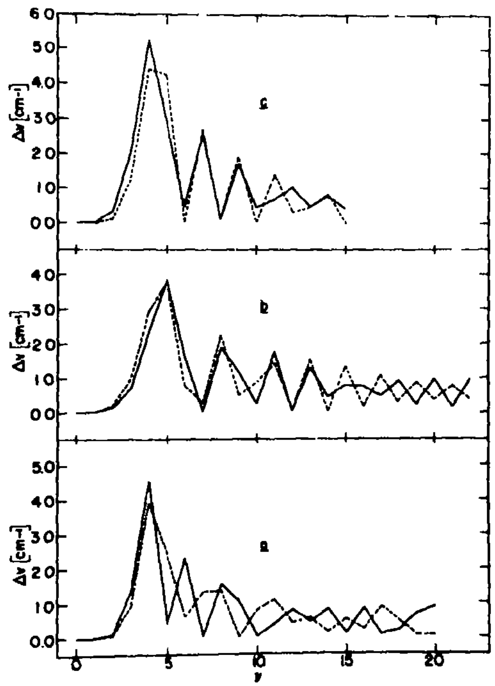

Fig. 6. Line broadening for the Schumann Runge spectrum of O_2. a for the RKR potential with ·· $E_0 = 2359$ cm^{-1}; --- $E_0 = 2604$ cm^{-1}; b for the harmonic potential with —— $E_0 = 2760$ cm^{-1}; --- $E_0 = 2610$ cm^{-1}; c for the Morse potential with —— $E_0 = 2468$ cm^{-1}; --- $E_0 = 2634$ cm^{-1}

ence of an inert gas at sufficiently high pressure to satisfy relation (2.9). Thus we can consider a decay process where the lowest vibrational level of the excited electronic state $^3\Sigma_u^-$ is optically populated and assuming that this electronically excited $^3\Sigma_u^-$ state arrives in thermal equilibrium before nonradiative (predissociated) decay. The microscopic rate constants, which are proportional to Δv_l (Eq. A.1), were

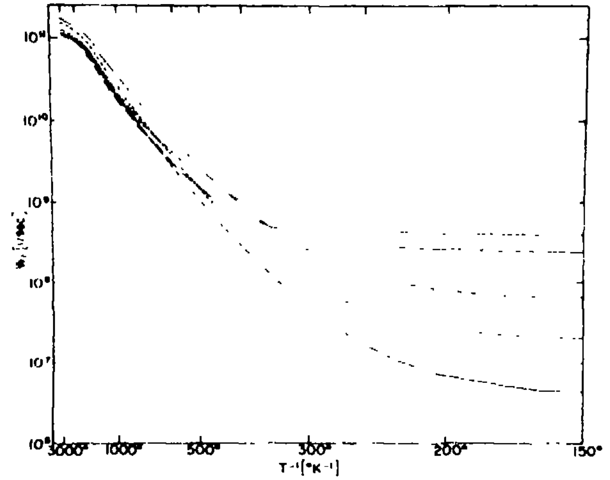

Fig. 7. Rate constants versus T^{-1} for the thermally induced predissociation of $O_2(^3\Sigma_u)$. For the RKR potential $E_0 = 2604$ cm^{-1}; ······ $E_0 = 2359$ cm^{-1}; for the harmonic potential: $E_0 = 2760$ cm^{-1}; · · $E_0 = 2610$ cm^{-1}; for the Morse potential; ··· $E_0 = 2648$ cm^{-1}; $E_0 = 2634$ cm^{-1}

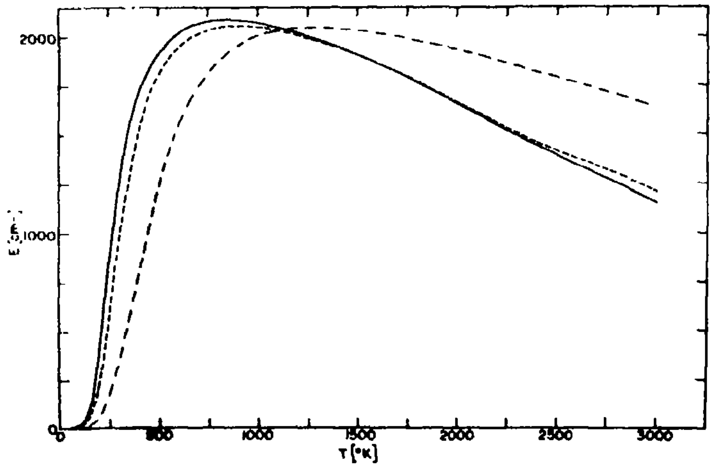

Fig. 8. Activation energy for the thermally induced predissociation of $O_2(^3\Sigma_u)$. General behaviour for - · - a harmonic potential; —— a Morse potential; – – – a RKR potential

used to calculate the thermally averaged rate constants and the activation energies. The results are given in Figs. 7 and 8. As expected, the rate constants are of the same order of magnitude for the different potentials chosen and yield zero activation energy for low temperatures while at high temperatures the energy value corresponding to the crossing point of the two potential surfaces is obtained. These results for thermally induced predissociation of an excited electronic state of a diatomic molecule concern with the results of our general analysis.

References

1. a Robinson,G.W.: J. chem. Physics **47**, 1967 (1967).
   b Bixon,M., Jortner,J.: J. chem. Physics **48**, 715 (1960).
   c Rhodes,W.: J. chem. Physics **50**, 2885 (1969).
   d Jortner,J.: J. Chim. Physique **67**, 1 (1970).
2. Rosen,N.: J. chem. Physics **1**, 319 (1933).
3. Langer,R.M.: Physic. Rev. **34**, 92 (1929).
4. Rice,O.K.: J. chem. Physics **1**, 375 (1933).
5. Mies,F.M., Kraus,M.: J. chem. Physics **45**, 4455 (1966).
6. – J. chem. Physics **51**, 787 (1969).
7. – J. chem. Physics **51**, 798 (1969).
8. Stearn,A.E., Eyring,H.: J. chem. Physics **3**, 778 (1935).
9. Gill,E.K., Laidler,K.: Canad. J. Chemistry **36**, 13731 (1958).
10. Wieder,G.M., Marcus,R.A.: J. chem. Physics **37**, 1835 (1962).
11. Gladsstone,S., Laidler,K.J., Eyring,H.: The theory of rate processes. N.Y.: McGraw-Hill 1941.
12. Troe,J., Wagner,H.: Ber. Bunsenges. physikal. Chem. **71**, 937 (1967).
13. Arrthenius,S.: Z. physik. Chem. **4**, 226 (1889).
14. Landau,L.D.: Physics Z. Sovijet Union **1**, 88 (1932).
15. Zener,C.: Proc. Roy. Soc. (London) A **140**, 660 (1933).
16. Hinshelwood,C.N.: Proc. Roy. Soc. (London) A **113**, 230 (1927).
17. Kassel,L.S.: J. physic. Chem. **32**, 225 (1928).
18. Slater,N.B.: Theory of unimolecular reactions. Ithaca: Cornell University Press 1959.
19. a Gilbert,R.G.: Ph. D. thesis. Australia: University of Canberra 1970.
    b – Ross,I.G.: Austral. J. Chemistry **24**, 1451 (1971).
20. Landau,L.D., Lifshitz,E.M.: Quantum mechanics. London, New York: Pergamon Press 1958.
21. Coulson,C.A., Zalewsky,K.: Proc. Roy. Soc. (London), A **268**, 437 (1962).
22. Harris,R.A.: J. chem. Physics **39**, 978 (1963).
23. Child,M.S.: J. molecular Spectroscopy **33**, 487 (1970).
24. Murrell,J.N., Taylor,J.M.: Molecular Physics **16**, 609 (1969).
25. Nitzan,A., Jortner,J.: Chem. Physics Letters (in press).
26. Siebrand,W.: J. chem. Physics **46**, 440 (1967).
27. Levich,V.G.: Physical chemistry and advanced treatise, Vol. IXB, p. 985, edited by H. Eyring, Academic Press (1970).
28. Nikitin,E.E.: In: Chemische Elementarprozesse. Berlin: Springer Verlag 1968.
29. Sponer,H., Bonner,L.G.: J. chem. Physics **8**, 33 (1940).
30. Burland,D.M., Robinson,G.W.: J. chem. Physics **51**, 4548 (1969).
31. Olschewski,H.A., Troe. J., Wagner,H.Gg.: Ber. Bunsenges. physik. Chem. **70**, 450 (1966).
32. Kubo,R., Toyozawa,Y.: Progr. theoret. Physics **13**. 160 (1955).
33. Englman,R., Jortner,J.: Molecular Physics **28**, 145 (1970).
34. Lax,M.: J. chem. Physics **20**, 1752 (1952).
35. Lin,S.H.: J. chem. Physics **44**, 3759 (1966).
36. Marcus,R.A.: J. chem. Physics **24**, 966 (1956).
37. Libby,W.: J. physic. Chem. **56**, 863 (1952).

38. Herzberg, G.: Electronic spectra of polyatomic molecules. New York: D. Van Nostrand Company 1966.
39. Nitzan, A., Jortner, J.: J. chem. Physics, to be published.
40. Olschewski, H. A., Troe, J. A., Wagner, Gg: Ber. Bunsenges. physik. Chem. N.F. **45**, 329 (1965).
41. Ackerman, M., Biounne, F.: J. molecular Spectroscopy **35**, 73 (1970).
42. Commes, F. J., Wenning, M.: Chem. Physics Letters **5**, 199 (1970).

Dr. H. Gebelein
Institut für physikalische Chemie
Robert Mayer-Str. 11
D-6000 Frankfurt am Main
Germany

Theoret. chim. Acta (Berl.) 25, 169—180 (1972)
© by Springer-Verlag 1972

Ab initio Untersuchungen über Stabilität und Spektren des hypothetischen Moleküls Si_2H_2

BERND WIRSAM

Institut für Theoretische Physik, Justus Liebig-Universität, Gießen

Eingegangen am 14. September 1971

Ab initio Calculations on the Stability and the Spectra of the Hypothetic Molecule Si_2H_2

Ab initio SCF MO and CI calculations for the ground and excited states of the hypothetical molecule Si_2H_2 are carried out in order to obtain a theoretical description of the stability and the electronic spectrum of this system. The results are compared with the corresponding quantities of linear and bent acetylene.

Mit Hilfe von SCF und CI Rechnungen werden mit einem atomaren Basissatz von kontrahierten Gauß-Lobefunktionen am hypothetischen Molekül Si_2H_2 Absolutrechnungen durchgeführt. Es werden die Bindungsverhältnisse für lineare und gewinkelte Geometrien untersucht, das Spektrum berechnet und die Ergebnisse mit entsprechenden Daten des stabilen C_2H_2 verglichen.

1. Einführung

Über ein dem Acetylen entsprechendes Molekül Si_2H_2 liegen weder experimentell noch theoretisch hergeleitete Angaben vor. Allgemein nimmt man an, daß es zwischen Siliziumatomen keine Mehrfachbindungen gibt, und versucht dies mit der Größe der Siliziumatome plausibel zu machen. Diese Feststellung soll durch Absolutrechnungen nachgeprüft werden.

Die Frage nach der Existenz dieses Moleküls stellt sich quantentheoretisch als die Frage nach der Existenz und der Tiefe eines Minimums in der Potentialhyperfläche dieses Systems im Grundzustand. Dies bedeutet insbesondere, daß ein solches Molekül gegen die Auftrennung der Si-Si Bindung stabil sein muß. Es müssen daher zuerst diejenigen Potentialkurven berechnet werden, die durch Auseinanderrücken zweier SiH Radikale entstehen. Weitere Untersuchungen beschäftigen sich mit den angeregten Zuständen dieses Moleküls auch bei gewinkelten Geometrien, da die Kenntnis charakteristischer Eigenschaften des Spektrums eines hypothetischen Moleküls möglicherweise die Suche danach erleichtert.

2. Rechenmethoden

Eine quantenmechanische *ab initio* Behandlung von Molekülen hat gegenüber semiempirischen Methoden den großen Vorteil, daß man neben universellen Naturkonstanten keine zusätzlichen Informationen aus dem Experiment über das jeweils betrachtete System benötigt. Ihre Genauigkeit sollte bereits ausreichen, um für Moleküle, über die keine oder unsichere Daten bekannt sind, ausführliche Aussagen zu machen oder gar für bisher unbekannte Moleküle zuverlässige Hypothesen für ihre Eigenschaften aufzustellen.

Die hier benutzten Verfahren gehen von reinen Gauß-Lobefunktionen aus [1, 8, 12, 13]. Nach [11] wird der Lobeabstand mit dem Exponent wie folgt verknüpft: $R = \gamma\alpha^{-1/2}$, wobei $\gamma = 0.03$ sich als günstig erwiesen hat [7]. Der atomare Basissatz für das Si-Atom ähnelt dem, der in [11] verwendet wurde. Er enthält also nur *s*- und *p*-Funktionen und keine *d*-Funktionen, deren Einfluß auf Bindungen zwischen Atomen der zweiten Reihe des Periodensystems bedeutend sein kann. Dieser Einfluß soll hier aber nicht untersucht werden. Die einzelnen Gaußfunktionen werden zu einer Basis von sechs kontrahierten *s*-Gruppen und drei p_x, p_y, p_z-Gruppen für Silizium zusammengefaßt. Eine *s*-Gruppe wird für das Wasserstoffatom benutzt. Dabei wird der Skalenfaktor für die Exponenten $\eta^2 = 2.0$ gewählt.

Die SCF Rechnungen werden nach der Roothaan-Hall Methode durchgeführt [3, 4, 9, 10]. Die anschließende CI-Rechnung benutzt ein Verfahren, das von Buenker und Peyerimhoff [2] entwickelt und programmiert wurde.

3. Stabilität des Moleküls Si_2H_2

A. SCF-*Rechnungen*

Zur Beantwortung der Frage nach einem relativen Minimum für die Potentialkurve des Grundzustandes wird diese zunächst mit dem SCF Verfahren berechnet. Außer dem $^1\Sigma_g^+$ Grundzustand, der zur Konfiguration $4\sigma_g^2 4\sigma_u^2 5\sigma_g^2 2\pi_u^4$ (die inneren MO's sind nicht angeführt) gehört, wird noch die einer einfachen Anregung entsprechende Konfiguration $4\sigma_g^2 4\sigma_u^2 5\sigma_g^2 5\sigma_u^1 2\pi_u^3$ mit den Zuständen $^3\Pi_u$ und $^1\Pi_g$ betrachtet; weiterhin wird die Konfiguration, aus der der nächst höhere Zustand der Symmetrie $^1\Sigma_g^+$ hervorgeht, nämlich $4\sigma_g^2 4\sigma_u^2 5\sigma_g^2 5\sigma_u^2 2\pi_u^2$ berechnet, welche zu den Zuständen $^1\Delta_g, {}^3\Sigma_g^-, {}^1\Sigma_g^+$ führt. Somit können Überschneidungen von Energieflächen oder Kurven und deren gegenseitige Beeinflussung verfolgt werden. Der Si-H Kernabstand wird gleich 2.68 atomare Einheiten gesetzt. Diesen Wert erhält man, wenn vorausgesetzt wird, daß sich die Bindungslängen zwischen dem Siliziumatom und dem Wasserstoffatom ähnlich verhalten wie die entsprechenden Bindungsabstände bei den Kohlenwasserstoffen. Dort verkleinert sich beim Übergang von CH zu C_2H_2 der C-H Kernabstand geringfügig um den Faktor 0.935. Der experimentelle Abstand von 2.87 atomare Einheiten zwischen dem Siliziumatom und dem Wasserstoffatom beim SiH mit dieser Zahl multipliziert ergibt 2.68 atomare Einheiten. Mit diesem konstanten Si-H Abstand werden die SCF-Rechnungen für geschlossene und offene Schalen durchgeführt. Tabelle 1 gibt die so erhaltenen Gesamtenergien des linearen Si_2H_2 bei Variation des Si-Si Kernabstandes an, die dazugehörige grafische Darstellung ist Fig. 1.

Die Kurve für den Grundzustand besitzt demnach ein Energieminimum mit einer Energie von -578.6251 DRy. Mit dieser Energie ergibt sich eine Dissoziationsenergie von 1.36 eV für das Auflösen des ganzen Moleküls in seine ein-

Tabelle 1. Gesamtenergien des linearen Si_2H_2 bei Variation des Si-Si Kernabstandes. (Energienullpunkt: −578,0 DRy)

Konfiguration	Zustand	$R = 2{,}6$	3,4	4,2	5,0 at. Einheit
$5\sigma_g^2 4\sigma_u^2 1\pi_g^4 2\pi_u^4$	$^1\Sigma_g^+$	+0.0145	−0,5717	−0,6128	−0,5061
$5\sigma_g^2 5\sigma_u^1 1\pi_g^4 2\pi_u^3$	$^3\Pi_g$	+0,2648	−0,4326	−0,5788	−0,5547
	$^1\Pi_g$	+0,3020	−0,3915	−0,5377	−0,5149
$5\sigma_g^2 5\sigma_u^2 1\pi_g^4 2\pi_u^2$	$^3\Sigma_g^-$	+0,5585	−0,2512	−0,4998	−0,5548
	$^1\Delta_g$	+0,5919	−0,2220	−0,4744	−0,5320
	$^1\Sigma_g^+$	+0,6252	−0,1928	−0,4489	−0,5092

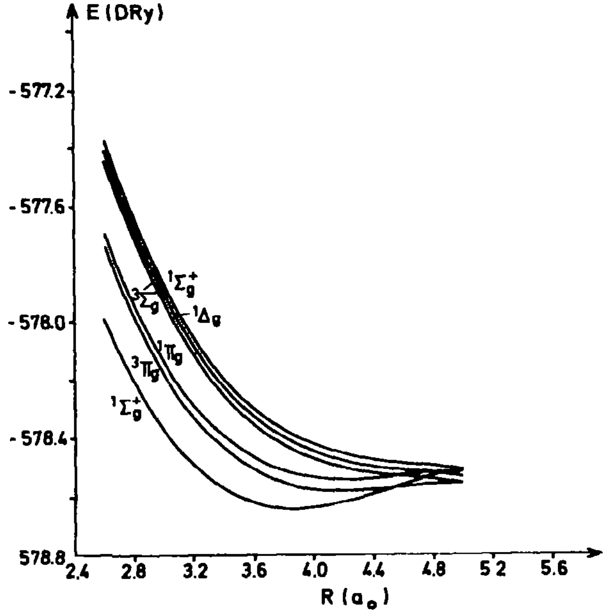

Fig. 1. Gesamtenergien (SCF-Werte) einiger Zustände des linearen Si_2H_2 bei Variation des Si-Si Kernabstandes

zelnen Atome. Aus der Betrachtung der SCF Potentialkurve des Grundzustandes allein könnte man schließen, daß das Molekül Si_2H_2 außerordentlich stabil gegen die Auftrennung der Si-Si Bindung sei. Vergleicht man jedoch die Energie des Minimums mit der aus einer völlig analogen SCF Rechnung erhaltenen Energie zweier getrennter SiH Radikale von −578,6300 DRy, so stellt man fest, daß die Energie der getrennten Bruchstücke um 0.14 eV unter der des Moleküls Si_2H_2 liegt. Dieser Vergleich spricht also gegen die Aussage, die man allein aus der Betrachtung der SCF Potentialkurve für den Grundzustand erhalten hatte, nämlich daß dieses Molekül im Grundzustand stabil gegen den Zerfall in zwei Radikale SiH ist.

Eine Ursache für diesen Widerspruch kann in der Vernachlässigung von 3*d* Funktionen liegen, da zu erwarten ist, daß sich ihr Beitrag zur Energie beim Molekül Si_2H_2 stärker auswirkt als beim Radikal SiH. Eine weitere Erklärung findet man, wenn man sich daran erinnert, daß SCF Rechnungen für offene Schalen wegen der in der Regel geringeren Korrelationsenergie relativ bessere Werte für die Energien liefern als vergleichbare SCF Rechnungen für abgeschlossene Schalen. Die SCF-MO-Rechnungen geben außerdem das Verhalten der wirklichen Potentialkurven für größere Abstände nicht immer richtig wieder, da der Grundzustand des vereinten Systems bei größer werdendem Abstand der Bruchstücke nicht in den Grundzustand des getrennten Systems überzugehen braucht. So geht der Grundzustand des Moleküls Si_2H_2 mit der Konfiguration $4\sigma_g^2 4\sigma_u^2 5\sigma_g^2 2\pi_u^4$ über in eine Mischung angeregter Zustände zweier SiH Radikale. Umgekehrt erhält man durch Kombination zweier Grundzustandskonfigurationen des SiH, $4\sigma^2 5\sigma^2 2\pi^1$ nur angeregte Konfigurationen des Si_2H_2 Moleküls, so zum Beispiel die Konfiguration $4\sigma_g^2 4\sigma_u^2 5\sigma_g^2 5\sigma_u^2 2\pi_u^2$, aus der der tiefste angeregte $^1\Sigma_g^+$ Zustand hervorgeht.

Aus Fig. 1 erkennt man, daß die Kurve dieses Zustands die entsprechende des $^1\Sigma_g^+$ Grundzustands schneidet. Dies ist möglich, da bei SCF Rechnungen Kreuzungsverbote von Potentialkurven gleicher Symmetrie nicht gelten. Eine quantentheoretische Berechnung, welche die Wechselwirkung zwischen den verschiedenen Konfigurationen berücksichtigt, sollte hier ein Ausweichen der beiden Kurven, bzw. einen Wechsel in der führenden Konfiguration ergeben. Das durch die SCF Rechnung erhaltene Minimum erscheint daher als fraglich, und es ist nötig, eine CI Rechnung durchzuführen.

B. CI-*Rechnung*

Bei der folgenden Rechnung soll es darauf ankommen, die Energiedifferenz zwischen dem Minimum des Grundzustandes von Si_2H_2 und der Energie zweier getrennter SiH Radikale zu bestimmen. Es sollen also lediglich Aussagen über die Trennungsenergie und die Stabilität des Moleküls Si_2H_2 erarbeitet werden, nicht aber die genaue Form der Potentialkurven, die daraus folgenden Schwingungsfrequenzen und andere spektroskopische Daten. Da bereits CI-Rechnungen für unendlichen Abstand vorliegen, nämlich die Rechnungen am SiH Radikal [14], genügt es, eine völlig analoge Berechnung für das Minimum des $^1\Sigma_g^+$ Grundzustandes von Si_2H_2 durchzuführen. Das SCF Minimum liegt etwas unterhalb von $R = 4.0$ atomaren Einheiten. In der Regel wird bei einer CI-Rechnung der berechnete Kernabstand für das Energieminimum gegenüber einer SCF Rechnung etwas vergrößert, so daß in unserem Fall $R = 4.0$ atomare Einheiten sicher in unmittelbarer Nähe des CI-Minimums liegt.

Analog zu dem Vorgehen beim SiH werden alle Konfigurationen gebildet, die entstehen, wenn man die Orbitale $1\sigma_g 1\sigma_u 2\sigma_g 2\sigma_u 3\sigma_g 3\sigma_u 1\pi_g 1\pi_u$ in den „core" und die Orbitale $4\sigma_g 4\sigma_u 5\sigma_g 5\sigma_u 2\pi_g 2\pi_u$ in den Valenzsatz aufnimmt. Aus den daraus resultierenden Zuständen werden alle 73 $^1\Sigma_g^+$ Zustände für die Berechnung des Grundzustandes herangezogen.

Mit dieser CI Funktion erhält man eine Gesamtenergie von -578.7055 DRy. Die analoge Energie zweier SiH Radikale beträgt -578.6468 DRy [14]. Daraus errechnet sich eine Trennungsenergie von 0.0587 DRy oder 1.60 eV.

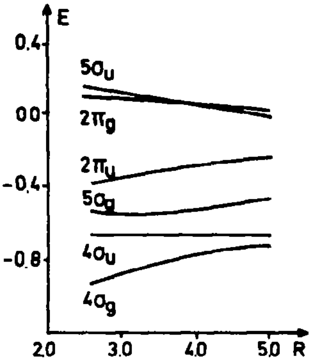

Fig. 2. Orbitalenergien der Valenzorbitale von Si_2H_2

Da die $3d$ Funktionen nicht berücksichtigt wurden, kann dieser Wert für die Trennungsenergie auch bei einer ausführlichen CI-Rechnung mit einem kleinen Fehler behaftet sein. Wie aber bereits angedeutet, sollte eine Hinzunahme von $3d$ Funktionen die Energie des Moleküls Si_2H_2 stärker senken als die Energie des SiH Radikals. Damit würde sich die Trennungsenergie und die Stabilität des Moleküls für den Zerfall in zwei SiH Radikale nur noch vergrößern. Die Stabilität des hypothetischen Moleküls Si_2H_2 konnte also bereits allein mit s- und p-Funktionen nachgewiesen werden.

Der Vergleich mit der aus einer entsprechenden CI Rechnung erhaltenen Trennungsenergie des Moleküls C_2H_2 von 8.14 eV läßt schon erkennen, daß die hier vorliegende Bindung nicht von der gleichen Stärke sein kann wie die chemisch feste Dreifachbindung beim Acetylen.

Um den Unterschied im Bindungscharakter näher zu untersuchen, werden die für die Bindung in Frage kommenden Orbitale in ihrem Verhalten und ihrer elektronischen Struktur genauer betrachtet. Fig. 2 gibt die Abhängigkeit der Orbitalenergien vom Si-Si Kernabstand wieder. Nach der qualitativen Molekülorbitaltheorie stellt man fest, daß die beiden Orbitale $4\sigma_g$ und $2\pi_u$ deutlich bindenden, die Orbitale $2\pi_g$ und $5\sigma_u$ stark antibindenden Charakter besitzen und die Orbitalenergien von $4\sigma_u$ und $5\sigma_g$ keine ausgeprägte Tendenz zeigen. Das Orbital $4\sigma_g$ bildet somit die σ-Bindung, das $2\pi_u$-Orbital ist für die doppelte π-Bindung verantwortlich. Die Elektronendichten für die beiden bindenden Orbitale sind in Fig. 3 und in Fig. 4 aufgezeichnet. Der Vergleich mit den Ladungsdichten der entsprechenden Orbitale beim C_2H_2 [6] zeigt, daß beim Acetylen die Ladungsdichten des σ-Orbitals in der Mitte zwischen den beiden C-Kernen auf über 0.2 steigt, während dieser Wert für Si_2H_2 nur bei ungefähr 0.03 liegt. Ähnlich verhält es sich mit der π-Bindung. Das Maximum der Ladungsdichten der π-Orbitale in der Ebene, die senkrecht zur Kernverbindungsachse durch deren Mitte geht, beträgt für C_2H_2 etwa 0.07, für Si_2H_2 dagegen nur 0.02. Diese geringeren Ladungsdichten bedeuten natürlich eine Verminderung der bindenden Kräfte.

Dreifachbindungen beim Si_2H_2 und beim C_2H_2 unterscheiden sich nach dieser theoretischen Betrachtung einzig in ihrer Stärke. Die geringen Bindungs-

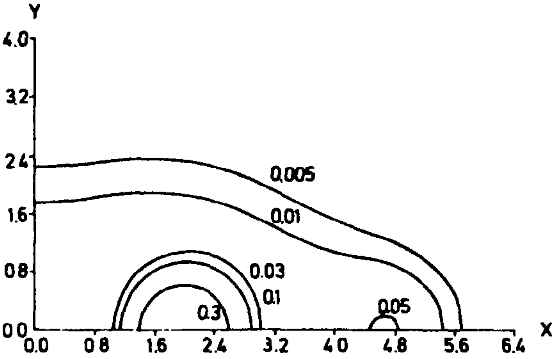

Fig. 3. Berechnete Elektronendichten des Orbitals $4\sigma_g$

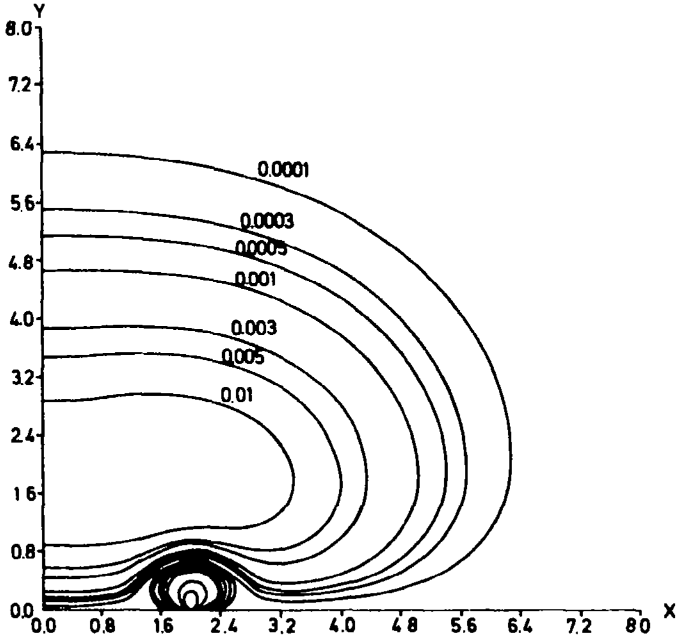

Fig. 4 Berechnete Elektronendichten des Orbitals $2\pi_u$

kräfte und eine mögliche Polymerisation zu Polysilin $(SiH)_n$ sollten dafür verantwortlich sein, daß die Existenz des Moleküls Si_2H_2 noch nicht festgestellt werden konnte.

4. Potentialkurven bei gewinkeltem Kerngerüst

Die Suche nach bisher experimentell nicht bekannten Molekülen wird erleichtert, falls einige charakteristische Eigenschaften des Spektrums und der Geometrie bekannt sind. Bisher wurde das Si_2H_2 Molekül nur im linearen Fall

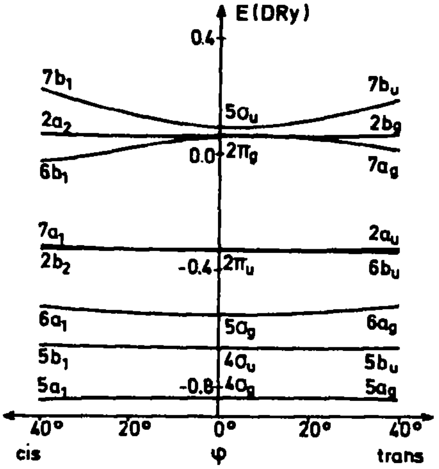

Fig. 5. Orbitalenergien der Valenzorbitale bei *cis*- und *trans*-Winkelungen von Si_2H_2

betrachtet, und daraus wurden Resultate hergeleitet. Das Molekül könnte aber ebensogut in einer der beiden gewinkelten Geometrien, d. h. in einer *trans*- oder *cis*-Form, vorliegen. Die jetzt folgenden Rechnungen sollen zeigen, daß das Si_2H_2 Molekül im Grundzustand tatsächlich linear vorliegt und somit die bisherigen Überlegungen zur Stabilität nachträglich gerechtfertigt werden.

Zugleich werden für die *cis*- und *trans*-Winkelungen auch angeregte Zustände betrachtet. Die Rechnungen für die gewinkelten Strukturen beschränken sich auf SCF Verfahren, da das für einen ersten Überblick voll ausreichende Ergebnisse liefert. Betrachten wir zunächst den Grundzustand, also den 1^1A_1 Zustand für die *cis*-Winkelung, den $^1\Sigma_g^+$ Zustand der linearen Geometrie und den 1^1A_g Zustand für die *trans* Winkelung. Dieser Zustand besitzt wie erwartet ein Minimum für die lineare Kernanordung (Fig. 6).

Der Verlauf der Orbitalenergien in Abhängigkeit von der Winkelung soll uns zunächst ohne viel Rechenaufwand Vorhersagen über den qualitativen Verlauf der Potentialkurven auch der angeregten Zustände liefern. In Fig. 5 sind diese Energien für die Valenzorbitale aufgetragen.

Man erkennt zunächst nur geringe Abhängigkeit der Energie der besetzten Orbitale von der Winkelung, dagegen zeigt das virtuelle $6b_1-2\pi_g-7a_g$ Orbital einen stark stabilisierenden Verlauf, sobald die beiden Wasserstoffatome aus der Geraden herausgedreht werden. Bei der Variation des Kernabstandes war dieses Orbital als stark antibindend aufgefallen. Somit verhält es sich ganz analog zu dem $3b_1-1\pi_g-4a_g$ Orbital des C_2H_2. Anregungen in dieses Orbital sollten dann auch zu Zuständen führen, deren Potentialkurven Minima zeigen, die zu *cis*- und *trans*-gewinkelten Geometrien gehören. Übergänge in das $2a_2-2\pi_g-2b_g$ Orbital dürften wenig Einfluß zugunsten einer Winkelung haben, dagegen sollte die Besetzung des $7b_1-5\sigma_u-7b_u$ Orbitals einen Effekt gerade in der umgekehrten Richtung bewirken. Bei Besetzung dieser Orbitale scheint eine Stabilisierung in Richtung auf lineare Geometrie zu verlaufen.

Tabelle 2. Gesamtenergien aus SCF-Rechnungen für *cis*- und *trans*-Winkelungen des Si_2H_2-Moleküls ($R_{SiH} = 2{,}68$, $R_{SiSi} = 3{,}4$ at. Einh. Energienullpunkt: $-578{,}0$ DRy. Energiewerte in DRy)

Anregung und Zustand						*cis*		linear	*trans*	
cis		linear		*trans*		40	20	0	20	40
–	$^1A_1$		$^1\Sigma_g^+$		^1A_g	−0,5089	−0,5546	−0,5717	−0,5703	−0,5629
$7a_1-6b_1$	$^3B_1$	$2\pi_u-2\pi_g$	$^3\Sigma_u^+$	$6b_u-7a_g$	^3B_u	−0,5070	−0,4958		−0,4708	−0,4863
$2b_2-6b_1$	$^3A_2$		$^3\Delta_u$	$2a_u-2b_g$	^3B_u	−0,4727	−0,4730	–	−0,4588	−0,4531
$2b_2-2a_2$	$^3B_1$			$2a_u-7a_g$	^3A_u	−0,3965	−0,4423		−0,4478	−0,4733
$7a_1-2a_2$	$^3A_2$		$^3\Sigma_u^-$	$6b_u-2b_g$	^3A_u	−0,3846	−0,4209		−0,4310	−0,4135
$7a_1-2a_2$	$^1A_2$		$^1\Sigma_u^-$	$6b_u-2b_g$	^1A_u	−0,3630	−0,4024		−0,4084	−0,3823
$2b_2-6b_1$	$^1A_2$		$^1\Delta_u$	$2a_u-7a_g$	^1A_u	−0,4454	−0,4449		−0,4293	−0,4532
$2b_2-2a_2$	$^1B_1$			$2a_u-2b_g$	^1B_u	−0,2556	−0,3014		−0,3179	−0,3122
$7a_1-6b_1$	$^1B_1$		$^1\Sigma_u^+$	$6b_u-7a_g$	^1B_u	−0,3970	−0,4011	–	−0,3260	−0,3390
$2b_2-7b_1$	$^3A_2$	$2\pi_u-5\sigma_u$	$^3\Pi_u$	$2a_u-7b_u$	^3B_g		–	−0,4326	−0,4073	−0,3288
$7a_1-7b_1$	$^3B_1$			$6b_u-7b_u$	^3A_g	–			−0,3995	−0,3040
$2b_2-7b_1$	$^1A_2$		$^1\Pi_g$	$2a_u-7b_u$	^1B_g		–	−0,3915	−0,3681	−0,2931
$7a_1-7b_1$	$^1B_1$			$6b_u-7b_u$	^1A_g	–			–	–

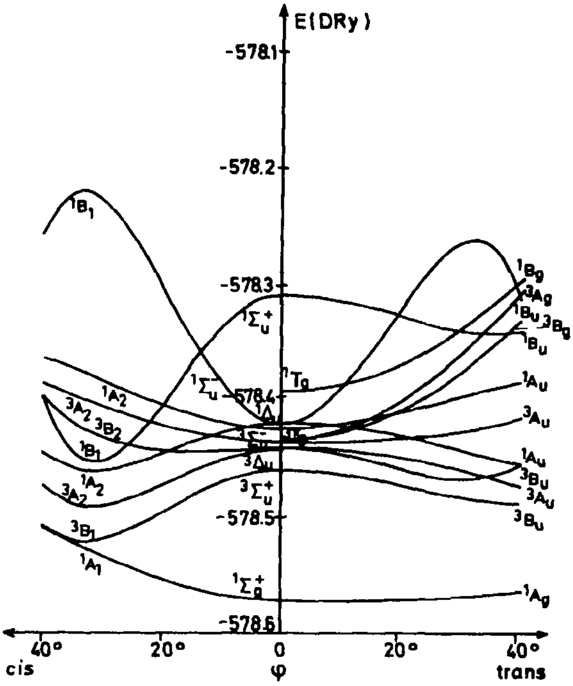

Fig. 6. Gesamtenergien aus SCF Rechnungen für *cis*- und *trans*-Winkelungen des Si_2H_2 Moleküls im Grundzustand und in angeregten Zuständen

Tabelle 2 faßt die Ergebnisse der SCF Rechnungen zusammen, in Fig. 6 wurden die aus diesen Werten durch Polynominterpolation erhaltenen Potentialkurven eingezeichnet. Zur besseren Gegenüberstellung mit dem Spektrum des Acetylens sind die Potentialkurven für dieses Molekül, berechnet nach dem CI Verfahren, aus einer Arbeit von Kammer [5] hier noch einmal in Fig. 7 wiedergegeben. Aus der grafischen Darstellung entnimmt man, daß tatsächlich alle Potentialkurven, die aus dem Übergang des höchsten besetzten MO's in das $6b_1 - 2\pi_g - 7a_g$ Orbital, nämlich die Zustände 1^3B_u, 1^1A_u, 1^3A_u, 1^1B_u für die *trans*-Winkelung und 1^3B_1, 1^3A_2, 1^1A_2, 1^1B_1 für die *cis*-Winkelung ein Minimum für gewinkelte Geometrien besitzen. Selbst die Asymmetrie des Verlaufes der MO-Energie von $7a_g$ und $6b_1$ bezüglich der beiden Winkelungen spiegelt sich in den Potentialkurven wieder. Die Minima auf der *cis*-Seite liegen deutlich tiefer als die auf der *trans*-Seite. Die Anregungen in das $2a_2 - 2\pi_g - 2b_g$ Orbital führen erwartungsgemäß zu Zuständen, deren Potentialkurven keine ausgeprägten Minima für *cis*- und *trans*-Winkelungen besitzen. Ebenso verhält es sich mit der einfachen Anregung in das $7b_1 - 5\sigma_u - 7b_u$ Orbital. Von den hieraus resultierenden Zuständen konnten auf der *cis*-Seite die Zustände 3^3A_2, 3^3B_1, 3^1A_2 und 3^1B_1, welche mit $^3\Pi_g$ und $^1\Pi_g$ korrelieren, nicht gerechnet werden, da das verwendete SCF Verfahren versagt, falls ein tieferes Orbital mit bestimmter Symmetrie nicht besetzt, dagegen ein höheres mit gleicher Symmetrie besetzt ist.

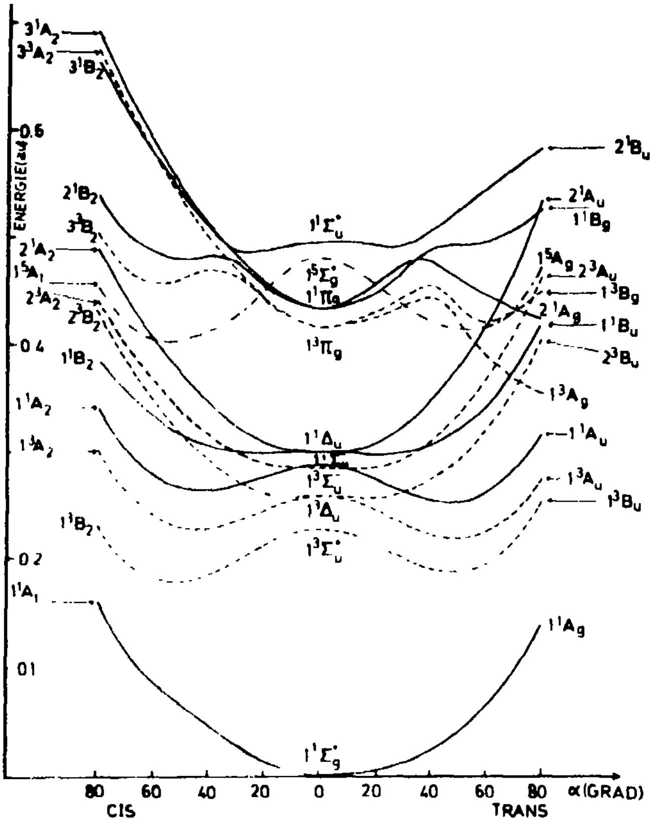

Fig. 7. Gesamtenergien aus CI Rechnungen für *cis*- und *trans*-Winkelungen des C_2H_2 Moleküls im Grundzustand und in angeregten Zuständen. (Aus der Arbeit von Kammer [5])

Die Ähnlichkeit zwischen dem $3b_1 - 1\pi_g - 4a_g$ Orbital des Acetylens und des $6b_1 - 2\pi_g - 7a_g$ Orbitals beim Si_2H_2 spiegelt sich auch im Verlauf der Potentialkurven wieder, die zu den Zuständen gehören, die bei Anregung dieses Orbitals auftreten. Fig. 7 ermöglicht den Vergleich mit den Potentialkurven des Acetylens. (Durch die Wahl eines anderen Koordinatensystems sind die Bezeichnungen von B_1 und B_2 Zuständen gerade umgekehrt wie in dieser Arbeit.)

Der tiefste angeregte Zustand ist in beiden Fällen $1^3B_1 - 1^3\Sigma_u^+ - 1^3B_u$, der bei *cis*- und *trans*-Winkelung ein Minimum zeigt. Der nächst folgende Zustand, $1^3A_2 - 1^3\Delta_u - 1^3A_u$, zeigt bei beiden Molekülen wieder ein ähnliches Verhalten. Dagegen treten bei den Zuständen, die mit dem $^1\Delta_u$ und dem $^1\Sigma_u^-$ korrelieren, also den Zuständen $2^1A_2 - 1^1\Sigma_u^- - 2^1A_u$ und $1^1A_2 - 1^1\Delta_u - 1^1A_u$ beim Molekül Si_2H_2 und den Zuständen $1^1A_2 - 1^1\Sigma_u^- - 1^1A_u$ und $2^1A_2 - 1^1\Delta_u - 2^1A_u$ beim C_2H_2 Unterschiede auf. Bei der SCF-Rechnung für das Si_2H_2 Molekül besitzt die energetisch tiefere Komponente des $1^1\Delta_u$ Zustandes ein deutliches Minimum, während in der entsprechenden CI-Rechnung für das C_2H_2 kein solches Minimum auftritt. Die Erklärung kann aus Fig. 8 abgelesen werden.

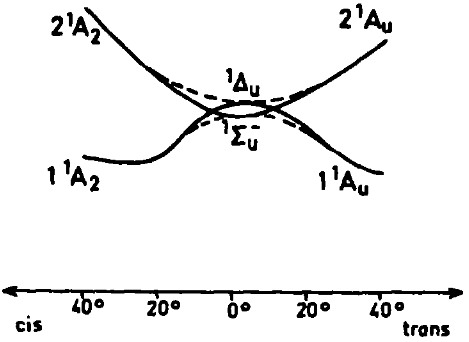

Fig. 8. Konfigurationswechselwirkung zweier Zustände

Eine Konfigurationswechselwirkung zwischen diesen beiden Zuständen tritt im linearen Fall nicht auf, da beide Zustände $^1\Delta_u$ und $^1\Sigma_u^-$ unterschiedliche Symmetrie besitzen. Diese Verhältnisse ändern sich, sobald zu einer der beiden gewinkelten Geometrien übergegangen wird. Nun kann die eine Komponente des ursprünglichen $^1\Delta_u$ Zustandes, der ^1A_u bzw. $^1A_2$ Zustand, mit dem ^1A_u bzw. $^1A_2$ Zustand, der aus dem $^1\Sigma_u^-$ Zustand hervorgeht, wechselwirken. Die Überschneidung der beiden Kurven, die bei der SCF Rechnung auftrat, wird in der CI Rechnung durch ein Ausweichen der beiden Kurven gleicher Symmetrie ersetzt. Das drückt sich in einem Wechsel der Konfigurationen aus. Bei 20° *cis* bzw. *trans* hat dieser Wechsel bereits stattgefunden, doch läßt sich die Tendenz der Konfigurationsverlagerung noch gut an den CI-Koeffizienten für C_2H_2 ablesen [6]. Die zweite Komponente des $^1\Delta_u$ Zustandes, der $^1B_1 - {}^1\Delta_u - {}^1B_u$ Zustand, weicht ebenfalls in der SCF Rechnung am Si_2H_2 erheblich von der CI-Rechnung am C_2H_2 ab. Nach unseren SCF Rechnungen schneidet dieser Zustand den $^1B_1 - {}^1\Sigma_u^+ - {}^1B_u$ Zustand, so daß auch hier mit einem Konfigurationswechsel gerechnet werden muß. Die Wirklichkeit verhält sich jedoch um einiges komplizierter, da diese beiden Zustände auch noch stark mit weiteren Konfigurationen mischen.

Der Vergleich zeigt große Ähnlichkeiten im Aufbau des Spektrums von Si_2H_2 und C_2H_2.

5. Zusammenfassung

SCF und CI Rechnungen zeigen, daß die Potentialkurve für den Grundzustand des hypothetischen Moleküls Si_2H_2 ein Minimum besitzt, und zwar für lineare Kerngeometrie. Daher sollte dieses Molekül zumindest kurzzeitig als stabiler Verband existieren können. Aufgrund der Elektronendichten und der Abhängigkeit der Orbitalenergien vom Si-Si Kernabstand stellte es sich heraus, daß die Bindung durch das $4\sigma_g$ und $2\pi_u$ Orbital verursacht wird. Die im Vergleich zum Acetylen geringe Trennungsenergie von 1.60 eV für das Aufbrechen der Si-Si Bindung sowie die viel geringeren Elektronendichten der bindenden Orbitale in der Mitte des Moleküls zeigen, daß sich „Dreifachbindungen" beim Si_2H_2

und beim C_2H_2 in ihrer Art zwar ähneln, aber in ihrer Stärke stark voneinander abweichen. Die Bindung beim Si_2H_2 sollte sich im Falle einer experimentellen Nachforschung als äußerst schwach erweisen.

Die Berechnung des Spektrums des gewinkelten Si_2H_2 ergibt große Ähnlichkeit mit dem entsprechenden Spektrum des Acetylens. Insbesondere besitzen beide Moleküle in einigen angeregten Zuständen Minima, die zu gewinkeltem Kerngerüst gehören.

Frau Prof. S. Peyerimhoff und Herrn Prof. R. Buenker möchte ich für Anregungen und Diskussionen sowie dafür danken, daß sie mir ihre Rechenprogramme zur Verfügung stellten. Mein Dank gilt ferner der Deutschen Forschungsgemeinschaft, durch deren finanzielle Unterstützung diese Untersuchungen ermöglicht wurden, und den Mitarbeitern des Rechenzentrums der Universität Gießen, wo die numerischen Berechnungen dieser Arbeit durchgeführt wurden.

Literatur

1 Boys, S. F.: Proc. Roy. Soc. (London) **200** A, 542 (1950).
2 Buenker, R. J., Peyerimhoff, S. D.: Theoret. chim. Acta (Berl.) **12**, 183 (1968).
3 Hartree, D. R.: Rept. Progr. Physics **11**, 113 (1948).
4 Huzinaga, S.: Physic. Rev. **120**, 866 (1960)
5 Kammer, W. E.: Chem. Physics Letters **6**, 529 (1970).
6. Dissertation Gießen (1971)
7 Petke, J. D., Whitten, J. L., Douglas, A. W.: J. chem. Physics **51**, 256 (1969).
8 Preuss, H.: Z. Naturforsch. **11**, 823 (1956)
9 Roothaan, C. C. J.: Rev. mod. Physics **23**, 69 (1951)
10. Rev. mod. Physics **32**, 179 (1960)
11 Shih, S., Buenker, R. J., Peyerimhoff, S. D., Wirsam, B.: Theoret. chim. Acta (Berl.) **18**, 277 (1970).
12 Whitten, J. L.: J. chem. Physics **39**, 349 (1963)
13 J. chem. Physics **44**, 359 (1966).
14 Wirsam, B.: Chem. Physics Letters **10**, 180 (1971).

Dr. B. Wirsam
Institut für Theoretische Physik
der Justus-Liebig-Universität
D-63 Gießen, Leihgesterner Weg 108
Deutschland

Theoret. chim. Acta (Berl.) 25, 181–188 (1972)
© by Springer-Verlag 1972

Relationes

Integral Hellmann-Feynman Investigations of *trans* Bent Acetylene

M. P. Melrose and P. J. Briggs
Department of Chemistry, King's College, London, W.C.2., England

Received September 20, 1971

The integral Hellmann-Feynman (IHF) theorem has been applied to various wavefunctions representing the ^1A_u state of acetylene with a view to testing traditional explanations of the excited state geometry. When LCAOSCF wavefunctions are used, the electronic energy changes associated with the individual corresponding orbitals (CMO's) are in sympathy with the trend in orbital (*i.e.* MO) energies suggested by Walsh. However, when LMO wavefunctions based on hybrid AO's are employed, the IHF results are against all experience; and imply that a change in hybridisation, from *sp* to sp^2, is not a viable model for the change in geometry.

Introduction

The experimental fact [1] that acetylene is *trans* bent in its first electronically excited state has long been of theoretical interest. The original qualitative explanation of Walsh [2] argues that, in so far as the change in molecular energy parallels the change in orbital energies, bending is favoured by the introduction of *s* character into the excited MO (π_g when CCH angle = 180°) which reduces the orbital energy until (when CCH angle = 90°) the a_g MO becomes almost non-bonding. This tendency is opposed by the b_u MO (corresponding to bonding π in the linear case) which becomes destabilised by increasing *s* character. The experimental bond angle [1] is almost exactly 120°, and it is tempting to suggest [3], in terms of localised molecular orbitals (LMO's), that these changes might equivalently be described by a change in hybridisation from *sp* to sp^2.

The first SCF calculation on acetylene to consider all the electrons was due to Burnelle [4] and confirmed the trend in $\pi_g - a_g$ orbital energy suggested by Walsh; but it failed to predict the correct geometry for the excited ^1A_u state from the total energy calculation, probably because of excessive integral approximations. Most of the theoretical studies of acetylene have since been concerned with the linear molecule, but recently Kammer [5] has reported SCF and CI calculations of linear and bent acetylene which agree extensively with the spectroscopic facts. Accurate *ab-initio* wavefunctions must provide the ultimate explanation for the shapes of molecules: but it may be difficult in some cases to relate the concepts of exact MO theory to the older, qualitative orbital theories. Peyerimhoff, Buenker and Allen [6] have shown that the success of the Walsh rules in predicting the geometries of AH_2 and AH_3 molecules with 6–9 valence electrons can be attributed to the fact that for these molecules changes in the sum of the SCF one electron energies are approximately parallel to changes in the total energy. On the other hand, Pan and Allen [7] have shown that in HCN, with ten valence electrons, the total energy and total orbital energy curves diverge as the bond angle is decreased from 180°. However, it must be pointed out that in the work cited above [6, 7] it has been assumed that the MO energies in Walsh diagrams are the one-electron eigenvalues of closed-shell SCF Hamiltonians. The geometries of open-shell molecules and of excited states are discussed using the lowest virtual orbitals – which do not have the same physical meaning as the MO's used in formulating the SCF Hamiltonians. Another difficulty in the interpretation of *ab-initio* wavefunctions arises in the localised orbital approach: that wavefunctions expressed in terms of extended atomic basis sets or, as in the calculations [5–7] cited above, in terms of gaussian lobe functions [8] may not be easy to visualise in terms of hybridisation.

In principle at least, the integral Hellmann-Feynman theorem (IHF), revived by Parr [9], offers a direct way of analysing the change in geometry from a one electron point of view. With a fixed CC bond length for each geometry, the change in electronic energy may be expressed as the difference of proton attraction operators integrated over the transition density between two configurations. The electronic energy change may then be analysed into contributions from the corresponding orbitals (CMO's) – the orbitals which diagonalise the 1-particle transition density matrix. Unfortunately, since the successful application of the IHF method to internal rotation in ethane [10], there has accrued considerable evidence [11–13] to suggest that simple LCAO wavefunctions do not give reliable IHF total energy differences. This, however, does not prevent the IHF theorem from giving insight into isoelectronic changes, particularly when the transition density is described in a way which is qualitatively correct [14]. Moreover, the error in an IHF calculation is entirely inherent in the wavefunctions used and, therefore, such calculations may be regarded as tests of the molecular models which the wavefunctions represent. One of the objects of the present study of *trans* bent acetylene was to see if the assumption of sp^2 hybridised carbon might account for the geometry of excited acetylene.

IHF Formula and the Configurations Considered

Within the framework of the Born-Oppenheimer approximation the IHF energy difference between linear and bent acetylene is given by

$$\Delta W_t = \frac{\langle \Phi_L | \Delta V_{ne} | \Phi_B \rangle}{\langle \Phi_L | \Phi_B \rangle} + \Delta V_{nn} \tag{1}$$

where Φ_L and Φ_B are electronic states associated with the linear and bent nuclear frames respectively. The normal and excited states of acetylene may be represented approximately by the following configurations:

$$^1\Sigma_g^+ \quad (1\sigma_g)^2 (1\sigma_u)^2 (2\sigma_g)^2 (2\sigma_u)^2 (3\sigma_g)^2 (\pi_u)^2 (\pi_u)^2 ,$$

$$^1A_u \quad (1a_g)^2 (1b_u)^2 (2a_g)^2 (2b_u)^2 (3a_g)^2 (3b_u)^2 (4a_g) (a_u) .$$

Now a direct substitution of the above wavefunctions for Φ_L and for Φ_B in (1) leads to a $\frac{0}{0}$ indeterminacy; and it was therefore decided to calculate instead the energy variation of the ^1A_u state ($^1\Delta_u$ in the linear case) as a function of CCH angle. No complication in applying (1) arises from the fact that the ^1A_u state formally requires two determinants. Since the singly occupied MO's are of different symmetry, there are no matrix elements of ΔV_{ne} between determinants which differ by an interchange of the spin factors of the $4a_g$ and a_u orbitals. Thus a single determinant is adequate for the IHF calculation. CMO's for state of the linear and bent nuclear frames were constructed by unitary transformations [10] of the MSO's with identical spin factors. In terms of single occupied CMO's Eq. (1) becomes

$$\Delta W_l = \sum_{i=1}^{i=14} \frac{\langle \hat{\psi}_i^L | \Delta V_{ne} | \hat{\psi}_i^B \rangle}{\langle \hat{\psi}_i^L | \hat{\psi}_i^B \rangle} + \Delta V_{nn}. \tag{2}$$

Geometry and Orbitals

Fig. 1 shows the nuclear frame and cartesian coordinates to which all wavefunctions are referred.

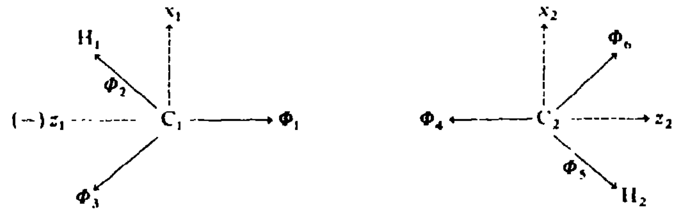

Fig. 1. Coordinate system and hybrid orbitals

The decision to fix the bond lengths was taken for an important reason. With bond lengths at their normal values (CH = 1.0568 Å; CC = 1.208 Å) a change in CCH angle of 60° produces a ΔV_{nn} value of 0.45358 a.u., which is *opposed* to bending. Thus in order to predict bending one is looking for a change in electronic energy, ΔE_l whose magnitude is about seven times as great as the ΔE_l magnitudes for the *rotation* of a bond in a comparable molecule [11]. The percentage error in the calculation of ΔE_l for the bending problem will thus be considerably smaller than for the rotation. (Of course, the algebraic sum $\Delta E_l + \Delta V_{nn}$, may be no more reliable than before.) If, however, the CC bond is allowed to relax (to the excited state value of 1.383 Å) simultaneously with the change in CCH angle, then at 120° the value of ΔV_{nn} is very small and actually in favour of the bent state. The value of ΔE_l might then also be very small – and too subtle for the wavefunctions envisaged here.

Three kinds of LCAO wavefunction were considered:-

a) The SCF MO's *of Burnelle*

Although these wavefunctions were calculated with integral approximations now regarded as too severe, the LCAO coefficients give reasonable populations [15] and are probably not very different from the coefficients of an exact minimal basis calculation. They were employed here because they appear to be the only MO's for bent acetylene which have been reported using a Slater-type AO basis. The orbital exponents were: C 1*s*, 5.7; C 2*s*, 1.59; C 2*p*, 1.59; and H 1*s*, 1.0.

b) Two Centre MO's *Constructed from Orthogonal Hybrids*

Employing precisely the same AO basis and bond lengths as in a), hybrid AO's were formed on each carbon atom according to

$$\Phi_i = (s + \lambda_i p_i) N_i \tag{3}$$

where Φ_i represents an sp^{λ_i} hybrid pointing in the direction (see Fig. 1) of a $2p_i$ orbital. Apart from normalising factors, Eqs. (3) contain six unknowns ($i = 1, 2, 3$) of which three may be eliminated by orthogonality criteria,

$$\langle \Phi_i | \Phi_j \rangle = \delta_{ij} \tag{4}$$

and the remaining three on the assumptions that Φ_1 and Φ_2 point along the CC and CH bonds respectively and that $\lambda_1 = \lambda_2$. With these assumptions the Φ_i take the usual forms of *sp* hybrids at 180° and sp^2 at 120°. Taking the inner shell MO's to be the C 1*s* orbitals themselves, two centre LMO's were constructed (ignoring normalising factors) as follows:

$$(\sigma_1)_{\mathrm{CH}} = k\Phi_2 + h_1 ,$$

$$(\sigma_2)_{\mathrm{CH}} = k\Phi_5 + h_2 ,$$

$$(\sigma)_{\mathrm{CC}} = \Phi_1 + \Phi_4\,(3a_g) ,$$

$$(\pi)_{\mathrm{CC}} = \Phi_3 - \Phi_6\,(3b_u) ,$$

$$(\pi^*)_{\mathrm{CC}} = \Phi_3 + \Phi_6\,(4a_g) .$$

The symbol *h* represents a hydrogenic 1*s* orbital. The MO designations refer to the linear molecule, while corresponding non-linear species are indicated in parentheses. The out-of-plane a_u orbital is identical with the π_y orbital throughout.

Only the factor *k* – the polarity of the CH bond – remains to be specified, and this was taken to be 1.09 [16]. It is interesting to note that in calculations by Woznicki [16] the expectation value of the ^1A_u state, calculated from the above MO's, gave a minimum in the energy curve when angle CCH = 120°. (The CC bond length in Woznicki's calculation was 1.383 Å, and the Mulliken approximation for polycentric integrals was used).

c) Two Centre LMO's *Constructed from Non-Orthogonal Hybrids*

As an alternative to the conventional sp^2 hybrids, it was decided to construct two centre MO's for the ^1A_u state at CCH = 120° from the hybrids theoretically determined in LMO studies [17] of ethylene from *ab-initio* LCAOSCF wavefunctions [18]. These hybrids may be represented approximately as $sp^{1.74}$, $sp^{1.85}$ and $sp^{1.85}$. These hybrids are not orthogonal, and the two which are equivalent lie at 1.2° to the line of the CH bonds. Referred to Fig. 1, they are

$$\begin{aligned}
\Phi_1 &= N_1\,(s+\sqrt{1.74}\,p_z)\\
\Phi_2 &= N_2\,[s+\sqrt{1.85}\,(p_x\cos 31.2^\circ - p_z\cos 58.8^\circ)]\\
\Phi_3 &= N_3\,[s+\sqrt{1.85}\,(-p_x\cos 31.2^\circ - p_z\cos 58.8^\circ)]\,.
\end{aligned}$$

With these hybrids instead of (3), two centre MO's for the bent state were constructed exactly as in b), except that k took the ethylenic value 1.13. For the linear molecule the recommended [17] hybrids were:

$$\Phi_1 = N_1\,(s+\sqrt{1.01}\,p_z);\qquad \Phi_2 = N_2\,(s-\sqrt{1.01}\,p_z);\qquad \Phi_3 = p_x\,;$$

and the value of k was 1.37.

Both procedures – b) and c) – give LMO's which are not orthogonal (the largest overlap is ~0.2), and prior to forming CMO's, the LMO's were Schmidt orthogonalised. These processes did not prevent the form of the hybrids from being approximately recognised in the final CMO's.

Overlap and nuclear attraction integrals over basis AO's – necessary for implementing (2) were calculated by methods discussed previously [11].

Results and Discussion

Table 1 gives the various contributions to ΔE_t for the change in CCH angle 180 → 120° *(trans)*, using the three different wavefunctions. (The symmetry designations are appropriate throughout because, in the LMO wavefunctions, inner shell and CH orbitals were symmetry adapted). Tables 2 and 3 show the LCAO coefficients for the CMO's derived from Burnelle's wavefunctions.

Table 1. Contributions to ΔE_t (a.u.) for 180° (linear) → 120° *(trans)*

CMO pair	LCAOSCF wavefunctions a) Contribution to ΔE_t		LMO wavefunctions b) Contribution to ΔE_t		LMO wavefunctions c) Contribution to ΔE_t	
	α	β	α	β	α	β
$1a_g$	−0.0360	−0.0440	−0.0365	−0.0356	−0.0339	−0.0330
$1b_u$	−0.0360	−0.0360	−0.0360	−0.0360	−0.0322	−0.0322
$2a_g$	0.0760	0.0069	−0.0432	−0.0963	−0.0553	−0.1268
$2b_u$	−0.0867	−0.0867	−0.0017	−0.0017	−0.0473	−0.0473
$3a_g$	−0.0876	−0.0561	−0.0705	−0.0818	−0.0691	−0.0788
$3b_u$	0.0230	0.0230	−0.0389	−0.0389	−0.0017	−0.0017
a_u	−0.0396		−0.0396		−0.0369	
$4a_g$		−0.0454		0.0639		0.0848
Total	−0.1869	−0.2483	−0.2664	−0.2264	−0.2774	−0.2360
ΔV_{nn}	0.4536		0.4536		0.4212	
ΔW_t	0.0176		−0.0392		−0.0922	

Table 2 Corresponding orbitals (α spin factors) from Burnelle's MO's, 180° (linear) → 120° *(trans)*

CMO pair	Overlap integral	Coefficients[a] C$_1$ 1*s*	C$_1$ 2*s*	C$_1$ 2*pz*	C$_1$ 2*px*	C$_1$ 2*py*	H$_1$ 1*s*
$1a_g$	0.99996	0.70572	0.00425	−0.00048	0.00000	0.0	0.00160
		0.70557	0.00652	−0.00199	0.00098	0.0	−0.00151
$1b_u$	0.99993	0.70497	0.01816	0.00541	0.00038	0.0	0.00036
		0.70466	0.02272	0.00754	0.00091	0.0	−0.00137
$2a_g$	0.85993	−0.07576	0.27100	−0.32145	0.00000	0.0	0.35193
		−0.06278	0.23379	−0.36578	0.13674	0.0	0.36132
$2b_u$	0.92334	0.10007	0.33241	−0.20515	0.26721	0.0	0.30779
		−0.11440	0.48657	−0.11937	0.11384	0.0	0.34372
$3a_g$	0.99883	0.14504	−0.36587	−0.38596	0.00000	0.0	0.03904
		0.14135	−0.32068	−0.41790	0.00355	0.0	−0.02095
$3b_u$	0.98468	−0.04835	0.16225	−0.10012	−0.54750	0.0	0.15022
		−0.05433	0.11427	−0.34478	−0.51949	0.0	−0.05075
a_u	1.00000	0.0	0.0	0.0	0.0	0.60923	0.0
		0.0	0.0	0.0	0.0	0.60923	0.0

[a] Coefficients of the other AO's may be found by symmetry.

Table 3 Corresponding orbitals (β spin factors) from Burnelle's MO's, 180° (linear) → 120° *(trans)*

CMO pair	Overlap integral	Coefficients[a] C$_1$ 1*s*	C$_1$ 2*s*	C$_1$ 2*pz*	C$_1$ 2*px*	C$_1$ 2*py*	H$_1$ 1*s*
$1a_g$	1.00000	0.64702	−0.23051	−0.20551	0.14463	0.0	0.00018
		0.64701	−0.23004	−0.20578	0.14484	0.0	−0.00043
$1b_u$	0.99993	0.70497	0.01816	0.00541	0.00038	0.0	0.00036
		0.70466	0.02272	0.00754	0.00091	0.0	−0.00137
$2a_g$	0.92956	−0.06895	0.24960	−0.31474	0.27165	0.0	0.33538
		−0.06263	0.24347	−0.38997	0.82680	0.0	0.35467
$2b_u$	0.92334	−0.10007	0.33241	−0.20515	0.26721	0.0	0.30779
		0.11440	0.48657	−0.11937	0.11384	0.0	0.34372
$3a_g$	0.99990	−0.31734	−0.30326	−0.26692	0.16737	0.0	−0.00018
		−0.31739	−0.30289	−0.26703	0.16767	0.0	−0.00065
$3b_u$	0.98468	−0.04835	0.16225	−0.10012	−0.54750	0.0	0.15022
		−0.05433	0.11427	−0.34478	−0.51949	0.0	−0.05075
$4a_g$	0.98689	0.02710	−0.02032	−0.19938	−0.80196	0.0	0.11360
		0.01444	0.13524	−0.30218	−0.74331	0.0	−0.10059

[a] Coefficients of the other AO's may be found by symmetry.

For the LCAOSCF wavefunctions a) the total ΔE_l is not quite large enough to cover ΔV_{nn} and so favour bending. However, it is believed that the contributions from the CMO's are qualitatively correct. The fact that there is some internal consistency in Burnelle's wavefunctions may be indicated by the fact that when

ΔE_l for 180° → 120° is compared to the value of ΔE_l for 180° → 150° *plus* ΔE_l for 150° → 120°, the result is conservative to within 1%. The contributions of the CMO pairs show a considerable agreement with the ideas of Walsh, who, it should be stressed, was thinking in terms of the change in orbital (*i.e.* self) energies rather than one-electron transition energies. Thus, the $4a_g$ CMO pair is in favour of bending, and the $3b_u$ opposes bending. From the coefficients in Table 2 it would appear that this is due to the introduction of p_z rather than s character into the π orbitals. Walsh's ideas are also supported by the behaviour of the $3a_g$ orbital (CC σ bond) which becomes less favourable to bending through the acquisition of p_x character (in the β set) than it is when dominated by s and p_z (in the α set). However, CMO's being unitary mixtures of MO's of the same symmetry, it is possibly unwise to look too closely at the form of individual CMO's; but rather one should compare the total contribution of the a_g orbitals when mixed with $4a_g$ (i.e. in the β set) with the total contribution of the a_g orbitals in the α set. The difference is nearly 0.1 a.u.

For the wavefunctions b) based on hybrid AO's, the results are quite different – and unacceptable. Firstly, the $4a_g$ CMO pair is opposed to bending, and the set of orbitals which contains the excited orbital (the β set) gives a smaller ΔE_l than the set which does not. Worse still, the orbitals of the α set actually represent, on this model, the orbitals of the closed shell ground state, ${}^1A_g$. Twice the value of ΔE_l for the α CMO's thus represents the change in electronic energy of the ${}^1A_g$ state, 180° → 120°. Since this quantity exceeds ΔV_{nn} in magnitude, the hybrid wavefunctions indicate a non-linear ground state for acetylene.

To show that these conclusions were not merely dependent on the arbitrary factors in the LMO wavefunctions b), the IHF calculations were repeated with various CH bond polarities. First the value of k was increased by 10%; then the hydrogenic exponent was changed to 1.2. Finally, the calculations were repeated using the excited CC bond length, 1.383 Å. Although the increase in bond length reduced the magnitudes of both ΔV_{nn} and ΔE_l, none of the changes mentioned materially affected the conclusions drawn from the second column of Table 2: the distribution of ΔE_l among the CMO's remained much the same; and the ground state orbitals were still more favourable to bending than the excited state orbitals.

The calculations using LMO wavefunctions c) were undertaken to counter possible objections to arbitrariness in the actual construction of the LMO's in b) – the two centre approximation; the hybridisation determined on CCH angle; and the Schmidt orthogonalisation which ignores orthogonality with the unoccupied LMO's. The hybrids and k values in wavefunctions c) were specially determined for two centre MO's on theoretical criteria [14], from *ab-initio* wavefunctions with carefully optimised exponents [15]. These exponents were used in the IHF calculation, together with bond lengths appropriate to ethylene [15]. The third column of Table 3 shows that the conclusions are the same as for wavefunctions b).

The calculations described in this work have employed very simple wavefunctions. It will be interesting to see if the conclusions are confirmed by LMO and IHF studies of more sophisticated wavefunctions, such as those reported by Kammer [4].

References

1. Ingold,C.K., King,G.W.: J. chem. Soc. **1953**, 2702.
2. Walsh,A.D.: J. chem. Soc. **1953**, 2288.
3. See for example, Murrell,J.N., Kettle,S.F.A., Tedder,J.M.: Valence theory, p. 192. John Wiley: 1965.
4. Burnelle,L.: J. chem. Physics **35**, 311 (1961).
5. Kammer,W.E.: Chem. Physics Letters **6**, 529 (1970).
6. Peyerimhoff,S.D., Buenker,R.J., Allen,L.C.: J. chem. Physics **45**, 734 (1966).
7. Pan,D.C., Allen,L.C.: J. chem. Physics **46**, 1797 (1966).
8. Whitten,J.L.: J. chem. Physics **44**, 359 (1966).
9. Parr,R.G.: J. chem. Physics **40**, 3726 (1964).
10. Wyatt,R.E.: J. chem. Physics **44**, 1529 (1966).
11. Melrose,M.P., Parr,R.G.: Theoret. chim. Acta (Berl.) **8**, 150 (1967).
12. Fink,W.H., Allen,L.C.: J. chem. Physics **46**, 3270 (1967).
13. Rothstein,S.M., Blinder,S.M.: Theoret. chim. Acta (Berl.) **8**, 427 (1967).
14. Marron,M.T.: J. chem. Physics **52**, 3600 (1970).
15. McLean,A.D., Ransil,B.J., Mulliken,R.S.: J. chem. Physics **32**, 1873 (1960).
16. Woznicki,W.: Bull. Acad. Polon. Sci., Ser. Sci. Math., Astr. et Phys. **9**, 273 (1961).
17. Newton,M.D., Switkes,E., Lipscomb,W.N.: J. chem. Physics **53**, 2645 (1970).
18. Switkes,E., Stevens,R.M., Lipscomb,W.N.: J. chem. Physics **51**, 5229 (1969).

Dr. M. P. Melrose
Department of Chemistry
King's College
London W.C.2., England

Theoret. chim. Acta (Berl.) 25, 189–195 (1972)
© by Springer-Verlag 1972

Application of Coulson's Contour Integral Method to Linear Finite Polymers

JOUKO J. KANKARE
Department of Chemistry, University of Turku, Turku, Finland

Received November 22, 1971

Coulson's contour integration method has been applied to calculate the charge and bond order matrices and total energies of conjugated systems composed of fragments whose Hückel secular equations have been solved. Integral formulas have been derived for the calculation of these quantities for two coupled conjugated systems and for linear polymers. A rapid method for the numerical evaluation of the integral formulas is presented and applied to a linear finite polyene.

Coulson [1] introduced in 1940 an integration method with which molecular orbital calculations can be performed without direct reference to the eigenvalues and eigenvectors of the secular problem. Recently, Linderberg [2] showed that this technique is useful in conjunction with computers. The purpose of this paper is to show that the contour integration method is particularly useful in calculating the properties of large molecules composed of fragments whose Hückel secular equations have been solved.

The results of Coulson and Linderberg are presented here in a somewhat different notation. For simplicity, overlap is not included and the coefficients of the atomic orbitals are assumed to be real. The calculations are performed in terms of a Hückel bond matrix $\boldsymbol{B}$ obtained from the normal Hückel matrix $\boldsymbol{H}$ by the transformation

$$\boldsymbol{B} = \frac{1}{\beta_0}(\boldsymbol{H} - \alpha_0 \boldsymbol{I}) \tag{1}$$

where α_0 and β_0 stand for the standard resonance parameter for the carbon-carbon bond and the Coulomb parameter of carbon, respectively. The equations of Coulson are converted into two general integral formulas.

Theorem 1. *The charge and bond order matrix* $\boldsymbol{P}$ *is given by the formula*

$$\boldsymbol{P} = \frac{1}{\pi i} \oint_{\text{occ}} (z\boldsymbol{I} - \boldsymbol{B})^{-1} dz \tag{2}$$

where "occ" means that the complex integral is taken over the contour enclosing the eigenvalues of $\boldsymbol{B}$ *corresponding to the occupied orbitals.*

The integrand is expanded as a sum of dyads

$$(z\boldsymbol{I} - \boldsymbol{B})^{-1} = \sum_j \frac{1}{z - \varepsilon_j} \boldsymbol{c}_j \boldsymbol{c}_j^T \tag{3}$$

where ε_j and c_j are, respectively, the eigenvalues and eigenvectors of $\boldsymbol{B}$. Application of the Cauchy integral formula gives

$$\frac{1}{2\pi i}\oint_{\mathrm{occ}}(z\boldsymbol{I}-\boldsymbol{B})^{-1}dz=\frac{1}{2\pi i}\sum_j \boldsymbol{c}_j\boldsymbol{c}_j^T\oint_{\mathrm{occ}}\frac{dz}{z-\varepsilon_j}=\sum_j \boldsymbol{c}_j\boldsymbol{c}_j^T=\frac{1}{2}\boldsymbol{P}.$$

Theorem 2. *The total π-electron energy in units of β_0 and assuming that $\alpha_0=0$ is given by the formula*

$$E=\frac{1}{\pi i}\oint_{\mathrm{occ}} z\,\mathrm{tr}(z\boldsymbol{I}-\boldsymbol{B})^{-1}dz. \tag{4}$$

This theorem is proved by dyadic expansion like the preceding.

Two Systems Coupled by One Bond

Let $\boldsymbol{B}_1$ and $\boldsymbol{B}_2$ be the Hückel bond matrices of two conjugated systems S_1 and S_2 containing n and m atoms, respectively. The bond matrix of the coupled system is

$$\boldsymbol{B}=\begin{pmatrix}\boldsymbol{B}_1 & \boldsymbol{K}\\ \boldsymbol{K}^T & \boldsymbol{B}_2\end{pmatrix}.$$

Two new matrices are now defined by

$$\boldsymbol{G}_1=(z\boldsymbol{I}-\boldsymbol{B}_1)^{-1}$$
$$\boldsymbol{G}_2=(z\boldsymbol{I}-\boldsymbol{B}_2)^{-1}.$$

It is easily shown that

$$\boldsymbol{G}=\begin{pmatrix}\boldsymbol{G}_1^{-1} & -\boldsymbol{K}\\ -\boldsymbol{K}^T & \boldsymbol{G}_2^{-1}\end{pmatrix}^{-1}=\begin{pmatrix}(\boldsymbol{I}-\boldsymbol{G}_1\boldsymbol{K}\boldsymbol{G}_2\boldsymbol{K}^T)^{-1}\boldsymbol{G}_1 & \boldsymbol{G}_1\boldsymbol{K}(\boldsymbol{I}-\boldsymbol{G}_2\boldsymbol{K}^T\boldsymbol{G}_1\boldsymbol{K})^{-1}\boldsymbol{G}_2\\ \boldsymbol{G}_2\boldsymbol{K}^T(\boldsymbol{I}-\boldsymbol{G}_1\boldsymbol{K}\boldsymbol{G}_2\boldsymbol{K}^T)^{-1}\boldsymbol{G}_1 & (\boldsymbol{I}-\boldsymbol{G}_2\boldsymbol{K}^T\boldsymbol{G}_1\boldsymbol{K})^{-1}\boldsymbol{G}_2\end{pmatrix}.$$

It is assumed that atom p in the system S_1 is bonded to atom q in the system S_2. Let the resonance parameter for the bond be k. The elements of $\boldsymbol{K}$ are then

$$K_{ij}=\delta_{ip}\delta_{jq}k.$$

With this matrix we obtain

$$(\boldsymbol{I}-\boldsymbol{G}_1\boldsymbol{K}\boldsymbol{G}_2\boldsymbol{K}^T)_{ij}=\delta_{ij}-(\boldsymbol{G}_1)_{ip}(\boldsymbol{G}_2)_{qq}\delta_{jp}k^2.$$

This matrix is inverted by partitioning [3]:

$$((\boldsymbol{I}-\boldsymbol{G}_1\boldsymbol{K}\boldsymbol{G}_2\boldsymbol{K}^T)^{-1})_{ij}=\delta_{ij}+\frac{k^2(\boldsymbol{G}_1)_{ip}(\boldsymbol{G}_2)_{qq}\delta_{jp}}{1-k^2(\boldsymbol{G}_1)_{pp}(\boldsymbol{G}_2)_{qq}}.$$

Hence

$$((\boldsymbol{I}-\boldsymbol{G}_1\boldsymbol{K}\boldsymbol{G}_2\boldsymbol{K}^T)^{-1}\boldsymbol{G}_1)_{ij}=(\boldsymbol{G}_1)_{ij}+\frac{k^2(\boldsymbol{G}_1)_{ip}(\boldsymbol{G}_1)_{pj}(\boldsymbol{G}_2)_{qq}}{1-k^2(\boldsymbol{G}_1)_{pp}(\boldsymbol{G}_2)_{qq}}. \tag{5}$$

Analogously we find that

$$((I - G_2K^TG_1K)^{-1}G_2)_{ij} = (G_2)_{ij} + \frac{k^2(G_2)_{iq}(G_2)_{qj}(G_1)_{pp}}{1 - k^2(G_1)_{pp}(G_2)_{qq}} \tag{6}$$

and

$$(G_2K^T(I - G_1KG_2K^T)^{-1}G_1)_{ij} = \frac{k(G_2)_{iq}(G_1)_{pj}}{1 - k^2(G_1)_{pp}(G_2)_{qq}}. \tag{7}$$

Application of Theorem 1 gives the differences in bond orders and electron densities between coupled and uncoupled systems. For instance, for the atoms of the system S_1 we obtain

$$(\Delta P_1)_{ij} = \frac{1}{\pi i} \oint_{\text{occ}} \frac{k^2(G_1)_{ip}(G_1)_{pj}(G_2)_{qq}}{1 - k^2(G_1)_{pp}(G_2)_{qq}} dz. \tag{8}$$

The total π-energy difference is given by

$$\Delta E = \frac{1}{\pi i} \oint_{\text{occ}} \frac{k^2 z}{1 - k^2(G_1)_{pp}(G_2)_{qq}} [(G_2)_{qq}(G_1^2)_{pp} + (G_1)_{pp}(G_2^2)_{qq}] dz. \tag{9}$$

Polymers

Recurrence relations for obtaining the elements of the matrix G for polymers are easily derived from Eqs. (5–7). In the case of identical monomer units, explicit formulas may be derived. Assuming that S_1 represents the monomer unit and S_2 the polymer, we derive from Eq. (5)

$$(G_2)_{qq}^{(n+1)} = (G_1)_{qq} + \frac{k^2(G_1)_{qp}^2(G_2)_{qq}^{(n)}}{1 - k^2(G_1)_{pp}(G_2)_{qq}^{(n)}}. \tag{10}$$

Here the same index q is used to label analogous positions in the monomer and n- and $n+1$-mers. Using the notation

$$Q_n = 1 - k^2(G_1)_{pp}(G_2)_{qq}^{(n)}$$

we have

$$Q_{n+1} = a + \frac{b}{Q_n} \tag{11}$$

where

$$a = 1 - k^2(G_1)_{pp}(G_1)_{qq} + k^2(G_1)_{qp}^2$$

$$b = -k^2(G_1)_{qp}^2.$$

This formula shows that Q_n is given by a terminating continuous fraction

$$Q_n = a + \frac{b}{a+}\,\frac{b}{a+}\cdots\frac{b}{Q_1}. \tag{12}$$

Eq. (9) is now brought into a more amenable form. Performing integration by parts, we obtain

$$\Delta E = -\frac{1}{\pi i} \oint_{\text{occ}} \ln(1 - k^2 (G_1)_{pp} (G_2)_{qq}) dz . \tag{13}$$

The energy change that occurs when one monomer unit is joined to an $n-1$-mer is obtained from

$$\Delta E^{(n)} = -\frac{1}{\pi i} \oint_{\text{occ}} \ln Q_{n-1} dz . \tag{14}$$

Hence the total π-energy of a polymer composed of n identical monomer units is obtained from

$$E^{(n)} = nE^{(1)} + \sum_{m=2}^{n} \Delta E^{(m)} = nE^{(1)} - \frac{1}{\pi i} \oint_{\text{occ}} \ln \prod_{m=1}^{n-1} Q_m dz . \tag{15}$$

From formula (11), it follows that

$$R_1^{(n-1)} = Q_{n-1} Q_{n-2} = a_1 Q_{n-2} + b_1 ,$$

$$R_2^{(n-1)} = Q_{n-1} Q_{n-2} Q_{n-3} = (a_1^2 + b_1) Q_{n-3} + a_1 b_1 ,$$

$$\dots\dots\dots\dots\dots\dots\dots\dots\dots\dots\dots\dots$$

$$R_m^{(n-1)} = \prod_{n-m-1}^{n-1} Q_i = a_m Q_{n-m-1} + b_m .$$

In these equations

$$a_1 = a, \ b_1 = b ,$$

$$a_m = a \cdot a_{m-1} + b_{m-1} ,$$

$$b_m = b \cdot a_{m-1} .$$

These simultaneous difference equations are transformed into a linear homogeneous second-order difference equation

$$a_{m+2} - a \cdot a_{m+1} - b \cdot a_m = 0 . \tag{16}$$

The general solution of this equation is

$$a_m = \alpha r_1^m + \beta r_2^m$$

where r_1 and r_2 are solutions of the characteristic equation

$$r^2 - ar - b = 0$$

and α and β are coefficients determined by the initial conditions. In this case the initial conditions obviously lead to equations

$$\alpha r_1 + \beta r_2 = a ,$$

$$\alpha + \beta = 1 .$$

Hence the solutions are

$$a_m = \frac{r_1^{m+1} - r_2^{m+1}}{r_1 - r_2},$$

$$b_m = b\,\frac{r_1^m - r_2^m}{r_1 - r_2}.$$

Thus we get

$$R_{n-2}^{(n-1)} = \prod_{m=1}^{n-1} Q_m = a_{n-2}Q_1 + b_{n-2} = \frac{r_1^{n-1} - r_2^{n-1}}{r_1 - r_2} + b\,\frac{r_1^{n-2} - r_2^{n-2}}{r_1 - r_2}. \tag{17}$$

Then, on the strength of the fact that $Q_1 = r_1 + r_2 - r_1 r_2$ and $b = -r_1 r_2$, the expression for the total energy is

$$E^{(n)} = nE^{(1)} - \frac{1}{\pi i} \oint_{\mathrm{occ}} \ln \frac{r_1^n(1-r_2) - r_2^n(1-r_1)}{r_1 - r_2}\,dz. \tag{18}$$

To obtain an explicit formula for the calculation of the electron densities, Eq. (5) is written as

$$(G_1)_{ii}^{(n)} = (G_1)_{ii} + \frac{(G_1)_{ip}^2}{(G_1)_{pp}} \left(\frac{1}{Q_{n-1}} - 1\right).$$

From Eq. (17) we derive

$$Q_{n-1} = \frac{R_{n-2}^{(n-1)}}{R_{n-3}^{(n-2)}} = \frac{r_1^n(1-r_2) - r_2^n(1-r_1)}{r_1^{n-1}(1-r_2) - r_2^{n-1}(1-r_1)}. \tag{19}$$

Hence the electron densities of the atoms of the terminal monomer unit in an n-mer are obtained from

$$(P_1)_{jj}^{(n)} = \frac{1}{\pi i} \oint_{\mathrm{occ}} \frac{(G_1)_{jp}^2 (r_1^{n-1} - r_2^{n-1})(1-r_1)(1-r_2)}{(G_1)_{pp}[r_1^n(1-r_2) - r_2^n(1-r_1)]}\,dz + (P_1)_{jj}^{(1)} \tag{20}$$

where $(P_1)_{jj}^{(1)}$ denotes the electron density of the atom j in the isolated monomer unit.

Numerical Calculation of Integrals

Proper choice of the integration path is essential to simplify the calculation of the integrals. The contour must enclose the eigenvalues corresponding to the occupied orbitals of both the coupled system and the subsystems. In the case of alternant hydrocarbons and most of their heteroanalogues, the "Coulson contour", i.e. the imaginary axis from $+\infty i$ to $-\infty i$ and the infinite semicircle to the right of the imaginary axis may be chosen. The integral taken over the infinite semicircle has a constant value. For example, by the substitution $z = iy$, Eq. (8) becomes

$$(\Delta P_1)_{ij} = \frac{1}{\pi} \int_{\infty}^{-\infty} \frac{k^2 (G_1)_{ip}(G_1)_{pj}(G_2)_{qq}}{1 - k^2 (G_1)_{pp}(G_2)_{qq}}\,dy. \tag{21}$$

The explicit expressions for the elements of the G-matrices are obtained by dyadic expansion (3).

Extremely cumbersome algebraic formulas are obtained when an attempt is made to separate the real and imaginary parts of the integrands. Therefore, the evaluation of the integrals is most easily performed using complex arithmetics with a computer. On substituting $y = x(1-x^2)^{-1/2}$, the integration limits change to $(-1,1)$ and we obtain generally

$$I = \frac{1}{\pi}\int_{-\infty}^{\infty} f(y)dy = \frac{1}{\pi}\int_{-1}^{1}(1-x^2)^{-1/2}(1+y(x)^2)f(y(x))dx \tag{22}$$

Chebyshev-Gauss quadrature utilizing the fact that $f(y)$ is an even function of y gives

$$I = \frac{1}{m}\sum_{i=1}^{m}\left(1+\tan^2\frac{2m-2i+1}{4m}\pi\right)f\left(\tan\frac{2m-2i+1}{4m}\pi\right). \tag{23}$$

This quadrature formula proved to be numerically very stable and rapidly converging.

Applications

The accuracy of the numerical integration was tested by applying Eq. (18) to the linear polyene $C_{60}H_{62}$. The total energy in this case is obtained from the explicit formula [4]:

$$E = \frac{2}{\sin\frac{\pi}{122}} - 2 = 75.67619648.$$

Energy is expressed in units of β_0 and assuming that $\alpha_0 = 0$. The total π-energy was also computed using Eqs. (18) and (23) taking ethylene as the monomer unit. Approximate values of the energy $E^{(30)}$ at a number of integration abscissas are shown in Table 1. We see that the convergence is fairly rapid.

The significance of Theorems 1 and 2 lies in the fact that they provide analytical expressions for quantities otherwise derivable only by comparatively slow diagonalization procedures. The rapidity of the numerical integration may be utilized in computing changes in, e.g., charges, bond orders, and total π-energies by

Table 1. Numerical calculation of the total π-electron energy of the linear polyene $C_{60}H_{62}$

m	$E^{(30)}$
1	75.51
2	76.015
4	75.788
8	75.699
16	75.6785
32	75.67624
64	75.67619649

Eqs. (8) and (9) when two coupled systems are rotated about the connecting bond. Eqs. (18) and (20) are perhaps the first explicit expressions to be proposed for the calculation of Hückel energies and charges of arbitrary linear finite polymers.

References

1. Coulson, C. A.: Proc. Cambridge Phil. Soc. 36, 201 (1940).
2. Linderberg, J.: Chem. Physics Letters 5, 134 (1970).
3. Faddeeva, V. N.: Computational methods of linear algebra, chapter 2. New York: Dover Publications, Inc. 1959.
4. Coulson, C. A.: Proc. Roy. Soc. (London) A 164, 383 (1938).

Dr. J.J. Kankare
Department of Chemistry
University of Turku
Turku, Finland

Theoret chim. Acta (Berl.) 25, 196—199 (1972)
© by Springer-Verlag 1972

Note on the Solution of Secular Problems with Two Non-Orthogonal Basis Functions

W. A. Bingel
Theoretical Chemistry Group, University of Göttingen, Göttingen, Germany

Received January 18, 1972

A convenient trigonometric expression for the eigenfunctions and eigenvalues of 2 × 2 secular problems including overlap is presented

1. Introduction

Secular equations occur in many applications of quantum mechanics to the electronic structure of atoms and molecules. Using symmetry-adapted basis functions, the secular determinant can often be factorised. The simplest non-trivial factor is a determinant with just 2 rows and columns. The solution of this problem is simple and is given in many textbooks [1–3]. Since the formulae for the coefficients (Eq. (5)) are somewhat awkward, it has become customary to use them in a more convenient trigonometric form [4]; which however is applicable only, if the two basis functions are orthogonal.

For a nonorthogonal basis, which often is required by the nature of the physical problem, no such convenient expressions seem to be available in the literature. They are therefore presented in this note.

2. Secular Problem with Orthogonal Basis

We collect here the pertinent formulae to facilitate a comparison with the results of the next section.

The wave function is written as a linear combination of the two orthonormal basis functions

$$\psi = c_1\varphi_1 + c_2\varphi_2 . \tag{1}$$

Minimization of the energy expectation value $\langle H\rangle_\psi$ with respect to c_1 and c_2 then leads to the secular equations

$$\begin{aligned} c_1(H_{11}-E)+c_2H_{12}&=0\\ c_1H_{12}^*+c_2(H_{22}-E)&=0 . \end{aligned} \tag{2}$$

From these we obtain the secular determinant

$$\begin{vmatrix} H_{11}-E & H_{12} \\ H_{12}^* & H_{22}-E \end{vmatrix} = 0 \tag{3}$$

with roots

$$E_\pm = \tfrac{1}{2}(H_{11}+H_{22}) \pm \sqrt{((H_{22}-H_{11})/2)^2+|H_{12}|^2} . \tag{4}$$

The coefficients are then obtained from Eq. (2) and the normalization condition $c_1^2 + c_2^2 = 1$

$$c_1 = \{\tfrac{1}{2} \pm (H_{22} - H_{11})/2\sqrt{[(H_{22} - H_{11})^2 + 4|H_{12}|^2]}\}^{\frac{1}{2}}\,, \tag{5a}$$

$$c_2 = \pm\{\tfrac{1}{2} \mp (H_{22} - H_{11})/2\sqrt{[(H_{22} - H_{11})^2 + 4|H_{12}|^2]}\}^{\frac{1}{2}}\,. \tag{5b}$$

The last two equations are somewhat awkward, especially if one does not wish to calculate the c_i, but only wants to get an idea of their magnitude from qualitative considerations.

If we write the two solutions (1) in the trigonometric form

$$\psi_- = \cos\theta\,\varphi_1 + \sin\theta\,\varphi_2\,, \tag{6a}$$

$$\psi_+ = \sin\theta\,\varphi_1 - \cos\theta\,\varphi_2\,, \tag{6b}$$

then the normalization of ψ_+ and ψ_- as well as their orthogonality are automatically assured and a comparison with Eqs. (5a, b) leads to

$$C\sin 2\theta = -H_{12}\,, \tag{7a}$$

$$C\cos 2\theta = (H_{22} - H_{11})/2\,, \tag{7b}$$

$$2C = \sqrt{(H_{22} - H_{11})^2 + 4|H_{12}|^2}\,, \tag{7c}$$

from which the angle parameter θ can be determined. The two energies (4) are now

$$E_\pm = \tfrac{1}{2}(H_{11} + H_{22}) \pm C\,. \tag{8}$$

The following points are useful for qualitative discussions of the solution (6a, b):

(a) We will assume that the basis functions φ_i are real and that φ_2 has the higher energy (i.e. $H_{22} \geq H_{11}$, H_{12} real).

(b) θ is then real and its sign is opposite to that of H_{12}. For H_{12} negative – the usual case in quantum chemistry – the wave function ψ_- with the lower energy is an in-phase-combination and ψ_+ an out-of-phase combination of the two basis functions. For positive H_{12} the situation is reserved.

(c) It follows from (7a, b) that for nondegenerate states ($H_{11} < H_{22}$) the angle $|\theta| < 45°$. This means that in the "lower" solution φ_1 and in the "higher" solution φ_2 makes the larger contribution. For degenerate states ($H_{11} = H_{22}$) $\theta = 45°$ and both solutions are 50 – 50-mixtures of φ_1 and φ_2.

3. Secular Problem with Non-Orthogonal Basis

Corresponding to Eqs. (2)–(4) we now have

$$\begin{aligned} c_1(H_{11} - E) + c_2(H_{12} - S_{12}E) &= 0 \\ c_1(H_{12}^* - S_{12}^*E) + c_2(H_{22} - E) &= 0\,, \end{aligned} \tag{2'}$$

$$\begin{vmatrix} H_{11} - E & H_{12} - S_{12}E \\ H_{12}^* - S_{12}^*E & H_{22} - E \end{vmatrix} = 0\,, \tag{3'}$$

$$\begin{aligned} E_\pm = {} & \frac{1}{1 - S_{12}^2}\{\tfrac{1}{2}(H_{11} + H_{22} - 2S_{12}H_{12}) \\ & \pm\sqrt{((H_{11} + H_{22} - 2S_{12}H_{12})/2)^2 + (1 - S_{12}^2)(H_{12}^2 - H_{11}\cdot H_{22})}\}\,. \end{aligned} \tag{4'}$$

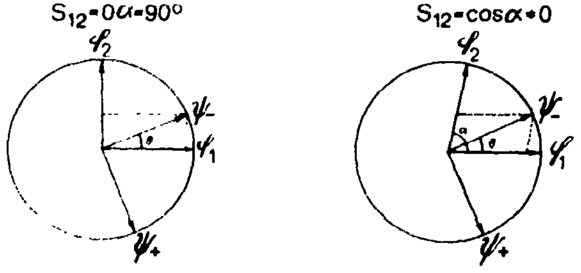

Fig. 1 Relation between basis functions φ_1, φ_2 and wave functions ψ_-, ψ_+ in a 2-dimensional vector space. Note that for both orthogonal and non-orthogonal basis functions ψ_+ is obtained from ψ_- by changing θ to $\theta - 90°$

The Eqs. (5′) for the coefficients are even more cumbersome and will therefore not be given.

The derivation of the trigonometric solution will only be sketched, since it is the final result only that is of interest.

The generalisation of Eqs. (6a, b) turns out to be (cf. Fig. 1)

$$\psi_- = (\sin(\alpha-\theta)\,\varphi_1 + \sin\theta\,\varphi_2)/\sin\alpha\,, \qquad (6a')$$

$$\varphi_+ = (\cos(\alpha-\theta)\,\varphi_1 - \cos\theta\,\varphi_2)/\sin\alpha \qquad (6b')$$

where

$$S_{12} = \cos\alpha\,.$$

To obtain the equations for the angle parameter θ corresponding to (7a, b) the following procedure different from that of Sect. 2 was found more convenient. One calculates the energy expection value with ψ_- of (6a′) and puts its derivative with respect to θ equal to zero. This procedure leads to

$$C\sin 2\theta = \sin\alpha(H_{11}\cos\alpha - H_{12})\,, \qquad (7a')$$

$$C\cos 2\theta = \cos\alpha(H_{11}\cos\alpha - H_{12}) + \tfrac{1}{2}(H_{22} - H_{11}) \qquad (7b')$$

$$C = \sqrt{\{(1-S_{12}^2)(H_{11}S_{12} - H_{12})^2 + ((H_{22} - H_{11})/2 + H_{11}S_{12}^2 - H_{12}S_{12})^2\}}\,.$$

The energy expression (4′) now becomes

$$E_\pm = [\tfrac{1}{2}(H_{11} + H_{22}) - H_{12}\cos\alpha \pm C]/\sin^2\alpha\,. \qquad (8')$$

These results can be checked by putting $\alpha = 90°$, i.e. $S_{12} = 0$ when the corresponding results of Sect. 2 are recovered.

The following points should be noted in using the trigonometric solution (6a′, b′):

(a′) With the assumptions of (a) of Sect. 2 we note, that we can choose the basis functions such that $S_{12} \geqq 0$, leading to $0 < \alpha \leqq \frac{\pi}{2}$.

(b′) θ is again real and from Eq. (7a′) its sign is the same as that of $H_{11}\cos\alpha - H_{12}$.

(c′) We still have the limitation $|\theta| \leqq 45°$; the contributions of φ_1 and φ_2 to ψ_+ and ψ_- for the nondegenerate case are given by the trigonometric ratios in Eqs. (6a′, b′). For the degenerate case $(H_{11} = H_{22})$, we obtain from Eqs. (7a′, b′), that $\theta = \alpha/2 < 45°$. In this case, Eqs. (6a′, b′) simplify to

$$\psi_- = (\varphi_1 + \varphi_2)/\sqrt{2(1 + S_{12})}$$

$$\psi_+ = (\varphi_1 - \varphi_2)/\sqrt{2(1 - S_{12})}$$

and (8′) becomes

$$E_\pm = \frac{H_{11} \mp H_{12}}{1 \mp S_{12}}$$

a wellknown result.

References

1. Slater, J. C.: Quantum theory of atomic structure, Vol. I, p. 119. New York: McGraw-Hill 1960.
2. Coulson, C. A.: Valence, p. 68; 2nd ed. Oxford: U. Press 1963.
3. Landau, L. D., Lifschitz, E. M.: Quantenmechanik, S. 141, 3. Aufl. Berlin: Akademie-Verlag 1967.
4. Carrington, A., McLachlan, A. D.: Introduction to magnetic resonance, p. 45. New York: Harper and Row 1969.

Prof. Dr. W. A. Bingel
Theoretical Chemistry Group
University of Göttingen
D-3400 Göttingen, Bürgerstr. 50a
Germany

Theoret. chim. Acta (Berl.) 25, 200 - 204 (1972)
© by Springer-Verlag 1972

SCF Calculations for H_2^+, Li_2^+ and LiH^+ with Atomic Basis Sets Enlarged by Bond Functions*

San Y. Chu

Department of Chemistry, Rice University, Houston, Texas 77001, USA

Received September 16, 1971/January 24, 1972

To simulate the charge distortion in the formation of a molecule from the separated atoms, a set of concentric *s*-type Gaussian functions is placed on the internuclear axis in addition to the *s*-type atomic basis functions to construct the molecular orbital for the one valence-electron systems H_2^+, Li_2^+ and LiH^+. This simple model gives 90.1%, 75.2% and 61.7%, respectively, of the improvement over minimal basis relative to Hartree-Fock energies.

1. Introduction

Based on the simple LCAO-MO approximation, the one-electron wavefunction for a diatomic molecule can be written as

$$\psi = N(\phi_a + \lambda\phi_b),$$

where ϕ_a and ϕ_b are the atomic basis functions. The charge density will have three contributions: two atomic contributions, ϕ_a^2 and $\lambda^2\phi_b^2$, and the interatomic interference term $2\lambda\phi_a\phi_b$. This interference term is often called the overlap charge [1]. For H_2^+, it has the spheroidal form $e^{-2(r_a+r_b)}$, with a maximum along the line joining the two nuclei, falling off as one goes away from the line. Since the total charge density is conserved, a buildup of the overlap charge in the bonding region implies a corresponding deletion of the atomic charges. In other words, the total charge has been distorted from the atomic region to the internuclear region. This charge distortion is an essential feature of the chemical bonding which can be shown even by a wavefunction approximated with the minimum basis functions. A calculation with a more extensive basis function set is better able to describe the charge distortion. For example, in the H_2^+ calculation [2], an *s* orbital and *p* orbital can mix to give direct atomic charge distortion in addition to the overlap charge. The purpose of the present study is to test a more economical way to represent the charge distortion. Instead of mixing the *s* atomic orbital with atomic orbitals of higher quantum number, the *p*, *d* and *f* orbitals, we adopt a set of concentric Gaussian *s*-type functions centered along the bond axis to simulate the charge distortion. In view of the reasonable validity of the united atom model [3], we expect the present "one-center" *s*-type orbitals to be effective basis functions complementary to the minimum atomic basis functions for the molecular wavefunction, especially those for the valence-electron part. In the present study, this model has been tested on systems containing one valence-electron, such as H_2^+, Li_2^+ and LiH^+, where there is a strong atomic charge distortion due to charge-

---

* Supported in part by a research grant to Rice University from the Robert A. Welch Foundation

induced dipole. However, this model can easily be generalized to include the electron-pair bond and polyatomic molecule. For these, a similar model has been proposed recently by Rothenberg and Schaefer [4]. A calculation on the closed shell system CH_4 was first performed using a small basis set containing only *s*, *p* orbitals on carbon and *s* orbital on hydrogen atoms. Then, by placing two *s*-type Gaussian functions with identical exponents along each C–H bond axis, they obtained about 60% of the energy improvement that was obtained by extending the basis set to include *d* orbitals on the carbon atom and *p* orbitals on the hydrogen atoms.

2. Calculation

The results reported in this paper were obtained using the MOLE Quantum Chemistry System [5]. This is a general purpose program for quantum-mechanical calculation of the electronic structure and electronic energy of molecules. The atomic basis sets used in this work are the grouped Gaussian orbitals suggested by Whitten [6]. For hydrogen the basis orbital is the five term 1*s*. For lithium the *s*-type basis orbitals are the four term 1*s*, three term 2*s*, and three term 3*s* grouped orbitals. A set of three rather diffuse concentric *s*-type Gaussian functions are used as the bond functions. Thus, the molecular orbital is a linear combination of the atomic basis functions and the bond functions.

$$\psi_j = \sum_i C_{ai}\phi_{ai} + \sum_i C_{bi}\phi_{bi} + \sum_i C_i \exp(-\alpha_i(r-R)^2) . \qquad (1)$$

The first two terms are summed over atomic functions and the third term is summed over the bond functions. The Roothaan's restricted open shell SCF method [7] is used. For convenience in choosing the value of the orbital exponent α_i, it is helpful to replace the orbital exponent α_i in Eq. (1) by

$$\alpha_i = 1/p_i^2 .$$

The parameter p_i has dimension of length and may be called an "orbital radius" [8]. It has the simple interpretation that the sphere of this radium contains about 74% of the orbital electron density. Thus, a reasonable way to choose a set of bond functions is to select values of p_i such that they are of the same order of magnitude as the size of the molecule.

At the beginning, several trial sets of bond functions were combined with atomic basis sets for the calculation. Each set of bond functions consists of five concentric bond functions with smoothly increasing exponents. From these we choose a set such that the magnitudes of the SCF coefficients show a rough Gaussian distribution. For example, the set chosen for H_2^+ has exponents 2.0, 1.0, 0.5, 0.1 and 0.05. Their magnitudes of coefficients from SCF results are 0.014, 0.084, 0.099, 0.325 and 0.030, respectively. This procedure reduces the possibility that we may miss important basis functions in the function selection, since basis functions whose exponents lie outside the prescribed range will have negligible SCF coefficients following the Gaussian distribution, while basis functions whose exponents lie inside the prescribed range are redundant functions, i.e. they have too big an overlap with the chosen functions. Subsequently, these five functions

Table 1. Results of total energy and valence orbital for H_2^+, Li_2^+ and LiH^+. (Calculation (*A*) uses five bond functions, (*B*) uses three bond functions, and *R* is the bond function to proton distance. For H_2^+ and Li_2^+, bond functions are at middle of the two nuclei)

	H_2^+ ($R_e = 2.0$ a. u.)		Li_2^+ ($R_e = 5.051$)		LiH^+ ($R_e = 3.014$)		
	(*A*)	(*B*)	(*A*)	(*B*)	$R = 0.9$	$R = 1.1$	$R = 1.3$
$1s_H$	0.648	0.650			0.911	0.940	0.965
$1s_{Li}$			−0.198	−0.199	−0.114	−0.118	−0.121
$2s_{Li}$			0.157	0.150	0.066	0.081	0.102
$s(\alpha = 2.00)$	0.014	-					
$s(\alpha = 1.00)$	0.084	0.051	−0.031	–			
$s(\alpha = 0.50)$	0.099	0.127	0.093	0.046	0.134	0.125	0.166
$s(\alpha = 0.10)$	−0.325	−0.362	0.591	0.635	0.060	0.048	0.040
$s(\alpha = 0.05)$	−0.030	–	0.178	0.151	−0.149	−0.166	−0.189
$s(\alpha = 0.01)$			−0.019	–			
E	0.59792	0.59778	14.70006	14.69976	7.72408	7.72427	7.72414
$-E_{HF}$	0.60262[a]		14.70971[b]			7.72943[c]	

[a] See Ref. [9]. [b] See Ref. [10]. [c] See Ref. [11].

are truncated to three functions by deleting the two functions with smallest and largest exponents. The loss in energy that results from this procedure is essentially negligible, 0.14×10^{-3} a.u. for H_2^+ and 0.30×10^{-3} a.u. for Li_2^+. The remaining three functions have orbital radii comparable in size to the internuclear distance. For example, three functions for H_2^+ with exponents 1.0, 0.5 and 0.1 have corresponding values of orbital radii 1.0, 1.4 and 3.1 comparable with the internuclear distance 2.0 a.u. By the same procedure, a set of functions with more diffused exponents 0.5, 0.1 and 0.05 are obtained for the Li_2^+. Their orbital radii 1.4, 3.1 and 4.5 are to be compared with the internuclear distance 5 a.u. for Li_2^+. The same set of functions has been used for the LiH^+ system with three different positions along the H-Li axis: 0.9, 1.1 and 1.3 a.u. from the proton. The difference in their energies is less than 0.2×10^{-3} a.u.

3. Discussion

The final results are shown in Table 1 and 2. From the reported data and several other numerical experiments, the conclusions we shall draw are:

(1) The energy improvement is insensitive to the choice of the set of bond function exponents as long as the whole set of orbital radii are complete enough to be able to cover the molecule. For the heternuclear diatomic molecule LiH^+, the choice of the center for the bond function is not critical. The change in energies is less than 0.2×10^{-3} a.u. for the three values of bond function – proton distance: 0.9, 1.1 and 1.3 a.u. This is probably due to the fact that the variation of each linear coefficient of the bond functions can compensate for the improper choice of the function center to a large extent.

(2) As shown in Table 2, the improvement in the energy resulting from this type of bond function is more important than the splitting of the atomic grouped Gaussian function which provides the additional flexibility. Splitting the single

Table 2. Comparison of the calculation with Gaussian basis and slater basis for H_2^+ ($R_e = 2.0$ a.u.)

Gaussian basis	$-E$	Slater basis[a]	$-E$
1*s* (5)	0.55373	$s(\alpha = 1.0)$	0.55377[b]
1*s*(4,1)	0.59047	s	0.58651[c]
1*s* (3.1.1)	0.59049	$s+p$	0.59980[c]
1*s* (5) + bond function	0.59778	$s+p+d$	0.60183[c]

[a] See Ref. [2].

[b] Slater exponent is frozen at unity.

[c] Slater exponents are scaled to minimize the energies.

Table 3. Comparison of various types of bond function for H_2^+ and Li_2^+. (Cases *a*, *b* and *c* use a set of concentric bond function; cases *d*, *e* and *f* use two sets of bond functions placed at 1/3 and 2/3 along bond distance)

Case	Number of bond function[a]	% of the energy improvement over minimum basis relative to Hartree-Fock	
		H_2^+	Li_2^+
a	3	90.1	75.2
b	2	88.5	73.1
c	1	69.3	73.1
d	(3,3)	90.6	70.0
e	(2,2)	87.8	67.8
f	(1,1)	70.2	67.7

[a] The set of bond functions used here are those in Table 1 with leading magnitudes of linear coefficients. The coefficients of bond functions are subjected to variation for each case here.

group of 1*s* orbitals with five Gaussian functions (denoted as 1*s* (5)) into two groups or three groups (denoted as 1*s* (4,1) or 1*s* (3,1,1)), gives an energy improvement of about 0.037 a.u. as compared with the value 0.044 a.u. by the present bond function method. The latter obtains 92% of the 0.048 a.u. improvement made by a rather accurate calculation with distorted atomic orbitals [2] where the *s* orbital is mixed with *p* and *d* orbitals with scaled Slater exponents. For the systems Li_2^+ and LiH^+, the present energies can reach 99.93% of the values calculated with extensive Slater-type atomic basis sets by Cade and Huo.

(3) For H_2^+, the number of bond-functions reduces from three to two, the energies improvement drops slightly, from 90.1–88.5% as shown in Table 3. However, one bond-function gives only 69.3% improvement. For Li_2^+, the energy improvement is rather insensitive to the number of bond functions. Furthermore, the concentric type of bond functions are compared with the new model where two sets of bond functions placed 1/3 and 2/3 along the internuclear distance. This model gives practically no improvement over former as shown in Table 3, case *d*, *e* and *f*. We shall conclude that the set of three concentric bond functions may be the optimal choice on account of the balance between effectiveness and economy.

The author is grateful to Professor E. F. Hayes for his interest in this work.

References

1. Slater, J. C.: Quantum theory of molecules and solids, Vol. I. New York: McGraw-Hill 1963.
2. Miller, R. L., Lykos, P. G.: J. chem. Physics **37**, 993 (1962).
3. Lennard-Jones, J. E.: Trans. Faraday Soc. **30**, 70 (1934).
4. Rothenberg, S., Schaefer, III, H. F.: J. chem. Physics **54**, 2764 (1971).
5. Kollman, P., Schwartz, M. E., Hayes, E. F., Allen, L. C.: Int. J. quant. Chem., Symp. 3, 715 (1970).
6. Whitten, J. L.: J. chem. Physics **44**, 359 (1966).
7. Roothaan, C. C. J.: Rev. mod. Physics **32**, 179 (1960).
8. Frost, A. A.: J. chem. Physics **47**, 3707 (1967).
9. Bates, D. P., Ledsham, K., Stewart, A. L.: Phil. Trans. Roy. Soc. (London) A **1953**, 246, 215. – Rosenthal, C. M., Wilson, E. B., Jr.: Physic. Rev. Letters **19**, 143 (1967).
10. LMSS (1967), Output of Laboratory of Molecular Structure and Spectra, University of Chicago. Attribution to the calculation was not given. See, Kreuss, M.: Compendium of *ab Initio* calculation of molecular energies and properties, Technical Note 438. Washington: National Bureau of Standards 1967.
11. Cade, P. E., Huo, W. M.: J. chem. Physics **47**, 614 (1967).

Dr. San Y. Chu
Chemistry Department
Rice University
Houston, Texas 77001, USA

Theoret. chim. Acta (Berl.) 25, 205—214 (1972)
© by Springer-Verlag 1972

Commentationes

Thomas-Fermi-Dirac Calculations for Molecules

II. One-Electron Energies for F_2

JERRY GOODISMAN*

Department of Chemistry, Syracuse University, Syracuse, N.Y. 13210, USA

Received July 6, 1971

The electrostatic potential derived from a solution to the molecular Thomas-Fermi-Dirac equation for F_2 is combined with the exchange potential and modified to give the correct behavior far from the nuclei. One-electron energy levels in this potential are calculated and are in qualitative agreement with SCF orbital energies. Similar computations are carried through for F and Ar, which correspond to the separated and united atoms for F_2. To compensate for errors in the potential, we subtract from molecular orbital energies the difference of TFD and SCF orbital energies for the separated atoms. Now all the orbital energies are correct to a few electron volts.

Das elektrostatische Potential, das sich für F_2 aus der Thomas-Fermi-Dirac Theorie ergibt, wird mit dem Austauschpotential kombiniert und so modifiziert, daß sich das richtige Verhalten in Kernnähe ergibt. Die berechneten Einelektronenenergien sind in qualitativer Übereinstimmung mit SCF-Werten. Analoge Rechnungen für F und Ar werden ausgeführt und als Grenzfälle für Korrekturen verwendet. Dann ergeben sich alle Orbitalenergien bis auf wenige eV richtig.

1. Introduction

The Thomas-Fermi-Dirac theory [1] gives a relation between electron density and electrostatic potential which, coupled with the Poisson equation, yields a differential equation from which either of these two quantities may be determined. This provides a simple route to approximate electron densities for many-electron systems, such as atoms and molecules. However, it appears [2] that the densities are not sufficiently accurate for many molecular properties, whose values are differences between nuclear and electronic contributions.

One may also consider using the results given by the theory for the potential seen by an electron at any point within the system. One can calculate the energy levels and wavefunctions of a single electron in this potential, and build up the atomic or molecular wavefunction from these. The energies are first approximations to the one-electron eigenvalues of the Hartree-Fock equations. By Koopman's Theorem, these approximate to ionization potentials, while differences between them may be related to the energies of electronic transitions [3]. For molecules, the variation of these energies with nuclear configuration is used to predict equilibrium nuclear positions and potential constants [4, 5].

In this article, we report the one-electron eigenvalues for diatomic fluorine near its equilibrium internuclear distance, using a potential derived from the solution to the Thomas-Fermi-Dirac equation. A number of calculations of this kind have been made in the past for atoms [1], but to our knowledge there is

---

* Supported by the National Science Foundation under Grant GP-20718.

only one for a molecule: Recknagel [6] in 1934, considered the term values of N_2 and N_2^+ using the Thomas-Fermi potential for the neutral homonuclear diatomic system of 13 electrons plus the Coulombic potential of two nuclei of charge $\frac{1}{2}e$. The energies of the lowest terms of N_2^+ and some excited terms of N_2 relative to ground state N_2 were calculated from differences of orbital energies (correcting for the change of equilibrium internuclear distance in the first case) and proved accurate to 1–2 eV.

The most complete tabulation of atomic results, for both the T–F and TFD fields, was given by Latter [7]. Unfortunately, he used an approximation to the TFD potential which means his eigenvalues are significantly changed. More recent workers [8] also used approximate potentials. An exception is Yonei [9], who treated K and Cs with a potential derived from a TFD calculation in which a Weizsäcker correction [1] (x 0.2) was used. Results were quite good for energies, and fair for calculated oscillator strengths. For the valence electron, a complicated modification of the exchange potential improved the results.

The computations are described in the next section. The results are discussed in Sect. 3. In Sect. 4, we investigate the use of atomic results to correct the molecular eigenenergies for the defects of the potential. The calculated atomic energy levels in the Thomas-Fermi-Dirac potential by Latter could not be used because of the approximations he introduced, and we have had to recalculate the results for atomic systems. Sect. 5 summarizes our conclusions.

2. Method of Calculation

The approximate solution of the Thomas-Fermi-Dirac equation for a homonuclear diatomic molecule, obtained by a relaxation method discussed and used by Sheldon [10], has been used [2] to generate approximate electron densities for several homonuclear diatomic systems. In terms of the function u used in those computations, the potential at some point in space r is given by:

$$V = u^2(R\xi\pi^2)^{-1} - (32\pi^2)^{-1}. \tag{1}$$

Here, R is the internuclear distance and $\xi^{-1} = r_A^{-1} + r_B^{-1}$, r_A and r_B being the distances to nuclei A and B. Atomic units are used ($e = \hbar = m = 1$), with the charge on the electron taken as -1.

It has been shown for many quantum mechanical calculations [11] that the exchange energy may be represented as the interaction of the electron density ϱ with an *exchange potential* $(3/2)(3/\pi)^{\frac{1}{3}}\varrho^{\frac{1}{3}}$. This is added to V. Expressing ϱ in terms of the function u gives for the total potential

$$V' = V + (3/4\pi^2)[1 + u(\tfrac{1}{2}\xi R)^{-\frac{1}{2}}]. \tag{2}$$

The exchange potential is set equal to zero outside the boundary of the system, where the electron density drops discontinuously to zero. Since V' does not approach a Coulombic potential as one goes far away from the nuclei, as it should, Latter suggested for atoms [7] that V' be used whenever it is greater than r^{-1} and that V' be replaced by r^{-1} when it drops below this. For the diatomic molecule, we maintain the expected shape of the problem by replacing V' by $\frac{1}{2}\xi^{-1}$ at all points in space where it goes below this quantity. It turns out that replacing $\frac{1}{2}\xi^{-1}$ by r_0^{-1}, r_0 being the distance from the molecular midpoint, changes our results little.

The equation which gives the eigenvalues is

$$-\tfrac{1}{2}\nabla^2\psi - V'\psi = \varepsilon\psi \tag{3}$$

and is treated by linear variation. The matrix elements are evaluated numerically, using crossed Gaussian quadrature formulas, over the two-dimensional grid of points used to determine u, extended to larger and smaller distances from the nuclei. Outside the boundary of the molecule, the potential is simply Coulombic, $V = \frac{1}{2}\xi^{-1}$. Close to the nuclei, where the molecular potential for F_2 is essentially that of the F atom, we use the atomic function ψ as a series in $r^{\frac{1}{2}}$ to compute V and add the corresponding exchange potential. The coordinates used [2] are ξ and η; if ξ is thought of as giving the distance from the nuclei and hence replacing r for a one-center system, η may be considered as giving angular position. Errors in the resulting eigenvalues could be due to numerical inaccuracies or to insufficiently flexible basis sets. The latter will make all the eigenvalues too high, according to the linear variational principle. The former probably would make them too low, since the use of sums for integrals is a removal of some restrictions on the trial function. The estimation of the overall error is discussed below.

It was thought originally that a reasonable and convenient set of basis functions would be

$$X_i = \xi^{j_i}\eta^{k_i}e^{-\alpha\xi} \tag{4}$$

(j and k positive integers, α a parameter to be determined) for σ_g orbitals, with multiplication by suitable factors of $e^{i\varphi}$, x, and r (distances from the midplane and from the symmetry axis) for orbitals of other symmetries. This turns out not to be so, because of the properties of the coordinate system, which can only be characterized as pathological. Sheldon [10] shows that the Laplacian of a φ-independent function f at the molecular midpoint ($\xi = \frac{1}{2}$, $\eta = 0$) is given by

$$\nabla^2 f = (\partial f/\partial\xi)_+ - (\partial f/\partial\xi)_-$$

where $(\partial f/\partial\xi)_\pm$ is the derivative for $\xi = \frac{1}{2} \pm \varepsilon$, $\varepsilon \to 0$. Thus any function which is continuous in ξ at this point has a zero kinetic energy here – an unnecessary restriction on the trial function. We decided to use the usual basis functions for the homonuclear diatomic problem.

For σ_g orbitals,

$$X_i = \lambda^{m_i}\mu^{n_i}e^{-\alpha\lambda} \tag{5}$$

with m_i an integer, n_i an even integer, and α to be determined. Here, λ and μ are the confocal ellipsoidal coordinates,

$$\lambda = (r_A + r_B)/R;\; \mu = (r_A - r_B)/R\,, \tag{6}$$

where r_A and r_B are distances to the nuclei A and B and R is the internuclear distance. For σ_u orbitals, (5) was used with n_i odd. For π_g orbitals, we used

$$X_i = \lambda^{m_i}\mu^{n_i}e^{-\alpha\lambda}e^{im\varphi}[(\lambda^2 - 1)(1 - \mu^2)]^{\frac{1}{2}} \tag{7}$$

Table 1. Eigenvalues in a two-center coulombic potential

Symmetry species	Our calculation α_{best}	Our calculation $-\varepsilon$(a.u.)	Exact[a] $-\varepsilon$(a.u.)
σ_g	0.92	0.9664	0.9619
σ_g	0.91	0.3327	0.3308
σ_g	0.95	0.2493	0.2494
σ_g	0.77	0.1674	0.1670
σ_u	1.22	0.7020	0.6966
σ_u	0.74	0.2551	0.2549
σ_u	0.60	0.1384	0.1364
σ_u	0.60	0.1330	0.1280
π_u	1.23	0.3994	0.3993
π_u	0.77	0.1943	
π_g	0.91	0.2299	0.2289
π_g	0.79	0.1335	

[a] Bates D. R., Ledsham, K., Stewart, A. L.: Philos. Trans. Roy. Soc. (London) A**246**, 215 (1953).

with n_i odd; for π_u orbitals, we used (7) with n_i even. Twelve basis functions were used initially in all the calculations reported here. In most cases, near linear dependencies reduced this number to nine or ten. For each eigenvalue, a series of calculations were made with different values of α until the energy as a function of α passed through a minimum. Three values were fitted to a parabola to determine the best α. All calculations were programmed in Fortran for the IBM 360.

In order to assess the accuracy of the calculation, we evaluated eigenvalues in the coulombic potential

$$V = \xi^{-1} = r_A^{-1} + r_B^{-1}$$

at an internuclear distance of 2.68 a_0. The energies of many of the states of this system, the H_2^+ molecular ion, are known from exact calculations. In Table 1 we give our results and compare with the exact values. It may be seen that our energies are correct to better than 0.01 a.u.

3. Results for F_2

For F_2 at an internuclear distance of 2.68 a_0, the same calculations were carried through, with results given in Table 2. We have also given the orbital energies from a matrix Hartree-Fock calculation. Atomic units (1 a.u. = 27.21 eV) are used for energies throughout. At the outset, we note that there is qualitative agreement for all the orbital energies.

The inner-shell energies are 1 a.u. too high, due to the fact that the Thomas-Fermi-Dirac model gives too high an electron density near the nuclei (at the nucleus the density is actually predicted to be infinite) so that V does not rise as rapidly as it should as one approaches a nucleus (the exchange potential is of minor importance here). For the energies of about -1 a.u., which include the highest filled levels, our results are several tenths of an a.u. too low. For the energies between these groups, the agreement with SCF is good.

Table 2. Orbital energies for F_2

Orbital	α_{best}	ε(a.u.)	ε(a.u.) from SCF[a]
$1\sigma_g$	11.9	−25.33	−26.423
$2\sigma_g$	5.4	− 1.828	− 1.757
$3\sigma_g$	4.2	− 1.091	− 0.746
$1\sigma_u$	11.2	−25.36	−26.422
$2\sigma_u$	5.4	− 1.573	− 1.495
$3\sigma_u$	4.4	− 0.791	--
$1\pi_u$	5.2	− 1.083	− 0.805
$1\pi_g$	5.3	− 0.943	− 0.663

[a] Wahl, A.C.: J. chem. Physics 41, 2600 (1964).

The order of the energy levels,

$$1\sigma_g = 1\sigma_u < 2\sigma_g < 2\sigma_u < 3\sigma_g < 1\pi_u < 1\pi_g < 3\sigma_u$$

is almost correct; $1\pi_u$ should actually be slightly below $3\sigma_g$. The difference of energies for $1\sigma_g$ and $1\sigma_u$ (the former should actually lie slightly lower) we take as an indication of the maximum numerical error in our calculation. These wavefunctions vary more rapidly in space than those for H_2^+. The experimental ionization potential is 0.599 a.u., which is in much better agreement with the SCF orbital energy for the highest occupied orbital (0.663 a.u.) than that from the TFD potential (0.943 a.u.). On the other hand, the error in all the higher orbital energies is roughly the same, so differences in these quantities, which may be related to spectra, are close to SCF values:

$$\varepsilon_{1\pi_g} - \varepsilon_{1\pi_u} = 0.14 \text{ a.u. (TFD)}, 0.14 \text{ a.u. (SCF)}$$

$$\varepsilon_{1\pi_u} - \varepsilon_{3\sigma_g} = 0.01 \text{ a.u. (TFD)}, -0.05 \text{ a.u. (SCF)}$$

$$\varepsilon_{1\pi_u} - \varepsilon_{2\sigma_u} = 0.49 \text{ a.u. (TFD)}, 0.69 \text{ a.u. (SCF)}$$

and so on.

The predicted electron affinity is the negative of the energy of the lowest unoccupied orbital, $-\varepsilon_{3\sigma_u} = 0.79$ a.u., and is undoubtedly at least three tenths of an atomic unit too high, but the energy of the lowest energy one-electron transition, $\varepsilon_{3\sigma_u} - \varepsilon_{1\pi_g} = 0.15$ a.u., should be much closer to the correct result. [Actually (see below) the errors in σ and π orbitals probably do not cancel as well as those between two σ orbitals or two π orbitals.] The experimental value for F_2 is not available, but, if we extrapolate results for I_2, Br_2, and Cl_2 from Herzberg, we may estimate a frequency of 20×10^3 cm^{-1} which corresponds to 0.09 a.u.

While a log-log plot of TFD orbital energies vs. SCF orbital energies doesn't look bad, it must be admitted that agreement is not good enough to be considered quantitative. The poblem now becomes correction of the defects in the potential which led to the inaccuracies. The problem close to the nucleus seems relatively easy to correct [12], but the incorrect behavior of the higher energies seems less so. It may be, however, that the problems with the potential are common to both atoms and molecules. For atoms, SCF calculations are readily available, while TFD calculations are easily performed. For large molecules, only the latter may be possible. If the molecular orbitals can be correlated with atomic orbitals, corrections derived from the atomic work can be applied to the molecular energies. Such correlations are of course part of every quantum chemist's education. As is shown below, this leads to a great improvement in predicted orbital energies.

4. Atomic Calculations

Latter [7] gives an extensive tabulation of "Atomic Energy Levels for the Thomas-Fermi and Thomas-Fermi-Dirac Potential". However, he replaced the TFD potential, which must be calculated separately for each atom, by an approximate universal potential. Its deviation from the correct potential, it is stated, is less than five per cent for $Z > 5$. This is too large for our purposes. As we will see below, the changes in orbital energies due to this approximation are tenths of atomic units. It was thus necessary to compute energies for the true TFD potential for several atoms.

The differential equation for the radial part of an atomic wavefunction of orbital angular momentum l is

$$\frac{d^2\psi}{dr^2} + \left[\frac{2m\varepsilon}{\hbar^2} - \frac{2mV(r)}{\hbar^2} + \frac{l(l+1)}{r^2}\right]\psi = 0 \tag{8}$$

where ψ is the radial wavefunction multiplied by r. Using the fact that $\psi(0)=0$, we may substitute for (8) the integral equation

$$\psi(r) = r\psi'(0) - \int_0^r (r-r')\left[\frac{2m\varepsilon}{\hbar^2} - \frac{2m}{\hbar^2}V(r') + \frac{l(l+1)}{r'^2}\right]\psi(r')\,dr'\,. \tag{9}$$

Since ψ goes as r^{l+1} as r approaches 0, $\psi'(0)$ is 0 except for s states. The overall normalization of ψ is irrelevant for our purposes. As did Latter, we solve (9) as a difference equation, using equal spacing in $r^{\frac{1}{2}}$. We evaluate all integrals using a Newton-Cotes five-point rule. The orbital energy ε is determined, generally to 0.01 a.u., by integrating outward from $r=0$ for successive trial values of ε until we obtain one too high and one too low, as judged by following the behavior of the functions for large r. The computations were carried out using the APL system of the 360 computer.

We first verified the accuracy of our procedure and choice of spacing of points by calculating energies for the F atom in Latter's approximate potential. Latter used different integration formulas in his work. Then we solved the TFD equation for this atom and determined energy levels in the correct potential (the TFD potential corrected for exchange and proper asymptotic behavior as in the previous section). Results are given in Table 3. It is seen that our energies agree with those given by Latter for his potential.

It is also seen that there are substantial differences between the energies in the two potentials. For the 1s, the TFD result is 1 a.u. closer to the SCF result than Latter's; for the 2s and 2p, there is a difference of 0.1 a.u. in the other direction. It may also be interesting to note that Herman and Skillman [13], performing SCF calculations with the exchange term replaced by a local potential proportional to $\varrho^{\frac{1}{3}}$, obtained -25.27, -1.318 and -0.625 a.u. for the orbital energies.

Table 3. One-electron energies for fluorine atoms

Orbital	Latter[a]	Energy (a.u.) Latter pot.[b]	TFD pot.	SCF[c]
1s	−24.18[d]	−24.25	−25.38	−26.383
2s	− 1.541	− 1.55	− 1.65	− 1.573
2p	− 0.858	− 0.857	− 0.96	− 0.730

[a] Latter, R.: Physic. Rev. 99, 510 (1955).

[b] Calculated with our programs using Latter's approximate potential.

[c] Clementi, E., Roothaan, C. C. J., Yoshimine, M.: Physic. Rev. 127, 1618 (1962).

[d] Not given by Latter; interpolated from his Table using $-\varepsilon = kZ^{*}$.

Table 4. One-electron energies for argon atom (a.u.)

Orbital	ε, TFD pot.	ε, SCF pot.[a]
2p	−9.31	−9.58
3s	−1.08	−1.28
3p	−0.62	−0.59
3d	−0.061	—

[a] Czyzak, S. J.: Astrophysic. J. Supp. 7, 53 (1962).

The TFD results are thus about as good (in the sense of approximating the SCF results) as these. In addition to the F atom, which represents the separated atoms for the F_2 molecule, we also want to consider the atom formed by F_2 when the internuclear distance approaches zero (united atom), Argon. Some energy levels calculated in the TFD potential for this atom are given in Table 4, and compared with SCF results.

The correlations of the molecular orbitals with orbitals of the united atom and separated atoms are easily obtained and are given in many sources [14]. It must be decided, for each orbital, whether the united atom or separated atom limit is more relevant. For the inner shell orbitals $1\sigma_g$ and $1\sigma_u$, there is little problem. When R is near the equilibrium internuclear distance these are essentially unaffected by the binding process. This is shown by comparing orbital energies for the molecule and the atoms, from the SCF or TFD calculations. The orbitals are $1s_A \pm 1s_B$, A and B denoting the two atoms, and the lack of substantial overlap between the atomic orbitals makes $\varepsilon_{1\sigma_g}$ and $\varepsilon_{1\sigma_u}$ close to equal. Of course, if the TFD results of Table 1 are corrected by addition of − 1.00 a.u., the difference between SCF and TFD energies for the F 1s orbitals, we obtain approximately correct energies for the $1\sigma_g$ and $1\sigma_u$ orbitals: $\varepsilon_{1\sigma_g} = \varepsilon_{1\sigma_u} = -26.35$. We have used the average. The last figure may be in error by several units, as indicated by $\varepsilon_{1\sigma_u}$ being 0.03 a.u. *lower* than $\varepsilon_{1\sigma_g}$ in the TFD results.

The remaining molecular orbitals correlate with the 2s and 2p orbitals of the separated atoms, and with 2s, 2p, 3s, 3p, 3d and 4s of the united atom. In general, one expects that the orbitals of lower energy, which are less diffuse, are more closely related to the separated atom limit, and the higher energy orbitals closer to the united atom. The orbital energies provide some guidance here. Thus, $2\sigma_g$ correlates

Table 5. Corrected orbital energies

Orbital	AO used for comparison	Corrected ε(a.u.)
$1\sigma_g$	F 1*s*	−26.36
$2\sigma_g$	F 2*s*	− 1.75
$3\sigma_g$	F 2*p*, Ar 3*s*	− 0.86, − 1.29
$1\sigma_u$	F 1*s*	−26.35
$2\sigma_u$	F 2*s*, Ar 3*p*	− 1.49, − 1.54
$3\sigma_u$	F 2*p*	− 0.56
$1\pi_u$	F 2*p*	− 0.85
$1\pi_g$	F 2*p*	− 0.71

Table 6 Ionization potentials for F_2 (eV)

State	Orbital energies This work, uncorrected	This work, corrected	Hartree-Fock calculation	Experimental[a] Ionization potential
$^2\Pi_g$	25.7	19.3	18.0	15.63 eV
$^2\Sigma_u^+$	29.7	23.4	20.3	17.35 eV
$^2\Pi_u$	29.5	23.1	21.9	18.46 eV

[a] Frost, D. C., McDowell, C. A., Vroom, D. A.: J. chem. Physics 46, 4255 (1967).

with the F 2*s* orbitals and the Ar 2*s* orbital. The energy of the latter is much too low, so $\varepsilon_{2\sigma_u}$ is corrected using the F results:

$$\varepsilon_{2\sigma_g} = -1.83 + (-1.57 + 1.65) = -1.75 .$$

Similarly, $1\pi_u$ has energy much closer to the separated atom limit $\varepsilon^{\mathrm{F}}_{2p} = -0.96$ than the united atom limit $\varepsilon^{\mathrm{Ar}}_{2p} = -9.31$, so its energy is corrected by addition of $(-0.73 + 0.96)$ to give -0.85. It has been noted [15] that the highest filled π_g and π_u orbitals resemble the separated atoms in the halogen molecules.

For $\varepsilon_{3\sigma_g}$ there is some ambiguity. The energy of -1.09 is fairly close to the separated atom $\varepsilon^{\mathrm{F}}_{2p} = -0.96$ but even closer to the united atom $\varepsilon^{\mathrm{Ar}}_{3s} = -1.08$. The former gives a correction of $+0.23$ and the latter a correction of -0.20, so only the former gives a satisfactory result. Both are included in Table 5. Except for the case just mentioned, we agree with the Hartree-Fock orbital energies to 0.08 a.u. or better. It is interesting that Recknagel [6], discussing his results for N_2, noted that certain orbitals resembled orbitals of the united atom, but not the orbitals with which they supposedly correlate. For instance, his $3\sigma_g$ MO resembled the united atom 2*s* rather than the 3*s*.

If we agree to use the corrections derived from separated atoms throughout, we may predict ionization potentials for F_2 going to several states of F_2^+. These may be compared with experimental results from photoelectron spectroscopy [16]. In Table 6 we give our results (orbital energies) without the atomic correction and with correction, the SCF results, and the experimental ionization potentials, in electron volts. The errors in the corrected values are about 30%, compared to errors of about half this for the SCF results.

As we have mentioned, orbital energies are used to predict nuclear configurations and related properties when total energies are not readily available [4]. The binding energy would be calculated as $\Sigma\varepsilon_i$ (separated atoms) $-\Sigma\varepsilon_i$ (molecule), the sums in each case running over occupied orbitals. When SCF calculations are treated this way, it may be shown [5] that the binding energy (B.E.) will be increased by $2\,(\mathrm{B.E.})-\Sigma Z_B\,\partial(\mathrm{B.E.})/\partial Z_B$ over the difference of total energies. The sum here is over the nuclei in the molecule, and the partial derivatives are small according to the isoelectronic principle. The difference of TFD orbital energies (atoms minus molecule) is 0.75 a.u.; the difference of SCF orbital energies is 0.43 a.u. The correct binding energy is 0.062 a.u.

5. Summary and Conclusions

Orbital energies for the F_2 molecule were calculated using the TFD potential plus an exchange potential, with the overall potential replaced by $\frac{1}{2}\left(\frac{1}{r_A}+\frac{1}{r_B}\right)$ when it dropped below this. This modification assures the correct boundary condition at large distances from the nuclei. The orbital energies were in qualitative agreement with SCF values. When they are corrected by comparing atomic eigenvalues for the F atom calculated by SCF with those calculated using the TFD potential, all the eigenvalues agree to about 1/20 a.u.

An error of 0.05 a.u. ($1\frac{1}{2}$ eV) is quite comparable to the difference between ionization potentials and Hartree-Fock orbital energies, and less than the errors made in atomic calculations when the exchange interaction is replaced by the free-electron approximation, *i.e.*, an exchange potential proportional to $\varrho^{\frac{1}{3}}$. Even with corrections, however, there are several unsatisfactory features.

The order of the eigenvalues of the outer shell F_2 orbitals, which all correlate with the $2p$ atomic orbital of Fluorine, is not quite correctly given. The $3\sigma_g$ energy is incorrectly lower than the $1\pi_u$ energy. Similarly, it may be noted in Table 6 that the ${}^2\Pi_g-{}^2\Pi_u$ spacing is identical to the SCF value, but the ${}^2\Sigma_g^+$ value is incorrect relative to these. We have remarked above that the potential is certainly in error near the nuclei, where the TFD density is known to be quite incorrect. (We have shown recently [12] how this error can be largely corrected in a simple way.) The π orbitals vanish at the nuclei, the σ orbitals do not. Thus the correction will affect them differently. This must be investigated.

References

1. General reference: Gombas, P.: Die statistische Theorie des Atoms und ihre Anwendungen. Vienna: Springer 1949.
2. Goodisman, J.: Physic. Rev. A 3, 1819 (1971).
3. Parr, R. G.: The quantum theory of molecular electronic structure. New York: W. A. Benjamin 1963.
4. Hoffmann, R., Lipscomb, W. N.: J. chem. Physics **36**, 2179 (1962). J. chem. Physics **39**, 1397 (1963). Walsh, A. D.: J. chem. Soc. **1953**, 2260, et seq.
5. Goodisman, J.: J. Amer. chem. Soc. **91**, 6552 (1969).
6. Recknagel, A.: Z. Physik **87**, 375 (1934).
7. Latter, R.: Physic. Rev. **99**, 510 (1955).

8. Tietz, T.: Z. Naturforsch. **23a**, 191 (1968); Muller, H. J. W.: Ann. Physik **16**, 255 (1965).
9. Yonei, K.: J. Physic. Soc. Japan **22**, 1127 (1967).
10. Sheldon, J. W.: Physic. Rev. **99**, 1291 (1955).
11. Slater, J. C.: Quantum theory of atomic structure. Vol. II, Chapt. 17. New York: McGraw-Hill 1960. Slater, J. C., Wood, J. H.: Int. J. quant. chemistry **4**, 3 (1971).
12. Goodisman, J.: Physic. Rev. **A2**, 1193 (1970).
13. Herman, F., Skillman, S.: Atomic structure calculations. Englewood Cliffs, N.Y.: Prentice-Hall 1963.
14. For example, Coulson, C. A.: Valence, Ch. IV 7. Oxford, London: 1958.
15. King, G. W., Richardson, A. W.: J. molecular Spectroscopy **21** 339 (1966).
16. Frost, D. C., McDowell, C. A., Vroom, D. A.: J. chem. Physics **46**, 4255 (1967).
17. Balint-Kurti, G. G., Karplus, M.: J. chem. Physics **50**, 478 (1969).

Prof. Dr. J. Goodisman
Department of Chemistry
Syracuse University
Syracuse, New York 13210, USA

Theoret. chim. Acta (Berl.) 25, 215–222 (1972)
© by Springer-Verlag 1972

Graphical Enumeration of the Coefficients of the Secular Polynomials of the Hückel Molecular Orbitals

HARUO HOSOYA
Department of Chemistry, Ochanomizu University, Bunkyo-ku, Tokyo, Japan

Received December 15, 1971

A general and simple method for graphical enumeration of the coefficients of the secular polynomials of the Hückel molecular orbitals is presented with examples. The essential procedure is to count for the graph and its subgraphs the non-adjacent numbers, $p(G, k)$'s, which appear as the coefficients of the Z-counting polynomial $Q(Y)$. Two composition principles are proposed and shown to simplify these procedures to a great extent. Application to biphenylene shows the superiority of this method to others, *e.g.*, the method of polygons.

Eine einfache und allgemeine Methode zur graphischen Bestimmung der Koeffizienten des Säkularpolynoms bei Hückelproblemen wird angegeben. Das Wesentliche für den Graphen und seine Untergraphen ist es, die Nichtnachbar-Zahlen abzuzählen. Letztere erscheinen im Z-zählenden Polynom. Zwei einfache Aufbau-Schemata werden vorgeschlagen. Am Beispiel von Biphenylen werden die Vorzüge diesen Verfahrens demonstriert.

Introduction

Since the secular determinant of the Hückel molecular orbitals for unsaturated hydrocarbons reflects only the neighbourship of the carbon atoms in molecules, it is closely related to what is called in the graph theory [1] an adjacency matrix but was named by Ham [2] a topological matrix [3, 4]. In this topological sense distinction between saturation and unsaturation in the C–C bonds is meaningless. There often arises a need for expanding the secular determinant into a polynomial $P(X)$, which is called a characteristic or secular polynomial. The method for deriving $P(X)$ from those of component subgraphs has been established [5, 6].

On the other hand "the method of polygons" has been proposed to count the coefficients in $P(X)$ graphically but with no generalised algorithm [7–10]. Very recently, however, it was shown that $P(X)$ for a tree graph, or a chain hydrocarbon, can be simply expressed by using the $p(G, k)$ numbers as,

$$P_G(X) = \sum_{k=0}^{m} (-1)^k \, p(G, k) \, X^{N-2k}, \qquad (1)$$

where $p(G, k)$ is the number of ways in which disjoint k bonds are chosen from graph G. This paper gives a generalised method for graphical enumeration of $P(X)$ of a given graph with or without rings.

Definitions

The followings are the necessary definitions for describing the enumeration method.

1) A graph **G** consists of points (vertices or atoms) and lines (edges or bonds) [1]. We are concerned with such connected non-directed graphs that have no loop (a line joining a point to itself) and no multiple lines (double or triple bonds).

2) An adjacency matrix **A** for graph G with N points is a square matrix of the order N with elements,

$$a_{ij}=\begin{cases}1 & \text{if the points } i \text{ and } j \text{ are neighbours,}\\ 0 & \text{otherwise.}\end{cases} \tag{2}$$

The matrix character is independent of the way of numbering the points.

3) A characteristic polynomial or a secular polynomial $P(X)$ is defined as

$$P(X)=\det|X\boldsymbol{E}+\boldsymbol{A}|=\sum_{i=0}^{N} C_i X^{N-i} \tag{3}$$

where **E** is a unit matrix of the same oder N as that of **A**, X is a scalar variable and C_i is the coefficient which we are going to obtain.

4) A non-adjacent number $p(G,k)$ is the number of ways in which disjoint k bonds are chosen from G; $p(G,0)$ being unity and $p(G,1)$ the number of lines.

5) A Z-counting polynomial $Q(Y)$ for G is defined as

$$Q_G(Y)=\sum_{k=0}^{m} p(G,k)\,Y^k \tag{4}$$

where m is the maximum number of k for G. Both for a single point and a vacant graph let us define $Q(Y)=1$. The integer $p(G,m)$ is the number of the Kekulé structures for an unsaturated hydrocarbon with the carbon skeleton G [11].

6. A topological index Z for G is defined as

$$Z_G=\sum_{k=0}^{m} p(G,k)=Q_G(1)\,. \tag{5}$$

Interesting properties of the quantities, $p(G,k)$, $Q(Y)$ and Z are discussed elsewhere [4].

Theorems

Fundamental Equation

The fundamental equation for the graphical enumeration of $P(X)$ from G is as follows:

$$\begin{aligned}P_G(X)=&\sum_{k=0}^{m}(-1)^k p(G,k)\,X^{N-2k}\\ &-2\sum_{i}^{G}\sum_{k=0}^{m_i}(-1)^{k+n_i}p(G-R_i,k)\,X^{N-n_i-2k}\\ &+2^2\sum_{i>j}^{G}\sum_{k=0}^{m_{ij}}(-1)^{k+n_i+n_j}p(G-R_i-R_j,k)\,X^{N-n_i-n_j-2k}\\ &-\cdots.\end{aligned} \tag{6}$$

$G-\boldsymbol{R}_i$: A subgraph of G derived by deleting a ring $\boldsymbol{R}_i$ and all the lines incident to $\boldsymbol{R}_i$. It may or may not be a disjoint graph.

$G-\boldsymbol{R}_i-\boldsymbol{R}_j$: A subgraph of G derived by deleting a pair of disjoint rings $\boldsymbol{R}_i$ and $\boldsymbol{R}_j$ and all the lines incident to $\boldsymbol{R}_i$ and/or $\boldsymbol{R}_j$.

n_i: The number of points in $\boldsymbol{R}_i$.

m_i: The maximum number of k for $G-\boldsymbol{R}_i$.

m_{ij}: The maximum number of k for $G-\boldsymbol{R}_i-\boldsymbol{R}_j$.

$\sum_i^G$: Summation over all the possible rings in G.

$\sum_{i>j}^G$: Summation over all the possible pairs of two disjoint rings in G.

If necessary, one can continue to write the right-hand side of Eq. (6) as far as he wishes. Note that the second term can be expressed as

$$-2\sum_i^G(-1)^{n_i}\left\{\sum_{k=0}^{m_i}(-1)^k p(G_i,k)\,X^{N_i-2k}\right\}$$

with $G_i=G-\boldsymbol{R}_i$ and $N_i=N-n_i$ and that the term in the brackets has quite the same form as the first term of Eq. (6). This is also the case for the remaining terms.

Now the problem is reduced to obtaining the $p(G,k)$ numbers for a given graph. It is easy to count the $p(G,k)$ numbers and therefore to write out $P(X)$ for graphs with smaller N or those of special classes as will be shown later. On the other hand, for most larger graphs the procedure for counting the $p(G,k)$ numbers is as formidable as that for expanding the determinant by minors.

By the aid of the Z-counting polynomial $Q(Y)$, the $p(G,k)$ numbers can be obtained rather mechanically. The following two Composition Principles are useful for this purpose.

Composition Principle I

Consider a graph G and choose from it a line l as exemplified in Fig. 1. 1) Delete line l and we get subgraphs L and M. 2) Delete all the lines in L and M that were incident to l and we get subgraphs $A, B, \ldots F$. The Z-counting polynomial Q_G

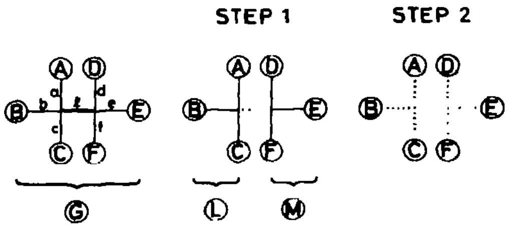

Fig. 1. Illustration for Composition Principle I. In this example no such lines are deleted that are constituents of a ring. See also Fig. 5 for the case where rings are opened by deletion of a line or a group of lines

for G can be expressed as

$$Q_G = Q_L Q_M + Y \cdot Q_A Q_B Q_C Q_D Q_E Q_F, \tag{7}$$

or more generally as

$$Q_G = \prod^{l} Q_L + Y \cdot \prod^{l+\{a\}} Q_A. \tag{8}$$

Multiplication l runs over all the subgraphs L's obtained by deleting bond l, while $l+\{a\}$ means deletion of l and all the bonds a's incident to l. The $p(G,k)$ numbers appear as the coefficients of the term Y^k in $Q_G(Y)$. If one deletes a line which is a constituent of a ring, a single subgraph L, instead of L and M, is obtained in step 1). In this case the first term of Eq. (8) is no longer a product but a single polynomial Q_L. This principle also applies to step 2) and Composition Principle II. Thus all the polynomials Q's following a product sign should be mutually disjoint.

By putting $Y=1$ into Eqs. (7) and (8) we get the expressions for the topological index Z.

$$Z_G = Z_L Z_M + Z_A Z_B Z_C Z_D Z_E Z_F \tag{9}$$

and

$$Z_G = \prod^{l} Z_L + \prod^{l+\{a\}} Z_A. \tag{10}$$

The proof is given in Appendix of Ref. [4].

Composition Principle II

Consider a graph G and choose from it a point p as exemplified in Fig. 2. The number of the lines incident to point p should be at least two, e.g., six as in this example. 1) Divide them into two groups. 2) Delete a group of lines a, b and c in G, and we get subgraphs A, B, C and M. 2) Delete another group of lines d, e and f in G, and we get subgraphs D, E, F and L. 4) Delete both the groups of lines $a, b, \ldots f$ in G, and we get subgraphs $A, B, \ldots F$. With these subgraphs we have

$$Q_G = Q_A Q_B Q_C Q_M + Q_D Q_E Q_F Q_L - Q_A Q_B Q_C Q_D Q_E Q_F{}^{1} \tag{11}$$

or more generally

$$Q_G = \prod^{(p)} Q_L + \prod^{(\bar{p})} Q_{\bar{L}} - \prod^{(p+\bar{p})} Q_A. \tag{12}$$

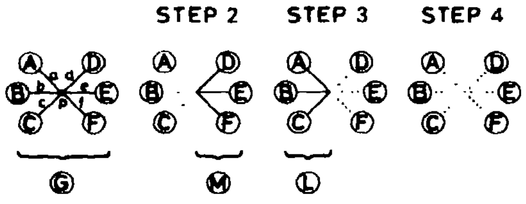

Fig. 2. Illustration for Composition Principle II. See also Fig. 3

---

[1] Eq. (11) may be expressed as

$$Q_G = Q_L Q_M - (Q_A Q_B Q_C - Q_L)(Q_D Q_E Q_F - Q_M) \tag{11'}$$

Multiplication $\{p\}$ runs over all the subgraphs L's obtained by deleting a group of lines incident to point p. The symbol $\{\bar{p}\}$ means deletion of the coset of $\{p\}$. The corresponding expressions for the topological index are

$$Z_G = Z_A Z_B Z_C Z_M + Z_D Z_E Z_F Z_L - Z_A Z_B Z_C Z_D Z_E Z_F{}^{2} \tag{13}$$

$$Z_G = \prod^{\{p\}} Z_L + \prod^{\{\bar{p}\}} Z_L - \prod^{\{p+\bar{p}\}} Z_A . \tag{14}$$

Examples

Tree Graphs

For tree graphs Eq. (6) turns out to be Eq. (1) since a tree has no ring.

1) *Linear Graphs (normal paraffins).* The carbon atom skeletons of n-paraffins form the most simplest series of graphs. If a linear graph with N points is denoted as $\bar{N}$, the $p(G, k)$ numbers for $\bar{N}$ are given by

$$p(\bar{N}, k) = {}_{N-k}C_k = (N-k)(N-k-1)\ldots(N-2k+1)/k! \tag{15}$$

and we have

$$Q_{\bar{N}}(Y) = \sum_{k=0}^{[\frac{N}{2}]} {}_{N-k}C_k Y^k \tag{16}$$

and

$$P_{\bar{N}}(X) = \sum_{k=0}^{[\frac{N}{2}]} (-1)^k {}_{N-k}C_k X^{N-2k} . \tag{17}$$

2) *Trees (branched paraffins).* Many examples for the application of Composition Principle I to tree graphs are given elsewhere [4, 12]. Therefore let us apply Compositon Principle II to a multi-branched tree graph, or 3,3-diethylpentane, in Fig. 3. By noticing the central point one can obtain the Z-counting polynomial Q as

$$\begin{aligned} Q(Y) &= 2(1+4Y+3Y^2)(1+Y)^2-(1+Y)^4 \\ &= 1+8Y+18Y^2+16Y^3+5Y^4 \end{aligned}$$

by decomposing the graph G into subgraphs as shown in Fig. 3 and by using Eq. (6). The $p(G, k)$ numbers appear as the coefficients of $Q(Y)$ and we get

$$P(X) = X^9 - 8X^7 + 18X^5 - 16X^3 + 5X$$

and $Z = 48$. The topological index Z is useful for checking the calculation of the polynomials Q and P.

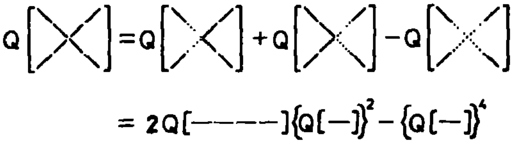

Fig. 3. Example of the application of Composition Principle II

---

[2] Eq. (13) may be expressed as

$$Z_G = Z_L Z_M - (Z_A Z_B Z_C - Z_L)(Z_D Z_E Z_F - Z_M) \tag{13'}$$

Non-Tree Graphs

1) ***Ring Graphs (cyclo-paraffins).*** The $p(G, k)$ numbers for an N-membered ring (denoted as N^0) are given by

$$p(N^0, k) = {}_{N-k}C_k N/(N-k) = \begin{cases} 1 & k=0 \\ N & k=1 \\ N(N-k-1)(N-k-2)\dots(N-2k+1)/k! & k>1 \end{cases} \qquad (18)$$

and we have

$$Q_{N^0}(Y) = \sum_{k=0}^{[\frac{N}{2}]} \{{}_{N-k}C_k N/(N-k)\}\, Y^k. \qquad (19)$$

Since in this case the ring R_1 is identical to G (namely $n_1 = N$), the second term of Eq. (6) becomes $-2(-1)^N$. Thus we have

$$P_{N^0}(X) = \sum_{k=0}^{[\frac{N}{2}]} (-1)^k p(N^0, k)\, X^{N-2k} - 2(-1)^N. \qquad (20)$$

The resultant polynomials for smaller rings are well known and not shown here [4–6, 13].

2) ***Multi-Ring Graphs.*** Consider a graph G in Fig. 4, or the carbon atom skeleton of biphenylene. See also Table 1 for explanation. The first step is to set up all the possible subgraphs G_i's ($i = 1-6$ in this example and marked with heavy lines, G_6 being a vacant graph) with N_i points by deleting from G a ring R_i (framed) and the lines (crossed) incident to it. Next try to find out the possibility if a pair of disjoint rings can be chosen from G. In this example we get a vacant graph G_7 by deleting two disjoint hexagons and two lines joining them. Continue this process until as many disjoint rings are chosen from G as possible. Write out the set of the polynomials $Q_{G_i}(Y)$'s together with that of the original graph

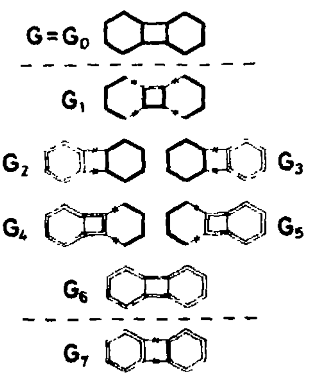

Fig. 4. Subgraphs for enumerating the characteristic polynomial of biphenylene. See also Table 1 for explanation

Table 1. Components of the characteristic polynomial $P_G(X)$ of biphenylene[a]

i[b]	l_i[c]	N_i[d]	Y-Expression, $Q_{G_i}(Y)$	Ref.	X-Expression[e]	Weight[f]
0	0	12	$1+14Y+71Y^2+162Y^3$ $+164Y^4+60Y^5+5Y^6$	Fig. 5 Eqs. (16) (19)	$X^{12}-14X^{10}+71X^8-162X^6$ $+164X^4-60X^2+5$	1
1	1	8	$(1+3Y+Y^2)^2$ $=1+6Y+11Y^2+6Y^3+Y^4$	Eq. (16)	$X^8-6X^6+11X^4-6X^2+1$	−2
2,3	1	6	$2(1+6Y+9Y^2+2Y^3)$	Eq. (19)	$2(X^6-6X^4+9X^2-2)$	−2
4, 5	1	4	$2(1+3Y+Y^2)$	Eq. (16)	$2(X^4-3X^2+1)$	−2
6	1	0	1	Def. 5)	1	−2
7	2	0	1	Def. 5)	1	4

[a] The characteristic polynomial $P_G(X)$ for biphenylene is obtained by adding the X-expressions with weights given in the last column.

[b] The suffix referring to the subgraph given in Fig. 4.

[c] The number of disjoint rings deleted from G to give G_i.

[d] The number of points in G_i.

[e] The polynomial begins with $(-1)^N(-X)^{N_i}$.

[f] $(-2)^{l_i}$.

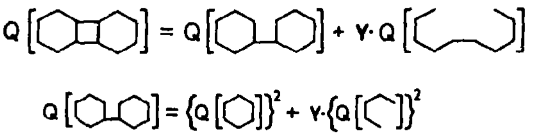

Fig. 5. Illustration for obtaining $Q_G(Y)$ of the carbon atom skeleton of biphenylene. By the use of Eqs. (16) and (19) the polynomial $Q_G(Y)$ is obtained as in Table 1

$G(\equiv_0)$ as in Table 1. The method for obtaining $Q_G(Y)$ is illustrated in Fig. 5. Now transfer each Y-expression into such an X-expression that begins with the term $(-1)^N(-X)^{N_i}$, descends in its power by two, alternates in the sign and has the same set of the coefficients $p(G,k)$'s. Finally add up all the X-expressions with weights $(-2)^{l_i}$ to get $P_G(X)$, where l_i is the number of the disjoint rings deleted from G to give G_i. In this example we get

$$\begin{aligned}P(X) &= X^{12}-14X^{10}+71X^8-162X^6+164X^4-60X^2+5\\ &\quad -2(X^8-4X^6+X^4+6X^2)+4\\ &= X^{12}-14X^{10}+69X^8-154X^6+162X^4-72X^2+9\,.\end{aligned}$$

Compare the present method with the "method of polygons" for the same example [8, 9] and find out the simplicity and generality of the former.

Acknowledgement. The author thanks Miss Keiko Kawasaki for programming and numerical checking of this material.

References

1. Harary, F.: Graph theory. Reading, Mass.: Addison-Wesley 1969.
2. Ham, N. S.: J. chem. Physics **29**, 1229 (1958).
3. Platt, J. R.: In: Encyclopedia of Physics, Vol. 37 (Molecule II) ed. by Flügge, S., pp. 173. Berlin: Springer-Verlag 1961.

4. Hosoya, H.: Bull. chem. Soc. Japan **44**, 2332 (1971).
5. Heilbronner, E.: Helv. chim. Acta **36**, 170 (1953).
6. Streitwieser, Jr., A.: Molecular orbital theory for organic chemists. New York: John Wiley 1961.
7. Samuel, I.: Compt. rend. **229**, 1236 (1949).
8. Coulson, C. A.: Proc. Cambridge phil. Soc. **46**, 202 (1950).
9. Gouarné, R.: Journal des recherches du C.N.R.S. **34**, 81 (1956).
10. Daudel, R., Lefebvre, R., Moser, C.: Quantum chemistry, methods and applications, p. 539. New York: Interscience Publishers 1959.
11. Ham, N. S., Ruedenberg, K.: J. chem. Physics **29**, 1199 (1958).
12. Mizutani, K., Kawasaki, K., Hosoya, H.: Natural Science Report of Ochanomizu Univ. (Tokyo) **22**, 39 (1971)
13. Kawasaki, K., Mizutani, K., Hosoya, H.: Natural Science Report of Ochanomizu Univ. (Tokyo) **22**, 181 (1972)

Professor H. Hosoya
Department of Chemistry
Ochanomizu University
Bunkyo-ku, Tokyo 112
Japan

Theoret. chim. Acta (Berl.) 25, 223–236 (1972)
© by Springer-Verlag 1972

Semiempirical SCF Theory with "Scaled" Slater Orbitals

II. Molecular Calculations

G. Klopman and R. Polak*

Department of Chemistry, Case Western Reserve University, Cleveland, Ohio 44106, USA

Received November 16, 1971

A new method is presented for the calculation of molecular properties in which the one center integrals are evaluated within their environment (scaled in the molecule) rather than carried over from atomic structures.

The procedure can be incorporated into any SCF scheme using a minimal basis set of atomic orbitals. In this paper an INDO framework was chosen to illustrate the results. Both heats of formation and bond distances for various types of molecules were found in satisfactory agreement with experiment.

Es wird eine neue Methode für die Berechnung von Moleküleigenschaften vorgeschlagen, in welcher die Einzentrenintegrale innerhalb ihrer Umgebung im Molekül bestimmt werden, statt sie von freien Atomen zu übernehmen.

Diese Methode kann bei jedem SCF Verfahren angewandt werden, das auf einer minimalen Basis von Atomorbitalen aufbaut. Zur Illustration der Ergebnisse in dieser Arbeit wird das INDO-Verfahren gewählt. Sowohl Bildungswärmen als auch Bindungsabstände von verschiedenen Molekülarten sind in guter Übereinstimmung mit den experimentellen Daten.

Une nouvelle méthode pour le calcul des propriétés moléculaires est presentée, dans laquelle les intégrales monocentriques sont evaluées dans leur environnement (ajustées à la molécule), au lieu d'être transférées du calcul atomique.

Le procédé peut être incorporé dans n'importe quel schema SCF qui utilise un «basis set» minimal.

Dans cet article, le procédé est illustré par l'utilisation d'un schema INDO.

Les chaleurs de formation et les distances de liaison pour plusieurs types de molécules sont trouvées en accord satisfaisant avec l'experience.

1. Introduction

The first semiempirical methods for the Self Consistent Field Calculation of σ bonded molecules were introduced six years ago [1]. Since then, several procedures specifically designed for the calculation of particular properties, have been proposed [2–6]. These procedures often utilize the original framework but differ from it sometimes by some minor adjustment of parameters or by some feature expecially designed to allow a specific property to be calculated, such as interaction of configuration for spectra [3].

---

* Present address: Institute of Physical Chemistry, Czechoslovak Academy of Sciences, Machova ul. 7, Praha 2, Czechoslovakia.

Although the approximations used for evaluating the various integrals are widely varied, the orbital energies and density matrices remain astonishingly similar in all these methods. A further remarkable similarity is that they consistently fail to account for ground and excited state properties consistently. Moreover, even for ground state molecules, it does not seem to be possible to obtain good values for bond distances and heats of formation simultaneously.

The total heat of formation of a molecule results from the intrinsic combination of electronic energy and core repulsions. Although the core repulsions are relatively easy to approximate and, if this is done (i.e., CNDO [4], INDO [2]), relatively good bond distances can be obtained (by minimization), the heats of formation are several orders of magnitude larger than those experimentally observed. If on the other hand, one wants to correlate the heats of formation, one has to decrease arbitrarily the core repulsion (*i.e.*, PNDO [5], MINDO [6]). By doing this, however, bond distances are usually found to be too short.

It thus appears that, at the present time, we are in possession of several powerful theoretical methods which are designed either for ground state energies, bond distances or transition energies calculations. However, one may argue that a sound method should be able to reproduce all three sets of properties. The fact that these methods do not, may mean that one is overlooking some important property which jeopardizes any new type of calculation such as the interpretation of NMR, IR or chemical reactivity data.

Numerous reasons may be invoked as responsible for such discrepancies including even the possibility that such crude methods cannot be expected to yield all these results. However, several routes which have not been investigated as yet, may still be open for improvement. One of these involves a reexamination of the "common to all semiempirical SCF methods" way of determining the one center integrals. These integrals are determined semiempirically by comparing the experimental and calculated ionization potentials of atoms. One may speculate however that such a procedure does not properly take into account the molecular environment and thus neglects the resulting expansion or contraction of the atomic orbitals on which the molecular orbitals are built. The neglect of this expansion of orbitals explains precisely the observed discrepancy between ground and excited states, and also the necessity of decreasing arbitrarily the nuclear interactions in order to obtain satisfactory bond energies.

In a previous communication [7], we have presented a new semiempirical method for the calculation of one center integrals involving scaled Slater orbitals. We now wish to present a method for the calculation of molecular properties in which the one center integrals are evaluated within their environment (scaled in the molecule) rather than treated as parameters carried over from atomic structures. The proposed method for the calculation of atomic terms might be, of course, incorporated in any numerical scheme using a minimum basis set of atomic orbitals, including an *ab initio* calculation method. In this article we are illustrating the procedure within an INDO [2] framework of approximations because of its intermediate complexity between the CNDO-type and *ab initio* type calculations. We believe with it, to gain a proper insight into the effect of using the variable exponent method to calculate molecular properties.

2. Theory

For a closed shell INDO type Hamiltonian, the elements of the Hartree-Fock matrix $F_{\alpha\beta}$ can be expressed as

$$F_{\alpha\beta} = H_{\alpha\beta} + G_{\alpha\beta}\,, \tag{1}$$

where, if $\alpha = \beta$ and the atomic orbital α is centered on atom I,

$$\begin{cases} H_{\alpha\alpha} = [\alpha| -\frac{1}{2}\Delta - V_{\mathrm{I}}|\alpha] + \sum\limits_{\mathrm{J}(\neq \mathrm{I})} [\alpha| - V_{\mathrm{J}}|\alpha]\,. \\ G_{\alpha\alpha} = \sum\limits_{\gamma\in(\mathrm{I})} P_{\gamma\gamma}\{[\alpha^2|\gamma^2]^{\mathrm{I}} - \frac{1}{2}[\alpha\gamma|\alpha\gamma]^{\mathrm{I}}\} \\ \qquad + \sum\limits_{\mathrm{J}(\neq \mathrm{I})} \sum\limits_{\kappa\in(\mathrm{J})} P_{\kappa\kappa}[\alpha^2|\kappa^2]^{\mathrm{I},\mathrm{J}} \end{cases} \tag{2}$$

and, if $\alpha \neq \beta$,

$$\begin{cases} H_{\alpha\beta} = h(\alpha,\beta)\,\beta_{\alpha\beta}\,, \\ G_{\alpha\beta} = \frac{1}{2}P_{\alpha\beta}\{(3[\alpha\beta|\alpha\beta]^{\mathrm{I}} - [\alpha^2|\beta^2]^{\mathrm{I}})\,\delta_{\mathrm{IJ}} - [\alpha^2|\beta^2]^{\mathrm{I},\mathrm{J}}(1-\delta_{\mathrm{IJ}})\}\,. \end{cases} \tag{3}$$

In these formulae, the Greek letters refer to atomic orbitals, the capital letters refer to atoms, the summation $\sum\limits_{\gamma\in(\mathrm{I})}$ extends over the AO's centered on atom I, P is the charge density – bond order matrix, and δ_{IJ} is the Kronecker symbol:

$$\delta_{\mathrm{IJ}} = \begin{cases} 1, \text{ if the AO's } \alpha \text{ and } \beta \text{ belong to the same atom} \\ 0, \text{ if the AO's } \alpha \text{ and } \beta \text{ belong to two different atoms I and J}\,. \end{cases}$$

All other symbols are the same as those used in Paper I of this series or will be specified later on. The total molecular energy can be expressed as

$$E_{\mathrm{tot}} = \tfrac{1}{2}\,(\mathrm{Tr}(\boldsymbol{H} + \boldsymbol{F})\,\boldsymbol{P}) + \text{Core-Core inter. terms.} \tag{4}$$

The problem which specifically interests us here consists in deriving a procedure for the minimization of the total energy of a molecule, E_{tot}, not only with respect to the coefficients of the atomic orbitals but also to the exponents of a minimal basis set of STO functions. In this paper, the treatment will be restricted to molecules composed only of first and second row elements. Due to the space invariance requirement, it will be necessary to assign identical exponents to the various p orbitals centered on any given atom. Thus, in addition to the usual quantities that are being optimized in classical SCF theories, *i.e.*, coefficients of atomic orbitals, one (for H atom) or two (for second row atoms) additional variational parameters will have to be optimized per atom. Assuming a first order approximation to the $\boldsymbol{P}$ matrix, the optimized atomic exponents might be determined according to the variation principle by setting the corresponding partial derivatives of the total molecular energy equal to zero.

For the sake of convenience, let us use the indices μ and λ (or Λ) for the s- and p-orbitals, respectively, and let the index v refer to either kind. If I defines the specific atom, the result of the variation procedure can be expressed as the following nonlinear system of equations of the s-orbital exponents $a_I(\mu)$ and the p-orbital exponents $a_I(\lambda)$ of all atoms ($I = A, B, \ldots K$) composing the molecule:

$$\begin{aligned} a_I(\mu) = K_s^I \Bigg\{ & \frac{Z_s^I}{N_s^I} - \frac{1}{4} P_{\mu\mu} \frac{\partial[\mu^2|\mu^2]^I}{\partial a_I(\mu)} \\ & + \left(\frac{\sum\limits_{A\in(I)} P_{\mu A}^2}{2P_{\mu\mu}} - \sum_{A\in(I)} P_{AA} \right) \frac{\partial[\mu^2|\lambda^2]^I}{\partial a_I(\mu)} \\ & + \frac{1}{2} \left(\sum_{A\in(I)} P_{AA} - \frac{3}{P_{\mu\mu}} \sum_{A\in(I)} P_{\mu A}^2 \right) \frac{\partial[\mu\lambda|\mu\lambda]^I}{\partial a_I(\mu)} - \frac{\partial U_s^I}{\partial a_I(\mu)} \Bigg\}, \end{aligned} \tag{5}$$

$$\begin{aligned} a_I(\lambda) = K_p^I \Bigg\{ & \frac{Z_p^I}{2} - \frac{1}{4} \frac{\sum\limits_{A\in(I)} P_{AA}^2}{\sum\limits_{A\in(I)} P_{AA}} \cdot \frac{\partial[\lambda^2|\lambda^2]^I}{\partial a_I(\lambda)} \\ & + \left(\frac{\sum\limits_{A\in(I)} P_{\mu A}^2}{2 \cdot \sum\limits_{A\in(I)} P_{AA}} - P_{\mu\mu} \right) \frac{\partial[\lambda^2|\mu^2]^I}{\partial a_I(\lambda)} \\ & + \frac{1}{2} \left(P_{\mu\mu} - \frac{3 \cdot \sum\limits_{A\in(I)} P_{\mu A}^2}{\sum\limits_{A\in(I)} P_{AA}} \right) \frac{\partial[\lambda\mu|\lambda\mu]^I}{\partial a_I(\lambda)} \\ & + \frac{1}{\sum\limits_{A\in(I)} P_{AA}} \left(\frac{\sum\limits_{A<A^*\in(I)}\sum P_{AA^*}^2}{2} - \sum_{A<A^*\in(I)}\sum P_{AA} \cdot P_{A^*A^*} \right) \frac{\partial[\lambda^2|\lambda^{*2}]^I}{\partial a_I(\lambda)} \\ & + \frac{1}{\sum\limits_{A\in(I)} P_{AA}} \left(\frac{1}{2} \sum_{A<A^*\in(I)}\sum P_{AA} \cdot P_{A^*A^*} - \frac{3}{2} \sum_{A<A^*}\sum P_{AA^*}^2 \right) \\ & \cdot \frac{\partial[\lambda\lambda^*|\lambda\lambda^*]^I}{\partial a_I(\lambda)} - \frac{\partial U_r^I}{\partial a_I(\lambda)} \Bigg\}, \end{aligned} \tag{6}$$

where

$$\begin{aligned} U_s^I = \sum_{J(\neq I)} \Bigg\{ & [\mu| - V_J|\mu] + 2\beta_{IJ} \frac{1}{P_{\mu\mu}} \sum_{\nu\in(J)} P_{\mu\nu} h(\mu, \nu) \\ & + [\mu^2|\mu'^2]^{I,J} \left(P_{\mu'\mu'} - \frac{P_{\mu\mu'}^2}{2 \cdot P_{\mu\mu}} \right) + [\mu^2|\lambda'^2]^{I,J} \qquad (\\ & \cdot \left(\sum_{A'\in(J)} P_{A'A'} - \frac{1}{2P_{\mu\mu}} \sum_{A'\in(J)} P_{\mu A'}^2 \right) \Bigg\} \end{aligned}$$

and

$$\begin{aligned} U_p^{\mathrm{I}} = \sum_{\mathrm{J}(\neq \mathrm{I})} \Bigg\{ & [\lambda| - V_{\mathrm{J}}|\lambda] + \frac{2\beta_{\mathrm{IJ}}}{\sum\limits_{\Lambda\in(\mathrm{I})} P_{\Lambda\Lambda}} \sum_{\substack{\Lambda\in(\mathrm{I}) \\ \nu\in(\mathrm{J})}} P_{\Lambda\nu} \cdot h(\Lambda,\nu) \\ & + [\lambda^2|\mu^2]^{\mathrm{I,J}} \left(P_{\mu'\mu'} - \frac{1}{2\cdot\sum\limits_{\Lambda\in(\mathrm{I})} P_{\Lambda\Lambda}} \sum_{\Lambda\in(\mathrm{I})} P_{\Lambda\mu'}^2 \right) \\ & + [\lambda^2|\lambda'^2]^{\mathrm{I,J}} \cdot \frac{1}{\sum\limits_{\Lambda\in(\mathrm{I})} P_{\Lambda\Lambda}} \sum_{\Lambda\in(\mathrm{I})} \sum_{\Lambda'\in(\mathrm{J})} (P_{\Lambda\Lambda} P_{\Lambda'\Lambda'} - \tfrac{1}{2} P_{\Lambda\Lambda'}^2) \Bigg\}. \end{aligned} \tag{8}$$

Again, the notation corresponding to atomic terms is the same as in paper I.

The numerical solution of the total variation problem can be achieved by means of a double iteration procedure, based alternatively on the minimization of the total energy with respect to the linear coefficients of the STO's and to exponents.

3. Evaluation of Integrals

a. Evaluation of Atomic Integrals

In the first paper of this series [7] two alternative parameter schemes were given, differing by the fact that either the effective nuclear charges Z_s and Z_p, or the kinetic factors K_s and K_p were treated as parameters. However, in all the cases that were investigated, it was found that within a uniquely defined molecular parameter scheme, both ground state energies and charge distributions do not differ substantially when calculated according to either the first or the second parameter scheme. Parameter scheme 1 however, seems sounder from a physical point of view and will therefore be used for the discussion and further calculations.

b. Evaluation of Molecular Integrals and Terms

The Coulomb integrals $[\alpha^2|\beta^2]^{\mathrm{I,J}}$ respresenting the interaction between electrons occupying orbitals α and β localized on centers I and J, respectively, are reduced to interactions involving exclusively s atomic orbitals as in the CNDO [4] and INDO [2] methods; the only difference being that, here, the corresponding Slater exponents $a_{\mathrm{I}}(\alpha)$, and $a_{\mathrm{J}}(\beta)$ are optimized.

The two-center electron-core attraction integrals are also calculated as in the CNDO or INDO methods, *i.e.*,

$$[\alpha|V_{\mathrm{J}}|\alpha] = Z_{\mathrm{J}}[\alpha^2|\eta^2]^{\mathrm{I,J}}, \tag{9}$$

where the α orbital with the varied orbital exponent $a_{\mathrm{I}}(\alpha)$ is centered on atom I and the s orbital η has a fixed exponent a_{av} calculated as a weighted average of the s- and p-atomic exponents a_s^0 and a_p^0, corresponding to the maximum multiplicity of atomic J, *i.e.*,

$$K = \text{Integer}\,(Z_{\mathrm{J}} + 7/6),$$

$$a_{\mathrm{av}} = \frac{K \cdot a_s^0 + (Z_{\mathrm{J}} - K)\, a_p^0}{Z_{\mathrm{J}}}, \tag{10}$$

where Z_J is the charge of the core J, equal to 1 for the H atom and equal to the atomic number diminished by 2 for all other atoms. (The numerical values of a_s^0 and a_p^0 are listed in Table 3 of Ref. [7].)

In addition, we define the total core-core interaction as

$$\text{Core-Core inter. terms} = \sum_{I<J}\sum \frac{Z_I Z_J}{R_{IJ}}. \tag{11}$$

A little longer discussion will be needed to estimate the best form of the resonance integrals corresponding to the off-diagonal terms of the H matrix defined in Eqs. (2) and (3).

Let us first assume that $h(\alpha, \beta)$ can be expressed as

$$h(\alpha, \beta) = -\{a(\alpha) + a(\beta)\}\, S_{\alpha\beta}, \tag{12}$$

where $S_{\alpha\beta}$ is the overlap integral between the corresponding STO functions having optimized exponents $a(\alpha)$ and $a(\beta)$. Such an expression accounts for the geometrical constraint appropriate to the resonance integrals and partly for the nature of orbitals as well. In addition, since all AO's localized on any given centre are orthonormal, only cofactors $\beta_{\alpha\beta}$ for AO's belonging to different atoms have to be considered. As $\beta_{\alpha\beta}$ then depends only on the type of atoms involved, it is possible to write

$$\beta_{\alpha\beta} = \beta_{IJ}.$$

The form of the cofactor β_{IJ} was estimated by comparing calculated and experimental heats of atomization of some diatomic and hydride molecules. However, since there are not enough suitable molecules for an unambiguous determination of all β_{IJ}'s, the fitting procedure was extended to several points of the Morse curves corresponding to a few of these diatomic molecules. The results are collected in Fig. 1 as a function β_{IJ} of the internuclear separation R between atoms I and J. Points corresponding to the same Morse curve are joined by a full tine.

The β-dependence on R for the hydrogen molecule was expressed analytically as

$$\beta_{HH} = F_H(R) + 0.06206, \tag{13}$$

where

$$F_H(R) = 0.12181/(R + 0.18609). \tag{14}$$

These numerical constants were chosen to fit exactly the points of the Morse curve of the H_2 molecule corresponding to the equilibrium distance and to the separations of the hydrogen nuclei of 1.0 and 2.0 a.u. The determination of the β-values for X-H bonds in polyatomic hydrides was carried out using the relationship (13) for the calculation of $H_{\mu\nu}$ elements.

From Fig. 1 it can be seen that for most types of bonds, (see however F_2) the β-values decrease with increasing bond distance along a specific pattern that seems to be describable by an expression such as:

$$\beta_{IJ}(R) = F(R) + C(Z), \tag{15}$$

where

$$
\begin{aligned}
Z &= Z_I, \quad \text{if} \quad Z_I \geqq Z_J, \\
Z &= Z_J, \quad \text{if} \quad Z_J \geqq Z_I,
\end{aligned}
\tag{16}
$$

$F(R)$ can thus be treated as a common function for all atoms. The constants $C(Z)$ are atomic parameters related for each bond to that atom having from both ones the larger core charge. Two exceptions only seem to violate these rules, the F_2 molecule and the Li_2 molecule, the latter corresponding to fitted values $\beta = 0.0344$ at $R = 4.5$ a.u., $\beta = 0.0374$ at $R = 5.051$ a.u., and $\beta = 0.0393$ at $R = 5.5$ a.u.

Accordingly, two versions of expressing $\beta_U(R)$ are suggested. In the Version-I no additional specific atomic parameters are introduced at all and we set

$$\beta_U(R) = F_H(R) + 0.0955 + (Z - Z_C) \cdot 0.016\,, \tag{17}$$

where Z_C is the charge of the carbon core and Z is defined by means of Eq. (16). We are clearly putting here preference to the hydrocarbons because the value 0.0955 is chosen to fit heats of atomization of hydrocarbons containing one and two carbon atoms. Of course, from Fig. 1 it can be seen that the β-dependence on R given by the functions $F_H(R)$ is not steep enough, at least for all bonds shorter than 2.3 a.u.

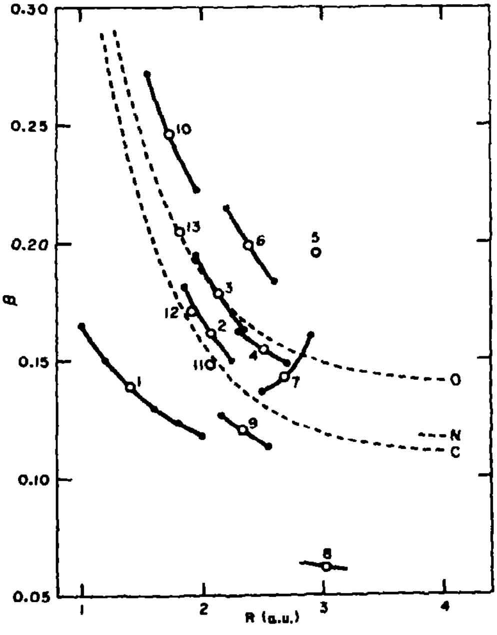

Fig. 1. β parameter as a function of internuclear distance R. Circles correspond to values matching experimental heats of atomization of corresponding molecules, full curves correspond to values fitted by means of Morse curves. (1, H_2; 2, N_2; 3, CO; 4, BeO; 5, LiF; 6, BF; 7, F_2; 8, LiH; 9, BH; 10, FH; 11, CH_4; 12, NH_3; 13, H_2O)

Alternatively, one may select a more appropriate function $F(R)$ for compounds composed of oxygen, nitrogen, carbon and hydrogen such as

$$F(R) = 1.1657 \cdot \exp(-1.5897 \cdot R) \tag{18}$$

and define in addition

$$\begin{aligned} C(4) &= 0.1090 \text{ (carbon)} \\ C(5) &= 0.1150 \text{ (nitrogen)} \\ C(6) &= 0.1390 \text{ (oxygen)}. \end{aligned} \tag{19}$$

The β_{HH} values remain as defined via Eqs. (13) and (14). The dependences of $\beta_{ij}(R)$ vs. R defined in this way correspond to Version-II and is represented in Fig. 1 for all three cases by dashed curves. Version-II is thus limited to calculations of molecules containing only hydrogen, carbon, nitrogen and oxygen atoms.

4. Numerical Solution

Since most of the time the numerical solution of the system of equations given by Eqs. (5) and (6) does not converge when a first order iteration process is used, the Crout's [8] modification of the Newton-Raphson procedure was applied for solving the problem. The proper solution of finding the stationary value of the total energy given by Eq. (4) consisted of a double iteration procedure composed successively of one iteration step considering the P matrix as variable with the Slater exponents fixed and of the next iteration step improving the exponents with the P matrix fixed. Of course, for the second iteration step first and second derivatives with respect to Slater exponents of all kinds of integrals are needed. Whereas the expressions of one-centre terms were calculated using analytical forms of the derivatives, all two-centre terms were calculated using numerical derivation, e.g.

$$\frac{\partial f(a,b)}{\partial a} = \frac{f(a+\Delta,b)-f(a-\Delta,b)}{2\Delta}. \tag{20}$$

It was found that such a procedure yields satisfactory numerical results for the derivatives of all integrals using the value $\Delta = 0.01$. A convergence criterion was imposed upon the total energy requiring the energy difference of two successive iteration steps to be smaller than 10^{-5} a.u. In order to get faster convergence for the calculations of molecules C_2N_2 and N_2O the criterion was lowered to 5×10^{-5} a.u.

The initial P matrix was obtained by solving a secular problem in which the $F_{\mu\mu}$ terms were replaced by the average ionization potentials (Table 2, Paper I) and $F_{\mu\nu}$, $(\mu \neq \nu)$ set equal to $H_{\mu\nu}$ calculated with atomic Slater exponents (cf. Table 3 and 4, Paper I).

On several examples of molecular calculations it was verified that the iteration procedure does not depend on the way it proceeds, particularly on the order of iteration steps. In addition, the authors believe that the initial values of Slater exponents taken as atomic ones ensure that this specific solution of the nonlinear system of Eqs. (5) and (6) by means of the proposed procedure is the physically meaningful solution among all possible ones.

All calculations were performed on the UNIVAC 1108 computer using a FORTRAN V program written by the authors.

5. Experimental Data

Most experimental data of both equilibrium geometries and heats of atomization at 0° K (or dissociation energies D_0^0 and eventually other "Morse curve" parameters of diatomics) were taken from JANAF Interim Thermochemical Tables [9]. Only equilibrium geometries of molecules CHN, C_2H_2, C_2H_4, C_2H_6 [10], the heat of atomization at 0° K for ethane [11], data for diatomics LiH and the D_0^0 value for F_2 [13] were taken elsewhere.

6. Results and Discussion

The general method of calculation of ground state properties described in the previous sections has been applied to a number of diatomic and polyatomic molecules as listed in Table 2. First of all, let us stress in comparison with other existing semiempirical all-valence electron methods (CNDO [4], INDO [2], PNDO [5], MINDO [6] *et al.*) that – besides the general function $F(R)$ – only one specific parameter per atom (Version-I) was introduced to extend the atomic SCF theory with "scaled" Slater exponents to molecular structures. The parameter scheme resembles the CNDO-2 or INDO scheme, but no presumptions concerning the values of Slater exponents needed to be made.

Table 1. Equilibrium geometries of calculated polyatomic molecules (in a.u.)

Molecule		Cartesian coordinates		
		x	y	z
H_2O	O	0.0	0.0	0.0
	H1	−1.431571	−1.109440	0.0
	H2	1.431571	−1.109440	0.0
NH_3	N	0.0	0.0	0.721183
	H1	−1.534653	−0.886033	0.0
	H2	1.534653	−0.886033	0.0
	H3	0.0	1.772065	0.0
CH_4	C	0.0	0.0	0.0
	H1	1.190341	1.190341	1.190341
	H2	1.190341	−1.190341	−1.190341
	H3	−1.190341	1.190341	−1.190341
	H4	−1.190341	−1.190341	1.190341
C_2H_2	C1	0.0	0.0	0.0
	C2	2.281	0.0	0.0
	H1	−2.002	0.0	0.0
	H2	4.283	0.0	0.0
CO_2	C	0.0	0.0	0.0
	O1	0.0	0.0	2.195904
	O2	0.0	0.0	−2.195904

Table 1 (continued)

Molecule		Cartesian coordinates		
		x	*y*	*z*
C_2H_4	C1	0.0	0.0	0.0
	C2	0.0	0.0	2.551160
	H1	1.751130	0.0	-1.011015
	H2	-1.751130	0.0	-1.011015
	H3	1.751130	0.0	3.562176
	H4	-1.751130	0.0	3.562176
C_2H_6 (st.)	C1	0.0	0.0	0.0
	C2	0.0	0.0	2.915876
	H1	1.961630	0.0	-0.699148
	H2	-0.980815	1.698822	-0.699148
	H3	-0.980815	-1.698822	-0.699148
	H4	-1.961630	0.0	3.615024
	H5	0.980815	-1.698822	3.615024
	H6	0.980815	1.698822	3.615024
C_2H_6 (ecl.)	C1	0.0	0.0	0.0
	C2			2.915876
	H1	1.961630	0.0	-0.699148
	H2	-0.980815	1.698822	-0.699148
	H3	-0.980815	-1.698822	-0.699148
	H4	1.961630	0.0	3.615024
	H5	-0.980815	1.698822	3.615024
	H6	-0.980815	-1.698822	3.615024
H_2CO	C	0.0	0.0	0.0
	O	2.286613	0.0	0.0
	H1	-1.090096	1.814224	0.0
	H2	-1.090096	-1.814224	0.0
HCN	C	0.0	0.0	0.0
	N	0.0	0.0	2.187
	H	0.0	0.0	-2.0
C_2N_2	C1	0.0	0.0	0.0
	C2	0.0	0.0	2.607872
	N1	0.0	0.0	-2.186455
	N2	0.0	0.0	4.794328
N_2O	N1	0.0	0.0	0.0
	N2	0.0	0.0	2.132030
	O	0.0	0.0	4.369887
HNO	H	0.0	-1.927558	0.0
	N	0.0	0.0	0.0
	O	2.131951	0.967994	0.0
HNO_2 *cis*	H	1.804502	-0.41602	0.0
	N	0.0	2.759053	0.0
	O1	0.0	0.0	0.0
	O2	2.071661	3.681416	0.0
O_3	O1	0.0	0.0	0.0
	O2	2.415117	0.0	0.0
	O3	-1.088921	2.155700	0.0

Table 2. Heats of atomization (in a.u.)

Molecule	Exptl.	INDO	Version-I	Version-II
H_2	0.1746	0.1972	0.1746	0.1746
Li_2	0.0419	0.5037	0.1131	–
LiH	0.0942	0.2098	0.1419	–
BH	0.1300	0.3437	0.1541	–
F_2	0.0594	0.2133	0.1716	–
HF	0.2247	0.2114	0.0829	–
LiF	0.2186	−0.0756	0.1766	–
BeO	0.1723	0.1876	0.2990	0.2136
BF	0.2980	0.3744	0.2521	
CO	0.4125	0.7043	0.4281	0.4124
N_2	0.3639	0.7279	0.4002	0.3254
H_2O	0.350	0.445	0.228	0.350
BH_3	0.345 0.414	1.081	0.464	
NH_3	0.441	0.772	0.428	0.445
CH_4	0.625	1.371	0.671	0.717
C_2H_2	0.618	1.689	0.685	0.673
C_2H_4	0.846	2.125	0.841	0.816
C_2H_6 (st.)	1.063	2.602	1.021	1.008
C_2H_6 (ecl.)		2.598	1.008	0.996
O_3	0.227	0.797	0.454	0.363
CH_2O	0.571	1.235	0.568	0.547
CHN	0.482	1.153	0.605	0.519
$(CN)_2$	0.782	2.220	–	0.756
CO_2	0.608	1.148	0.661	0.597
N_2O	0.402	1.102	0.469	0.418
HNO	0.317	0.762	·	0.391
HNO_2 *cis*	0.476	1.118		0.578

Heats of atomization calculated from our theory are shown in Table 2. It may be seen that the method, particularly its Version-II, works fairly well and its results compare much better to experimental values than the regular INDO-type calculations. Moreover, equilibrium distances come out very well, as can be seen from Fig. 2 and Fig. 3, where a few types of dependences of heats of formation on geometry variations are presented. These results seem to be very encouraging, since the correct energy - bond distance relationship was lacking in all semi-empirical methods described previously, unless ample parametrization is performed [14, 6].

On comparing the results of Table 3, concerning the frontier orbitals, with known experimental ionization potentials [15, 16], it may be noticed that the orbital energies of the highest occupied molecular orbital are bad estimates of the ionization potentials. This effect, of course, could have been expected, since the variation of orbital exponents might only violate the validity of the Koopmans' theorem. If correct theoretical ionization potentials were to be calculated, the exponents of the ionized state would also have to be optimized.

Due to similar reasons *i.e.*, orbital exponents variation, it is also hard to draw relevant conclusions from a conventional "population analysis" procedure based on the charges listed in Table 3. The charges cannot be assigned entirely

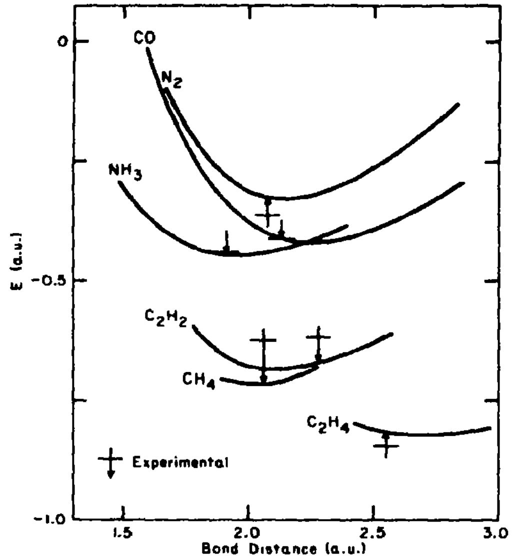

Fig. 2. Heats of atomization as functions of bond distances. Experimental values corresponding to equilibrium geometries are represented by points of intersection of horizontal and vertical lines. For molecules C_2H_2 and C_2H_4, the C C bond is varied. In all cases of bond variation the equilibrium symmetry has been retained

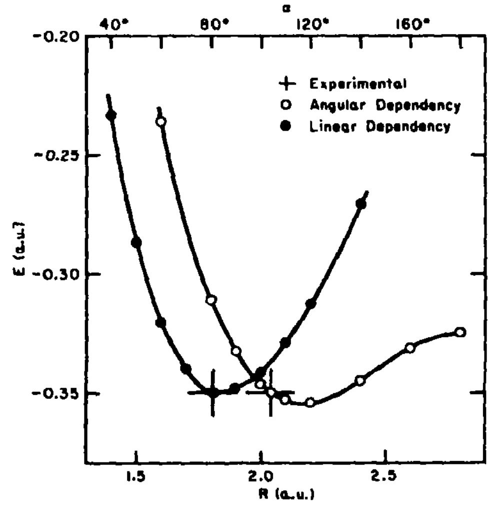

Fig. 3. Heat of atomization of water molecule plotted versus OH bond distance (at the equilibrium bond angle), A, and bond angle (at equilibrium OH bond distance), B, respectively. Experimental values are represented by points of intersection of horizontal and vertical lines

Table 3. Frontier orbital energies (in a.u.), charge densities and optimized exponents (calculated by mean of Version-II)

Molecule	ε_h	ε_l	Atom	P_{vv}				$a(s)$	$a(p)$
				s	p_x	p_y	p_z		
CO	−0.5018	0.1235	C	1.78	0.92	0.58	0.58	2.15	1.55
			O	1.82	1.48	1.42	1.42	2.12	1.95
N_2	−0.5367	0.0845	N	1.80	1.20	1.0	1.0	2.41	1.70
H_2O	−0.6132	0.3777	O	1.78	1.40	1.62	2.0	2.60	1.90
			H	0.60	—	-	–	1.28	
NH_3	−0.5825	0.2868	N	1.61	1.40	1.40	1.79	2.17	1.58
			H	0.60	–	-	-	1.20	—
CH_4	−0.6762	0.2388	C	1.39	1.45	1.45	1.45	1.83	1.31
			H	0.56		—	—	1.11	
C_2H_2	−0.5554	0.1309	C	1.28	0.95	1.0	1.0	2.11	1.50
			H	0.76	—	–	—	1.12	
CO_2	−0.6390	0.1106	C	1.08	0.54	0.54	0.69	2.35	1.82
			O	1.88	1.73	1.73	1.23	2.65	1.92
C_2H_4	−0.4691	0.1281	C	1.25	1.08	1.0	0.98	2.09	1.55
			H	0.84	-	—	- -	1.07	—
C_2H_6 (st.)	−0.4803	0.1523	C	1.205	1.103	1.103	0.992	2.061	1.57
			H	0.866	—	—	-	1.045	-
C_2H_6 (ecl.)	−0.4786	0.1544	C	1.203	1.096	1.096	0.989	2.068	1.57
			H	0.872	–	-		1.044	- -
H_2CO	−0.4692	0.0920	C	1.22	0.86	0.98	0.62	2.18	1.62
			O	1.87	1.24	1.93	1.38	2.66	1.93
			H	0.95	-	--	-	1.06	–
HCN	−0.5787	0.0975	C	1.31	0.91	0.91	1.00	2.15	1.48
			N	1.83	1.09	1.09	1.04	2.40	1.64
			H	0.82	–	- -		1.06	–
C_2N_2	−0.5296	0.0219	C	1.30	0.84	0.84	0.85	2.17	1.58
			N	1.84	1.16	1.16	1.02	2.36	1.64
N_2O	−0.6638	−0.0806	N1	1.86	1.30	1.30	0.79	2.40	1.68
			N2	1.41	0.90	0.90	0.87	2.53	1.77
			O	1.89	1.81	1.81	1.17	2.48	1.76
HNO	−0.4835	0.0231	H	0.85	–	-		1.17	
			N	1.77	1.08	1.23	0.72	2.42	1.78
			O	1.90	1.40	1.78	1.28	2.68	1.92
HNO_2	−0.5518	0.0194	H	0.58	-	-	-	0.96	-
			N	1.88	0.90	0.67	0.55	2.58	1.95
			O1	1.85	1.56	1.57	1.93	2.60	1.88
			O2	1.90	1.45	1.67	1.52	2.62	1.96
O_3	−0.5939	−0.1209	O1	1.87	1.19	1.28	0.95	2.83	2.12
			O2	1.95	0.92	1.95	1.53	2.66	1.95
			O3	1.95	1.66	1.21	1.53	2.66	1.95

to specific centers anymore since the orbitals vary in size from molecule to molecule and the corresponding density functions may have their maxima at different distances from the nucleus. In addition, it is known from *ab initio* calculations that an energy optimization with respect to orbital exponents mostly leads to a deterioration of values of dipole moments [17].

In conclusion, we should like to express that we are aware of the fact that there might exist other better molecular parameter schemes for incorporating our basic ideas developed in Paper I, that is the proper consideration of atomic environment and atomic contributions to electron correlation. From that point of view, this paper has thus to be considered as preliminary.

Acknowledgement. The authors gratefully acknowledge support of this work by a grant from the National Science Foundation, Grant No. GP-19985.

References

1. Klopman, G.: J. Amer. chem. Soc. **86**, 1463, 4550 (1964); **87**, 3300 (1965); Pohl, H. A., Appel, R., Appel, K.: J. chem. Physics **41**, 3385 (1964); Pople, J. A., Santry, D. P., Segal, G. A.: J. chem. Physics **43**, S 129 (1965).
2. Pople, J. A., Beveridge, D. L., Dobosh, P. A.: J. chem. Physics **47**, 2026 (1967).
3. Del Bene, J., Jaffé, H. H.: J. chem. Physics **48**, 1807 (1968).
4. Pople, J. A., Segal, G. A.: J. chem. Physics **44**, 3289 (1966).
5. Dewar, M. J. S., Klopman, G.: J. Amer. chem. Soc. **89**, 3089 (1967).
6. Baird, N. C., Dewar, M. J. S.: J. chem. Physics **50**, 1262 (1969).
7. Klopman, G., Polak, R., Theoret. chim. Acta (Berl.) **22**, 130 (1971)
8. Crout, P. D.: Trans. American Inst. of Electrical Engineers **60**, 1235 (1941).
9. JANAF Interim thermochemical tables, Midland, Michigan: 1960 and revised Tables, 1965.
10. Palke, W. E., Lipscomb, W. N.: J. Amer. chem. Soc. **88**, 2384 (1966).
11. Selected values of chemical thermodynamic properties. Circular of the National Bureau of Standards 500 Washington: U.S. Government Printing Office 1952.
12. Herzberg, H.: Molecular spectra and molecular structure, Vol. I. Toronto: D. Van Nostrand Company, Inc 1967.
13. Klopman, G.: J. Amer. chem. Soc. **86**, 4550 (1964).
14. Sichel, J. M., Whitehead, M. A.: Theoret. chim. Acta (Berl.) **11**, 220 (1968).
15. Cermak, V.: Coll. Czech. Chem. Commun. **33**, 2739 (1968).
16. Whitehead, M. A.: Sigma molecular theory, ed. by O. Sinanoglu and K. B. Wiberg, p. 49. New Haven and London: Yale University Press 1970.
17. Urban, M.: Private communication.

Prof. Dr. G. Klopman
Department of Chemistry
Case Western Reserve University
Cleveland, Ohio 44106, USA

Theoret. chim. Acta (Berl.) 25, 237—247 (1972)
© by Springer-Verlag 1972

The Influence of Solvation on the Calculated Activation Energy for the Reaction $CH_3F + F^-$

P. Cremaschi, A. Gamba, and M. Simonetta

Institute of Physical Chemistry, University of Milano, Milano, Italy

Received December 3, 1971

The influence of the solvent on the activation energy of the synchronous, concerted, narcissistic reaction: $CH_3F + F^- \rightarrow |CH_3F_2|^- \rightarrow FCH_3 + F^-$, has been investigated by means of CNDO/2 method. The reaction path has been fully followed *in vacuo*, and at a suitable point only, of reaction coordinate, in solution. The geometries of H_2O, F^-, CH_3F, and $|CH_3F_2|^-$, *in vacuo* and in different hydrated cages, have been optimized.

Der Einfluß des Lösungsmittels auf die Aktivierungsenergie der synchronverlaufenden Reaktionen $CH_3F + F^- \rightarrow |CH_3F_2|^- \rightarrow FCH_3 + F^-$, wurde mit der CNDO/2 Methode geprüft. Der Reaktions-Ablauf wurde in Vakuum vollkommen und in der Lösung an einem geeigneten Punkt der Reaktionskoordinate durchgeführt. Die Geometrien von H_2O, F^-, CH_3F, und $|CH_3F_2|^-$ im Vakuum und in verschiedenen hydrierten Käfigen wurden optimalisiert.

L'influence du solvent sur l'énergie d'activation de la réaction synchronique, concertée, narcissistique: $CH_3F + F^- \rightarrow |CH_3F_2|^- \rightarrow FCH_3 + F^-$ a été examinée par la méthode CNDO/2. On a suivie l'entier chemin de réaction *in vacuo*, alors qu'on a observé un seul point convenable de la coordonée de réaction en solution. On a optimize les géometries de H_2O, F^-, CH_3F, et $|CH_3F_2|^-$ *in vacuo* et en differentes cages hydratés.

Introduction

The electronic structure of initial and transition states for nucleophilic substitution reactions have been extensively investigated in the past few years [1–5]. The symmetrical SN 2 reaction:

$$F^- + CH_3F \rightarrow [CH_3F_2]^- \rightarrow FCH_3 + F^- \qquad (1)$$

is a case in which reactants and products are identical, and is an example of synchronous, concerted narcissistic reaction [6].

The reaction path in the vacuo has been studied by Veillard *et al.* [7–8] through *ab initio* MO calculation on Gaussian basis, that is each atomic orbital is a linear combination of gaussian functions (GTO).

Particular attention has been given to the choice of the basis set. When no polarization functions were included in the basis the transition state was found to be more stable than the reactants. An activation energy of 7.9 kcal/mole has been found when *d* orbitals on carbon and fluorine atoms were introduced. On other hand it has been pointed out that the variation of solvation energy is generally competitive, and in the present case prevailing on the variation of inner energy of the system, in determining the activation energy.

The role of the solvent on the energy and electronic structure of initial and transition states for reaction (1), is here investigated by means of theoretical calculations. The complexity of the system and the amount of computational time discourage from employing *ab initio* methods; consequently the study of the reaction:

$$F^-_{aq} + CH_3F_{aq} \rightarrow [CH_3F_2]^-_{aq} \qquad (2)$$

has been performed within the framework of a semiempirical MO LCAO method; namely the energy of these systems have been calculated by the CNDO/2 method [9] as a function of bond-lengths and bond-angles.

Calculations

CNDO calculations have been performed following the standard procedure with a program written by Santry [10], and using the parameters assigned by Pople and Segal [9]. The geometry and the electronic structure for H_2O, F^-, CH_3F, and $CH_3F_2^-$ systems, *in vacuo* and in different hydration cages, have been optimized through an energy minimizing process. When more complex systems are involved we have been forced to limit the number of geometrical parameters to be optimized following criteria that will be discussed at due time. In a first stage of calculations an indicative value for the hydration energy has been obtained as the difference between the energy of the hydrated cage and that of the corresponding isolated units. To study the path followed by the system in going from reactants to products and to evaluate the energy changes, several points have been calculated along the reaction path. For the hydrated system only one intermediate point has been determined for a suitable value of the reaction co-ordinate.

Results

1. $(H_2O)_n$ $(n = 1, 2, 4, 6)$

The isolated water molecule, the dimer, tetramer and hexamer have been considered. The structures taken into consideration are drawn schematically in Fig. 1, where the point group symmetry, the variables to be optimized and the net-charges for the optimized geometry are also reported.

The minimum-energy geometry for isolated water corresponds to a bond-length (r) of 1.029 Å and a bond angle (θ) of 104° 30′ [1]. For the oligomers the O–H bond-lengths not involved in hydrogen bridges were kept constant at $r = 1.029$ Å in all our calculations.

The minimum-energies (in a.u.), stabilization energy (in kcal/mole) and the optimized geometrical parameters for the different structures are collected in Table 1.

---

[1] This result agrees with the values obtained by Burton and Daly [11].

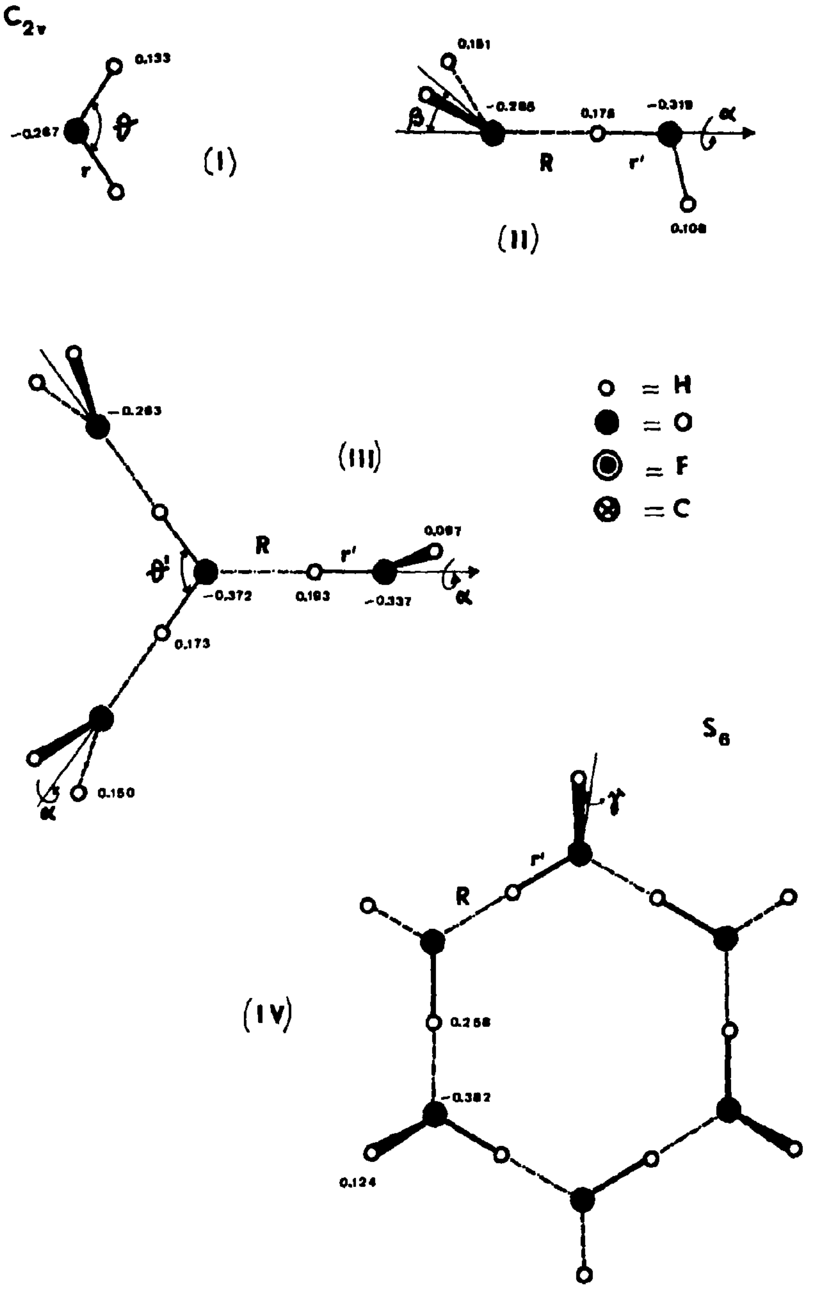

Fig. 1. Optimized geometries for water oligomers. Letters indicate the optimized variables and figures the net-charges

Table 1. Minimum and stabilization energies, and optimized geometry for water (distances in Å; angles in degree)

	E (a.u.)	ΔE (kcal/mole)	r	θ	R	r'	θ'	α	β	γ
I	- 19.8912		1.029[a]	104° 30′						
II	- 39.7960	4.30			1.498	1.043		0°	0°	
III	- 79.6074	6.68			1.487	1.036	105° 12′	0°		
IV	- 119.4593	11.72			1.357[b]	1.068				52°

[a] Experimental values. $r = 0.9571$ Å, $\theta = 104°\ 32'$ [13a].

[b] The calculated distance O O for IV is intermediate between the experimental values found for ice (2.76 Å) [14] and polywater (2.3 Å) [15].

It seems interesting that in the case of structure (IV), the planar model (C_6 symmetry) is less stable than the no planar one (S_6 symmetry) [12]. By inspection of energy data reported in Table 1, a value of about 10–12 kcal/mole may be assigned to the stabilization energy for a mole of solvated water. This value can be favourably compared with the evaporation-heat of water (10.5 kcal/mole [16]).

2. $F^- \cdot nH_2O$ ($n = 0, 2, 4, 6, 8, 12$)

The calculated energy for fluoride ion is −27.4841 a.u. The hydration of the fluoride ion has been studied considering several complexes in which F^- is bound with two, four (tetrahedral cage), six (octahedral cage), eight (cubic cage), and twelve (dodecahedral cage) molecules of water respectively.

The total energy was minimized with respect to the distances r_0 and R_0, shown in Fig. 2, where the complex with $n = 4$ is schematically drawn. The bond-angle and the O H distance of water not interested in hydrogen-bonds were kept constant, that is equal to the values obtained for water molecule.

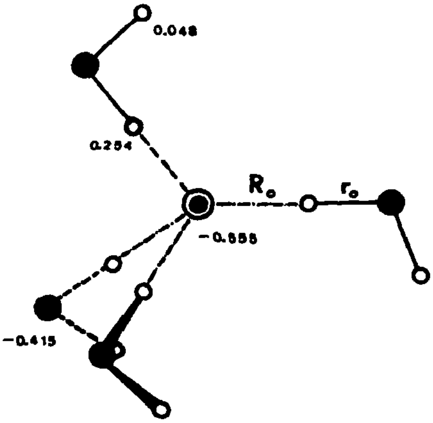

Fig. 2. Geometry for tetrahedral cage of fluoride ion

Table 2. Minimum and stabilization energies, optimized geometries and net-charge on fluorine for $F^- \cdot n H_2O$ systems

$F^- \cdot n H_2O$	E(a.u.)	ΔE(kcal/mole)	r_0(Å)[a]	R_0(Å)[a]	q_F
$n=0$	− 27.4841				−1.00
2	− 67.4559	118.85	1.101	1.221	−0.601
4	−107.3101	163.98	1.067	1.315	−0.555
6	−147.1334	189.57	1.054	1.389	−0.547
8	−186.9248	195.22	1.047	1.481	−0.577
12	−266.4755	186.37	1.042	1.680	−0.660

[a] r_0 and R_0 are defined in Fig. 2.

The more significant calculated data, that is, minimum-energy, stabilization-energy, optimized geometrical parameters, and net-charge on the fluorine atom for the different systems are collected in Table 2.

The most stable packing corresponds to a cage of eight water molecules; the calculated stabilization-energy (187 kcal/mole) overextimates, as expected, the experimental hydration energy (120 kcal/mole) [17]. On other hand, a more realistic value of solvation-energy should be calculated as the difference between the energy of the n-hydrated complex and the energy of n suitably packed molecules of water. Assuming (see the preceeding section) a value of 12 kcal/mole for the stabilization energy of a molecule of solvated water, the complexes with four and six water units show the maximum stabilization, and the corresponding hydration-energy are 128 and 117 kcal/mole respectively, in nice agreement with the experimental value (120 kcal/mole) and a theoretical value previously evaluated (126.7 kcal/mole) [18], considering the difference between the systems

$$F^- + (H_2O)_5 \text{ and } H_2O + [F(H_2O)_4]^- .$$

By inspection of the last column of Table 2 it appears that the charge-transfer from fluorine to the solvent for the different structures, shows a regular trend, with the strongest delocalization for the octahedral cage.

3. $CH_3F \cdot n H_2O$ ($n = 0, 3, 4, 7$)

The geometry of the isolated system has been optimized minimizing the total energy with respect to the bond-distances r_{C-F} and r_{C-H} and the bond-angles θ (see Fig. 3–I).

Afterwards the system in which fluorine atom is bound to three water molecules has been considered.

The calculated geometry shows that one further molecule can be placed around the fluorine atom. Keeping fixed the geometry of methyl group, as found for isolated molecule, the variables indicated in Fig. 4 have been optimized.

Two conformations (oxigen atoms staggered or eclypsed in respect with methyl protons) have been considered and the total-energy of the staggered conformation is lower by 5.15 kcal/mole than that of the eclypsed one. The system in which in addition the methyl group is hydrated have been also considered. The optimized parameters are reported in Fig. 5 where the more stable eclypsed conformation is shown.

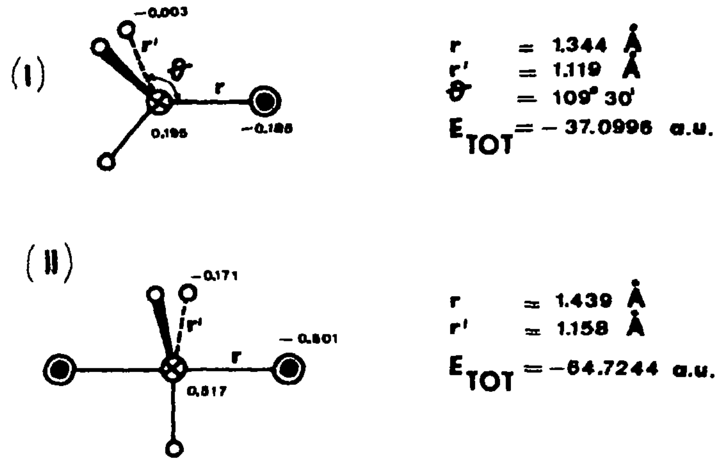

Fig. 3 Optimized geometry, energy, and net-charges for CH_3F (I) and CH_3F_2 (II)

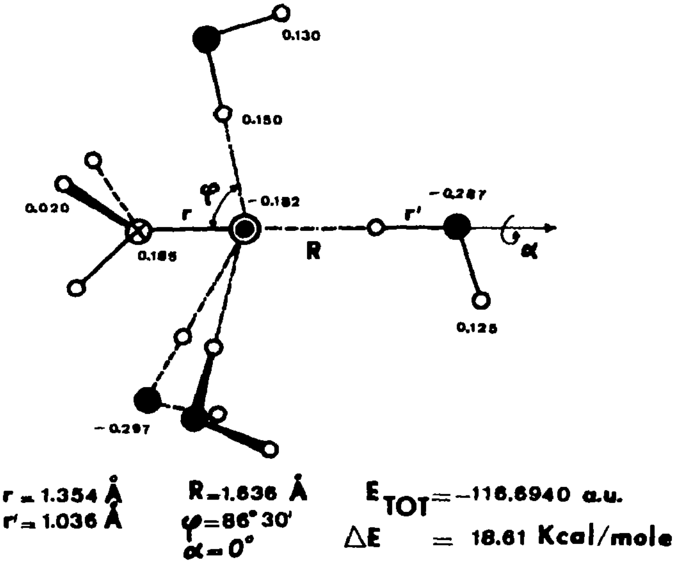

Fig. 4. Optimized geometry, energy, and net-charges for $CH_3F \cdot 4\,H_2O$. After the optimization of the variables r, R, r', and θ it has been verified that the total energy is in a *minimum* when $\alpha = 0$, that is the external proton of water molecule lying along the C–F bond, is in the symmetry plane of the system

Net-charges for all atoms in CH_3F, $CH_3F \cdot 4\,H_2O$, and $CH_3F \cdot 7\,H_2O$ systems are shown in the proper figures (3–I; 4 and 5).

The geometry of the CH_3F molecule ($r_{C-F} = 1.344$ Å; $r_{C-H} = 1.119$ Å; and $\theta = 109°\,30'$) as obtained by CNDO calculations accords well both with exper-

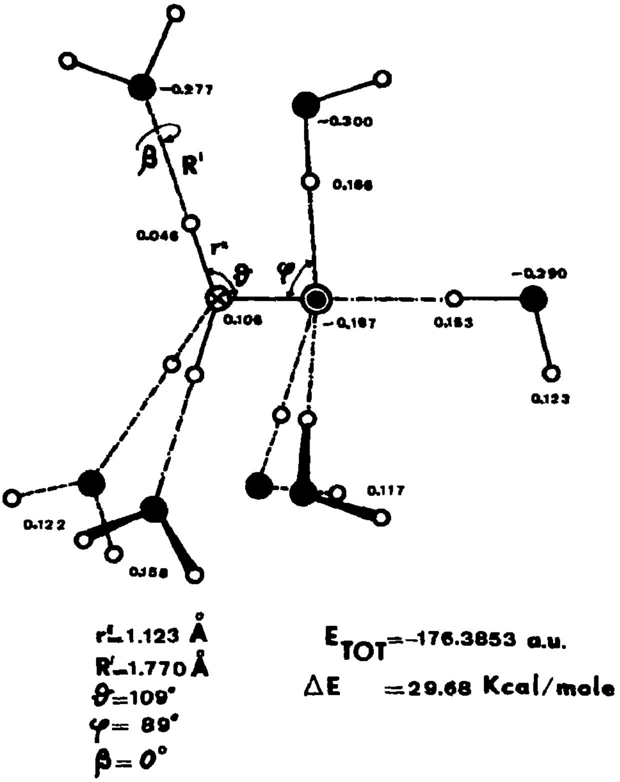

Fig. 5. Optimized geometry, energy, and net-charges for $CH_3F \cdot 7H_2O \cdot \beta$ is equal to 0° when the water molecule lies in the symmetry plane of the system

imental data ($r_{C-F} = 1.385$ Å; $r_{C-H} = 1.109$; $\theta = 110°$) [13b], and with the geometry obtained by an *ab initio* calculation ($r_{C-F} = 1.42$ Å, $r_{C-H} = 1.08$ Å, $\theta = 107° 30'$) [8].

Calculated stabilization energies for $CH_3F \cdot 4\,H_2O$ and $CH_3F \cdot 7\,H_2O$ systems are 18.6 and 29.7 kcal/mole respectively and may be related to the experimental value of the hydration value: $\Delta H_S = 14.94$ kcal/mole [19].

4. $CH_3F_2^- \cdot nH_2O$ ($n = 0, 8, 11$)

The geometry of the isolated system has been optimized minimizing the total energy with respect to the bond-distances r_{C-F} and r_{C-H} (see Fig. 3–II).

The same criteria followed for the energy-minimization of $CH_3F \cdot nH_2O$ systems, have been adopted for the transition state. The systems hydrated by eight and eleven water molecules respectively, are schematically drawn in Figs. 6 and 7, where the optimizing variables and the most relevant calculated results are collected.

In the case in which the fluorine atom only is hydrated, the staggered conformation is favoured of 3.45 kcal/mole. However the eclypsed conformation is more

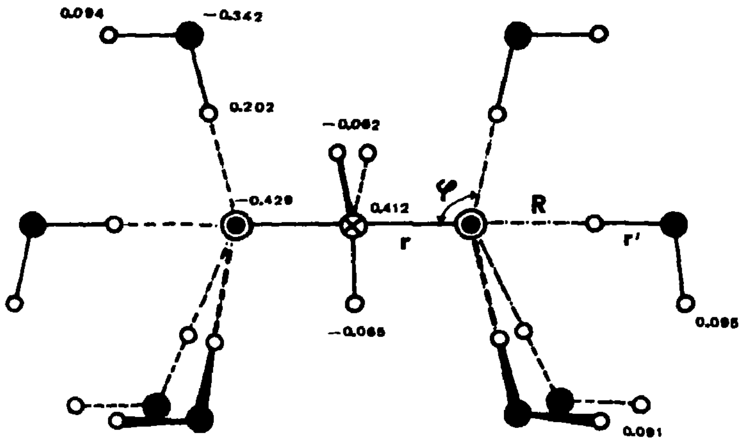

r = 1.466 Å
R = 1.482 Å
r' = 1.047 Å
φ = 104°

$E_{TOT} = -224.0341$ a.u.
ΔE = 113.01 Kcal/mole

Fig. 6. Optimized geometry, energy, and net-charges for $CH_3F_2 \cdot 8\,H_2O$

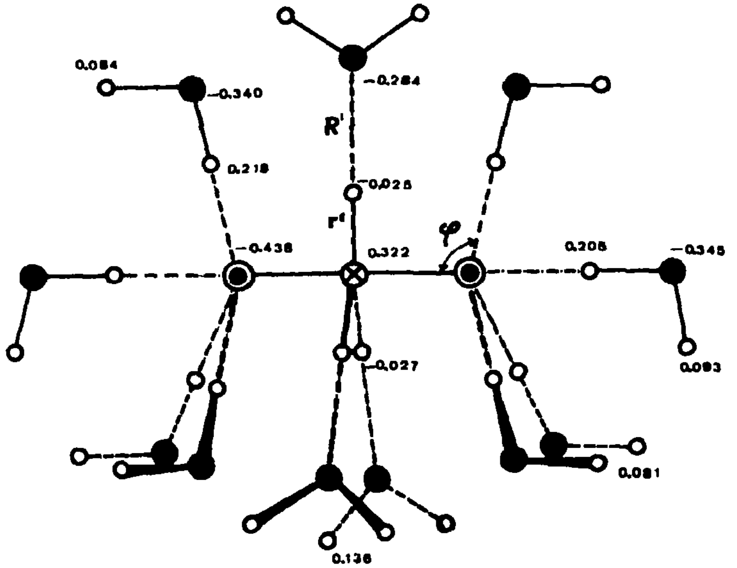

r' = 1.157 Å
R' = 1.732 Å
φ = 106°

$E_{TOT} = -283.7342$ a.u.
ΔE = 131.53 Kcal/mole

Fig. 7. Optimized geometry, energy, and net-charges for $CH_3F_2^- \cdot 11\,H_2O$

stable (18.72 kcal/mole) when three water molecules hydrate also the methyl group. It is interesting to observe how the stabilization energy for transition state falls between fluoride ion and CH_3F's stabilization energies; this finding is in accord with expectation as the transition state is charged, unlike CH_3F, but the charge is more spread than in the case of fluoride ion (see net-charges in Figs. 2, 4, 6, 7).

Reaction Path

Activation energies have been evaluated for the system *in vacuo* and for different degrees of solvated systems; numerical values are collected in Table 3.

The reaction path *in vacuo* has been calculated for several values of reaction coordinate. Activation energy, net-charge on the nucleophilic fluorine atom, and geometrical parameters are shown in Table 4.

Table 3. Activation energies for the system *in vacuo* and in different hydrated cages

	Reactions	ΔE(kcal/mole)
a	$CH_3F + F^- \rightarrow [CH_3F_2]^-$	− 88.29
b	$CH_3F(H_2O)_4 + [F(H_2O)_4]^- \rightarrow [CH_3F_2(H_2O)_8]^-$	− 18.82
c	$CH_3F(H_2O)_4 + [F(H_2O)_6]^- \rightarrow [CH_3F_2(H_2O)_8]^- + 2\,H_2O$	+ 6.34
d	$CH_3F(H_2O)_4 + [F(H_2O)_8]^- \rightarrow [CH_3F_2(H_2O)_8]^- + 4\,H_2O$	+ 12.49
e	$CH_3F(H_2O)_7 + [F(H_2O)_4]^- \rightarrow [CH_3F_2(H_2O)_{11}]^-$	− 24.35
f	$CH_3F(H_2O)_7 + [F(H_2O)_6]^- \rightarrow [CH_3F_2(H_2O)_{11}] + 2\,H_2O$	+ 1.32
g	$CH_3F(H_2O)_7 + [F(H_2O)_8]^- \rightarrow [CH_3F_2(H_2O)_{11}] + 4\,H_2O$	+ 6.96

Table 4. Energy and geometrical data for the reaction path in the vacuo at different values of reaction coordinate (ϱ)[a]

ϱ(Å)[b]	∞	3	2	1.8	1.6	1.439
r (Å)	1.344	1.349	1.374	1.391	1.418	1.439
r' (Å)	1.119	1.119	1.120	1.131	1.144	1.158
θ	109° 30′	109° 12′	102° 42′	98° 6′	93° 24′	90°
q_F	− 1	− 0.998	− 0.886	− 0.768	− 0.621	− 0.501
E(a.u.)	− 64.5837	− 64.5955	− 64.6277	− 64.6584	− 64.7025	− 64.7244

[a] ϱ is the distance between the carbon atom and the incoming fluoride ion.

[b] The geometrical parameters are defined in Fig. 3.

Discussion

To evaluate the influence of the solvent on the activation energy the reaction (2) has been studied by the CNDO method. The calculated geometry of CH_3F, as reported in a previous section is in agreement with experiment. In the case of the transition state, where no comparison with experiment is possible, we can only observe that C–F bond-length (1.439 Å), obtained by CNDO calculations is remarkably shorter than the corresponding *ab initio* value (1.80 Å).

Table 5. Energy and geometry parameters for the reaction in the solvent (case b) at different values of reaction-coordinate (ϱ)

ϱ [a]	∞ $[F(H_2O)_4]^-$	∞ $CH_3F \cdot (H_2O)_4$	2.00 (Å)	Equilibrium $[CH_3F_2(H_2O)_8]^-$
r		1.354	1.378	1.466
R		1.636	1.574	1.482
R_0	1.315		1.348	
θ		109° 30′	105° 36′	90°
Φ		86° 30′	104°	104°
Φ'	109° 30′		90° 24′	
E(a.u.)	− 224.0041		− 224.0155	− 224.0341

[a] The geometrical parameters are defined in Figs. 2, 4 and 6.
θ = FCH in $CH_3F \cdot 4\,H_2O$.
Φ' = OFO in $F \cdot 4\,H_2O$.

In the absence of solvent, our calculations, as *ab initio* ones [8, 20], when no polarization functions are included in the basis set predict the reactants to be less stable than the transition state. The activation energies for the series of models in which different number of water molecules have been introduced, are collected in Table 3. Solvation stabilizes the transition state much more than the reactants and if a sufficient number of water molecules is included in the system a reasonably value for the activation energy of reaction in solution is obtained.

The calculated values may be compared with a value of 20 kcal/mole extimated by Bertier *et al.* [8].

Among the data reported in Table 3, the difference of 70 kcal/mole between activation energies for the system *in vacuo* (*a*) and a system with a minimum number of molecules of water (*b*) is the most significant result. It is evident that solvation energy plays an important role on the determination of activation energy.

The reaction path has been fully followed for the reaction *in vacuo* (the relevant data are shown in Table 4). It is evident that the departure of the leaving fluorine atom is rather late: when the incoming F^- ion is at 2.0 Å from the carbon atom, the leaving F atom has moved by only 0.03 Å. An analogous result has been obtained by *ab initio* calculations where for $\varrho = 2.1$ Å, the leaving fluorine atom is moved by 0.08 Å. The presence of the solvent does not modify this situation as reported in Table 5 for the single point calculated on the reaction path ($\varrho = 2.0$ Å) for the hydrated system.

Financial aid from Italian "Centro Nazionale delle Ricerche" is gratefully acknowledged.

References

1. Ritchie, C. D., King, H. F.: J. Amer. chem. Soc. **88**, 1069 (1966).
2. — — J. Amer. chem. Soc. **90**, 825 (1968).
3. — — J. Amer. chem. Soc. **90**, 833 (1968).
4. — — J. Amer. chem. Soc. **90**, 838 (1968).
5. Lowe, J. P.: J. Amer. chem. Soc. **93**, 301 (1971).

6. Salem, L., Durup, J., Bergeron, G., Cazes, D., Chapuisat, X., Kagan, H.: J. Amer. chem. Soc. **92**, 4472 (1970).
7. Dedieu, A., Veillard, A.: Chem. Physics Letters **5**, 328 (1970).
8. Bertier, G., David, D. I., Veillard, A.: Theoret. chim. Acta (Berl.) **14**, 329 (1969).
9. Pople, J. A., Santry, D. P., Segal, G. A.: J. chem. Physics **43**, S 129 (1965).
— Segal, G. A.: J. chem. Physics **43**, S 136 (1965).
— — J. chem. Physics **44** 3289 (1966).
10. Segal, G. A.: CNDO/2, molecular calculations with complete neglecte of differential overlap, Program 91, Quantum Chemistry Program Exchange, Indiana University (1966).
11. Burton, R. E., Daly, J.: Trans. Faraday Soc. **66**, 1281 (1970).
12. Del Bene, J., Pople, J. A.: Chem. Physics Letters **4**, 426 (1969).
13. a Tables of interatomic distances and configurations in molecules and ions. London: Spec. Publ. n° 11, Scient. Ed. Sutton. The Chemical Society (1958), M 37 s.
b ibidem, M 112.
14. Pimentel, G. C., McClellan, A. L.: The hydrogen bond, p. 260. San Francisco: W. H. Freeman and Co., 1960.
15. Pedersen, L.: Chem. Physics Letters **4**, 280 (1969).
16. Hougen, O. A., Watson, K. M., Ragatz, R. A.: Chemical process principles, Part. I, p. 279. New York: John Wiley and Sons, Inc., 1954.
17. Morris, D. F. C.: Structure and bonding, Vol. IV, p. 63. Berlin: Springer 1968. (Eds. C. K. Jørgensen, J. B. Neilands, R. S. Nyholm, D. Reineu, R. J. P. Williams).
18. Lischka, H., Plesser, Th., Schuster, P.: Chem. Physics Letters **6**, 263 (1970).
19. Glew, D. N., Moelwyn-Hughes, E. A.: Discuss Faraday Soc. **15**, 150 (1953).
20. Duke, A. J., Bader, R. F. W.: Chem. Physics Letters **10**, 631 (1971).

Prof. Dr. M. Simonetta
Institute of Physical Chemistry
University of Milano
I-20133 Milano, Italy

Theoret chim. Acta (Berl.) 25, 248 - 253(1972)
© by Springer-Verlag 1972

On the Evaluation of the Energies of Hybridized Valence States

TOSINOBU ANNO

Laboratory of Chemistry, College of General Education,
Kyushu University, Ropponmatsu, Fukuoka, 810 Japan

Received September 9, 1971

The method of evaluation of the valence-state energy from the observed term values, as proposed originally by Moffitt [1] for unhybridized valence state and extended by Öpik [3] to the hybridized one, is critically reviewed. It is shown for the hybridized valence states that off-diagonal terms, corresponding to interactions among multiplets of the same symmetry arising from different configurations participating in the hybridized valence state, must also be considered in addition to the diagonal terms considered in Öpik's method. Actual procedure of doing this is given. A numerical example given shows that the improvement of Öpik's method proposed here may be ignored in a crude theory but is worth considering in order that the accurate value of the valence-state energy be obtained.

Das Verfahren zur Berechnung der Energie von Valenzzuständen, wie es von Öpik für den Fall hybridizierter Orbitale erweitert wurde, wird bezüglich der Behandlung von Nichtdiagonalelementen kritisiert. Es wird gezeigt, daß solche Terme, die der Wechselwirkung von Multipletts gleicher Symmetrie, aber verschiedener Konfiguration entsprechen, nur bei verhältnismäßig groben Rechnungen vernachlässigt werden dürfen. Anhand eines Beispiels wird gezeigt, daß sie bei größeren Ansprüchen an die Genauigkeit eingeschlossen werden sollten.

1. Introduction

The concept of valence state has been often used in the literature. Conceptually, the valence state is defined as the state in which an atom is supposed to exist within a molecule. Moffitt [1] has presented an elegant way of defining the valence state. He has also given a way to calculate the valence state energy (VSE) and has presented a table of coefficients which give the VSE if they are multiplied by the term values and the products are summed up. Anno and Sakai [2] have shown that the most appropriate account can be taken of the effect of correlation energy upon the energy of the valence states defined by Moffitt, if the VSE is evaluated directly from the observed term values by using this table. However, Moffitt [1] and Anno and Sakai [2] have been concerned with the unhybridized valence states arising from the configurations of the $s^m p^n$ $(m = 0, 1, 2;\ n = 0, 1, \ldots, 6)$ type only. As for the hybridized valence states, Öpik [3] has presented a similar table and Orloff and Sinanoğlu [4] have discussed such valence states with reference to the correlation energy. A characteristic feature of a hybridized valence state is that more than one spectroscopic state wave functions of the same symmetry but of different configurations may be found, if the wave function of the hybridized valence state is expanded into wave functions of various spectroscopic states. It seems to the present author that Öpik's treatments (which is followed by Orloff and Sinanoğlu) of such states of the same symmetry is not necessarily appropriate. It is the purpose of the present paper to describe how to improve Öpik's method.

2. Remarks on the Moffitt-Öpik Method

For practical purpose, Moffitt's method [1] of defining the valence state can be described in terms of the wave functions as follows:

(i) Construct the wave function of Molecule M in the valence-bond (VB) approximation.

(ii) Expand those parts of this wave function which correspond to a given atom A in terms of the wave functions of Atom A in its various spectroscopic states as expressed in orbital approximation.

(iii) Let the lengths of all the bonds starting from Atom A be infinite and drop out those parts of the wave function which do not correspond to Atom A. The resulting function $\tilde{\Phi}_V$ will be a linear combination of wave functions of Atom A in its various spectroscopic states as expressed in orbital approximation:

$$\tilde{\Phi}_V = \sum_{r=1}^{N} c_r \tilde{\psi}_r , \tag{1}$$

where $\tilde{\psi}_r$ is the wave function of the rth spectroscopic state of Atom A in orbital approximation and c_r is the coefficient.

(iv) Φ_V, which is obtained by replacing $\tilde{\psi}_r$ in Eq. (1) with ψ_r, the *exact* wave function of the rth spectroscopic state of Atom A, is *defined* as the exact wave function of the valence state V of Atom A in Molecule M:

$$\Phi_V = \sum_{r=1}^{N} c_r \psi_r . \tag{2}$$

From this definition of the valence state, the "exact" energy E_V of Atom A in its valence state V can be obtained as

$$E_V = \langle \Phi_V | \mathscr{H} | \Phi_V \rangle = \sum_{r=1}^{N} |c_r|^2 \langle \psi_r | \mathscr{H} | \psi_r \rangle = \sum_{r=1}^{N} |c_r|^2 E_r . \tag{3}$$

where E_r is the exact energy of Atom A in its rth spectroscopic state and may be obtained as the observed spectroscopic term value T_r. It is to be noted that no cross term occurs in Eq. (3), because ψ_r is the eigenfunction of the total Hamiltonian $\mathscr{H}$ of Atom A by definition. Although original definition of Moffitt [1] covers unhybridized valence states only, Öpik [3] uses Eq. (2) for the definition of hybridized valence states as well. Orloff and Sinanoğlu's analysis [4] of the correlation energy of the carbon hybridized valence states is also based on Eq. (2). We shall show that this is not necessarily appropriate, by confining ourselves to those valence states which arise from the configurations of the $s^m p^n$ type for brevity.

As was mentioned in Introduction, a characteristic feature of a hybridized valence state is that more than one spectroscopic state wave functions of the same symmetry but belonging to different configurations may be found if the wave function of the hybridized valence state is expanded. For example, $(t_1^2 t_2 t_3 t_4)$ in Öpik's notation can be expanded in terms of the wave functions of spectroscopic states belonging to configurations s^2p^3, sp^4, and p^5. Of these spectroscopic states, two of ${}^2P$ are involved, one arising from s^2p^3 and the other from p^5. Let $\tilde{\psi}_s$ and $\tilde{\psi}_t$

be the wave functions, within the orbital approximations, of such a pair of states having the same symmetry. Eq. (1) in this case reads:

$$\tilde{\Phi}_V = \sum_{\substack{r=1 \\ r \neq s,t}}^{N} c_r \tilde{\psi}_r + c_s \tilde{\psi}_s + c_t \tilde{\psi}_t \,. \tag{4}$$

It is to be noted that r extends, in Eq. (1), over only those states which belong to one configuration if V is unhybridized, but r may extend over more than one configuration in the case of a hybridized valence state, with which we are now concerned. Therefore, N in Eqs. (1), etc. is the number of spectroscopic states belonging to the configuration to which V belongs if V is unhybridized, but N is the total number of spectroscopic states belonging to several configurations if V is hybridized. Öpik evaluates the VSE in just the same way as in the case of unhybridized valence states:

$$E_V = \sum_{r=1}^{N} |c_r|^2 T_r = \sum_{\substack{r=1 \\ r \neq s,t}}^{N} |c_r|^2 T_r + |c_s|^2 T_s + |c_t|^2 T_t \,. \tag{5}$$

This is tantamount to assume that

$$\Phi_V = \sum_{\substack{r=1 \\ r \neq s,t}}^{N} c_r \psi_r + c_s \psi_s + c_t \psi_t \,. \tag{6}$$

Now, an important point we must remember is the fact that the concept of hybridization is based on the orbital approximation, in which the s^2p^n, sp^{n+1}, and the p^{n+2} configurations are regarded as independent configurations, whereas the interaction between s^2p^n and p^{n+2} ($n = 3$ for the example quoted above) is incorporated in ψ_s and ψ_t. Therefore, the method adopted by Öpik is not consistent with the original method of Moffitt, since Moffitt's definition of the valence state is based on the orbital approximation as was mentioned before.

3. A Proposal of a Modification of Öpik's Method

To remove the inconsistency with Moffitt's method pointed out above for Öpik's method, Eq. (6) must be replaced by

$$\Phi_V = \sum_{\substack{r=1 \\ r \neq s,t}}^{N} c_r \psi_r + c_s \psi_s' + c_t \psi_t' \,, \tag{7}$$

where ψ_s' and ψ_t' are "semi-exact" wave functions in which all but $\tilde{\psi}_s - \tilde{\psi}_t$ interactions are included. The exact value of VSE is then the expectation value of the Hamiltonian $\mathscr{H}$ with respect to Φ_V given by Eq. (7), not by Eq. (6):

$$\begin{aligned} E_V = \langle \Phi_V | \mathscr{H} | \Phi_V \rangle = & \sum_{\substack{r=1 \\ r \neq s,t}}^{N} |c_r|^2 \langle \psi_r | \mathscr{H} | \psi_r \rangle + |c_s|^2 \langle \psi_s' | \mathscr{H} | \psi_s' \rangle \\ & + |c_t|^2 \langle \psi_t' | \mathscr{H} | \psi_t' \rangle + (c_s^* c_t + c_t^* c_s) \langle \psi_s' | \mathscr{H} | \psi_t' \rangle \,. \end{aligned} \tag{8}$$

Of the various matrix elements appearing in the right-hand side of Eq. (8), $\langle\psi_r|\mathscr{H}|\psi_r\rangle$ $(r=1,2,\ldots,N;r\neq s,t)$ may be equated to the observed term value T_r. The other matrix elements may be obtained as follows.

Now, from the definitions of ψ_s, ψ_t, ψ'_s, and ψ'_t, it is obvious that

$$\left.\begin{aligned}\psi_s&=a_{11}\psi'_s+a_{12}\psi'_t\\ \psi_t&=a_{21}\psi'_s+a_{22}\psi'_t\end{aligned}\right\},\tag{9}$$

where a_{ij} $(i,j=1,2)$ are numerical coefficients to be determined variationally, leading to the secular equation

$$\begin{vmatrix}\langle\psi'_s|\mathscr{H}|\psi'_s\rangle-E & \langle\psi'_s|\mathscr{H}|\psi'_t\rangle\\ \langle\psi'_t|\mathscr{H}|\psi'_s\rangle & \langle\psi'_t|\mathscr{H}|\psi'_t\rangle-E\end{vmatrix}=0\,.\tag{10}$$

The roots of this secular equation are equal to $\langle\psi_s|\mathscr{H}|\psi_s\rangle$ and $\langle\psi_t|\mathscr{H}|\psi_t\rangle$ which can now be equated to T_s and T_t, respectively. Therefore, $\langle\psi'_s|\mathscr{H}|\psi'_s\rangle$ and $\langle\psi'_t|\mathscr{H}|\psi'_t\rangle$ may be evaluated if the value of $\langle\psi'_s|\mathscr{H}|\psi'_t\rangle$ $[\equiv\langle\psi'_t|\mathscr{H}|\psi'_s\rangle]$ is known.

For the evaluation of $\langle\psi'_s|\mathscr{H}|\psi'_t\rangle$, we use an orbital approximation

$$\langle\psi'_s|\mathscr{H}|\psi'_t\rangle\approx\langle\tilde{\psi}_s|\mathscr{H}|\tilde{\psi}_t\rangle\,,\tag{11}$$

which is expected to be a good approximation for such an off-diagonal matrix element of fairly small magnitude. For hybridized valence states, which Öpik has dealt with, one member, say ψ_s, of a pair of wave functions which are of the same symmetry, always belongs to the configuration s^2p^n, if the other member, say ψ_t, of the same pair belongs to the configuration s^0p^{n+2} $(0\leqq n\leqq 4)$. In such cases, it can always be shown that $\langle\tilde{\psi}_s|\mathscr{H}|\tilde{\psi}_t\rangle$ has the following form:

$$\langle\tilde{\psi}_s|\mathscr{H}|\tilde{\psi}_t\rangle=fG^1(sp)\,,\tag{12}$$

where f is a factor depending upon the valence state and the symmetry of ψ_s (and ψ_t) and $G^1(sp)$ is a Slater-Condon parameter. This factor can easily be calculated algebraically while $G^1(sp)$ is to be obtained from the Slater type treatment of the observed term values of the configuration sp^{n+1}. It is to be added that we use the $\langle\psi'_s|\mathscr{H}|\psi'_t\rangle$ value thus determined also in Eq. (8).

4. Discussions

We shall now discuss the difference in VSE's evaluated with Öpik's method (Eq. (5)) on the one hand and with our method (Eq. (8)) on the other. These VSE's will be distinguished by denoting them $E_V(I)$ and $E_V(II)$, respectively. There is no difference between Eqs. (5) and (8) as far as the first term in the right-hand side is concerned. Therefore,

$$\begin{aligned}E_V(I)-E_V(II)=&|c_s|^2\{\langle\psi_s|\mathscr{H}|\psi_s\rangle-\langle\psi'_s|\mathscr{H}|\psi'_s\rangle\}\\ &+|c_t|^2\{\langle\psi_t|\mathscr{H}|\psi_t\rangle-\langle\psi'_t|\mathscr{H}|\psi'_t\rangle\}\\ &-(c_s^*c_t+c_t^*c_s)\langle\psi'_s|\mathscr{H}|\psi'_t\rangle\,.\end{aligned}\tag{13}$$

As a numerical example, a valence state which is called $(t_1^2 t_2 t_3 t_4)$ by Öpik will be considered for the neutral nitrogen atom. As was mentioned in Section 2, the neglected term in Öpik's treatment is the interaction between $s^2p^3\,{}^2P$ and $p^5\,{}^2P$, which will be assigned to the sth and the tth "states", respectively, in our analysis. An algebraic calculation shows that

$$\langle\tilde{\psi}_s|\mathscr{H}|\tilde{\psi}_t\rangle = -(\sqrt{2}/3)\,G^1(sp)\,, \tag{14}$$

$$\left.\begin{aligned} |c_s|^2 &= (1/8)\,\{(1-\lambda_1)^2-\lambda_2^2-\lambda_3^2-\lambda_4^2\} \\ |c_t|^2 &= (1/4)\,\{(1-\lambda_1)^2-\lambda_2^2-\lambda_3^2-\lambda_4^2\} \\ c_s^* c_t + c_t^* c_s &= (1/2\sqrt{2})\,\{(1-\lambda_1)^2-\lambda_2^2-\lambda_3^2-\lambda_4^2\} \end{aligned}\right\}, \tag{15}$$

where λ_i is the amount of s character of $t_i\,(i=1,2,3,4)$ as defined by Öpik [3]. To be more realistic, let us take

$$\left.\begin{aligned} t_1 &= (1+\lambda^2)^{-\frac{1}{2}}(\lambda s + x) \\ t_2 &= [2(1+\lambda^2)^{-\frac{1}{2}}\,[s-\lambda x-(1+\lambda^2)^{\frac{1}{2}}y] \\ t_3 &= [2(1+\lambda^2)^{-\frac{1}{2}}\,[s-\lambda x+(1+\lambda^2)^{\frac{1}{2}}y] \\ t_4 &= z \end{aligned}\right\}, \tag{16}$$

where s, x, y, and z represent $2s, 2p_x, 2p_y$, and $2p_z$ AO, respectively, and λ is a parameter specifying the hybrid character of t_i's. It is to be noted that t_1, t_2, and t_3 in Eq. (16) becomes three equivalent sp^2 hybrid AO's lying in the xy plane for $\lambda = 1/\sqrt{2}$ and $(t_1^2 t_2 t_3 t_4)$ then becomes the valence state in which a nitrogen atom is expected to be found in the ground state of the nitrogen-containing heterocyclic molecules [5]. By expressing λ_i's involved in Eq. (15) in terms of λ of Eq. (16), it can be shown that

$$\left.\begin{aligned} |c_s|^2 &= 1/\{16(1+\lambda^2)^2\} \\ |c_t|^2 &= 1/\{8(1+\lambda^2)^2\} \\ c_s^* c_t + c_t^* c_s &= 1/\{4\sqrt{2}(1+\lambda^2)^2\} \end{aligned}\right\}. \tag{17}$$

For the numerical work, we use the following data [6, 7][1]:

$$G^1(sp) = 73\,111\ \text{cm}^{-1}\,, \tag{18}$$

$$T(s^2p^3\,{}^2P) = 28\,840\ \text{cm}^{-1}\,, \tag{19}$$

$$T(p^5\,{}^2P) = 234\,690\ \text{cm}^{-1}\,. \tag{20}$$

The value of $\langle\psi_s'|\mathscr{H}|\psi_t'\rangle$ can be obtained immediately from Eqs. (11), (14), and (18):

$$\langle\psi_s'|\mathscr{H}|\psi_t'\rangle = -34\,465\ \text{cm}^{-1}\,. \tag{21}$$

The values given in Eqs. (19) and (20) are supposed to be the expectation values of $\mathscr{H}$ with respect to the exact wave functions of the sth and the tth state and to be the roots of the secular equation (10) as measured from the ground state of the nitrogen atom:

---

[1] The $G^1(sp)$ value has been taken from [6]. The term values have been obtained from Moore's table [7] by averaging out fine structure, each component of a particular term being given a weight of $2J+1$. Since ${}^2P$ of $1s^2 2p^5$ is not given for N in Moore's table, its term value has been obtained by a linear extrapolation along isoelectronic series.

$$\langle\psi_s|\mathscr{H}|\psi_s\rangle = 28840\ \mathrm{cm}^{-1}, \tag{22}$$

$$\langle\psi_t|\mathscr{H}|\psi_t\rangle = 234690\ \mathrm{cm}^{-1}. \tag{23}$$

Therefore, $\langle\psi'_s|\mathscr{H}|\psi'_s\rangle$ and $\langle\psi'_t|\mathscr{H}|\psi'_t\rangle$ are obtained by the method described in Section 3, using (21), as

$$\langle\psi'_s|\mathscr{H}|\psi'_s\rangle = 34782\ \mathrm{cm}^{-1}, \tag{24}$$

$$\langle\psi'_t|\mathscr{H}|\psi'_t\rangle = 228748\ \mathrm{cm}^{-1}. \tag{25}$$

From Eqs. (13), (17), (21)–(25), $E_V(I) - E_V(II)$ is found to be

$$E_V(I) - E_V(II) = 2873\ \mathrm{cm}^{-1} = 0.356\ \mathrm{eV}, \tag{26}$$

for $\lambda = 1/\sqrt{2}$ (sp^2 hybridization). This value is rather small as compared with the one-center electron repulsion integral, which is obtained from the energy change in the course of electron-transfer reaction involving the atoms in their valence states [2, 8], and may be ignored in a crude theory. However, essential achievement of evaluation of the VSE directly from the observed term values is that one can expect a high degree of accuracy of evaluation and the difference shown by Eq. (26) is not negligible from this point of view. Therefore, it may safely be concluded that the improvement of Öpik's method suggested in the present paper is worth considering.

Acknowledgements. The author expresses his thanks to Dr. Uno Öpik of the Queen's University, Belfast, for his correspondence and reading the draft of the present paper. He is also grateful to Miss Yoshiko Sakai for her discussions, which have been very useful in improving the present paper.

References

1. Moffitt, W.: Repts. Progr. Phys. **17**, 173 (1954).
2. Anno, T., Sakai, Y.: Some remarks on the semi- and the nonempirical values of the Slater-Condon parameters and the parametrization for the one-center electron repulsion integrals in the semi-empirical molecular orbital method. J. chem. Physics (in press).
3. Öpik, U.: Molecular Physics **4**, 505 (1961).
4. Orloff, M. K., Sinanoğlu, O.: J. chem. Physics **43**, 49 (1965).
5. Anno, T.: J. chem. Physics **29**, 1161 (1958).
6. Teruya, H.: Theoret. chim. Acta (Berl.) **21**, 127 (1971).
7. Moore, C. E.: Atomic energy levels as derived from the analyses of optical spectra. Vol. I. Washington, D. C.: National Bureau of Standards (U.S.), Circular No. 467, 1949.
8. Pariser, R.: J. chem. Physics **21**, 568 (1953).

Professor Dr. Tosinobu Anno
Laboratory of Chemistry
College of General Education
Kyushu University
Ropponmatsu, Fukuoka, 810 Japan

Theoret. chim. Acta (Berl.) 25, 254 258 (1972)
© by Springer-Verlag 1972

Sulphur Dioxide. Notes on the Electronic Changes which Occur on Coordination

P. D. Dacre and M. Elder

Chemistry Department, The University, Sheffield S 3 7 HF, England

Received October 21, 1971

The sulphur dioxide molecule and the two negative ions, SO_2^- and SO_2^{2-} are studied by *ab initio* SCF MO methods using a small but flexible gaussian orbital basis set. The calculations were performed for two different geometries and allow some understanding of the electronic changes that accompany the formation of complexes in which the SO_2 molecule acts as a ligand.

Das Schwefeldioxid-Molekül und die beiden negativen Ionen SO_2^- und SO_2^{2-} werden mit Hilfe einer *ab initio* SCF MO Methode, die einen kleinen aber flexiblen Gauß-Basissatz benutzt, studiert. Die Rechnungen werden für 2 verschiedene Geometrien durchgeführt und erlauben ein näherungsweises Verständnis der Änderungen der Elektronenparameter, die die Bildung von Komplexen mit dem SO_2-Molekül als Ligand begleiten.

Introduction

In this paper we present the results of some calculations on the sulphur dioxide molecule. These calculations were performed with the aim of providing some information about the electronic changes which occur in the molecule when it coordinates to transition metal complexes. There is a great deal of experimental information about the stereochemistry and electronic arrangement of such ligands as CO, NO, O_2, SO_2, olefins, allyls and acetylenes bonded to transition metal complexes, derived mainly from X-ray crystallographic and spectroscopic observations. There have been a number of theories of a largely qualitative nature produced to explain the bonding in such complexes [1–6], but few calculations have been performed. It seems reasonable to suppose that SCF calculations upon such molecules should provide much information about the bonding in them. In the main, the size of the complexes precludes the possibility of MO SCF calculations by present methods, although $Ni(\pi\text{-}C_3H_5)_2$ [7], $Ni(CO)_4$ [8] and CrO_8^{3-} [9] have been studied recently. Calculations upon a system such as $RhCl(CO)(SO_2)[P(C_6H_5)_3]_2$ are not yet possible, so that a first attempt at understanding the bonding seems to be to study the electronic structure of the ligand of interest, SO_2 in this case, and the possible changes that occur upon coordination.

SO_2 coordinates in two different ways to transition metal systems. On the one hand there is the complex $[RuCl(NH_3)_4SO_2]Cl$ [10] where the $Ru–SO_2$ group is planar and symmetric, and the Ru–S bond is short at 2.072 Å. On the other hand, the reversible coordination of the complexes characterised by $RhCl(CO)(SO_2)[P(C_6H_5)_3]_2$ [11] with a long Rh–S bond (2.450 Å) and the SO_2 group bonded symmetrically, but with an angle of 30.3° between the Rh–S bond

Table 1. The geometry of SO_2 as the free molecule and in various complexes

Compound	S–O (Å)	O–S–O (deg.)
SO_2 [13]	1.431 (1)[a]	119.0 (5)
$[RuCl(NH_3)_4(SO_2)]Cl$ [10]	1.43 (1)	114 (6)
$RhCl(CO)(SO_2)[P(C_6H_5)_3]_2$ [11]	1.451 (4)	113.8 (3)
$S_2O_4^{2-}$ [12]	1.50 (2)	108

[a] The estimated experimental error in the last significant figure is given parenthetically.

and the normal to the SO_2 plane. This latter coordination parallel that in the dithionite ion, $S_2O_4^{2-}$ [12] which has a very long S–S bond (2.39 Å) linking, at a similar angle, two SO_2 groups, with overall C_{2v} geometry. The geometries of the SO_2 group in these various complexes are listed in Table 1. The variations in geometry that are indicated in the table, together with the different modes of coordination described above, suggest considerable electronic differences between the SO_2 group in the various complexes. The calculations presented here are aimed at going some way toward elucidating these differences.

Calculations

MO–SCF–LCAO calculations were performed for the SO_2 molecule and the negative ions SO_2^- and SO_2^{2-} at two different geometries. The calculation designated (I) employed the geometry obtained for gaseous SO_2 from electron diffraction data [13]. This geometry is identical with that found in an X-ray study of the solid [14]. The second calculation (II) employed the geometry of the SO_2 group in the dithionite ion, determined by an X-ray crystallographic analysis of $Na_2S_2O_4$ [12], averaging the two S–O distances, which agreed within error in the experiment. Details of these two geometries are given in Table 1.

A basis set of 48 uncontracted gaussian functions was employed in all calculations. This is equivalent to two gaussian functions per atomic orbital. A (6*s*, 4*p*) set of gaussian functions for sulphur determined by optimization against the total energy of the ^3P ground state of the sulphur atom (total energy −395.262 a.u.) [15] was supplemented by two *d*-type functions with exponents 0.4 and 2.0. For the oxygen atoms a (4*s*, 2*p*) set was optimized to give a total energy for the atom of −73.900 a.u. [15]. All one- and two-electron integrals were computed exactly. The SCF calculations were carried out by repeated diagonalization, making use of molecular symmetry [16]. All calculations were performed on an ICL 1907 computer using programs written by the authors.

Results and Discussion

Three *ab initio* calculations on SO_2 have been reported in the literature, and it is instructive to compare the results of the present work with these calculations, in order to assess the accuracy of our wavefunction. Some of the results of these

Table 2. Results of some *ab initio* SCF calculations on SO_2

	This work	Ref. [17]	Ref. [18]	Ref. [19]	Observed
Total energy (a u.)	−543.340	−541.008	−546.831	−547.209	
Dissociation energy (eV)	7.56		5.77	3.85	11.18[a]
Ionization potential (a.u.)	0.413	0.444	0.466	0.491	0.454[b]
Dipole moment (Debye)	−1.26	−0.81	−2.17	−2.28	1.61[c]
S 3*d* population	1.33	1.17	0.55	0.43	

[a] Ref [19]. [b] Ref. [20] [c] Ref. [21].

calculations are presented in Table 2. Column 2 gives values obtained by Hillier and Saunders [17] who employed a basis set of 72 gaussian functions contracted in groups of three to a minimal (3*s*, 2*p*, 1*d*) basis for sulphur and (2*s*, 1*p*) for oxygen. It is significant that the present calculation, which uses a smaller basis set of 48 gaussians, yields a total energy some 2.3 a.u. lower, partially as a result of the greater flexibility of the non-minimal bais set, but mainly because the smaller basis set has been subjected to optimization for the free atoms. Columns 3 and 4 give results from the considerably more accurate GTO calculations of Roos and Siegbahn [18] and Rothenberg and Schaefer [19], who both included 3*d* functions of oxygen as well as sulphur, and used considerably more accurate expansions for the core orbitals. These calculations give lower sulphur 3*d* populations, which, as Hillier and Saunders pointed out, is to be expected since the participation of the 3*d* orbitals in both the present calculation and the 3- GTO minimal basis calculation is certain to be exaggerated because of the incomplete *s* and *p* orbital basis sets. The fact that the present calculation apparently gives the best dissociation energy, from comparison with the experimental value, can be explained by this exaggerated 3*d* participation in the wave function, which allows an improved description of the sulphur core orbitals and hence artifically lowers the binding energy. The Koopmans' theorem ionization potential, and the dipole moment calculated from the present wavefunction are in reasonable agreement with the experimental values. Final confirmation of the quality of this wavefunction is given by the energy level ordering it exhibits, which is the same as that of the Roos and Siegbahn wavefunction.

For geometry (II) total energies of −543.340, −543.264 and −542.831 a.u. were obtained for SO_2, SO_2^- and SO_2^- respectively. The figures for geometry (II) were −543.349, −543.304 and −542.903 respectively. The two additional electrons in the SO_2^{2-} calculations resided in the level $3b_1$, whilst the $^2B_1$ wavefunction was the most stable state found for both SO_2^- calculations.

The total energies for the SO_2 ground state in the two different geometries are separated by 0.009 u.a. with the experimental geometry giving rise to the higher figure. This indicates an energy plateau as far as small, symmetric deformations of the isolated molecule are concerned, and we feel that the apparent slight increase in stability when the S–O bonds are stretched and the OSO angle decreased is an artifact of the limited basis set used in the calculations. The most stable virtual orbital of the SO_2 calculations has b_1 symmetry. It is centred mainly on the sulphur atom but with some 2*p* character, and has the symmetry of a

p-orbital perpendicular to the SO_2 plane. The orbital is S–O π-antibonding and O–O π-bonding. When electrons are added to this orbital it is evidently considerably more stable in geometry (II) rather than (I). The orbital energies for this orbital in both the SO_2^- and SO_2^{2-} calculations are 0.031 a.u. lower in (II) than their corresponding values in (I). This is confirmed by the total energies which indicate SO_2^- (II) to be 0.040 a.u. more stable than SO_2^- (I) whilst the difference between the SO_2^{2-} energies is 0.072 a.u. These differences are considerably larger than the small difference between the SO_2 energies, and they agree with the experimental observations of the geometry change in SO_2 when it coordinates as a Lewis acid [11]. The $3b_1$ orbital has the correct symmetry for σ-bond formation between sulphur and another atom in such complexes as $S_2O_4^{2-}$ and $RhCl(CO)(SO_2)(P(C_6H_5)_3)_2$ where the SO_2 group is oriented such that the normal to the SO_2 plane is at about 30° from the line of the S–S or S–Rh bond. In both the SO_2^- calculations the molecular orbital $3b_1$ has atomic orbital components which are 54% sulphur $3p_z$, 17% sulphur $3d_{xz}$ and 29% oxygen $2p_z$ where the SO_2 molecule lies in the xy-plane with the x-axis the 2-fold axis. The presence of electrons in this orbital, whether in the SO_2 and SO_2^{2-} ion, or in complexes where the orbital is involved in σ-overlap with a suitably directed doubly-occupied metal orbital, will decrease the amount of S–O π-bonding and increase the O–O π-bonding over that found in free SO_2. The geometry changes which will enhance the stability of a system where the SO_2 $3b_1$ orbital is occupied will therefore be S–O bond lengthening and the decrease of the angle between the two S–O bonds. We observe that the other two orbitals which are more stable in the geometry calculations (II), namely $6a_1$ and $8a_1$, are both S–O antibonding and O–O bonding in character, whilst the orbital $5b_2$ and $1a_2$ which are antibonding between the oxygens are less stable in the geometry (II) calculations.

The orbital $8a_1$ is the obvious source of the electron pair needed for σ-bond formation in complexes such as $[RuCl(NH_3)_4SO_2]Cl$ where the SO_2 group acts as a Lewis base. As Roos and Siegbahn have pointed out, this orbital can not be characterized as a lone pair orbital on sulphur, since it has a large oxygen $2p$ component (58% in our calculation) and is S–O antibonding. However, withdrawal of electrons from this orbital on complex formation will stabilize the S–O σ-bonding and will favour back-donation from appropriately directed occupied metal d-orbitals into the vacant $3b_1$ orbital on SO_2 which has the right symmetry for metal-sulphur π-bond formation. Thus we suggest that the electronic configuration of SO_2 in the ruthenium amine complex will resemble that in an excited state of SO_2 that can be qualitatively described as $\ldots(1a_2)^2(8a_1)^1(3b_1)^1$. Since both the orbitals $8a_1$ and $3b_1$ are S–O antibonding and O–O bonding we would expect little or no change in the geometry of the SO_2 group on complex formation of this type. The relevant crystallographic data for $[RuCl(NH_3)_4SO_2]Cl$ (see Table 1) confirm that, within error, the SO_2 geometry is the same as that in the free molecule, whilst the short Ru–S distance indicates the presence of a double bond between these atoms.

Acknowledgements. We thank Professor R. Mason and Professor R. McWeeny for their advice and encouragement, and the staff of the Sheffield University computer centre for their assistance. This work was supported financially by the S.R.C.

References

1. Dewar, M. J. S.: Bull. Soc. chim. France **18**, C71 (1951).
2. Chatt, J., Duncanson, L. A.: J. chem. Soc. **1953**, 2939.
3. Mason, R.: Nature **217**, 543 (1968).
4. McWeeny, R., Mason, R., Towl, A. D. C.: Discuss. Faraday Soc. **1969**, 20.
5. Kettle, S. F. A., Mason, R.: J. organometallic Chem. **5**, 573 (1966).
6. Blizzard, A. C., Santry, D. P.: J. Amer. chem. Soc. **90**, 5749 (1968).
7. Veillard, A.: Chem. Comm. **1969**, 1022.
8. Hillier, I. H., Saunders, V. R.: Chem. Physics Letters **9**, 642 (1971).
9. Dacre, P. D., Elder, M.: J. chem. Soc. Dalton, in press.
10. Vogt, L. H., Katz, J. L., Wiberley, S. E.: Inorg. Chem. **4**, 1157 (1965).
11. Muir, K. W., Ibers, J. A.: Inorg. Chem. **8**, 1921 (1969).
12. Dunitz, J. D.: Acta crystallogr. **9**, 579 (1956).
13. Haase, J., Winnewisser, M.: Z. Naturforsch. **23a**, 61 (1968).
14. Post, B., Schwartz, R. S., Fankucyen, I.: Acta crystallogr. **5**, 372 (1952).
15. Cook, D. B.: Private communication.
16. Dacre, P. D.: Chem. Physics Letters **7**, 47 (1970).
17. Hillier, I., Saunders, V. R.: Chem. Physics Letters **4**, 163 (1969).
18. Roos, B., Siegbahn, P.: Theoret. chim. Acta (Berl.) **21**, 368 (1971).
19. Rothenberg, S., Schaefer, H. F.: J. Amer. chem. Soc., in press.
20. N.B.S. Technical Note: 270–3 (1968).
21. McClellan, A. L.: Tables of experimental dipole moments. San Francisco and London: Freeman 1963

Dr. M. Elder
The University
Sheffield S 3 7 HF, England

Theoret. chim. Acta (Berl.) 25, 259—267 (1972)
© by Springer-Verlag 1972

Analyse conformationnelle théorique de la diméthylsulfone, $(CH_3)_2SO_2$

GERMAINE ROBINET, FRANÇOIS CRASNIER, JEAN-FRANÇOIS LABARRE
et CLAUDE LEIBOVICI

Laboratoire Associé au C.N.R.S. n° 160, Université Paul Sabatier,
38, rue des 36 Ponts, 31-Toulouse, France

Reçu le 15 décembre 1971

Theoretical Conformational Analysis of the Dimethylsulfone, $(CH_3)_2SO_2$

The conformational analysis of $(CH_3)_2SO_2$ is investigated within the framework of the CNDO/2 approximation. The preferred conformation of heavy atoms (C, S, O) is found to be the one which was proposed by Jacob and Lide in 1971 on the basis of microwave measurements. The map of iso-energy curves was drawn, describing the variation of energy as a result of mutual rotation of the two methyl groups. This showed that the equilibrium symmetry for the complete molecule, including the hydrogens, was C_{2v}. The rotational barrier for one CH_3 group is 3.65 kcal/mole, in good agreement with the experimental value (3.4 kcal/mole [10]). A bicentric energy partitioning shows that at least 70 per cent of the variation in total energy is reflected by the single sum, Σ *E*(S–H), of the spatial interaction terms between sulphur and the six hydrogens. This result, which is consistent with previous work, strongly supports the classical concept of hyperconjugation.

La méthode SCF–LCAO–MO dans l'approximation CNDO/2 est utilisée pour l'étude de l'analyse conformationnelle de la diméthylsulfone $(CH_3)_2SO_2$. On montre ainsi que, parmi les déterminations géométriques les plus récentes, celle obtenue par Jacob et Lide en 1971 au moyen de la spectroscopie de micro-ondes semble devoir être retenue. La carte de potentiel, décrivant la rotation simultanée des deux groupements méthyle autour des liaisons (S–C), est tracée: elle montre que la molécule $(CH_3)_2SO_2$ appartient bien au groupe de symétrie C_{2v}, non seulement au niveau des atomes lourds (C, S, O) mais aussi à celui des hydrogènes. La barrière à la rotation d'un CH_3 est ainsi trouvée égale à 3,65 kcal/mole (expérimentalement: 3,4 kcal/mole [10]). Un découpage bicentrique de l'énergie totale montre enfin que 70% des variations de cette grandeur sont dus à la seule somme, Σ *E*(S–H), des interactions dans l'espace entre l'atome de soufre et les six atomes d'hydrogène. Ce résultat éclaire d'un jour nouveau le concept qualitatif d'hyperconjugaison.

Die Konformationsanalyse von $(CH_3)_2SO_2$ wird im Rahmen der CNDO/2-Näherung untersucht. Die bevorzugte Konformation der schweren Atome (C, S, O) ergibt sich als diejenige, die von Jacob und Lide 1971 auf der Grundlage von Mikrowellenmessungen vorgeschlagen wurde. Die iso-energetischen Kurven wurden angegeben; sie beschreiben die Variation der Energie als ein Ergebnis der gleichzeitigen Rotation der beiden Methylgruppen. Dies zeigte, daß für das Gesamtmolekül – die Wasserstoffatome eingeschlossen – im Gleichgewicht C_{2v}-Symmetrie besteht. Die Rotationsschwelle für eine CH_3-Gruppe ist 3,65 kcal/mole, in guter Übereinstimmung mit dem experimentellen Wert (3,4 kcal/mole [10]). Eine bizentrische Energieaufspaltung zeigt, daß mindestens 70% der Variation der totalen Energie auf die eine Summe Σ *E*(S–H) der räumlichen Wechselwirkungsterme zwischen Schwefel und den sechs Wasserstoffatomen entfallen. Dieses Ergebnis – in Übereinstimmung mit früheren Arbeiten – erhärtet von neuem das klassische Konzept der Hyperkonjugation.

Introduction

La résolution de l'équation de Schrödinger par une méthode variationnelle – visant la détermination de fonctions propres dont la connaissance permet d'atteindre en particulier la distribution électronique au sein d'une molécule donnée – peut s'effectuer dans le cadre d'un grand nombre d'approximations plus ou moins grossières allant de celles de Hückel à celles sur lesquelles reposent les formalismes dits *ab initio*.

Dans le domaine de la chimie minérale moléculaire – et plus particulièrement en chimie de coordination - il est apparu très vite que seules les méthodes semi- et non-empiriques pouvaient être raisonnablement utilisées, ces dernières ayant, si l'on en juge par un examen de la littérature la plus récente, la préférence des quanto-chimistes.

S'il est aisé de comprendre l'origine d'un tel état de fait, il nous a paru toutefois nécessaire de réexaminer le bien-fondé de l'affirmation selon laquelle seule une méthode *ab initio* permet d'atteindre la structure électronique d'un composé de coordination.

Que signifie en fait le vocable *ab initio* ? Celà veut dire en toute rigueur qu'une méthode de calcul ainsi qualifiée recherche *à la fois* une minimisation de l'énergie et la détermination *de facto* de la géométrie optimale de la molécule. On peut donc dire que, comme son nom l'indique, une véritable méthode *ab initio* n'impose *a priori* aucune "contrainte" géométrique au système qui est étudié (hormis, bien sûr, l'existence des liaisons chimiques).

Or, en fait, ces méthodes nécessitent un tel potentiel en moyens de calcul que, dans l'immense majorité des cas, les auteurs étudient des systèmes dont la géométrie a été préalablement déterminée d'une manière aussi précise que possible par voie expérimentale et portent en fait uniquement leurs efforts sur la minimisation de l'énergie du système ainsi constitué. Pour peu alors que la géométrie retenue soit entachée d'erreurs *mêmes minimes* , un temps de calcul souvent considérable sera ainsi dépensé sinon en pure perte du moins avec des avantages discutables si l'on compare les résultats ainsi obtenus avec ceux déduits d'une étude semi-empirique resposant sur une géométrie plus proche de la réalité.

La connaissance aussi approfondie que possible des géométries est donc actuellement un des buts fondamentaux vers lesquels il est nécessaire de tendre avant d'envisager ce qui sera certainement possible dans un futur proche - l'utilisation systématique des méthodes non-empiriques pour l'approche des distributions électroniques réelles.

C'est dans cet esprit que le tout récent article de Jacob et Lide [1] sur la géométrie de la diméthylsulfone $(CH_3)_2SO_2$ a retenu l'attention de notre groupe.

Il s'avère en effet que cette molécule étalon des composés tétracoordonnés du soufre (auxquels nous prêtons attention depuis plusieurs années tant du point de vue de leur physico-chimie que de leur intérêt en chimie théorique [2]) a fait l'objet d'un certain nombre d'études spectroscopiques dont les données les plus récentes figurent dans le Tableau 1. On s'accorde généralement en chimie moléculaire pour attribuer une confiance égale aux paramètres fournis par la diffraction électronique et la spectroscopie de micro-ondes. Or le Tableau 1 montre à l'évidence qu'il n'en est pas ainsi dans le cas de la molécule étudiée puisque – et ce fût l'objet essentiel du récent article de Jacob et Lide [1] – l'angle $\widehat{OSO}$ par exemple vaut respectivement 127°1 [3] et 120°8 *ou* 122°0 [1].

Il serait sans grand fondement en pareil cas d'effectuer un triple calcul par une méthode *ab initio* pour départager les deux études expérimentales que nous venons de citer. C'est ici que les méthodes semi-empiriques trouvent l'une des justifications de leur utilité, la seule condition restrictive étant que les énergies

Tableau 1

	Micro-ondes (Jacob et Lide [1])		Diffraction électronique (Oberhammer et Zeil [3])
	Géométrie A	*Géométrie* B	*Géométrie* C
r_{S-O} (Å)	1,433	1,425 (fixé)	1,425
r_{S-C} (Å)	1,770 (fixé)	1,780	1,770
r_{C-H} (Å)	1,085 (fixé)	1,085 (fixé)	1,077
∢ OSO (degrés)	120,82	122,02	127,1
∢ CSC (degrés)	103,45	102,68	102,5
∢ CSO (degrés)	-	-	106,2
∢ HCS (degrés)	110,8 (fixé)	110,8 (fixé)	
∢ HCH (degrés)			109,8

totales obtenues soient suffisamment distinctes d'une géométrie à l'autre pour que le choix qu'elles permettent soit sans équivoque.

Parmi ces méthodes semi-empiriques, la méthode de Hückel généralisée [4] a été écartée d'entrée de jeu en raison de ce qu'elle ne permet guère d'effectuer une analyse des mécanismes des barrières à la rotation, analyse qui constitue l'une des parties essentielles de notre travail.

Les résultats encourageants auxquels nous sommes tout récemment parvenus au moyen de la méthode CNDO/2 de Pople et Segal [5] lors d'une analyse conformationnelle de certains composés organiques [6, 7] et minéraux [8, 9] nous ont incités à retenir cette même méthode pour le problème ici posé.

Résultats

Nous nous sommes donc dans un premier temps attaché à voir laquelle des géométries du Tableau 1 conduit à une valeur minimale de l'énergie. Le Tableau 2 rassemble les résultats obtenus et appelle les remarques suivantes:

1° Pour chacune des géométries, la conformation la plus stable est celle, (60,60)[1], dans laquelle un hydrogène de chaque groupement méthyle se trouve dans le plan CSC et pointe dans la direction des oxygènes: nous rediscuterons

Tableau 2

		Géométrie A	Géométrie B	Géométrie C	Expérience
nergie totale n kcal/mole)	Conformation (60,60)[a]	−41657,520	−41649,731	−41646,313	
	Conformation (0,60)	−41653,867	−41646,179	−41642,488	
	Conformation (0,0)	−41649,157	−41641,545	−41637,442	
oment dipolaire n Debyes)	Conformation (60,60)	4,176	3,984	3,618	4,44 [2c], 4,50
	Conformation (0,60)	4,243	4,050	3,695	
	Conformation (0,0)	4,274	4,084	3,736	

[a] La *conformation de reference*, notée (0,0), est celle dans laquelle un hydrogène de chaque groupement méthyle se trouve dans le plan CSC et pointe *vers l'intérieur* de l'angle $\widehat{CSC}$. Lorsque ces deux hydrogènes particuliers tournent autour de la liaison (C-S) correspondante, l'un de l'angle θ l'autre de l'angle φ, on obtient alors la conformation (θ, φ): dans ces conditions, la conformation (60,60) par exemple est celle dans laquelle ce sont deux des hydrogènes *voisins des précédents* qui se trouvent alors dans le plan CSC *mais pointant maintenant vers l'extérieur* de l'angle $\widehat{CSC}$ (cf. Fig. 3).

---

[1] On trouvera une explication de cette symbolique dans la note qui figure en pied du Tableau 2.

d'ailleurs en détail le caractère privilégié d'une telle conformation à la fin de ce Mémoire;

2 pour cette conformation, l'énergie la plus basse est obtenue pour la structure A de Jacob et Lide [1] dans laquelle la longueur de la liaison (S–C) a été fixée *a priori* à la valeur 1,770 Å;

3 la géométrie de Oberhammer et Zeil [3] semble par contre la plus défavorable;

4 on peut remarquer enfin que la méthode CNDO/2 permet d'incliner – au sein des travaux mêmes de Jacob et Lide – vers la géométrie A plutôt que vers celle, B, dans laquelle ces auteurs se sont imposé une longueur de liaison (SO) égale à 1,425 Å.

Il est en outre remarquable de constater que ce que nous venons de dire en termes d'énergie peut être transcrit au niveau des moments dipolaires calculés et de leur comparaison à l'expérience (les valeurs 4,44 et 4,50 D provenant de mesures effectuées en solution dans le dioxane [2c] et par effect Stark [1]).

En résumé de cette partie, non seulement une méthode semi-empirique permet de discerner à peu de frais en ce qui concerne le temps de calcul – dans un ensemble de donnés expérimentales la géométrie à retenir pour un éventuel calcul *ab initio*, mais encore elle permet de lever certaines ambiguïtés auxquelles se heurtent les spécialistes des micro-ondes, ambiguïtés qui reposent sur le fait que dans ce domaine (comme d'ailleurs dans celui des constantes de force en infra-rouge) il arrive souvent que le nombre d'équations soit inférieur à celui des inconnues, obligeant ainsi à faire certaines hypothèses de travail.

Mais la méthode CNDO/2 permet encore d'aller plus loin. L'analyse des spectres de diffraction électronique [3] et de micro-ondes [1] a été conduite dans l'hypothèse où la molécule appartiendrait au groupe C_{2v}, les deux groupements méthyle étant alors l'image l'un de l'autre dans le plan σ_v. Jacob et Lide ont bien senti l'approximation ainsi faite puisqu'ils ne parlent pour leur part que d'une «probable symétrie C_{2v}, au moins en ce qui concerne les atomes lourds» [1].

Il était donc intéressant d'utiliser la méthode CNDO/2 pour progresser quelque peu sur ce point.

Partant alors de la géométrie A proposée par Jacob et Lide, il a été procédé à une analyse tridimensionnelle de la conformation des deux groupements méthyle: pour une conformation donnée ($\theta = C^{te}$) de l'un des méthyles, nous avons fait subir à l'autre méthyle une rotation de 60° (ψ variable). Les résultats concernant l'énergie totale de la molécule ont été reproduits dans le Tableau 3.

Tableau 3. Energie totale de la molécule (à-41640 kcal/mole près)

θ ψ	0	10	20	30	40	50	60
0	− 9.16	− 9.48	−10.36	−11.55	−12.72	−13,56	−13,87
10	− 9.48	− 9,73	−10.55	−11,70	−12,87	−13,75	−14,11
20	−10.36	−10,55	−11.29	−12,38	−13,52	−14,39	−14,79
30	−11.55	−11.70	−12,38	−13.40	−14,47	−15,31	−15,70
40	−12.72	−12,87	−13,52	−14,47	−15,47	−16,26	−16,61
50	−13,56	−13,75	−14,39	−15,31	−16,26	−16.97	−17,28
60	−13.87	−14,12	−14,79	−15,70	−16,61	−17,28	−17,52

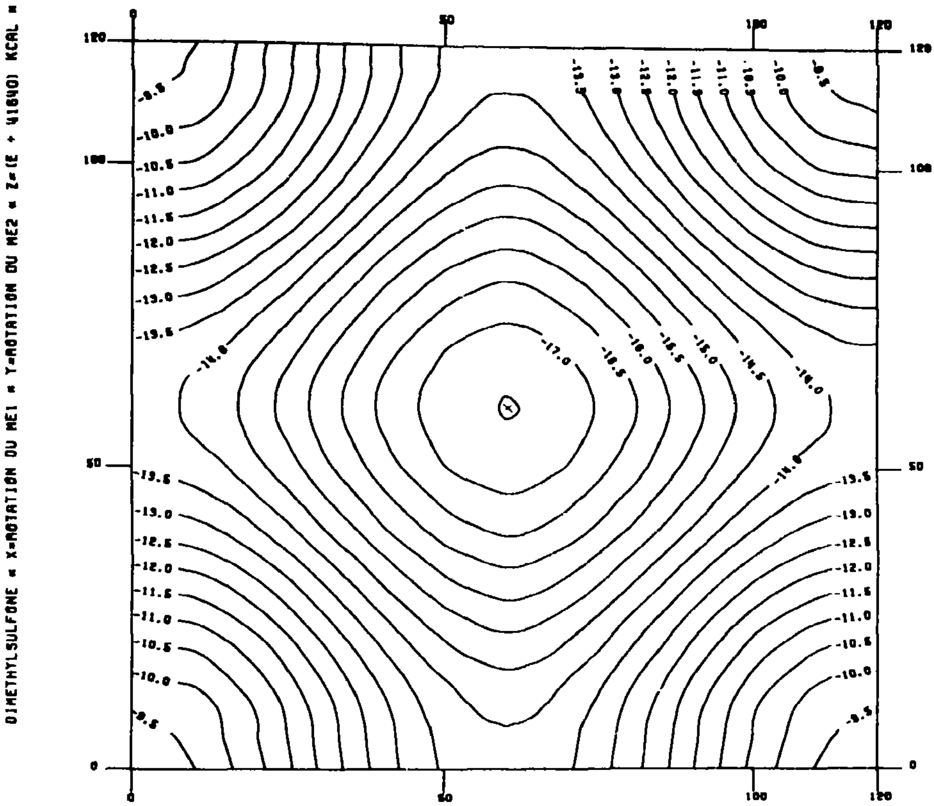

Fig. 1

La Fig. 1 rassemble les courbes d'iso-énergies correspondantes, la surface de potentiel ainsi définie ayant pour équation

$$
\begin{aligned}
E(\theta, \varphi) = & -41.649{,}157 - 2{,}355\,[(1-\cos 3\theta) + (1-\cos 3\varphi)] \\
& - 0{,}0195\,[(1-\cos 6\theta) + (1-\cos 6\varphi)] \\
& + 0{,}007625\,((1-\cos 6\theta)(1-\cos 3\varphi) + (1-\cos 3\theta)(1-\cos 6\varphi)) \\
& + 0{,}26425\,(1-\cos 3\theta)(1-\cos 3\varphi) \\
& + 0{,}06331\,(1-\cos 6\theta)(1-\cos 6\varphi)\,.
\end{aligned}
$$

Cette fonction mathématique permet de reproduire l'ensemble des résultats avec une incertitude au plus égale à 0,05 kcal/mole.

Il ressort de ces résultats que la conformation la plus stable est bien celle pour laquelle les groupements méthyle sont images l'un de l'autre dans le plan de symétrie des atomes lourds et tels que chaque méthyle présente un hydrogène dans le plan CSC qui pointe vers les oxygènes (Fig. 2): *la molécule de diméthylsulfone appartient donc bien au groupe* C_{2v}.

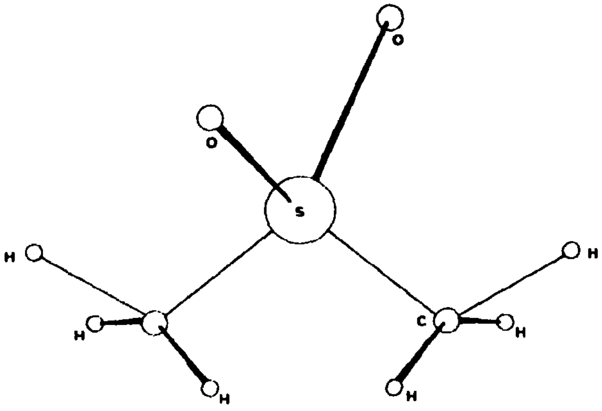

Conformation stable de la diméthylsulfone

Fig. 2

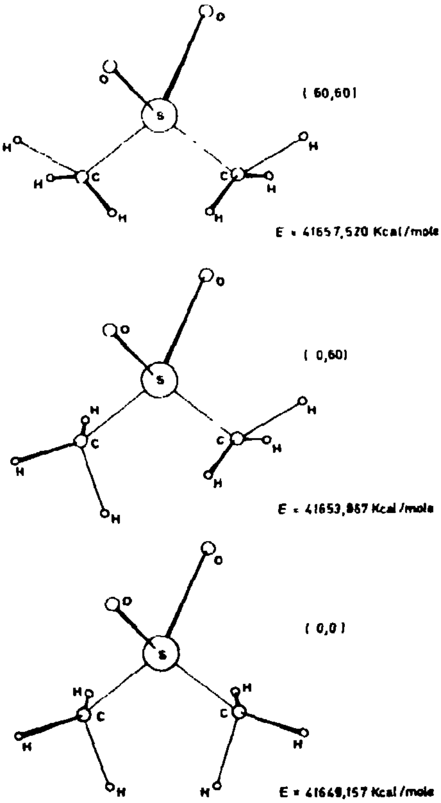

Fig. 3

La Fig. 3 rassemble en outre les données numériques relatives à trois conformations particulièrement intéressantes : $(\theta = 60, \psi = 60)$, $(\theta = 0, \psi = 60)$ et $(\theta = 0, \psi = 0)$; l'examen de cette figure indique en effet que, partant de la conformation (60,60) qui est la plus stable, la barrière à la rotation d'un groupement méthyle est égale à

$$\Delta E^{\dagger} = E(0{,}60) - E(60{,}60) = 3{,}65 \text{ kcal/mole}$$

en excellent accord avec la valeur estimée tout récemment par Clever et Westrum [10] (3,4 kcal/mole) au moyen des spectres de micro-ondes et dans des conditions d'entropie idéales.

Il résulte donc de tout ce qui précède que la conformation la plus stable de la molécule de diméthylsulfone est bien celle, (60, 60), de symétrie C_{2v}, correspondant à la géométrie A des atomes lourds proposée par Jacob et Lide. Les Tableaux 4 et 5 rassemblent, les charges électroniques et les populations de Wiberg [11] relatives à cette conformation.

Tableau 4. Distribution des charges électroniques pour la conformation (60,60)

S	$3s$	1,222	O	$2s$	1,784
	$3p_x$	0,829		$2p_x$	1,574
	$3p_y$	0,821		$2p_y$	1,560
	$3p_z$	0,810		$2p_z$	1,339
	$3d_{z^2}$	0,505		Total	6,257
	$3d_{xz}$	0,397			
	$3d_{yz}$	0,394	O	$2s$	1,784
	$3d_{x^2-y^2}$	0,467		$2p_x$	1,574
	$3d_{xy}$	0,194		$2p_y$	1,560
	Total	5,639		$2p_z$	1,339
				Total	6,257
C	$2s$	1,063	C	$2s$	1,063
	$2p_x$	1,013		$2p_x$	1,007
	$2p_y$	1,007		$2p_y$	1,013
	$2p_z$	1,002		$2p_z$	1,002
	Total	4,085		Total	4,085
H	$1s$	0,953	H	$1s$	0,953
H (dans le plan CSC)	$1s$	0,933	H (dans le plan CSC)	$1s$	0,933
H	$1s$	0,953	H	$1s$	0,953

Tableau 5. Populations de liaison selon Wiberg pour la conformation (60,60)

Liaison	Population de liaison
S–O	2,188
S–C	1,092
C–H (pour les hydrogènes hors du plan CSC)	0,958
C–H (pour les hydrogènes dans le plan CSC)	0,947

Ceci étant, une dernière question méritait d'être posée quant à *l'origine* de la barrière à la rotation que nous avons évoquée ci-dessus.

Ce problème a été résolu d'une manière maintenant classique [6–9] en procédant à un découpage bicentrique de l'énergie totale de la molécule selon l'expression

$$E = \sum_{\mathrm{A}} E_{\mathrm{A}} + \sum_{\mathrm{A<B}} E_{\mathrm{AB}}$$

que l'on peut grossièrement écrire sous la forme

$$E = E_b + E_{nb}$$

avec

$$E_b = \sum_{\mathrm{A}} E_{\mathrm{A}} + \sum_{\mathrm{A-B}} E_{\mathrm{AB}} \qquad \text{(A et B chimiquement liés)}$$

$$E_{nb} = \sum_{\mathrm{A\cdots B}} E_{\mathrm{AB}} \qquad \text{(A et B non chimiquement liés)}.$$

Une première analyse de la variation des termes E_b et E_{nb} en fonction de la conformation montre que c'est au terme E_{nb} que la courbe d'énergie totale doit sa forme.

Une analyse de l'évolution de chacun des 66 termes qui définissent l'énergie totale de la molécule montre qu'en fait les variations de cette dernière sont principalement liées à celles du terme global $\Sigma\, E(\mathrm{S{-}H})$ qui traduit les interactions entre l'atome de soufre et les six hydrogènes méthyliques; à elle seule, la variation de ce premier terme permet de rendre compte d'environ 70% du phénomène. Les 30% restants sont expliqués de façon quasi complète par la variation des seuls termes $\Sigma\, E(\mathrm{O{-}H})$ et $\Sigma\, E(\mathrm{H{-}H})$ (interaction entre les hydrogènes d'un méthyle avec ceux de l'autre); à eux seuls, ces trois termes permettent d'expliquer 95% de la variation d'énergie (Fig. 4).

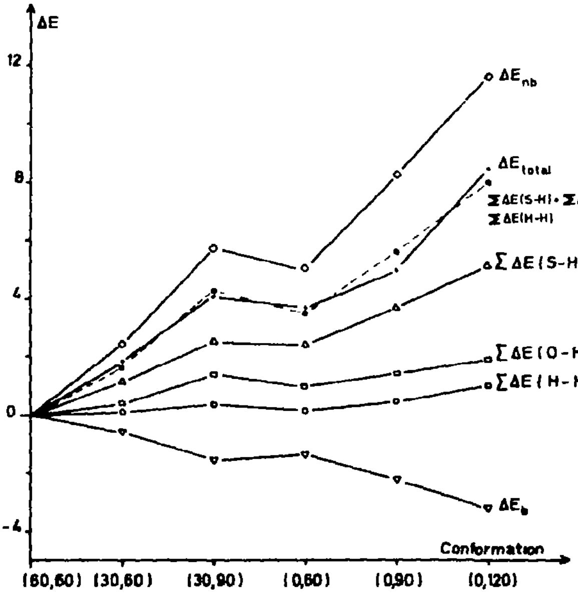

Fig. 4

On retrouve ici en quelque sorte, d'une manière toutefois plus atténuée, une origine de barrière à la rotation très comparable à celle qui nous a permis d'analyser la conformation des complexes de Lewis $F_3P \cdot BH_3$ et $F_2HP \cdot BH_3$ [8]: dans ces deux cas en effet, 98% de la barrière à la rotation autour de la liaison (P.B) étaient dus à une interaction dans l'espace entre l'atome de phosphore et les trois hydrogènes liés au bore, ce résultat traduisant d'ailleurs d'une manière quantitative le concept souvent évoqué par les expérimentateurs d'« hyperconjugaison du BH_3 ».

L'analyse de $\Delta E^\dagger$ dans le cas de la dimethylsulfone suggère une certaine analogie avec le travail dont nous venons de faire état et repose donc d'une manière nouvelle le problème de l'hyperconjugaison au sens large du terme.

Remerciements. Les auteurs tiennent à remercier très vivement le Professeur C. A. Coulson pour l'intérêt qu'il a bien voulu porter à ce travail et pour les suggestions positives qu'il a faites aussi bien quant au fond qu'à la forme de ce Mémoire.

Références

1. Jacob, F. J., Lide, D. R., Jr.: J. chem. Physics **54**, 4591 (1971).
2. a. Gallais, F., Voigt, D.: Bull. Soc. chim. France **1963**, 1935.
   b. Robinet, G., Dagnac-Amans, P., Labarre, J.-F.: J. Chim. physique **66**, 63 (1969).
   c. Fayet, J.-P., Labarre, J.-F., Mauret, P.: J. Chim. physique **66**, 459 (1969).
   d. Dagnac, P., Castan, P., Labarre, J.-F.: J. Chim. physique **67**, 522 (1970).
   e. Voigt, D., Dagnac, P., Castan, P., Labarre, J.-F.: J. Chim. physique **67**, 1817 (1970).
3. Oberhammer, H., Zeil, W.: J. molecular Structure **6**, 399 (1970).
4. Hoffmann, R.: J. chem. Physics **39**, 1397 (1963).
5. Pople, J. A., Segal, G. A.: J. chem. Physics **44**, 3289 (1966).
6. Pelissier, M., Serafini, A., Devanneaux, J., Labarre, J.-F., Tocanne, J.-F.: Tetrahedron **27**, 3271 (1971).
7. Leibovici, C., Labarre, J.-F.: Tetrahedron Letters **40**, 3759 (1971).
8. Labarre, J.-F., Leibovici, C.: Int. J. quant Chemistry, sous presse.
9. J. Chim. physique **68**, 1618 (1971).
10. Clever, H. L., Westrum, E. F.: J. physic. Chem. **74**, 1309 (1970).
11. Wiberg, K.: Tetrahedron **24**, 1083 (1968).

Dr. J.-F. Labarre
Laboratoire Associé au C.N.R.S. n 160
Université Paul Sabatier
38, rue des 36 ponts
F-31 Toulouse, France

SF_2

From thermochemical estimates made by O'Hare [16], HATX(SF_2) = 174.8 kcal/mole. Johnson and Powell [21] have determined from its microwave spectrum that SF_2 is a C_{2v} species with R(SF) = 1.589 Å, ∢ FSF = 98°16′.

SF_4

In a recent study of thiazyl tri- and monofluorides, O'Hare, Hubbard, Glemser and Wegener [22] pointed out that experimental values of $\Delta H_f^0(SF_4, g)$ range from −162 to −208 kcal/mole. Previously, O'Hare [16] had favored a mean of −182.1 kcal/mole, which value has been adopted in the present work. A compatible HATX(SF_4) is 330.7 kcal/mole.

The geometry of SF_4 is well established [23, 24]. The data used in our calculations are those of Tolles and Gwinn [23], as employed in the calculations of Brown and Peel [8]: $R(SF)_{ax} = 1.646$ Å, $R(SF)_{eq} = 1.545$ Å, ∢ $FSF_{ax} = 87.8°$, ∢ $FSF_{eq} = 101.5°$. Results of calculations run with data given by Kimura and Bauer [24] differed insignificantly.

SF_6

From well established data [16] a value HATX = 484.5 kcal/mole can be deduced. The internuclear distance R(SF) = 1.564 Å [25] seems preferable to that employed by Brown and Peel.

$S{=}SF_2$ *and* FSSF

Geometries of these species are well known [26]. Data used in our calculations include, for $S{=}SF_2$: R(SF) = 1.598 Å, R(SS) = 1.860 Å, ∢ SSF = 107.5°, ∢ FSF = 92.5°; for FSSF: R(SF) = 1.635 Å, R(SS) = 1.888 Å, ∢ FSS = 108.3°, ϕ(dihedral) = 87.9°. From thermochemical arguments O'Hare [16] estimated heats of formation for both species. With these and observed fundamental vibrational frequencies, values of HATX(SSF_2) = 266.3 kcal/mole and HATX(FSSF) = 258.7 kcal/mole were computed.

S_2F_{10}

The geometry of S_2F_{10} is believed to be that of two $C_{4v}SF_5$ pyramids linked through a long S–S bond, with hindered rotation about that bond [27]. Bond distances used in our calculations are: R(SF) = 1.56 Å, R(SS) = 2.209 Å.

From three indirect ΔH_f^0 values estimated by O'Hare [16], a value HATX(S_2F_{10}) = 869.9 kcal/mole was obtained. In one of his thermochemical schemes O'Hare estimated D(SS) in the molecule to be 55 ± 5 kcal/mole with an empirical relation between force constants, bond distances and bond energies. The proposed relative weakness of this bond is substantiated by the S_2F_{10} thermal decomposition studies of Trost and McIntosh [28], indicating a S–S bond-breaking activation energy of 49.2 kcal/mole.

S_2

Data employed for diatomic S_2 include $D_0^0 = 101.0$ kcal/mole [29, 30] and R(SS) = 1.889 Å [31], both of which values now appear to be well accepted.

Calculations and Results

In our initial approach CNDO/2-based binding energies in atomic units were plotted against experimental heats of atomization HATX (see Fig. 1). An acceptable linear relationship obviously obtained for molecules with only SF bonds, but equally obviously was invalid for molecules combining both SS and SF bonds, a result indicating that a rescaling factor common to both types was inappropriate.

To assist analysis of the situation the CNDO/2 program was adapted to permit computation of all diatomic contributions, E_{AB}, to the total molecular energy, as defined by Pople and Beveridge [2] for closed shell systems:

$$E_{AB} = \sum_{\mu}^{A} \sum_{\nu}^{B} P_{\mu\nu} \{F_{\mu\nu} + H_{\mu\nu}\} + \{P_{AA}P_{BB} - P_{AA}Z_B - P_{BB}Z_A\} \gamma_{AB} + Z_A Z_B / R_{AB} . \quad (1)$$

Previously Brown and Peel [8], working with their VESCF-MO theory (based on NDDO and entirely different integral approximations) defined as a "bond energy" a quantity like the first term of Eq. (1), and attempted to correlate these quantities with bond-stretching force constants. Fischer and Kollmar [15] with a modified CNDO method found that both the total bicentric energy E_{AB} and a subsidiary quantity,

$$E_{AB}^{R} = 2 \sum_{\mu}^{A} \sum_{\nu}^{B} P_{\mu\nu} H_{\mu\nu} \quad (2)$$

termed the resonance energy, were suitable qualitative measures of chemical bond strengths in a series of hydrocarbons; however, these authors were reluctant to compare E_{AB} directly with experimental dissociation energies. More recently Ehrenson and Seltzer [14] reexamined Wiberg's results with energy partitioning schemes and found that sums over "bond indices" defined according to Eq. (2) gave within original CNDO/2 parametrization a quite good correlation with heats of atomization. These authors furthermore (1) justified Wiberg's linear relation-

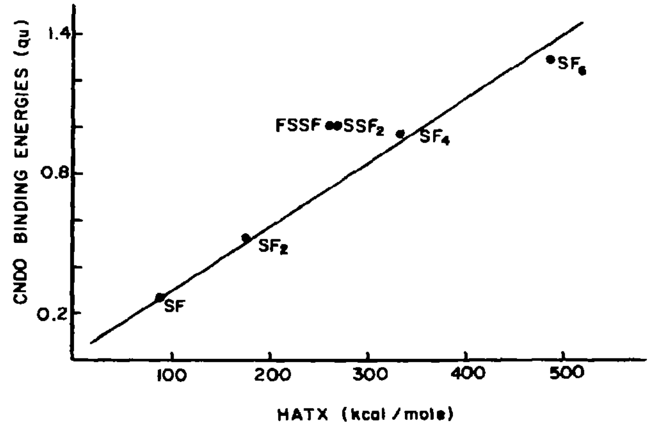

Fig. 1. Theoretical (CNDO) versus experimental (HATX) heats of atomization of sulfur-fluorine compounds

ships for many hydrocarbons including the perturbing variation in intercepts, (2) concluded that one-center contributions E_A to the total molecular energy were relatively constant per atom over a large family of hydrocarbons, (3) expressed belief that the bond index had some dependence on the $\sigma - \pi$ character of the bond, (4) concluded that for hydrocarbons all other contributions to E_{AB} beyond those reflected in Eq. (2) either cancel or are insignificant, and (5) found that, for hydrocarbons, interactions between non-bonded AB atom pairs were negligible.

In our own analysis on compounds of sulfur and fluorine we found (1) that E_A values were sufficiently constant to justify neglect of atomic promotional energy contributions in our rescaling process, (2) that contributions to E_{AB} from terms other than E^R_{AB} amounted in some instances to 10% of E^R_{AB} (and consequently rescaling was performed on total E_{AB} values), (3) that no significant dependence of E_{AB} on single-double bond character was observed within the limits of the available experimental data, and (4) that interaction between conventionally non-bonded atoms (such as F, F) appeared to be significant when summed over the molecule.

Two rescaling procedures of partitioned E_{AB} values were considered. In method *A* only total E_{AB} values between canonically bonded atoms were considered. E_{SF} was proportionally rescaled with 1/6 HATX(SF_6), the best established of experimental values, and E_{SS} was calibrated with HATX(S_2) (see Table 1). Theoretical heats of atomization for all others species were obtained as appropriate sums of these quantities.

In method *B* all bicentric E_{AB} values (where AB = SS, SF and FF) were summed for each molecule, including smaller attractions and repulsions between non-bonded pairs. HATX(SF_4) was used as a third calibrating factor. Results are again illustrated in Table 1.

Method *A* though yielding a less satisfactory correlation with HATX values is intrinsically somewhat more appealing, since it requires only two bonds for calibration. Furthermore it avoids, as observed in method *B*, a critical dependence of the repulsive E_{FF} interaction on the HATX values used for calibration. However, results of method *B* are much closer to estimated thermochemical values and indicate the importance of including all interactions in molecules of this type.

Since the total molecular energy is the sum over all bicentric E_{AB} and monocentric E_A terms, the success of this recalibration process (and the failure of the attempted single parameter rescaling procedure indicated in Fig. 1) establish conclusively that with the usual CNDO/2 parametrization the relative weights of bond contributions from chemically different atom pairs must be improperly reflected in the total CNDO molecular energies (and consequently in the bonding energies). Hence conclusions about geometry or conformation based on either of these quantities *for molecules of mixed-row atoms* must be suspect. On the other hand, with energy partitioning and external rescaling (or appropriate internal reparametrization) quite reasonable chemical results may be obtained.

Binding energies for the molecule ions were computed with the same rescaling factors used for neutral molecules.

Use of energy partitioning methods to estimate energies of the molecule ions permits circumvention of one problem observed during the course of this work. In the usual CNDO approach, binding energies are obtained as the difference

Table 1. Rescaled bond energies and heats of atomization

Species	E_{SF} (a.u.)	E_{SS} (a.u.)	Rescaled E_{SF} (kcal/mole)		Rescaled E_{SS} (kcal/mole)	ΣE_{SF} (a.u.)	ΣE_{FF} (a.u.)	Predicted heats of atomization (kcal/mole)		HATX (kcal/mole)
			Method *A*	Method *B*				Method *A*	Method *B*	
SF	−0.9079	—	78.4	85.2	—	−0.9079	—	78.4	85.2	87.1
SF^+	−0.9940	—	85.9	93.2	—	−0.9940	—	85.9	93.2	—
SF^-	−0.7362	—	63.6	69.1	—	−0.7362	—	63.6	69.1	—
SF_2	−0.9226	—	79.7	86.5	—	−1.8452	+0.0095	159.4	171.1	174.8
SF_2^+	−0.9966	—	86.1	93.5	—	−1.9931	+0.0024	172.3	186.4	—
SF_2^-	−0.7655	—	66.2	71.8	—	−1.5310	+0.0254	132.3	138.4	—
SF_4	−0.8874 (ax)	—	76.7	83.2	—	−3.7005	+0.0804	319.9	(330.7)	330.7
	−0.9628 (eq)	—	83.2	90.3	—					
SF_4^+	−0.7614 (ax)	—	65.8	71.4	—	−3.5079	+0.0243	303.2	324.1	—
	−0.9925 (eq)	—	85.8	93.1	—					
SF_4^-	−0.7886 (ax)	—	68.2	74.0	—	−3.2982	+0.1613	285.1	276.5	—
	−0.8605 (eq)	—	74.4	80.7	—					
SF_6	−0.9342	—	80.7	87.6	—	−5.6049	+0.2022	(484.5)	(484.5)	484.5
SF_6^+	−0.8506	—	73.5	79.8	—	−5.1039	+0.0574	441.2	467.0	—
SF_6^-	−0.8555	—	74.0	80.2	—	−5.1332	+0.3832	443.7	403.4	—
S_2	—	−1.4127	—	—	103.1	—	—	(103.1)	(103.1)	103.1
FSSF	−0.8736	−1.4585	75.7	81.9	106.3	−1.7624	+0.0065	257.4	270.3	258.6
SSF_2	−0.8994	−1.4503	77.7	84.3	105.7	−1.8010	+0.0137	261.2	271.9	266.3
S_2F_{10}	−0.9226	−0.5687	79.7	86.5	41.5	−9.4915	+0.3601	840.9	858.3	869.9
	−0.9338 (ax)		80.7	87.6						

Parentheses denote values used for calibration. Scaling factors are, for method *A*: 1 E_{SS} unit = 72.91 kcal/mole, 1 E_{SF} unit = 86.44 kcal/mole; for method *B*, 1 E_{SS} unit = 72.91 kcal/mole, 1 E_{SF} unit = 93.79 kcal/mole, 1 E_{FF} unit = 203.8 kcal/mole.

Table 2. Vertical ionization energies and electron affinities

Molecule	Ionization energies		Electron affinities	
	Method A (in eV)	Method B (in eV)	Method A (in eV)	Method B (in eV)
SF	10.0	10.0	2.8	2.8
SF_2	9.6	9.7	2.3	2.0
SF_4	11.1	10.6	1.9	1.1
SF_6	12.2	11.1	1.7	−0.07

between total molecular energies and summed energies of isolated atoms (or ions), the latter calculated with approximations similar to those used in the total energy computation. Under these approximations, however, $E(F^-)$ appears to be higher than $E(F)$, leading to an incorrect description of the electron affinity process of the fluorine atom and consequent errors in binding energies of species with F^- as a dissociation product.

For SF^+ and SF^-, results of both methods A and B are consistent with qualitative predictions based on increase or decrease in the number of antibonding electrons on the SF molecule.

With the computed binding energies and the experimental quantities $I(S) = 10.357$ eV [32], $EA(F) = 3.457$ eV [33], the ionization energy and electron affinity of SF may be computed according to the equations:

$$\begin{aligned} I(SF) &= BE(SF) + I(S) - BE(SF^+), \\ EA(SF) &= BE(SF^-) + EA(F) - BE(SF). \end{aligned} \tag{3}$$

Results obtained from rescaling methods A and B are essentially equivalent for this species: $I(SF) = 10.0$ eV, $EA(SF) = 2.8$ eV, both in excellent agreement with the *ab initio* results of O'Hare and Wahl [18].

Note in Table 1 that individual SF bonds in the SF_2 molecule are predicted to be stronger than those in the SF radical. This most likely reflects the engagement of the antibonding odd electron on SF in an additional bond. Vertical ionization energies and electron affinities for SF_2 as computed from appropriate analogs of Eq. (3) are listed in Table 2.

Rescaled binding energies of ions of SF_4 and SF_6 are listed in Table 1 and vertical ionization energies and electron affinities in Table 2. In the SCF iterations on these ions the total molecular energies and density matrices converged rapidly (within 40 cycles) for all species except SF_6^+. Although after 200 cycles a reasonable convergence of total energy resulted, a small asymmetry persisted in the density matrix. The E_{SF} value listed in Table 1 for SF_6^+ is the average over six bonds, while the sums are exact. A possible reason for the convergence difficulty may be that in the ionization process one electron is removed from the filled triply-degenerate $3t_{1u}$ level, and small density changes are induced over the whole molecule. In contrast, no difficulty was experienced with the SF_6^- calculation. Here the electron attached enters the non-degenerate $3a_{1g}$ MO, markedly increasing the 3s electron density on the sulfur atom. Santry and Segal [34] have previously commented on the low occupation predicted for this orbital in SF_6.

d orbital occupancy remains almost constant during both ionization and electron attachment processes for SF_4 and SF_6 (near 1.5 and 1.8 respectively). CNDO calculations thus do not support the suggestion of Harland and Thyne [35] that the relatively long lifetimes observed for SF_4^- and SF_6^- ions may be attributed to the ease with the captured electron may be accomodated in the *d* orbitals. The SF_6 electron affinity predicted by method *B* (close to zero) is consistent with the recent conclusions of Lifshitz, Hughes and Tiernan [36]. These authors, from studies of negative-ion charge-transfer reactions of SF_6, contend that the electron affinity of this molecule is much smaller than the value 1.49 eV indicated by previous experiments [37].

Although predicted electron affinities decrease gradually from SF to SF_6 (Table 2), the ionization energies as calculated by both rescaling methods increase smoothly except for an interruption in the trend at SF_2.

In his thermochemical analysis of the FSSF molecule, O'Hare [16], basing his arguments on the similarity of bond lengths and stretching constants, assumed equivalent bond energies for SF in FSSF and axial SF in SF_4. Table 1 values roughly substantiate this assumption. D(SS) in FSSF was deduced to be about 20 kcal/mole lower than that in diatomic S_2, and similarly D(SS) in SSF_2 was estimated at 10 kcal/mole lower than that of S_2. The partitioned energies of Table 1 contradict this, indicating rather an increase in S–S bond strength in both FSSF and SSF_2 over that of diatomic S_2. The qualitative reason for this may be much like that governing the well known fact that $D(O_2^+) > D(O_2)$. In both these molecules electrons that were unpaired and antibonding in S_2 are in part drawn off by the fluorine atoms.

Within both rescaling methods the gauche D_{4d} form of S_2F_{10} was predicted to be slightly more stable than that of the eclipsed D_{4h} form. The energy partitioned value for the S–S bond energy (41.5 kcal/mole) is in reasonable accord with previously mentioned experimental estimates, 55 ± 5 kcal/mole [16] and 49.2 kcal/mole [28].

Calculations in progress on other inorganic halides combining first and second row atoms indicate that the methods proposed here may permit prediction of equally satisfactory values of bond energies and related properties of several important families.

Acknowledgement. The author is grateful for support provided by a grant from the National Science Foundation and for a generous grant of computer time by the Graduate School of Illinois Institute of Technology. Dr. Y. P. Hsia and Mr. K. K. Lin assisted with the programming.

References

1. Hoffmann, R.: Extended Hückel theory calculations, Program 30, Quantum chemistry program exchange, Indiana University; Hoffmann, R.: J. chem. Physics **39**, 1397 (1963).
2. Dobosh, P. A.: CNINDO: CNDO and INDO molecular orbital program, Program 141, Quantum chemistry program exchange, Indiana University; Pople, J. A., Beveridge, D. L.: Approximate molecular orbital theory, New York: McGraw-Hill Book Company 1970.
3. Jug, K.: Theoret. chim. Acta (Berl.) **14**, 91 (1969).
4. Kaufman, J.: J. chem. Physics **43**, 152 S (1965).
5. Manne, R.: Theoret. chim. Acta (Berl.) **6**, 299 (1966).

6. Fenske, R. F., Radtke, D. D.: Inorg. Chem. **7**, 479 (1968).
7. Hillier, I. H.: J. chem. Soc. (London) **1969** A, 878.
8. Brown, R. D., Peel, J. B.: Austral. J. Chem. **21**, 2589, 2605, 2617 (1968).
9. Roby, K. R.: Theoret. chim. Acta (Berl.) **16**, 175, 194, 278, (1970).
10. Sichel, J. M., Whitehead, M. A.: Theoret. chim. Acta (Berl.) **7**, 32 (1967); **11**, 220, 239 (1968).
11. Yeranos, W.: Theoret. chim. Acta (Berl.) **13**, 346 (1969).
12. Pearson, R. G., Mawby, R. J.: Halogen chemistry, Vol. 3, p. 55, New York: Academic Press 1967.
13. Wiberg, K. B.: J. Amer. chem. Soc. **90**, 59 (1968).
14. Ehrenson, S., Seltzer, S.: Theoret. chim. Acta (Berl.) **20**, 17 (1971).
15. Fischer, H., Kollmar, H.: Theoret. chim. Acta (Berl.) **16**, 163 (1970).
16. O'Hare, P. A. G.: Argonne National Laboratory Report, ANL-7315, July 1968.
17. Carrington, A.: J. chem. Physics **50**, 2726 (1969).
18. O'Hare, P. A. G., Wahl, A. C.: J. chem. Physics **53**, 2834 (1970).
19. Glemser, O., Muller, A., Bohler, D., Krebs, B.: Z. Anorg. Allgem. Chem. **357**, 184 (1968).
20. Marriott, J. W., Cragg, J. D.: Electrical Research Associates, Tech. Report L/T-301 (1953).
21. Johnson, D. R., Powell, F. X.: Science **164**, 950 (1969). The author is grateful to Dr. K.-P. Wanczek for pointing out this and other more recent references on the SF_2 molecule.
22. O'Hare, P. A. G., Hubbard, W. N., Glemser, O., Weggener, J.: J. Chem. Thermo. **2**, 17 (1970).
23. Tolles, W. M., Gwinn, W. D.: J. chem. Physics **36**, 1119 (1962).
24. Kimura, K., Bauer, S. H.: J. chem. Physics **39**, 3172 (1963).
25. Ewing, V. C., Sutton, L. E.: Trans. Faraday Soc. **59**, 1241 (1963).
26. Kuczkowski, R. L.: J. Amer. chem. Soc. **86**, 3617 (1964); Kuczkowski, R. L., Wilson, E. B.: J. Amer. chem. Soc. **85**, 2028 (1963).
27. Harvey, R. B., Bauer, S. H.: J. Amer. chem. Soc. **75**, 2840 (1953).
28. Trost, W. R., McIntosh, R. L.: Canad. J. Chem. **29**, 508 (1951).
29. Berkowitz, J., Chupka, W. A.: J. chem. Physics **50**, 4245 (1969).
30. Budininkas, P., Edwards, R. K., Wahlbeck, P. G.: J. chem. Physics **48**, 2859 (1968).
31. Herzberg, G.: Spectra of diatomic molecules. Princeton, N. J.: D. Van Nostrand and Co. Inc. 1950.
32. Moore, Ch. E.: Atomic energy levels, Vol. I, Circular 467, Washington, D.C.: National Bureau of Standards 1949
33. Berry, R. S., Riemann, C. W.: J. chem. Physics **38**, 1540 (1963).
34. Santry, D. P., Segal, G. A.: J. chem. Physics **47**, 158 (1967).
35. Harland, P. W., Thynne, J. C. J.: Inorg. Chem. Letters **7**, 29 (1971).
36. Lifshitz, C., Hughes, B. M., Tiernan, T. O.: Chem. Physics Letters **7**, 469 (1970).
37. Kay, J., Page, F. M.: Trans. Faraday Soc. **60**, 1042 (1964).

Prof. Dr. A. L. Companion
Department of Chemistry
Illinois Institute of Technology
Chicago, Illinois 60616, USA

Theoret. chim. Acta (Berl.) 25, 277—288 (1972)
© by Springer-Verlag 1972

The Electronic Structure of Groups of Isomeric Heteroaromatic Systems

IV. Structure and Spectra of Pyridones and Their N-Methyl Derivatives

M. Cignitti and L. Paoloni

Laboratories of Chemistry, Istituto Superiore di Sanità, Roma,
Gruppo Chimica Teorica, Università, Palermo, Italy

Received February 22, 1971

Using the CNDO procedure, an all-valence electron study, including configuration interaction, was made of the three pyridone isomers and their N-methyl derivatives. The calculated dipole moments were found to be in reasonable agreement with the available experimental data, and the value predicted for N-methyl-3-pyridone was 7.2 D.

Transition energy, intensity and assignment were compared with ultraviolet spectra, recorded for the first time on all the N-methyl substituted isomers under similar conditions in non-aqueous solvents. The agreement is satisfactory for the 2- and 4-pyridone isomers, less so for N-methyl-3-pyridone.

Mit Hilfe der CNDO-Methode wurden die drei Pyridonisomeren und ihre N-methyl-Derivate untersucht. Die berechneten Dipolmomente sind in befriedigender Übereinstimmung mit den experimentellen Daten; der berechnete Wert für N-methyl-3-Pyridon war 7,2 D. Die berechneten Übergangsenergien, Intensitäten und Zuordnungen wurden mit dem experimentellen UV-Spektrum verglichen, das zum ersten Mal für alle N-methyl-substituierten Isomeren unter ähnlichen Bedingungen in nichtwäßrigen Lösungsmitteln aufgenommen wurde. Die Übereinstimmung ist zufriedenstellend für die 2- und 4-Pyridon-Isomeren, jedoch weniger gut für N-methyl-3-Pyridone.

On donne les résultats d'un calcul CNDO avec interaction des configurations, sur tous les électrons des pyridones isomères et leurs derivés N-méthylés. Les moments dipolaires calculés sont en bon accord avec les données expérimentales. La valeur 7.2 D est prévue pour le moment du N-méthyl-3-pyridone.

L'energie, l'intensité et les attributions des transitions calculées sont comparées avec les spectres d'absorption dans l'ultraviolet des N-méthyl-pyridones isomères. Ces spectres ont été mésurés sous des conditions rigueurésement comparables en solution non-aqueuse pour la prémière fois. L'accord est satisfaisant pour les derivés du 2- et du 4-pyridone, moins pour le derivé du 3-pyridone.

A previous comparative study of the π-electron structure of the three pyridone isomers [1] has shown that a substantial similarity was to be expected in their ground-state properties and, in particular, that there was no reason to doubt the existence of the isomer 3-pyridone and its derivatives. These conclusions were the starting-point for the work which led to the synthesis of N-methyl-3-pyridone, reported in the same paper [1].

A localization transformation of the π-electron MO's was described in a subsequent paper [2], and their analysis showed that the classic formulae are a realistic representation of the π-electronic structure of pyridones since the double-bond localization in I, II, and III agrees with the maximum π-electron localization of their MO's.

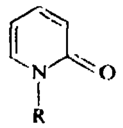

I

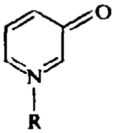

II

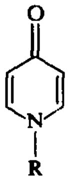

III

The present paper describes an all-valence electron study of the same compounds ($R=H, CH_3$), carried out for testing our previous conclusions [1] – based only on the π-electrons – and also for obtaining reliable predictions of their dipole moments and electronic transitions.

Within this scope we found it necessary to record the UV spectra of I, II, and III ($R=CH_3$) in non-aqueous solvents under comparable conditions. The spectra of the O- and N-methyl derivatives of the hydroxy-pyridine isomers seem in fact to have been studied mainly for identifying the tautomeric forms present in their aqueous solutions [3–8]. Thus, e.g., the spectrum of 3-hydroxy-pyridine methoiodide has been reported in aqueous solution at various pH's [6] and in neutral, acidic, and alkaline ethanol [5], and the spectrum of its methochloride has been studied in water, in dioxane[1], and in water-dioxane mixtures [4c].

These spectral data have been regarded by a number of authors as supporting the existence of a species of "salt-like character", the zwitter-ion [4] or phenol-betain [5] structure IV, with the stated [7] or implied presumption that the structure II could not exist, and with the extensive conclusion that the zwitter ion formulae represented the normal amido tautomers of this group of compounds [4, 8].

This interpretation of the spectral data is still widely accepted in the literature [9], and the writing of structure II is considered impossible as a matter of course [10].

Another object of the work here reported was, therefore, to see to what extent a formulation like IV can be based on a realistic evaluation of the molecular electron density distribution.

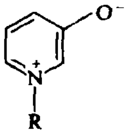

IV

---

[1] From Ref. [4c] it is not apparent whether this spectrum has been recorded on the salt dissolved in pure dioxane or on its water solution diluted with a large excess of dioxane.

Method of Calculation

The MO's of the isomers I, II, and III ($R = H$, CH_3), were obtained by the CNDO procedure [11] extended by configuration interaction as proposed by Del Bene and Jaffé [12]. The program, based on their parameters and including the lowest 40 mono-excited configurations, was made available to us by Professor Leibovici, to whom we express our thanks. The computation of the ground-state properties, also carried out with the CNDO/2 program – written by Segal (QCPE n. 91) – gave equivalent results.

Three different rotational positions of the methyl group were considered for each isomer in order to examine the influence of N-methyl substitution and to determine the configuration of lowest energy. The ring bond lengths and angles were the same as in Ref. [1]. For other details see the Appendix.

Results

A. Ground State

The molecular charge diagrams of pyridones and their N-methyl derivatives, given in Fig. 1, show that the nitrogen atom bears a small negative charge in all compounds except the 3-pyridones, whose nitrogen is positively charged. However, this electron deficiency, about +0.1, is 2.5–4 times smaller than that of the carbon atom bound to the substituent oxygen. This latter possesses in all cases a negative charge of about 0.5 e.

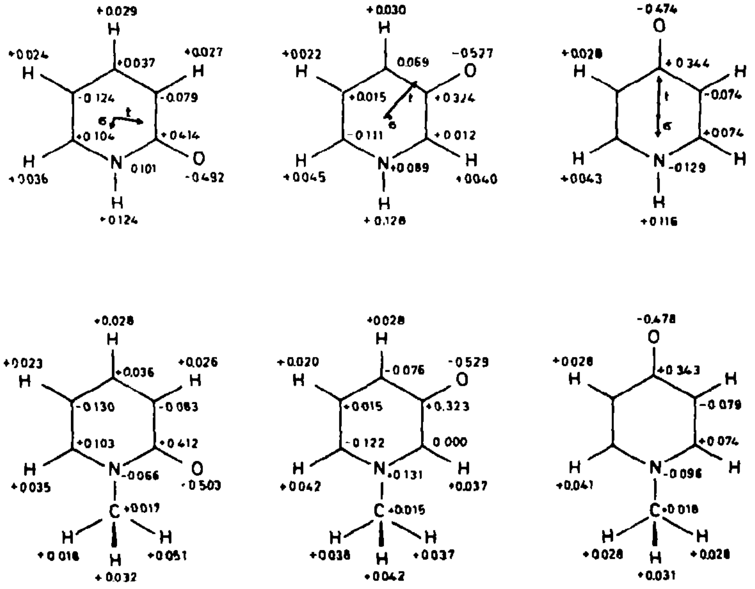

Fig. 1. Net total charges, total dipole moment and its μ_σ component of pyridones and their N-methyl-derivatives

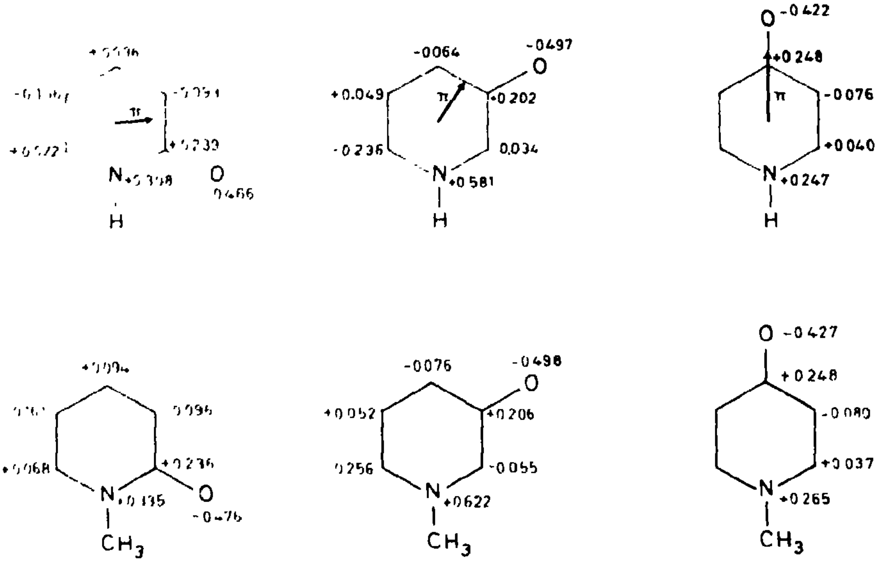

Fig 2 Net π-charges and μ_π component of dipole moment of pyridones and their N-methyl derivatives

The total net charges are the result of a complex balance that can be seen by examining separately the contribution of the π-electrons, shown in Fig. 2. The negative charge of the extracyclic oxygen derives almost entirely from the π-electron migration. The small contribution, 5 -10%, from the σ-electrons increases in the order 2- < 3- < 4-pyridone, and seems not affected by the N-methyl substitution. The π-electron loss of the nitrogen atom in the 2- and 4-pyridone isomers is smaller than the negative charge due to the σ-electron migration. This migration is the largest with 3-pyridone, about 20% greater, but it is not sufficient to compensate for a π-electron loss nearly double of that occurring in the other isomers.

An interesting point is that the largest negative charge in the pyridine ring is located on the carbon atom *para* to the substituent oxygen. This negative charge results from the accumulation of π-electrons which is neutralized only in part (20% for C (5) in 2-pyridone and 50% for C (6) in 3-pyridone) by the loss of σ-electrons. This net π-migration on the ring position *para* to the oxygen atom might explain why the 4-pyridone nitrogen shows the lowest π-electron vacancy and the 3-pyridone nitrogen the highest π-electron vacancy: the π-migration brings in a compensation in the first molecule and an accumulation of the π-electron losses in the second.

This analysis of the molecular electron distribution shows that the zwitter-ion formulae, like IV, approximately represent the polarization of the π-electrons in the oxygen and nitrogen $p\pi$ atomic orbitals. However, a more realistic image of the molecular polarities, based on the total charges, should localize the positive charge on the carbon atom bound to the substituent oxygen, because it is the carbon end of the C=O group which loses both σ- and π-electrons and has therefore the largest electron vacancy in the molecule.

The molecular polarity is largely determined by the π-electron distribution. This follows from the comparison of the total dipole moments, reported in Table 1, and their σ- and π-components, shown in Figs. 1 and 2. The centroid of the positive charge is progressively displaced away from the nitrogen atom when the substituent oxygen moves to the positions 2, 3 and 4.

Table 1. Calculated and experimental[a] dipole moments, D

R		2-oxo	3-oxo	4-oxo
H	μ_x	−4.78	−4.78	0
	μ_y	0.68	−5.78	−7.26
	$\mu_{tot.}$	4.83	7.49	7.26
	$\mu_{exper.}$	1.95	—	5.3
CH_3	μ_x	−4.76	−4.75	0
	μ_y	0.36	−6.28	−7.55
	$\mu_{tot.}$	4.78	7.88	7.55
	$\mu_{exper.}$	4.04	—	6.9

[a] See Ref. [13]. The experimental values of the R=H compounds do not represent the value of the isolated molecule because of strong hydrogen bonded association [17] and solvent-solute interactions [18].

Table 2. Energy levels of pyridone isomers and their N-methyl derivatives, eV

	2-oxo		3-oxo		4-oxo	
	NH	NMe	NH	NMe	NH	NMe
π	2.714	2.812	3.110	3.242	3.124	3.208
π	0.804	0.884	0.782	0.909	0.411	0.481
π	− 0.300	− 0.186	− 1.211	− 0.936	− 0.159	− 0.013
π	− 9.769	− 9.608	− 8.825	− 8.715	− 9.870	− 9.657
n	−11.206	−11.043	−10.165	−10.030	−10.445	−10.343
π	−12.880	−12.429	−12.610	−12.370	−11.944	−11.862
π	−13.781	−13.636	−14.199	−13.745	−14.329[a]	−13.779
σ	−14.221	−14.079	−14.209	−13.990	−14.184[a]	−13.995
σ	−14.663	−14.433	−14.621	−14.463	−14.908	−14.702
σ	−16.590	−16.106	−16.772	−16.397	−16.768	−16.338[a]
π	−17.523	−16.215	−17.576	−16.468	−17.171	−16.268[a]
σ	−18.142	−16.688	−17.720	−16.889	−17.564	−16.488
σ	−18.686	−17.559	−19.042	−18.145	−18.864	−18.195
σ	−19.886	−18.727	−20.270	−18.479	−20.130	−18.778
π (Me)	–	−19.911	–	−20.426		−19.967
σ	−22.861	−20.475	−22.783	−20.744	−22.795	−20.787
σ	−26.888	−22.237	−26.864	−22.285	−26.584	−21.165
σ	−27.684	−25.189	−28.162	−25.527	−27.174	−26.255
σ	−32.310	−27.871	−31.826	−27.598	−33.746	−27.768
σ	−37.202	−30.920	−36.877	−30.895	−34.864	−28.919
σ	−42.000	−32.425	−43.038	−32.922	−42.945	−34.983
σ	−47.485	−39.039	−47.434	−38.347	−46.754	−36.561
σ		−42.068		−43.359		−43.408
σ		−48.304		−48.068		−47.298

[a] σ and π assignment reversed with respect to the other isomers.

Table 3. Singlet-singlet electronic transitions of pyridone isomers and their N-methyl derivatives

R	ΔE, eV	f	Polarization		Assignment[*]	
			x	y		
2-oxo						
H	3.78	0	—		$n \to \pi^*$	
	4.19	0.11	−0.83	−0.56	$\pi \to \pi^*$	
	5.37	0.18	−0.73	0.68	$\pi \to \pi^*$	
	5.88	0	—	—	$n \to \pi^*$	
CH_3	3.78	0		—	$n \to \pi^*$	
	4.15	0.10	0.79	0.61	$\pi \to \pi^*$	
	5.28	0.16	0.76	−0.65	$\pi \to \pi^*$	
	5.82	0	—	—	$n \to \pi^*$	
3-oxo						
H	3.00	0.11	−0.90	0.44	$\pi \to \pi^*$	
	3.17	0		—	$n \to \pi^*$	
	3.91	0	—	—	$n \to \pi^*$	
	4.45	0.14	−0.84	−0.54	$\pi \to \pi^*$	
CH_3	3.06	0.11	−0.89	0.45	$\pi \to \pi^*$	
	3.22	0			$n \to \pi^*$	
	3.95	0		—	$n \to \pi^*$	
	4.45	0.13	−0.85	−0.52	$\pi \to \pi^*$	
4-oxo						
H	3.01	0			$n \to \pi^*$	A_2
	4.51	0.011	1	0	$\pi \to \pi^*$	B_2
	5.09	0.26	0	1	$\pi \to \pi^*$	A_1
	5.30	0			$n \to \pi^*$	B_1
CH_3	3.04	0			$n \to \pi^*$	A_2
	4.41	0.016	1	0	$\pi \to \pi^*$	B_2
	4.96	0.26	0	1	$\pi \to \pi^*$	A_1
	5.27	0	–	—	$n \to \pi^*$	B_1

[*] The transitions of the 4-pyridone isomers are labelled also with the C_{2v} irreducible representations of the excited state.

The experimental dipole moments of N-methyl-2-pyridone and N-methyl-4-pyridone, measured in benzene solution, are [13] 4.04 and 6.9 *D* respectively, about 0.7 *D* smaller than the calculated values. If this difference is regarded as due to the approximations of the method, then the best prediction for the N-methyl-3-pyridone dipole moment is 7.2 *D*.

The sequence of the energy levels, shown in Table 2, is the same for all the isomers, with minor differences for the 4-pyridone compounds. The highest occupied MO is of π-character, but the next below is largely localized on the non-bonding AO of oxygen. The lowest occupied π MO of the N-methyl derivatives has its population mainly distributed on the methyl group. The so-called hyperconjugation is therefore embodied in the procedure, and the non-symmetric orientation of the methyl group is favoured with respect to those orientations which have one hydrogen atom lying in the plane of the ring. The energy gain due to methyl rotation (see Table 4) is 0.19, 0.13, and 0.32 (or 0.54, 0.20, and 0.32) eV

Table 4. Total energies of pyridones and their N-methyl derivatives, eV

N-substituent[a]	2-oxo	3-oxo	4-oxo
H	−858.92	−855.57	−863.41
CH_3, 0°	−933.98	−936.56	−944.76
+90°	−933.79	−936.43	−944.44
−90°	−933.44	−936.36	−944.44

[a] The 0° angle of methyl group corresponds to a C—H bond in the plane perpendicular to the ring plane. Rotation is negative towards the side of the oxygen atom.

respectively, for each conformation of the 2-, 3-, and 4-pyridone isomers. The charge distribution is only slightly affected by the rotation of the methyl group, and the alteration of the dipole moment is negligible ($\simeq 0.02$ *D*).

B. Excited States

The four lowest calculated singlet-singlet transitions and their assignment is shown in Table 3. The 2-oxo and the 4-oxo isomers show the same pattern: a lowest $n \rightarrow \pi^*$ followed by two $\pi \rightarrow \pi^*$ transitions. This sequence changes in the 3-oxo isomer, where the lowest $\pi \rightarrow \pi^*$ is followed by two $n \rightarrow \pi^*$ transitions.

The N-methyl substitution has a small effect, bathochromic on the $\pi \rightarrow \pi^*$ and negligible or hypsochromic on the $n \rightarrow \pi^*$ transitions of the 2-oxo and 4-oxo isomers. The same substitution appears to have an hypsochromic effect on all the transitions of the 3-oxo isomer.

The comparison of the calculated transitions with the recorded spectra is shown in Fig. 3. The agreement is very satisfactory for the position and relative intensity of the N-methyl-2-pyridone spectrum. The experimental assignment based on the band shift in aqueous solutions, seems to correspond with that deduced from the transition moment and the electron population analysis.

The calculated $\pi \rightarrow \pi^*$ transitions of the N-methyl-4-pyridone compare very well with the observed bands. Reasonable evidence for the $n \rightarrow \pi^*$ transitions predicted at 5.30 eV is the remarkable difference between the absorption intensity of the H_2O and that of the NaOH solutions in the 45000 cm^{-1} region. The lowest $n \rightarrow \pi^*$ is however predicted at about 24000 cm^{-1} (400 nm), a region where we have not found any appreciable absorption down to $\varepsilon \simeq 10$.

The agreement is relatively poor with the spectrum of the N-methyl-3-pyridone, whose lowest calculated transition, predicted $\pi \rightarrow \pi^*$, falls just outside the first absorption band, whose prevailing character is $n \rightarrow \pi^*$. It is possible that a marked hypsochromic shift of this band may be due to a strong dipole-dipole interaction with acetonitrile. The spectra of the liquid film and of the saturated solution in cyclohexane (5 cm, unknown concentration) show a pronounced shoulder at 390 nm and the maximum is displaced to 365 nm.

There are no spectral data to be compared with the singlet-triplet transitions listed in Table 5. Although these predictions are in general less reliable than those for the singlet-singlet, it is remarkable and, we believe, significant that 3-pyridone

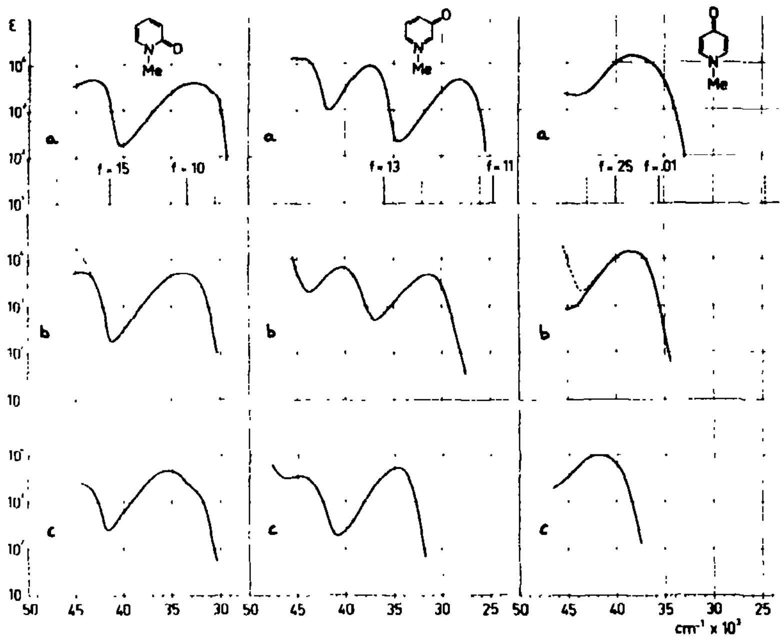

Fig. 3a–c. Absorption spectra of N-methyl pyridones. Solvents: a Acetonitrile; b - - water; - - - - - 0.1 N NaOH; c 0.1 N HCl. The calculated transitions and their oscillator strengths *f* are shown on the base-line of a. The broken lines mark here the forbidden transitions

Table 5. Singlet-triplet electronic transitions of pyridone isomers and their N-methyl derivatives, eV

N-substituent	2-oxo		3-oxo		4-oxo	
H	2.47	$\pi \rightarrow \pi^*$	0.89	$\pi \rightarrow \pi^*$	2.76	$\pi \rightarrow \pi^*$
	3.48	$\pi \rightarrow \pi^*$	2.96	$n \rightarrow \pi^*$	3.02	$\pi \rightarrow \pi^*$
	3.78	$n \rightarrow \pi^*$	3.17	$n \rightarrow \pi^*$	3.02	$n \rightarrow \pi^*$
CH_3	2.49	$\pi \rightarrow \pi^*$	1.00	$\pi \rightarrow \pi^*$	2.74	$\pi \rightarrow \pi^*$
	3.46	$\pi \rightarrow \pi^*$	2.98	$n \rightarrow \pi^*$	2.99	$\pi \rightarrow \pi^*$
	3.80	$n \rightarrow \pi^*$	3.22	$n \rightarrow \pi^*$	3.05	$n \rightarrow \pi^*$

and its N-methyl derivative should absorb in the near infrared, having their lowest triplet level lowered towards the ground-state by a factor of 2.5 or 3 compared with the other isomers. This circumstance could be related to the rapid alteration of the compound when, even for a short time, it is heated above 100° C.

The analysis of the electron distribution of the singlet excited states reveals several interesting features mainly concerning the C=O group and the nitrogen atom. The polarization induced by the $\pi \rightarrow \pi^*$ transitions causes a shift of 0.3–0.5 e within the π-orbitals but leaves unchanged the ground state σ-electron distribution. In all compounds the $\pi \rightarrow \pi^*$ transitions occur with a net transfer of π-electrons from the extra-cyclic oxygen to the ring atoms, and the corresponding reduction of the negative charge on oxygen varies from 0.1–0.25 e. The nitrogen $2p\pi$-orbital population of the 2-oxo and 4-oxo compounds is also reduced by the $\pi\rightarrow\pi^*$ transitions and the net negative total charge of the ground state is reversed in some cases. The opposite occurs in the 3-oxo compound, where the $2p\pi$ nitrogen population is increased and the net positive charge of the ground state reversed because the balance now gives about -0.15. Therefore as a consequence of the $\pi\rightarrow\pi^*$ transitions the electron vacancy of the nitrogen $2p\pi$-orbital is increased in the 2-oxo and 4-oxo, and decreased in the 3-oxo compounds.

About 75% of the $n\rightarrow\pi^*$ transition electron transfer comes from the in-plane $2p$ orbitals of oxygen, whereas its $2s$ population remains nearly constant at about 1.72 e, for all the isomers. As a consequence, the oxygen atom acquires a net positive charge of about 0.15. The simultaneous change of the ring core polarization is rather small, with shifts never larger than 0.08 e on a single orbital. The n-electron migration from oxygen is partly balanced by a donation to its $2p\pi$-orbitals, whose negative charge increases by about 0.05 in the 3-oxo to a maximum of 0.15 in the 4-oxo compound. The nitrogen $2p\pi$-orbitals receive the largest share of n-electrons in the 3-oxo compound, which in the $n\rightarrow\pi^*$ excited states acquires on nitrogen a negative net charge comparable to that of the other isomers. More uniformly, the strong positive charge of the C=O-group carbon atom in all isomers is reduced to about half of its ground state value.

Discussion and Conclusions

Our previous calculations [1], based on the π-electrons only, suggested that 2-pyridone was the most stable among the three isomers. The total energies of our present calculations, including all the valence electrons (Table 4), indicate 4-pyridone as the lowest-energy isomer. In both cases 3-pyridone is the intermediate term in the series.

It should be stressed, however, that the comparison cannot be decisive because of the uncertainties in the bond angles and distances, which were assigned average values, based on the data available for N-methyl-2-pyridone and similar molecules[2].

Concerning more specifically the case of 3-pyridones and the structural peculiarities that the experimental chemists have assigned to it [7, 8], we think it convenient to collect here several theoretical peculiarities, which might be typical of these compounds:

i) the total π-orbital of the ring nitrogen shows the largest π-vacancy (about 0.6); the migration of σ-electrons, which is sufficient to make the nitrogen of the other isomers negative, leaves the atom slightly positive;

ii) the compound has the largest dipole moment, where the σ-component adds to the π-component with an increasing instead of a decreasing effect;

---

[2] For this same reason we have not made a comparison between the total energies of the oxo- and hydroxy-tautomers. Establishing a stability sequence for isomeric molecules with atoms of different valence state is likely beyond the limit of reliability of the CNDO procedure, unless the dimensional parameters of the molecules are known.

iii) its lowest singlet-singlet transition is predicted $\pi \rightarrow \pi^*$, and not $n \rightarrow \pi^*$ as in the other pyridones;

iv) its lowest singlet-triplet transition is in the near infrared;

v) its ionization potential, as measured by the energy of the highest occupied MO is nearly 1.0 eV lower than that of the other terms.

Although the spectral predictions regarding 3-pyridone and its N-methyl-derivative are apparently less reliable than the others here made[3], we believe that the whole results show that 3-pyridone should be affected by radiation, heat or reagents much more easily than its isomers.

The method of calculation is another aspect of our results which requires a few comments. The data we have discussed so far have been obtained by using the Pariser-Parr formulae for the γ_{pq} integrals. The alternative use of the Nishimoto-Mataga procedure leads to minor differences in the charge distribution of the ground state. Marked differences are found instead for the excited state. The lowest transition is always red-shifted by 0.2–0.4 eV; the others are less affected. For comparison we report here the transitions calculated for N-methyl-3-pyridone: 2.84 eV ($f = 0.0$ $n \rightarrow \pi^*$); 3.10 ($f = 0.11$, $\pi \rightarrow \pi^*$); 3.71 ($f = 0$; $n \rightarrow \pi^*$); 4.47 ($f = 0.16$, $\pi \rightarrow \pi^*$).

The $n \rightarrow \pi^*$ transitions are the most affected by the Nishimoto-Mataga γ_{pq} integrals, and the result seems worst with respect to the spectral data: e.g., for N-methyl-2-pyridone 3.41 eV ($f = 0$, $n \rightarrow \pi^*$), to be compared with 3.78 eV in Table 3. Moreover, the Nishimoto-Mataga integrals slow down the convergence, increasing the computing time by a factor of about 10.

A final comparison can be made with the Pariser-Parr-Pople, π-electron method. The molecular diagrams (Fig. 2) are similar to those of our previous work [1][4]. The spectral predictions, based on 12 monoexcited configurations, which were not published at that time, gave the lowest $\pi \rightarrow \pi^*$ at 4.92, 3.77, and 4.88 eV, respectively, for 2-, 3-, and 4-pyridone. The corresponding transitions in Table 3 are 5.35, 3.02, and 4.51 eV, within accepted limits of approximation for the 2-oxo and the 4-oxo-compounds.

Appendix

Theoretical

The following additions have to be made to the geometry adopted in Ref. [1]: ring C–H: 1.075 Å; methyl C–H: 1.09 Å; N–H: 1.02 Å; and N–CH_3: 1.48 Å.

---

[3] An explanation of this apparent failure of the method may be found in the uncertainties of the dimensional parameters of the molecule, which might differ significantly from those we have assumed. Moreover, the CNDO approximation might fail with a high polar molecule because the core polarization accounted for in the procedure can be inadequate [14].

[4] In that paper we observed a quantitative relationship between the nitrogen net π-charge and the relative displacement of the methyl proton magnetic resonance absorption. We have now measured the PMR shift of N-methyl-4-pyridone: PPM 3.07 in $(CD_3)_2CO$; 3.64 in D_2O; 3.76 in $D_2O + NaOD$, and 4.13 in $D_2O + DCl$. Comparison of these with the previous data [1] shows that the qualitative trend with the net π-charges is maintained, although the relationship does not hold.

Experimental

Preparation of N-methyl-3-pyridone has been somewhat modified with respect to Ref. [1]. The liquid which separates after saturation with potassium carbonate was repeatedly extracted with acetone, which was then evaporated from the extract in the shortest possible time. The residue was maintained at 95 -100° C at reduced pressure ($\simeq$10 mm Hg) during 30 min. All these operations were performed away from light to avoid any photochemical alteration of the product[5]. N-methyl-3-pyridone thus obtained with better yield was identical in all respect to the material previously described and more suitable for recording UV spectra.

N-methyl-4-pyridone was obtained by methylation of the 4-pyridone according to the procedure of Ruzicka and Fornasir [16]. The free base was purified by repeated distillation of the product in a vacuum line and kept in a sealed tube.

The commercial N-methyl-2-pyridone (Schuchardt, München) was purified by distillation at reduced pressure and immediately used for recording the spectra.

The IR, the PMR spectra and the analysis of the products were consistent with their structure and in agreement with those reported in the literature.

Ultraviolet spectra were recorded using a Cary Md. 11 M.S. instrument, with spectrograde solvents checked before their use.

Acknowledgements. This work was carried out with the financial support of the Consiglio Nazionale delle Ricerche, Rome. The Authors are grateful to Dr. M. L. Tosato for her help in the synthetic work and to Mr. A. Verdecchia, B. Giuli, and P. Corradini, Computing Centre, Istituto Superiore di Sanità, for their cooperation.

References

1. Paoloni, L., Tosato, M. L., Cignitti, M.: Theoret. chim. Acta (Berl.) **14**, 221 (1969).
2. Berthier, G., Lévy, B., Paoloni, L.: Theoret. chim. Acta (Berl.) **16**, 316 (1970).
3. Metzler, D. E., Snell, E. E.: J. Amer. chem. Soc. **77**, 2431 (1955).
4. Mason, S. F.: (a) J. chem. Soc. (London) **1959**, 1240; (b) **1959**, 1247; (c) **1959**, 1253; (d) **1959**, 1263; (e) **1959**, 1269.
5. Saxena, J. P., Stafford, W. H., Stafford, W. L.: J. chem. Soc. (London) **1959**, 1579.
6. Harris, S. A., Webb, T. T., Folkers, K.: J. Amer. chem. Soc. **62**, 3198 (1940).
7. Albert, A.: Heterocyclic chemistry, An Introduction, p. 56, London: The Athlone Press 1959.
8. Mason, S. F.: Physical methods in heterocyclic chemistry, ed. by A. R. Katritzky, p. 47, New York: Academic Press 1963.
9. Evleth, E. M.: Theoret. chim. Acta (Berl.) **11**, 145 (1968).
10. Bodor, N., Dewar, M. J. S., Harget, A. J.: J. Amer. chem. Soc. **92**, 2929 (1970).
11. Pople, J. A., Segal, G. A.: J. chem. Physics **44**, 3289 (1966).
12. Del Bene, J., Jaffé, H. H.: J. chem. Physics **48**, 1807, 4050 (1968).
13. See Ref. [7], Table 21, and Krachov, M. H., Lee, C. M., Mautner, H. G.: J. Amer. chem. Soc. **87**, 892 (1965).
14. Cusach, L. C.: Int. J. quant. Chemistry, Symp. **1**, 301 (1967), discussion on the paper by Pople, J. A., Beveridge, D. L., Ostlund, N. S.: Int. J. quant. Chemistry, Symp. **1**, 293 (1967).

---

[5] The acetone solution of the compound becomes blue when exposed to light, and the colour deepens to violet, and a brown oil separates, after prolonged exposure. The thin layer chromatography of this oil shows that it contains about 50% of the starting material and another component which has not yet been identified. Photochemical reactions have been reported also for the 2- and the 4-pyridone [15].

15. (a) Slomp, C., Mac Kellar, S. A., Paquette, L. A.: J. Amer. chem. Soc. **83**, 4472 (1961); (b) Corey, E. J., Streith, J.: J. Amer. chem. Soc. **86**, 950 (1964); (c) Kulevsky, N., Reineke, W.: J. physic. Chem. **72**, 339 (1968). (d) Sang Chul Shim: C. A. **68**, 113787 (1968).
16. Ruzicka, L., Fornasir, V.: Helv. chim. Acta **3**, 806 (1920).
17. Hammes, G. G., Spivey, H. O.: J. Amer. chem. Soc. **88**, 1621 (1966).
18. Bellamy, L. J., Rogash, P. E.: Spectrochim. Acta **16**, 30 (1960).

Prof. Dr. L. Paoloni
Gruppo Chimica Teorica Università
Via Archirafi 20
I-90123 Palermo, Italy

Theoret. chim. Acta (Berl.) 25, 289 308 (1972)
© by Springer-Verlag 1972

Störungstheoretische Berechnung von Ionisierungsenergien und Elektronenaffinitäten mit Hilfe der Greenschen Zweipunktfunktion*

FRANZ ECKER** und GEORG HOHLNEICHER
Institut für Physikalische Chemie und Elektrochemie der Technischen Universität München

Eingegangen am 30. März 1971

Calculations of Ionisation Energies and Electron Affinities by Means of the One Particle Green's Function

The values of ionization energy and electron affinity of a system of *n* electrons belonging to an atom or a molecule are related to the negative value of the real part of the poles of the one particle Green's function connected with this system. An approximate calculation of the position of the poles can be made via a perturbation treatment of the one particle Green's function. In zero order approximation one chooses as one particle wavefunctions the canonical Hartree-Fock orbitals. In this case the results concide with Koopmans's theorem. Deviations from Koopmans's theorem, which are induced by reorganization and correlation effects, can be calculated in higher order via the Dyson equation, by means of the so-called self-energy operator.

In the present paper the self-energy operator is expanded up to the second order of the perturbation. The results are discussed qualitatively. They agree with the observations, which have been made, when experimentally determined ionization energies were compared to values, derived from *ab-initio* calculations via Koopmans's Theorem.

Der negative Realteil der Pole der dem N-Elektronensystem eines Atoms oder Moleküls zugeordneten Greenschen Zweipunktfunktion entspricht den Ionisierungsenergien bzw. Elektronenaffinitäten dieses Systems. Mit Hilfe einer störungstheoretischen Entwicklung der Greenschen Zweipunktfunktion kann die Lage dieser Pole näherungsweise berechnet werden. Die nullte Näherung kann dabei so gewählt werden, daß das Ergebnis mit dem Koopmansschen Theorem übereinstimmt. Abweichungen vom Koopmansschen Theorem, die durch Reorganisations- und Korrelationseffekte hervorgerufen werden, können in höherer Ordnung über die Dysongleichung mit Hilfe des sog. Massenoperators erfaßt werden.

In der vorliegenden Arbeit wird der Massenoperator bis zur zweiten Ordnung störungstheoretisch entwickelt. Das erhaltene Resultat wird qualitativ diskutiert. Die Ergebnisse dieser Diskussion stehen in Einklang mit den Beobachtungen, die beim Vergleich experimenteller Ionisierungsenergien mit den unter Anwendung des Koopmansschen Theorems berechneten Werten gemacht werden.

La partie réelle négative du pôle de la fonction de Green à une particule du système électronique d'un atome ou d'une molécule fournit le potentiel d'ionisation ou l'affinité électronique d'un tel système. La position de ces pôles peut être obtenue d'une manière approchée par un développement de perturbation de la fonction de Green. On peut choisir l'approximation d'ordre zéro de manière à ce que le théorème de Koopmans soit vérifié. L'écart au théorème de Koopmans provoqué par les effets de réorganisation et de corrélation peut être évalué aux ordres supérieurs à l'aide de l'équation de Dyson faisant intervenir opérateur de self energy.

---

* Auszugsweise vorgetragen auf der "Conference on Photoionization Phenomena and Photoelectrospectroscopy", Oxford, 14.–16. September 1970.

** Auszug aus der von der Fakultät für allgemeine Wissenschaften der Technischen Universität München genehmigten Dissertation des Dipl. Phys. Franz Ecker. Dissertation eingereicht am 27. 1. 1970. Neue Anschrift: Siemens AG, München 2, Wittelsbacherplatz .

Dans ce travail l'opérateur de self energy est développé par perturbation jusqu'au second ordre. Le résultat obtenu est discuté d'une manière qualitative. Le résultat de cette discussion est en accord avec les observations que l'on peut faire par comparaison du potentiel d'ionisation expérimental avec les termes calculés par application du théorème de Koopmans.

1. Einleitung

Nach dem Theorem von Koopmans [1] sind die Energieeigenwerte des Hartree-Fock-Operators je nach Besetzung des entsprechenden Eigenzustandes gleich den negativen Ionisierungsenergien bzw. Elektronenaffinitäten des betrachteten N-Elektronensystems.

Die Näherungen unter denen das Koopmanssche Theorem abgeleitet ist, wurden bereits mehrfach – zuletzt von Richards [2] – diskutiert. In diesen Diskussionen wird immer wieder darauf hingewiesen, daß die neben den relativistischen Effekten vernachlässigten Reorganisations- und Korrelationseffekte durchaus merkliche Beiträge liefern können.

Das große Interesse, das in jüngster Zeit der theoretischen Behandlung von Ionisierungsprozessen entgegengebracht wird und auf das auch die neuen Diskussionen um das Koopmanssche Theorem zurückzuführen sind, hängt mit der Entwicklung der Photoelektronenspektroskopie zusammen [3, 4]. Mit dieser neuen Art von Spektroskopie ist es möglich, auch höhere Ionisierungsenergien, bei denen das $(N-1)$-Elektronensystem in einem mehr oder minder hoch angeregten Zustand zurück bleibt, mit großer Genauigkeit zu messen. Dabei werden in erster Linie solche Ionisierungen beobachtet, die im Einteilchenbild der Entfernung eines Elektrons aus einem der besetzten Hartree-Fock-Orbitale entsprechen. Die zugehörigen angeregten Zustände des $(N-1)$-Teilchensystems können im Einteilchenbild durch folgenden Anregungstyp charakterisiert werden.

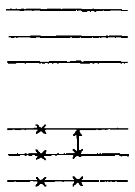

Die bisher mit der Photoelektronenspektroskopie gewonnenen Ergebnisse haben gezeigt, daß das Koopmanssche Theorem im allgemeinen gut dazu geeignet ist, um Photoelektronenspektren mit den Ergebnissen von Rechnungen zu korrelieren. Quantitativ treten jedoch merkliche – und zwar nichtsystematische – Abweichungen auf. Tabelle 1 gibt für einige Beispiele einen Vergleich zwischen den im PE-Spektrum gemessenen vertikalen Ionisierungsenergien und den mit *ab-initio*-Rechnungen erhaltenen Orbitalenergien.

Die wesentliche Alternative zur Anwendung des Koopmansschen Theorems bildet die direkte Berechnung von Ionisierungsenergien (I_k) und Elektronenaffinitäten (A_k) als Differenz der Gesamtenergien der beteiligten Zustände:

$$I_k = E_k^{(N-1)} - E_0^{(N)},$$

$$A_k = E_0^{(N)} - E_k^{(N+1)}.$$

Tabelle 1. Vergleich von berechneten (Koopmanssches Theorem) und vertikalen experimentellen Ionisierungsenergien

	Acetylen			N_2			Formaldehyd	
	ber. [22]	exp.		ber. [23]	exp.		ber. [22]	exp.
$1\pi_u$	11.26	11.40	$3\sigma_g$	17.36	15.58	$2b_2$	11.98	10.88
$3\sigma_g$	18.62	16.6	$1\pi_u$	17.10	16.92	$1b_1$	14.47	14.39
$2\sigma_u$	20.88	18.62	$2\sigma_u$	20.92	18.76	$3a_1$	17.38	16.01
						$1b_2$	19.13	ca 16.8
						$2a_1$	23.60	20

Da sich die gesuchten Größen in diesem Fall als Differenz zweier großer Zahlen ergeben, muß die Energie der beteiligten Zustände mit großer Genauigkeit bestimmt werden. Berechnet man die Energie der beiden Zustände auf dem Hartree-Fock-Niveau, so erfaßt man im Prinzip den Einfluß der Reorganisation, aber nicht den der Korrelation. Bei der Bildung der Differenz zwischen den Hartree-Fock-Energien des (N)- und des $(N-1)$- bzw. $(N+1)$-Elektronensystems tritt jedoch folgende Schwierigkeit auf: Mindestens eines der beiden Systeme – Ausgangsmolekül oder Ion – ist immer ein open-shell-System. Behandelt man das open-shell-System im Rahmen eines restricted-Hartree-Fock-Verfahrens, so vernachlässigt man einen Teil der Wechselwirkungen, die man im closed-shell-Fall berücksichtigt. Verwendet man dagegen ein unrestricted-Hartree-Fock-Verfahren, bei dem man entweder zuerst minimisiert und dann projiziert oder besser zuerst projiziert und dann minimisiert, so erfaßt man bereits einen Teil der Korrelation. In jedem Fall bildet man also die Differenz zwischen zwei Gesamtenergien, die mit unterschiedlichen Näherungsannahmen berechnet wurden.

Aufgrund dieser Situation haben wir uns die Frage gestellt, ob es nicht möglich ist, die bei Anwendung des Koopmansschen Theorems vernachlässigten Einflüsse von Reorganisation und Korrelation im Rahmen einer störungstheoretischen Entwicklung zu erfassen. Eine ähnliche Fragestellung wurde bereits von Brailsford [5] aufgegriffen, der versucht hat, mit Hilfe eines elektrostatischen Modells den Einfluß der Reorganisation abzuschätzen.

Das Ergebnis unserer Überlegungen ist ein störungstheoretisches Verfahren zur Berechnung von Ionisierungsenergien und Elektronenaffinitäten, bei dem das Theorem von Koopmans die nullte Näherung darstellt. In der vorliegenden Arbeit wird die Herleitung des Verfahrens, das auf der Anwendung Greenscher Funktionen basiert, erläutert und das Ergebnis diskutiert, das man erhält, wenn der sog. Massenoperator bis zur zweiten Ordnung entwickelt wird. In zwei weiteren Arbeiten werden wir über Möglichkeiten zur Verallgemeinerung der störungstheoretischen Entwicklung [6] sowie über numerische Resultate [7] berichten.

2. Ionisierungsenergien und Elektronenaffinitäten als Pole der Greenschen Zweipunktfunktion

Die *Greensche Zweipunktfunktion* ist definiert als Erwartungswert eines zeitgeordneten Produkts von Operatoren im Grundzustand $|E_0(N)\rangle$ eines N-Teilchensystems [8]:

$$G_{ij}(t,t') = -i\langle E_0(N)|\, T\{a_i(t)a_j^+(t')\}\,|E_0(N)\rangle\,. \tag{1}$$

Die $a_i^+(t)$ bzw. $a_i(t)$ bezeichneten *Erzeugungs-* bzw. *Vernichtungsoperatoren* von Fermiteilchen in der Heisenberg-Darstellung:

$$a_i^+(t) = e^{iHt} a_i^+ e^{-iHt}; \qquad a_i(t) = e^{iHt} a_i e^{-iHt};$$
$$a_i^+ \equiv a_i^+(0); \qquad a_i \equiv a_i(0).$$

Für $t = t'$ erfüllen diese Operatoren die Antivertauschungsrelationen:

$$\{a_i, a_j^+\}_+ \equiv a_i a_j^+ + a_j^+ a_i = \delta_{ij},$$
$$\{a_i^+, a_j^+\}_+ \equiv \{a_i, a_j\}_+ = 0.$$

Das *Wicksche Zeitordnungssymbol* T ist für Fermionen folgendermaßen definiert:

$$T\{a_i(t) a_j^+(t')\} = \begin{cases} a_i(t) a_j^+(t') & t > t' \\ -a_j^+(t') a_i(t) & t \leqq t'. \end{cases}$$

Im Fall zeitlicher Translationsinvarianz des betrachteten Systems hängt $G_{ij}(t, t')$ nur von der Zeitdifferenz $(t - t')$ ab, d. h. man erhält alle Informationen bereits aus der Funktion $G_{ij}(t) \equiv G_{ij}(t, 0)$.

Schiebt man in (1) für $t > 0$ die Zustände $|E_k(N+1)\rangle$ des $(N+1)$-Teilchensystems und für $t \leqq 0$ die Zustände $|E_k(N-1)\rangle$ des $(N-1)$-Teilchensystems als Zwischenzustände ein, so ergibt sich

$$G_{ij}(t) = \begin{cases} -i \sum\limits_k e^{i(E_0^{(N)} - E_k^{(N+1)})t} \langle E_0(N)| a_i |E_k(N+1)\rangle \langle E_k(N+1)| a_j^+ |E_0(N)\rangle & t > 0 \\ i \sum\limits_k e^{i(E_0^{(N)} - E_k^{(N-1)})t} \langle E_0(N)| a_j^+ |E_k(N-1)\rangle \langle E_k(N-1)| a_i |E_0(N)\rangle & t \leqq 0. \end{cases} \tag{2}$$

Geht man mit

$$G_{ij}(\omega) = \int\limits_{-\infty}^{\infty} G_{ij}(t) e^{i\omega t} dt \tag{3}$$

zur *Spektraldarstellung* über, so folgt für $G_{ij}(\omega)$ aus (2)

$$\begin{aligned} G_{ij}(\omega) = {} & \sum_k \frac{\langle E_0(N)| a_i |E_k(N+1)\rangle \langle E_k(N+1)| a_j^+ |E_0(N)\rangle}{\omega - (E_k^{(N+1)} - E_0^{(N)}) + i\eta} \\ & + \sum_k \frac{\langle E_0(N)| a_j^+ |E_k(N-1)\rangle \langle E_k(N-1)| a_i |E_0(N)\rangle}{\omega - (E_0^{(N)} - E_k^{(N-1)}) - i\eta}. \end{aligned} \tag{4}$$

η ist hierbei eine reelle, positive, infinitesimale Größe, die bei der Fourier-Rücktransformation gewährleistet, daß sich die richtige Zeitabhängigkeit von $G_{ij}(t)$ ergibt.

Ist $|E_0(N)\rangle$ im speziellen Fall der Grundzustand eines N-Elektronensystems, so sind die Zwischenzustände $|E_k(N+1)\rangle$ bzw. $|E_k(N-1)\rangle$ Elektronenzustände eines Systems mit $N+1$ bzw. $N-1$ Elektronen. Ist insbesondere $|E_0(N)\rangle$ der Singulett-Grundzustand eines closed-shell-Systems, so liefern nur die reinen Spin-Dublett-Zustände $|E_k(N+1)\rangle$ und $|E_k(N-1)\rangle$ der open-shell-Systeme mit $(N+1)$ und $(N-1)$ Elektronen einen Beitrag zu $G_{ij}(\omega)$.

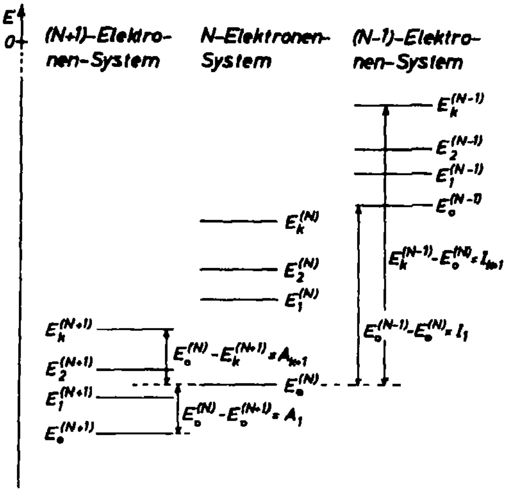

Fig. 1. Zusammenhang zwischen den Ionisierungsenergien (I) und Elektronenaffinitäten (A) eines N-Elektronensystems und den Energiezuständen des $(N+1)$-, N- und $(N-1)$-Elektronensystems

Die im Nenner von $G_{ij}(\omega)$ auftretenden Energiedifferenzen

$$I_k = E_k^{(N-1)} - E_0^{(N)}, \tag{5a}$$

$$A_k = E_0^{(N)} - E_k^{(N+1)} \tag{5b}$$

sind definitionsgemäß die Ionisierungsenergien (I_k) und die Elektronenaffinitäten (A_k) des N-Elektronensystems (Fig. 1). Vorausgesetzt, daß nicht zufälligerweise der Zähler verschwindet, folgt damit aus (4):

Die infinitesimal oberhalb der reellen Achse der komplexen ω-Ebene bei

$$\omega = -I_k + i\eta \quad \text{mit} \quad \mathrm{Re}(\omega) \leqq -I_0 \tag{6a}$$

liegenden Pole der Greenschen Zweipunktfunktion $G_{ij}(\omega)$ entsprechen gerade den Ionisierungsenergien, während die bei

$$\omega = -A_k - i\eta \quad \text{mit} \quad \mathrm{Re}(\omega) \geqq -A_0 \tag{6b}$$

infinitesimal unterhalb der reellen Achse liegenden Pole die Elektronenaffinitäten liefern.

Das Problem, die Ionisierungsenergien und Elektronenaffinitäten eines Moleküls zu berechnen, geht folglich im Rahmen des hier verwendeten Formalismus in das Problem über, die entlang der reellen Achse der komplexen ω-Ebene liegenden Pole der dem N-Elektronensystem des Moleküls zugeordneten Greenschen Zweipunktfunktion $G_{ij}(\omega)$ zu ermitteln. Da die Funktion $G_{ij}(\omega)$ für ein System wechselwirkender Teilchen ebensowenig exakt angegeben werden kann, wie die Wellenfunktion selbst, ist man auf eine näherungsweise Behandlung des Problems angewiesen. Hierfür bieten sich zwei Möglichkeiten an:

1) Stellt man die Bewegungsgleichung der Greenschen *Zweipunktfunktion* auf, so ergibt sich eine Verknüpfung mit der *Vierpunktfunktion*. Diese wiederum wird

durch die Bewegungsgleichung mit der *Sechspunktfunktion* verknüpft usw. [9]. Man erhält ein System von gekoppelten Gleichungen, das sich durch geeignete *Entkopplung* näherungsweise lösen läßt. Diese Art des Vorgehens wird z.B. in den Arbeiten von Linderberg und Öhrn [10–13] verwendet.

2) Ausgehend von einem ungestörten Problem, beschrieben durch einen Hamiltonoperator H_0, für das die Greensche Zweipunktfunktion exakt angegeben werden kann, wird mit Hilfe einer *störungstheoretischen Entwicklung* die Greensche Funktion des vollständigen Systems näherungsweise berechnet.

In der vorliegenden Arbeit verwenden wir das zweite Verfahren, da es in einfacher Weise die Möglichkeit bietet, vom Koopmansschen Theorem als nullter Näherung auszugehen. In [6] werden wir jedoch zeigen, daß bei störungstheoretischer Entkopplung des Gleichungssystems der Ansatz 1) zum gleichen Ergebnis führt.

3. Störungstheoretische Berechnung der Greenschen Zweipunktfunktion

3.1. Allgemeiner Formalismus

In diesem Abschnitt wird kurz der Formalismus erläutert, auf dem eine störungstheoretische Berechnung der Greenschen Zweipunktfunktion basiert. Eine eingehende Darstellung des hier nur andeutungsweise skizzierten Vorgehens findet sich z.B. in [14].

Voraussetzung für eine störungstheoretische Berechnung der Greenschen Zweipunktfunktion ist, daß sich der Hamiltonoperator

$$H = H_0 + H_w \tag{7}$$

so in zwei Teile zerlegen läßt, daß die Greensche Zweipunktfunktion für das sog. ungestörte Problem ($G_{ij}^0(t)$), das durch H_0 charakterisiert ist, exakt angegeben werden kann. Die freie Greensche Funktion $G_{ij}^0(t)$ beschreibt ein System nicht wechselwirkender Quasiteilchen. Bei entsprechender Wahl von H_0 können an die Stelle dieser Quasiteilchen auch die freien Teilchen treten.

Um die Greensche Funktion $G_{ij}(t)$ des vollen Problems durch $G_{ij}^0(t)$ auszudrücken, geht man zunächst von der Schrödingerdarstellung, in der das System durch den Grundzustand $|\Phi(t)\rangle$ und die Wechselwirkung H_w beschrieben wird, in das Wechselwirkungsbild über

$$H_w \to H_w(t) = e^{iH_0t} H_w e^{-iH_0t}\,, \tag{8}$$

$$|\Phi(t)\rangle \to |\Phi_w(t)\rangle = e^{iH_0t} |\Phi(t)\rangle\,. \tag{9}$$

Die Bewegungsgleichung für $|\Phi_w(t)\rangle$

$$i\frac{\partial}{\partial t}|\Phi_w(t)\rangle = H_w(t)|\Phi_w(t)\rangle \tag{10}$$

oder

$$|\Phi_w(t > t_1)\rangle = |\Phi_w(t_1)\rangle + \frac{1}{i}\int_{t_1}^{t} H_w(t')|\Phi_w(t')\rangle\, dt' \tag{11}$$

hat die formale Lösung

$$|\Phi_w(t)\rangle = S(t,t')|\Phi_w(t')\rangle \tag{12}$$

mit

$$S(t,t') = \sum_{n=0} \frac{(-i)^n}{n!} \int_t^{t'} \cdots \int_t^{t'} T\{H_w(t_1)\dots H_w(t_n)\}\, dt_1 \dots dt_n\,, \tag{13}$$

$$S(t,t')\cdot S(t',t'') = S(t,t''), \tag{14}$$

$$S(t,t')^{-1} = S(t',t). \tag{15}$$

Um nun die Zustände des Wechselwirkungsbildes in die Zustände des Heisenbergbildes überführen zu können, nimmt man an, daß die Störwechselwirkung H_w hinreichend langsam eingeschaltet wird (adiabatisches Einschalten)

$$H_w(t) \rightarrow H_w(t)e^{-\eta|t|} \qquad \eta \text{ hinreichend klein.} \tag{16}$$

Zur Zeit $t = -\infty$ setzt man den Wechselwirkungszustand gleich dem Heisenbergzustand des ungestörten Systems $|\Phi_H^0\rangle$, d.h. man tut so, als existiere zu diesem Zeitpunkt das durch $G_{ij}^0(t)$ beschriebene System nichtwechselwirkender Quasiteilchen

$$|\Phi_w(-\infty)\rangle = |\Phi_H^0\rangle\,. \tag{17}$$

Überträgt man jetzt noch die Zeitabhängigkeit auf die Operatoren

$$F(t) \rightarrow S^{-1}(t)\cdot F(t)\cdot S(t) \quad \text{mit} \quad S(t) = S(t,-\infty), \tag{18}$$

so wird:

$$\begin{aligned} G_{ij}(t) &= -i\langle\Phi_H(N)|T\{a_i(t)a_j^+\}|\Phi_H(N)\rangle \\ &= \begin{cases} -i\langle\Phi_H^0(N)|S^{-1}(t)a_i(t)S(t)S^{-1}(0)a_j^+\,S(0)|\Phi_H^0(N)\rangle & t>0 \\ +i\langle\Phi_H^0(N)|S^{-1}(0)a_j^+\,S(0)S^{-1}(t)a_i(t)S(t)|\Phi_H^0(N)\rangle & t\leqq 0\,. \end{cases} \end{aligned} \tag{19}$$

Da der Grundzustand nicht entartet ist, erfolgt bei hinreichend langsamem Einschalten eine Grundzustandsänderung ohne Beteiligung von angeregten Zuständen, d. h.

$$|\Phi_w(\infty)\rangle = |\Phi_H^0\rangle\langle\Phi_H^0|\Phi_w(\infty)\rangle = |\Phi_H^0\rangle\langle\Phi_H^0|S(\infty)|\Phi_H^0\rangle\,. \tag{20}$$

Nach Einsetzen von (20) ergibt sich unter Berücksichtigung von (14) und (15)

$$G_{ij}(t) = -i\frac{\langle\Phi_H^0(N)|T\{a_i(t)a_j^+\,S(\infty)\}|\Phi_H^0(N)\rangle}{\langle\Phi_H^0(N)|S(\infty)|\Phi_H^0(N)\rangle} \tag{21}$$

mit

$$T\{a_i(t)a_j^+\,S(\infty)\} = \begin{cases} S(\infty,t)a_i(t)S(t,0)a_j^+\,S(0) & t>0 \\ -S(\infty,0)a_j^+\,S(0,t)a_i(t)S(t) & t\leqq 0\,. \end{cases}$$

Zur expliziten Behandlung dieses Ausdruckes wird die Entwicklung von $S(\infty)$ bis zu einer bestimmten Ordnung eingesetzt. Die auftretenden Terme werden unter

Anwendung des *Wick'schen Theorems* [15] mit Hilfe von *Feynmangraphen* ausgewertet. Den in den Graphen vorkommenden Symbolen ist folgende Bedeutung zugeordnet:

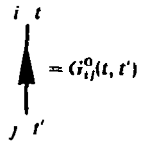

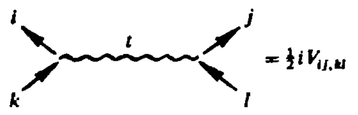

Die bei der Auswertung von (21) auftretenden Graphen lassen sich in zwei Kategorien einteilen, nämlich in *verkettete* (z.B. a) und *unverkettete* (z.B. b) Graphen.

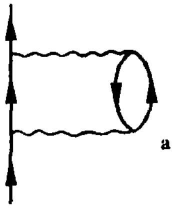
a

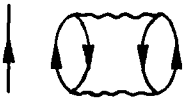
b

Man kann zeigen, daß sich bei Fortsetzung der störungstheoretischen Entwicklung bis zu unendlicher Ordnung alle in der Entwicklung des Zählers von (21) auftretenden unverketteten Graphen gerade gegen die Gesamtheit der bei der Entwicklung des Nenners vorkommenden Graphen wegheben (linked cluster theorem [16]). Demzufolge kann man schreiben

$$G_{ij}(t) = -i\langle \Phi^0_H(N) | T\{a_i(t) a_j^+ S(\infty)\} | \Phi^0_H(N)\rangle \quad \text{verkettet.} \qquad (23)$$

Bei den in höherer Ordnung auftretenden Graphen läßt sich eine weitere Klassifizierung vornehmen. Man findet Graphen folgender Struktur:

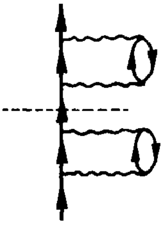

Diese Graphen zerfallen beim Durchschneiden einer einzigen G_0-Linie (angedeutet durch --------) in zwei miteinander nicht verbundene Teile. Solche Graphen bezeichnet man als *reduzibel;* Graphen, die sich auf diese Weise nicht in zwei Teile zerlegen lassen als *irreduzibel.* Die Gesamtheit der irreduziblen Graphen, bei denen die beiden äußeren G_0-Linien entfernt wurden, bezeichnet man als *Massenoperator* $\mathbb{M}$.

Den Beitrag aller Graphen zu $G_{ij}(t)$, die man bei Fortsetzung der Störungstheorie bis zu unendlicher Ordnung erhält, findet man, indem man den Massenoperator unendlich oft in eine G_0-Linie einsetzt [8]:

$$\begin{aligned}\mathbb{G} &= \mathbb{G}^0 + \mathbb{G}^0\,\mathbb{M}\mathbb{G}^0 + \mathbb{G}^0\,\mathbb{M}\mathbb{G}^0\,\mathbb{M}\mathbb{G}^0 + \ldots \\ &= \mathbb{G}^0 + \mathbb{G}^0\,\mathbb{M}\underbrace{(\mathbb{G}^0 + \mathbb{G}^0\,\mathbb{M}\mathbb{G}^0 + \ldots)}_{\mathbb{G}}\,.\end{aligned} \tag{24}$$

Man erhält die Dysongleichung

$$\mathbb{G} = \mathbb{G}^0 + \mathbb{G}^0\,\mathbb{M}\mathbb{G}$$

oder

$$G_{ij}(t) = G^0_{ij}(t) + \sum_{kl} \iint G^0_{ik}(t,t')M_{kl}(t',t'')G_{lj}(t'')\,dt'dt''\,.$$

In der ω-Darstellung lautet die Dysongleichung

$$G_{ij}(\omega) = G^0_{ij}(\omega) + \sum G^0_{ik}(\omega)M_{kl}(\omega)G_{lj}(\omega)$$

oder

$$G^{-1}_{ij}(\omega) = G^{0^{-1}}_{ij}(\omega) - M_{ij}(\omega)\,. \tag{25}$$

Gleichung (25) bildet den Ausgangspunkt unserer weiteren Überlegungen: Wenn es möglich ist eine Zerlegung des Hamiltonoperators zu finden, die es gestattet, die freie Greensche Funktion exakt anzugeben, so besteht die wesentliche Aufgabe darin, den Massenoperator bis zu einer bestimmten Ordnung der störungstheoretischen Entwicklung zu berechnen. Das Aufsuchen derjenigen ω-Werte, für die $G^{-1}_{ij}(\omega)$ nach Einsetzen des so gewonnenen Massenoperators Eigenwerte vom Betrag Null besitzt, liefert neue, bis zur entsprechenden Ordnung verbesserte Werte für die Ionisierungsenergien und Elektronenaffinitäten. Obwohl der Massenoperator nur in endlicher Ordnung berechnet wird, werden bei dieser Art des Vorgehens bestimmte Graphen, d.h. bestimmte störungstheoretische Terme bis zu unendlicher Ordnung berücksichtigt.

3.2. Wahl des ungestörten Problems

Für ein closed-shell System mit $N = 2n$ Elektronen kann man immer einen Ansatz wählen, bei dem die Einteilchenfunktionen den Hartree-Fock-Operator

$$\boldsymbol{F} = \sum_{ij}\left[h_{ij} + \sum_{j'=1}^{N}(V_{ij',jj'} - V_{ij',j'j})\right]\tilde{\boldsymbol{a}}_i^+\tilde{\boldsymbol{a}}_j \tag{26}$$

diagonalisieren, so daß gilt

$$\boldsymbol{F} = \sum_i \varepsilon_i \boldsymbol{a}_i^+ \boldsymbol{a}_i\,. \tag{27}$$

Die Indices i, j usw. sollen auch die Spinindices σ_i und σ_j enthalten. Für die Matrixelemente gilt dann folgende Vereinbarung

$$h_{ij} = \int d\tau\,\varphi_i^*(\boldsymbol{r})\,(T + V(\boldsymbol{r}))\,\varphi_j(\boldsymbol{r})\,\delta\sigma_i\sigma_j\,, \tag{28}$$

$$V_{ij,lk} = \iint d\tau\,d\tau'\,\varphi_i^*(\boldsymbol{r})\,\varphi_j^*(\boldsymbol{r})\,V(\boldsymbol{r},\boldsymbol{r}')\,\varphi_l(\boldsymbol{r})\,\varphi_k(\boldsymbol{r})\,\delta\sigma_i\sigma_l\,\delta\sigma_j\sigma_k\,. \tag{29}$$

Die Eigenzustände φ_i von $\boldsymbol{F}$ werden als *kanonische Hartree-Fock-Orbitale bezeichnet.*

Da nach dem Theorem von Koopmans die Orbitalenergien ε_i der kanonischen Hartree-Fock-Orbitale nullte Näherungen für Ionisierungsenergien und Elektronenaffinitäten darstellen, liegt es nahe, bei einer störungstheoretischen Entwicklung von eben diesen Orbitalen auszugehen, d.h. wir setzen

$$\boldsymbol{H}_0 = \boldsymbol{F} = \sum_i \varepsilon_i \boldsymbol{a}_i^+ \boldsymbol{a}_i \,. \tag{30}$$

Für die zugehörige freie Greensche Funktion $G_{ij}^0(t)$ erhalten wir

$$\begin{aligned} G_{ij}^0(t) &= -i\langle E_0^0(N)|\boldsymbol{T}\{\boldsymbol{a}_i(t)\boldsymbol{a}_j^+\}|E_0^0(N)\rangle \\ &= \begin{cases} -i\langle E_0^0(N)|e^{iH_0t}\boldsymbol{a}_i e^{-iH_0t}\boldsymbol{a}_j^+|E_0^0(N)\rangle & t>0 \\ i\langle E_0^0(N)|\boldsymbol{a}_j^+ e^{iH_0t}\boldsymbol{a}_i e^{-iH_0t}|E_0^0(N)\rangle & t\leqq 0 \end{cases} \\ &= \begin{cases} -ie^{-i\varepsilon_j t}\delta_{ij} & j\notin\{\text{bes.}\}, t>0 \\ +ie^{-i\varepsilon_j t}\delta_{ij} & j\in\{\text{bes.}\}, t\leqq 0 \,. \end{cases} \end{aligned} \tag{31}$$

{bes} ist die Menge der im Grundzustand zweifach besetzten Orbitale. In der ω-Darstellung wird

$$G_{ij}^0(\omega) = \underset{j\notin\{\text{bes}\}}{\frac{\delta_{ij}}{\omega-\varepsilon_j+i\eta}} + \underset{j\in\{\text{bes}\}}{\frac{\delta_{ij}}{\omega-\varepsilon_j-i\eta}} \,. \tag{32}$$

Die freie Greensche Funktion reproduziert das mit der speziellen Wahl von $\boldsymbol{H}_0$ implizierte Ergebnis: Die Orbitalenergien der besetzten kanonischen Hartree-Fock-Orbitale sind nullte Näherungen für die Ionisierungsenergien und die der unbesetzten kanonischen Hartree-Fock-Orbitale nullte Näherungen für die Elektronenaffinitäten.

Um die bei Anwendung des Koopmansschen Theorems vernachlässigten Reorganisations- und Korrelationseffekte wenigstens teilweise zu berücksichtigen, müssen wir den Massenoperator näherungsweise berechnen. Dazu formen wir den Hamiltonoperator des vollen Problems

$$\boldsymbol{H} = \sum_{ij} h_{ij}\tilde{\boldsymbol{a}}_i^+\tilde{\boldsymbol{a}}_j + \tfrac{1}{2}\sum_{\substack{i,j\\k,l}} V_{ij,kl}\tilde{\boldsymbol{a}}_i^+\tilde{\boldsymbol{a}}_j^+\tilde{\boldsymbol{a}}_l\tilde{\boldsymbol{a}}_k \tag{33}$$

in folgender Weise um

$$\begin{aligned} \boldsymbol{H} = {}& \sum_{ij}\left[h_{ij} + \sum_{j'=1}^{N}(V_{ij',jj'} - V_{ij',j'j}) - \sum_{j'=1}^{N}(V_{ij',jj'} - V_{ij',j'j})\right]\tilde{\boldsymbol{a}}_i^+\tilde{\boldsymbol{a}}_j \\ &+ \tfrac{1}{2}\sum_{i,j,k,l} V_{ij,kl}\tilde{\boldsymbol{a}}_i^+\tilde{\boldsymbol{a}}_j^+\tilde{\boldsymbol{a}}_l\tilde{\boldsymbol{a}}_k \,. \end{aligned}$$

Mit der Abkürzung

$$v_{ij} = \sum_{j'=1}^{N}(V_{ij',jj'} - V_{ij',j'j}) \tag{34}$$

und unter Berücksichtigung von (27) wird

$$H=\sum_i \varepsilon_i a_i^+ a_i-\sum_{ij} v_{ij} a_i^+ a_j+\tfrac{1}{2}\sum_{i,j,k,l} V_{ij,kl}\, a_i^+ a_j^+ a_l a_k\,. \tag{35}$$

Aus (7), (35) und (30) erhalten wir schließlich

$$H_w=-\sum_{i,j} v_{ij} a_i^+ a_j+\tfrac{1}{2}\sum_{\substack{i,j\\k,l}} V_{ij,kl}\, a_i^+ a_j^+ a_l a_k\,. \tag{36}$$

3.3. *Berechnung des Massenoperators bis zur zweiten Ordnung*

Um den Massenoperator in einer bestimmten Ordnung zu berechnen hat man die Entwicklung von $S(\infty)$ aus (23) bis zur entsprechenden Ordnung in (21) einzusetzen und alle bei der Auswertung des Zählers auftretenden irreduziblen Graphen zu ermitteln. Geht man bei der Entwicklung von $S(\infty)$ bis zu den Gliedern zweiter Ordnung in H_w, so erhält man folgende Terme:

$$\begin{aligned}
&-i\langle \Phi_H^0(N)|\,T\{a_i(t)a_j^+\,S(\infty)\}\,|\Phi_H^0(N)\rangle\\
&=-i\langle \Phi_H^0(N)|\,T\{a_i(t)a_j^+\}\,|\Phi_H^0(N)\rangle-\int_{-\infty}^{+\infty}\langle \Phi_H^0(N)|\,T\{a_i(t)a_j^+H_w(t_1)\}\,|\Phi_H^0(N)\rangle\, dt_1 \qquad (37)\\
&+\frac{i}{2}\int_{-\infty}^{\infty}\int_{-\infty}^{\infty}\langle \Phi_H^0(N)|\,T\{a_i(t)a_j^+H_w(t_1)H_w(t_2)\}\,|\Phi_H^0(N)\rangle\, dt_1\, dt_2\,.
\end{aligned}$$

Zur Auswertung dieser Terme ordnen wir der in H_w auftretenden Wechselwirkung v_{ij} folgendes Symbol zu:

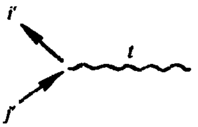

$= iv_{i'j'}$

Damit und mit den in (22) definierten Symbolen lassen sich diejenigen Beiträge der störungstheoretischen Entwicklung, die in H_w von erster Ordnung sind, folgendermaßen darstellen:

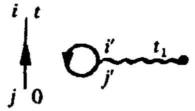

I

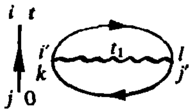

II

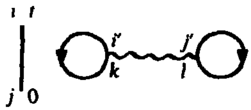

III

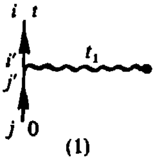

(1)

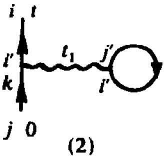

(2)

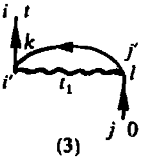

(3)

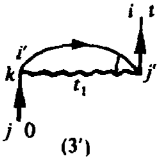

(3')

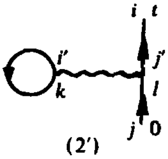

(2')

Da nach (23) die unverketteten Graphen I, II und III für die störungstheoretische Entwicklung von $G_{ij}(t)$ nicht in Betracht zu ziehen sind, haben wir im weiteren nur die verketteten Graphen zu diskutieren. Durch Umbenennung des Summationsindizes läßt sich zeigen, daß die Graphen 2 und 2' sowie 3 und 3' den gleichen Beitrag liefern. Zwischen den verbleibenden Graphen besteht aber wegen der Definition von v_{ij} aus (34) folgende Beziehung:

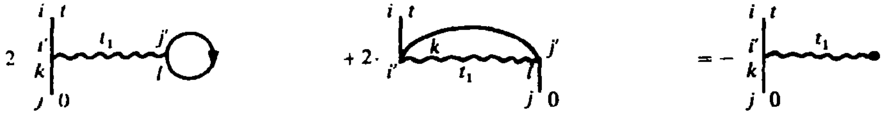

d.h. die Terme erster Ordnung liefern keinen Beitrag zur Entwicklung von $G_{ij}(t)$. In zweiter Ordnung treten folgende irreduzible Graphen auf:

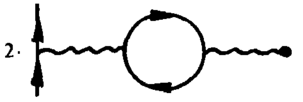

a

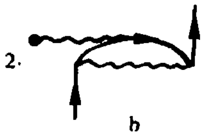

b

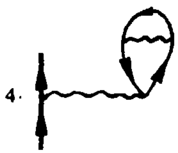

c

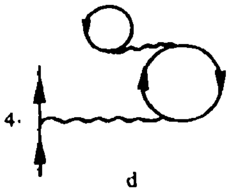

d

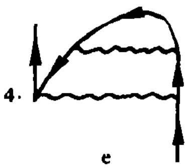

e

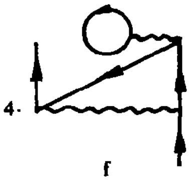

f

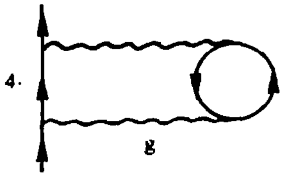

g

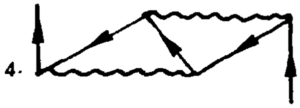

h

Wegen der Gültigkeit von (39) heben sich die Graphen a gegen die Graphen c und d, und die Graphen b gegen e und f weg. Folglich liefern in zweiter Ordnung nur die Graphen g und h einen Beitrag zur störungstheoretischen Entwicklung von $G_{ij}(t)$. Nach Entfernung der beiden äußeren G^0-Linien erhalten wir als Beiträge zum Massenoperator zweiter Ordnung:

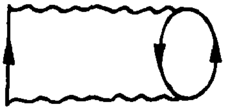

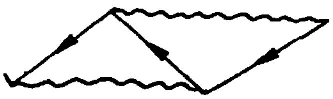

Nach Ausführung der Fouriertransformation wird:

$$\begin{aligned} M_{ij}^{(2)}(\omega) = & \sum_{j' \in \{\mathrm{bes}\}} \sum_{k,l \notin \{\mathrm{bes}\}} (V_{ij',kl} - V_{ij',lk}) V_{lk,j'j} \frac{1}{\varepsilon_{j'} - \varepsilon_k - \varepsilon_l + \omega + i\eta} \\ & + \sum_{j' \notin \{\mathrm{bes}\}} \sum_{k,l \in \{\mathrm{bes}\}} (V_{ij',kl} - V_{ij',lk}) V_{lk,j'j} \frac{1}{\varepsilon_{j'} - \varepsilon_k - \varepsilon_l + \omega - i\eta} . \end{aligned} \tag{40}$$

Durch Einsetzen von $M_{ij}^{(2)}(\omega)$ aus (40) und von $G_{ij}^{0}(\omega)$ aus (32) in die Dysongleichung (25) erhalten wir schließlich:

$$G_{ij}^{(2)^{-1}}(\omega) = (\omega - \varepsilon_i)\delta_{ij} - M_{ij}^{(2)}(\omega) . \tag{41}$$

Sind die kanonischen Lösungen des Hartree-Fock-Problems in einer bestimmten Näherung bekannt, so läßt sich $M_{ij}^{(2)}(\omega)$ auf dem Niveau dieser Näherung berechnen. Das Aufsuchen der Nullstellen von $\mathfrak{G}^{(2)^{-1}}$, d.h. die Ermittlung derjenigen ω-Werte, für die die Matrix der $G_{ij}^{(2)^{-1}}$ Eigenwerte vom Betrag Null besitzt, liefert dann die gesuchten neuen Werte für Ionisierungsenergien und Elektronenaffinitäten. Wegen der ω-Abhängigkeit von $M_{ij}^{(2)}$ führt das Aufsuchen der Nullstellen allerdings auf ein nichtlineares Problem. Auf die Behandlung dieses Problems werden wir im Zusammenhang mit numerischen Rechnungen in [7] eingehen. In der vorliegenden Arbeit wollen wir uns darauf beschränken, einige qualitative Folgerungen zu diskutieren, die sich aus den Gln. (32), (40) und (41) ableiten lassen.

4. Diskussion

Ziel unserer Untersuchungen war es, die Pole der Greenschen Zweipunktfunktion mit Hilfe einer störungstheoretischen Entwicklung zu berechnen. In nullter Ordnung entsprechen die Pole den Energien derjenigen Quasiteilchen, die durch die freie Greensche Funktion G_{ij}^{0} beschrieben werden. Das Verschwinden des Massenoperators erster Ordnung, das dazu führt, daß auch die Pole von $G_{ij}^{(1)}$ durch die gleichen Quasiteilchenenergien bestimmt werden, ist eine Folge der speziellen Wahl der für die störungstheoretische Entwicklung verwendeten Basis: Wären wir nicht von den kanonischen Lösungen des Hartree-Fock-Problems ausgegangen, sondern z.B. von den nicht wechselwirkenden Teilchen mit

$$H_0 = \sum_{ij} h_{ij} a_i^{+} a_j ,$$

so hätte eine selbstkonsistente Entwicklung in erster Ordnung gerade auf die Quasiteilchen geführt, die durch die Hartree-Fock-Gleichungen beschrieben werden [17].

Verallgemeinert heißt das, daß eine selbstkonsistente Entwicklung in erster Ordnung das gleiche Ergebnis liefert, wie das Koopmanssche Theorem:

$$\begin{aligned} I_i^{(1)} &= -\varepsilon_i \qquad i \in \{\mathrm{bes}\} , \\ A_i^{(1)} &= -\varepsilon_i \qquad i \notin \{\mathrm{bes}\} . \end{aligned} \tag{42}$$

Berücksichtigt man, daß den Ionisierungsenergien und Elektronenaffinitäten Übergänge vom Grundzustand des N-Teilchensystems in Zustände des $(N-1)$-

bzw. $(N+1)$-Teilchensystems entsprechen, so bedeutet das, daß in erster Ordnung über die Greensche Zweipunktfunktion nur solche angeregte Zustände des $(N-1)$- bzw. $(N+1)$-Teilchensystems erfaßt werden, die im Hartree-Fock-Bild durch Einloch- (43a) bzw. Einteilchenanregungen (43b) beschrieben werden.

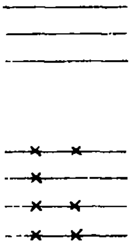
(43a)

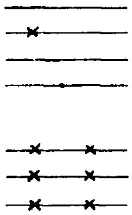
(43b)

Alle anderen angeregten Zustände des $(N-1)$- bzw. $(N+1)$-Teilchensystems müssen folglich bei Fortsetzung der störungstheoretischen Entwicklung über den Massenoperator erfaßt werden.
Zu Beginn dieser Arbeit wurde darauf hingewiesen, daß in der Photoelektronenspektroskopie in erster Linie die Ionisierungen beobachtet werden, die zu angeregten Zuständen des $(N-1)$-Teilchensystems führen, welche gerade den *Einlochanregungen* vom Typ (43a) entsprechen. Für die Interpretation der Photoelektronenspektren und für das theoretische Verständnis der gegenüber dem Koopmansschen Theorem auftretenden Abweichungen ist es demzufolge von besonderem Interesse zu untersuchen, inwieweit die Pole von $G_{ij}^{(2)}$ mit denen von $G_{ij}^{(1)}$ korreliert und inwieweit allgemeine Aussagen über eventuell auftretende Verschiebungen gemacht werden können.

4.1. *Einfluß des Massenoperators in 2. Ordnung*

Aus (40) ist ersichtlich, daß der Massenoperator selbst Pole besitzt. Diese liegen oberhalb bzw. unterhalb der reellen Achse der komplexen ω-Ebene bei

$$\omega = \varepsilon_l + \varepsilon_k - \varepsilon_{j'} \pm i\eta\,. \tag{44}$$

Bezeichnen wir das höchste besetzte Orbital des N-Elektronensystems mit φ_m und die Energielücke zwischen φ_m und dem niedrigsten unbesetzten Orbital φ_{m+1} mit

$$\Delta = \varepsilon_{m+1} - \varepsilon_m\,, \tag{45}$$

so folgt für die aus dem ersten Term von (40) resultierenden Pole, die wir mit M^+ bezeichnen wollen,

$$\operatorname{Re} M^+ \geqq \varepsilon_{m+1} + \varepsilon_{m+1} - \varepsilon_m = \varepsilon_{m+1} + \Delta\,, \tag{46a}$$

d.h. der energetisch niedrigste Pol dieser Art liegt gerade um Δ oberhalb von $-A_1^{(1)}$ (vgl. Fig. 2). Entsprechend gilt für die aus dem zweiten Term von (40) hervorgehenden Pole

$$\operatorname{Re} M^- \leqq \varepsilon_m + \varepsilon_m - \varepsilon_{m+1} = \varepsilon_m - \Delta\,. \tag{46b}$$

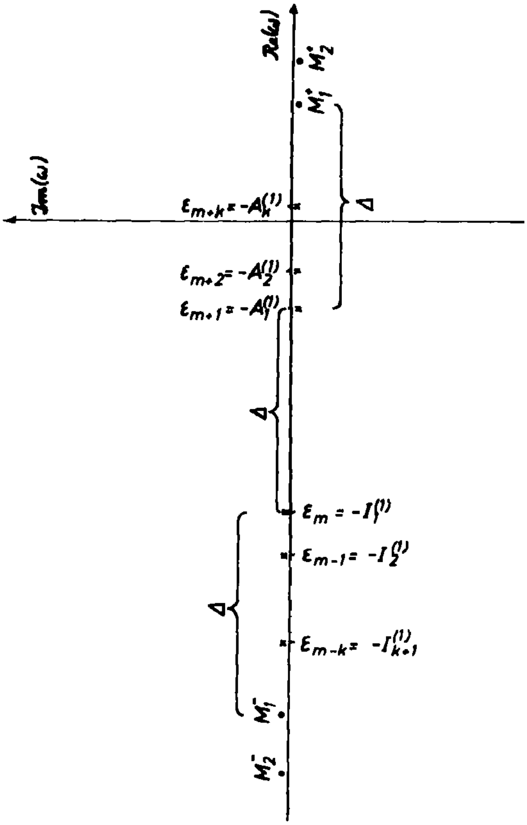
Re(ω)
Im(ω)
M_2^+
M_1^+
Δ
$\varepsilon_{m+k} = -A_k^{(1)}$
$\varepsilon_{m+2} = -A_2^{(1)}$
$\varepsilon_{m+1} = -A_1^{(1)}$
Δ
$\varepsilon_m = -I_1^{(1)}$
$\varepsilon_{m-1} = -I_2^{(1)}$
Δ
$\varepsilon_{m-k} = -I_{k+1}^{(1)}$
M_1^-
M_2^-

Fig. 2. Lage der Pole der freien Greenschen Funktion $\mathbb{G}^0$ und des Massenoperators zweiter Ordnung $\mathbb{M}^{(2)}$ in der komplexen ω-Ebene

Diese Pole liegen mindestens um Δ unterhalb von $-I_1^{(1)}$. Da der energetische Abstand zwischen φ_m und φ_{m+1} bei neutralen Molekülen mit abgeschlossener Schale in den meisten Fällen erheblich größer ist, als der Abstand zwischen den obersten der besetzten und zwischen den niedrigsten der unbesetzten Orbitale, liegen bei diesen Systemen im allgemeinen mehrere Nullstellen von $G_{ij}^{0^{-1}}$, d.h. mehrere $-I^{(1)}$ und $-A^{(1)}$ zwischen M_1^+ und M_1^- (Fig. 2).

Im Hartree-Fock-Bild stehen die Pole M^+ mit Einteilchenzuständen in Beziehung, bei denen sich relativ zum Grundzustand des N-Teilchensystems (47a) ein zusätzliches Teilchen im Orbital φ_k befindet und gleichzeitig ein Teilchen aus dem Orbital $\varphi_{l'}$ in das Orbital φ_l überführt ist. Umgekehrt entsprechen die Pole M^- solchen Zuständen, bei denen ein Teilchen aus dem Orbital φ_k entfernt und ein anderes aus dem Orbital $\varphi_{l'}$ in das Orbital φ_l gebracht ist. Ist insbesondere k gleich $m+1$ (47b) bzw. $m-1$ (47c) so entspricht ein Übergang aus dem Grundzustand des $(N+1)$- bzw. $(N-1)$-Teilchensystems (47d und 47e) in einen der Zustände (47b) bzw. (47c) einer Einteilchenanregung. Es ist bekannt, daß diese

Einteilchenanregungen sehr wesentlich zu energetisch niedrig liegenden elektronisch angeregten Zuständen von Radikalionen beitragen. Übergänge, die in diese Zustände führen, sind in vielen Fällen optisch erlaubt und dementsprechend in den Elektronenspektren gut zu beobachten [18]. Geht man dagegen vom Grundzustand des N-Teilchensystems (47a) aus, so entspricht der in der Photoelektronenspektroskopie im allgemeinen nicht zu beobachtende Übergang in einen der Zustände (47b) oder (47c) einem Zweiteilchenprozeß.

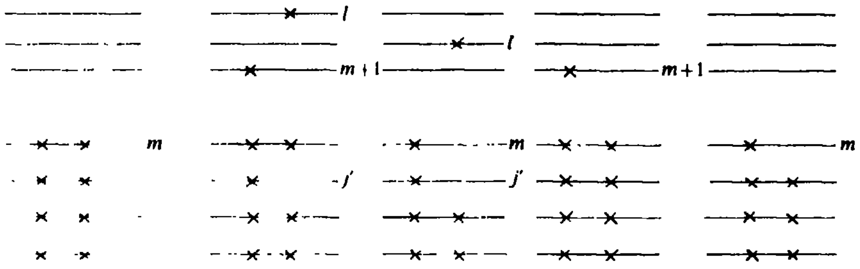

(47a) (47b) (47c) (47d) (47e)

Untersuchen wir jetzt den Einfluß des Massenoperators (40) auf diejenigen Pole der freien Greenschen Funktion (32), die zwischen M_1^- und M_1^+ liegen. Wir gehen dabei von der Voraussetzung aus, daß die Nichtdiagonalelemente $M_{ij}^{(2)}$ von $\mathbb{M}^{(2)}$ klein sind gegenüber der Differenz zwischen den Orbitalenergien ε_i und ε_j. Wie sich zeigt [7] ist diese Voraussetzung fast immer erfüllt, wenn es sich nicht um entartete oder fast entartete Orbitale handelt. $G_{ij}^{(2)\,-1}$ ist dann in der Umgebung von $\omega=\varepsilon_i$ im wesentlichen durch den Diagonalterm $M_{ii}^{(2)}(\omega)$ von $\mathbb{M}^{(2)}$ bestimmt:

$$G_{ij}^{(2)\,-1}(\omega\approx\varepsilon_i)\approx\omega-\varepsilon_i-M_{ii}^{(2)}\cdot\delta_{ij}=-M_{ii}^{(2)}\cdot\delta_{ij}\,. \tag{48}$$

Durch Ausführung der Spinsummation und Umformung erhält man für die beiden formal äquivalenten Terme von $M_{ii}^{(2)}$

$$\begin{aligned}&\sum_{j'}\sum_{k,l}(V_{ij',kl}-V_{ij',lk})V_{lk,j'i}\frac{1}{\varepsilon_{j'}-\varepsilon_k-\varepsilon_l+\omega}\rightarrow\\ &\qquad\sum_{j'}\sum_{k}V_{ij',kk}^2\frac{1}{\varepsilon_{j'}-2\varepsilon_k+\omega}\\ &\qquad+\sum_{j'}\sum_{k<l}\frac{1}{\varepsilon_{j'}-\varepsilon_k-\varepsilon_l+\omega}\left(V_{ij',kl}^2+V_{ij',lk}^2+(V_{ij',kl}-V_{ij',lk})^2\right).\end{aligned}\tag{49}$$

Aus (49) folgt, daß das Vorzeichen der beiden Terme von $M_{ii}^{(2)}$ nur durch den Resonanznenner bestimmt wird. Für den rechtsseitigen Grenzwert von M_1^- erhält man

$$\lim_{\eta\to 0}\operatorname{Re}M_{ii}^{(2)}(M_1^-+\eta)\quad=+\infty$$

und für den linksseitigen Grenzwert von M_1^+

$$\lim_{\eta\to 0}\operatorname{Re}M_{ii}^{(2)}(M_1^+-\eta)\quad=-\infty\,.$$

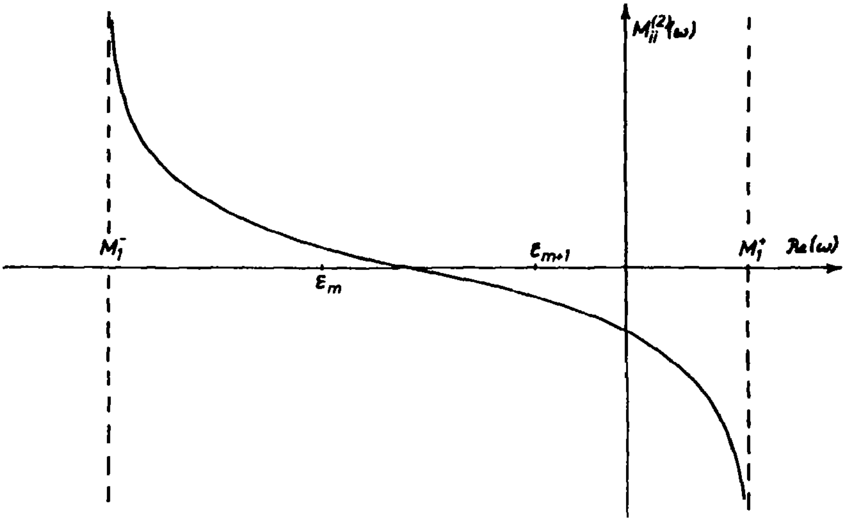

Fig. 3. Qualitatives Verhalten eines Diagonalterms von $\mathbb{M}^{(2)}$ im Bereich zwischen M_1^- und M_1^+

Da die V-Terme selbst nicht von ω abhängen, ist $M_{ii}^{(2)}(\omega)$ im Bereich zwischen M_1^- und M_1^+ außerdem eine monotone Funktion von ω. Für das qualitative Verhalten von $M_{ii}^{(2)}(\omega)$ ergibt sich damit im untersuchten Bereich das in Fig. 3 dargestellte Bild. Ist der Beitrag der beiden Summen in (40) von gleicher Größenordnung, so liegt der Nulldurchgang von $M_{ii}^{(2)}$ zwischen $\omega = \varepsilon_m$ und $\omega = \varepsilon_{m+1}$.

Zusammen mit (48) lassen sich aus Fig. 3 folgende Konsequenzen ziehen:

a) Solange der Betrag von $M_{ii}^{(2)}$ kleiner ist als der Betrag des Abstandes von ε_i zum Pol M_1^+ oder M_1^-, kann der Pol von $G_{ij}^{(2)}$ als ein Pol betrachtet werden, der durch Verschiebung aus einem Pol von G_{ij}^0 hervorgeht.

b) Erfolgt der Nulldurchgang von $M_{ii}^{(2)}(\omega)$ zwischen $\omega = \varepsilon_m$ und $\omega = \varepsilon_{m+1}$, so wird der entsprechende Pol von G^0 zu größeren ω-Werten hin verschoben, wenn ε_i zwischen M_1^- und ε_m liegt. Liegt der Pol von G^0 dagegen zwischen ε_{m-1} und M_1^+, so erfolgt eine Verschiebung in Richtung kleinerer ω-Werte. Die durch den Massenoperator 2. Ordnung hervorgerufenen Verschiebungen wirken sich in diesem Bereich so aus, daß die Ionisierungsenergien gegenüber dem Koopmansschen Theorem verkleinert und die Elektronenaffinitäten vergrößert werden.

c) $M_{ii}^{(2)}(\omega)$ hängt über die V-Terme vom gerade betrachteten ε_i ab. Sind die V-Terme für verschiedene ε_i von gleicher Größenordnung, so ist die Verschiebung gegenüber der nullten Ordnung wegen der ω-Abhängigkeit von $M_{ii}^{(2)}$ umso größer, je näher das betrachtete ε_i an den Polen M_1^- oder M_1^+ liegt. Es ist jedoch durchaus denkbar, daß sich die Größenordnung der V-Terme für verschiedene Orbitale, insbesondere z.B. für π- und σ-Orbitale, deutlich unterscheidet. Es ist deshalb nicht generell damit zu rechnen, daß – wie in den von Basch *et al.* untersuchten Beispielen [18] – die Abweichung vom Koopmansschen Theorem umso größer wird, je höher die Ionisierungsenergie ist. Man vergleiche als Gegenbeispiel die in Tabelle 1 für Formaldehyd angegebenen Daten.

d) Für Orbitale, deren Energie im Bereich $\varepsilon_i < M_1^-$ oder $\varepsilon_i > M_1^+$ liegt, gelten die hier durchgeführten Betrachtungen nicht. In diesem Bereich sind durchaus gegenläufige Verschiebungen möglich. Eine eingehende Analyse dieses Bereichs erfolgt in [21].

Die Aussagen b) und c) stimmen qualitativ mit dem überein, was man beim Vergleich experimenteller Ionisierungsenergien mit den unter Anwendung des Koopmansschen Theorems berechneten Werten beobachtet. Inwieweit die auftretenden Abweichungen mit den hier entwickelten Näherungen auch quantitativ erfaßt werden können, d.h. welcher Teil der Reorganisations- und Korrelationseffekte bei Entwicklung des Massenoperators bis zur zweiten Ordnung tatsächlich erfaßt wird, läßt sich erst abschätzen, wenn eine größere Zahl von numerischen Rechnungen vorliegt.

4.2. *Gültigkeitsbereich*

Prinzipiell ist der verwendete Formalismus sowohl auf closed-shell- als auch auf open-shell-Systeme anwendbar. Zur Ableitung der speziellen Näherungen wurde jedoch in (27) vorausgesetzt, daß die verwendete Basis den Hartree-Fock-Operator diagonalisiert. Diese Voraussetzung ist in voller Allgemeinheit nur für closed-shell-Systeme erfüllt. Demzufolge ist die Beziehung (40) nur dann anwendbar, wenn das N-Elektronensystem, dessen Ionisierungsenergien und Elektronenaffinitäten berechnet werden sollen, ein closed-shell-System ist.

Beim Vergleich mit experimentellen Daten ist außerdem zu beachten, daß das Hartree-Fock-Problem parametrisch von den Kernkoordinaten abhängt. Wird es für einen bestimmten Satz von Kernkoordinaten gelöst, so werden die über $\boldsymbol{H}_w$ erfaßten Wechselwirkungen für die gleichen Kernkoordinaten berechnet. Sind diese Koordinaten die Gleichgewichtskoordinaten des Grundzustands des N-Elektronensystems, so heißt das, daß die in höherer Ordnung berechneten Pole analog zur Anwendung des Koopmansschen Theorems mit *vertikalen* Ionisierungsenergien und Elektronenaffinitäten zu identifizieren sind.

4.3. *Konvergenz der störungstheoretischen Entwicklung*

Konvergenzprobleme treten ganz allgemein deshalb auf, weil man die störungstheoretische Entwicklung notgedrungenermaßen an irgend einer Stelle abbrechen muß. Ein solcher Abbruch bedeutet, daß man in der Entwicklung nur bestimmte Graphen berücksichtigt. Jeder Graph entspricht aber im Prinzip – bei wirklich vollständiger Basis – einer unendlichen Summe und man kann nicht davon ausgehen, daß jede dieser Summen für sich konvergiert. So divergiert z.B. beim dreidimensionalen Elektronengas der Beitrag, den das *Ringdiagram* zweiter Ordnung (50) liefert [19]. Um Konvergenz zu erhalten, muß man in diesem Fall die Beiträge aller Ringdiagramme bis zu unendlicher Ordnung aufsummieren (RPA-Näherung).

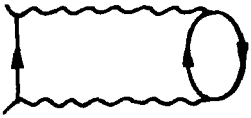

Mit dieser Näherung werden allerdings nur im *high-density-Fall* wesentliche Beiträge der störungstheoretischen Entwicklung erfaßt [20]. Von high density spricht man, wenn der mittlere Abstand zwischen den Teilchen klein ist gegenüber der mittleren Reichweite der Wechselwirkung zwischen diesen Teilchen. Ist umgekehrt der mittlere Abstand der Teilchen groß gegenüber der mittleren Reichweite der Wechselwirkung, *(low-density-Fall)*, so liefern die Ringdiagramme keinen entscheidenden Beitrag. Hier spielen die sogenannten Leitergraphen die wesentliche Rolle.

Für den Fall der *intermediate-density*, der bei Molekülen realisiert ist, ist kein allgemeines Lösungsschema wie bei den beiden oben genannten Grenzfällen bekannt. Es ist jedoch nicht zu erwarten, daß der Beitrag, den der Ringgraph zweiter Ordnung zum Massenoperator liefert, in diesem Fall divergiert. Sollten dennoch Schwierigkeiten auftreten, so lassen sich diese dadurch umgehen, daß man ausgehend vom Massenoperator zweiter Ordnung das Problem in selbstkonsistenter Weise löst [21].

5. Zusammenfassung

In der vorliegenden Arbeit wurde ein störungstheoretisches Verfahren entwickelt, das es ermöglicht, die durch Reorganisations- und Korrelationseffekte hervorgerufenen Abweichungen vom Koopmansschen Theorem direkt zu erfassen. Gegenüber der Berechnung von Ionisierungsenergien und Elektronenaffinitäten als Differenz von Gesamtenergien hat ein solches Verfahren den Vorteil, daß nur eine relativ kleine Korrekturgröße berechnet werden muß. Darüberhinaus bleibt das Einteilchenbild, das einen Zusammenhang mit Molekülorbitalen herstellt und dadurch eine anschauliche Interpretation von Ionisierungsenergien ermöglicht, weitgehend erhalten. Sollte es sich zeigen, daß die hier vorgeschlagene Näherung – oder eine eventuelle Erweiterung – die beobachteten Abweichungen auch quantitativ ausreichend beschreibt, so ist es durchaus denkbar, daß dieses Verfahren auch bei semiempirischen Rechnungen, wie man sie heute in großem Umfang zur Interpretation von Photoelektronenspektren größerer Moleküle heranzieht, angewandt werden kann.

*

Wir danken den Herren F. Metz und L. Cederbaum für ihre intensive Mitarbeit; Frau Dr. Liselotte Becker für viele anregende Diskussionen und der Deutschen Forschungsgemeinschaft für die gewährte finanzielle Unterstützung.

Literatur

1. Koopmans, T.: Physica 1, 104 (1933).
2. Richards, W. G.: J. Mass spectrom. Ion Physics 2, 419 (1969).
3. Turner, D. W., Baker, C., Baker, A.-D., Brundle, C. R.: Molecular photoelectron spectroscopy. London: Wiley Interscience 1970.
4. Siegbahn, K., *et al.*: ESCA – atomic, molecular and solid state structure studied by means of electron spectroscopy. Uppsala: Almquist & Wiksells 1967.
5. Brailsford, B. F., Ford, B., Hall, G. G.: Lecture given at the conference on Photoionization Phenomena and Photoelectron Spectroscopy held at the University of Oxford, 14.–16. September 1970. In diesem Vortrag wurde von B. F. Brailsford ebenfalls auf die Möglichkeit hingewiesen, Greensche Funktionen für die Berechnung von Ionisierungsenergien zu verwenden.

6. Metz, F., Cederbaum, L., Hohlneicher, G.: In Vorbereitung; Metz, F.: Dissertation TU München, 1971.
7. Cederbaum, L., Peyerimhoff, S., Hohlneicher, G.: Chem. Physics Letters **11**, 421 (1971).
8. Nozières, P.: Theory of interacting fermi systems, S. 190. New York-Amsterdam: W. A. Benjamin 1964.
9. Puff, R. D.: Ann. Physik **13**, 317 (1961).
10. Linderberg, J., Öhrn, Y.: Proc. Roy. Soc. (London) A **285**, 445 (1965).
11. Öhrn, Y., Linderberg, J.: Physic. Rev. **139**, A 1065 (1965).
12. Linderberg, J., Öhrn, Y.: J. chem. Physics **49**, 710, 716 (1968).
13. Chem. Physics Letters **1**, 295 (1967).
14. Abrikosov, A., Gor'kov, L., Dzyaloshinskii, J.: *Quantum field theoretical methods in statistical physics*. Oxford · Pergamon Press 1965.
15. Wick, G. C.: Physic. Rev. **80**, 268 (1950).
16. Thouless, D. J.: Quantenmechanik der Vielteilchensysteme. Mannheim: Bibliographisches Institut, 1964.
17. Quantenmechanik der Vielteilchensysteme, S. 64. Mannheim: Bibliographisches Institut 1964
18. Basch, H., Robin, M. B., Kuebler, N. A., Baker, C., Turner, D. W.: J. chem. Physics **51**, 52 (1969).
19. Mattuck, R. D.: A guide to feynman diagrams in the many-body problem. London: McGraw-Hill 1967
20. Gell-Mann, M., Brueckner, K. A.: Physic. Rev. **106**, 364 (1957).
21. Cederbaum, L.: *Dissertation TU München (in Vorbereitung).*
22. Peyerimhoff, S. D., Buenker, R. J.: Private Mitteilung.
23. Cade, P. E., Sales, K., Wahl, A. C.: J. chem. Physics **44**, 1973 (1966).

Dr. G. Hohlneicher
Institut für Physikalische Chemie
und Elektrochemie der TH München
D-8000 München 2, Arcisstr. 21
Deutschland

Instructions to Authors

1. *Manuscripts* should be submitted in duplicate, typed in double-line spacing on one side of the paper only. Form and content should be carefully checked to exclude the need for corrections in proof. To speed up publication, authors will receive only one set of proofs: provisionally numbered page proofs. Authors are requested to correct typographical errors only; they will be charged for corrections involving changes, additions or deletions to the original manuscript.

Formulae should be typewritten whenever possible, special attention being given to the placing of indices and exponents so that they are recognizable as such even though there is no difference in size. Formulae should preferably be written in a "linear" form (e.g. $\exp(-\varepsilon/kT)$ instead of $e^{-\frac{\varepsilon}{kT}}$). Special typefaces (Greek, Script) should be shown by underlining in color. To avoid confusing the printer, please use red for Greek and green for Script, and underline in brown for bold face. Characters which are easily confused, e.g. 0 (zero) and capital O (letter) or 1 (figure one) and small *l* (letter), should have some special distinguishing mark. When formulae are inserted by hand, small letters should be underlined once and capital letters twice.

2. *Illustration copies* (graphs and structural formulae) should be drawn in Indian ink in clean uniform lines and sent in on separate sheets. Please mark in the margin of the manuscript where diagrams and tables should be inserted. Captions, which should be brief, should be typed separately and attached to the manuscript.

3. Original papers should be preceded by a *summary* (not more than 100 words) in English, German and French. (The editorial staff is willing to translate English summaries if asked.) Short notes need only an English summary. Papers not written in English should have an *English title* for use by such journals as Current Contents.

4. *Literature references* should be numbered and listed at the end of the paper. They should be cited as follows: *journal papers* — names and initials of all authors, journal in the accepted abbreviation, volume and page number, year; *books* — names of authors, full title, edition, place, publisher and year. References should be cited in the text by number.

5. 75 *offprints* of each paper will be supplied free of charge; additional copies may be ordered at cost price.

6. *Editorial enquiries* should be addressed to:
Prof. Dr. Hermann Hartmann, Theoretica Chimica Acta, Institut für physikalische Chemie der Universität, Robert-Mayer-Straße 11, D-6000 Frankfurt am Main 1

Manuscripts should be sent to the Editor or to one of the Co-editors:

Prof. Dr. Carl J. Ballhausen, Chemical Laboratory IV, H. C. Ørstedinstitutet, Universitetsparken 5, København Ø, Danmark,
Prof. Dr. Ronald D. Brown, Monash University, Department of Chemistry, P. O. Box 92, Clayton, Victoria, Australia 3168,
Prof. Dr. Edgar Heilbronner, Physikalisch-Chemisches Institut der Universität Basel, CH-4000 Basel, Klingelbergstraße 80, Switzerland,
Prof. Dr. J. Jortner, Department of Chemistry, Tel-Aviv University, Tel-Aviv, Israel,
Prof. Dr. Jan A. A. Ketelaar, Laboratory for Electrochemistry, Plantage Muidergracht 14, Amsterdam-C, The Netherlands,
Prof. Dr. Masao Kotani, 36-4 Sanno 3 chome, Ota-ku, Tokyo 143, Japan,
Prof. Dr. Jaroslav Koutecký, Československá Akademie Věd. Ústav Fyzikální Chemie, Praha 2-Vinohrady, Máchova 7, ČSSR,
Prof. Dr. Jack W. Linnett, Department of Physical Chemistry, Lensfield Road, Cambridge, England,
Prof. Dr. E. E. Nikitin, Institute of Chemical Physics, Academy of Sciences, Vorobyevskoye Chaussée 2b, Moskwa V-334, USSR,
Prof. Dr. Ralph G. Pearson, Department of Chemistry, Northwestern University, Evanston, Illinois 60201, USA,
Prof. Dr. Bernard Pullman, Université de Paris, Institut de Biologie physico-chimique, 13, rue Pierre Curie, Paris V, France,
Prof. Dr. Klaus Ruedenberg, Department of Chemistry, Iowa State University of Science and Technology, Ames, Iowa 50010, USA,
Prof. Dr. Camille Sandorfy, Université de Montréal, Case Postale 6128, Montréal, Canada,
Prof. Dr. Massimo Simonetta, Istituto di Chimica Fisica dell'Università di Milano, Via Saldini, 50, Milano, Italia,
Prof. Dr. Oktay Sinanoğlu, Department of Chemistry, Yale University, 225 Prospect Street, New Haven, Conn. 06520, USA.

Hinweise für die Autoren

1. *Manuskripte* werden mit einer Kopie, auf einseitig beschriebenen Blättern mit doppeltem Zeilenabstand erbeten. Die Manuskripte müssen formal wie inhaltlich so durchgearbeitet sein, daß Änderungen in den Korrekturfahnen unnötig sind. Zur Abkürzung der Publikationszeit erhalten die Autoren nur *eine* Seitenkorrektur mit provisorischen (*kursiven*) Seitenzahlen. Es sollen darin nur Satzfehler berichtigt werden. Nachträgliche (vom Manuskript abweichende) Korrekturen müssen den Autoren berechnet werden.

Alle Formeln sind möglichst mit der Maschine zu schreiben. Dabei ist darauf zu achten, daß Indices und Exponenten trotz des fehlenden Größenunterschiedes genau als solche zu erkennen sind. Besondere Lettern (griechische, Script) sind durch farbige Unterstreichungen zu kennzeichnen. Zur Vereinfachung für den Setzer wird gebeten, griechische Buchstaben rot, Scripttypen grün und halbfette braun zu unterstreichen. Auch einander ähnliche Zeichen, z. B. 0 (Null) und O (Buchstabe) oder 1 (Eins) und *l* (Buchstabe) sind besonders zu kennzeichnen. Bei handgeschriebenen Formeln ist bei allen vorkommenden Alphabeten zwischen Groß- und Kleinbuchstaben (durch doppeltes bzw. einfaches Unterstreichen) zu unterscheiden.

2. *Abbildungsvorlagen* werden als Tuschezeichnungen mit tiefschwarzem einheitlichen Strich auf besonderen Blättern erbeten. Am Manuskriptrand ist deutlich ihre Plazierung und die von Tabellen zu vermerken. Kurze Abbildungsunterschriften sollen am Schluß des Manuskripts beigefügt werden.

3. Bei Originalarbeiten wird um je eine *Zusammenfassung* (nicht über 100 Wörter) in Englisch, Deutsch und Französisch, bei Kurzmitteilungen um eine in Englisch gebeten. (Übersetzung ins Französische kann in der Redaktion vorgenommen werden.) Nichtenglischen Arbeiten soll außerdem eine englische Titelübersetzung beigefügt werden.

4. *Literaturangaben* sind am Schluß der Arbeit zusammenzustellen und zu numerieren. Sie enthalten Namen und nachgestellte Initialen aller Autoren, den nach den internationalen Regeln gekürzten Zeitschriftentitel, Band-, Seiten- und Jahreszahl; bei *Büchern* Autorennamen, vollen Titel, Auflage, Ort, Verlag und Jahr. Zitierung im Text erfolgt mit Nummer.

5. Von jeder Arbeit werden 75 *Sonderdrucke* kostenlos zur Verfügung gestellt. Weitere Separata können von den Autoren zum Selbstkostenpreis bezogen werden.

6. *Redaktionelle Anfragen* sind zu richten an:
Theoretica Chimica Acta, Prof. Dr. HERMANN HARTMANN.
Manuskripte können an alle Mitherausgeber eingesandt werden. Adressen umstehend.

Indications pour les auteurs

1. Les *manuscripts* seront envoyés en deux exemplaires dactylographiés au recto seulement. Tant la forme extérieure que le contenu doivent avoir leur aspect définitif, afin que des corrections sur les épreuves ne soient plus nécessaires. Afin d'accélérer la publication, les auteurs ne recevront qu'une seule épreuve dont les pages seront numérotées provisoirement. Seul les fautes de typographie devront être corrigées; toute autre correction entraînant des modifications, additions ou suppressions au texte original sera facturée aux auteurs. Dans la mesure du possible les formules doivent être tapées à la machine. On veillera à ce que les indices et les exposants soint facilement reconnaissables lorsqu'ils ne sont pas différenciés par leur taille. Sinon, ils devront être inscrits à la main. Les lettres spéciales (grecques, script) doivent être soulignées en couleur. Pour simplifier le travail du typographe on recommande de souligner en rouge les lettres grecques et en vert les script. Les lettres grasses seront soulignées en brun. Dans la mesure où des caractères manuscrits sont utilisés on distinguera (même pour les caractères latins) les majuscules, qu'on soulignera deux fois, des minuscules, soulignées une fois. Des difficultés spéciales naissent du fait que les machines à écrire ne font pas, en général, de différence entre 0 (zéro) et O (lettre) ainsi qu'entre 1 (un) et *l* (lettre). Dans ce cas, des signes distinctifs sont absolument indispensables.

2. Des *graphiques* et des formules développées doivent être tracés en lignes noires à l'encre de Chine. Veuillez indiquer dans la marge du manuscrit où les graphiques et les tableaux doivent être disposés.

3. Les travaux originaux doivent comporter de brefs *résumés* (100 mots maximum), rédigés dans les 3 langues: anglais, français et allemand. Le résumé des communications brèves doit être rédigé en anglais. (Sur demande, le résumé original peut être traduit par la rédaction, en allemand). Pour faciliter la documentation un titre anglais doit être ajouté à chaque article n'étant pas écrit en anglais.

4. Les *références* bibliographiques seront numérotées et rassemblées à la fin du texte. Les citations se présenteront comme suit: noms et initiales de tous les auteurs, titre du journal abrégé selon les règles internationales, tome, numéros des pages et année. Les *livres* seront cités précédés du nom de l'auteur, titre complet, édition, lieu de publication, éditeur et date de parution. Les références dans le texte doivent être indiquées par des numéros.

5. 75 *tirés à part* de chaque article seront remis gratuitement aux auteurs. Pour les exemplaires supplémentaires le prix de revient sera facturé aux auteurs.

6. *Les demandes au rédacteur* doivent être adressées à
Theoretica Chimica Acta, Prof. Dr. HERMANN HARTMANN.
Les *manuscrits* peuvent être envoyés à tous les co-éditeurs (adresses susmentionnées).

Theoret. chim. Acta (Berl.) 25, 309--318 (1972)
© by Springer-Verlag 1972

Commentationes

Chemical Applications of Topology and Group Theory

VI. Polyhedral Water Networks in Clathrates and Semiclathrates

R. B. King

Department of Chemistry, University of Georgia, Athens, Georgia 30601, USA

Received February 16, 1972

Possible convex polyhedra for three-dimensional water networks in clathrate and semiclathrate hydrates are discussed in this paper. All such polyhedra have all vertices of order three. Therefore, the number of vertices (v), edges (e), and faces (f) must satisfy the equalities $e = 3v/2$ and $f = (4 + v)/2$. Possible polyhedra of this type with exclusively quadrilateral, pentagonal, and hexagonal faces and with up to 18 faces are examined. Many of these polyhedra are duals of various triangulated coordination polyhedra studied in previous papers of this series. In order to minimize angular strain, polyhedra with the maximum number of pentagonal faces are favored for water networks in clathrate and semiclathrate hydrates subject to the presence of sufficiently large cavities to accommodate the guest molecule.

In dieser Arbeit werden mögliche konvexe Polyeder für dreidimensionale Wasser-Netzwerke in Klathrat- und Semiklathrathydraten diskutiert. Daher muß die Anzahl der Scheitelpunkte (v), Kanten (e) und Flächen (f) den Gleichungen $e = 3v/2$ und $f = (4 + v)/2$ genügen. Es werden mögliche Polyeder dieses Typs mit bis zu 18 Flächen, die ausschließlich quadrilateral, pentagonal und hexagonal sein sollen, untersucht. Viele dieser Polyeder sind Zwillinge von verschiedenen, aus Dreiecken zusammengesetzten Koordinationspolyedern, die in früheren Arbeiten dieser Reihe untersucht wurden. Um die Winkeldeformation auf ein Mindestmaß zurückzuführen, werden im Falle von Wassernetzwerken in Klathrat- und Semiklathrathydraten Polyeder mit der maximalen Anzahl von pentagonalen Flächen bevorzugt, weil so ausreichend große Hohlräume zur Aufnahme des Gastmoleküls entstehen.

Introduction

In recent years the structural chemistry of a novel class of organic hydrates, the clathrate hydrates [2, 3], has received considerable attention. These clathrate hydrates contain a relatively large number of water molecules for each guest molecule. The water molecules in these clathrate hydrates are joined by hydrogen bonding into networks of fused polyhedra. In cases where the guest molecule is an amine, one or more nitrogen atoms of the guest molecule may also be bonded to the fused polyhedral network of water molecules resulting in "semiclathrates" rather than true clathrates [2, 3]. Some of the observed polyhedra [2] in the clathrate and semiclathrate hydrates are rather peculiar ones not otherwise encountered in chemical systems. This paper examines the generation of the polyhedra observed in clathrate and semiclathrate hydrates by appropriate modifications of the techniques successfully used in earlier papers for the study of coordination polyhedra [4, 5], metal clusters [1], and polyhedral cage boron hydrides [1]. In the polyhedra of the clathrate and semiclathrate hydrates the vertices correspond to tetrahedral or nearly tetrahedral oxygen atoms and the edges to hydrogen bonds between pairs of oxygen atoms.

Generation of Possible Polyhedra

The problem of the generation and evaluation of possible polyhedra for water networks in clathrates and semiclathrates is a more complex problem than the generation and evaluation of possible coordination polyhedra [4, 5], metal cluster polyhedra [1], or boron hydride polyhedra [1] for the following three reasons:

1. There is no inherent direct limitation on the size[1] of polyhedra in clathrate and semiclathrate water networks as in the case of coordination polyhedra where both steric considerations and the number of available orbitals on the central atom impose strict limits on the coordination number and hence on the number of vertices and the size[1] of possible coordination polyhedra [4–6]. Closed metal cluster [1] and boron hydride polyhedra also have an inherent size[1] limitation based on the presence of only triangular faces for maximization of bond delocalization [1] combined with limitations on the maximum vertex order imposed by restrictions on the number of available metal or boron orbitals. Aspecific example of an extremely large polyhedron found in a clathrate is the irregular 116, 174, 60-polyhedron found[2] [7] in $[(n\ C_4H_9)_3S]\,F \cdot 23\,H_2O$. This polyhedron has 2 quadrilateral faces, 48 pentagonal faces, and 10 hexagonal faces. However, this polyhedron has reentrant edges and hence is not a convex polyhedron but instead a concave polyhedron.

2. The polyhedra in clathrate and semiclathrate water networks are not discrete but instead are joined in an infinite three-dimensional lattice. The space filling properties of convex polyhedra [8] in such infinite three-dimensional lattices indirectly limit the size[1] of polyhedra in water networks. A large convex polyhedron (i.e. one with large v, e, and f values) can be approximated by a sphere. Packing spheres into a three dimensional network always leaves relatively small spaces which correspond to small polyhedra with considerable angular strain. Thus, if only convex polyhedra are considered for the three-dimensional polyhedral network, the size and shape of the relatively small polyhedra necessary to fill the gaps in packing large polyhedra will introduce increasing amounts of angular strain as the size of the large polyhedra increases. A similar limitation on the maximum size of concave polyhedra with one or more reentrant edges does not obtain. However, concave polyhedra may be regarded as derived from the fusion of two or more smaller convex polyhedra such that the volumes of the convex polyhedra overlap. The portions of the convex polyhedra inside the resulting concave polyhedron (i.e. those which bound the region of overlap) are then lost.

---

[1] As used here the "size" of a polyhedron refers to its volume relative to its edge length. In general a polyhedron with a larger "size" has a larger number of vertices, edges, and faces.

[2] This notation indicates the number of vertices, edges, and faces, respectively, in various polyhedra as introduced in Ref. [4]. The notation used to indicate the number of faces with various numbers of sides is described by Wells, A. F.: The third dimension in chemistry, London: Oxford University Press 1962, and is also used in Table III of Ref. [2].

3. In the semiclathrate hydrates of the alkylamines, the nitrogen atoms of the alkylamine guest molecules form hydrogen bonds with the oxygen atoms of the network of fused water polyhedra. However, since each polyhedron contains only one alkylamine molecule, since the alkylamines forming semiclathrate hydrates contain only one nitrogen atom, and since the polyhedra large enough to enclose the alkylamine guest molecule contain at least twelve vertices, this effect can involve no more than about 10% of the vertices of the water network polyhedra. The perturbations introduced by hydrogen bonding of the nitrogen atoms of the alkylamine guest molecules to the polyhedral water network are small relative to those introduced by the packing properties of polyhedra and therefore may be neglected in this treatment as long as the alkylamine guest molecules contain no more than one nitrogen atom. However, in hexamethylenetetramine hexahydrate [9] where the amine contains four nitrogen atoms, of which three participate in hydrogen bonding, the hydrogen bonding of the hexamethylenetetramine to the water network is significant enough to destroy the basic polyhedral structure, although a regular network is still maintained. The treatment in this paper, therefore, is limited to clathrate hydrates and semiclathrate hydrates where the guest molecule (an alkylamine in all of the known cases) contains no more than one atom which forms hydrogen bonds with the water network. For the reasons stated above such semiclathrate hydrates can be treated as if they were true clathrate hydrates ignoring the single hydrogen bonding interaction between each guest molecule and the polyhedral three-dimensional water network.

For the first two reasons discussed above consideration of possible polyhedra for water networks in clathrates and semiclathrates can be limited to convex polyhedra and restricted to polyhedra with no more than a given number of faces. Such a restriction is also necessary to keep the scope of the problem within manageable limits. The maximum number of faces of polyhedra considered in this work is 18, since this is sufficient to include all known convex polyhedra found water networks in clathrates. The only larger polyhedra found in such water networks are the 26-hedron [10] in $4(CH_3)_3N \cdot 41\,H_2O$ and the irregular 116, 174, 60-polyhedron[2] [7] found in $[(n\text{-}C_4H_9)_3S]\,F \cdot 23\,H_2O$. Both of these large polyhedra are concave with the 26-hedron being formed by fusion of two 14-hedra ($5^{12}6^2$) sharing a common hexagonal face.

The tetrahedral hybridization of the oxygen atoms in hydrogen-bonded water molecules imposes the following basic conditions that all polyhedra for water networks in clathrates must satisfy:

1. *All vertices of the polyhedron must have an order of exactly three.* Each oxygen atom in these water networks has exactly four hydrogen atoms bonded to it. However, only three of the hydrogen bonds attached to any oxygen atom are so directed (i.e. on the same side of a supporting plane (Stutzeben) [11] through the oxygen atom) that they can be edges of the same polyhedron. This indicates a maximum order of three for vertices of polyhedra for water networks in clathrates. Furthermore, geometrical considerations require that each vertex in any three-dimensional polyhedron has an order of at least three. For these reasons, all vertices of polyhedra for water networks in clathrates must have an order of exactly three.

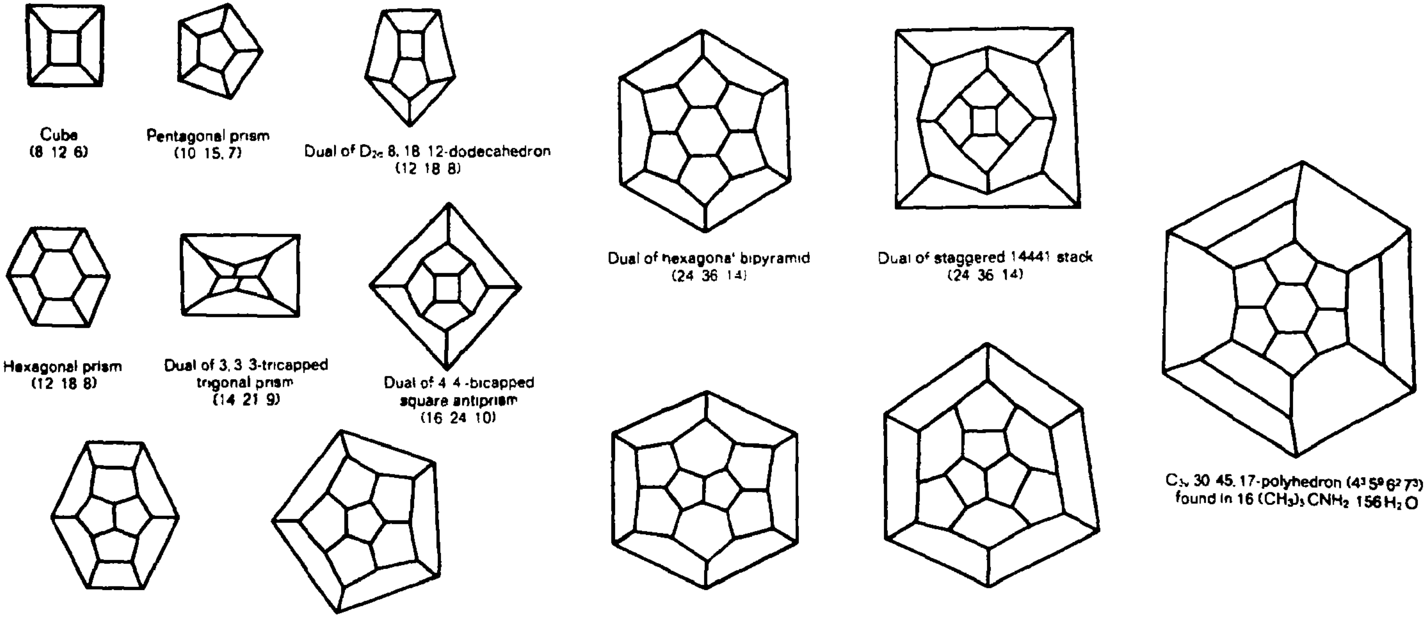

Cube
(8 12 6)

Pentagonal prism
(10 15, 7)

Dual of D_{2d} 8, 18 12-dodecahedron
(12 18 8)

Dual of hexagonal bipyramid
(24 36 14)

Dual of staggered 14441 stack
(24 36 14)

Hexagonal prism
(12 18 8)

Dual of 3, 3 3-tricapped trigonal prism
(14 21 9)

Dual of 4 4-bicapped square antiprism
(16 24 10)

C_{3v} 30 45, 17-polyhedron $(4^3 5^9 6^2 7^3)$
found in 16 $(CH_3)_3CNH_2$ 156 H_2O

Dual of $B_{11}H_{11}^{2-}$ polyhedron
(18, 27, 11)

Pentagonal dodecahedron
(20, 30 12)

15-Hedron of Allen
(26 39 15)

16-Hedron of Allen
(28 42 16)

Fig. 1. Schlegel diagrams of some of the polyhedra listed on Table 1

2. *No face of the polyhedron can be triangular and pentagonal faces are greatly favored.* The bond angle for an unstrained tetrahedral atom is 109°28′. This is closest to the 108° interior angle in a regular pentagon. An equilateral triangle has an interior angle of only 60° which is so far from the tetrahedral angle that excessive angular strain prevents the occurrence of triangular faces in polyhedra for water networks. Quadrilateral and hexagonal faces with interior angles of 90° and 120°, respectively, for these polygons when regular have a much smaller and more tolerable amount of angular strain. Furthermore, in the hexagon (as well as in polygons with larger number of sides) possible nonplanarity of the faces provides possibilities for relief of some of the angular strain. Angular strain considerations suggest that the relative tendency for various types of polygonal faces to occur in polyhedra for water networks in clathrates decreases in the following sequence:

Pentagon (most favorable) > hexagon > quadrilateral $\gg$ triangle (least favorable).

In the actual polyhedra many of the faces will not be regular polygons and the angles will not correspond exactly to the $[(n-2)/n]\ 180°$ values required for a regular polygon with n sides. However, the sum of the interior angles of even an irregular (but still planar) polygon with n sides must be a constant $(n-2)\ 180°$. Therefore, as long as planarity is preserved, deviations in one interior angle of a polygon because of irregularity will be compensated by opposite deviations in the other angles. Thus, the angular strain is not appreciably changed by moderate deviations from regularity. Extreme deviations from regularity can only increase the angular strain.

A further complication is that faces of polyhedra with five or more edges need not be planar. Bending of a face can serve to reduce the angular strain in faces with six or more edges. However, bent faces cannot be a major factor in the construction of convex polyhedra for three-dimensional water networks in clathrate hydrates for the following reasons:

1. Incorporation of an outwardly bent face (i.e. one bent in a direction to increase the area enclosed by the polyhedron) introduces reentrant angles into the polyhedron thereby making it concave. Such concave polyhedra may be decomposed into two or more smaller convex polyhedra with overlapping volumes as discussed above. As the concavity of the large concave polyhedron increases, the volume of the convex polyhedra into which the concave polyhedron can be decomposed relative to the volume of the original concave polyhedron decreases and the degree of overlap of the convex polyhedra into which the concave polyhedron can be decomposed decreases. Concave polyhedra can be excluded from consideration in this paper since all concave polyheadra can be decomposed into two or more convex polyhedra of types included in the treatment of this paper.

2. Incorporation of an inwardly bent face (i.e. one bent in a direction to decrease the area enclosed by the polyhedron) will decrease the ability for a given polyhedron to enclose a guest molecule. Hence, inwardly bent faces will only occur when necessary for the polyhedron to remain closed.

These considerations suggest that simple angular strain as discussed above is the major factor in determining the polygons to be found as faces of polyhedra

Table 1. Some possible polyhedra for water networks in clathrates

No. of elements[a]			Name of Polyhedron (if any)	Types of faces[a]			Point group[b]	Examples of clathrates containing this polyhedron
v	e	f		$f_4(=q)$	f_5	f_6		
8	12	6	Cube	6	0	0	O_h	
10	15	7	Pentagonal prism	5	2	0	D_{5h}	
10	15	7		6	0	1		
12	18	8	Dual of D_{2d}-8,18,12-dodecahedron	4	4	0	D_{2d}	16 $Me_3CNH_2 \cdot 156\ H_2O$ (empty)
12	18	8		5	2	1		
12	18	8	Hexagonal prism	6	0	2	D_{6h}	10 $Me_2CHNH_2 \cdot 80\ H_2O$ (empty)
14	21	9	Dual of 3,3,3-tricapped trigonal prism	3	6	0	D_{3h}	
14	21	9		4	4	1		
14	21	9	Dual of 252 stack[c]	5	2	2	C_{2v}	
14	21	9		6	0	3		
16	24	10	Dual of 4,4-bicapped square antiprism	2	8	0	D_{4d}	
16	24	10	Dual of staggered 136 stack[c]	3	6	1	C_{3v}	
16	24	10	Dual of 262 stack	4	4	2	D_{2h}	
16	24	10	Dual of staggered 343 stack[c]	5	2	3	C_{2v}	
16	24	10		6	0	4		
18	27	11	Existence questionable	1	10	0		
18	27	11	Dual of $B_{11}H_{11}^{2-}$ polyhedron	2	8	1	C_{2v}	16 $PrNH_2 \cdot 104\ H_2O$ (empty)
18	27	11		3	6	2		
18	27	11	Dual of 1622 stack[c]	4	4	3	C_{2v}	
18	27	11		5	2	4		
18	27	11	Dual of staggered 353 stack[c]	6	0	5	C_{2v}	
20	30	12	Pentagonal dodecahedron	0	12	0	I_h	4 $Me_3N \cdot 41\ H_2O$ and many others
20	30	12		1	10	1		
20	30	12		2	8	2		
20	30	12	Dual of staggered 363 stack[c]	3	6	3	D_{3h}	
20	30	12	Dual of 22422 stack[c]	4	4	4	D_{2h}	
20	30	12		5	2	5		
20	30	12		6	0	6		
22	33	13		0	12	1		
22	33	13		1	10	2		
22	33	13		2	8	3		
22	33	13		3	6	4		
22	33	13		4	4	5		
22	33	13		5	2	6		
22	33	13	Dual of 16222 stack[c]	6	0	7	C_{2v}	
24	36	14	Dual of hexagonal bipyramid[f]	0	12	2	D_{6d}	16 $PrNH_2 \cdot 104\ H_2O$
24	36	14		1	10	3		

24	36	14	Dual of staggered 14441 stack[f]	2	8	4	D_{4h}	10 $Me_2CHNH_2 \cdot 80\ H_2O$
24	36	14		3	6	5		
24	36	14		4	4	6		
24	36	14		5	2	7		
24	36	14	Dual of 22622 stack	6	0	8	D_{2h}	
26	39	15	15-Hedron of Allen[e]	0	12	3	D_{3h}	4 $Me_3N \cdot 41\ H_2O$
26	39	15		1	10	4		
26	39	15		2	8	5		
26	39	15	[d]	3	6	6		
26	39	15		4	4	7		
26	39	15		5	2	8		
26	39	15	Dual of omnistaggered 33333 stack[c]	6	0	9	D_{3h}	
28	42	16	16-Hedron of Allen[e]	0	12	4	T_d	10 $Me_2CHNH_2 \cdot 80\ H_2O$
28	42	16		1	10	5		
28	42	16		2	8	6		
28	42	16		3	6	7		
28	42	16	Dual of staggered 14641 stack[c]	4	4	8	D_{2h}	
28	42	16		5	2	9		
28	42	16		6	0	10		
30	45	17	Dual of staggered 15551 stack[c]	0	12	5	D_{5h}	
30	45	17		1	10	6		
30	45	17		2	8	7		
30	45	17		3	6	8		
30	45	17		4	4	9		
30	45	17		5	2	10		
30	45	17		6	0	11		
32	48	18	Dual of omnistaggered 3663 stack[c]	0	12	6	D_{3d}	12 $Et_2NH \cdot 104\ H_2O$
32	48	18		1	10	7		
32	48	18		2	8	8		
32	48	18		3	6	9		
32	48	18		4	4	10		
32	48	18		5	2	11		
32	48	18		6	0	12		

---

[a] For an explanation of these symbols and nomenclature see the text and King, R. B.: J. Amer. chem. Soc. 91, 7211 (1969).

[b] The point groups listed here represent the maximum possible symmetry. In actual cases this may be lowered in a three-dimensional network by various distortions.

[c] For an explanation of the "stack" nomenclature see King, R. B.: J. Amer. chem. Soc. 92, 6460 (1970).

[d] For a diagram of the $B_{11}H_{11}{}^{2-}$ polyhedron see Fig. 5 of Klanberg, F., Muetterties, E. L.: Inorg. Chem. 5, 1955 (1966).

[e] For a description of these polyhedra see Allen, K. W.: J. chem. Physics 41, 840 (1964).

[f] This polyhedron is the 14-hedron of Allen (see footnote e).

in three-dimensional water networks and that relief of strain by bending will not cause polygons with more sides than those favored by angular strain considerations to become predominant as faces in the construction of such polyhedra.

The first paper of this series [4] listed relationships between the parameters describing closed convex three-dimensional polyhedra with only triangular and quadrilateral faces. The following are the analogous relationships between the parameters describing closed convex-dimensional polyhedra with all vertices of order three:

1. Euler's Relationship [12]: $e+2=v+f$.
2. Relationship between the Edges and Vertices: $3v=2e$.
3. Relationship between the Edges and Faces: $\sum_i if_i=2e$. Here f_i refers to the numbers of faces with i sides or edges. Thus f_4 refers to the number of quadrilateral faces (designated as q in the first paper of this series [4]).
4. Totality of Faces: $\sum_i f_i=f$.

For any closed convex three-dimensional polyhedron with all vertices of order three the numbers of edges and faces for a given number of vertices are uniquely defined by the relationships $e=3v/2$ and $f=(4+v)/2$. This reduces drastically the number of sets of v, e, and f values which have to be considered. For a given set of v, e, and f values there are many possible polyhedra corresponding to different solutions of the equations $\sum_i if_i=2e$ and $\sum_i f_i=f$.

Table 1 summarizes the possible closed convex three-dimensional polyhedra with all vertices of order three, with no more than eighteen faces, and with only quadrilateral, pentagonal, and hexagonal faces. Figure 1 shows Schlegel diagrams [12] of some of the more important of these polyhedra in the chemistry of clathrate water networks.

Identification of the actual polyhedra corresponding to various sets of v, e, f, and f_n values is relatively difficult in many cases but has been achieved for the polyhedra of greatest potential importance in polyhedral water networks in clathrates. The relationship of duality [13], briefly cited in the first paper of this series [4], is of considerable value in the identification of the polyhedra listed in Table 1. In a pair of (mutually) dual polyhedra P_a and P_b the vertices of one of the polyhedra correspond to the faces of the other and vice versa. Both P_a and P_b belong to the same symmetry point group. Furthermore, the following relationships are satisifed where the subscripts a and b refer to the dual polyhedra P_a and P_b, respectively: $v_b=f_a$; $e_b=e_a$; $f_b=v_a$. The correspondence of a vertex of a polyhedron P_a to a face of a polyhedron P_b and vice versa also mean that the following relationships must be satisifed for all n: $(j_n)_a=(f_n)_b$ and $(f_n)_a=(j_n)_b$. One obvious consequence of the latter set of relationships is that the polyhedra with all vertices of order three generated in Table 1 all are duals of some triangulated polyhedron [4]. Triangulated polyhedra are of interest as coordination polyhedra [4, 5], metal cluster polyhedra [1], and cage boron hydride polyhedra [1] and thus were discussed in earlier papers of this series. Many of the polyhedra in Table 1 can be identified as duals of previously observed triangulated polyhedra. The "parallel plane method" for generating polyhedra [5] is useful for generating duals of polyhedra in Table 1. The existence of the 18, 27, 11-polyhedron ($4^1 5^{10}$)

is regarded as unlikely (although not yet rigorously disproved) since all previous attempts during the study on polyhedra for high coordination numbers [5] to find its dual (i.e. an 11, 27, 18-polyhedron with no vertices of order six or higher) were unsuccessful.

Discussion

The pentagonal dodecahedron is the optimum polyhedron for water networks in clathrates and semiclathrates since it is the only polyhedron with all vertices of order three where all faces are the favored pentagons with minimum angular strain. The pentagonal dodecahedron cannot be packed into a lattice if it is kept regular with idealized I_h symmetry [14]. However, if the pentagonal 108° angles in the pentagonal dodecahedron are distorted slightly to the tetrahedral value of 109°28′, then pentagonal dodecahedra can form a network with cubic symmetry. This network also contains larger 28, 42, 16-polyhedral ($5^{12}6^4$) holes which represent a distorted C_{2v} version of the idealized T_d polyhedron of this type. In another packing of pentagonal dodecahedra larger holes are also generated which correspond to the 24, 36, 14-polyhedron ($5^{12}6^2$), i.e., the dual of the hexagonal bipyramid, and to the 26, 39, 15-polyhedron ($5^{12}6^3$). These water networks with pentagonal dodecahedra are found in numerous clathrate hydrates and gas hydrates [2, 3]. The water networks containing pentagonal dodecahedra may also contain the 14-hedra, 15-hedra, and 16-hedra with the maximum numbers of the favored pentagonal faces.

A pentagonal dodecahedron in a water network has a volume of about 170 A^3 [15]. Some types of guest molecules in a clathrate or semiclathrate hydrate will be either too large or of the wrong shape to fit into a cavity of this size and shape. In some cases the guest molecules can be accommodated in the somewhat larger 24, 36, 14-polyhedra ($5^{12}6^2$) (volume $\sim 220\ A^3$) or 26, 39, 15-polyhedra ($5^{12}6^3$) (volume $\sim 240\ A^3$) which form the larger cavities in one of the packings of pentagonal dodecahedra. The still larger 28, 42, 16-polyhedron ($5^{12}6^4$) is found in isopropylamine hydrate $10(CH_3)_2CHNH_2 \cdot 80\,H_2O$ [16].

Clathrate and semiclathrate hydrates of relatively bulky amines contain still larger polyhedra. Thus, the water network of diethylamine hydrate, $12(C_2H_5)_2NH \cdot 104\,H_2O$, contains D_{3d} 32, 48, 18-polyhedra ($5^{12}6^6$); the diethylamine molecules fit relatively well into these ellipsoidal cavities [17]. This network of 32, 48, 18-polyhedra ($5^{12}6^6$) contains no pentagonal dodecahedral cavities but instead some irregular concave 29, 44, 17-polyhedra ($4^3 5^8 6^6$) which because of their concavity contain one vertex of order four. The water network of t-butylamine hydrate, $16(CH_3)_3CNH_2 \cdot 156\,H_2O$, the only known amine clathrate hydrate without hydrogen bonding of the amine to the water network, contains unusual C_{3v} 30, 45, 17-polyhedra ($4^3 5^9 6^2 7^3$); [18] this is the only polyhedron with heptagonal faces encountered in clathrate hydrates (polyhedra with heptagonal faces have been omitted from Table 1, since consideration of such polyhedra increases the possibilities to an unmanageable number). Packing these 30, 45, 17-polyhedra ($4^3 5^9 6^2 7^3$) into a three-dimensional network leaves small cavities of 12, 18, 8-polyhedra ($4^4 5^4$); this polyhedron is the dual of the D_{2d} 8, 18, 12-dodecahedron which is the most common coordination polyhedron for eight-coordinate complexes [4, 19]. The 12, 18, 8-polyhedra ($4^4 5^4$) in $16(CH_3)_3CNH_2 \cdot 156\,H_2O$ are far too small to accommodate any guest molecules. However, the 30, 45, 17-polyhedron ($4^3 5^9 6^2 7^3$) has a free volume about 30% larger than that of the 28, 42, 16-polyhedron ($5^{12} 6^4$); this additional volume may be necessary to accommodate the relatively bulky t-butylamine molecule. Furthermore, the failure of the t-butylamine in its clathrate hydrate to form hydrogen bonds with the polyhedral water network may make a larger polyhedron necessary to enclose it in to keep the t-butylamine molecules beyond the bonding distances to the atoms in the water network. Most of the faces of both the 32, 48, 18-polyhedra ($5^{12} 6^6$) and the 30, 45, 17-polyhedra ($4^3 5^9 6^2 7^3$) are the favored pentagons.

The theory developed in this paper suggests that the normal water network for clathrates and semiclathrates contains the very favorable pentagonal dodecahedron. However, if the guest molecules are too large to fit into the cavities of pentagonal dodecahedra (e.g. diethylamine and t-butylamine), then alternative water networks with larger polyhedra will be formed. This suggests that clathrate and semiclathrate hydrates of relatively large and non-spherical molecules which do not fit into the polyhedra with up to 18 faces discussed in this paper are most likely to contain unusual polyhedra. However, a limiting factor in the preparation of clathrate hydrates of large molecules of appropriate polarity is likely to be the difficulty of packing large convex polyhedra into a three-dimensional network because of the concurrent need in such networks for strained small polyhedra both to fill the gaps between the large polyhedra and to accommodate the fourth hydrogen bond to each oxygen atom.

References

1. For Part V of this series see King, R. B.: J. Amer. chem. Soc. **94**, 95 (1972).
2. Jeffrey, G. A · Accts. Chem. Research **2**, 344 (1969).
3. -- McMullan, R. K.: Progr. Inorg. Chem. **8**, 43 (1967).
4. King, R. B : J Amer. chem. Soc. **91**, 7211 (1969)
5. J. Amer. chem. Soc. **92**, 6460 (1970).
6. -- J. Amer. chem. Soc. **92**, 6455 (1970).
7. Beurskens, P. T., Jeffrey, G. A.: J. chem. Physics **40**, 906, 2800 (1964).
8. For a definition of convex polyhedra see Grünbaum, B.: Convex polytopes, New York: Interscience Publishers 1967.
9. Mak, T. C. W.: J. chem. Physics **43**, 2799 (1965).
10. Panke, D.: J. chem. Physics **48**, 2990 (1968).
11. Alexandrow, A. D.: Konvexe Polyeder, p. 14, Berlin: Akademie-Verlag 1958.
12. Ref. [8], pp. 42–46.
13. Ref. [8], pp. 46–48.
14. Claussen, W. F.: J. chem. Physics **19**, 259 (1951).
15. Feil, D., Jeffrey, G. A.: J. chem. Physics **35**, 1863 (1961).
16. Panke, D., McMullan, R. M.: Abstracts of american crystallographic association meeting, No. K 7. Tucson, Arizona: February 1968.
17. Jordan, T. H., Mak, T. C. W.: J. chem. Physics **47**, 1222 (1967).
18. McMullan, R. K., Jeffrey, G. A., Jordan, T. H.: J. chem. Physics **47**, 1229 (1967).
19. Lippard, S. J.: Progr. Inorg. Chem. **8**, 109 (1967).

Prof. Dr. R. B. King
Department of Chemistry
University of Georgia
Athens, Georgia 30601, USA

Theoret. chim. Acta (Berl.) 25, 319—330 (1972)
© by Springer-Verlag 1972

Angenäherte Berechnung der Dreizentren-Kernanziehungsintegrale in LCAO–MO-Verfahren für Koordinationsverbindungen

J. REINHOLD und E. HOYER
Sektion Chemie der Karl-Marx-Universität, Leipzig, DDR

Eingegangen am 13. August 1971

Approximation of Three-Center Nuclear Attraction Integrals in LCAO-MO-*Methods for Coordination Compounds*

At the calculation of non-diagonal elements in LCAO-MO-methods for coordination compounds arise three-center nuclear attraction integrals of type $\left(\chi_a \middle| \frac{1}{r_c} \middle| \chi_b\right)$. We give a simple method for the approximate calculation of these integrals which is based on the high symmetry of the coordination compounds. The three-center integrals are reduced to a sum of few special two-center integrals.

Bei der Berechnung der Nichtdiagonalelemente in LCAO-MO-Verfahren für Koordinationsverbindungen treten Dreizentren-Kernanziehungsintegrale vom Typ $\left(\chi_a \middle| \frac{1}{r_c} \middle| \chi_b\right)$ auf. Wir geben ein einfaches Verfahren zur näherungsweisen Berechnung dieser Integrale an, das auf der hohen Symmetrie der Koordinationsverbindungen beruht. Die Dreizentrenintegrale werden auf eine Summe von wenigen speziellen Zweizentrenintegralen zurückgeführt.

1. Einleitung

Das von Wolfsberg u. Helmholz [1] angegebene Verfahren zur Berechnung von Übergangsmetallkomplexen wurde mannigfach modifiziert und kritisch untersucht, um seine Mängel und seinen Anwendungsbereich kennenzulernen. Es zeigte sich, daß die Resultate stark von den gewählten Parametern abhängen; das Problem der Reihenfolge und des Metall-Ligand-Charakters der Orbitale beim Permanganat-Ion ist dafür typisch (siehe etwa [2]). Will man die Rechnungen auf eine theoretisch fundiertere Stufe heben, so muß man nichtempirische Verfahren anstreben. Dies erfordert die Berechnung der Matrixelemente. Während die Behandlung der auftretenden Ein- und Zweizentrenintegrale keine prinzipiellen Schwierigkeiten bereitet, ist die der Drei- und Vierzentrenintegrale außerordentlich kompliziert und zeitaufwendig. Im allgemeinen werden sie vernachlässigt, durch Hilfsformeln berücksichtigt oder mit Hilfe der Mulliken-Näherung [3] auf Zweizentrenintegrale zurückgeführt. Fenske *et al.* [4] berechneten auch Dreizentrenintegrale und konnten die Unzulänglichkeit der einfachen Hilfsformeln für die Nichtdiagonalelemente zeigen [5].

Für exaktere, „parameterfreie“ Verfahren müssen also Mehrzentrenintegrale berechnet werden. Das schränkt die allgemeine Anwendung solcher Verfahren ganz wesentlich ein. Wir beschreiben in der vorliegenden Arbeit ein bereits kurz vorgestelltes [6] Verfahren zur näherungsweisen Berechnung der Dreizentren-Kernanziehungsintegrale vom Typ $\left(\chi_a \middle| \frac{1}{r_c} \middle| \chi_b\right)$ in Komplexmolekülen, das sich die hohe Symmetrie dieser Moleküle zunutze macht. Es führt die Dreizentren-Kernanziehungsintegrale auf Zweizentrenintegrale zurück und ermöglicht dadurch eine breitere Anwendung exakterer Methoden.

2. Die Dreizentren-Kernanziehungsintegrale

Für das Nichtdiagonalelement zwischen den Atomorbitalen $\chi_{k'}$ am Liganden k' und χ_M am Zentralion M schreiben wir

$$(\chi_{k'}|H|\chi_M) = (\chi_{k'}|-\tfrac{1}{2}\Delta + V_M|\chi_M) + \sum_{k \neq k'} (\chi_{k'}|V_k|\chi_M) + (\chi_{k'}|V_{k'}|\chi_M) .$$

Eine ausführliche Diskussion der einzelnen Teile des Hamiltonoperators im Hinblick auf ihre Verwendung in den Matrixelementen findet man bei Fenske *et al.* [4]. Das Potential V_k der Liganden k im zweiten Term des obigen Ausdrucks läßt sich in guter Näherung als Punktladungspotential auffassen:

$$\sum_{k \neq k'} (\chi_{k'}|V_k|\chi_M) = \sum_{k \neq k'} \left(\chi_{k'} \middle| \frac{-q_k}{r_k} \middle| \chi_M\right) . \tag{1}$$

Das ist eine Summe von $L-1$ Dreizentren-Kernanziehungsintegralen; L ist die Anzahl der Liganden.

Wir spalten nun die Summe (1) nicht in Einzelintegrale auf, wie es gewöhnlich getan wird; bei den hochsymmetrischen Anordnungen, an denen wir interessiert sind, ist es zweckmäßig, die Summe (1) als Ganzes zu behandeln. Zunächst formen wir (1) identisch um zu

$$\sum_{k=1}^{L} \left(\chi_{k'} \middle| \frac{-q_k}{r_k} \middle| \chi_M\right) - \left(\chi_{k'} \middle| \frac{-q_{k'}}{r_{k'}} \middle| \chi_M\right) . \tag{2}$$

Die Summe über k enthält jetzt auch das Glied $k = k'$, das rechts wieder subtrahiert wird. Dieses Glied ist ein simples Zweizentrenintegral, das lediglich als Hilfsgröße dient. Es ist kein Zweizentren-Kernanziehungsintegral im Sinne von (1), da für den Zweizentren-Fall die Punktladungsnäherung nicht anwendbar ist. Für die Summe in (2) schreiben wir

$$\left(\chi_{k'} \middle| \sum_{k=1}^{L} \frac{-q_k}{r_k} \middle| \chi_M\right) = (\chi_{k'}|V|\chi_M) . \tag{3}$$

Jede Punktladung hatte bisher ihr eigenes Koordinatensystem. Ab jetzt verwenden wir jedoch ein einheitliches Koordinatensystem mit dem Ursprung am Ort des Zentralions M. Drücken wir das Potential V in diesem Koordinatensystem aus, so haben wir die Mehrzentrenintegrale in (3) formal schon auf ein Zweizentrenintegral zurückgeführt.

3. Das Potential der Liganden

Durch die identische Umformung von (1) in (2) haben wir das Ligandenfeldpotential V (das Potential aller Liganden) in die Betrachtung einbezogen. Dadurch können wir jetzt den Formalismus der Ligandenfeldtheorie anwenden[1].

Das Potential von L Punktladungen $-q_k$ an den Orten $\boldsymbol{R}_k = (R_k, \Theta_k, \Phi_k)$ (Koordinatenursprung am Ort des Zentralions) ist am Aufpunkt $\boldsymbol{r} = (r, \vartheta, \varphi)$

$$V(\boldsymbol{r}) = \sum_{k=1}^{L} \frac{-q_k}{|\boldsymbol{R}_k - \boldsymbol{r}|}.$$

Nimmt man die Ladungen $-q_k$ und die Abstände R_k der Liganden vom Zentralion als gleich an ($q_k = q$ und $R_k = R$ für alle k) und entwickelt $|\boldsymbol{R}_k - \boldsymbol{r}|^{-1}$ in der üblichen Weise nach Kugelflächenfunktionen, so erhält man

$$V(\boldsymbol{r}) = -q \sum_{k=1}^{L} \sum_{\lambda=0}^{\infty} \sum_{\varkappa=-\lambda}^{+\lambda} \frac{4\pi}{2\lambda+1} \frac{r_<^{\lambda}}{r_>^{\lambda+1}} Y_{\lambda\varkappa}(\vartheta, \varphi)\, Y^*_{\lambda\varkappa}(\Theta_k, \Phi_k).$$

Für das Potential innerhalb einer Kugel mit dem Radius R gilt (mit $r_< = r$ und $r_> = R$)

$$V^{\text{inn}}(\boldsymbol{r}) = -q \sum_{k} \sum_{\lambda} \sum_{\varkappa} \frac{4\pi}{2\lambda+1} \frac{r^{\lambda}}{R^{\lambda+1}} Y_{\lambda\varkappa}(\vartheta, \varphi)\, Y^*_{\lambda\varkappa}(\Theta_k, \Phi_k).$$

Mit diesem Potential arbeitet die Ligandenfeldtheorie, da die Aufenthaltswahrscheinlichkeit der $3d$-Elektronen des Zentralions außerhalb R vernachlässigt werden kann. Wir benötigen das Potential V jedoch zur Bildung der Matrixelemente (3) zwischen Metall- und Ligandfunktionen, d. h. wir müssen auch das Potential außerhalb R berücksichtigen ($r_< = R, r_> = r$):

$$V^{\text{auß}}(\boldsymbol{r}) = -q \sum_{k} \sum_{\lambda} \sum_{\varkappa} \frac{4\pi}{2\lambda+1} \frac{R^{\lambda}}{r^{\lambda+1}} Y_{\lambda\varkappa}(\vartheta, \varphi)\, Y^*_{\lambda\varkappa}(\Theta_k, \Phi_k).$$

Wir fassen V^{inn} und $V^{\text{auß}}$ zusammen zu

$$V(\boldsymbol{r}) = \Theta(R - r)\, V^{\text{inn}}(\boldsymbol{r}) + \Theta(r - R)\, V^{\text{auß}}(\boldsymbol{r}).$$

Dabei ist Θ eine Sprungfunktion, definiert durch

$$\Theta(x) = \begin{cases} 1 & \text{für} \quad x > 0 \\ 0 & \text{für} \quad x < 0. \end{cases}$$

$V(\boldsymbol{r})$ wird damit zu

$$V(\boldsymbol{r}) = -q \sum_{k} \sum_{\lambda} \sum_{\varkappa} \frac{4\pi}{2\lambda+1} \left[\frac{r^{\lambda}}{R^{\lambda+1}} \Theta(R - r) + \frac{R^{\lambda}}{r^{\lambda+1}} \Theta(r - R) \right] Y_{\lambda\varkappa}(\vartheta, \varphi)\, Y^*_{\lambda\varkappa}(\Theta_k, \Phi_k).$$

Das schreibt man zweckmäßig als

$$V(\boldsymbol{r}) = \sum_{\lambda=0}^{\infty} \sum_{\varkappa=-\lambda}^{+\lambda} A_{\lambda\varkappa} \left[r^{\lambda} \Theta(R - r) + \frac{R^{2\lambda+1}}{r^{\lambda+1}} \Theta(r - R) \right] Y_{\lambda\varkappa}(\vartheta, \varphi) \qquad (4)$$

---

[1] Wir lehnen uns eng an das Buch von Schläfer und Gliemann „Einführung in die Ligandenfeldtheorie“ [7] an, benutzen insbesondere im wesentlichen die dortige Bezeichnungsweise.

mit

$$A_{\lambda\varkappa} = -\frac{q}{R^{\lambda+1}}\,\frac{4\pi}{2\lambda+1}\sum_{k=1}^{L} Y^{*}_{\lambda\varkappa}(\Theta_k, \Phi_k)\,. \tag{5}$$

Im Falle hochsymmetrischer Ligandenanordnungen reduziert sich die Anzahl der Summenglieder in (4). Wir greifen den Fall eines oktaedrischen Ligandenfeldes heraus, d. h. wir betrachten das Potential von $L = 6$ Punktladungen $-q$, die sich im Abstand R vom Zentralion an den Ecken eines regulären Oktaeders befinden. Da das Potential (4) invariant bezüglich aller Symmetrieoperationen der Oktaedergruppe sein muß, bleiben nur folgende Terme der Potentialentwicklung:

$$\begin{aligned} V(r) = {} & A_{00}\left| r^0\,\Theta(R-r) + \frac{R}{r}\,\Theta(r-R)\right| Y_{00} \\ & + A_{40}\left| r^4\,\Theta(R-r) + \frac{R^9}{r^5}\,\Theta(r-R)\right| \left(Y_{40} + \sqrt{\tfrac{5}{14}}\,(Y_{44} + Y_{4,-4})\right) \\ & + \cdots \end{aligned}$$

mit

$$A_{00} = -12\sqrt{\pi}\, q/R\,, \qquad A_{40} = -7\sqrt{\pi}\, q/3R^5\,. \tag{6}$$

Der Ausdruck kann weiter vereinfacht werden, wenn man bedenkt, daß das Potential in Matrixelementen mit $\chi_{k'}$ und χ_M verwendet wird. Die Integration über φ liefert nur dann einen nichtverschwindenden Wert, wenn $\varkappa = 0$ ist. Damit bleibt nur

$$\begin{aligned} V(r) = {} & A_{00}\left| r^0\,\Theta(R-r) + \frac{R}{r}\,\Theta(r-R)\right| Y_{00} \\ & + A_{40}\left| r^4\,\Theta(R-r) + \frac{R^9}{r^5}\,\Theta(r-R)\right| Y_{40} \\ & + \cdots \end{aligned} \tag{7}$$

als wirksamer Teil der Entwicklung. Mit diesem Potential werden wir im folgenden arbeiten. In der vorliegenden Arbeit betrachten wir nur die Glieder mit $\lambda \leq 4$[2].

4. Zur Berechnung von Zweizentrenintegralen

Aus Gründen der Bezeichnungsweise muß zunächst einiges zur Berechnung von Zweizentrenintegralen in elliptischen Koordinaten gesagt werden. Sind $(r_a, \vartheta_a, \varphi_a)$ die Koordinaten eines Punktes bezüglich eines Zentrums a und $(r_b, \vartheta_b, \varphi_b)$ diejenigen bezüglich eines Zentrums b, so sind die elliptischen Koordinaten λ, μ, φ definiert als

---

[2] Wir bemerken, daß in der Ligandenfeldtheorie die zusätzliche Bedingung $\lambda \leq 4$ gilt. Das Potential wird dort in Matrixelementen $(3d|V|3d)$ verwendet, die als Faktor ein Integral über drei Kugelflächenfunktionen enthalten. Allgemein ist aber $(Y_{lm}|Y_{\lambda\varkappa}|Y_{l'm'})$ nur dann von Null verschieden, wenn $l + l' + \lambda$ gerade und $|l - l'| \leq \lambda \leq |l + l'|$ ist. Für den Fall der Ligandenfeldtheorie ($l = l' = 2$) liefert das $\lambda \leq 4$. Für unsere Zwecke ist dieser Satz nicht anwendbar. Wir brauchen V zur Bildung von Matrixelementen zwischen Metall- und Ligandfunktionen, d. h. die enthaltenen Kugelflächenfunktionen gehören zu verschiedenen Zentren; dann gilt aber der Satz nicht mehr.

$$\lambda = \frac{1}{R}(r_a + r_b), \qquad \mu = \frac{1}{R}(r_a - r_b), \qquad \varphi = \varphi_a = \varphi_b$$

mit $1 \leqq \lambda < \infty$, $-1 \leqq \mu \leqq +1$ und $0 \leqq \varphi \leqq 2\pi$.

Bildet man mit Slater-Atomorbitalen

$$\chi_{nlm} = \sqrt{\frac{2^{2n+1}}{(2n)!}} \left(\frac{\zeta}{a_0}\right)^{(2n+1)/2} r^{n-1} \exp\left\{-\frac{\zeta}{a_0} r\right\} Y_{lm} \tag{8}$$

Überlappungsintegrale und geht zu elliptischen Koordinaten über, dann erhält man nach Integration über φ die bekannten Formeln von Mulliken *et al.* [8], Jaffé und Doak [9, 10]. Als willkürliches Anschauungsbeispiel dient

$$\begin{aligned}(2p\sigma|1s) &= \tfrac{1}{8} p^4(1+t)^{5/2}(1-t)^{3/2}\left[\int\int (1+\lambda\mu)(\lambda^2-\mu^2)e^{-p\lambda}e^{-pt\mu}\,d\lambda\,d\mu\right] \\ &= \tfrac{1}{8} p^4(1+t)^{5/2}(1-t)^{3/2}\left[A_3B_1 + A_2B_0 - A_1B_3 - A_0B_2\right]\end{aligned}$$

mit

$$A_k(p) = \int_1^\infty \lambda^k e^{-p\lambda}\,d\lambda \quad \text{und} \quad B_k(pt) = \int_{-1}^{+1} \mu^k e^{-pt\mu}\,d\mu \tag{9}$$

und

$$p = \tfrac{1}{2}\,\frac{R}{a_0}(\zeta_a + \zeta_b), \qquad t = \frac{\zeta_a - \zeta_b}{\zeta_a + \zeta_b}\,.$$

Wir verwenden für alle analogen Formeln die pauschale Schreibweise

$$(n_a l_a m_a|n_b l_b m_b) = F(n_a l_a m_a, n_b l_b m_b; p, t)\,[n_a l_a m_a, n_b l_b m_b; p, pt]\,. \tag{10}$$

Die Faktoren $F(n_a l_a m_a, n_b l_b m_b; p, t)$ sind Funktionen von p und t. $[n_a l_a m_a, n_b l_b m_b; p, pt]$ bezeichnet Integrale über λ und μ; die Integranden sind Polynome in λ und μ, multipliziert mit Exponentialfunktionen. Sie lassen sich in den Hilfsintegralen (9) ausdrücken; dann sind die $[n_a l_a m_a, n_b l_b m_b; p, pt]$ Summen von Produkten $A_k(p)\,B_l(pt)$.

Wir werden im folgenden immer für die Ligandfunktionen das Zentrum a und für die Metallfunktionen das Zentrum b verwenden. Eine solche Vorschrift ist nicht üblich; im allgemeinen können natürlich die Zentren willkürlich gewählt werden. Für unsere Zwecke macht sich jedoch eine einheitliche Festlegung erforderlich.

5. Das Näherungspotential

Die Zweizentrenintegrale $(\chi_{k'}|V|\chi_M)$ in (3) enthalten das exakte Potential (7). In dieser Form läßt sich das Potential nicht in geschlossener Weise durch elliptische Koordinaten ausdrücken, und der obige Lösungsformalismus (Zurückführen auf die leicht zugänglichen Hilfsintegrale (9)) ist nicht anwendbar. Wir wollen nun aber gerade eine solche Gestalt für V suchen, daß das möglich wird. Dazu müssen wir die Sprungfunktionen in (7) beseitigen und geschlossene Ausdrücke für die Klammern suchen.

Betrachten wir aber zunächst die Kugelflächenfunktionen in (7): Y_{00} ist nur eine Konstante; aus der zweiten Klammer ziehen wir r^4 heraus, denn $r^4\,Y_{40}$ läßt sich als Polynom in λ und μ schreiben:

$$r_b^4\, Y_{40} = \frac{3}{16}\, \frac{1}{\sqrt{\pi}}\, r_b^4 (8 \cos^4 \vartheta_b - 24 \cos^2 \vartheta_b \sin^2 \vartheta_b + 3 \sin^4 \vartheta_b)$$

$$= y_4\, V_4$$

mit

$$y_4 = \frac{3}{16}\, \frac{1}{\sqrt{\pi}} \left(\frac{R}{2}\right)^4 \tag{11}$$

und

$$V_4 = 8(1 - \lambda\mu)^4 - 24(1 - \lambda\mu)^2 (\lambda^2 - 1)(1 - \mu^2) + 3(\lambda^2 - 1)^2 (1 - \mu^2)^2 . \tag{12}$$

(Es sei daran erinnert, daß die Metallfunktionen und somit auch das Potential V zum Zentrum b gehören sollen.)

Dann bleiben

$$\left| r^0\, \Theta(R - r) + \frac{R}{r}\, \Theta(r - R) \right| \quad \text{und} \quad \left[r^0\, \Theta(R - r) + \frac{R^9}{r^9}\, \Theta(r - R) \right] .$$

Der gesuchte Ausdruck für diese Klammern kann Potenzen von r enthalten; in elliptischen Koordinaten ergibt das $\left(\frac{R}{2}\right)^i (\lambda - \mu)^i$. Wir können deshalb Polynome in r als Näherungsausdrücke für die Klammern ansetzen:

$$\sum_{i=0}^{n_0} \hat{b}_{0i}\, r^i \quad \text{und} \quad \sum_{i=0}^{n_4} \hat{b}_{4i}\, r^i .$$

In der vorliegenden Arbeit haben wir zunächst quadratische Polynome verwendet, d. h. $n_0 = n_4 = 2$; höhere Potenzen vergrößern den Rechenaufwand.

Eine wesentliche Verbesserung ohne Mehraufwand erreicht man aber durch einen Faktor $e^{-\hat{a}r}$. Damit kann der Abfall des Potentials für $r > R$ auf Null gut angenähert werden. Beim Übergang zu elliptischen Koordinaten wird dieser Faktor von den Exponentialfunktionen in (10) mit aufgenommen (siehe später, Abschn. 7).

Wir setzen damit für das Potential (7) folgende Näherung an:

$$\begin{aligned} V(r) = {} & A_{00}[e^{-\hat{a}_0 r}(\hat{b}_{00} + \hat{b}_{01} r + \hat{b}_{02} r^2)]\, Y_{00} \\ & + A_{40}[e^{-\hat{a}_4 r}(\hat{b}_{40} + \hat{b}_{41} r + \hat{b}_{42} r^2)]\, r^4\, Y_{40} \\ & + \cdots . \end{aligned} \tag{13}$$

Die Koeffizienten $\hat{a}_0$, $\hat{b}_{0i}$, $\hat{a}_4$ und $\hat{b}_{4i}$ sind so zu bestimmen, daß (13) mit (7) bestmöglich übereinstimmt.

6. Bestimmung der Koeffizienten des Näherungspotentials

Zur Bestimmung der Koeffizienten in (13) verwenden wir die Methode der kleinsten Quadrate. Für die erste Klammer fordern wir, daß das Integral

$$M = \int_0^{3R/2} \left[e^{-\hat{a}_0 r}(\hat{b}_{00} + \hat{b}_{01} r + \hat{b}_{02} r^2) - \left(\Theta(R - r) + \frac{R}{r}\, \Theta(r - R) \right) \right]^2 dr$$

einen minimalen Wert annimmt.

Das Potential V wird in Matrixelementen $(\chi_{k'}|V|\chi_M)$ verwendet. Da unser Ziel die näherungsweise Berechnung dieser Integrale und nicht die des Potentials ist, müßten wir die Ausdrücke im Integranden von M eigentlich mit dem r-abhängigen Teil des Produkts $\chi_{k'}\chi_M$ wichten. Dann würde aber für jedes spezielle Funktionenpaar $\chi_{k'}$, χ_M ein neues Problem entstehen. Wir verwenden deshalb einheitlich für alle $\chi_{k'}$, χ_M für $0 \leqq r \leqq \frac{3}{2} R$ das Gewicht 1 und für $r > \frac{3}{2} R$ das Gewicht 0 (dort verschwindet das Produkt $\chi_{k'}\chi_M$ im wesentlichen). Wir versuchen also, im Intervall $0 \leqq r \leqq \frac{3}{2} R$ das Potential (13) möglichst gut an (7) anzunähern, um damit auch gute Übereinstimmung der Matrixelemente zu erzielen.

Das Extremalproblem liefert ein nichtlineares Gleichungssystem für die optimalen Koeffizienten $\hat{a}_0$, $\hat{b}_{0i}$. Durch Übergang zu neuen Koeffizienten

$$a_0 = \frac{R}{2}\,\hat{a}_0\,, \qquad b_{0i} = \left(\frac{R}{2}\right)^i \hat{b}_{0i} \tag{14}$$

kann man erreichen, daß die Gleichungen R nicht mehr explizit enthalten. Man braucht also das Extremalproblem nur einmal zu lösen; das Ergebnis gilt für jeden Metall-Ligand-Abstand R. Die optimalen Koeffizienten sind

$$\begin{aligned} a_0 &= 0{,}981\,, \\ b_{00} &= 1{,}0478\,, \\ b_{01} &= 0{,}5485\,, \\ b_{02} &= 1{,}1288\,. \end{aligned} \tag{15}$$

Die Beziehungen zu den eigentlichen Potentialkoeffizienten $\hat{a}_0$, $\hat{b}_{0i}$ sind durch (14) gegeben.

Wir bestimmen nun die Koeffizienten der zweiten Klammer in (13). Dazu verwenden wir das Integral

$$M = \int\limits_0^{3R/2} \left| e^{-\hat{a}_4 r}(\hat{b}_{40} r^4 + \hat{b}_{41} r^5 + \hat{b}_{42} r^6) - \left(r^4\,\Theta(R-r) + \frac{R^9}{r^5}\,\Theta(r-R) \right) \right]^2 dr\,.$$

Den Faktor r^4 im Potential (7) und (13) können wir als Gewicht verwenden, da er keine Schwierigkeiten bereitet; im übrigen gelten die Bemerkungen zum ersten Problem. Wir benutzen den gleichen Lösungsformalismus wie oben, d. h. wir führen die R-unabhängigen Koeffizienten

$$a_4 = \frac{R}{2}\,\hat{a}_4\,, \qquad b_{4i} = \left(\frac{R}{2}\right)^i \hat{b}_{4i} \tag{16}$$

ein. Als optimale Werte erhalten wir

$$\begin{aligned} a_4 &= 4{,}012\,, \\ b_{40} &= 1025{,}7\,, \\ b_{41} &= -2516{,}3\,, \\ b_{42} &= 1482{,}0\,. \end{aligned} \tag{17}$$

Einen Vergleich zwischen den korrekten Potentialtermen in (7) und den Näherungen in (13) zeigt die Fig. 1. Man sieht, daß das Potential (7) mit dem Ansatz (13) gut angenähert werden kann.

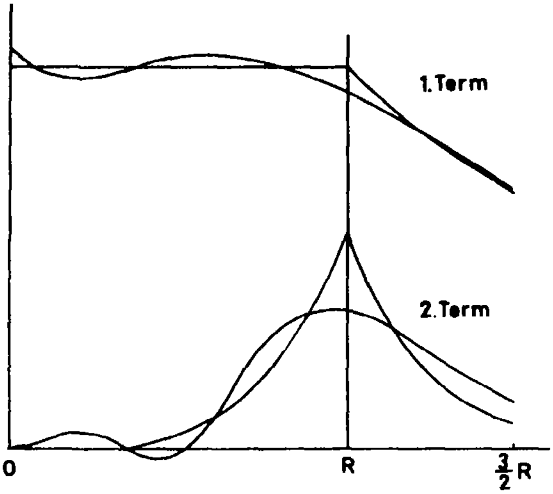

Fig. 1 Vergleich zwischen den exakten Termen der Potentialentwicklung und den Näherungen mit den Koeffizienten (15) und (17)

7. Die Integrale $(\chi_{k'}|V|\chi_M)$

Wir sind nun mit dem Potentialausdruck (13) – in der Lage, die Integrale $(\chi_{k'}|V|\chi_M)$ in (3) in geschlossener Form in elliptischen Koordinaten auszudrücken und auf die Hilfsintegrale (9) zurückzuführen. Allgemein schreiben wir

$$\begin{aligned}(\chi_a|V|\chi_b) = {} & (\chi_a|A_{00}[e^{-\hat{a}_0 r_b}(\hat{b}_{00}+\hat{b}_{01}r_b+\hat{b}_{02}r_b^2)]\,Y_{00}|\chi_b) \\ & +(\chi_a|A_{40}[e^{-\hat{a}_4 r_b}(\hat{b}_{40}+\hat{b}_{41}r_b+\hat{b}_{42}r_b^2)]\,r_b^4\,Y_{40}|\chi_b) \\ & +\cdots .\end{aligned} \tag{18}$$

Diese Ausdrücke zerfallen in Einzelintegrale, die r_b^i als Faktor enthalten. Da die Funktion χ_b zur Hauptquantenzahl n die Potenz r_b^{n-1} enthält (zufolge (8)), so bewirkt der Faktor r_b^i eine formale Erhöhung der Hauptquantenzahl von χ_b um i (bei unverändertem Orbitalexponent).

Beim Übergang zu elliptischen Koordinaten wird aus jedem r_b ein $\frac{R}{2}(\lambda-\mu)$. $r_b^4\,Y_{40}=y_4 V_4$ ist in (11) und (12) gegeben. Analog dazu schreiben wir auch für die Konstante Y_{00}

$$Y_{00}=y_0 V_0, \quad \text{mit} \quad y_0=1/2\sqrt{\pi} \quad \text{und} \quad V_0=1 .$$

Wir betrachten nun die Exponentialfunktionen in (18). Ihr Produkt mit den Exponentialfunktionen aus χ_a und χ_b ergibt

$$\exp\left\{-\hat{a}\,\frac{R}{2}(\lambda-\mu)\right\}\exp\{-p\lambda\}\exp\{-pt\mu\}=\exp\{-(p+a)\lambda\}\exp\{-(pt-a)\mu\} . \tag{19}$$

Die Einführung von e^{-ar} in den Näherungsausdruck (13) bewirkt also lediglich eine Verschiebung der p- und pt-Werte.

In einer Schreibweise, entsprechend der bei den Überlappungsintegralen in Abschn. 4 eingeführten, wird damit aus (18)

$$\begin{aligned}(n_a l_a m_a|V|n_b l_b m_b) \\ = A_{00} y_0 \sum_{i=0}^{2} \left(\frac{R}{2}\right)^i \hat{b}_{0i} F(n_a l_a m_a, n_b l_b m_b; p, t)\,[n_a l_a m_a, (n_b+i) l_b m_b; p+a_0, pt-a_0] \qquad (20) \\ + A_{40} y_4 \sum_{i=0}^{2} \left(\frac{R}{2}\right)^i \hat{b}_{4i} F(n_a l_a m_a, n_b l_b m_b; p, t)\,[n_a l_a m_a, V_4, (n_b+i) l_b m_b; p+a_4, pt-a_4] \\ + \cdots .\end{aligned}$$

Zichen wir aus $A_{\lambda 0} y_\lambda$ einen Faktor $-q/R$ heraus, so erhalten wir konstante, symmetrietypische Vorfaktoren $s_\lambda = -\frac{R}{q} A_{\lambda 0} y_\lambda$. Für das Oktaeder wird mit (6) und (11)

$$s_0 = 6, \qquad s_4 = \tfrac{7}{256}. \qquad (21)$$

Damit nimmt (20) folgende endgültige Form an:

$$\begin{aligned}(n_a l_a m_a|V|n_b l_b m_b) = -\frac{q}{R} F(n_a l_a m_a, n_b l_b m_b; p, t) \\ \times \Bigg\{ s_0 \sum_{i=0}^{2} b_{0i}[n_a l_a m_a, (n_b+i) l_b m_b : p+a_0, pt-a_0] \qquad (22) \\ + s_4 \sum_{i=0}^{2} b_{4i}[n_a l_a m_a, V_4, (n_b+i) l_b m_b; p+a_4, pt-a_4] \\ + \cdots \Bigg\}.\end{aligned}$$

Der Faktor $F(n_a l_a m_a, n_b l_b m_b; p, t)$ hat die gleiche Gestalt wie bei den Überlappungsintegralen. $[n_a l_a m_a, (n_b+i) l_b m_b; p+a_0, pt-a_0]$ hat ebenfalls die gleiche Gestalt wie bei den Überlappungsintegralen, lediglich die Exponentialfunktionen ändern sich gemäß (19), d. h. die Hilfsintegrale (9) sind zu bilden als $A_k(p+a_0)$ und $B_k(pt-a_0)$. $[n_a l_a m_a, V_4, (n_b+i) l_b m_b; p+a_4, pt-a_4]$ hat, als Integral über λ und μ ausgedrückt, eine Form wie in den Formeln (10), nur werden alle Integranden mit (12) multipliziert; die Hilfsintegrale sind zu bilden als $A_k(p+a_4)$ und $B_k(pt-a_4)$.

Man sieht in (19) und (20), daß die R-abhängigen Koeffizienten $\hat{a}_0$, $\hat{b}_{0i}$, $\hat{a}_4$ und $\hat{b}_{4i}$ beim Übergang zu elliptischen Koordinaten gerade so mit Potenzen von $R/2$ multipliziert werden, daß die R-unabhängigen Koeffizienten (14) und (16) entstehen. Für die Berechnung der Matrixelemente $(\chi_{k'}|V|\chi_M)$ werden also nicht die im Potentialansatz (13) befindlichen R-abhängigen Koeffizienten verwendet, sondern die R-unabhängigen Koeffizienten (14) und (16) mit den für alle Fälle konstanten Werten (15) und (17).

Mit (22) als Näherungsausdruck für (3) können also die Dreizentren-Kernanziehungsintegrale (1) in den Nichtdiagonalelementen auf Zweizentrenintegrale zurückgeführt werden, die nicht schwieriger handhabbar sind als Überlappungsintegrale.

8. Genauigkeit des Näherungsverfahrens

Da uns kein Rechenprogramm für Dreizentrenintegrale zur Verfügung stand, überprüften wir die Genauigkeit der Näherung (22) an den von Fenske, Caulton, Radtke und Sweeney [4] durchgeführten Berechnungen der Dreizentren-Kernanziehungsintegrale beim $[\mathrm{TiF}_6]^{3-}$. In Tabelle 3 von [4] sind die Werte der Integrale $(\chi_{k'} | r_k^{-1} | \chi_M)$ für die bei der Behandlung des $[\mathrm{TiF}_6]^{3-}$ benötigten Funktionen $\chi_{k'}$ und χ_M gegeben. Die Werte für die Dreizentrenintegrale ($k \neq k'$) haben wir addiert zu

$$I_{\text{exakt}} = \sum_{k \neq k'} \left(\chi_{k'} \middle| \frac{1}{r_k} \middle| \chi_M \right). \tag{23}$$

Das entspricht, bis auf $-q_k$, dem Ausdruck (1) in den Nichtdiagonalelementen.

Mit der Näherungsformel (22) für den ersten Term in (2) berechneten wir

$$I_{\text{approx}} = -\frac{1}{q} (\chi_{k'} | V | \chi_M) - \left(\chi_{k'} \middle| \frac{1}{r_{k'}} \middle| \chi_M \right). \tag{24}$$

Um mit I_{exakt} vergleichen zu können, benutzten wir die gleichen Basisfunktionen $\chi_{k'}$ und χ_M wie in [4], Ti^{2+}-Funktionen von Richardson *et al.* [11, 12] und F^--Funktionen von Sugano und Shulman [13]. Die für I_{approx} berechneten Werte werden in der Tabelle 1 mit den exakten verglichen.

Die Übereinstimmung ist - unter Beachtung der für I_{approx} gemachten Annahmen und Vernachlässigungen, besonders bezüglich der Gewichte in Abschn. 6 überraschend gut.

Es gibt zwei Möglichkeiten zur Verbesserung des Verfahrens. Einmal kann man die Potentialterme durch höhere als quadratische Polynome annähern. Jeder optimale Koeffizientensatz $b_{00}, \ldots, b_{0n_0}$ bzw. $b_{40}, \ldots, b_{4n_4}$ erfordert die (einmalige) Lösung eines Extremalproblems in der in Abschn. 6 angegebenen Weise. Eine zweite Möglichkeit zur Steigerung der Genauigkeit besteht in der Berücksichtigung höherer Glieder der Potentialentwicklung (7). Dazu müssen (wiederum einmalig) Koeffizientensätze $b_{6i}, b_{8i}, \ldots$ berechnet werden. Die Formel (22) wird entsprechend erweitert; d. h. die Anzahl der entstehenden Zweizentrenintegrale steigt. Gegenwärtig untersuchen wir systematisch den Einfluß dieser beiden Wege.

Tabelle 1. Vergleich der näherungsweise berechneten Integrale mit den exakten Werten von Fenske *et al.* [4]

	I_{exakt}	I_{approx}	Δ	Δ (%)
$(2s \vert V \vert 4s)$	6,083	5,871	−0,212	−3,5
$(2s \vert V \vert 4p\sigma)$	9,632	9,239	−0,393	−4,1
$(2s \vert V \vert 3d\sigma)$	3,989	3,809	−0,180	−4,5
$(2p\sigma \vert V \vert 4s)$	4,769	4,805	+0,036	+0,8
$(2p\sigma \vert V \vert 4p\sigma)$	5,395	5,427	+0,032	+0,6
$(2p\sigma \vert V \vert 3d\sigma)$	3,703	3,708	+0,005	+0,1
$(2p\pi \vert V \vert 4p\pi)$	5,465	5,435	−0,030	−0,5
$(2p\pi \vert V \vert 3d\pi)$	3,120	3,129	+0,009	+0,3

9. Anwendungsmöglichkeiten

Die Näherungsformel (22) mit den Koeffizienten (15) und (17) wurde zunächst nur für sechs oktaedrisch angeordnete Punktladungen $-q$ abgeleitet. Sie gilt aber unverändert auch für vier tetraedrisch angeordnete Punktladungen, da sich die Form der Potentialentwicklung (7) nicht ändert. Mit

$$A_{00}(\text{Tetr.}) = -8\sqrt{\pi}\, q/R, \qquad A_{40}(\text{Tetr.}) = 28\sqrt{\pi}\, q/27 R^5 \tag{25}$$

erhält man lediglich andere symmetrietypische Koeffizienten

$$s_0 = 4, \qquad s_4 = -\tfrac{7}{576}. \tag{26}$$

Für vier Punktladungen an den Ecken eines Quadrates (D_{4h}-Symmetrie) ist in der Potentialentwicklung (4) auch $A_{20} \neq 0$. Das erfordert die Bestimmung eines optimalen Koeffizientensatzes $b_{20}, b_{21}, \ldots$; die Näherungsformel (22) ist um ein Glied

$$s_2 \sum_{i=0}^{n_2} b_{2i}[n_a l_a m_a, V_2, (n_b + i) l_b m_b; p + a_2, pt - a_2]$$

zu erweitern.

Das angegebene Näherungsverfahren für die Dreizentren-Kernanziehungsintegrale eignet sich naturgemäß – Entwicklung des Ligandenfeldpotentials nach Kugelflächenfunktionen – nur für hochsymmetrische Anordnungen der Liganden. Insbesondere sollen alle Liganden gleich und (wenigstens näherungsweise) als Punktladungen auffaßbar sein. Wir hoffen aber, daß das Verfahren auch bei solchen Koordinationsverbindungen Dienste leisten kann, bei denen wenigstens die Ligatoren die obigen Bedingungen erfüllen, außerhalb aber noch Chelatringe oder andere symmetrieerniedrigende Gruppen vorhanden sind.

Für den praktischen Gebrauch der Methode hat man ein Computer-Programm zur Berechnung von Überlappungsintegralen gemäß den Erläuterungen zu Formel (22) zu modifizieren. Wir hoffen, daß das Verfahren wegen seiner Unkompliziertheit der breiteren Anwendung exakterer Methoden dienen kann.

Dank. Wir danken Herrn Professor Dr. G. Weber (Jena) für die kritische Durchsicht des Manuskripts.

Literatur

1. Wolfsberg, M., Helmholz, L.: J. chem. Physics **20**, 837 (1952).
2. Canadine, R. M., Hillier, I. H.: J. chem. Physics **50**, 2984 (1969).
3. Mulliken, R. S.: J. Chim. physique **46**, 497, 675 (1949).
4. Fenske, R. F., Caulton, K. G., Radtke, D. D., Sweeney, C. C.: Inorg. Chem. **5**, 951 (1966).
5. Radtke, D. D., Fenske, R. F.: J. Amer. chem. Soc. **89**, 2292 (1967).
6. Reinhold, J., Hoyer, E.: Proceedings of the XIIIth International Conference on Coordination Chemistry, Cracow-Zakopane, Poland, Sept. 14–22, 1970, No. 356.
7. Schläfer, H. L., Gliemann, G.: Einführung in die Ligandenfeldtheorie. Frankfurt am Main: Akademische Verlagsgesellschaft 1967.

8. *Mulliken, R.S., Rieke, C.A., Orloff, D., Orloff, H.: J. chem. Physics* **17**, *1248 (1949).*
9. *Jaffé, H.H.: J. chem. Physics* **21**, *258 (1953).*
10. - Doak, G.O.: J. chem. Physics **21**, 196 (1953).
11. Richardson, J.W., Nieuwpoort, W.C., Powell, R.R., Edgell, W.F.: J. chem. Physics **36**, 1057 (1962).
12. - Powell, R.R., Nieuwpoort, W.C.: J. chem. Physics **38**, 796 (1963).
13. Sugano, S., Shulman, R.G.: Physic Rev. **130**, 517 (1963).

Dr. J. Reinhold
Sektion Chemie
Karl-Marx-Universität
DDR-701 Leipzig, Liebigstraße 18

Theoret. chim. Acta (Berl.) 25, 331—337 (1972)
© by Springer-Verlag 1972

Low Temperature Absorption Spectra of TcO_4^- and ReO_4^- in $KClO_4$

H. U. GÜDEL* and C. J. BALLHAUSEN

Chemical Laboratory IV, H.C. Ørsted Institute, University of Copenhagen, Denmark

Received December 22, 1971

The low temperature spectra of TcO_4^- and ReO_4^- both show two band systems with pronounced vibrational structures. The bands are identified as ${}^1A_1 \to {}^1T_2$ transitions. No other bands are observed with certainty. It seems likely that the $KClO_4$ crystals contain $KReO_4$ crystallites. They are therefore not pure mixed crystals. It is concluded that the virtual orbital ($2e$) used in the construction of the low lying states resembles an atomic nd orbital more and more when going from $n = 3$, Mn to $n = 5$, Re.

Die Tieftemperaturspektren von TcO_4 und ReO_4 zeigen beide zwei Bandensysteme mit ausgeprägten Schwingungsstrukturen. Die Banden werden als ${}^1A_1 \to {}^1T_2$-Übergänge identifiziert. Keine anderen Banden werden mit Sicherheit beobachtet. Es scheint wahrscheinlich, daß die $KClO_4$-Kristalle $KReO_4$-Kristallite enthalten und deswegen keine reinen Mischkristalle sind. Es wird geschlossen, daß das virtuelle Orbital ($2e$), welches zur Konstruktion der tiefliegenden Zustände gebraucht wird, in der Reihe $n = 3$, Mn bis $n = 5$, Re immer weitgehender einem nd-Atomorbital ähnelt.

Introduction

In view of the continued interest in the electronic absorption spectra of tetrahedrally coordinated d^0 transition metal ions it seemed natural to study the low temperature spectra of TcO_4^- and ReO_4^-. The solution spectra of these ions have recently been reported [1], but it was anticipated that more detail would emerge by recording the spectra of single crystals at low temperatures. As a result, we can now offer a somewhat better analysis of the vibrational band structures than was previously possible. Some conjectures regarding the non-appearance in these ions of the so-called "Teltow band" have also been made.

Experimental

$KClO_4$ crystals containing 0.5, 1.5, and 3 mol-% respectively of TcO_4^- were prepared by the following procedure: a 0.1 M solution of ammonia in water was saturated with $KClO_4$(BDH) at 60° C, and an appropriate amount of a 0.26 M solution of $NH_4Tc^{99}O_4$ (Amersham Radiochemical Centre, England) in 0.1 M ammonia was added. The container was then tightly closed and placed in a thermostat the temperature of which was set to decrease at 2° C per day for 25 days. Plate-shaped crystals were individually picked out of the solution and used for the measurements.

---

* Nachwuchsstipendiat, Schweizerischer Nationalfonds.

For the $KClO_4$ crystals doped with ReO_4^- the same procedure was employed. Aqueous solutions of $KReO_4$ (purity $\geq 99.9\%$, Koch Light Laboratories Ltd.) and $KClO_4$ with perrhenate contents ranging from 0.5–4.0 mol-% were used.

Absorption spectra were measured at temperatures between 2.5° K and 77° K using both a Cary 14 spectrometer (dispersion 32 – 12 Å/mm) and a Zeiss 2 m grating spectrograph (dispersion 8 Å/mm). The Zeiss spectra were recorded on Kodak 103-F and SWR films. For the spectra measured between 2.5 and 4.2° K an immersion dewar with a device to pump on the liquid helium was employed. The spectra between 4.2 and 77° K were obtained using a helium gas-flow dewar. The cryostat described by Morris *et al.* [2] was modified for spectroscopic use.

For the experiments with polarized radiation the crystals were oriented using X-ray diffraction photographs taken with a Buerger precession camera. The incident light beam was always parallel to the *a* axis of the $KClO_4$ host crystal, with the electric vector either parallel to *b* or to *c* using the setting of the crystallographic axes given by Donnay [3]. Glan-Thompson prisms were used to polarize the light.

General Features of the Absorption Spectra

As has already been observed in the solution spectra [1] of TcO_4^- and ReO_4^- the main feature of the absorption spectra in the UV region are two strong, overlapping band systems. We shall call the lower and higher energy systems band system I and II respectively. In the crystal spectra of both compounds both band systems exhibit vibrational structure. Due to the overlap, only an estimate of the origin of system II can be made. On the high energy side of system II in

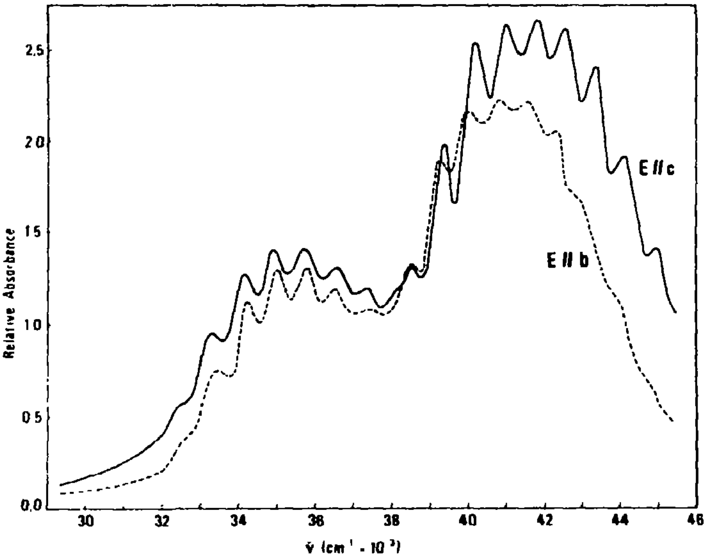

Fig. 1. UV absorption spectrum of TcO_4^- in a $KClO_4$ host lattice at liquid helium temperature

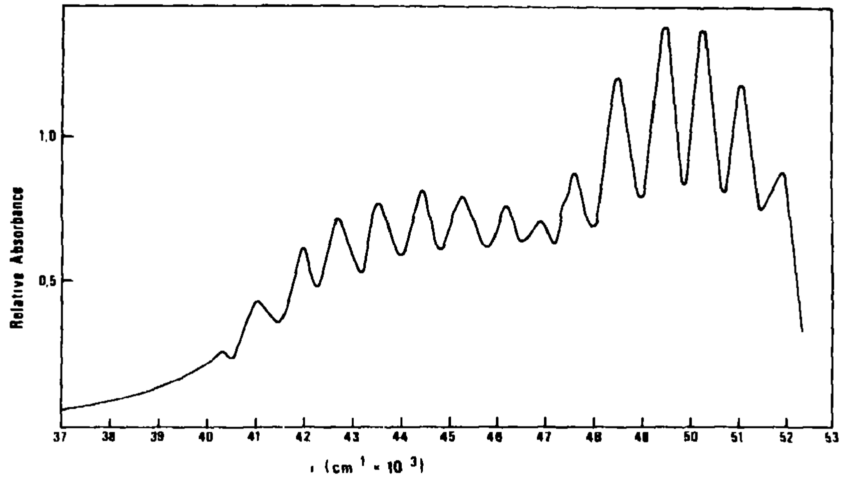

Fig. 2. UV absorption spectrum of ReO_4^- in a $KClO_4$ host lattice at liquid helium temperature

TcO_4^- the absorbance increases slightly without, however, reaching a maximum in the wavelength region covered in this study. On the low energy side of system I both TcO_4^- (Fig. 1) and ReO_4^- (Fig. 2) show very weak, broad and structureless absorption.

The region on the low energy side of band systems I has been examined very carefully (2 m Zeiss, resolution ~ 1 Å/mm; temperature 2.5° K; "concentration" of the crystals up to 4 mol-%, in both compounds). No sharp absorption lines comparable to those observed in permanganate crystal spectra [4–6] could be found between 32000 cm^{-1} and 25000 cm^{-1} in TcO_4^- and between 40000 cm^{-1} and 30000 cm^{-1} in ReO_4^-. There seems to be, however, structureless broad absorption, best seen in Cary spectra, in the ascent to the first component of the band systems I.

Analysis of the TcO_4 Spectra

Band System I

Progressions in 795 cm^{-1} and 806 cm^{-1} are observed $\parallel$ and $\perp$ (with the electric vector parallel and perpendicular) respectively to the symmetry plane of the site group C_s. The vibrations responsible for these progressions are undoubtedly totally symmetric vibrations ν_1 of the pertechnetate ion in the excited states. ν_1 for a regular tetrahedral TcO_4^- ion in the ground state [7] is 912 cm^{-1}. It is thus diminished by 11.6–12.8% in the excited state, compared to 9.1% in the corresponding state of MnO_4^-.

The values given in Table 1 for the origins, 32677 cm^{-1} $\parallel$ and 32576 cm^{-1} $\perp$, are not very accurate because they occur only as shoulders. Based on the most intense "components" 3, 4, and 5, a splitting $E\parallel - E\perp$ of about 70 cm^{-1} between the absorption maxima of the spectra in the two polarization directions can be measured. The corresponding value for MnO_4^- in the same host lattice is [4] some 20 cm^{-1}.

Table 1. Vibrational structure in the absorption spectrum of TcO_4 dissolved in $KClO_4$

‖ b ("Crystal Data" setting) (E ‖ to the symmetry plane of the site group C_s) Positions of Maxima (cm^{-1})	Δ	‖ c ("Crystal Data" setting) (E ⊥ to the symmetry plane of the site group C_s) Positions of Maxima (cm^{-1})	Δ
Band system I			
32677 sh	0	32576 sh	0
33435	(758)	33372	(796)
34237	802	34159	787
35020	783	34944	785
35804	784	35751	807
36561	757	36593	842
37408	847	37402	809
		38334 sh	(932)
Average	795	Average	806
Band system II			
38544 sh	0	38619	0
39254	(710)	39432	813
40023	769	40234	802
40823	800	41062	828
41599	776	41846	784
42364	765	42614	768
43135	771	43400	786
43885	750	44150	750
		44951	801
		45756 sh	(805)
		46624 sh	(868)
Average	772	Average	791

Band System II

Progressions in 772 cm^{-1} and 791 cm^{-1} are observed ‖ and ⊥ respectively. These values indicate a decrease of ν_1 by 15.3% (‖) and 13.3% (⊥) respectively compared to the ground state of pertechnetate. The components in the ‖ spectrum are somewhat broader than the corresponding bands in the ⊥ spectrum. This probably indicates that each ‖ component is composed of at least two unresolved peaks. With a site group of C_s for the TcO_4 ions in the $KClO_4$ crystal two origins are expected in the spectrum measured with the electric vector perpendicular to the z axis. The progression frequencies are 15-23 cm^{-1} smaller than in the first band system, compared to 18 cm^{-1} and 20 cm^{-1} in the spectra of permanganate and perrhenate respectively. The differences of the positions of the absorption maxima in the two polarization directions, $E\|-E\perp$, indicate a large site group splitting. For the most intense components the average splitting is -253 cm^{-1}, much larger and of opposite sign to that in the first band system. Splittings of this order of magnitude have not been observed in diluted $KMnO_4/KClO_4$ crystals, but have been recorded in diluted $LiMnO_4 \cdot 3H_2O/LiClO_4 \cdot 3H_2O$ and in $Ba(MnO_4)_2 \cdot 3H_2O/Ba(ClO_4)_2 \cdot 3H_2O$ crystals [8, 9].

Table 2. Vibrational structure in the absorption spectrum of $KReO_4/KClO_4$ crystals

Positions of Maxima (cm^{-1})	Δ
Band system I	
40066	0
40933	867
41795	862
42630	835
43461	831
44315	854
45155	840
46018 sh	(863)
Average	848
Band system II	
45934 sh	0
46775	(841)
47393 sh	(618)
47582	807 (189)
48237 sh	(655)
48418	836 (181)
49227	809
50052	825
50878	826
51685	807
Average	818

The different behaviour of MnO_4^- and TcO_4 ions in a $KClO_4$ host lattice is understandable when the M-O distances are compared: Cl–O = 1.46 Å, Mn-O = 1.63 Å, Tc-O = 1.73 Å. The latter value has not been experimentally determined but can be reasonably estimated [10]. While $KClO_4$ and $KMnO_4$ are isomorphous and orthorhombic, $KTcO_4$ (as well as $KReO_4$) crystallizes with a tetragonal scheelite structure [11].

Therefore, the environmental forces acting on a pertechnetate ion "dissolved" in a potassium perchlorate lattice are certainly greater than in diluted $KMnO_4/KClO_4$ crystals and can well be responsible for the observed large site splitting.

Analysis of the ReO_4^- Spectrum

Band System I

A regular progression in 848 cm^{-1} is built upon the origin at 40066 cm^{-1}. Since the totally symmetric vibration of regularly tetrahedral ReO_4^- in the ground state [7] is 971 cm^{-1} the decrease in frequency in going to the excited state is thus 12.7%. Attempts were made to record spectra with polarized radiation. However, due to experimental limitations this was only possible for the first five "components". The positions of the absorption maxima were the same with both polarizations. This might mean that the site group splitting is too small to be detected. However, remembering that the splitting was larger in pertechnetate than in permanganate and noting that the Re–O distance [10] is 1.76 Å it seems more probable that we are not dealing with mixed crystals but with $KClO_4$ crystals containing $KReO_4$ crystallites. In other words, what has effectively been measured is a powder spectrum of potassium perrhenate in a matrix of potassium perchlorate.

Band System II

The overlap with band system I is very great and the assignment of the components in the overlap region is difficult. The third and fourth components attributed to band system II each have a shoulder on the low energy side that is certainly genuine and which probably has nothing to do with the overlapping band system I. The average spacing between the absorption maxima is 818 cm^{-1}, 30 cm^{-1} smaller than in the first band system and 15.8% smaller than ν_1 in the ground state of perrhenate.

There are possibly more components of this band system beyond our experimental limit of 52000 cm^{-1}.

Comparison of the Band Systems I of MnO_4^-, TcO_4^-, ReO_4^-

In the first strong band system of the permanganate crystal spectra a great deal of fine structure can be resolved. However, the spectra of TcO_4^- and ReO_4^- in $KClO_4$ exhibit only one progression in each case. The half widths of the "components" of these progressions are ~600 cm^{-1} for both compounds, compared to 200–300 cm^{-1} in the permanganate under similar experimental conditions.

A second striking observation is the relative intensities of the "components" of each progression. We observe a shift of maximum intensity towards higher components in the sequence MnO_4^-, TcO_4^-, ReO_4^-.

Discussion

The calculations of Dahl and Johansen [12] indicate that in permanganate the two low-lying absorption bands with pronounced vibrational structure are to be assigned [8, 9] as ${}^1A_1 \rightarrow {}^1T_2(t_1 \rightarrow 2e)$ and ${}^1A_1 \rightarrow {}^1T_2(3t_2 \rightarrow 2e)$. The two ${}^1T_2$ states are of course mixed, and also contain admixtures of higher lying ${}^1T_2$ states. In T_d symmetry electric dipole transitions are allowed only to the ${}^1T_2$ states. Both of the electronic excitations $(t_1 \rightarrow 2e)$ and $(3t_2 \rightarrow 2e)$ will also produce ${}^1T_1$ states. These are placed on the red side of the ${}^1T_2$ states [5, 6], and the first ${}^1T_1$ is responsible for the "Teltow band" found in the MnO_4^- and $CrO_4^=$ ions.

Calculations by Ziegler [13] show the $3t_2$ orbital to be a nearly-pure ligand orbital in MnO_4^-, TcO_4^-, and ReO_4^-; by symmetry the t_1 orbital is a pure ligand orbital. On the other hand the $2e$ orbital is given by a mixture $\psi(2e) = \alpha(d_e) + \beta(\Sigma$ ligand orbitals). In the INDO approximation scheme the separation $E({}^1T_2) - E({}^1T_1)$ will therefore be proportional to β^2, and the same will be the case for the interaction term between the two ${}^1T_2$ states and the two ${}^1T_1$ states. To a first approximation we can therefore assume that the smaller the value of β, the closer can the states approach each other and the smaller will the energy separation be between the "Teltow band" and the first structured allowed

$^1A_1 \rightarrow {}^1T_2$ transition. Indeed, for $\beta = 0$, the $^1A_1 \rightarrow {}^1T_1$ transition is calculated to lie on the blue side of the $^1A_1 \rightarrow {}^1T_2$ transition [5].

The mixing parameter β is expected to decrease through the series MnO_4^-, TcO_4^-, and ReO_4^-, since the energy separations between the oxygen ligand orbitals and the metal nd-orbitals, $n = 3$, 4, and 5, become larger. Consequently in ReO_4^-, $\psi(2e)$ is expected to be nearly pure $5d_e$, and both the allowed transitions $^1A_1 \rightarrow {}^1T_2(1)$ and $^1A_1 \rightarrow {}^1T_2(2)$ should be found close together possessing identical band shapes. This is indeed what is observed experimentally. The absence of a "Teltow band" is also explained, since we should expect it to be hidden under the first strong $^1A_1 \rightarrow {}^1T_2$ transition.

The spectrum of TcO_4^- is intermediate between the spectrum of MnO_4^- and ReO_4^-. Again the appearance of the "Teltow band" is probably obscured by the first strong transition. Furthermore, from an overall examination of the absorption spectrum it seems as if the characteristics of the first permanganate band are mirrored in the second pertechnetate band and those of the second permangante band in the first pertechnetate band. Evidently the potential surface of the $^1T_2(1)$ state found in MnO_4^- is closer to the second $^1T_2$ potential surface of TcO_4^- than it is to the first.

In both TcO_4^- and ReO_4^- the spectral measurements reveal a tail stretching towards the red at the bottom of the first $^1A_1 \rightarrow {}^1T_2$ band. We take this to indicate the presence of some spin forbidden, $S = 0 \rightarrow 1$, transitions. Such transitions are expected [14] on the red side of $^1A_1 \rightarrow {}^1T_2(1)$, and the high value of the spin-orbit coupling constant in ReO_4^- should certainly make them more pronounced here than in, say, MnO_4^-. Since, however, we can observe no spectral details, we offer no further comment on this aspect.

Acknowledgements. We wish to thank Dr. S. Christensen for his assistance in the preparation of the pertechnetate crystals and Dr. T. Ziegler for helpful discussions. The financial support of the Swiss National Research Foundation in the form of a Nachwuchsstipendium (H.U.G) is gratefully acknowledged.

References

1. Mullen, P., Schwochau, K., Jørgensen, C. K.: Chem. Physics Letters **3**, 49 (1969).
2. Morris, I. C., Read, D. A., Temple, B. K.: Scient. Instruments **3**, 343 (1970).
3. Donnay, I. D. H. (Ed.): Crystal data, American Crystallographic Assoc. Monograph **5** (1963).
4. Teltow, J.: Z. physik. Chem. B **40**, 397 (1938); — Z. physik. Chem. B **43**, 198 (1939).
5. Ballhausen, C. J., Dahl, J. P., Trabjerg, I.: Coll. Int. Cen. Nat de la Recherche Sci. **191**, 69 (1970).
6. Day, P., DiSipio, L., Oleari, L.: Chem. Physics Letters **5**, 533 (1970).
7. Müller, A., Krebs, B.: Z. Naturforsch. B **20**, 1127 (1965).
8. Johnson, L. W., McGlynn, S. P.: J. chem. Physics **55**, 2985 (1971).
9. – – Chem. Physics Letters **10**, 595 (1971).
10. Kalman, A.: J. chem. Soc. (A) **1971**, 1858.
11. McDonald, B. J., Tyson, G. J.: Acta crystallogr. **15**, 87 (1962).
12. Dahl, J. P., Johansen, H.: Theoret. chim. Acta (Berl.) **11**, 8 (1968).
13. Ziegler, T.: Thesis, Copenhagen 1971.
14. Ballhausen, C. J.: Theoret. chim. Acta (Berl.) **1**, 285 (1963).

Prof. Dr. C. J. Ballhausen
Louisiana State University
College of Chemistry
Baton Rouge, Louisiana 70803, USA

Theoret. chim. Acta (Berl.) 25, 338–345 (1972)
© by Springer-Verlag 1972

Das Kastenmodell als Grundlage für ein *ab initio*-Verfahren

III. Ergebnisse für das Wasserstoff- und Heliumatom

ERNST-ALBRECHT REINSCH
Institut für theoretische Chemie der Johann Wolfgang Goethe-Universität in Frankfurt am Main

Eingegangen am 3. Dezember 1971

The Box Model as a Basis for an ab initio Procedure

III. Results for the Hydrogen and the Helium Atom

The results of the procedure developped in [1] are given in the case of the hydrogen and the helium atom. On the basis of these results conclusions can be drawn on the applicability of the whole method.

Es werden die Resultate des in [1] entwickelten Verfahrens für den Fall des Wasserstoff- und des Heliumatoms mitgeteilt und diskutiert. Mit diesen Daten lassen sich Rückschlüsse auf die Anwendbarkeit des Verfahrens allgemein ziehen.

1 Einleitung

In den beiden vorangegangenen Arbeiten [1, 2] wurde ein Verfahren zur Berechnung der Gesamtenergie von Molekülen mittels einer Störungsrechnung aufgezeigt. Es stellt sich nun die Frage, ob die Qualität der Ergebnisse dazu anregt, den eingeschlagenen Weg weiter zu verfolgen. Deshalb sollen an dieser Stelle die Resultate von Testrechnungen mitgeteilt werden.

Da bei dieser Methode die Zahl der Elektronen nicht vom Ansatz für die Wellenfunktion her eingeht, hat man zwar den Vorteil, daß der damit verbundene numerische Aufwand mit zunehmender Zahl der Elektronen nicht wie n^4 ansteigt. Umgekehrt stellt aber selbst ein so einfaches Gebilde wie ein ungebundenes Wasserstoffatom keinen trivialen Fall dar und kann deshalb als ein echter Test gelten. Mit ihm soll begonnen werden.

2. Einatomige Moleküle

Allgemeines

Die Durchführung der Rechnung erfolgt für alle „ungebundenen“ Atome auf die gleiche Weise. Sie kann deshalb zunächst in allgemeiner Form skizziert werden. Als erstes ist die Art, in der die Atome zum Gitter angeordnet werden, festzulegen. Da sie möglichst gleichförmig im Raum verteilt werden sollen, wurde die Form der hexagonal dichtesten Kugelpackung gewählt. Der Abstand zweier benachbarter Atome wird mit $2A$ bezeichnet; er ist der einzige Parameter für die Anordnung. Bei vollständig durchgeführter Störungsrechnung – Konvergenz vorausgesetzt – würde die Energie pro Atom für große A gegen die (gesuchte) Energie des isolierten Atoms gehen. Das ist bei Abbruch der Störreihe nicht der Fall. Die Frage bleibt aber, ob sich die Näherung soweit an den wahren Verlauf anschmiegt, daß ein Bereich von A existiert, in dem die Energie leidlich konstant gegenüber Änderungen von A ist.

Ist Z die Kernladung des behandelten Atoms, so ist die Zahl der Elektronen m je Elementarzelle ebenfalls Z und das Volumen der Zelle $a = 4\sqrt{2}\,A^3$. Unter diesen Umständen gilt [vgl. Gl. (II.11)] für die Energie pro Atom in erster Näherung

$$E^{(0)} + E^{(1)} = \frac{3\varkappa^2}{10}\,\frac{Z^{5/2}}{A^2} - \alpha\,\frac{Z^2}{A} - \frac{3\varkappa}{4\pi}\,\frac{Z^{4/3}}{A} \tag{1}$$

wobei

$$\varkappa = \sqrt[3]{\frac{3\pi^2}{4\sqrt{2}}}$$

und

$$k_F = \varkappa\,\frac{Z^{1/3}}{A}\,.$$

α ist eine Art Madelungsche Konstante:

$$\alpha = -\frac{1}{2}\left[\sum_{\substack{j'\\(\neq 0)}} \frac{1}{|\varrho_{j'}|} - \frac{1}{4\sqrt{2}}\int \frac{dv'}{|\varrho'|}\right]$$

mit $\varrho' = A r'$, $\varrho_{j'} = A r_{j'}$ ($\Sigma(j')$ geht über alle Gitterplätze). Die numerische Auswertung ergibt

$$\alpha = 0{,}8065\,.$$

Bildung der n-Summen

Für die höheren Ordnungen von E sind Summen über die Gittervektoren des reziproken Gitters [vgl. die Gl. (II.12 u. 13)] zu bilden. Da dies numerisch zu geschehen hat, ist es unvermeidbar, an geeigneter Stelle abzubrechen. Der Fehler, der dadurch entsteht, soll am Beispiel des V_K^2-Terms im Fall von $Z = 2$ diskutiert werden.

Das reziproke Gitter ist ebenfalls das Gitter einer hexagonal dichtesten Kugelpackung, und es ist am bequemsten, die Summation jeweils über Schichten von Gitterpunkten, die die Oberfläche einer ständig wachsenden hexagonalen Bipyramide bilden, vorzunehmen. Diese Schichten werden mit n nummeriert und $n = 0$ sei der Gitterpunkt im Ursprung. In Fig. 1 ist der Logarithmus des Beitrages der n-ten Schicht (bis auf eine Konstante) gegen $\log n$ aufgetragen. Die Ausgleichsgerade zeigt – wie erwartet – die Steigung -4 [vgl. II. Abschn. 5]. Man kann aus ihr den Faktor für die $1/n^4$-Terme entnehmen; in unserem Beispiel ergibt sich 3,058.

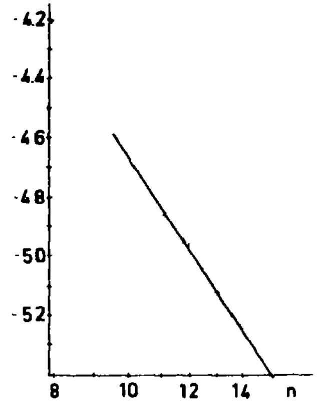

Fig. 1. Logarithmus des Beitrages der n-ten Schicht gegen log n beim Graph V_g^2 für Helium

In Tabelle 1 ist die Summe der Beiträge für $n_{\max} = 8$, 10, 12 und 14 zusammengestellt. Man kann den Fehler infolge Abschneidens bei $n = 14$ recht genau ermitteln, wenn man

$$\sum_{15}^{\infty} \frac{3.058}{n^4}$$

berechnet. Mit der Riemannschen ζ-Funktion ergibt sich

$$3{,}058\left(\zeta(4) - \sum_{1}^{14} \frac{1}{n^4}\right) = 0{,}00034,$$

und man kann damit den Beitrag auf $n_{\max} \to \infty$ extrapolieren. Die Tabelle 1 zeigt weiter, daß der Fehler auch für $n_{\max} = 8$ schon sehr viel kleiner als die erforderliche Genauigkeit, deren Größenordnung 0,01 a.E. beträgt, ist.

Um den Fehler auch ohne das Legen einer Ausgleichsgeraden gering zu halten, kann man nach dem von Bulirsch u. Stoer [3] angegebenen Verfahren mit einer rationalen Funktion extrapolieren. Derartig extrapolierte Ergebnisse sind in der letzten Spalte der Tabelle angegeben. Man sieht, daß sich dann schon bei $n_{\max} = 8$ recht gute Extrapolationswerte ergeben und daß die n-Summe hier spätestens nach $n_{\max} = 10$ abgebrochen werden kann.

Tabelle 1. Fehler durch Abbrechen der n-Summen (V_g^2 im Fall Helium)

$n_{\max}$	Summe der Beiträge	Fehler	extrapol. nach B.S. [3]
8	−0,44570	−0,00164	−0,44739
10	−0,44646	−0,00088	−0,44731
12	−0,44681	−0,00053	−0,44731
14	−0,44700	−0,00034*	−0,44731
∞	−0,44734		—

* Berechnet auf die im Text angegebene Weise.

Für den Beitrag der Graphen $V_K^2 V_E^1$ liegen die Verhältnisse noch günstiger, da die Beiträge der Schichten hier proportional $1/n^6$ sind – also die Summe noch schneller konvergiert. Die Extrapolation erwies sich in diesem Fall als überflüssig. Die n_1, n_2-Summen, die in dem Ausdruck für den Graphen V_K^3 auftreten, machen aber den Abbruch bei $n_{\max} = 8$ notwendig, weil die Zahl der Paare von Gittervektoren insgesamt wie n^6 ansteigt. In diesem Fall mußte auf die Extrapolation zurückgegriffen werden.

Berechnung von V_E^2 und V_E^3

Bezüglich der Integrale $\mathscr{I}_1$ bis $\mathscr{I}_6$ sei auf das in Teil II [2] Gesagte verwiesen. Offen bleiben lediglich noch die Terme V_E^2 und V_E^3. Gell-Mann u. Brueckner [4] haben den k_F-unabhängigen und den $\ln k_F$-Term für Elektronengase berechnet. Sie geben für die Energie pro Elektron den Ausdruck

$$0{,}0622 \ln r_s - 0{,}096 \quad [\text{Rydberg}]$$

an, wobei

$$r_s = \sqrt[3]{\frac{9}{4}\pi}\,\frac{1}{k_F}\,.$$

Die Umrechnung auf Energie pro Elementarzelle [in a.E.] und die Einführung von k_F führt zu

$$V_E^2 = m \cdot (-0{,}0311 \ln k_F - 0{,}028)\,, \tag{3}$$

wobei m die Zahl der Elektronen pro Elementarzelle, hier also Z ist.

Die nächsthöheren Terme findet man – unvollständig – bei Carr u. Mardudin [5]. Sie lauten

$$0{,}018\, r_s \ln r_s - 0{,}036\, r_s\,,$$

wobei das noch auftretende, unbekannte E'_3 wie in der zweiten Hälfte von [5] selbst gleich Null gesetzt wurde. Eine zu V_E^2 analoge Umrechnung führt dann zu

$$V_E^3 = \frac{m}{k_F} \cdot (-0{,}017 \ln k_F - 0{,}023)\,. \tag{4}$$

3. Ergebnisse für das Wasserstoffatom

Führt man die Rechnung für $Z = 1$ aus, so ergeben sich folgende Terme (in a.E.)

$$\left.\begin{aligned}
E^{(0)} + E^{(1)} &= \frac{0{,}9043}{A^2} - \frac{1{,}2210}{A}\\
V_K^2 &= -0{,}0458\\
V_E^2 &= 0{,}0311 \ln A - 0{,}045\\
V_K^3 &= -0{,}0112\, A\\
V_K^2 V_E^1 &= -0{,}0006\, A\\
V_E^3 &= 0{,}0098\, A \ln A - 0{,}0184\, A\,.
\end{aligned}\right\} \tag{5}$$

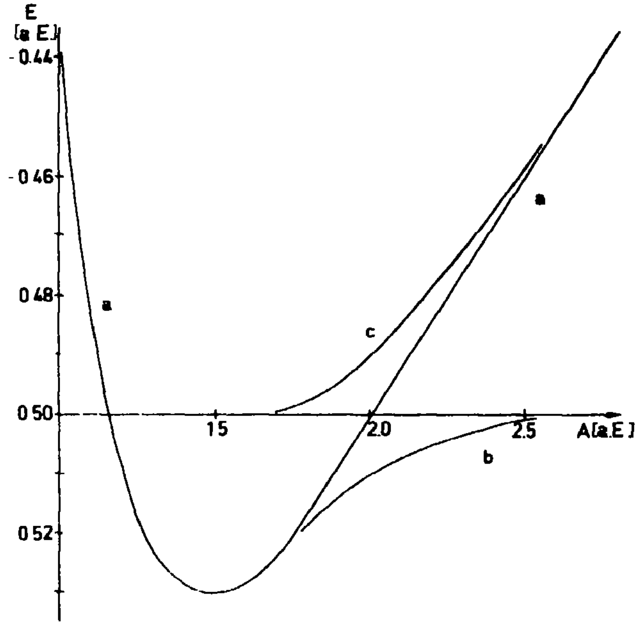

Fig. 2 a Berechnete Gesamtenergie für das Wasserstoffatom in Abhängigkeit des Gitterparameters A. b Angenommene obere Schranke für den Energieverlauf einschließlich Gitterenergie. c Untere Schranke für den Fehler infolge Abbruchs der Störreihe durch Differenzbildung

Für $A = 1{,}5$ a.E. beispielsweise lauten die Werte

$$\begin{aligned} E^{(0)} + E^{(1)} &= -0{,}4121 \\ E^{(2)} &= -0{,}0783 \\ E^{(3)} &= -0{,}0404\,. \end{aligned}$$

Durch die Gln. (5) ist die Energie pro Atom in Abhängigkeit von A gegeben. Fig. 2 (Kurve a) zeigt ihren Verlauf, der den Erwartungen entspricht: Der linke Kurvenast ist durch die ansteigende Gitterenergie, der rechte durch den Fehler infolge der rasch abnehmenden Konvergenz der Störungsrechnung bestimmt.

Zunächst kann man feststellen, daß die Gesamtenergie für Werte von A zwischen 1,1 und 2,2 a.E. in der richtigen Größenordnung liegt. Der Fehler beträgt in diesem Bereich maximal etwa ± 6%. Außerhalb dieses Bereiches haben die Resultate für das Wasserstoffproblem keinen Sinn mehr, weil sie entweder durch die Existenz der Gitterwechselwirkungen oder durch die Unzulänglichkeit des Verfahrens vollständig bestimmt sind.

Leider ist es nicht möglich, diese Resultate direkt mit entsprechenden experimentell erhaltenen Werten zu vergleichen, da Wasserstoff ja keine metallartigen Gitter bildet. Man kann über den Fehler des Verfahrens deshalb nur auf Umwegen Aussagen machen. Die Gesamtenergie stellt so, wie sie hier berechnet wird, eine obere Schranke dar, denn bei Einschluß der Terme dritter Ordnung läßt sie sich als Erwartungswert der Energie der Zustandsfunktion von erster Ordnung auffassen und liegt somit nach dem Variationsprinzip höher als der tiefste Eigenwert.

Es ist klar, daß bei richtigem Verhalten die Energie für große *A* asymptotisch gegen den Grenzwert $E = -0{,}5$ ginge. Man wird deshalb einen Verlauf, der etwa der Kurve *b* in Fig. 2 entspricht, als eine geschätzte obere Schranke für die wahre Energie annehmen können. Das führt zu der Kurve *c* in Fig. 2 als unterer Grenze für den Fehler des Verfahrens bei Abbruch nach den Graphen dritter Ordnung.

Man kann dann den Kurven *b* und *c* entnehmen, daß – im Fall des Wasserstoffatoms – die Gitterenergie bis zu *A*-Werten von etwa 2,2 eine kaum zu vernachlässigende Rolle spielt. Andererseits zeigt es sich, daß der Fehler infolge Abbruchs der Störreihe bereits bei *A*-Werten von 1,9 schon beträchtlich ist. Die untere Schranke der beiden Fehlerquellen ist bei $A = 2$ jeweils 0,01 a.E.

Man könnte also im Fall des *H*-Atoms zu der Meinung kommen, daß sich dieses System tatsächlich auf die beschriebene Weise mit einer Genauigkeit von 0,01 a.E. (6 kcal/mol) behandeln läßt. Das eigentliche Problem besteht aber darin, daß der Bereich von *A*, in welchem die Fehler die angegebene Größe nicht wesentlich überschreiten, sehr eng ist. Die zwei Bereiche, in denen die beiden Fehler die Energie beeinflussen, schließen aneinander an und es fehlt eine Zone, in der sich *E* an die Abzisse 0,5 anschmiegt. So hat man im allgemeinen Fall kein Indiz mehr dafür, daß man bei der Wahl von *A* eine gute Mitte zwischen beiden Fehlerquellen eingehalten hat.

4. Ergebnisse für das Heliumatom

Als nächstes soll die Frage untersucht werden, wie die Methode auf Vergrößerung der Kernladungszahl *Z* reagiert. Sie kann and Hand von Rechnungen zum Fall des Heliumatoms eine vorläufige Antwort finden. Die Berechnung ist analog zu derjenigen für das Wasserstoffatom durchgeführt worden und das Resultat ist in Fig. 3 enthalten.

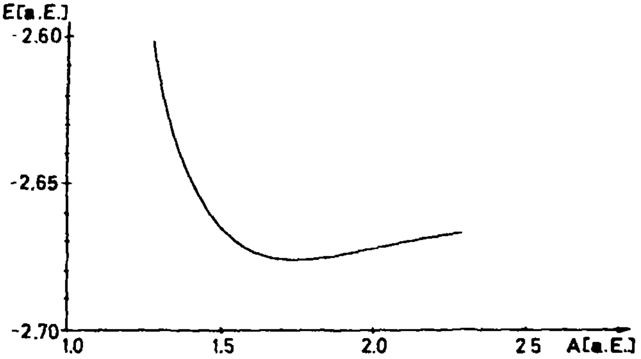

Fig. 3. Berechnete Gesamtenergie für das Heliumatom in Abhängigkeit von *A*

Das Minimum dieser Kurve liegt bei einem A von 1,75, entsprechend einem Abstand zweier Atome von 1,85 Å. Die Energie je Atom ist an dieser Stelle $-2{,}67$ a.E., während der theoretische Wert $-2{,}9037$ a.E. beträgt [6]. Der Fehler liegt somit bei etwa 8%, nicht gerechnet die schwer erfaßbare Beeinflussung durch den Einschluß von Gitterenergie. Diese dürfte jedoch im Vergleich zum Wasserstoffatom gering sein, weil Helium ein Edelgas ist und sein Siedepunkt sehr tief liegt.

Bei Helium wird also der theoretische Wert zwar ungefähr getroffen, aber der Fehler beträgt bereits 0,23 a.E. und liegt damit außerhalb der Toleranzschranke der theoretischen Chemie. Es kann als sicher gelten, daß die Genauigkeit bei noch größeren Kernladungen weiter abnimmt.

5. Diskussion

Abschließend läßt sich sagen, daß das Verfahren nur für den Fall mit der geringsten Störung Werte liefert, die mit einem tragbaren Fehler behaftet sind. Geringe Störungen sind dann gegeben, wenn

(i) die Kernladungen klein und
(ii) die Gitterabstände eng sind.

Beides tendiert in Richtung möglichst geringer Schwankungen des Kernpotentials.

Es zeigt sich dann, daß man bei Abbruch der Störreihe nach den Graphen dritter Ordnung nur im Fall von Kernen der Ladung 1, d.h. für Wasserstoff, einigermaßen akzeptable Werte erhält; ihr Wert wird allerdings eingeschränkt durch die Tatsache, daß das Gitter so eng gewählt werden muß, daß die – hier unerwünschte Gitterenergie eine nicht mehr zu vernachlässigende Rolle spielt.

Geht man mit der Kernladung auf 2, d. h. zu Helium über, so verschlechtern sich die Ergebnisse so weit, daß der Fehler auch im günstigsten Bereich der Gitterabstände auf 8% ansteigt. Das führt zu der Festellung, daß das Verfahren für die Chemie nicht als brauchbar gewertet werden kann; denn es würde mindestens die Behandlung von Kernladungen bis zu 8 (Sauerstoff) notwendig sein, um einen Großteil wenigstens der organischen Chemie erfassen zu können.

Es liegt nahe, die Störungsrechnung noch um eine Ordnung weiterzutreiben. Aber nach den hier gemachten Erfahrungen muß ein Erfolg bezweifelt werden. Einerseits würden die mathematischen und numerischen Probleme hinsichtlich der Graphen vierter Ordnung ein Vielfaches der der dritten Ordnung betragen und einige der Summen in den Beiträgen sind Summen über Tripel von reziproken Gittervektoren. Andererseits steht nach diesen Erfahrungen zu erwarten, daß die Resultate auch dann noch nicht die erforderliche Genauigkeit erreichen würden.

Die recht umfangreichen Rechnungen sind sowohl im Deutschen Rechenzentrum, Darmstadt, als auch im Rechenzentrum der Bayerischen Akademie der Wissenschaften, München, durchgeführt worden. Der Sonderforschungsbereich Theoretische Chemie stellte die notwendigen finanziellen Mittel zu Verfügung.

Literatur

1. **Reinsch, E. A.**: Theoret. chim. Acta (Berl.) **23**, 155 (1971).
2. -- Theoret. chim. Acta (Berl.) **24**, 290 (1972).
3. **Bulirsch, R., Stoer, J.**: Numer. Math. **6**, 413 (1964).
4. **Gell-Mann, M., Brueckner, K. A.**: Physic. Rev. **106**, 364 (1957).
5. **Carr, W. J., Maradudin, A. A.**: Physic. Rev. **133A**, 371 (1964).
6. **Moore, C. E.**: Atomic energy levels, Vol. I. Washington: National Bureau of Standards 1949.

Dr. Ernst-Albrecht Reinsch
Institut für theoretische Chemie
Universität Frankfurt am Main
D-6000 Frankfurt am Main 1
Robert-Mayer-Straße 11
Deutschland

Theoret. chim. Acta (Berl.) 25, 346–351 (1972)
© by Springer-Verlag 1972

Finite Electric Field Valence-Shell Calculations of Molecular Hyperpolarizabilities

N. S. HUSH* and M. L. WILLIAMS

Department of Inorganic Chemistry, University of Bristol, U.K.

Received June 21, 1971

Using the Finite Electric Field CNDO/II method discussed previously (Chem. Physics Letters 5, 507, (1970)), components of the first hyperpolarizability tensor β_{ijk} are calculated for a series of linear molecules, for H_2O and NH_3 and for methane and its fluorinated derivatives. These are compared, where possible, with results of previous calculations and with experimental results.

Mit Hilfe der zuvor diskutierten CNDO/II-Methode, bei der endliche Werte des störenden elektrischen Feldes Verwendung finden (Chem. Physics Letters 5, 507 (1970)), werden die Komponenten des ersten Hyperpolarisierbarkeitstensors β_{ijk} für eine Reihe von linearen Molekülen, für H_2O, NH_3 und für Methan und seine fluorierten Derivate berechnet. Soweit möglich, werden die Ergebnisse mit früheren Rechnungen und experimentellen Werten verglichen.

In a previous communication [1a] concerned mainly with electronic polarizabilities, we mentioned briefly preliminary calculations of components of the first hyperpolarizability tensor [2] β_{ijk} for the diatomic molecules CO and NO. These have now been extended.

Several sets of *ab initio* calculations of hyperpolarizabilities have previously been reported. O'Hare and Hurst [3], using an uncoupled Hartree-Fock perturbation scheme calculated hyperpolarizability tensor components for a series of First-Row polar diatomic molecules using several sets of zero-order wavefunctions. The finite-field technique has been employed by McLean and Yoshimine [4, 5] for a number of linear molecules, while Moccia *et al.*, [6], used a coupled Hartree-Fock perturbation method for H_2O, NH_3, CH_4 and CH_3F.

One fact which the results of these calculations reveal is the sensitivity of the hyperpolarizability components to the form of the basis set used and to the form of the zeroorder wave-function employed. A critical evaluation of the theoretical results is difficult at present due to the paucity of experimental data[1]. Where values are available, the experimental difficulties often allow only order of magnitude estimates to be made.

It is of interest to see whether semi-empirical calculations, with a valence orbital basis set, are capable of yielding useful predictions of hyperpolarizabilities. Using the Finite-Electric-Field CNDO/II method described earlier [1] we have extended our previous work to include calculations of first hyperpolarizability components for several linear ($C_{\infty v}$) molecules, for H_2O, NH_3, CH_4 and its fluorinated derivatives.

---

* Present address: Department of Theoretical Chemistry, The University of Sydney, Sydney, N.S.W., Australia.

[1] For a comprehensive survey of experimental methods and results the reader is referred to the review by Buckingham and Orr [2].

The perturbed SCF equations in the CNDO/II approximation are given in Ref. [1a] and these are used to calculate the perturbed dipole moment μ. The latter is expanded in the familiar Taylor series in powers of the external field F:

$$\mu_i = \mu_i^0 + a_{ij}F_j + \tfrac{1}{2}\beta_{ijk}F_jF_k + \cdots \tag{1}$$

where α_{ij} is the electronic polarizability tensor. The nonzero components of β_{ijk} are determined by the molecular point group symmetry and are listed elsewhere [2]. For example, in the case of a $C_{\infty v}$ molecule the non-zero components are β_{zzz} and $\beta_{xxz} = \beta_{yyz}$ where z is the highest symmetry axis. In the finite field method, the components of the perturbing electric field are chosen to induce the component of the dipole moment appropriate to the β_{ijk} component it is required to calculate.

Thus to calculate β_{xxz} for a $C_{\infty v}$ molecule the field is applied purely in the x direction and, since β_{ijk} is symmetric in the suffices, $\tfrac{1}{2}\beta_{xxz}$ is then the coefficient of F_x^2 in the expansion of μ_z. The components of β were determined in this way by calculating the appropriate dipole component for several values of the field and obtaining the quadratic coefficients from a least-squares analysis. The results are discussed in the sections below.

1) Linear ($C_{\infty v}$) Molecules

For these molecules we have calculated the non-zero components β_{zzz} and $\beta_{xxz} (= \beta_{yyz})$. These, along with available comparison calculations, are listed in Table 1. Also listed in Table 1 are the corresponding values of the anisotropy, $\Delta\beta$, of the hyperpolarizability tensor [2] defined as

$$\begin{aligned}\Delta\beta &= \beta_{zzz} - \tfrac{3}{2}\beta_{xxz} - \tfrac{3}{2}\beta_{yyz} \\ &= \beta_{zzz} - 3\beta_{xxz}\end{aligned}$$

for $C_{\infty v}$ molecules.

We note firstly that agreement with the finite-field calculations of McLean and Yoshimine [5] is reasonably good (CO, LiF, FCCH and HF)[2]. The values for β_{zzz} obtained by O'Hare and Hurst [3] from different zero-order wavefunctions cover a wide range for each molecule studied; for CO and HF these ranges include the values obtained by us and McLean and Yoshimine. The general agreement is best for HF. For the molecule BF however, our value for β_{zzz} $(-0.0624 \times 10^{-50}\,\mathrm{C^3m^3J^{-2}})$ differs in sign from the range of values $(0.289 - 1.834 \times 10^{-50}\,\mathrm{C^3m^3J^{-2}})$ calculated by O'Hare and Hurst.

Our calculated values of β_{xxz} are also shown in Table 1, and compared with the calculations of O'Hare and Hurst for CO, HF and BF. The three sets of wavefunctions used by O'Hare and Hurst give reasonably consistent values of β_{xxz} for HF and BF whereas for both these molecules the CNDO wavefunctions yield a value with the opposite sign. For the other molecule where a comparison can be made, namely CO, the range of values quoted by O'Hare and Hurst $(0.0794$ to $-0.0698 \times 10^{-50}\,\mathrm{C^3m^3J^{-2}})$ includes our value $(-0.0635 \times 10^{-50}\,\mathrm{C^3m^3J^{-2}})$.

---

[2] Comparison values have, wherever necessary, been converted to S.I. units.

Table 1. Hyperpolarizabilities of linear ($C_{\infty v}$) molecules[a] (Units: $\times 10^{-50} C^3 m^3 J^{-2}$)

Molecule	μ(cm $\times 10^{30}$) (calc.)[b]	β_{zzz}		$\beta_{xxz} = \beta_{yyz}$		$\Delta\beta(\beta_{zzz} - 3\beta_{xxz})$	
		This work	Comparison	This work	Comparison[c]	This work	Comparison[c]
CO	3.1986	0.0731	0.0705 [5]	−0.0635	–	0.2603	
			0.9273 [3]		−0.0794		−0.6891
			−0.3759 [3]		−0.0698		−0.1692
			−0.3648 [3]		−0.0564		−0.1956
NO	−0.0153	0.0831	—	−0.0120	—	0.1191	—
LiF	−16.0719	0.1980	0.1002 [5]	0.262	—	−0.588	—
FCCH	3.1916	−0.1990	−0.2969 [5]	0.157	—	−0.670	—
HF	−4.4968	−0.0865	−0.0275 [5]	0.0193	—	−0.1444	—
			−0.1050 [3]		−0.0119		−0.0963
			−0.2342 [3]		−0.0434		−0.1040
			−0.0618 [3]		−0.0200		−0.0018
BF	7.4232	−0.0624	1.834 [3]	−0.2930	0.1974	0.8166	1.2418
			0.372 [3]		0.1221		0.0057
			0.289 [3]		0.0817		0.0439

[a] Atoms lie along positive z axis, with atom on the left at origin (F at origin in FCCH)

[b] Positive in sense A^-B^+.

[c] Ref. [3]. All bond lengths as in Ref. [1b].

Using a simple charged sphere model of a polar diatomic molecule, Buckingham and Orr [2] have shown that for this extreme limit $\beta_{zzz} = 3\beta_{xxz}$ or $\Delta\beta = 0$. Such a model might roughly represent a highly polar molecule such as HCl but would form a poor representation of, for example, CO. From the values of $\Delta\beta$ listed in Table 1 it is clear that in general for both the present and comparison calculations, this simple relationship is not well obeyed. However for two molecules, namely HF and BF, one of the values of $\Delta\beta$ calculated by O'Hare and Hurst is indeed very small.

2) $CH_4(T_d)$

The only non-zero component of β_{ijk} in this case is β_{xzy} where the x, y and z axes are co-incident with the three twofold axes. Our calculated value can be compared with an approximate experimental one [2], and also with the theoretical values of Buckingham and Stephen [7] and Moccia *et al.* [6]:

This work	Previous calculations	Experimental	(Units: $\times 10^{-50} C^3 m^3 J^{-2}$)
-0.00779	-0.0779 [7] $+0.0148$ [6] $+0.0071$ [6]	$\lvert\beta_{xyz}\rvert \simeq 0.0037$ [2]	
($r_{C-H} = 1.094$ Å; $< HCH = 109°\,28'$)			

Moccia *et al.* calculate a positive sign for this quantity, in disagreement with the negative sign obtained in the present work and that of Buckingham and Stephen.

3) $NH_3(C_{3v})$

With the reference frame such that the z-axis is the three-fold axis with the $y-z$ plane one of the planes of symmetry, the non-zero components are β_{zzz}, $\beta_{yyy} = -\beta_{yxx}$ and $\beta_{yyz} = \beta_{xxz}$. Our values for these can be compared with those of Moccia *et al.* [6]. We can also compare values for the quantity β defined [2] as

$$\beta = \tfrac{3}{5}(\beta_{xxz} + \beta_{yyz} + \beta_{zzz})$$

for which an approximate experimental value has been quoted [2]. There is agreement of sign for both β_{zzz} and β_{yyz} but not for the β_{yyy} components. Both sets of calculated values of β have the same sign as the approximate experimental quantity but are smaller in absolute magnitude. It should also be noted that β is independent of β_{yyy}.

	This work	Moccia *et al.*	Expt.
β_{zzz}	-0.0488	-0.000798 -0.00854	
β_{yyz}	-0.00980	-0.00924 -0.0203	
β_{yyy}	-0.00490	$+0.0173$ $+0.0283$	
β	-0.0419	-0.0116 -0.0304	ca. -2.6

(Units: $\times 10^{-50} C^3 m^3 J^{-2}$)
($r_{N-H} = 1.016$ Å, $<HNH = 107°$)

4) $H_2O(C_{2v})$

The non-zero components here are β_{zzz}, β_{xxz} and β_{yyz} with z as the two-fold axis and yz as the molecular plane. Again our results for these can be compared with Moccia *et al.* [6]. For the β_{xxz} component there is a disagreement in sign. The β_{zzz} values are in reasonable agreement and the β_{yyz} values agree in sign; however, there is a marked difference in Moccia's calculations performed with two different sized basis sets which emphasises the sensitivity of these calculations to choice of orbital basis.

	This work	Moccia *et al.* [6]	(Units: $\times 10^{-50} C^3 m^3 J^{-2}$)
β_{xxz}	-0.1532	0.1086 0.8974	
β_{yyz}	-0.1232	-0.00006 -0.01026	
β_{zzz}	0.1274	0.06372 0.08032	

($r_{O-H} = 0.958$ Å, $<HOH = 104° 27'$)

5) Fluorinated Derivatives of Methane

There is an unfortunate lack of experimental data for the molecules mentioned above; consequently appraisal of the various theoretical methods employed in the calculation of β's is difficult. Recently however, experimental estimates of hyperpolarizability components for CH_3F, CH_2F_2 and CHF_3 have become available through the work of Buckingham and Orr [8] on the temperature dependence of the first Kerr virial coefficient. The experimentally determined parameter is β (defined as in Section 3 above) and our calculated values for this quantity are compared with the experimental values in Table 2. Also included for comparison is a calculation by Moccia *et al.* [6] of β for CH_3F.

The most precise experimental value for β is that for $CH_2F_2(-0.041 \pm 0.01 \times 10^{-50} C^3 m^3 J^{-2})$ and our calculated value of $-0.0254 \times 10^{-50} C^3 m^3 J^{-2}$ is in fair agreement with this. For both CH_3F and CHF_3 the experimental and calcu-

Table 2. Hyperpolarizabilities of fluorinated methanes (Units: $- \times 10^{-50} C^3 m^3 J^{-2}$)[a]

Molecule	μ_z(cm $\times 10^{30}$) (calc.)	β_{zzz}	β_{xxz}	β_{yyz}	β_{xyz}	β(calc.)	β(expt.)
CH_3F	-5.7310	-0.0186	-0.0067	-0.0067	0.0	-0.0192[b]	-0.19 ± 0.1
CH_2F_2	6.6283	-0.0121	-0.0130	-0.0173	0.0	-0.0254	-0.041 ± 0.01
CHF_3	5.7557	0.0221	0.0076	0.0076	0.0	0.0224	0.27 ± 0.1
CF_4	0.0	0.0	0.0	0.0	0.0043	–	–

[a] Axis system is right-handed, with carbon at origin; z is the highest symmetry axis and the fluorine atom(s) always constitute the negative end of the dipole. In CH_2F_2 the CH_2 fragment is in the yz plane.

[b] Moccia *et al.* [6] calculate $\beta = -0.0594 \times 10^{-50} C^3 m^3 J^{-2}$

[c] Ref. [8].

Bond Lengths and angles:

CH_3F: $< HCH = 110$ $r_{C-H} = 1.109$ Å $r_{C-F} = 1.385$ Å
CH_2F_2: $< HCH = 109.5°$ $< FCF = 108.5°$ $r_{C-H} = 1.093$ Å $r_{C-F} = 1.360$ Å
CHF_3: $< FCF = 108.8°$ $r_{C-H} = 1.098$ Å $r_{C-F} = 1.332$ Å
CF_4: $r_{C-F} = 1.317$ Å $< FCF = 109.5°$

lated β values have the same sign but even allowing for the appreciable uncertainty in the experimental value, the calculated β for CHF_3 is an order of magnitude different from that reported. The calculated β for CH_3F is of the same order of magnitude as the upper estimated experimental limit for this molecule, as also is the calculated value of Moccia *et al.* [6].

It is clearly difficult at present to draw general conclusions from these results. Two points may however (with caution) be regarded as encouraging: these are firstly, the reasonable agreement for the axial hyperpolarizability components of linear molecules calculated by two finite-field methods (ours and that of Ref. [5]) and secondly, the quite good agreement for β with the best-established experimental value (i.e., that for CH_2F_2).

Acknowledgement. This work was carried out during the tenure of a maintenance grant from the Science Research Council by one of us (M.L.W.).

References

1. Hush, N.S., Williams, M.L.: (a) Chem. Physics Letters **5**, 507 (1970). (b) Chem. Physics Letters **6**, 163 (1970).
2. Buckingham, A.D., Orr, B.J.: Quart. Rev. **21**, 195 (1967).
3. O'Hare, J.M., Hurst, R.P.: J. chem. Physics **46**, 2356 (1967).
4. McLean, A.D., Yoshimine, M.: J. chem. Physics **46**, 3682 (1967).
5. — Compendium of *Ab Initio* calculations of Molecular properties, U.S. National Bureau of Standards, Technical Note 438, (1967).
6. Arrighini, G.P., Maestro, M., Moccia, R.: Symposia of the Faraday Soc., No. 2, 48 (1968).
7. Buckingham, A.D., Stephen, M.J.: Trans. Faraday Soc. **53**, 884, (1957).
8. — Orr, B.J.: Trans. Faraday Soc. **65**, 673, 1969.

Prof. N. S. Hush
Department of Theoretical Chemistry
The University of Sydney
Sydney, N.S.W., Australia

Theoret. chim. Acta (Berl.) 25, 352–359 (1972)
© by Springer-Verlag 1972

Geometry and Force Constant Determination from Correlated Wave Functions for Polyatomic Molecules: Ground States of H_2O and CH_2*

DONALD R. MCLAUGHLIN** and CHARLES F. BENDER
Lawrence Radiation Laboratory, University of California, Livermore, California 94550, USA

HENRY F. SCHAEFER III***
Department of Chemistry, University of California, Berkeley, California 94720, USA

Received September 9, 1971

Ab initio calculations including electron correlation are reported for the water and methylene molecules as a function of geometry. A large contracted gaussian basis set is used and the multiconfiguration wave functions, optimized by the iterative natural orbital procedure, include 277 and 617 configurations for H_2O and CH_2 respectively. The method of selecting configurations, yielding "first-order" wave functions, is discussed in some detail. For H_2O, the SCF geometry is $r = 0{,}942$ Å, $\theta = 105{,}8$, the correlated result is $r = 0{,}968$ Å, $\theta = 103{,}2$, and the experimental $r = 0{,}957$ Å, $\theta = 104{,}5$. The water stretching force constants, in millidynes/Å, are 8,72 (SCF), 8,75 (CI), and 8,4 (experiment). Bending force constants are 0,88 (SCF), 0,83 (CI), and 0,76 (experiment). For methylene the SCF geometry is $r = 1{,}072$ Å, $\theta = 129{,}5$, while the result from first-order wave functions is $r = 1{,}088$ Å, $\theta = 134$ The predicted CH_2 force constants are 6,16 (SCF) and 6,13 (CI) for stretching and 0,44 (SCF) and 0,33 (CI) for bending.

Es wird über *ab initio*-Rechnungen mit Berücksichtigung der Elektronenkorrelation berichtet, die an Wasser- und Methylenmolekülen als Funktion der Geometrie durchgeführt worden sind. Dazu benutzt man einen großen kontrahierten Gauß-Basissatz. Die Multikonfigurationswellenfunktionen, die unter Benutzung von natürlichen Orbitalen nach der iterativen Prozedur optimiert werden, enthalten für H_2O 277 Konfigurationen und für CH_2 617. Die Auswahlmethode, die zu Wellenfunktionen 1. Ordnung führt, wird diskutiert. Im Falle des Wassers erhält man die SCF-Geometrie zu $r = 0{,}942$ Å, $\theta = 105{,}8$, das korrelierte Resultat ist: $r = 0{,}968$ Å, $\theta = 103{,}2$ und das experimentelle $r = 0{,}957$ Å, $\theta = 104{,}5$. Für Wasser ergeben sich die Valenzkraftkonstanten (in Millidyn Å^{-1}) 8,72 (SCF), 8,75 (CI) und 8,4 (Experiment). Die Deformationskonstanten sind 0,88 (SCF), 0,83 (CI) und 0,76 (Experiment). Im Falle des Methylens ist die SCF-Geometrie $r = 1{,}072$ Å, $\theta = 129{,}5$, während man mit Wellenfunktionen 1. Ordnung $r = 1{,}088$ Å und $\theta = 134^\circ$ erhält. Die CH_2-Kraftkonstanten werden für die Valenzschwingung zu 6,16 (SCF) und 6,13 (CI) bzw. für die Deformationsschwingung zu 0,44 (SCF) und 0,33 (CI) vorausgesagt.

Introduction

The correlation energy of a many-electron system arises from the instantaneous repulsions between pairs of electrons [1] and can be quantitatively defined [2] as the difference between the Hartree-Fock (or best single configuration) energy

---

* Work performed under the auspices of the U.S. Atomic Energy Commision.

** Permanent address: Department of Chemistry, University of New Mexico, Albuquerque, New Mexico.

*** Supported by the grants from the Research Corporation and the University of California Committee on Research.

and the nonrelativistic exact energy. In recent years molecular calculations using near-Hartree-Fock wave functions have given theoretical chemists a fairly clear picture of the merits of the single configuration self-consistent-field (SCF) approach [3–6]. Going beyond the Hartree-Fock approximation, the picture is less clear. The question most frequently raised is how much electron correlation must be considered to reach a given level of reliability. For diatomic molecules rather thorough investigations have been made of the effect of correlation on predicted dipole moments [7–9] and potential energy curves [10, 11]. However, most of chemistry is concerned with polyatomic molecules and very few through examination of the effects of configuration interaction (CI) have been carried out [12].

In this paper we consider two simple molecules, H_2O and CH_2, and study the influence of correlation on the predicted geometries and force constants.

The correlated "first-order wave functions" used here have proved useful in calculations (employing smaller basis sets) on other small molecules [3, 13–15]. The agreement with experiment obtained for H_2O will give us an estimate of the reliability of our predictions concerning CH_2. Although it is now clear that the $^3B_1$ ground state of methylene is bent [16–18] the experimental bond angles are not yet of quantitative accuracy.

Basis Set

If one intends to draw general conclusions from an *ab initio* calculation, it is necessary that the results be independent of basis set.The *s*, *p* basis sets on oxygen and carbon atoms in the present work are the 10*s* 6*p* gaussian sets of Huzinaga [19]. This basis set has been carefully contracted to five *s* and three *p* functions (5*s* 3*p*) by Dunning [20]. For the ^3P ground state of carbon Dunning finds [20] the contracted energy to be −37.68716 hartrees while the uncontracted energy is −37.68732, and the Hartree-Fock energy −37.6886. For the hydrogen atom Huzinaga's 5*s* set [19] is contracted following Dunning [20] to 3*s*. Dunning has also investigated the gaussian representation of polarization functions [21], and following his suggestions we have used single gaussian p_x, p_y, and p_z functions (with exponents 1.00 for CH_2 and 1.16 for H_2O) on each hydrogen atom. *d* functions on the central atoms were linear combinations of two gaussians chosen to least-squares fit a single Slater function (with exponent 2.00 in CH_2 and 2.01 in H_2O). The final basis set, designated (5*s* 3*p* 1*d*/3*s* 1*p*), yields an SCF energy for H_2O at equilibrium of −76.05 hartrees, to be compared with the estimated Hartree-Fock limit −76.065.

Selection of Configurations

Using a basis set as large as that detailed above it is not feasible to carry out a full configuration interaction. In fact, using the much smaller (4*s* 2*p*/2*s*) basis set and including only the SCF configuration plus all single, double, triple, and quadruple excitations yields 6779 configurations for H_2O [22]. A full configuration interaction for water would have to include up through 10 electron excitations. In this work we have used two configuration selection schemes. Both schemes have the virtue of being nonarbitrary in the sense that, having set down the general rules [13], the selection of configurations for a particular molecule is automatic.

To clarify the selection process it is useful to write down the SCF electron configurations for the two molecules (assuming C_{2v} symmetry)

$$\begin{array}{lll} {}^3B_1 & \mathrm{CH_2} & 1a_1^2\,2a_1^2\,1b_2^2\,3a_1\,1b_1 \\ {}^1A_1 & \mathrm{H_2O} & 1a_1^2\,2a_1^2\,1b_2^2\,3a_1^2\,1b_1^2\,. \end{array}$$

The molecular orbitals are fruitfully divided into four categories:

a) The core orbitals P. In both molecules there is only a single orbital of this type, namely $1a_1$, which is essentially the $1s$ atomic orbital on the central atom.

b) The occupied valence orbitals Q. $2a_1$, $1b_2$, $3a_1$, and $1b_1$ for both H_2O and CH_2.

c) The unoccupied (in the SCF configuration) valence orbitals R. For CH_2 these are the $3a_1$ and $1b_1$ orbitals (only singlyoccupied in the ${}^3B_1$ state) and for both molecules the $4a_1$ and $2b_2$ orbitals fall in this category.

d) The unoccupied higher orbitals S. These are the remaining functions in the basis set, in this case $5a_1$ through $16a_1$, $1a_2$ and $2a_2$, $2b_1$ through $5b_1$, and $3b_2$ through $9b_2$.

With these definitions the form of our two CI wave functions which we have referred to [13] as MC1 and MC2 is easy to specify:

MC1 includes the SCF configuration, all single excitations of the type $Q_i \to R_j$ and double excitations of the type $Q_iQ_j \to R_kR_l$. This type of wave function is in the spirit of the "optimized valence configurations" approach of Wahl and Das [23].

MC2 includes all the configurations in MC1 plus all single excitations of the type $Q_i \to S_j$ and all double excitations $Q_iQ_j \to R_kS_l$. This is our approximate first-order wave function, which has been discussed elsewhere [11, 13–15, 24].

We do not list the configurations included here for H_2O and CH_2 since explicit examples have previously been given for several molecules [11, 13–15]. For H_2O MC1 includes 18 and MC2 277 configurations. The analogous methylene calculations include 32 and 617 configurations.

Method of Calculation

A self-consistent-field calculation is the first step in our computational procedure. Rather that the usual methods for solving the SCF equations [25], the iterative natural orbital technique [26, 27] is used to annihilate single excitations relative to the SCF configuration. Iterations are continued until the coefficients of the singly-excited configurations vanish and the natural orbital (NO) occupation numbers [28] become integers. The orbitals obtained via this method are not the canonical SCF orbitals [25], so we use a simple unitary transformation employing the properties of Koopmans' theorem to yield to canonical orbitals, which are eigenfunctions of the Fock operator.

Before proceeding to the final NO iterations, the virtual orbitals are transformed so as to correspond to the single particle states of the molecular positive ion. This gives us a well defined starting point for the final NO iterations, which are carried out on the full first-order wave functions (617 configurations for CH_2) until the energy reaches a minimum. Typically this requires four iterations.

Results

The calculated total energies are given in Table 1. From the calculated energies, the equilibrium geometries and quadratic force constants have been determined as described elsewhere [29]. These results are given in Table 2.

For water all three calculations give good agreement with experiment [30–32] for both geometry and force constants. The SCF bond distance is 0.015 Å shorter than experiment, while the first-order value is 0.011 Å too long. We anticipate [11] that further expansion of the basis set will make both the SCF and first-order bond distance smaller. The SCF bond angle is 1.3° too large and the first-order value 1.1° too small. Thus it is seen that for both bond distance and bond angle the first-order results are in slightly better agreement with experiment than the SCF values. The SCF and first-order stretching force constants are both 104% of experiment, while for the bending force constant the theoretical values are 116% and 109% of experiment. The errors (4% and 9%) in the force constants

Table 1. Theoretical energies for the ground states of CH_2 and H_2O. Bond angles are in degrees and bond distances in bohr radii

θ	R(CH)	E(SCF)	E(MC1)	E(MC2)
$^3B_1$ CH_2				
124	1.95	−38.92961		
124	2.00	−38.93183		
124	2.05	−38.93193		
124	2.10	−38.93019		
128	1.95	−38.93026	−38.96421	−39.00686
128	2.00	−38.93239	−38.96788	−39.01027
128	2.05	−38.93238	−38.96941	−39.01155
128	2.10	−38.93054	−38.96911	−39.01102
132	1.95	−38.93036	−38.96454	−39.00755
132	2.00	−38.93235	−38.96811	−39.01083
132	2.05	−38.93225	−38.96956	−39.01200
132	2.10	−38.93031	−38.96918	−39.01135
136	1.95	−38.92986	−38.96438	−39.00774
136	2.00	−38.93178	−38.96790	−39.01092
136	2.05	−38.93158	−38.96927	−39.01198
136	2.10	−38.92955	−38.96880	−39.01123
140	1.95	−38.92892	−38.96386	−39.00754
140	2.00	−38.93073	−38.96729	−39.01065
140	2.05	−38.93043	−38.96859	−39.01156
140	2.10	−38.92830	−38.96805	−39.01071
$^1A_1$ H_2O				
99.52	1.7589	−76.05717	−76.10676	−76.17031
99.52	1.8089	−76.05724	−76.10910	−76.17316
99.52	1.8589	−76.05449	−76.10870	−76.17312
104.52	1.7589	−76.05847	−76.10736	−76.17099
104.52	1.8089	−76.05826	−76.10943	−76.17349
104.52	1.8589	−76.05525	−76.10872	−76.17322
109.52	1.7589	−76.05837	−76.10653	−76.17029
109.52	1.8089	−76.05791	−76.10838	−76.17251
109.52	1.8589	−76.05467	−76.10745	−76.17196

Table 2. Predicted geometries and force constants for the ground states of CH_2 and H_2O. SCF refers to our self-consistent-field wave functions, MC1 to the configuration interaction including SCF plus all promotions to valence orbitals and MC2 to the approximate first-order wave functions. Experimental values are given in parentheses

	H_2O			CH_2		
	SCF	MC1	MC2	SCF	MC1	MC2
Bond distance (Å)	0.942	0.964	0.968 (0.957)[a]	1.072	1.092	1.088
Bond angle (degrees)	105.8	103.2	103.4 (104.5)[a]	129.5	131.7	134.0 (136 ± 8)[b]
Interpolated total energy (hartrees)	76.05876	-76.1096	-76.1738	-38.9327	-38.9696	-39.0121
Stretching force constant (md/Å)	8.72	8.61	8.75 (8.4)[c]	6.16	6.09	6.13
Bending force constant (md/Å)	0.88	0.84	0.83 (0.76)[d]	0.44	0.23	0.33

[a] Benedict, W. S., Gailar, N., Plyer, E. K.: J. chem. Physics **24**, 1139 (1956).

[b] Wasserman, E., Yager, W. A., Kuck, V. J.: Chem. Physics Letters **7**, 409 (1970).

[c] Nibler, J. W., Pimentel, G. C.: J. molecular Spectroscopy **26**, 294 (1968).

[d] Duncan, J. L., Mills, I. M.: Spectrochim. Acta **20**, 523 (1964).

from first-order wave functions are about what we have seen for diatomic molecules O_2 [11], BeO [14], KrF^+ [33], and BH [34]. However, H_2O is unusual with respect to the SCF force constants, since these are often in poor agreement with experiment [35].

The geometry of CH_2 has been of considerable interest to theoreticians since increasingly accurate *ab initio* calculations [36–38] have predicted a bent triplet ground state, while experimentalists generally accepted Herzberg's spectroscopic determination of linearity [39]. However, recent electron-spin resonance measurements at 4 K have demonstrated that CH_2 is bent [16, 17, 40, 41], a conclusion which can be understood in terms of predissociation in the gas phase absorption spectrum of CH_2 [18, 39]. The ESR measurements have been used to determine bond angles for CH_2 of 136° [17, 40] and 137.7° [41]. However these "experimental" bond angle determinations cannot be taken literally since they assume that one of the two unpaired electrons ($1b_1$) is in a $2p_x$ orbital perpendicular to the plane while the other electron occupies a hybrid orbital oriented along the bisector of the H–C–H angle [41]. As has been pointed out to the authors by Hoffman [42], hybridization is not a physical phenomenon and thus the experimental determinations are by no means rigorous. In light of the above, the most reliable experimental value for the bond angle may be Herzberg's experimental range of 128–148.

The present calculations predict bond angles of 129.5, 131.7°, and 134.0 from SCF, MC1, and MC2 wave functions. The SCF bond angle agrees with the value 129 recently obtained by Allen and Franceschetti [43] using a slightly smaller basis set. The angle predicted from first-order wave functions is expected to be the most reliable. To aid in our evaluation of the expected reliability of this 134° CH_2 angle, we point out that comparable first-order calculations [44] on the ground $^2B_1$ and first-excited $^2A_1$ states of NH_2 yielded bond angles differing by 0.6° and 0.7° from experiment. In light of these results and the H_2O results discussed above, we estimate that our theoretical bound angle of 134° is reliable to within 2°. Thus we feel that the present calculations provide the most reliable value to date theoretical or experimental, for the bond angle of the $^3B_1$ ground state of methylene.

Table 3. Important spatial configurations in the first-order wave functions for CH_2 and H_2O. The "degeneracy" of a spatial configuration is the number of linearly independent spin eigenfunctions arising. The coefficients tabulated incorporate the effects of all proper spin eigenfunctions associated with a given spatial configuration

Excitation	Coefficient	Energy criterion $[= \Sigma c_i^2 (H_{ii} - H_{11})]$
$^3B_1$ CH_2 $R = 2.05$ bohrs, $\theta = 132°$		
1. $1a_1^2 2a_1^2 1b_2^2 3a_1 1b_1$	0.9796	
2. $2a_1 1b_2 \rightarrow 4a_1 2b_2$	0.0618	0.0074
3. $1b_2^2 \rightarrow 2b_2^2$	0.0552	0.0056
4. $2a_1 \rightarrow 4a_1$	0.0660	0.0044
5. $2a_1^2 \rightarrow 4a_1^2$	0.0453	0.0041
6. $1b_2 1b_1 \rightarrow 2b_2 2b_1$	0.0482	0.0040
7. $1b_2^2 \rightarrow 4a_1^2$	0.0505	0.0038
8. $1b_2 3a_1 \rightarrow 2b_2 5a_1$	0.0448	0.0036
$^1A_1$ H_2O $R = 1.8089$ bohrs, $\theta = 104.52°$		
1. $1a_1^2 2a_1^2 1b_2^2 3a_1^2 1b_1^2$	0.9815	
2. $1b_2 3a_1 \rightarrow 4a_1 2b_2$	0.0765	0.0131
3. $1b_2 1b_1 \rightarrow 2b_2 2b_1$	0.0698	0.0122
4. $3a_1 1b_1 \rightarrow 4a_1 2b_1$	0.0696	0.0121
5. $1b_2^2 \rightarrow 2b_2^2$	0.0630	0.0084
6. $2a_1 1b_2 \rightarrow 2b_2 5a_1$	0.0464	0.0070
7. $3a_1^2 \rightarrow 4a_1^2$	0.0576	0.0069
8. $2a_1 3a_1 \rightarrow 4a_1 5a_1$	0.0455	0.0065

Table 4. Natural orbital occupation numbers (≥ 0.001) for CH_2 and H_2O at the geometries given in Table 3

	CH_2	H_2O
$1a_1$	2.000	2.000
$2a_1$	1.972	1.944
$3a_1$	0.997	1.975
$4a_1$	0.025	0.025
$5a_1$	0.004	0.005
$6a_1$	0.002	0.001
$7a_1$	0.002	
$1a_2$	0.002	0.001
$1b_1$	0.996	1.989
$2b_1$	0.004	0.010
$3b_1$	0.002	
$1b_2$	1.970	1.974
$2b_2$	0.021	0.028
$3b_2$	0.002	0.001

The SCF, MC 1, and MC 2 stretching force constants are essentially the same, as was the case for H_2O, and all three values should be fairly reliable. There are considerable differences between the three calculated values of the bending force constant. It is clear, however, that this force constant is small, less than half that for H_2O.

Some detailed information concerning the electronic structure of H_2O and CH_2 is given in Tables 3 and 4. Table 3 gives the coefficients of the eight most important configurations in the final CI expansions and Table 4 the corresponding natural orbital occupation numbers. The fact that the coefficient of the SCF configuration is 0.9796 for CH_2 and 0.9815 for H_2O is a verification of the essential correctness of the molecular orbital model for these molecules. The same qualitative conclusion is seen in the nearly integer values of the occupation numbers in Table 4 for the SCF orbitals. Table 4 also shows that the most important orbitals besides the SCF orbitals are the $4a_1$ and $2b_2$ valence orbitals. Higher orbitals (those which cannot be constructed from a minimum basis) are seen to be relatively unimportant.

Acknowledgements. We thank Professor Roald Hoffmann for helpful correspondence regarding the reliability of the experimental CH_2 ground state bond angle.

References

1. Löwdin, P. O.: Advances chem. Physics **2**, 207 (1959).
2. Clementi, E.: J. chem. Physics **38**, 2248 (1963).
3. Wahl, A. C.: J. chem. Physics **41**, 2600 (1964).
4. Cade, P. E., Huo, W. M.: J. chem. Physics **47**, 614, 649 (1967).
5. Yoshimine, M., McLean, A. D.: Int. J. quant. Chemistry **1** S, 313 (1967).
6. Neumann, D., Moskowitz, J. W.: J. chem. Physics **49**, 2056 (1968).
7. Grimaldi, F., Lecourt, A., Moser, C.: Int. J. quant. Chemistry **1** S, 153 (1967).
8. Bender, C. F., Davidson, E. R.: J. chem. Physics **49**, 4222 (1968).
9. Green, S.: J. chem. Physics **54**, 827 (1971).
10. Das, G., Wahl, A. C.: Physic. Rev. Letters **24**, 440 (1970).
11. Schaefer, H. F.: J. chem. Physics **54**, 2207 (1971).
12. Potential surfaces have been obtained (using wave functions including electron correlation) for systems containing very few electrons. See, for example, Edmiston, C., Doolittle, J., Murphy, K., Tang, K. C., Willson, W.: J. chem. Physics **53**, 3419 (1970).
13. Schaefer, H. F., Bender, C. F.: J. chem. Physics **55**, 1720 (1971).
14. J. chem. Physics **55**, 176 (1971).
15. O'Neil, S. V., Pearson, P. K., Schaefer, H. F.: Chem. Physics Letters **10**, 404 (1971).
16. Bernheim, R. A., Bernard, H. W., Wang, P. S., Wood, L. S., Skell, P. S.: J. chem. Physics **53**, 1280 (1970).
17. Wasserman, E., Kuck, V. J., Hutton, R. S., Yager, W. A.: J. Amer. chem. Soc. **92**, 7491 (1970).
18. Herzberg, G., Johns, J. W. C.: J. chem. Physics **54**, 2276 (1971).
19. Huzinaga, S.: J. chem. Physics **42**, 1293 (1965).
20. Dunning, T. H.: Gaussian Basis Functions for Use in Molecular Calculations III Contraction of (10s 6p) Atomic Basis Sets for the First-Row Atoms, to be published.
21. — — Gaussian Basis Functions for Use in Molecular Calculations IV. The Representation of Polarization Functions for the First-Row Atoms and Hydrogen, to be published.
22. Hosteny, R. P., Gilman, R. R., Dunning, T. H., Pipano, A., Shavitt, I.: Chem. Physics Letters Vol. 7, 325 (1970).
23. Wahl, A. C., Das, G.: Advances quant. Chem. **5**, 261 (1970).
24. Schaefer, H. F., Klemm, R. A., Harris, F. E.: Physic. Rev. **181**, 137 (1969).

25. Roothaan, C. C. J.: Rev. mod. Physics **23**, 69 (1951); **32**, 179 (1960).
26. Bender, C. F., Davidson, E. R.: J. physic. Chemistry **70**, 2675 (1966).
27. — — Physic. Rev. **183**, 23 (1969).
28. Löwdin, P. O.: Physic. Rev. **97**, 1474 (1955).
29. Bender, C. F., Schaefer, H. F.: J. molecular Spectroscopy **37**, 423 (1971).
30. Benedict, W. S., Gailar, N., Plyer, E. K.: J. chem. Physics **24**, 1139 (1956).
31. Nibler, J. W., Pimentel, G. C.: J. molecular Spectroscopy **26**, 294 (1968).
32. Duncan, J. L., Mills, I. M.: Spectrochim. Acta **20**, 523 (1964).
33. Lin, B., Schaefer, H. F.: J. chem. Physics **55**, 2369 (1971).
34. Pearson, P. K., Bender, C. F., Schaefer, H. F.: J. chem. Physics **55**, 5235 (1971).
35. Freed, K. F.: J. chem. Physics **52**, 253 (1970).
36. Foster, J. M., Boys, S. F.: Rev. mod. Physics **32**, 305 (1960).
37. Harrison, J. F., Allen, L. C.: J. Amer. chem. Soc. **91**, 807 (1969).
38. Bender, C. F., Schaefer, H. F.: J. Amer. chem. Soc. **92**, 4984 (1970).
39. Herzberg, G.: Proc. Roy. Soc. (London) A **262**, 291 (1961)
40. Wasserman, E., Yager, W. A., Kuck, V. J.: Chem. Physics Letters **7**, 409 (1970).
41. Bernheim, R. A., Bernard, H. W., Wang, P. S., Wood, L. S., Skell, P. S.: J. chem. Physics **54**, 3223 (1971).
42. Hoffman, R.: Personal communication.
43. Allen, L. C., Franceschetti, D. R.: To be published.
44. Bender, C. F., Schaefer, H. F.: J. chem. Physics **55**, 4798 (1971).

Dr. C. F. Bender
Lawrence Radiation Laboratory
University of California
P.O. Box 808
Livermore, California 94550
USA

Theoret. chim. Acta (Berl.) 25,360 – 371 (1972)
© by Springer-Verlag 1972

Electronic Structure of Long Polyene Chains with an Impurity Atom

I. I. UKRAINSKY

Division of Molecular Quantum Mechanics, Sector of Theoretical Biophysics, Institute for Theoretical Physics, Academy of Sciences of the Ukrainian S.S.R., 252130 Kiev, USSR

G. F. KVENTSEL

Division of Heterogeneous Catalysis, L. V. Pisarzhevsky Institute of Physical Chemistry, Academy of Sciences of the Ukrainian S.S.R., 252028 Kiev, USSR

Received July 20, 1971

The influence of an impurity atom on the π-electronic structure of long polyenes is considered using the unrestricted Hartree-Fock (UHF) method. It is shown that the substitution of a carbon atom in a long polyene chain is a local perturbation in spite of the nonlinearity of the UHF Hamiltonian. The conditions under which the local states appear in the forbidden zone of long polyenes are stated. Some experiments are proposed to elucidate the nature of the forbidden zone in the π-electron spectra of long polyene chains.

Der Einfluß eines Fremdatoms auf die π-Elektronenstruktur langer Polyene wird mit Hilfe der uneingeschränkten Hartree-Fock-Methode (UHF) untersucht. Es wird gezeigt, daß die Substitution eines C-Atoms in einer langen Polyenkette eine lokale Störung darstellt, obwohl der UHF-Hamiltonoperator nicht linear ist. Die Bedingungen, unter denen die lokalen Zustände in der verbotenen Zone für die langen Polyene erscheinen, werden dargestellt. Einige Experimente zur Aufklärung der Natur der verbotenen Zonen in den π-Elektronen-Spektren langer Polyenketten werden vorgeschlagen.

La méthode Hartree-Fock sans restrictions (UHF) est utilisée pour étudier l'influence d'une impureté atomique sur la structure électronique π des grands polyènes. On montre que la substitution d'un atome de carbone dans une longue chaîne polyénique est une perturbation locale en dépit de la non linéarité de l'hamiltonien UHF. On énonce les conditions d'apparition des états locaux dans la zone interdite des longs polyènes. Certaines expériences sont proposées pour élucider la nature de la zone interdite dans le spectre d'électrons π des longues chaînes polyéniques.

Introduction

The optical experiments have shown [1] that the frequency of the first electronic transition in polyenes tends to a non-zero value when the polyene chain is lengthened. Until recently this energy gap was supposed to arise from the instability of the equal-bond polyene configuration with respect to the bond alternation [2, 3]. Nevertheless, it has recently been shown that the unrestricted Hartree-Fock (UHF) method taking into account electron correlation can be used to describe[1] the π-electronic spectra of large conjugated systems (polyenes, cumulenes, polyacenes, graphite) [4–11]. The papers [4, 9–11] have dealt with the electronic structure of ideal polyene chains consisting of an even [4, 9] or odd [10, 11] number of carbon atoms.

---

[1] Effect of projecting of the UHF wave function on the pure spin state is considered in Ref. [22] for the case of large systems.

Comparing with experiment only the values of energy gaps, obtained in the two different models, do not make it clear which of these models (or their combination [12]) is more realistic. One of the possible methods of investigating the electronic structure of periodic systems is to study the influence of the appropriately introduced defects on the energy spectra of these systems. That is why, to study the effect of disturbed periodicity on the electronic structure of polyene chains by means of the UHF method is of interest. The same problem has been discussed in [13–15] under the assumption that the energy gap is due to the bond alternation.

The UHF Solution for Long Polyene Chains with an Impurity Atom

The UHF equations for an ideal polyene chain have the following form in the orthogonal AO representation [4, 9–11]

$$\begin{aligned}\left(\alpha_0+\frac{\gamma}{2}+\varepsilon_k^{(j)}\right)C_{k\sigma}^{(j)}(\mu)&=\sum_{\nu=1}^{N}H_\sigma(\mu,\nu)\,C_{k\sigma}^{(j)}(\nu)\\&\equiv[\alpha_0+\gamma n_{\mu,\sigma}^{(0)}]\,C_{k\sigma}^{(j)}(\mu)+\beta[(1-\delta_{\mu,1})\,C_{k\sigma}^{(j)}(\mu-1)+(1-\delta_{\mu,N})\,C_{k\sigma}^{(j)}(\mu+1)]\,,\end{aligned}\tag{1}$$

where α_0 and β are the Coulomb and resonance integrals, γ is the electron repulsion integral, $n_{\mu\sigma}^{(0)}=\sum\limits_{k<\frac{\pi}{2}}[C_{k\sigma}^{(1)}(\mu)]^2$ are the electron populations of the μ-th AO with σ-spin, $\sigma=\uparrow,\downarrow$.

The solution of (1) is defined by the relations

$$C_{k\sigma}^{(1)}(\mu)=\sqrt{\frac{2}{N}}\,[1+(-1)^{\mu+1}\xi_k\tau_\sigma]\sin\mu k/\sqrt{1+\xi_k^2}\,,\tag{2a}$$

$$C_{k\sigma}^{(2)}(\mu)=\sqrt{\frac{2}{N}}\,[(-1)^{\mu+1}-\xi_k\tau_\sigma]\sin\mu k/\sqrt{1+\xi_k^2}\,,\tag{2b}$$

$$\varepsilon_k^{(1)}=-\varepsilon_k^{(2)}=-\sqrt{4\beta^2\cos^2k+a^2}\,,\tag{3}$$

where $N\gg1$ is the number of carbon atoms in the chain. The self-consistent value of a is found from the equation

$$\begin{aligned}&\frac{\gamma}{\pi}\int_0^{\pi/2}dk(4\beta^2\cos^2k+a^2)^{-1/2}=1\,;\\&\tau_\sigma=\begin{cases}1, & (\sigma=\uparrow)\\-1, & (\sigma=\downarrow)\end{cases}\end{aligned}\tag{4}$$

$$\xi_k=[2\beta\cos k+\sqrt{4\beta^2\cos^2k+a^2}]/a\,.\tag{5}$$

The width of the forbidden zone between the energy levels $\varepsilon_k^{(1)}$ occupied in the ground state and empty levels $\varepsilon_k^{(2)}$ is equal to $2a$. It follows from (2)–(5) that

$$n_{\mu\sigma}^{(0)}=\frac{1}{2}+(-1)^{\mu+1}\frac{2\tau_\sigma\gamma}{\pi}\int_0^{\pi/2}dk\frac{\sin^2\mu k}{\varepsilon_k^{(2)}}=\frac{1}{2}+(-1)^{\mu+1}\delta_\mu\,.\tag{6}$$

As is seen from (6) the values of δ_μ depend on an atom number μ. The analysis of (6) shows that this dependence occurs near the chain boundary:

$$\delta_\mu \approx \delta + (\tfrac{1}{2})^{\mu-1}\Delta\delta\,, \tag{7}$$

where $\delta = a/\gamma = 0.21$, $\Delta\delta = 0.06$ ($\beta = -2.4$ eV, $\gamma = 5{,}4$ eV [4]).

Using the UHF method we now consider the electronic structure of a long polyene chain with the ν-th atom substituted. We make an assumption that such a substitution can be approximated by changing an appropriate Coulomb integral as: $\alpha_\nu = \alpha_0 + t$. As seen from (1), the change of γ corresponding to perturbed atom can be taken into account by an appropriate change of the effective value of α. We shall consider here such substitutions which can be described by the change of the parameters α and γ only, i.e. the values of β are considered to be close to those for ideal polyenes. There are a number of substitutions which satisfy the above conditons, e.g. $H \rightarrow CH_3$, $C \rightarrow N$.

The UHF Hamiltonian for polyenes (1) is a non-linear operator since it contains $n_{\mu\sigma}^{(0)}$ (6). Therefore, a direct application of the local-perturbation theory [16] developed for linear Hamiltonians [17, 18] (e.g., for the tight binding method) requires an justification. The correct solution involves an iteration procedure usual for the calculations by the SCF methods. Consequently, one can use the local-perturbation theory for each iteration. The equation for eigenfunctions and eigenvalues in the case of long polyenes with the substitution has the following form for the first iteration (e.g., see [17])

$$(\hat{H}_\sigma + t\hat{A} - z_\sigma)\varphi_\sigma = 0\,, \tag{8}$$

where $\hat{H}_\sigma$ is given by (1), the operator $\hat{A}$ is defined by

$$(g, \hat{A}\varphi) \equiv \sum_{\mu,\mu'} g^*(\mu)A(\mu,\mu')\varphi(\mu') = g^*(\nu)\varphi(\nu)\,. \tag{9}$$

Let us present some general results which follow from [17]. Eigenvalues $z_{q\sigma}^{(i)}$ of the Eq. (8) are determined by

$$1 + t\sum_{k,j} \frac{[C_{k\sigma}^{(j)}(\nu)]^2}{\varepsilon_k^{(j)} - z_{q\sigma}^{(i)}} = 0\,. \tag{10}$$

It follows from (10) that a perturbation of type (9) gives rise to the infinitesimal shifts of zone levels:

$$z_{k\sigma}^{(i)} = \varepsilon_k^{(i)} + \frac{\pi}{N}\,\frac{d\varepsilon_k^{(i)}}{dk}\,\Theta_{k\sigma}^{(i)}\,. \tag{11}$$

The perturbation of the type (9) can also give rise to a local state splitting off zones. This question will be discussed in the next section. Now, we consider the effect of the substitution of an atom placed near the end of polyene chain ($\nu \ll N$). Then the shifts in a quasi-continuous spectrum are determined by the equation (see Appendix)

$$\operatorname{ctg}\pi\Theta_{k\sigma}^{(i)} = -\frac{\sin 2k}{2\lambda L_{k\sigma}^{(i)}(\nu)\sin^2 \nu k}\left[1 - \lambda L_{k\sigma}^{(i)}(\nu)\frac{\sin 2\nu k}{\sin 2k}\right], \tag{12}$$

where $\lambda = t/|\beta|$,

$$L_{k\sigma}^{(i)}(\nu) = \frac{1}{2|\beta|}\left[\varepsilon_k^{(i)} + (-1)^{\nu} a\tau_\sigma\right]. \tag{13}$$

The eigenfunctions corresponding to the eigenvalues (11) can be written as (for the derivation, see Appendix)

$$\varphi_{k\sigma}^{(i)}(\mu) = \sqrt{\frac{2}{N}}\,\tilde{C}_{k\sigma}^{(i)}(\mu)\sin(k^*\mu - \pi\Theta_{k\sigma}^{(i)}), \qquad (\mu > \nu), \tag{14}$$

$$\varphi_{k\sigma}^{(i)}(\mu) = \sqrt{\frac{2}{N}}\,\tilde{C}_{k\sigma}^{(i)}(\mu)\sin(\nu k - \pi\Theta_{k\sigma}^{(i)})\sin\mu k/\sin\nu k, \qquad (\mu < \nu), \tag{15}$$

$$\varphi_{k\sigma}^{(i)}(\nu) = \sqrt{\frac{1}{2N}\,\frac{d\varepsilon_k^{(i)}}{dk}}\,\sin\pi\Theta_{k\sigma}^{(i)}/(t\tilde{C}_{k\sigma}^{(i)}(\nu)\sin k\nu), \tag{16}$$

where $C_{k\sigma}^{(i)}(\mu) = \sqrt{\frac{2}{N}}\,\tilde{C}_{k\sigma}^{(i)}(\mu)\sin\mu k$, $k^* = k + \frac{\pi}{N}\Theta_{k\sigma}^{(i)}$. It follows from (14) that the perturbation results in the phase shift of the eigenfunctions for $\mu > \nu$. In order to define under what conditions the relations (10) (16) correspond to the self-consistent solution of Eq. (8) we evaluate $n_{\mu\sigma}$. Transforming (14) yields for the zone-state density at the μ-th atom

$$\begin{aligned}[n_{\mu\sigma}^{(1)}]_{\text{zone}} = \sum_k [\varphi_{k\sigma}^{(1)}(\mu)]^2 &= \frac{1}{2} + (-1)^{\mu+1}\delta_\mu\tau_\sigma \\ &+ \frac{a}{\pi}\int_0^{\pi/2} dk\left[\cos(2\mu k - 2\pi\Theta_{k\sigma}^{(i)})\right]/\varepsilon_k^{(2)} \qquad (\mu > \nu).\end{aligned} \tag{17}$$

Comparing (17) with (6) one can see that the perturbation effect on the zone-state density is transferred along the chain in the same way as the influence of its boundary, i.e. it sharply attenuates ($2^{|\mu-\nu|}$ times at the distance $|\mu - \nu|$). Thus, if $\mu - \nu \gg 1$ then (17) leads to $n_{\mu\sigma}^{(1)} = n_{\mu\sigma}^{(0)}$. It means that regardless of the non-linearity of the UHF equations, the impurity effect is local as in the case of linear Hamiltonians. Following [17] one can obtain for the electron density at the impurity atom (see Appendix)

$$n_{\nu\sigma}^{(1)} = \frac{d}{dt}\sum_k (z_{k\sigma}^{(1)} - \varepsilon_k^{(1)}). \tag{18}$$

Taking into consideration Coulson's and Lonquet-Higgins' relation [19], we reduce the expression (18) to the form

$$n_{\nu\sigma}^{(1)} = \frac{d}{dt}\,\frac{1}{2\pi i}\oint_C z\,d\ln\left[M_\sigma(z)/M_\sigma^{(0)}(z)\right], \tag{19}$$

where the integration is in the positive direction along the infinite half-circle ($\mathrm{Re}\,z < 0$) and imaginary axis in the complex plane z; $M_\sigma(z)$ and $M_\sigma^{(0)}(z)$ are determinants which vanish at the points $z = z_{k\sigma}^{(i)}$ and $z = \varepsilon_k^{(1)}$, respectively. The expression (19) can be written as [20]

$$\begin{aligned} n_{\nu\sigma}^{(1)} &= \frac{d}{dt}\,\frac{1}{2\pi i}\oint_C z\,d\ln[1-tG_{0\sigma}(\nu,\nu;z)] \\ &= -\frac{1}{2\pi i}\oint_C dz\,\frac{d}{dt}\ln[1-tG_{0\sigma}(\nu,\nu;z)]\,, \end{aligned} \tag{20}$$

where the function

$$G_{0\sigma}(\nu,\mu;z)=\sum_{kj}\frac{C_{k\sigma}^{(j)}(\nu)\,C_{k\sigma}^{(j)}(\mu)}{z-\varepsilon_k^{(j)}} \tag{21}$$

is the Green function:

$$\sum_{\mu'=1}^{N}[H_\sigma(\mu,\mu')-z\delta_{\mu\mu'}]\,G_{0\sigma}(\mu',\nu;z)=-\delta_{\mu\nu}\,.$$

The equivalence of expressions (19) and (20) results from the fact that in accordance with (10) the functions in bracets in (19) and (20) have simple poles and zeroes at the same points. Having failed to obtain general analytical expressions for (17) or (19) we now discuss some limiting cases. Let $|\lambda| \ll 1$. Then the integrand in (20) can be expanded in the series of λ

$$n_{\nu\sigma}^{(1)}=\frac{1}{2\pi i}\oint_C dz\,G_{0\sigma}(\nu,\nu;z)\sum_{n=0}^{\infty}[\lambda|\beta|\,G_{0\sigma}(\nu,\nu;z)]^n\,. \tag{22}$$

According to (21) $|\beta G_{0\sigma}(\nu,\nu;z)|<1$ if $z\in C$. Therefore, the series in (22) converges regularity if $|\lambda|<1$ and $z\in C$. As a consequence, integrating (22) term by term yields

$$n_{\nu\sigma}^{(1)}=\sum_k[C_{k\sigma}^{(1)}(\nu)]^2\sum_{n=0}^{\infty}[\lambda L_{k\sigma}^{(1)}(\nu)\sin 2\nu k/\sin 2k]^n\,. \tag{23}$$

It follows from (23) that

$$n_{\nu\sigma}^{(1)}=n_{\nu\sigma}^{(0)}+O(\lambda),\ |\lambda|\ll 1\,. \tag{24}$$

Thus, if $|\lambda|$ is small, the solution of (8) given by (10)–(18) and corresponding to the first iteration of the self-consistency procedure for a long polyene chain with impurity is a self-consistent one. The equation of second iteration has the following form

$$\sum_{\mu'=1}^{N}\{H_\sigma(\mu,\mu')+tA(\mu,\mu')+\gamma[n_{\mu\sigma}^{(1)}-n_{\mu\sigma}^{(0)}]\,\delta_{\mu\mu'}-z\delta_{\mu\mu'}\}\,\varphi_\sigma(\mu')=0\,. \tag{25}$$

Let us consider this equation for the case $\nu=1$, i.e. when the perturbation is localised at the first atom of the chain. It follows from (23) that

$$n_{1\sigma}^{(1)}-n_{1\sigma}^{(0)}=\sum_{n=1}^{\infty}\lambda^n(-1)^n f_{n\sigma}=-\lambda\Delta^{(1)}/\gamma\,, \tag{26}$$

where $\Delta^{(1)} > 0$,

$$f_{n\sigma} = \frac{1}{\pi} \int_0^{\pi/2} dk \sin^2 k \frac{(\sqrt{\cos^2 k + d^2} + d\tau_\sigma)^{n+1}}{\sqrt{\cos^2 k + d^2}} .$$

As seen from (26), the correction $-\lambda\Delta^{(1)}$ to the perturbation has the opposite sign to the initial perturbation $\lambda|\beta|$. Consequently, if λ is finite, the impurity is screened with zone electrones, as one should expect. It means that the effective value of the perturbation parameter $|\lambda'|$ is less than $|\lambda|$. It is easy to verify using (23) that this result is also valid if $\nu \neq 1$.

In order to evaluate differences $n_{\mu\sigma}^{(1)} - n_{\mu\sigma}^{(0)}$ for $\mu > \nu$ we now concider another limiting case: $|\lambda| \to \infty$. Then it follows from (12) that $\pi\Theta_{k\sigma}^{(i)} \to \nu k$. Hence, the relations (14)–(16) take the form

$$\lim_{|\lambda| \to \infty} \varphi_{k\sigma}^{(i)}(\mu) = \begin{cases} C_{k\sigma}^{(i)}(\mu - \nu), & (\mu > \nu) \\ 0 & (\mu \leqq \nu) . \end{cases} \tag{27}$$

It follows from (27) that a strong perturbation tears the link consisting of ν atoms off the chain. It is obvious that the functions (27) are self-consistent for the chain consisting of $N - \nu \approx N$ atomes because they coincide with the self-consistent zone functions of an ideal polyene chain. Substituting (27) into (17) and using (6) and (7) we obtain

$$|n_{\mu\sigma}^{(1)} - n_{\mu\sigma}^{(0)}| = |\delta_{\mu-\nu} - \delta_\mu| \leqq |\delta_1 - \delta_2| = 0.09 . \tag{28}$$

It means that the changes of values $n_{\mu\sigma}(\mu > \nu)$ are small even though the parameter $|\lambda|$ changes from zero to infinity. Thus, in order to obtain the zone functions $\varphi_{k\sigma}^{(i)}(\mu)$ of a long polyene chain with the ν-th atom substituted ($\nu \ll N$) as $\mu > \nu$, it is quite sufficient to restrict oneself to the first iteration of the self-consistency procedure for any value of the perturbation parameter λ. In particular, if $\nu = 1$ one can suppose that $n_{\mu\sigma}^{(1)} - n_{\mu\sigma}^{(0)} = \delta_{\mu 1} \left(\frac{-\lambda\Delta^{(1)}}{\gamma} \right)$. It means that the non-linearity of Eq. (8) can be neglected except for the fact that an initial perturbation parameter λ is to be replaced by its effective value λ', $|\lambda'| < |\lambda|$. On the other hand, if $\nu \neq 1$ and $|\lambda| \gg 1$ then functions $\varphi_\sigma(\mu)$ $(\mu < \nu)$ are to be close to the corresponding functions of a short polyene chain consisting of $\nu - 1$ atoms. It should be also noted that calculating $n_{\mu\sigma}^{(1)}$-values, we neglect the contribution of local-state functions, which have the amplitude (see Appendix):

$$|\varphi_{p\sigma}(\mu)| = C(e^{-\frac{1}{2}|\mu-\nu|q_0} + e^{-\frac{1}{2}(\mu+\nu)q_0}) , \tag{29}$$

where $q_0 > 0$. Hence it is clear that the functions are localized near the substituted atom. If $|\lambda| \gg 1$ then $q_0 \gg 1$, i.e. $\varphi_{p\sigma}(\mu) \sim \delta_{\mu\nu}$, if $|\lambda| \ll 1$ then $\varphi_{p\sigma}(\mu) \sim \lambda$ (see Appendix, the relation (A 17)). Thus, taking into account the local-state functions does not affect the relations (24) and (28).

Local States

General results obtained in the preceeding section can be used to consider the local electronic states in polyene chains with impurity.

As stated by Lifshits [17] and Koster and Slater [18], the wave functions of local states are determined by the equations

$$\varphi_\sigma(\nu) = -\sum_{\mu,\mu'} G_{0\sigma}(\nu,\mu';z)\, t_{\mu'\mu}\,\varphi_\sigma(\mu)\,. \tag{30}$$

Here $t_{\mu\nu}$ is the matrix of perturbation produced by substitution. If, for example, only one of the Coulomb integrals $\alpha_\nu \to \alpha_{\nu_0} + t\Delta\alpha_{\nu_0}$ changes, then $t_{\mu\mu'} = t\delta_{\mu\mu'}\delta_{\mu\nu_0}$. To solve (30) the following relation should be satisfied

$$\mathrm{Det}\left[\delta_{\mu\mu'} + t_{\mu\mu'}\, G_{0\sigma}(\mu,\mu';z)\right] = 0\,. \tag{31}$$

The relation (31) gives the equation for evaluating the energies of local states. Substituting $\varepsilon_k^{(j)}$ and $C_{k\sigma}^{(j)}(\mu)$ from (2)–(3) into (21) one can obtain expressions for $G_{0\sigma}(\mu,\nu;z)$ for the most interesting case of local states in the forbidden zone:

$$\begin{aligned}
&G_{0\sigma}(2\mu,2\nu;z_\sigma) = (z_\sigma - a\tau_\sigma)(2\beta^2\,\mathrm{sh}\,\Theta)^{-1}(-1)^{\mu-\nu}\left[e^{-|\mu-\nu|\Theta} - e^{-|\mu+\nu|\Theta}\right]\\
&G_{0\sigma}(2\mu-1,2\nu-1;z_\sigma) = (z_\sigma + a\tau_\sigma)(2\beta^2\,\mathrm{sh}\,\Theta)^{-1}(-1)^{\mu-\nu}\left[e^{-|\mu-\nu|\Theta} + e^{-|\mu+\nu|\Theta}\right]\\
&G_{0\sigma}(2\mu-1,2\nu;z_\sigma) = (-1)^{\mu-\nu}(\beta\,\mathrm{sh}\,\Theta)^{-1}\left[\mathrm{sh}\,\mu\Theta - \mathrm{sh}(\mu-1)\Theta\right] \quad (\nu \geqq \mu)\\
&G_{0\sigma}(2\mu-1,2\nu;z_\sigma) = (-1)^{\mu-\nu}(\beta\,\mathrm{sh}\,\Theta)^{-1}\left[1 - e^{\Theta}\right]e^{-\mu\Theta}\,\mathrm{sh}\,\mu\Theta \quad (\nu < \mu)
\end{aligned} \tag{32}$$

where Θ is given by the relation $\mathrm{ch}\,\Theta = -\dfrac{-(z_\sigma^2 - a^2 - 2\beta^2)}{2\beta^2}$.

The Green functions determined by (32) are identical with those for a diatomic (... A – B – A – B ...) chain with equal bonds in tight binding approximation (see the expressions (9a)–(9g) in [15] for $\beta_1 = \beta_2$ and $z = a\tau_\sigma$). If the values of $n_{\nu\sigma}$ were independent of ν this fact would be concidered as trivial because the Hamiltonian (1) and that of [15] are identical. However, as follows from (6), $n_{\nu\sigma}$ depends on ν and the self-consistent field near the end of a chain differs from the one in the middle of a chain. Thus, the Hamiltonian (1) differs from the Hamiltonian of [15] and coincides with the tight binding Hamiltonian for the diatomic chain in the case of the specific change of the Coulumb integrals $\alpha_{\mu A}$ and $\alpha_{\mu B}$ when μ increases. As the Green functions of [15] and (32) are identical, one can use the results of [15] to consider the conditions under which the local states arise. These conditions corresponding to the simplest perturbation, which is described by the change of the Coulomb integral of an atom or resonance integral of a bond, can be formulated as follows.

The infinitesimal change $\Delta\alpha$ of the Coulomb integral of an odd atom is sufficient to give rise to a local state in the forbidden zone.

On the other hand, the perturbation of an even atom with number $2l$ generates the local state in the forbidden zone only if

$$|\Delta\alpha| > 2\beta^2\left[\sqrt{a^2 + 4\beta^2} \pm a\right]^{-1}\frac{1}{l}\,. \tag{33}$$

The wave function and the energy of the local state caused by the perturbation of the first atom will be considered in more detail. Substituting $\nu = 1$ and $t_{\mu\nu} = t\delta_{\mu\nu}\delta_{\mu 1}$ into (31) one can obtain

$$0 = 1 + \lambda\left[\tilde{z}_{p\sigma} - d\tau_\sigma\right](1 + e^{-q_0})/\mathrm{sh}\,q_0\,, \tag{34}$$

with

$$\operatorname{ch} q_0 = 1 + 2(d^2 - \tilde{z}_{p\sigma}^2); \quad z_{p\sigma} = \frac{z_{p\sigma}}{|2\beta|} < d\,, \tag{35}$$

and

$$0 = 1 - \lambda[\tilde{z}_{p\sigma} - d\tau_\sigma](1 - e^{-Q_0})/\operatorname{sh} Q_0\,, \tag{36}$$

with

$$\operatorname{ch} Q_0 = 2[\tilde{z}_{p\sigma}^2 - d^2] - 1; \quad |\tilde{z}_{p\sigma}| > \sqrt{1 + d^2}\,. \tag{37}$$

As seen from (34), the infinitesimal change of the Coulumb integral of the first atom actually leads to the local state appearing in the forbidden zone. Its energy distance from the edge of the gap is equal to

$$|\tilde{z}_{p\sigma} - a| \approx a\lambda^2 = 1{,}1\,\lambda^2\,(\mathrm{eV})\,.$$

In the case of large perturbations $\lambda \to \pm\infty$ the Eq. (36) gives for the energy of local state: $\tilde{z}_{p\sigma} \to \pm\infty$.

Using the general Eq. (30) one can obtain the wave function of a local state, the first atom being perturbed

$$\varphi_{p\sigma}(\mu) = \tau_{p\sigma}(-1)^{\frac{\mu-1}{2}} e^{-\frac{\mu-1}{2} q_0}\,, \qquad (\mu \text{ is odd}) \tag{38}$$

$$\varphi_{p\sigma}(\mu) = \tau_{p\sigma}\lambda(-1)^{\frac{\mu}{2}} e^{-\frac{\mu}{2} q_0}\,. \qquad (\mu \text{ is even})\,. \tag{39}$$

Here $\tau_{p\sigma} = (1 - e^{-2q_0})/(1 + \lambda^2 e^{-2q_0})$ and q_0 are determined by (35). In accordance with (36) the greater the perturbation parameter the higher the degree of the localisation of the wave function of the impurity level in the region of impurity. It can be shown that the situation is exactly the same when $\nu \neq 1$.

If the perturbation of a chain can be simulated by a small change of the resonance integral of a bond, then it does not cause the local states to splitt off the allowed bands.

Discussion

Derived in the preceding section properties of local states differ essentially from those obtained under the assumption that the energy gap in the spectra of long polyene chains is due to the bond alternation [13]. In the latter case the perturbation giving rise to the local state in the forbidden zone is $\sim 1/l$ (l is the number of a perturbed atom) both for even and odd l. Thus, in contrast to the above model, the generation of a "surface" state ($l = 1$) is most difficult. In addition, the appropriate change of the resonance integral of a bond (weakening of a stronger bond or strengthening of a weaker bond) leads to two local states appearing in the forbidden zone.

The recent theoretical results [6, 12, 21, 22] provide an evidence in favour of the electron-correlation nature of the polyene-spectrum gap. But it appears likely that the question still remains doubtful [see, e.g., 23–25]. The above mentioned differences in the properties of local states can be used to investigate experimentally whether the energy gap is due to electron correlations or its appearence is a consequence of the bond alternation.

The results obtained seem to be useful in the study of the following question. In contrast to polyenes, the first optical transition frequency in the symmetric cyanide dyes tends to zero when the conjugated chain of the dye is lengthened [26]. Nevertheless, the long conjugated chains cyanine dyes and polyenes differ by their end groups only. Then, it is natural to correlate the above difference in the optical spectra of these molecules with the effect of nitrogenium atoms of the end groups of cyanine dyes. Indeed, the insertion of nitrogenium atoms into the chain can give rise to a local state near the bottom of an empty zone. As a consequence, the first optical transition corresponds to the transition of an electron from this local level[2] to an empty zone. The energy of this transition is small for long chains. Then, the extrapolation of experimental data can give zero value (or nearly zero value) of the first transition frequency.

Appendix

In this section we deal with the derivation of main relations used in the previous section. At first, we shall consider the sum in (10).

$$-G_{0\sigma}(\nu,\nu;z_{q\sigma}^{(i)}) \equiv \sum_{kj} \frac{|C_{k\sigma}^{(j)}(\nu)|^2}{\varepsilon_k^{(j)} - z_{q\sigma}^{(i)}} = \frac{4}{N} \sum_{k} \frac{\sin^2 k\nu[\varepsilon_q^{(i)} + a\tau_\sigma(-1)^\nu]}{\varepsilon_k^2 - \varepsilon_q^2 - 2\pi \frac{1}{N} \Theta_{q\sigma}^{(i)} \varepsilon_q^{(i)} \frac{d\varepsilon_q^{(i)}}{dq}} \tag{A 1}$$

$$+0\left(\frac{1}{N}\right) \equiv [\varepsilon_q^{(i)} + (-1)^\nu a\tau_\sigma] S^{(i)}(q,\sigma),$$

where we have used (11). To calculate $S^{(i)}(q,\sigma)$ we shall use the method developed by Lifshits [17]. Let us denote

$$S^{(i)}(q,\sigma) = S_1^{(i)}(q,\sigma) + S_1^{(i)}(q,\sigma) \tag{A 2}$$

and evaluate apart each of the two sums.

$$S_1^{(i)}(q\sigma) = \frac{4}{N^2} \sum_{k \neq q} \frac{2\pi\Theta_{q\sigma}^{(i)} d\varepsilon_q^{(i)}/dq\,\varepsilon_q^{(i)} \sin^2 k\nu}{(\varepsilon_k^2 - \varepsilon_q^2)\left(\varepsilon_k^2 - \varepsilon_q^2 - 2\frac{\pi}{N}\Theta_{q\sigma}^{(i)} \frac{d\varepsilon_q^{(i)}}{dq}\right)}$$

$$-\frac{2}{\pi} \frac{\sin^2 q\nu}{\Theta_{q\sigma}^{(i)} \varepsilon_q^{(i)} \frac{d\varepsilon_q^{(i)}}{dq}} = \frac{2\sin^2 q\nu}{\frac{d\varepsilon_q^{(i)}}{dq}\varepsilon_q^{(i)}} \left\{\frac{2}{N^2} \sum_{k\neq q} \frac{\pi\Theta_{q\sigma}^{(i)}}{(k-q)\left(k-q-\frac{\pi}{N}\Theta_{q\sigma}^{(i)}\right)} - \frac{1}{\pi\Theta_{q\sigma}^{(i)}}\right\}$$

$$+0\left(\frac{1}{N}\right) \approx \frac{2\sin^2 q\nu}{\varepsilon_q^{(i)} \frac{d\varepsilon_q^{(i)}}{dq}} \left\{\sum_{n\neq 0} \frac{\pi\Theta_{q\sigma}^{(i)}}{\pi n(\pi n - \pi\Theta_{q\sigma}^{(i)})} - \frac{1}{\pi\Theta_{q\sigma}^{(i)}}\right\} \tag{A 3}$$

$$= -2\sin^2 q\nu \operatorname{ctg}\pi\Theta_{q\sigma}^{(i)}/(\varepsilon_q^{(i)} d\varepsilon_q^{(i)}/dq);$$

$$S_2^{(i)}(q,\sigma) = \frac{4}{N} \sum_{k\neq q} \frac{\sin^2 k\nu}{\varepsilon_k^2 - \varepsilon_q^2} = \frac{1}{2\pi\beta^2} \fint_0^{\pi} \frac{1-\cos\nu k}{\cos k - \cos 2q}\,dk + 0\left(\frac{1}{N}\right), \tag{A 4}$$

---

[2] The conjugated chains of cyanine dyes consist of an odd number of atoms (N). But, the number of π-electrons N_e is even: $N_e = N \mp 1$. If $N_e = N + 1$ then the local state considered above is occupied in the ground state. If $N_e = N - 1$ then there is a hole in a valency zone of cyanine dye and the explanation of optical experiments is trivial.

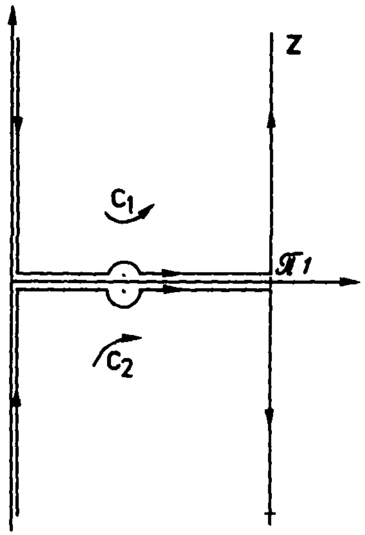

Fig. 1. The contours for the evaluation of integrals in (A 6)

where $⨍$ denotes the value principale (V.p.) of a corresponding integral. In order to evaluate (A 4) it needs to calculate

$$⨍_0^\pi \frac{\cos \nu k}{\cos k - \cos 2q} dk = I_1 + I_2 \equiv I\,, \tag{A 5}$$

where

$$\begin{aligned} I_1 &= \frac{1}{2} ⨍_0^\pi dx \frac{e^{i\nu x}}{\cos x - \cos q}\,, \\ I_2 &= \frac{1}{2} ⨍_0^\pi dx \frac{e^{-i\nu x}}{\cos x - \cos q}\,. \end{aligned} \tag{A 6}$$

The integrals (A 6) can be evaluated by means of the residuum theory. The integral I_1 is taken along the contour C_1, I_2-along C_2. The contours C_1 and C_2 are given on Fig. 1. After the calculations required performed one can obtain

$$I = \frac{\pi i}{2} \operatorname{res}\left(\frac{e^{i\nu z} - e^{-i\nu z}}{\cos z - \cos q}\right)\Big/_{z=q} = \pi \frac{\sin \nu q}{\sin q}\,. \tag{A 7}$$

The substitution (17) into (A 5) and (A 4) results in the relation

$$S_2^{(i)}(q, \sigma) = -\frac{1}{2\beta^2} \frac{\sin 2\nu q}{\sin 2q}\,. \tag{A 8}$$

The Eq. (12) can be obtained from (A 3), (A 8), (A 1) and (10). The eigenfunctions of (8) are defined as [17]

$$\varphi_{q\sigma}^{(i)}(\mu) = -t\tau_{q\sigma}^{(i)} \sum_{k,j} \frac{C_{k\sigma}^{(j)}(\mu) C_{k\sigma}^{(j)}(\nu)}{\varepsilon_k^{(j)} - z_{q\sigma}^{(i)}}\,. \tag{A 9}$$

The sum which stands in (A 9) is calculated just like as $S^{(i)}(q, \sigma)$. Let us evaluate a normalisation constant $\tau_{q\sigma}^{(i)}$.

$$\sum_{\mu=1}^{N} [\varphi_{q\sigma}^{(i)}(\mu)]^2 = \left| \frac{\tilde{C}_{q\sigma}^{(i)}(\nu)\sin q\nu}{d\varepsilon_q^{(i)}/dq} t\tau_{q\sigma}^{(i)} \right|^2 \frac{2}{N} \sum_k \frac{1}{\left(k - q - \frac{\pi}{N}\Theta_{q\sigma}^{(i)}\right)^2}$$
$$+ 0\left(\frac{1}{N}\right) = 2N(t\tau_{q\sigma}^{(i)})^2 \left| \frac{\tilde{C}_{q\sigma}^{(i)}(\nu)\sin q\nu}{(d\varepsilon_q^{(i)}/dq)\sin \pi\Theta_{q\sigma}^{(i)}} \right|^2 = 1\,. \tag{A 10}$$

Substituting $\tau_{q\sigma}^{(i)}$ from (A 10) into (A 9) one obtains (14)- (16). It follows from (A 10) that

$$[t\tau_{q\sigma}^{(i)}]^2 = \sum_{k,j} \left| \frac{C_{k\sigma}^{(j)}(\nu)}{\varepsilon_k^{(j)} - z_{q\sigma}^{(i)}} \right|^2$$
$$= \left| \frac{dz_{q\sigma}^{(i)}}{dt} \right|^{-1} \frac{d}{dt} \sum_{k,j} \frac{C_{k\sigma}^{(j)}(\nu) C_{k\sigma}^{(j)}(\nu)}{\varepsilon_k^{(j)} - z_{q\sigma}^{(i)}} = - \frac{1}{t^2} \left| \frac{dz_{q\sigma}^{(i)}}{dq} \right|^{-1}. \tag{A 11}$$

Taking also into account that in accordance with (A 9) and (10) $\varphi_{q\sigma}^{(i)}(\nu) = \tau_{q\sigma}^{(i)}$, one obtains (18).

Now let us consider functions $G_{0\sigma}(\nu, \mu; z)$, where $\frac{|z|}{2|\beta|} \notin [d, \sqrt{1 + d^2}]$, i.e. for states splitting off zones. Using (2), (3) one obtains

$$G_{0\sigma}(\nu, \nu; z) = - \sum_{k,j} \frac{[C_{k\sigma}^{(j)}(\nu)]^2}{\varepsilon_k^{(j)} - z}$$
$$= \frac{\tilde{z} + (-1)^\nu d\tau_\sigma}{\pi|\beta|} \int_0^\pi dk(1 - \cos \nu k)/(\cos k + \alpha)\,, \tag{A 12}$$

where

$$\tilde{z} = z/2|\beta|; \quad d = a/2|\beta|; \quad \alpha = 1 + 2(d^2 - \tilde{z}^2)\,.$$

The integral in (A 12) is calculated like as the integral (A 5) except the poles of the integrand are in the complex plane k on the lines $\mathrm{Re}\,k = 0$ ($\tilde{z}^2 > 1 + d^2$) and $\mathrm{Re}\,k = \pi$ ($|\tilde{z}| < d$). Having carried out the calculations required one obtains

$$\int_0^\pi dk \frac{\cos \nu k}{\cos k + \alpha} = \begin{cases} (-1)^\nu \pi e^{-\nu q_0}/\mathrm{sh}\, q_0, & (\alpha > 0) \\ \pi e^{-\nu Q_0}/\mathrm{sh}\, Q_0, & (\alpha < 0) \end{cases} \tag{A 13}$$

where

$$\mathrm{ch}\, q_0 = 1 + 2(d^2 - \tilde{z}^2), \quad (\tilde{z}^2 < d^2)$$
$$\mathrm{ch}\, Q_0 = 2(\tilde{z}^2 - d^2) - 1, \quad (z^2 > 1 + d^2)\,.$$

Using (A 13) one can calculate all functions $G_{0\sigma}(\nu, \mu, z)$ with $\tilde{z}^2 > 1 + d^2$ or $\tilde{z}^2 < d^2$. In particular, one can obtain equations for local energies

$$1 - tG_{0\sigma}(\nu, \nu; z_{p\sigma}) = 0 \tag{A 14}$$

and for corresponding functions

$$\varphi_{p\sigma}(\mu) = t\tau_{p\sigma} G_{0\sigma}(\mu, \nu; z_{p\sigma})\,. \tag{A 15}$$

The relations (29), (32), (34)–(39) results from (A 14) and (A 15). If $|\lambda| \gg 1$, then it follows from (A 13) and (A 14) that $q_0(Q_0) \gg 1$. Using (29) and (16) one can see that if $|\lambda| \ll 1$ then

$$\tau_{p\sigma}^2 \sim t^{-2}(1 - e^{-2q})\operatorname{sh}^2 q\,, \quad (q = q_0, Q_0)$$

hence

$$|\varphi_{p\sigma}(v)|^2 \sim \lambda^2\,. \tag{A 16}$$

References

1. Murrel, J. N.: The theory of electronic spectra of organic molecules, p. 78. New York-London: 1963.
2. Lonquet-Higgins, H. C., Salem, L.: Proc. Royal Soc. (London) A **251**, 172 (1959)
3. Ooshika, Y.: J. physic. Soc. Japan **12**, 1246 (1957).
4. Misurkin, I. A., Ovchinnikov, A. A.: Teor. i Eksperim. Khim. **3**, 431 (1967).
5. — — Teor. i Eksperim. Khim. **4**, 3 (1968).
6. — — Theoret. chim. Acta (Berl.) **13**, 115 (1969).
7. Fukutome, H.: Progr. theoret. Physics (Kyoto) **40**, 998, 1227 (1968).
8. Berggren, K.-F., Johansson, B.: Int. J. quant. Chemistry **2**, 483 (1968).
9. Johansson, B., Berggren, K.-F.: Physic. Rev. **181**, 855 (1969).
10. Ukrainsky, I. I., Kruglyak, Yu. A.: Ukr. Fiz. Zh. **15**, 1068 (1970).
11. Kruglyak, Yu. A., Ukrainsky, I. I.: Int. J. quant. Chemistry **4**, 57 (1970).
12. Popov, N. A.: Zh. Strukt. Khim. **10**, 533 (1969).
13. Kventsel, G. F.: Teor. i Eksperim. Khim. **4**, 291 (1968).
14. — Kruglyak, Yu. A.: Theoret. chim. Acta (Berl.) **12**, 1 (1968).
15. – Teor. i Eksperim. Khim. **5**, 435 (1969).
16. – Ukrainsky, I. I.: Ukr. Fiz. Zh. **16**, 615 (1971).
17. Lifshits, I. M.: Zh. Eksperim. i Teor. Fiz. **17**, 1017, 1076 (1947); Nuovo Cim. Suppl. **4**, 716 (1956).
18. Koster, G. F., Slater, J. C.: Physic. Rev. **95**, 1167 (1954).
19. Coulson, C. A., Lonquet-Higgins, H. C.: Proc. Royal Soc. (London) A **191**, 39 (1947).
20. Maradudin, A. A., Montroll, F. W., Weiss, G. M.: Theory of lattice dynamics in the harmonic approximation, Chapt. Y. New York-London: 1963.
21. Harris, R. A., Falicov, L. M.: J. chem. Physics **51**, 5034 (1969).
22. Ukrainsky, I. I.: Int. J. quant. Chemistry (in press).
23. Salem, L.: J. chem. Physics **52**, 1115 (1970).
24. Harris, R. A., Falikov, L. M.: J. chem. Physics **52**, 1115 (1970).
25. Van-Catledge, F. A., Allinger, N. L.: J. Amer. chem. Soc. **91**, 2582 (1969).
26. Platt, J. R.: J. chem. Physics **25**, 80 (1956).

Dr. I. I. Ukrainsky
Institute of Theoretical Physics
Academy of Sciences of the Ukraine
252130 Kiev, Ukraine
USSR

Theoret. chim. Acta (Berl.) 25, 372–381 (1972)
© by Springer-Verlag 1972

Theoretical Study of the Photodimerization of Pyrimidine Bases

J. Bertran

Instituto de Biología Fundamental, Universidad Autónoma de Barcelona,
Avd. San Antonio Mª Claret 171, Barcelona-13, Spain

Received January 7, 1972

The experimental results are correctly interpreted as from the delocalized model of the transition state and the theory of perturbations. The surfaces of the energy of interaction between both molecules in function of different coordinates of reaction make it possible to discuss the concerted nature of photodimerization and permit the two conjugated systems to be added between carbon atoms 5 and 6 of both molecules.

Die experimentellen Resultate werden mit Hilfe eines delokalisierten Modells des Übergangszustandes und der Störungstheorie richtig interpretiert. Die Energiehyperfläche der Wechselwirkung zwischen den beiden Molekülen als Funktion verschiedener Reaktionskoordinaten erlaubt die Diskussion des konzertierten Ablaufs der Photodimerisation und der Addition der beiden konjugierten Systeme, die zwischen den Kohlenstoffatomen 5 und 6 der beiden Moleküle stattfindet.

Les résultats expérimentaux sont correctement interprétés à partir du modèle delocalisé de l'état de transition et de la théorie des perturbations. Les surfaces de l'énergie d'interaction entre les deux molécules en fonction aux différentes coordonnées de réaction permettent de discuter le caractère concerté de la photodimerisation et que l'addition des deux systèmes conjugués se réalise entre les carbones 5 et 6 des deux molécules.

1. Introduction

The research activities in photochemistry of the pyrimidine bases of the DNA during the last few years can be seen in frequent review articles [1–5]. From the results thus obtained, one can cite the following.

The photodimerization of the thymine, discovered some ten years ago [6] has also been observed in the other pyrimidine bases, uracil [7, 8] and cytosine [9, 10].

The formation of mixed dimers has also been observed [9, 11].

Experimentation with DNA of different composition has shown the following relative efficiency in the formation of dimers: $\widehat{TT} > \widehat{CT} > \widehat{CC}$ [12].

Theoretically, four conformations of final products are possible (Fig. 1). In this study, the nomenclature *cis-syn*, *trans-syn*, *cis-anti*, and *trans-anti* has been adopted to designate them [13]. In certain conditions, the four conformations are obtained [14, 15], whilst in other cases, the *cis-syn* conformation is predominant [16, 17].

The analysis by x-ray diffraction techniques has permitted the determination of the geometry of the dimers [18–23]. In the *cis-syn* conformation, the planes of both bases are not parallel, the bases have turned around the bonds 5–6, opening themselves, furthermore, the cyclobutane formed in the dimerization

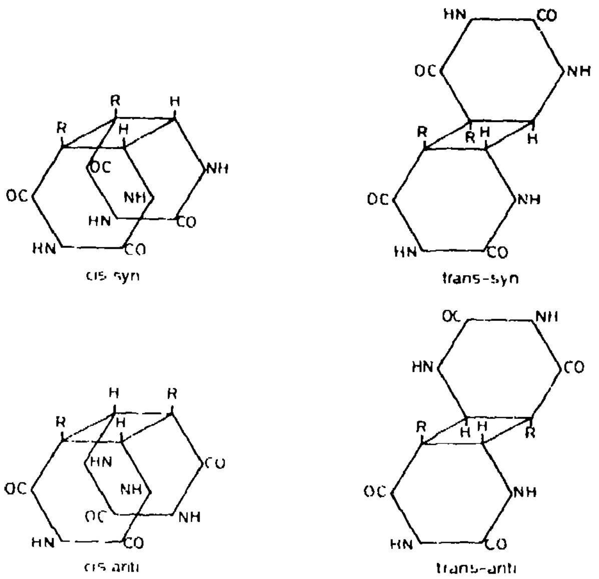

Fig. 1. Possible conformations of thymine and uracil dimers ($R = CH_3$ thymine dimers; $R = H$ uracil dimers)

is twisted by a turn of some 28° around the axis which unites the two midpoints of the 5–6 bonds.

The reaction seems to be concerted with both new bonds, closing itself simultaneously [24]. The bimolecular process results when one base, in a fundamental electronic state, interacts with another, in its first excited state. A metastable dimer in an excited state appears to be the intermediate product [25].

$$P + P^* \xrightarrow[a]{} \widehat{PP}^* \xrightarrow[b]{} \widehat{PP}\,.$$

One supposes that the determining step of the velocity of reaction is the *a*. The intervention of the first singlet excited state or the first triplet state depends upon the conditions of reaction [15]. In diluted solutions, one deals, without doubt, with the first excited triplet state, due to its longer life span [26–28]. In a solid phase and in concentrated solutions, the intervention of the first excited singlet state seems assured [15, 29, 30].

Following the pioneering works of Pullman and Mantione [31, 32] the reaction of the photodimerization of the pyrimidine bases has been interpreted from the diminishing with the excitation of the bond index between the carbons 5 and 6 [33–36]. This carries a notable increase of the free valence above these centres in the first excited state. This static index is characteristic for reactions of addition. Also, one has underlined the high spin density about the carbons 5 and 6 in the first excited state. This corresponds to grand coefficients in these centres in the semioccupied orbitals. The electronic excitation is found to be highly localized in the double bond between the carbons 5 and 6, which are the points of photodimerization.

Other theoretic works try to interpret the photodimerization of the pyrimidine bases by evaluating the energy of interaction between the monomers through the perturbation theory, limiting itself to the frontier orbitals [37], or including all the orbitals π, and the overlaps, explicitly [38].

In this present work, one is trying to interpret the experimental facts previously enumerated from the dynamic indices. One adopts the delocalized model of the transition state, and one studies the interaction of one base in a fundamental state with another in an excited state, at the beginning of the reaction, through the theory of perturbations. By always using a monoelectronic operator, the distinction between the first single excited state, and the triplet is not considered. Finally, one has to underline the kinetic nature of the present study, and this differentiates it from the energetic studies made on the stability of the different conformations of the final products [13, 19].

2. Method of Calculation

The calculations based on the delocalized model of the transition state were carried out according to the method previously described [40]. The conditions under which this method can be applied to cycloadditions of two conjugated systems have been exposed, by studying the photodimerization of the anthracene [41]. Faced with the Wheland model, this model of the transition state corresponds to an extension of the delocalization. This is suitable for rapid reactions in which the transition state does not separate itself far away from the reactants. At intermolecular distances which are great, the Hamiltonian operator in each conjugated molecule differs only slightly from the original, in a manner in which the σ/π separation would still be practically valid. The wave function of the transition state can be constructed from molecular orbitals covering all the system for the electrons π of both molecules, whilst the electrons σ remain localized in each molecule, acting as a hard core which forbids too close an approach. The extension of the Hückel method to the whole delocalized system of electrons is based on an orbital overlap argument, and not on a symmetry one. This can be done because the idea of delocalized bond does not include any element of symmetry.

The delocalization energy is the difference in energy, in units of β, between the transition state containing the whole delocalized system in its first excited state and the inital state of two molecules of pyrimidine bases, one in its ground state and the other in its first excited state. The larger the value of delocalization energy, the lower in energy is the transition state for formation of the photodimer. In some calculations the resonance integrals between carbons 5 and 6 of both molecules have been only taken into account. The resonance integrals are assumed to be equal to 0.5. This value corresponds to "σ" type overlap of 0.125 between two carbon $2p$ SCF orbitals with atoms 3 Å apart. This distance is common for all charge transfer electronic delocalization. In other calculations all the resonance integrals between atomic $2p_z$ orbitals of both molecules have been taken into account. These resonance integrals are assumed to be proportional to overlap integrals [42]. The intermonomer overlaps were obtained in the following way: for every pair of atoms, spreading over both monomers, the $2p_z$ orbitals were decomposed into components of σ and π mutual symmetry. The overlap of the components with a $\sigma-\sigma$ symmetry was calculated by equations suggested by Roothaan [43]. The contribution of the components with the $\pi-\pi$ symmetry to the overlap was disregarded. Finally eigenvalues and wavefunctions of bases in a Hückel approximation have been obtained by using the parameters suggested by Hoffman and Ladik [44].

The calculations based on the theory of perturbations has been done using the approximation proposed by Salem [45]. The energy of interaction between the conjugated systems is expressed in function of the overlaps between the atomic orbitals $2p_z$ of both molecules. Two limitations are imposed. Each atomic centre only interacts with one centre of the other molecule. The resonance integrals are small when compared with the unit (i.E. $\leqq 0.2$).

One supposes that both molecules have orbital bands σ and π well separated. One only evaluates the energy of interaction coming from the molecular orbitals π. The contribution to the stabilisation of the orbitals σ will be depreciable, since it comes from terms of perturbation of the 2° order between molecular orbitals occupied by one molecule and vacant orbitals of the other. In the denominator the difference of energy between the orbitals considered will be elevated, and a small term will figure in the numerator, which corresponds to a weak overlapping.

The extended Hückel method [46] is also used for calculating comparatives.

3. Results and Discussion

The Table 1 presents the energy of delocalization for the photodimerization of the pyrimidine bases. Only the resonance integrals between the carbons 5 and 6 of both molecules have been taken into account.

Table 1. Delocalization energies

	Syn	*Anti*
Uracil	0.703	0.608
Thymine	0.699	0.618
Cytosine	0.588	0.464
Cytosine-thymine	0.600 C*	0.503 C*
	0.700 T*	0.603 T*

The delocalization energy of the anthracene in the photodimerization is 0.566 [41]. Attending only to this factor, the photodimerization is presented as more favourable for the pyrimidine bases. The relative efficiency in the formation of dimers between the cytosine and the thymine [12] agrees well with the delocalization energies evaluated. Take note that the delocalization energy of the mixed photodimer will distinct, following that the excited reactant molecule will be that of the cytosine (C*), or the thymine (T*). One must signal the difference between theoretic results, and experimental values. The latter correspond to equilibrium constants, whilst the former are in regard to constants of velocity of the direct reaction of the dimerization.

By virtue of the delocalization energies obtained, the formation of *syn* conformations (head-to-head) will be kinetically more favourable than the formation of *anti* conformations (head-to-tail). This result, already previously obtained for the thymine [37], has a general character. To study the conformations *cis* (endo) and *trans* (exo) it is necessary to consider the interactions between all the centres of both molecules. The Table 2 presents the results obtained for the uracil and cytosine. The uracil was selected to avoid the problems stemming from the methyl group of the thymine. The calculations have been done with the two bases in parallel planes at a distance of 2.8 Å. Later on, this selection will be justified. Using Slater orbitals at this distance, one obtains lower values for the overlap integrals with respect to those obtained with atomic orbitals SCF. The Table 2 also contains the interaction energy evaluated by the theory of perturbations, and the increase of energy between the transition state and reagents evaluated by the extended Hückel method.

Table 2

	Delocalization energies		Interaction energies		ΔE^{*} computed by EHMO	
Uracil	Exc.	Fund.	Exc.	Fund.	Exc.	Fund.
Cis-syn	0.446	0.038	0.224	−0.130	−0.191	0.997
Trans-syn	0.362	0.030	0.229	−0.059	−0.144	0.755
Cis-anti	0.300	0.069	0.116	−0.102	0.248	0.868
Trans-anti	0.306	0.037	0.184	−0.050	−0.064	0.716
Cytosine						
Cis-syn	0.412	0.034	0.196	−0.139	---	—
Trans-syn	0.309	0.032	0.169	−0.051	--	
Cis-anti	0.251	0.069	0.072	−0.100		-
Trans-anti	0.265	0.044	0.102	−0.043		

The delocalization and interaction energies are given in units of β and ΔE^{*} in eV.

The energies obtained by the three methods present a displacement, introduced in the theory of perturbations by repulsive terms resulting from the interaction of orbitals π doubly occupied of both molecules, owing to the overlapping, and in the Hückel extended method, by the repulsion of σ orbitals. It is interesting to note that relative results between the different conformations in the photodimerization and the dimerization, with both molecules in a fundamental state, remain practically constant. One must note that the results of the extended Hückel method come given in the eV and not in β units. The *cis-syn* conformation is the most favoured. The inclusion of all valence electrons does not modify this result. However, when using a monoelectronic operator, one does not bear in mind the electrostatic interaction between both molecules. An exploratory calculation with the distribution of the π charges gives a high repulsion in the *cis-syn* conformation, in such a way that the electrostatic factor comes in to compensate the energy differences between the different conformations. To discuss the conformation kinetically most favoured, it appears to be indespensable to introduce a bielectronic

Hamiltonian operator, as has already been done for reactions with both molecules in the fundamental state [47, 48]. It is necessary to give only a provisional value to the results obtained with a monoelectronic operator.

Experimentally, the *cis-syn* conformation presents a double rotation around the 5–6 bonds, and the line which unites the midpoints of the 5–6 bonds. One tries to study whether the improving reaction initiate these rotations which present the geometry of the final product. The theory of perturbations is inadequate to study the rotation around the line which unites the two mid-points of the 5–6 bonds, by excluding the interaction between 3 or more centers in the approximation used.

One has evaluated the delocalization energy by turning the upper base to the distance of 2.8 Å. In the transition state of the photodimerization of the uracil, there was an energetic minimum presented at 9° of rotation, 0.004 β underneath the starting position. On the other hand, the electrostatic repulsion diminishes with the rotation. Because of this, it appears that one can be sure that the rotation around the line which unites the mid-points of the 5–6 bonds is already initiated in the transition state. A similar result, but with a higher rotation of 28°, had been discovered earlier by another method [38].

The angle formed by the two planes of the bases at coming together can be studied by constructing the interaction energy surface in function of the distance and the angle of the turn. The analytical expression of the interaction energy in function to the overlap integrals between the orbitals $2p_z$ of both molecules permits a rapid evaluation of the points of the surface. Table 3 contains said equations for the *cis-syn* and *cis-anti* conformations of uracil, of the thymine and the cytosine. S_{rp} indicates the overlap integral between the $2p_z$ orbitals of the centre r of one molecule, and the centre p of another. The numeration which has been adopted for the different centres is to be found in Fig. 2. The expressions for the second order terms have been truncated, owing to their length. So for example, the equation for the uracil *cis-syn* contains 44 terms.

Table 3. Equations of interaction energy in function of overlap integrals

Uracil

$$\textit{Cis-syn}\ \Delta E = 1{,}060\ S_{11} + 0{,}109\ S_{22} + 0{,}198\ S_{33} + 0{,}282\ S_{44} + 1{,}915\ S_{55} + 1{,}668\ S_{66} + 0{,}470\ S_{77} + 0{,}299\ S_{88} - 5{,}692\ S_{11}^2 - 1{,}421\ S_{11}S_{22} - \cdots$$

$$\textit{Cis-anti}\ \Delta E = -0{,}440\ S_{14} + 0{,}131\ S_{23} + 0{,}131\ S_{32} - 0{,}440\ S_{41} + 1{,}402\ S_{56} + 1{,}402\ S_{65} + 0{,}117\ S_{14}^2 - 1{,}176\ S_{14}S_{23} - \cdots$$

Thymine

$$\textit{Cis-syn}\ \Delta E = 1{,}034\ S_{11} + 0{,}104\ S_{22} + 0{,}203\ S_{33} + 0{,}320\ S_{44} + 1{,}891\ S_{55} + 1{,}663\ S_{66} + 0{,}489\ S_{77} + 0{,}288\ S_{88} + 0{,}001\ S_{99} + 0{,}006\ S_{1010} - 5{,}688\ S_{11}^2 - 1{,}426\ S_{11}S_{22} - \cdots$$

$$\textit{Cis-anti}\ \Delta E = -0{,}462\ S_{14} + 0{,}125\ S_{23} + 0{,}125\ S_{32} - 0{,}462\ S_{47} + 1{,}441\ S_{56} + 1{,}441\ S_{65} + 0{,}083\ S_{14}^2 - 1{,}181\ S_{14}S_{23} - \cdots$$

Cytosine

$$\textit{Cis-syn}\ \Delta E = 1{,}027\ S_{11} + 0{,}050\ S_{22} + 0{,}530\ S_{33} + 0{,}735\ S_{44} + 1{,}290\ S_{55} + 1{,}362\ S_{66} + 0{,}659\ S_{77} + 0{,}347\ S_{88} - 5{,}466\ S_{11}^2 - 1{,}191\ S_{11}S_{22} - \cdots$$

$$\textit{Cis-anti}\ \Delta E = -0{,}689\ S_{14} + 0{,}124\ S_{23} + 0{,}124\ S_{32} - 0{,}689\ S_{41} + 0{,}798\ S_{56} + 0{,}798\ S_{65} + 0{,}481\ S_{11}^2 - 1{,}286\ S_{14}S_{23} - \cdots$$

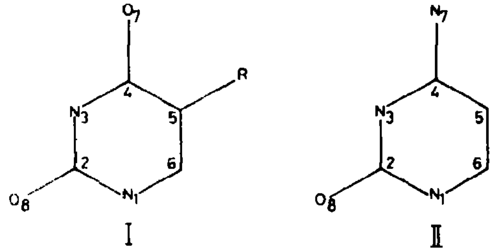

Fig. 2. The numeration of centres. I. R = H uracil, R = CH$_3$ thymine; II. cytosine

At great distances, the terms of the first order will be predominant. Among these, those which affect the 5 and 6 centres have the highest coefficients, owing to the high coefficients of the frontier orbitals in these positions. The Figs. 3, 4, and 5 present the interaction energy surfaces for the uracil *cis-syn*, the uracil *cis-anti* and the cytosine *cis-syn*. The most favourable path of reaction will be perpendicular to the isoenergetic lines, in the direction of the higher interaction energies. This path is the one which corresponds to the maximum stabilisation. In the Figs. 3, 4, and 5, a dotted line has been drawn for the most favourable path of reaction, starting from a position parallel to both molecules at great distances. The molecules come together in parallel until the distance of 2.8 Å. After this distance, the approximation is accompanied by a rapid turn of both molecules around the 5–6 bonds. A rapid decrease in the interaction energy impedes a parallel approximation after the distance indicated. If one had used the SCF

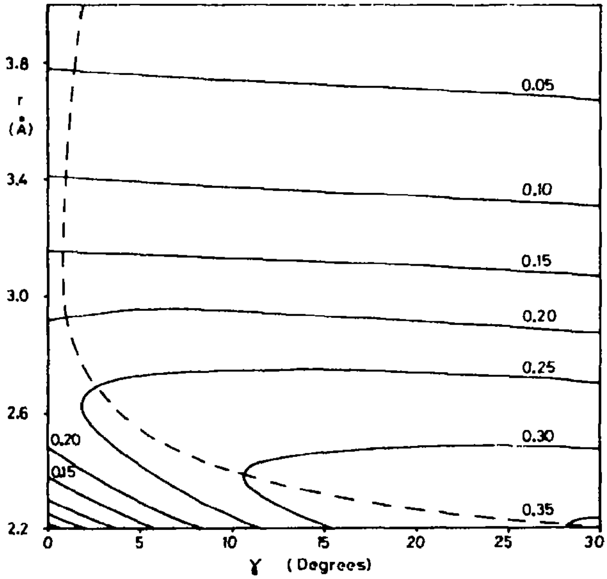

Fig. 3. Interaction energy surface between two *cis-syn* uracils, r distance between 5–6 bonds of both molecules, γ angle formed by the two planes of the bases

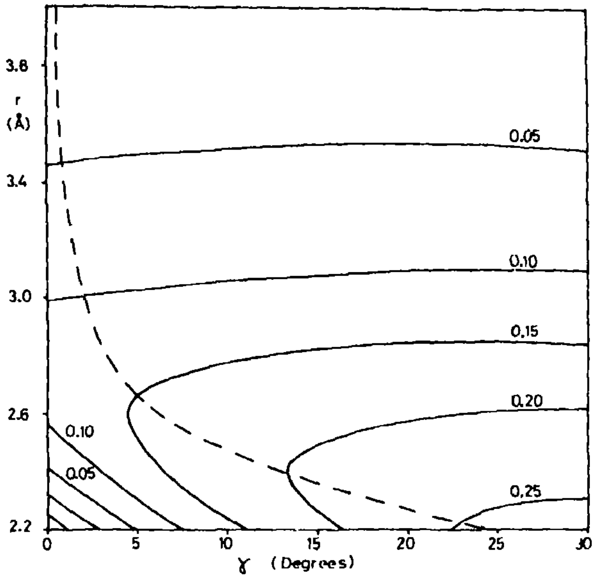

Fig. 4. Interaction energy surface between two *cis-anti* uracils, r and γ as in Fig. 3

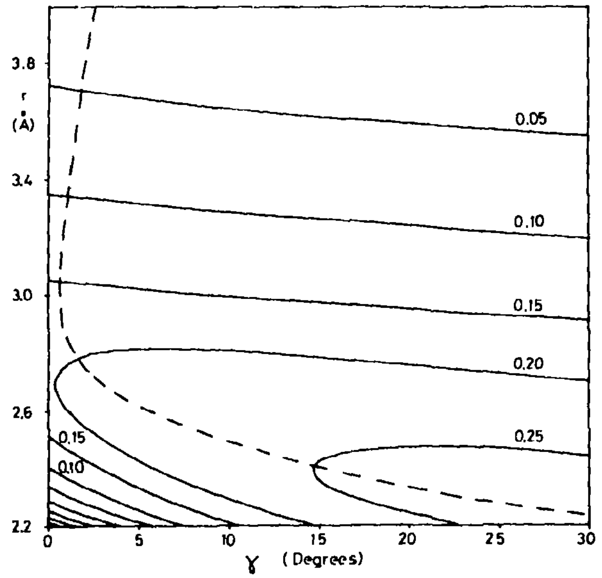

Fig. 5. Interaction energy surface between two *cis-syn* cytosines, r and γ as in Fig. 3

atomic orbitals instead of the Slater orbitals to evaluate the overlap integrals, one would have found a greater distance. Even though the interaction surface represents only one of the components of the potential surface, the path of reaction found, seems to be qualitively correct, since other factors, such as the electrostatic repulsion, confirm it.

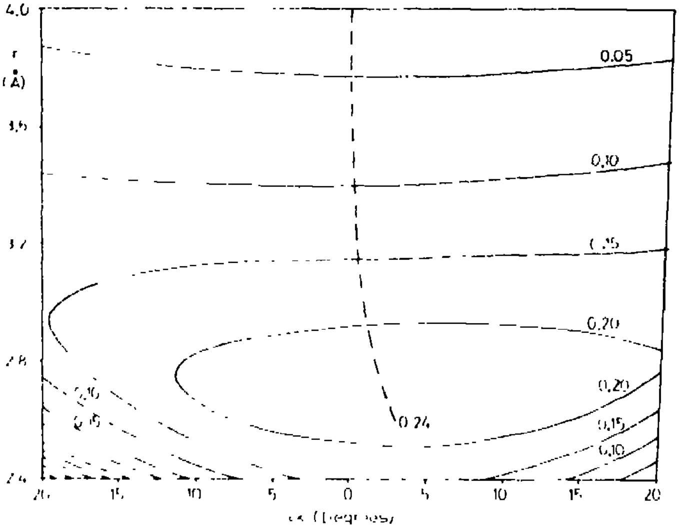

Fig. 6. Interaction energy surface between two *cis-syn* uracils, *r* distance between the midpoints of 5-6 bonds of both molecules, α angle formed by the two 5-6 bonds of the bases

The equations of the interaction energy permit the study also of the concerted character of the process of photodimerization. For the *anti* conformations it is undoubtable that the new bonds are formed at the same velocity, since there is an axis of symmetry in existance, but for the *syn* conformations, this is open to question. Fig. 6 presents the interaction energy surface in function of the distance between the two midpoints of the 5-6 bonds, and the angle formed by these two bonds. For positive values, the 6-6 bond is formed more rapidly, and vice-versa, the 5-5 bond for negative values. It can be seen that if both 5-6 bonds are parallel at great distances, they remain in parallel in the course of the reaction. Even if both bonds for a certain angle at great distances they will follow on adapting a parallel conformation as the reaction advances, since the no-null angles appear to have a high diminishing of the interaction energy, as the distance between the two bases decreases. The concerted character of the reaction seems, therefore, to be confirmed by this theoretic study.

Acknowledgement. The author is grateful to the European Molecular Biology Organization for financial support to visit Quantum Chemistry Group of Uppsala University where some calculations were carried out.

References

1. McLaren, A. D., Shugar, D.: Photochemistry of proteins and nucleic acids, Oxford: Pergamon 1964.
2. Setlow, J. K.: Current Topics Rad. Res. 2, 195 (1966).
3. Smith, K. C.: Radiation Res. Suppl. C, 54 (1966).
4. Setlow, R. B.: Progress in Nucleic Acid Res. and Mol. Biol. 8, 257 (1968).
5. Burr, J. G.: Advances Photochemistry 6, 193 (1968).
6. Beukers, R., Berends, W.: Biochim. Biophys. Acta 41, 550 (1960).

7. Swensen, P. A., Setlow, R. B.: Photochem. Photobiol. **2**, 419 (1963).
8. Brown, I. H., Freeman, K. B., Johns, H. E.: J. molecular Biol. **15**, 640 (1966).
9. Smith, K. C.: Photochem. Photobiol. **2**, 503 (1963).
10. Freeman, K. B., Hariharan, P. V., Johns, H. E.: J. molecular Biol. **13**, 833 (1965).
11. Ben-Ishai, R., Ben-Hur, E., Hornfeld, Y.: Israel J. Chem. **6**, 769 (1968).
12. Setlow, R. B., Carrier, W. L.: J. molecular Biol. **17**, 237 (1966).
13. Jordan, F., Pullman, B.: Theoret. chim. Acta (Berl.) **10**, 423 (1968).
14. Weinblum, D., Johns, H. E.: Biochim. Biophys. Acta **114**, 450 (1966).
15. Fisher, G. J., Johns, H. E.: Photochem. Photobiol. **11**, 429 (1970).
16. Johns, H. E., Helleincer, C. W., Pearson, M. L., LeBlanc, J. C.: J. molecular Biol. **9**, 503 (1964).
17. Blackburn, G. M., Davies, R. J. H.: Tetrahedron Letters **37**, 4471 (1966).
18. Camerman, N., Nyburg, S. C., Weinblum, D.: Tetrahedron Letters **42**, 4127 (1967).
19. Einstein, J. R., Hosszu, J. L., Longworth, J. W., Rahn, R. O., Wei, C. H.: Chem. Comm. **20**, 1063 (1967).
20. Adman, E., Gordon, M. P., Jensen, L. H.: Chem. Comm. **21**, 1019 (1968).
21. Camerman, N., Camerman, A.: Science **160**, 1451 (1968).
22. Karle, I. L.: Acta crystallogr. B **25**, 2119 (1969).
23. Camerman, N., Camerman, A.: J. Amer. chem. Soc. **92**, 2523 (1970).
24. Corey, E. J.: J. Amer. chem. Soc. **86**, 5570 (1964).
25. Lamola, A. A.: Photochem. Photobiol. **7**, 619 (1968).
26. - Eisinger, J.: Proc. nat. Acad. Sci. USA **59**, 46 (1968).
27. Whillans, D. W., Johns, H. E.: Photochem. Photobiol. **9**, 323 (1969).
28. Wagner, P., Bucheck, D.: J. Amer. chem. Soc. **92**, 181 (1970).
29. Eisinger, J., Schulman, R. G.: Proc. nat. Acad. Sci. USA **58**, 895 (1967).
30. Sutherland, B. M., Sutherland, J. C.: Biophys. J. **9**, 292 (1969).
31. Mantione, M. J., Pullman, B.: Biochim. Biophys. Acta **91**, 387 (1964).
32. Pullman, B., Mantione, M. J.: Biochim. Biophys. Acta **95**, 668 (1965).
33. Danilov, V. I.: Photochem. Photobiol. **6**, 233 (1967).
34. Denis, A., Pullman, A.: Theoret. chim. Acta (Berl.) **7**, 110 (1967).
35. Kuprievich, V.: Int. J. quant. Chemistry **1**, 561 (1967).
36. Pullman, B.: Photochem. Photobiol. **7**, 525 (1968).
37. Nagata, C., Imamura, Y., Tagashira, M., Kodama, M., Fukuda, N.: J. theoret. Biology **9**, 357 (1965).
38. Sayre, R., Harlos, J., Rein, R.: Molecular orbital studies in chemical pharmacology, ed. by L. B. Kier, p. 207. N. Y.: Springer-Verlag 1970.
39. Camerman, N., Nyburg, S.: Theoret. chim. Acta (Berl.) **13**, 162 (1969).
40. Bertrán, J., Chalvet, O., Daudel, R., McKillop, T. F., Schmid, G. H.: Tetrahedron **26**, 339 (1970).
41. — Schmid, G. H.: Tetrahedron **27**, 5191 (1971).
42. Mulliken, R. S.: J. Chim. physique **46**, 497, 675 (1949).
43. Roothaan, C. J.: J. chem. Physics **19**, 1445 (1951).
44. Hoffmann, T. A., Ladik, J.: Advances chem. Physics **7**, 84 (1964).
45. Salem, L.: J. Amer. chem. Soc. **90**, 543, 553 (1968).
46. Hoffman, R.: J. chem. Physics **39**, 1397 (1963).
47. Devaquet, A., Salem, L.: J. Amer. chem. Soc. **91**, 3793 (1969).
48. Sustmann, R., Binsch, G.: Molecular Physics **20**, 1, 9 (1971).

Dr. J. Bertran
Instituto de Biología Fundamental
Universidad Autónoma de Barcelona
Avd. San Antonio Mª Claret 171
Barcelona – 13, Spain

Theoret. chim. Acta (Berl.) 25, 382--390 (1972)
© by Springer-Verlag 1972

A CNDO/2 Calculation on a Complex between Ethylene and Chlorine

BENGT NELANDER
Thermochemistry Laboratory, Chemical Center, University of Lund, S-220 07 Lund, Sweden

Received November 26, 1971

CNDO/2 calculations have been carried out for an ethylene chlorine complex, with the halogen orthogonal or parallel to the C-C bond. For comparison similar calculations were also carried out for ethylene and fluorine. The results are compared to estimates from experiments on related complexes and from Mulliken's resonance theory. It is concluded that the CNDO/2 calculations grossly overestimate the ethylene-chlorine interaction in particular if *d*-orbitals on chlorine are included in the AO-basis. The explanation for this may be the too high *d*-orbital exponent used here and the wrong asymptotic behaviour of the Slater orbitals.

Es werden CNDO/2-Rechnungen für zwei Konformationen eines Äthylen-Chlor-Komplexes und eines Fluor-Analogens berichtet und die Resultate mit der Resonanztheorie von Mulliken und mit experimentellen Daten verglichen. Es ergibt sich, daß bei CNDO/2-Rechnungen die Chlor-Äthylen-Wechselwirkung stark überschätzt wird, insbesondere, wenn *d*-Orbitale eingeschlossen werden. Letzteres könnte auch an einem großen Exponenten bei diesen Funktionen oder am falschen asymptotischen Verlauf von Slater-Funktionen liegen.

Calculs CNDO/2 pour un complexe ethylène-chlore avec l'halogène orthogonal ou parallèle à la liaison C-C. A titre de comparaison des calculs analogues ont été aussi effectués pour l'éthylène et le fluor. Les résultats sont comparés à des estimations expérimentales sur des complexes voisins et à des estimations provenant de la théorie de la résonance de Mulliken. La conclusion est que les calculs CNDO/2 surestiment beaucoup l'interaction éthylène-chlore, en particulier lorsque l'on inclut des orbitales *d* dans la base des orbitales atomiques. La raison peut s'en trouver dans les exposants trop élevés des orbitales *d* et dans le mauvais comportement asymptotique des orbitales de Slater.

Introduction

At present, experimental results on charge transfer complexes are in general interpreted using Mulliken's resonance theory [1]. While this theory has made it possible to systematize a large body of experimental results, it is quite often difficult to apply. It is for instance not easy to estimate the relative importance of pure electrostatic and charge transfer contributions to the energy of formation [2], or to find out the extent to which the complex forming molecules are deformed upon complex formation.

In recent years the CNDO approximation of Pople and coworkers [3] has been successfully applied to a large number of different problems. In view of these successful applications it seemed worth-while to calculate a number of properties of a simple charge transfer complex from the CNDO approximation in order to get an idea of the usefulness of such calculations. While this work was in progress a CNDO calculation on the benzene TCNE complex appeared

[4]. Its results, a too short equilibrium distance and a too large energy of formation are in general accord with the results of this paper.

Since there is available a large body of experimental results on halogen complexes, chlorine was chosen as electron acceptor as being the only complex forming halogen for which parameters are available. Ethylene was used as electron donor, since work is presently carried out in this laboratory on ethylene complexes [5].

Calculations

The calculations were carried out at the UNIVAC 1108 computer of the University of Lund computing centre. The CNDO/2 program used is based on QCPE 100, by Clarke and Ragle, supplied by the Quantum Chemistry Program Exchange, Indiana University, Bloomington, Indiana. The program was rewritten to allow calculations with second row atoms, as described by Segal and Santry [6]. For these atoms calculations may be carried out both using basis sets with no *d*-orbitals and with *d*-orbitals (*sp*- and *spd*-approximations of Ref. [6]). The orbital exponent of the *d*-orbitals was the same as of the *s*- and *p*-orbitals on the same atom. Excitation energies were calculated in the virtual orbital approximation as described by Kroto and Santry [7]. Oscillator strengths were calculated using the formula of Giessner-Prettre and A. Pullman [8]. The parameters used were the original parameters of Pople and Segal [9] and Segal and Santry [6]. Vibration frequencies were obtained by fitting parabolas, or (in the case of ethylene-chlorine *sp*-approximation) a paraboloid to the energy values calculated within 0.02 (Cl–Cl-distance) or 0.03 Å from the equilibrium position. The use of Fues-potentialfunctions ($A + B/R + C/R^2$), which fit the calculated energies much further from the minimum than parabolas do, was found to have no effect on the calculated frequencies.

Results

Calculations were carried out for complexes between ethylene and fluorine or chlorine. In all calculations the experimental geometry of ethylene was used [10] and the fluorine internuclear distance was kept at the experimental value [11]. The chlorine internuclear distance was varied both for the most stable complex and for free chlorine. Two different relative orientations of the two interacting molecules were considered. In one series of calculations the halogen molecule was parallel to the C–C bond and the CCClCl plane was orthogonal to the ethylene plane (resting model). In the other series of calculations the halogen molecule was placed on the symmetry axis of ethylene, orthogonal to the ethylene plane (axial model). For each orientation the halogen ethylene distance was varied.

Ethylene-Fluorine

a) Axial Model. A minimum in the energy of 0.0584 a.u. (*ca.* 37 kcal/mole) below the energy of the free components was found for $R = 1.456$ Å (R, the distance between the nearest chlorine atom and the midpoint of the C–C bond). From the variation in the CNDO-charges, Q_A, ($Q_A = Z_A - \sum_{i \in A} P_{ii}$, where Z_A is the core charge of atom A and P_{ii} is the diagonal element of the CNDO density matrix for the i-th atomic orbital) with the fluorine ethylene distance, it was found that the charge transfered from ethylene to fluorine increases as the distance decreases, and that all charge transfered to the fluorine molecule becomes localised on the fluorine atom farthes away from the ethylene molecule. In fact the other fluorine atom even becomes positively charged. The charge transfered within the fluorine molecule is between one third and half of the charge transfered from ethylene to fluorine, depending on distance. The dipole moment rises rapidly with decreasing distance, reaching 3.58 D at the energy minimum.

b) Resting Model. As might be expected the energy rises rapidly when the fluorine ethylene distance is decreased. In fact, in this conformation the ethylene molecule acts as an electron acceptor, a rather unfavorable situation. Between 1.66 and 1.65 Å the calculated ground state changes abruptly from two interacting molecules to a highly deformed state of 1,2 difluoroethane. In the first excited state, where one electron is excited from the highest occupied to the lowest virtual orbital the energy changes smoothly from an excited state of the two interacting molecules to an excited state of difluoroethane. This kind of behavior was expected from considerations of orbital symmetry [12].

Ethylene-Chlorine

a) Axial Model, sp-Approximation. The energy decreases as the chlorine molecule is brought closer to the C–C bond (keeping the Cl_2 distance fixed) and reaches a minimum for $R = 2.259$ Å, the minimum energy is 0.00983 a.u. (*ca.* 6.2 kcal/mole) below the energy of the free components. When the chlorine internuclear distance was varied the energy minimum was found for $R = 2.242$ Å and $R_{ClCl} = 2.000$ Å (compared to 1.980 Å for free chlorine in the *sp*-approximation) and the energy was 0.00986 a.u. below the energy of the free components[1]. The axial energy minimum was found to be stable to small simultaneous variations of the parameters describing the relative orientations of the two interacting molecules. A number of properties calculated at equilibrium are given in Table 1a and 1b. As was found for the fluorine case, the only atom, which gains charge as the distance is decreased is the outer chlorine atom. In this case the charge transfer within the chlorine molecule is approximately equal to the ethylene chlorine charge transfer. Since the equilibrium distance obtained was much shorter than might be expected a number of properties were also calculated at a more reasonable distance, 3.25 Å, the results are given in Table 1.

The energy of the three lowest excited states of the complex, in the virtual orbital approximation, were also calculated as a function of distance. The two lowest states may be described as an excited chlorine molecule interacting with ethylene. Their energy curves are indistinguishable except at small distances. These states are repulsive. There is a very small dip in the energy at *ca.* 3 Å which should not be taken seriously, since no variation of the chlorine distance was carried out. The vertical excitation energy is given in Table 1b for the *sp*-minimum. The third lowest excited state is obtained upon excitation of an electron from an orbital which is essentially a combination of the $2p\pi$ orbital of ethylene and the $3p\sigma$ orbital of chlorine to the $3p\sigma^*$ orbital of chlorine. It thus involves charge transfer from ethylene to chlorine and may therefore be identified with the charge transfer band of Mulliken's theory.

---

[1] *The value in Table 1 has been corrected for the zero point vibration energy of the Cl_2 ... ethylene vibration, 237 cm^{-1}.*

As expected the equilibrium distance of this excited state is somewhat shorter than for the ground state, 1.97 Å compared to 2.26 Å for the ground state. The

Table 1a. Calculated properties of the ethylene-chlorine complex

	$r_e(Cl_2)$ Å	$-\Delta E$ kcal/mole	Dipole moment D	$\nu(Cl_2)$ cm^{-1}	$(\nu_0 - \nu)/\nu_0$	Dipole moment derivative D/Å(amu)$^{1/2}$
CNDO (*sp*-approx. equilibr.)	2.000	5.8	1.52	913	0.070	1.32
CNDO (*sp*-approx. 3.25 Å)	1.980	0.46	0.06	980	0.0005	0.031
CNDO (*spd*-approx. 3.25 Å)	-	2.74	0.15			
CNDO (*spd*-approx. 3.25 Å Cl_2 distance relaxed)	1.752	2.6	0.13	1305	0.0021	0.013
CNDO Cl_2 (*sp* approx.)	1.980	—	-	981		
CNDO Cl_2 (*spd* approx.)	1.751	—	-	1308	–	
Estimates (see text)[a]	-	2.2[d]	0.4		0.011	0.16
Benzene-Cl_2 (experimental)	1.99[b]	1.1[e]	0.5 – 0.7[e]	526[f]	0.028	0.20[g]
Cl_2 (experimental)	1.988[c]	--		541[g]		--

[a] The energy of formation was estimated by adding the resonance and van der Waal's energies calculated above.

[b] Hassel, O., Strømme, Knut: Acta chem. scand. 13, 1781 (1959).

[c] Herzberg, G.: Spectra of Diatomic Molecules, 2nd Ed. Princeton N.J.: Van Nostrand 1950.

[d] The resonance contribution was 1.4 kcal/mole.

[e] Estimated by Lippert, Joseph L., Hanna, Melvin W., Trotter, Philip J.: J. Amer. chem. Soc. 91, 4035 (1969).

[f] Collin, J., D'Or, L.: J. chem. Physics 23, 397 (1955).

[g] Friedrich, H. Bruce, Person, Willis B.: J. chem. Physics 44, 2161 (1966).

Table 1b. Calculated excitation energies of the ethylene-chlorine complex

	ν "Cl_2" kK	Oscillator strength	CT-abs kK	Oscillator strength
CNDO (*sp*-approx. equilibr.)	40.0	0.026	80.43	1.65
CNDO (*sp*-approx. 3.25 Å)	37.2	0.031	105.00	0.58
Cl_2, CNDO (*sp*-approx.)	36.8	0.030	-	--
Experimental	-		43.4[b]	0.19[c]
Experimental, Cl_2	30.5[a]	0.0017[a]		

[a] Seery, D.J., Britton, D.: J. physic. Chemistry 68, 2263 (1964).

[b] Dubois, J.E., Garnier, F.: Spectrochim. Acta 23A, 2279 (1967).

[c] Estimated, see text.

O–O excitation energy is 0.343 a.u.[2] (75.1 kK) compared to the vertical excitation energy of 0.366 a.u.

b) Resting Model, sp-Approximation. The potential curve obtained for this model has a very insignificant minimum around 3 Å, the energy is *ca.* 0.0007 a.u. (*ca.* 0.4 kcal/mole) below the energy of the free components. Inside this minimum the energy rises rapidly. As for the resting model of the fluorine complex, ethylene here acts as an electron acceptor.

c) Axial and Resting Models, spd-Approximation. For both models the calculated potential curves had very deep minima at very short equilibrium distances. For the axial model the energy is 0.23 a.u. (*ca.* 140 kcal/mole) below the energy of the free components at the equilibrium distance of *ca.* 1.7 Å. The energy minimum of the resting model is at *ca.* 1.9 Å and the stabilisation energy is *ca.* 0.14 a.u.

The inclusion of *d*-orbitals allows charge to be back donated from the outer to the inner chlorine atom, and thus the strong polarisation of the chlorine molecule in the *sp*-approximation is absent. The inclusion of *d*-orbitals also transforms the chlorine molecule into an electron acceptor in the resting conformation.

Because of the very poor results for stabilitsation energies and equilibrium distances, the *spd*-approximation was only used to calculate a few properties of the axial complex at 3.25 Å. The results are included in Table 1.

Estimates

At present, only the charge transfer band of ethylene chlorine complex has been observed experimentally [13]. It was therefore necessary to estimate other properties for comparison with the results of the CNDO calculation.

All estimates, except of the van der Waal's energy were made for an axial complex with $R = 3.5$ Å. The van der Waal's energy was calculated as a function of R as described by Eliel *et al.* [14]. A very flat minimum was found at $R = 3.3$ Å, where the interaction energy was -0.8 kcal/mole.

In order to estimate the resonance energy, the experimentally observed relation between ionisation potential and position of the charge transfer band was used as a startingpoint.

$$\begin{aligned} h\nu_{CT} &= I - C_1 + C_2/(I - C_1) \\ C_2 &= \beta_0^2 + \beta_1^2 . \end{aligned} \tag{1}$$

(For detailed information on the physical interpretation of the parameters, and their values in different cases see Refs. [1] and [15].) The value of C_2 for the iodine complexes, given by Briegleb [15] was used directly, but the value of C_1 was changed to take into account the differences in electron affinity and in electrostatic interaction between the ethylene iodine and chlorine complexes. The change in vertical electron affinity was taken from Person [16]. The difference in electrostatic energy was calculated from a simple point charge model for the excited state of the complex, and the assumption that the ground states do not contribute.

---

[2] This is only a crude approximation to the true CNDO O–O excitation energy, since no variation in the internal structure of ethylene or chlorine was carried out.

The halogen ethylene distances were taken to be the sum of the van der Waal's radii [17] and the charges were divided even between the halogen atoms, and the two carbon atoms of ethylene. The resulting parameters were: $\beta_0 = -4.5$ kK, $\beta_1 = -8.8$ kK and $C_1 = 42$ kK. These parameters and formulas given in Ref. [1] were used to calculate the values given in Table 1. For the position of the charge transfer band, these parameters give 45.0 kK compared to the experimental value 43.4 kK.

Discussion

For ethylene and chlorine all calculations predict the existence of a stable complex with the chlorine molecule on the C_2 axis orthogonal to the ethylene plane. This structure is also expected from considerations of overlap between donor and acceptor orbitals. For the *sp*-approximation the equilibrium distance is 2.24 Å, which lies between the CCl single bond length 1.77 Å, and the sum of the van der Waal's radii, 3.5 Å [17]. However, since the ionisation potential of ethylene is higher than for benzene, the ethylene complex is expected to be weaker than the benzene-chlorine complex, and thus the equilibrium distance is expected to be longer than that of benzene chlorine complex, which is 3.28 Å in the crystal [18]. Considering the possibility that the benzene chlorine distance found by Hassel and Strømme may represent the average value of a long and a short distance [1] the ethylene-chlorine equilibrium distance may be shorter than 3.28 Å, but it seems very unlikely that it is shorter than 3.0 Å. The failure of the CNDO approximation to give reasonable equilibrium distances for complexes is in contrast to the reasonable bond distances which are obtained from such calculations.

It is very difficult to make any precise statements about the energy of formation of the ethylene-chlorine complex, in the gas phase. Olefin-iodine complexes have enthalpies of formation of about −1 to −2 kcal/mole at room temperature in solution [15]. Chlorine complexes are in general weaker and therefore should have more positive enthalpies of formation. Lippert *et al.* [2] estimate the energy of formation of the chlorine benzene complex to be −1.1 kcal/mole in solution, compared to −1.3 kcal/mole for the benzene-iodine complex. The energies of formation in the gas phase are expected to be more negative than in solution since van der Waal's interactions between the complex forming molecules are no longer compensated for by interactions with the solvent [1]. The van der Waal's energy of the ethylene complex was estimated above to be 0.8 kcal/mole. If this contribution is added to the experimental values for the olefine-iodine complexes and the change from iodine to chlorine is assumed to have no effect, the energy of formation of the ethylene chlorine complex is estimated to be −2 to −3 kcal/mole.

The resonance energy contribution to the energy of formation was estimated above to be *ca.* 1.4 kcal/mole, if the van der Waal's energy is added the energy of formation is estimated as *ca.* −2.2 kcal/mole. From these estimates it seems as if the calculated energy of formation −5.8 kcal/mole (*sp*-approximation) is at least too low by a factor two.

The interaction energy between axial chlorine calculated for 3.25 Å, −0.5 kcal/mole, seems too close to zero, while the interaction energies from the *spd*-approximation seem to be reasonable (−2.7 and −2.6 without and with relaxation of the Cl–Cl distance respectively).

As is seen from Table 1 the Cl–Cl stretching frequency decreases upon complex formation. A comparison with the frequency shift for the benzene-chlorine complex and with the estimated shift from the resonance theory makes it rather obvious that the shifts calculated at 3.25 Å are all too small, while the *sp*-approximation at equilibrium gives a much too large shift. It should be pointed out here that the calculations for the *sp*-minimum indicate a very strong coupling between the Cl_2–C_2H_4 vibration and the Cl–Cl vibration in the complex. If the Cl–Cl frequency shift is calculated from the corresponding force constant alone the relative change is only 0.040 compared to 0.070 when this coupling is included. The coupling although much exagerated by the CNDO calculation should be of importance also in real halogen complexes. A decrease in the halogen donor distance will increase the charge transfer to the halogen, and therefore weaken the halogen-halogen bond.

For the I_2 hexamethylenetetramine complex, Ichiba *et al.* [19] found that 0.37 electrons were transfered from the iodine closest to nitrogen to the outer iodine, while only 0.08 electrons were transfered from the donor to the iodine molecule. Of course the hexamethylenetetramine iodine complex is much stronger than the ethylene chlorine complex, which makes any extrapolations from the results of Ichiba *et al.* to this complex dangerous. It seems, however, that the *spd*-approximation grossly under estimates the importance of the halogen polarisation relative to that of the charge transfer.

When the overlap integrals were calculated between the free molecules and the axial complex at a distance close to the minimum (2.3 Å) in the *sp*-approximation, it was found that most orbitals of chlorine and ethylene are quite unaffected by complex formation. Two things should be noted, first the contribution of the $3p\sigma^{*}$-orbital of chlorine to the two highest occupied orbitals of a_1-symmetry of the complex. (Overlap integrals 0.145 and 0.069.) These contributions are responsible for the polarisation of the chlorine molecule, and also for the charge transfer. Second the strong mixing of the $2p\pi$-orbital of ethylene and the $3p\sigma$ orbital of chlorine. They contribute approximately equally to the two highest a_1 orbitals of the complex. This mixing leads to repulsion and therefore helps to precent the two molecules to get too close to each other.

Qualitatively, the calculated UV-spectra agree with experimental observations on halogen complexes. The chlorine absorption is shifted towards higher wavenumbers by *ca.* 3.4 kK. This shift may be compared to a shift of the visible iodine band of *ca.* 2.3 kK in the ethylene iodine complex at 20 K [5]. The shift of the chlorine band, although it seems a little too large, is thus of the expected magnitude. The calculated charge transfer excitation energy is much too high.

Conclusion

From the results of the calculations discussed above, it will seem as if the CNDO approximation gives a qualitatively correct picture of the structure of the complex, and of some of its properties, at least if *d*-orbitals are left out. The quantitative results are rather poor however. In view of the qualitative agreement it may be possible to obtain useful results from comparisons between calculations on closely related complexes. However, if the CNDO approximation is to be useful for more general investigations of molecular complexes, some changes in the method of calculation seem necessary. From the successful CNDO calculations on stable molecules it seems as if the approximations involved in the setting up of the F matrix balance each other at the relatively short distances between bonded atoms and next neighbour atoms. At the much longer distances involved in molecular complexes, the Slater orbitals used to calculate the overlap matrix go to zero much faster than Hartree Fock orbitals. This probably creates an unbalance in the approximations, since the exchange repulsion will be underestimated compared to nuclear repulsion and electron nuclear attraction, which may be the reason for the too short equilibrium distances etc. It might be of interest to calculate the overlap matrix using orbitals which approximate Hartree Fock orbitals more closely at large distances from the nucleus.

Another point which is of importance for chlorine complexes is the role of the *d*-orbitals. From an extrapolation of the trend in stabilisation energies of the fluorine and chlorine complexes in the *sp*-approximation it seems as if bromine and in particular iodine should be very weak acceptors compared to chlorine, while experimentally it is the other way around. This reverse of the trend may perhaps be due to the increasing importance of the *d*-orbitals when going from chlorine to bromine and iodine. The results of the calculations are very dependent on the *d*-orbital exponent, which makes the choice of the latter a very important problem. It may perhaps be as has been argued by Craig *et al.* [20] that the *d*-orbitals contract upon bond formation, which would make them sensitive to environment and make it more or less impossible to choose the correct orbital exponents in actual cases. Recently Keeton and Santry [21] stated from an investigation of the *d*-orbital exponents of phosphorus and sulfur, using minimal basis sets, that the *d*-orbital exponent is 0.9 of the 3*s* orbital exponent quite independently of the atoms surrounding the phosphorus or sulfur atom. There may thus be some hope that a "best" set of *d*-orbitals may be found.

References

1. Mulliken, R. S., Person, W. B.: Molecular complexes. New York: Wiley-Interscience 1969.
2. Lippert, J. L., Hanna, M. W., Trotter, Ph. J.: J. Amer. chem. Soc. **91**, 4035 (1969).
3. Pople, J. A., Beveridge, D. L.: Approximate molecular orbital theory. New York: McGraw-Hill 1970.
4. Chesnut, D. B., Wormer, P. E. S.: Theoret. chim. Acta (Berl.) **20**, 250 (1971).
5. Fredin, L.: Private communication.
6. Santry, D. P., Segal, G. A.: J. chem. Physics **47**, 158 (1967).
7. Kroto, H. W., Santry, D. P.: J. chem. Physics **47**, 792 (1967).
8. Giessner-Prettre, C., Pullman, A.: Theoret. chim. Acta (Berl.) **13**, 265 (1969).
9. Pople, J. A., Segal, G. A.: J. chem. Physics **44**, 3289 (1966).
10. Herzberg, G.: Electronic spectra of polyatomic molecules. Princeton, N.J.: Van Nostrand 1966.
11. — Spectra of diatomic molecules, 2nd Ed. Princeton, N.J.: Van Nostrand 1950.
12. Woodward, R. B., Hoffman, R.: The conservation of orbital symmetry. Weinheim/Bergstr.: Verlag Chemie, GmbH. 1970.
13. Dubois, J. E., Garnier, F.: Spectrochim. Acta **23A**, 2279 (1967).
14. Eliel, E. L., Allinger, N. L., Angyal, S. J., Morrison, G. A.: Conformational Analysis. New York: Wiley-Interscience 1965.

15. Briegleb, G.: Elektronen-Donator-Acceptor-Komplexe. Berlin: Springer-Verlag 1961.
16. Person, W. B.: J. chem. Physics **38**, 109 (1963).
17. Pauling, L.: Nature of the chemical bond. 3rd Ed. Ithaca, N.Y.: Cornell University Press 1960.
18. Hassel, O., Strømme, K.: Acta chem. scand. **13**, 1781 (1959).
19. Ichiba, S., Sakai, H., Negita, H., Maeda, Y.: J. chem. Physics **54**, 1627 (1971).
20. Craig, D. P., Maccoll, A., Nyholm, R. S., Orgel, L. E., Sutton, L. E.: J. chem. Soc. **332** (1954).
21. Keeton, M., Santry, D. P.: Chem. Physics Letters **7**, 105 (1970).

Dr. B. Nelander
Themochemistry Laboratory
Chemical Center
University of Lund
S-220 07 Lund
Sweden

Theoret. chim. Acta (Berl.) 25, 391–395 (1972)
© by Springer-Verlag 1972

Nuclear Mass Effect in Many-Electron Atoms*

B. W. N. Lo and S. Fraga

Division of Theoretical Chemistry, Department of Chemistry, University of Alberta,
Edmonton 7, Alberta, Canada

Received February 23, 1972

The total nuclear mass effect, including the normal mass and the mass polarization corrections, have been evaluated, from existing analytical Hartree-Fock functions, for the positive ions, neutral systems, and negative ions of all the atoms from He through Kr. The formulation for the mass polarization effect is presented in detail.

Mit Hilfe existierender analytischer Hartree-Fock-Funktionen wurde der totale Kernmasseneffekt einschließlich der Korrekturen für normale Massen und Massenpolarisation für positive und negative Ionen und neutrale Systeme für alle Atome von He bis Kr berechnet. Der Formalismus für den Massenpolarisationseffekt wird im einzelnen dargelegt.

Introduction

The electronic state functions of atoms are determined under the assumption of an infinite nuclear mass. The corresponding energies must then be modified by inclusion of the corrections for the finite mass of the nucleus and its motion (Bethe and Salpeter [1]). These corrections, although small, give rise to the so-called mass-dependent isotopic shift, that can be observed experimentally.

The purpose of this work is to present the formulation for this correction and the numerical values obtained for all the positive ions, neutral systems, and negative ions of all the atoms from He through Kr, using existing analytical Hartree-Fock functions, in order to complete the research project[1] undertaken at this Laboratory on the determination of atomic Hartree-Fock parameters [4].

Theoretical Formulation

It is customary to consider separately the two contributions, normal mass effect and mass polarization effect, to the isotopic shift. The corresponding formulations are presented below.

Normal Mass Effect

This correction arises from the use of the Rydberg constant, R_M, for the nucleus under consideration. Taking into account that

$$R_M = [M/(m+M)]\,R_\infty ,$$

---

* This work has been supported in part by the National Research Council of Canada.

[1] The complete spin-orbit and electron spin-spin contact interactions and the mass variation and Darwin relativistic corrections have been reported recently [6–8]. For details on previous work see Ref. [4].

where m and M are the masses of the electron and the nucleus, respectively, one obtains

$$\Delta E_n = -[m/(m+M)]\,R_\infty E_\infty$$

for the normal nass correction to the energy; E_∞ represents the electronic energy evaluated for infinite nuclear mass.

Mass Polarization Effect

The correction corresponding to this effect, also denoted as specific mass effect, is given by

$$\Delta E_s = -[2m/(m+M)]\,R_M \langle \Psi | \sum_{i<j} \Lambda_i \cdot \Lambda_j | \Psi \rangle\,,$$

where Ψ represents the total electronic function for the state under consideration and the summations extend over all the electrons in the system.

Taking into account (Innes and Ufford [5]) that

$$\Lambda = \frac{\partial}{\partial r} C^{(1)} - \frac{\sqrt{2}}{r} (C^{(1)} l)^{(1)}\,,$$

where $C^{(1)}$ is the modified spherical harmonics tensor operator of rank 1 and l is the orbital angular momentum vector operator, one can write

$$\begin{aligned} \Lambda_i \cdot \Lambda_j = {} & \frac{\partial^2}{\partial r_i \partial r_j} (C_i^{(1)} \cdot C_j^{(1)}) - \frac{\sqrt{2}}{r_i} \frac{\partial}{\partial r_j} \{(C^{(1)} l)_i^{(1)} \cdot C_j^{(1)}\} \\ & - \frac{\sqrt{2}}{r_j} \frac{\partial}{\partial r_i} \{C_i^{(1)} \cdot (C^{(1)} l)_j^{(1)}\} + \frac{2}{r_i r_j} \{(C^{(1)} l)_i^{(1)} \cdot (C^{(1)} l)_j^{(1)}\}\,. \end{aligned}$$

The general matrix element between 2-electron states may then be written as

$$\begin{aligned} & \langle l_a l_b L M_L S M_S | \mathscr{A}^\dagger (\Lambda_i \cdot \Lambda_j) \mathscr{A} | l_c l_d L' M'_{L'} S' M'_{S'} \rangle \\ & \quad = \{\langle \Lambda \cdot \Lambda \rangle_d + \langle \Lambda \cdot \Lambda \rangle_e\}\, \delta(L M_L S M_S, L' M'_{L'} S' M'_{S'})\,, \end{aligned}$$

where $\langle \Lambda \cdot \Lambda \rangle_d$ and $\langle \Lambda \cdot \Lambda \rangle_e$ stand for the direct and exchange contributions; $\mathscr{A}$ is the antisymmetrizing operator.

Using the relation

$$\langle l \| (C^{(k)} l)^{(k)} \| l' \rangle = [l(l+1) - k(k+1) - l'(l'+1)]\,[2k(2k+2)]^{-1/2} \langle l \| C^{(k)} \| l' \rangle\,,$$

one can write for the direct contribution

$$\begin{aligned} \langle \Lambda \cdot \Lambda \rangle_d = {} & (-1)^{L+l_b+l_c} \begin{Bmatrix} L & l_b & l_a \\ 1 & l_c & l_d \end{Bmatrix} \langle l_a \| C^{(1)} \| l_c \rangle \langle l_b \| C^{(1)} \| l_d \rangle \\ & \{T(ab, cd) - \tfrac{1}{2}[l_a(l_a+1) - l_c(l_c+1) - 2]\, U(ab, cd) \\ & - \tfrac{1}{2}[l_b(l_b+1) - l_d(l_d+1) - 2]\, U(ba, dc) \\ & + \tfrac{1}{4}[l_a(l_a+1) - l_c(l_c+1) - 2]\,[l_b(l_b+1) - l_d(l_d+1) - 2]\, Q(ab, cd)\}\,. \end{aligned}$$

The exchange interaction may be obtained from the above expression by exchanging first the subindices a and b and then multiplying by $(-1)^{L+S+l_a+l_b}$.

The radial integrals are defined by

$$T(ab, cd) = \int_0^\infty \int_0^\infty r_1^2 dr_1 r_2^2 dr_2 R_a(1) R_b(2) \frac{\partial^2}{\partial r_1 \partial r_2} R_c(1) R_d(2),$$

$$U(ab, cd) = \int_0^\infty \int_0^\infty r_1^2 dr_1 r_2^2 dr_2 R_a(1) R_b(2) \frac{1}{r_1} \frac{\partial}{\partial r_2} R_c(1) R_d(2),$$

$$Q(ab, cd) = \int_0^\infty \int_0^\infty r_1 dr_1 r_2 dr_2 R_a(1) R_b(2) R_c(1) R_d(2),$$

R being the radical function of the shell denoted by the subscript.

Using the generalized 2-particle coefficients of franctional parentage one can now derive the expression of the total correction for a many-electron configuration. Restricting the discussion to functions obtained within the one-electron function approximation, it is found that the intrashell interaction and the direct term of the intershell interaction vanish due to the parity restriction in the double-barred matrix elements. The interaction[2] between two shells, when at least one of them is closed, can be written as

$$\begin{aligned} \langle A \cdot A \rangle = (-1)^{l_a + l_b} n_a n_b [2(2l_a+1)(2l_b+1)]^{-1} \langle l_a \| C^{(1)} \| l_b \rangle^2 \\ \{T_{ba} - \tfrac{1}{2}[l_a(l_a+1) - l_b(l_b+1) - 2] U_{ab} \\ - \tfrac{1}{2}[l_b(l_b+1) - l_a(l_a+1) - 2] U_{ba} \\ + \tfrac{1}{4}[l_a(l_a+1) - l_b(l_b+1) - 2][l_b(l_b+1) - l_a(l_a+1) - 2] Q_{ba}\}, \end{aligned}$$

where n_a and n_b are the occupation numbers of the two shells involved. For simplicity, the notation of the radial integrals has been changed to T_{ab}, U_{ab}, and Q_{ab}, with the convention $T_{ab} = T(ab, ba)$, $U_{ab} = U(ab, ba)$, and $Q_{ab} = Q(ab, ba)$.

In order for this interaction not to vanish, it is necessary that l_a and l_b differ by ± 1. In such a case the above expression simplifies to

$$\begin{aligned} \langle A \cdot A \rangle = - n_l n_{l+1} (l+1) [2(2l+1)(2l+3)]^{-1} \\ [T_{l+1,l} + (l+2) U_{l,l+1} - l U_{l+1,l} - l(l+2) Q_{l+1,l}]. \end{aligned}$$

The total interaction for the configuration considered is then obtained by summing all the intershell contributions.

Results and Discussion

The calculations have been carried out for the positive ions, neutral systems, and negative ions for all the atoms from He through Kr.

The normal mass effect has been evaluated for the most abundant isotope of each atom; for simplicity the values[3] are not presented here as their calculation is straightforward. For the atoms considered here, this correction varies from 86 cm^{-1} for He to 3996 cm^{-1} for Kr.

---

[2] The derivation parallels that given for the electron spin-spin contact interaction [6] and for that reason it is omitted here.

[3] The values for both corrections for all the systems considered are available upon request.

Table 1. Values (in a.u.) of $\langle A \cdot A \rangle$ for positive ions, neutral atoms, and negative ions

Configuration[a]	State	Positive ions		Neutral atoms		Negative ions	
		System		System		System	
$2p^1$	^2P	C	0.88085	B	0.40491		
$2p^2$	^3P	N	2.54998	C	1.39425	B	0.53604
	^1D		2.50114		1.35552		0.49119
	^1S		2.42858		1.29785		0.51252
$2p^3$	^4S	O	5.21731	N	3.17939	C	1.60538
	^2D		5.13555		3.11391		1.54622
	^2P		5.08115		3.07051		1.50570
$2p^4$	^3P	F	8.94324	O	5.84933	N	3.36944
	^1D		8.88588		5.80080		3.32681
	^1S		8.79700		5.72740		3.26152
$2p^5$	^2P	Ne	14.06424	F	9.71118	O	6.12790
$2p^6$	^1S	Na	20.78773	Ne	14.97543	F	10.08886
$3s^1$	^2S	Mg	27.58848	Na	20.80104		
$3s^2$	^1S	Al	35.39230	Mg	27.60894	Na	20.80392
$3p^1$	^2P	Si	44.56300	Al	35.59283		
$3p^2$	^3P	P	55.08558	Si	44.82954	Al	35.66672
	^1D		55.06518		44.81350		35.46262
	^1S		55.03452		44.78686		35.60850
$3p^3$	^4S	S	67.05839	P	55.42108	Si	44.95406
	^2D		67.02311		55.39441		44.93002
	^2P		67.00054		55.37640		44.90803
$3p^4$	^3P	Cl	80.50782	S	67.41237	P	55.55414
	^1D		80.49627		67.39138		55.53360
	^1S		80.44737		67.36053		55.50495
$3p^5$	^2P	A	95.59085	Cl	80.94511	S	67.59899
$3p^6$	^1S	K	112.3869	A	96.10217	Cl	81.18783
$4s^1$	^2S	Ca	130.1744	K	112.4413		
$4s^2$	^1S			Ca	130.2436	K	112.4485
$3d^1$	^2D			Sc	150.6497		
$3d^2$	^3F	Sc	151.4151	Ti	173.2858	Sc	151.3041
$3d^3$	^4F	Ti	174.1834	V	198.1598	Ti	174.0642
$3d^4$	^5D	V	199.1627	Cr	225.3846	V	199.0490
$3d^5$	^6S	Cr	226.5326	Mn	255.0946	Cr	226.3239
$3d^6$	^5D	Mn	256.1654	Fe	287.1840	Mn	256.0124
$3d^7$	^4F	Fe	288.4189	Co	322.0240	Fe	288.2575
$3d^8$	^3F	Co	323.3581	Ni	359.7512	Co	323.1725
$3d^9$	^2D	Ni	360.9808	Cu	400.0073		
$3d^{10}$	^1S	Cu	401.6254				
$4s^1$	^2S	Zn	443.5981	Cu	401.4520	Ni	367.0901
$4s^2$	^1S	Ga	487.8287	Zn	443.4911	Cu	401.4083
$4p^1$	^2P	Ge	534.8446	Ga	488.0597		
$4p^2$	^3P	As	584.4249	Ge	535.1090	Ga	488.1461
	^1D		584.4121		535.1055		488.1216
	^1S		584.3779				
$4p^3$	^4S	Se	636.7640	As	584.7467	Ge	535.2614
	^2D		636.6319		584.7188		535.2159
	^2P		636.6039		584.7112		535.2054
$4p^4$	^3P	Br	691.5456	Se	637.0015	As	584.8960
	^1D		691.5312		636.9765		584.8695
	^1S		691.4848		636.9552		584.8337
$4p^5$	^2P	Kr	749.1885	Br	691.9457	Se	637.1991
$4p^6$	^1S			Kr	749.6405	Br	692.1783

[a] The positive ions of the transition elements (from Sc through Cu) have configurations $4s^0 3d^n$.

The evaluation of the interaction $\langle \Lambda \cdot \Lambda \rangle$ has been carried out using the analytical Hartree-Fock functions of Clementi [2] and Malli [9]. It has been considered more convenient to report in this case only the values of $\langle \Lambda \cdot \Lambda \rangle$, as in this way the mass polarization effect[3] may then be calculated at any time for any desired isotope; the corresponding values are collected in Table 1. This contribution is more important, varying from a value of $-4.40\,\mathrm{cm}^{-1}$ for B to a value of $-1067\,\mathrm{cm}^{-1}$ for Kr.

The accuracy of the values for the mass polarization effect parallels the accuracy of the electronic functions used. Taking into account the characteristics ($\Delta l = \pm 1$) mentioned above, it is evident that introduction of angular correlation will affect the values. This fact is clearly evident in those systems (He, Li, Be) with s^n configurations, where the Hartree-Fock value vanishes. (Calculations have been carried out for some of these systems using correlated functions [3, 10–12].)

References

1. Bethe, H., Salpeter, E. E.: Quantum mechanics of one- and two-electron systems. New York: Academic Press 1957.
2. Clementi, E.: Tables of atomic functions. San Jose: IBM 1965.
3. Dalgarno, A., Parkinson, E. M.: Physic. Rev. **176**, 73 (1968).
4. Fraga, S., Thorhallsson, J., Fisk, C.: Canad. J. Physics **47**, 1415 (1969).
5. Innes, F. R., Ufford, C. W.: Physic. Rev. **111**, 194 (1958).
6. Lo, B. W. N., Saxena, K. M. S., Fraga, S.: Theoret chim. Acta (Berl.) **24**, 71 (1972).
7. Theoret. chim. Acta (Berl.) (in press).
8. Theoret. chim. Acta (Berl.) (in press).
9. Malli, G.: Canad. J. Physics **44**, 3121 (1966).
10. Prasad, S. S., Stewart, A. L.: Proc. Physic. Soc. **87**, 159 (1966).
11. Schiff, B., Lifson, H., Pekeris, C. L., Rabinowitz, P.: Physic. Rev. **140**, A 1104 (1965).
12. Stewart, A. L.: Advanc. Physics **12**, 299 (1963).

Dr. S. Fraga
Division of Theoretical Chemistry
Department of Chemistry
University of Alberta
Edmonton 7, Alberta
Canada

Theoret. chim. Acta (Berl.) 25, 396—399 (1972)
© by Springer-Verlag 1972

Relationes

The Electronic Structure of the Silyl Halides

D. R. ARMSTRONG, J. JAMIESON, and P. G. PERKINS
Department of Pure and Applied Chemistry, University of Strathclyde, Glasgow, C. 1, Scotland

Received December 3, 1971

Calculations have been performed on the silyl and methyl halides, using the CNDO method and the photoelectron spectra of the silyl halides are interpreted from the results. Inclusion of *d* orbitals on silicon is found to be necessary so that the calculated ionisation potentials of silyl bromide and chloride are greater than the corresponding methyl compounds, in agreement with observation.

Introduction

A recent publication by Cradock and Ebsworth dealing with the photoelectron spectra of the silyl halides [3] gave the observed band positions for electrons believed to be excited from the halogen "lone pair" orbitals orthogonal to the Si–X axis. The authors concluded, moreover, from the presence of vibrational bands in the photoelectron spectra, that there is bonding between these lone pair halogen electrons and the silicon 3*d* orbitals. However, an *ab initio* calculation on SiH_3F [2] has suggested that the first ionisation potential should occur at a much lower energy than that reported in Ref. [3], and it therefore seemed of interest to calculate the electronic structure of the silyl halides, SiH_3F, SiH_3Cl and SiH_3Br, to examine the nature of the molecular orbitals which give rise to the photoelectron spectra, and to evaluate the extent of the postulated $(d_\pi - p_\pi)$ π-bonding.

Our method of calculation used a modified [1] version of the CNDO/2 method [5]. The parameters used in the calculation were taken from previous work [4] and the relevant interatomic distances were abstracted from Ref. [6].

The parameter k used in the construction of the offdiagonal elements of the H matrix

$$H_{\mu\nu} = k S_{\mu\nu} (I_\mu I_\nu)^{\frac{1}{2}}$$

was varied in the calculations on silyl fluoride so as to obtain a set of eigenvalues comparable with the eigenvalues given by the *ab initio* calculation [2].

Results and Discussion

Calculations were attempted on silyl fluoride using a wide range of k values, and we found that in no case did the energy of the highest filled molecular orbital approach the value quoted (16.1 eV) by Cradock and Ebsworth. However, the

Table 1. Valence orbital eigenvalues (eV) for silyl and methyl halides

Eigenvalue	1	2	3,4		5		6,7
CH_3F	−45.41	−31.15	−19.48		−13.98		−12.75
SiH_3F	−40.43	−24.83	−16.76		−12.34		−12.33
SiH_3F^a	−39.52	−24.68	−16.66	$\Psi_{5,6}$	−11.66	Ψ_7	−11.50
CH_3Cl	−41.30	−24.68	−20.23		−12.41		−10.77
SiH_3Cl	−32.77	−25.26	−17.47		−12.14		−11.30
SiH_3Cl^a	−32.61	−24.27	−17.60		−11.24		−10.11
CH_3Br	−37.16	−23.97	−18.47		−11.73		−10.27
SiH_3Br	−29.78	−24.77	−16.62		−11.46		−10.95
SiH_3Br^a	−29.45	−23.36	−16.21		−10.18		− 9.75

[a] Without *d* orbitals on silicon.

Table 2. Experimental lone pair ionisation potentials (eV) for silyl and methyl halides

Halide	Methyl[a]	Silyl[b]
fluoride	17.0	16.1
chloride	11.28	11.61
bromide	10.70	11.03

[a] Ref. [7]. – [b] Ref. [3].

latter quantity correlated well in energy with the third and fourth molecular orbitals (a degenerate bonding pair). These have some halogen lone pair character (see later). Our finding also agreed with the *ab initio* work of Ref. [2] when a value of $k = 1.15$ was chosen.

Using this k value of 1.15, calculations were next performed on the silyl and methyl halides, both including and neglecting the silicon 3*d* orbitals. The eigenvalues and the experimental ionisation potentials assigned to the "lone pair" electrons are given in Table 1 and 2 respectively. From these values it can readily be seen that the experimental "lone pair" ionisation potentials correlate with the energies of molecular orbitals 3 and 4 for both methyl and silyl fluoride, whilst for the chloride and bromide they correspond to the 6th and 7th eigenvalues. Both these pairs are degenerate and examination of their eigenvector elements (Table 3) reveals that orbitals 3 and 4 are bonding in nature while the 6th and 7th are antibonding orbitals orthogonal to the Si–X axis. Table 3 shows that on going from the fluoride to the bromide the contribution of the halogen "π" orbitals to the bonding orbital decreases whereas it increases in the antibonding orbital. The LCAO MO approach which we have used no doubt somewhat overestimates the conjugation of these halogen lone pairs but some delocalisation certainly occurs and the degenerate orbitals incorporate substantial amounts of the halogen "$p\pi$" orbital. Moreover, the calculations show that the energies of the 6th and 7th orbitals show only a gradual trend over the halide series and, therefore, a band at 12.3 eV should be expected in the photoelectron spectrum of silyl fluoride having characteristics similar to those of the bromide and chloride.

Table 3. Atomic orbital coefficients for silicon and halogen p orbitals in the degenerate molecular orbitals of the silyl halides

Molecular orbital number	3		6	
	C(Si)	C(X)	C(Si)	C(X)
SiH_3F	0.62	0.59	0.26	0.84
SiH_3Cl	0.63	0.50	0.26	0.84
SiH_3Br	0.65	0.40	0.19	0.89

Table 4 Contribution to total bond order (%) of each type of π-bonding present in the methyl and silyl halides between carbon (silicon) and halogen

	$Mp\pi$-$Xp\pi$	$Mp\pi$ $Xd\pi$	$Md\pi$ $Xd\pi$	$Md\pi$ $Xp\pi$
CH_3F	7.1			
CH_3Cl	6.1	22.8		
CH_3Br	4.0	19.3		
SiH_3F	9.7			10.2
SiH_3Cl	7.5	14.2	0.5	17.1
SiH_3Br	6.7	11.9	0.3	18.2

An interesting aspect of the calculations is that for the chloro- and bromo-compounds the silyl derivative has a larger ionisation potential than the methyl halide only when d orbitals are included in the calculation. This agree with experiment and would seem to indicate that d orbitals are important in the bonding in silyl halides. The calculations also reveal the degree of each type of π-type bonding (i.e., involving d or p orbitals) present between silicon (carbon) and the particular halogen, and these data are given in Table 4. The $p\pi - d\pi$ and $d\pi - p\pi$ components of the bond order are numerically quite substantial, although it must be remembered that, physically, the important quantity is the bond energy and the $p\pi - d\pi$ and $d\pi - p\pi$ fractions of this term will certainly be much smaller.

Table 5. The overall charge distribution in the methyl and silyl halides

	M	X	H
SiH_3F	0.46	−0.31	−0.05
SiH_3Cl	0.21	−0.16	−0.02
SiH_3Br	0.16	−0.09	−0.02
CH_3F	0.14	−0.23	0.03
CH_3Cl	0.06	−0.23	0.06
CH_3Br	−0.02	−0.11	0.04

The overall charge distributions in all the halides are presented in Table 5. The results correlate with those expected from simple electronegativity principles, although the charge on chlorine in methyl chloride is somewhat anomalous and is clearly due to the *d* orbital occupancy of chlorine.

One of us (J.J.) thanks the Scottish Education Department for a Maintenance Grant.

References

1. Armstrong, D. R., Perkins, P. G., Stewart, J. J. P.: J. chem. Soc. (London) A (in press).
2. Breeze, A., Collins, G. A. D., Cruickshank, D. W. J.: J. chem. Soc. (London) D **1971**, 445.
3. Cradock, S., Ebsworth, E. A. V.: J. chem. Soc. (London) D **1971**, 57.
4. Levison, K., Perkins, P. G.: Theoret. chim. Acta (Berl.) **14**, 206 (1969).
5. Pople, J. A., Santry, D. P., Segal, G. A.: J. chem. Physics **43**, S 129 (1965).
6. Sutton, L. E.: Ed. Tables of interatomic distances and configurations in molecules and ions, Special Publication No. 11. London: The Chemical Society 1958.
7. Turner, D. W., Baker, C., Baker, A. D., Brundle, C. R.: Molecular photo-electron spectroscopy. London, New York, Sydney, and Toronto: Wiley Intersciences 1970.

Dr. D. R. Armstrong
Department of Pure and Applied Chemistry
University of Strathclyde
Glasgow, C. 1
Scotland

Theoret. chim. Acta (Berl.) 25, 400–402 (1972)
© by Springer-Verlag 1972

Charge Distributions in Polyatomic Ions

M. F. C. Ladd
Department of Chemical Physics, University of Surrey, Guildford, Surrey, England

Received February 8, 1972

The determination of charge distributions in polyatomic ions through both energetic and quantum mechanical (CNDO/2) methods is discussed. Results from both methods are shown to be in good agreement

In an earlier paper [1], a method for evaluating the charge distribution in polyatomic ions in inorganic salts was presented. The purpose of this note is to consider an extension of that work, and to give an indication of the precision of the method through a comparison with quantum mechanical calculations.

In a study of alkali-metal cyanides [1], the various factors involved in bringing two polymorphs on to a common internal energy basis were discussed. It seems possible to relax these requirements slightly, and yet retain a reasonably precise result.

Early calculations of the cohesive energies of inorganic salts containing polyatomic ions treated the polyatomic ion as a point charge at the centre of gravity of the ion-group (the point-charge model). More refined calculations consider the distribution of the total ionic charge among the atomic species present in the ion (the distributed-charge model).

In the cyanides, the decrease in cohesive energy for the distributed-charge model is 5–10% of that found for the point-charge model. The change occurs mainly in the electrostatic part of the cohesive energy. From those and other (including the present) studies, it seems that provided $\Sigma|z_i| \simeq Z$, where z_i are the charges on the atoms in a polyatomic ion of total charge Z, the greater the spread of the charge, the lower is the numerical value of the electrostatic energy. This takes place through a decrease in the value of the Madelung constant. If, however, $\Sigma|z_i| > Z$, while $|\Sigma z_i| = Z$ (necessarily), then wider variations in the Madelung term may be obtained.

Calculations have been carried out on the calcite (c1), aragonite (c2) and vaterite (c3) forms of calcium carbonate. The Madelung terms $A(L)/L$, where L is the shortest interatomic distance in the crystal, have been evaluated by the Bertaut-Templeton expressions [2–4], as a function of z_0, the charge, including sign, on the oxygen atom; the charge z_c on the carbon atom is $(-2-3z_0)$. A linear distribution function was employed together with a summation limit of about 1.2 reciprocal space units. The results are illustrated by Fig. 1. The curves are approximately parabolic and may be represented by the similar Eqs. (1)–(3),

Table 1. Energy parameters and charge distributions for polymorphs of calcium carbonate

	ϱ/L, Å^{-1}	$-U$, kcal mol^{-1}	$-U'$, kcal mol^{-1}	$A(L)/L$, Å^{-1}	Z_0, e. units
Calcite (c 1)	0.10	640	589	1.97	−0.763
Aragonite (c 2)	0.11	624	574	1.93	−0.755
Vaterite (c 3)	0.11^a	642	591	2.00	−0.794
					Mean z_0 = −0.77

^{a} Estimated value.

with average r.m.s. errors ε_i $(i = 1, 2, 3)$:

$$\mathrm{c1}: A(L)/L = 2.1422 + 4.5391\, z_0 + 5.6546\, z_0^2 \qquad \varepsilon_1 = 3.7 \times 10^{-3} \tag{1}$$

$$\mathrm{c2}: A(L)/L = 2.1068 + 4.3201\, z_0 + 5.4193\, z_0^2 \qquad \varepsilon_2 = 6.3 \times 10^{-3} \tag{2}$$

$$\mathrm{c3}: A(L)/L = 2.1679 + 4.6551\, z_0 + 5.5989\, z_0^2 \qquad \varepsilon_3 = 3.1 \times 10^{-3} \tag{3}$$

Crystal cohesive energies have been calculated from Eqs. (4) and (5), where the terms used have their usual significances.

$$U(L) = -(A(L)e^2/L)\{1 - (\varrho/L)\}, \tag{4}$$

$$(\varrho/L) = (A(L)e^2/L)/\{(9V/\beta) + (2A(L)e^2/L)\}. \tag{5}$$

Crystal data were taken from Wyckoff [5] and compressibilities from the International Critical Tables [6]. The point-charge model values of U are listed in Table 1. If we accept a decrease of about 8% of the cohesive energy U, as suggested by the work on the cyanides, then the energies, U', for the distributed-

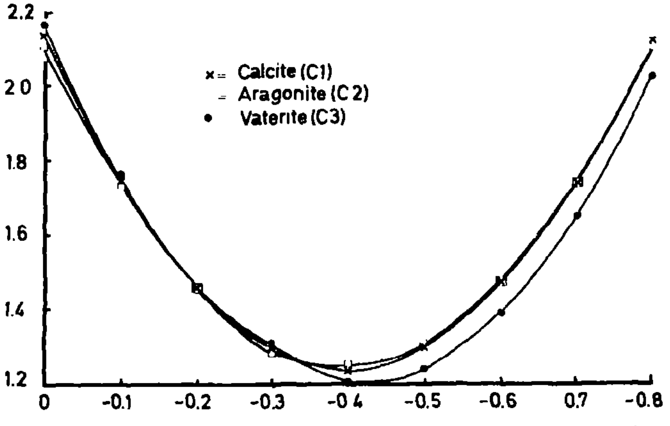

Fig. 1. Variation of the Madelung term, $A(L)/L$, with charge, z_0, on oxygen in three polymorphs of $CaCO_3$

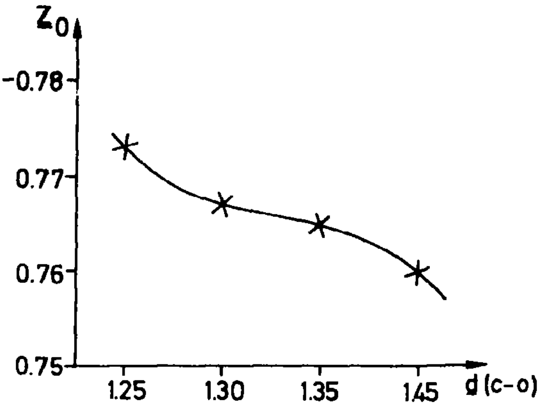

Fig. 2. Variation of z_0 with bond distance d(C–O) in the carbonate ion

charge model may be obtained through Eqs. (4) and (5). The appropriate Madelung terms are obtained and from Fig. 1, the corresponding values of z_0; all of these values are listed in the table. The alternative values for z_0, lying between -0.03 and -0.05 electron units, are rejected as unrealistic.

Quantum mechanical calculations of the charge distribution in the carbonate ion (symmetry, $\bar{6}m2$) have been carried out by the CNDO/2 method [7, 8] as a function of the C–O distance, d. The results are illustrated in Fig. 2. For the calcium carbonate structures, d is approximately 1.26 Å, whence z_0 is -0.771.

The agreement between the values of z_0 obtained by these two independent procedures is very good, and leads one to place reliance upon these methods of calculating charge distributions in simple polyatomic ions.

The author is grateful to Dr. R. Grinter of the University of East Anglia for assistance with the quantum mechanical calculations.

References

1. Ladd, M. F. C.: Trans. Faraday Soc. 65, 2712 (1969).
2. Bertant, F.: J. Physics Radium 13, 499 (1952).
3. Templeton, D. H.: J. chem. Physics 23, 1629 (1955).
4. Jones, R. E., Templeton, D. H.: J. chem. Physics 25, 1062 (1956).
5. Wyckoff, R. W. G.: Crystal structures, Vol. 2, 1967.
6. International critical tables. Vol. 3, 1928.
7. Pople, J. A., Santry, D. P., Segal, G. A.: J. chem. Physics 43, S 129 (1965).
8. Jaffe, H. H., Del Bene, J.: J. chem. Physics 48, 1807 (1968).

[illegible]
38963
[illegible] 24.4.80

Dr. M. F. C. Ladd
University of Surrey
Guildford, Surrey
England